NEUROIMMUNOLOGY OF THE INNER EAR

EDITED BY: Agnieszka J. Szczepek, Paola Perin, Franca Marino and Isabel Varela-Nieto

PUBLISHED IN: Frontiers in Neurology, Frontiers in Immunology and Frontiers in Neuroscience

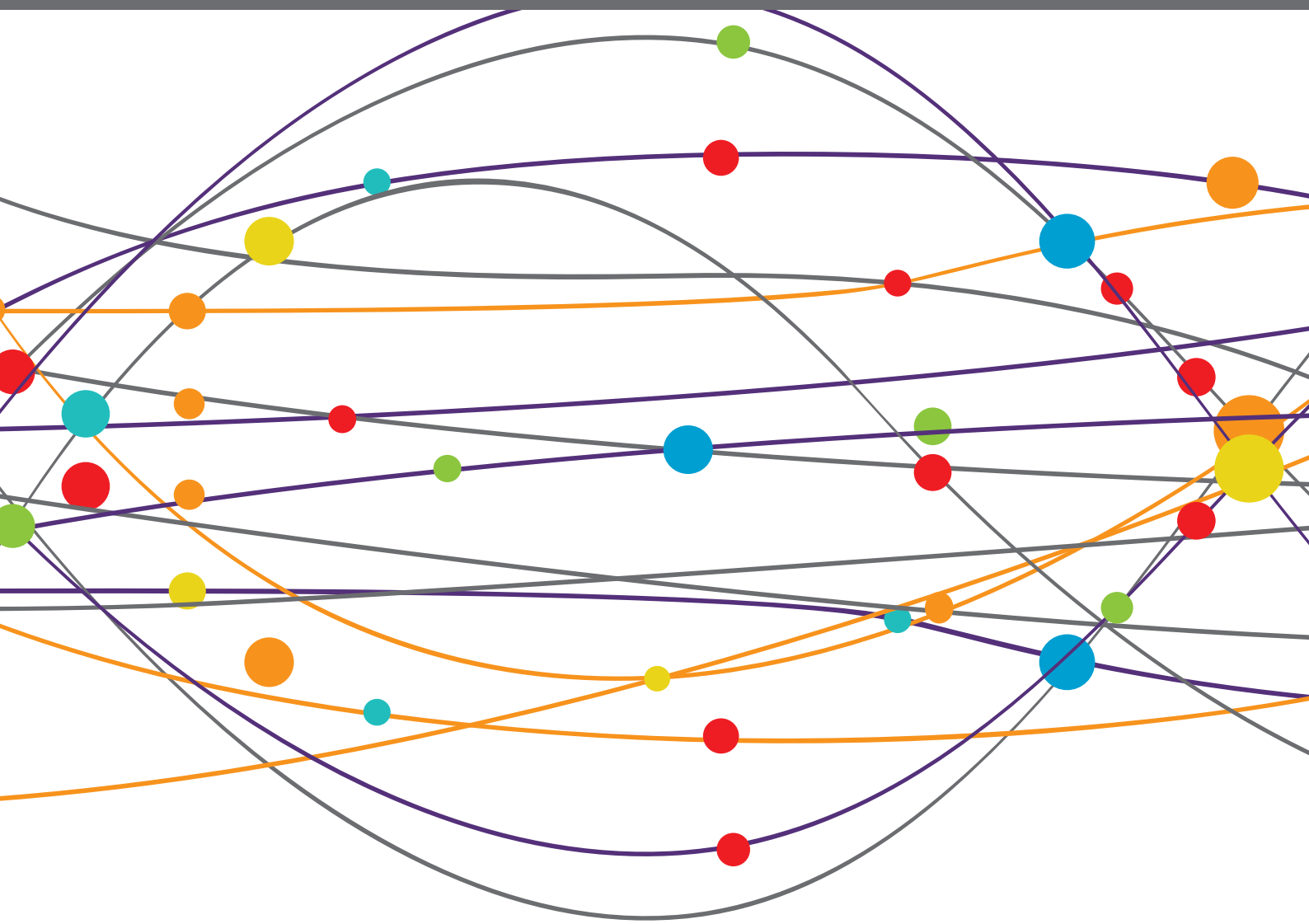

frontiers Research Topics

ISSN 1664-8714
ISBN 978-2-88966-590-7
DOI 10.3389/978-2-88966-590-7

About Frontiers

Frontiers is more than just an open-access publisher of scholarly articles: it is a pioneering approach to the world of academia, radically improving the way scholarly research is managed. The grand vision of Frontiers is a world where all people have an equal opportunity to seek, share and generate knowledge. Frontiers provides immediate and permanent online open access to all its publications, but this alone is not enough to realize our grand goals.

Frontiers Journal Series

The Frontiers Journal Series is a multi-tier and interdisciplinary set of open-access, online journals, promising a paradigm shift from the current review, selection and dissemination processes in academic publishing. All Frontiers journals are driven by researchers for researchers; therefore, they constitute a service to the scholarly community. At the same time, the Frontiers Journal Series operates on a revolutionary invention, the tiered publishing system, initially addressing specific communities of scholars, and gradually climbing up to broader public understanding, thus serving the interests of the lay society, too.

Dedication to Quality

Each Frontiers article is a landmark of the highest quality, thanks to genuinely collaborative interactions between authors and review editors, who include some of the world's best academicians. Research must be certified by peers before entering a stream of knowledge that may eventually reach the public - and shape society; therefore, Frontiers only applies the most rigorous and unbiased reviews.
Frontiers revolutionizes research publishing by freely delivering the most outstanding research, evaluated with no bias from both the academic and social point of view. By applying the most advanced information technologies, Frontiers is catapulting scholarly publishing into a new generation.

What are Frontiers Research Topics?

Frontiers Research Topics are very popular trademarks of the Frontiers Journals Series: they are collections of at least ten articles, all centered on a particular subject. With their unique mix of varied contributions from Original Research to Review Articles, Frontiers Research Topics unify the most influential researchers, the latest key findings and historical advances in a hot research area! Find out more on how to host your own Frontiers Research Topic or contribute to one as an author by contacting the Frontiers Editorial Office: frontiersin.org/about/contact

NEUROIMMUNOLOGY OF THE INNER EAR

Topic Editors:
Agnieszka J. Szczepek, Charité – Universitätsmedizin Berlin, Germany
Paola Perin, University of Pavia, Italy
Franca Marino, University of Insubria, Italy
Isabel Varela-Nieto, Consejo Superior de Investigaciones Científicas (CSIC), Spain

Citation: Szczepek, A. J., Perin, P., Marino, F., Varela-Nieto, I., eds. (2021). Neuroimmunology of the Inner Ear. Lausanne: Frontiers Media SA.
doi: 10.3389/978-2-88966-590-7

Table of Contents

05 ***Editorial: Neuroimmunology of the Inner Ear***
Paola Perin, Franca Marino, Isabel Varela-Nieto and Agnieszka J. Szczepek

11 ***Differential Proinflammatory Signature in Vestibular Migraine and Meniere Disease***
Marisa Flook, Lidia Frejo, Alvaro Gallego-Martinez, Eduardo Martin-Sanz, Marcos Rossi-Izquierdo, Juan Carlos Amor-Dorado, Andres Soto-Varela, Sofia Santos-Perez, Angel Batuecas-Caletrio, Juan Manuel Espinosa-Sanchez, Patricia Pérez-Carpena, Marta Martinez-Martinez, Ismael Aran and Jose Antonio Lopez-Escamez

22 ***Anti-inflammatory and Oto-Protective Effect of the Small Heat Shock Protein Alpha B-Crystallin (HspB5) in Experimental Pneumococcal Meningitis***
Silvia T. Erni, Gabriella Fernandes, Michelle Buri, Michael Perny, Rolf Jan Rutten, Johannes M. van Noort, Pascal Senn, Denis Grandgirard, Marta Roccio and Stephen L. Leib

37 ***Lack of Fractalkine Receptor on Macrophages Impairs Spontaneous Recovery of Ribbon Synapses After Moderate Noise Trauma in C57BL/6 Mice***
Tejbeer Kaur, Anna C. Clayman, Andrew J. Nash, Angela D. Schrader, Mark E. Warchol and Kevin K. Ohlemiller

53 ***Defining the Inflammatory Microenvironment in the Human Cochlea by Perilymph Analysis: Toward Liquid Biopsy of the Cochlea***
Athanasia Warnecke, Nils K. Prenzler, Heike Schmitt, Kerstin Daemen, Jana Keil, Martin Dursin, Thomas Lenarz and Christine S. Falk

63 ***Human Inner Ear Immune Activity: A Super-Resolution Immunohistochemistry Study***
Wei Liu, Charlotta Kämpfe Nordström, Niklas Danckwardt-Lilliestrom and Helge Rask-Andersen

77 ***Early Diagnosis of Hearing Loss in Patients Under Methadone Maintenance Treatment***
Arash Bayat, Nader Saki, Golshan Mirmomeni and Ali Yadollahpour

83 ***Nfatc4 Deficiency Attenuates Ototoxicity by Suppressing Tnf-Mediated Hair Cell Apoptosis in the Mouse Cochlea***
Yanping Zhang, Diyan Chen, Liping Zhao, Wen Li, Yusu Ni, Yan Chen and Huawei Li

94 ***Main Aspects of Peripheral and Central Hearing System Involvement in Unexplained HIV-Related Hearing Complaints***
Marrigje Aagje de Jong, Ari Luder and Menachem Gross

100 ***Age-Related Changes in Immune Cells of the Human Cochlea***
Kenyaria V. Noble, Ting Liu, Lois J. Matthews, Bradley A. Schulte and Hainan Lang

113 ***Subcellular Abnormalities of Vestibular Nerve Morphology in Patients With Intractable Meniere's Disease***
Pengjun Wang, Huaming Zhu, Wen Lu, Qiang Song, Zhengnong Chen, Yaqin Wu, Hui Wang, Dongzhen Yu, Haibo Ye, Haibo Shi and Shankai Yin

123 ***Cytokine Levels in Inner Ear Fluid of Young and Aged Mice as Molecular Biomarkers of Noise-Induced Hearing Loss***
Lukas D. Landegger, Sasa Vasilijic, Takeshi Fujita, Vitor Y. Soares, Richard Seist, Lei Xu and Konstantina M. Stankovic

137 ***Biomarkers in Vestibular Schwannoma–Associated Hearing Loss***
Luis Lassaletta, Miryam Calvino, Jose Manuel Morales-Puebla, Pablo Lapunzina, Lourdes Rodriguez-de la Rosa, Isabel Varela-Nieto and Victor Martinez-Glez

144 ***Early Development of Resident Macrophages in the Mouse Cochlea Depends on Yolk Sac Hematopoiesis***
Ippei Kishimoto, Takayuki Okano, Koji Nishimura, Tsutomu Motohashi and Koichi Omori

157 ***Vertigo and Severe Balance Instability as Symptoms of Lyme Disease—Literature Review and Case Report***
Magdalena Jozefowicz-Korczynska, Ewa Zamyslowska-Szmytke, Anna Piekarska and Oskar Rosiak

162 ***Csf1 Signaling Regulates Maintenance of Resident Macrophages and Bone Formation in the Mouse Cochlea***
Takayuki Okano and Ippei Kishimoto

170 ***Correlations Between Vestibular Function and Imaging of the Semicircular Canals in DFNA9 Patients***
Berina Ihtijarevic, Sebastien Janssens de Varebeke, Griet Mertens, Sven Dekeyzer, Paul Van de Heyning and Vincent Van Rompaey

177 ***Intracochlear Perfusion of Tumor Necrosis Factor-Alpha Induces Sensorineural Hearing Loss and Synaptic Degeneration in Guinea Pigs***
Sachiyo Katsumi, Mehmet I. Sahin, Rebecca M. Lewis, Janani S. Iyer, Lukas D. Landegger and Konstantina M. Stankovic

189 ***Genetic Hearing Loss Associated With Autoinflammation***
Hiroshi Nakanishi, Pragya Prakash, Taku Ito, H. Jeffrey Kim, Carmen C. Brewer, Danielle Harrow, Isabelle Roux, Seiji Hosokawa and Andrew J. Griffith

196 ***Immune Response After Cochlear Implantation***
Edi Simoni, Erica Gentilin, Mariarita Candito, Giulia Borile, Filippo Romanato, Milvia Chicca, Sara Nordio, Marta Aspidistria, Alessandro Martini, Diego Cazzador and Laura Astolfi

211 ***Cannabinoids, Inner Ear, Hearing, and Tinnitus: A Neuroimmunological Perspective***
Paola Perin, Alex Mabou Tagne, Paolo Enrico, Franca Marino, Marco Cosentino, Roberto Pizzala and Cinzia Boselli

frontiers in Neurology

EDITORIAL
published: 09 February 2021
doi: 10.3389/fneur.2021.635359

Editorial: Neuroimmunology of the Inner Ear

Paola Perin[1]*, *Franca Marino*[2], *Isabel Varela-Nieto*[3,4,5] and *Agnieszka J. Szczepek*[6,7]*

[1] Department of Brain and Behavioural Sciences, University of Pavia, Pavia, Italy, [2] Center of Research in Medical Pharmacology University of Insubria, Varese, Italy, [3] Institute for Biomedical Research "Alberto Sols" (IIBM), Spanish National Research Council-Autonomous University of Madrid (CSIC-UAM), Madrid, Spain, [4] Rare Diseases Networking Biomedical Research Centre, Centro de Investigación Biomédica en Red, Carlos III Institute of Health, Madrid, Spain, [5] La Paz Hospital Institute for Health Research (IdiPAZ), Madrid, Spain, [6] Department of Otorhinolaryngology, Head and Neck Surgery, Charité-Universitätsmedizin Berlin, Corporate Member of Freie Universität Berlin, Humboldt-Universität zu Berlin, and Berlin Institute of Health, Berlin, Germany, [7] Faculty of Medicine and Health Sciences, University of Zielona Gora, Zielona Gora, Poland

Keywords: inner ear, immunology, neuroimmunology, balance, hearing, disorders

Editorial on the Research Topic

Neuroimmunology of the Inner Ear

OPEN ACCESS

Edited by:
Michael Strupp, Ludwig Maximilian University of Munich, Germany

Reviewed by:
Göran Frans Emanuel Laurell, Uppsala University, Sweden
Akira Ishiyama, University of California, Los Angeles, United States
Peter S. Steyger, Creighton University, United States

***Correspondence:**
Paola Perin
pperin@unipv.it
Agnieszka J. Szczepek
agnes.szczepek@charite.de

Specialty section:
This article was submitted to Neuro-Otology, a section of the journal Frontiers in Neurology

Received: *30 November 2020*
Accepted: *07 January 2021*
Published: *09 February 2021*

Citation:
Perin P, Marino F, Varela-Nieto I and Szczepek AJ (2021) Editorial: Neuroimmunology of the Inner Ear. Front. Neurol. 12:635359. doi: 10.3389/fneur.2021.635359

Although the term was first officially used in 1982 (1), neuroimmunology is now a mature field that has gained immense traction in the past decade. Thanks to novel technological advances, the cellular and molecular mechanisms that mediate the crosstalk between the immune and nervous systems are increasingly appreciated in both physiological and pathological states (1).

Similar to the brain, the inner ear has long been considered an "isolated" system devoted to auditory and vestibular signal processing and protected by a blood-labyrinth barrier (BLB) (2–5), and the early neuroimmunology of the inner ear was mainly focused on autoimmunity (6, 7), and on the role of macrophages in cochlear damage (8, 9). In parallel to the brain, awareness about non-neural cells and molecules affecting inner ear functions has been steadily growing[1], and neuro-immunological studies of the inner ear face multiple challenges, including an overwhelming number of cellular and molecular interactions, which will require a systems biology approach to grasp their full functionality. In addition, the inner ear poses unique difficulties due to its tight bone encasing and complex fluid regulation.

Like most organs, including the brain, the inner ear immune cells are dominated by several populations of macrophages [reviewed in (10, 11)], which largely contribute to both inflammatory/phagocytic and regenerative/protective responses. However, several questions are still open, such as:

- What are the signals exchanged between immune cells and inner ear cells in healthy and pathological settings?
- How much communication is there between the inner ear and surrounding tissues and fluids?
- What is the neuroimmune role of the endolymphatic sac?
- What are the roles, nature, and location of several immune cell populations and subpopulations, e.g., mast cells (12), lymphocytes (13), or other leukocytes (14)?
- How are local and systemic immune responses regulated—and especially dysregulated- in various kinds of damage (e.g., infection, noise trauma, and ototoxicity)?
- How do neuroimmune interactions translate in the modulation of inner ear functions?

[1] PUBMED search with the query "(inner ear OR cochlea OR vestibular) AND (neuroimmune OR neuroimmunology)" only retrieves 14 results, but this reflects the still sparse use of "neuroimmune", since the related queries "(inner ear OR cochlea OR vestibular) AND (immune OR macrophage OR cytokine)" and "(inner ear OR cochlea OR vestibular) AND (inflammatory OR inflammation)" retrieve 1,734 and 2,043 results, respectively.

The articles collected in this Research Topic reflect this increasingly diverse field in several main threads, broadly divided into immune cell characterization, responses to diseases or damage, biomarkers, and immune molecular targets (**Figure 1**). Both human and animal studies are included in this Special Topic. The system's complexity at both cellular and functional levels requires the integration of invasive approaches only possible in animals and testing of functions and markers that may be incompletely overlapping between humans and other animals. **Table 1** summarizes the main points that were contributed by human and animal studies within this Research Topic.

Five papers published in this Research Topic focus on the description of the immune cells of the inner ear, with a predominance of studies regarding cochlear macrophages, consistent with their role as leading players both by number and function, as reviewed in (10, 11).

The paper "Early Development of Resident Macrophages in the Mouse Cochlea Depends on Yolk Sac Hematopoiesis" describes the presence of two resident macrophage populations in the mouse cochlea, derived respectively from the yolk sac and fetal liver (Kishimoto et al.). These populations are different in their Csf1-dependence and final cochlear localization. The origin of macrophages may be reflected in their various shapes in the adult cochlea, as seen in human samples in the following two papers. The first, "Age-Related Changes in Immune Cells of the Human Cochlea," describes macrophage populations associated with various parts of the human cochlea and the aging-dependent changes occurring in these cells (Noble et al.). Similarly, the paper "Human Inner Ear Immune Activity: A Super-Resolution Immunohistochemistry Study," describes immune cells (mainly macrophages and to a lesser extent T lymphocytes) associated with the human cochlea and endolymphatic sac (Liu et al.). Both papers observed an association between cell shapes and their localization in the inner ear. Finally, two groups studied macrophage-related gene knock-out effects on the inner ear function and anatomy using the mouse model. "Csf1 Signaling Regulates Maintenance of Resident Macrophages and Bone Formation in the Mouse Cochlea" underlines the impact of the Csf1op/op genotype (where no Csf1 is produced) on cochlear bone remodeling and cochlear macrophages, therefore pointing to a possible connection between immune responses and bony capsule metabolism (Okano and Kishimoto). On the other hand, the paper "Lack of Fractalkine Receptor on Macrophages Impairs Spontaneous Recovery of Ribbon Synapses After Moderate Noise Trauma in C57BL/6 Mice" demonstrates the negative impact of knocking-out the fractalkine receptor on ribbon synapse recovery after noise trauma, suggesting a protective role for auditory nerve-associated macrophages (Kaur et al.).

Eight other papers in this Research Topic studied immune responses in the inner ear in a pathological context, three of which (two in humans and one in a rat model) focus on infectious diseases. Passive barriers strongly protect the inner ear, but pathogens may enter it through its connections with CSF and middle ear, plus vascular and neural routes additionally available for viruses (15). Moreover, even systemic responses to pathogens may affect the ear indirectly, due to immune crossreactivity (as suggested after viral or fungal infection, reviewed in (16) or BLB impairment opening the way to ototoxic factors into the inner ear (17–19).

The review "Main Aspects of Peripheral and Central Hearing System Involvement in Unexplained HIV-Related Hearing Complaints" presents an interesting study on the auditory consequences of HIV viral infection (which show similarities to age-induced hearing impairment), an aspect not well-understood and of enormous importance (de Jong et al.). The paper "Vertigo and Severe Balance Instability as Symptoms of Lyme Disease—Literature Review and Case Report" describes the effects of neuroborreliosis, which can target the 8th nerve, on the human vestibular system from a clinical point of view (Jozefowicz-Korczynska et al.). The work described in "Anti-inflammatory and Oto-Protective Effect of the Small Heat Shock Protein Alpha B-Crystallin (HspB5) in Experimental Pneumococcal Meningitis" demonstrates in a rat model that inner ear damage due to meningococcal infection goes together with an increase of proinflammatory cytokines in CSF, and rise in the numbers of cochlear neutrophils and macrophages (Erni et al.). The cytokine (but not the cellular) response could be reduced by intracisternal injection with the small heat shock protein alpha B-crystallin (HspB5), which also ameliorated hearing loss.

Besides infections, the inner ear can be affected by exposure to stress factors (including noise, drugs, and surgery), aging, genetic defects, or pathologies of unclear etiology, such as Menière's disease (MD). Many of these settings are accompanied by inflammation—a classical response to damage that is beneficial *per se* but may become detrimental if dysregulated, further damaging the inner ear [reviewed in (20, 21)]. Moreover, inflammation related to invasive inner ear intervention, such as cochlear implantation (CI), may lead to fibrosis and bone neoformation (22, 23), which degrade residual hearing. An effective otoprotective strategy in CI is the use of dexamethasone-eluting electrodes (24–26). However, understanding the otoprotective mechanisms of dexamethasone in CI is difficult since steroids can block all inflammatory response phases (20). Interestingly, CI influences the composition of macrophages subsets in animals (27, 28) and humans (29, 30). In the animal model, where the entire inflammatory process can be followed, macrophages have been found in the inflammatory, cytotoxic phenotype (27), and in the reparative phenotype, which is associated to matrix deposition and remodeling, and therefore to fibrosis (28). Moreover, a protective macrophage subpopulation has been observed in rodents' spiral ganglion (31) and suggested to exist in humans (29). The foreign-body responses may also induce the macrophages to form giant multinucleated cells with osteoblast-like properties (32). Finally, CI may also recruit B and T lymphocytes (33). The manuscript "Immune Response After Cochlear Implantation" shows that dexamethasone-eluting electrodes reduce both the cellular and cytokine signature of acute inflammatory response and fibrosis associated with implantation in a guinea pig, a well-established animal model for CI (Simoni et al.).

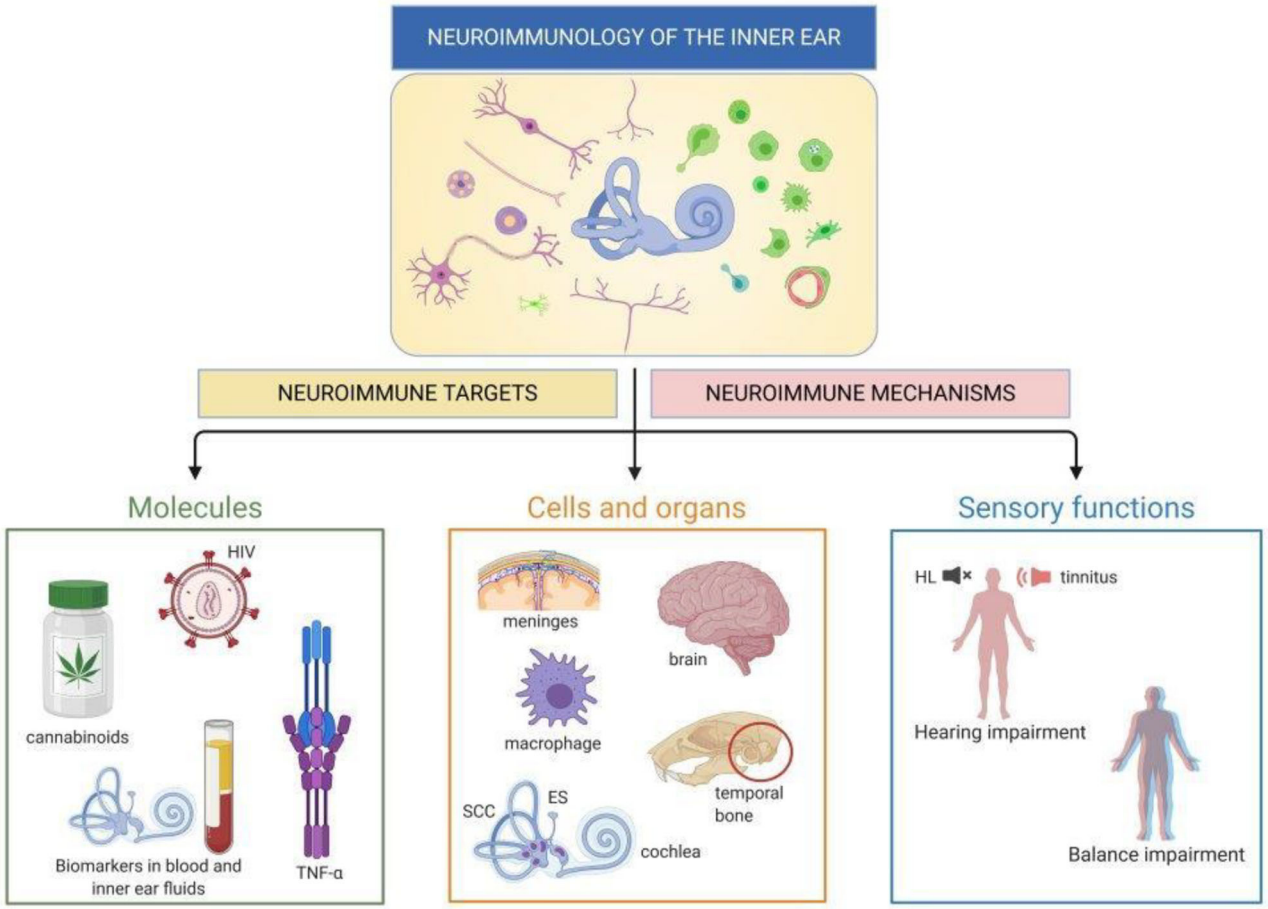

FIGURE 1 | Neuroimmunology of the inner ear. Visual abstract of this Research Topic: each paper within this Topic explores molecules, cells and/or functions related to inner ear neuroimmune interactions. HL, hearing loss; ES, endolymphatic sac; SCC, semicircular canals. Created with Biorender.com.

The paper "Genetic Hearing Loss Associated With Autoinflammation" describes deafness correlated with mutations affecting the NLRP3 inflammasome and other genes that influence macrophages (Nakanishi et al.). Inflammation of strial blood vessels was suggested, among other possible causes, in ototoxicity secondary to methadone treatment in humans in the paper "Early Diagnosis of Hearing Loss in Patients Under Methadone Maintenance Treatment" by Bayat et al..

Finally, two papers focus on the immune-inflammatory response in Menière's disease. As of today, MD diagnosis and monitoring are based on clinical symptoms, and no selective biomarker is available (34, 35). Endolymphatic hydrops has been long associated (although not exclusively) with MD, and endolymph-producing and reabsorbing structures in the ear are being targeted in treatment options [reviewed in (34, 35)]. Also, recent studies show a breakdown of the human utricular BLB in MD due to increased vesicular transport in endothelial cells and pericytes (36). Therefore, perilymph production appears to be affected, as well. In fact, a diagnostic tool based on gadolinium-enhanced MRI is being considered for MD (37, 38).

MD etiology is still debated and includes a combination of genetic, immune, inflammatory, environmental, hemodynamic, and hormonal factors (39). Immune-inflammatory responses seem however central, given that several genes linked to MD belong to immune or inflammation pathways (40), and that a significant percentage of patients with MD is also affected by other autoimmune diseases (41), or displays enhanced and anomalous inflammatory responses (42). Moreover, the endolymphatic sac, which is involved in endolymph reabsorption and displays morphological changes in MD (43), is the primary immune structure of the inner ear (44), and inner ear vasculature permeability is strongly affected by inflammation (45). Finally, MD immune-inflammatory model explains the effectiveness of steroid treatment (46). However, as for other immune diseases, treatment of subjects non-responsive to steroids requires personalized approaches that depend on the particular pathway being deranged (40).

The report "Subcellular Abnormalities of Vestibular Nerve Morphology in Patients with Intractable Menière's Disease" found the presence of structures associated to neurodegeneration

TABLE 1 | A summary of data published in the Research Topic "Neuroimmunology of the Inner Ear" based on the type of manuscript and the research model used.

References	Type of manuscript	Discovery	Model
ANIMAL STUDIES			
"Early Development of Resident Macrophages in the Mouse Cochlea Depends on Yolk Sac Hematopoiesis" (Kishimoto et al.)	Original Research	Two resident macrophage populations derived from the yolk sac and fetal liver	Mouse
"Csf1 Signaling Regulates Maintenance of Resident Macrophages and Bone Formation in the Mouse Cochlea" (Okano and Kishimoto)	Original Research	The influence of Csf1op/op genotype (where no Csf1 is produced) on cochlear bone remodeling and cochlear macrophages, pointing to a possible connection between immune responses and bony capsule metabolism	Mouse
"Lack of Fractalkine Receptor on Macrophages Impairs Spontaneous Recovery of Ribbon Synapses After Moderate Noise Trauma in C57BL/6 Mice" (Kaur et al.)	Original Research	The negative impact of knocking-out the fractalkine receptor on ribbon synapse recovery after noise trauma - a protective role for auditory nerve-associated macrophages	Mouse
"Anti-inflammatory and Oto-Protective Effect of the Small Heat Shock Protein Alpha B-Crystallin (HspB5) in Experimental Pneumococcal Meningitis" (Erni et al.)	Original Research	Protective effect of alpha B-crystallin (HspB5) on the inner ear damage due to meningococcal infection	Rat
"Immune Response After Cochlear Implantation" (Simoni et al.)	Original Research	Dexamethasone-eluting electrodes reduce the inflammatory response induced by cochlear implantation	Guinea pig
"Cytokine Levels in Inner Ear Fluid of Young and Aged Mice as Molecular Biomarkers of Noise-Induced Hearing Loss" (Landegger et al.)	Original Research	Discovered reduced concentrations of IL-1β and TNF-α in the perilymph of 2-year-old mice compared to adolescent mice. Discovered that exposure to noise associates with increased levels of the chemokine (C-X-C motif) ligand 1, IL-6 and TNF-α in the perilymph of adolescent mice.	Mouse
"Intracochlear Perfusion of Tumor Necrosis Factor-Alpha Induces Sensorineural Hearing Loss and Synaptic Degeneration in Guinea Pigs" (Katsumi et al.)	Original Research	TNF-α perfusion rapidly induced synaptic loss and CAP reduction	Guinea pig
"Nfatc4 Deficiency Attenuates Ototoxicity by Suppressing Tnf-Mediated Hair Cell Apoptosis in the Mouse Cochlea" (Zhang et al.)	Original Research	Expression of Nfatc4 in the auditory hair cells associates with TNF-dependent apoptosis	Mouse
CLINICAL STUDIES			
"Vertigo and Severe Balance Instability as Symptoms of Lyme Disease—Literature Review and Case Report" (Jozefowicz-Korczynska et al.)	Case report and literature review	The effects of neuroborreliosis on the human vestibular system	Human
"Age-Related Changes in Immune Cells of the Human Cochlea" (Noble et al.)	Original Research	Macrophage populations associated with various parts of the human cochlea in respect of aging	Human (cochlea)
"Human Inner Ear Immune Activity: A Super-Resolution Immunohistochemistry Study" (Liu et al.)	Original Research	Macrophages and T lymphocytes in the inner ear	Human (cochlea and endolymphatic sac)
"Early Diagnosis of Hearing Loss in Patients Under Methadone Maintenance Treatment" (Bayat et al.)	Original Research	Mechanisms of ototoxicity secondary to methadone treatment	Human
"Subcellular Abnormalities of Vestibular Nerve Morphology in Patients with Intractable Menière's Disease" (Wang et al.)	Original Research	Presence of structures associated to neurodegeneration in the vestibular nerve of Meniere's disease patients	Human
"Differential Proinflammatory Signature in Vestibular Migraine and Meniere Disease" (Flook et al.)	Original Research	Cytokine expression pattern from peripheral blood mononuclear cells discriminating between healthy controls, vestibular migraine patients, and two subgroups of Meniere's disease	Human
"Defining the Inflammatory Microenvironment in the Human Cochlea by Liquid Biopsy and Perilymph Analysis" (Warnecke et al.)	Original Research	Analysis of human perilymph obtained during cochlear implantation demonstrated feasibility of method and identified potential biomarkers differentiating between the patients with residual hearing and complete deafness	Human
"Correlations Between Vestibular Function and Imaging of the Semicircular Canals in DFNA9 Patients" (Ihtijarevic et al.)	Original Research	Demonstrated and association between CT and MRI abnormalities in DFNA9 patients carrying the P51S mutation in the gene encoding cochlin	Human
REVIEWS (CLINICAL STUDIES)			
"Biomarkers in Vestibular Schwannoma–Associated Hearing Loss" (Lassaletta et al.)	Mini Review	Synthesis of knowledge about biomarkers characterizing sporadic vestibular schwannoma and VS associated with neurofibromatosis type 2	Human
"Main Aspects of Peripheral and Central Hearing System Involvement in Unexplained HIV-Related Hearing Complaints" (de Jong et al.).	Review	auditory consequences of HIV viral infection	Human
REVIEWS (CLINICAL AND ANIMAL STUDIES)			
"Genetic Hearing Loss Associated With Autoinflammation" (Nakanishi et al.)	Review	Review of evidence associating the NLRP3 inflammasome with deafness	Human, mouse
"Cannabinoids, inner ear, hearing and tinnitus: a neuroimmunological perspective" (Perin et al.).	Review	Review of effects of cannabinoid on the brain-related and ear-related immune system with emphasis on tinnitus and hearing loss	Human, mouse, rat

(corpora amylacea, lipofuscin, microglia) in the vestibular nerve of MD patients (Wang et al.). On the other hand, the paper "Differential Proinflammatory Signature in Vestibular Migraine and Meniere Disease" describes a cytokine subset whose expression level in peripheral blood mononuclear cells can discriminate between healthy controls, vestibular migraine patients, and two subgroups of MD patients, thus yielding the basis for a blood test helping MD diagnosis (Flook et al.).

Two papers focused on a hot spot in auditory research: biomarkers for various types of inner ear diseases. "Cytokine Levels in Inner Ear Fluid of Young and Aged Mice as Molecular Biomarkers of Noise-Induced Hearing Loss" approaches the connection between noise-induced and age-related hearing loss using the mouse model (Landegger et al.). The second paper, "Biomarkers in Vestibular Schwannoma–Associated Hearing Loss," reviews the proteins and genes that could potentially be included in the clinical evaluation panel of vestibular schwannoma (Lassaletta et al.).

The paper "Defining the Inflammatory Microenvironment in the Human Cochlea by Liquid Biopsy and Perilymph Analysis" studied human perilymph from patients assigned for CI, observing the expression of a panel of immune-related and growth factor-related proteins (Warnecke et al.). Finally, in the paper "Correlations Between Vestibular Function and Imaging of the Semicircular Canals in DFNA9 Patients," MRI was used to visualize abnormalities of the semicircular canals that were attributed to cochlin deposits and fibrosis in the light of functional deficiencies (Ihtijarevic et al.).

Regarding molecular targets for neuroimmune signaling in the ear, most papers in this Research Topic confirmed an essential role for TNF signaling [see discussion in (47)]. Two papers focused on that issue. "Intracochlear Perfusion of Tumor Necrosis Factor-Alpha Induces Sensorineural Hearing Loss and Synaptic Degeneration in Guinea Pigs" found that TNF-α perfusion rapidly induced synaptic loss and CAP reduction, which resembled primary cochlear neuropathy (Katsumi et al.), whereas "Nfatc4 Deficiency Attenuates Ototoxicity by Suppressing Tnf-Mediated Hair Cell Apoptosis in the Mouse Cochlea" describes the expression of Nfatc4 in the auditory hair cells being linked to TNF-dependent apoptosis (Zhang et al.).

The last paper, "Cannabinoids, inner ear, hearing and tinnitus: a neuroimmunological perspective" reviews cannabinoid effects on the immune system and their possible roles in tinnitus and hearing loss, for which only neuronal effects have been considered so far (Perin et al.).

By exploring several consolidated or novel mechanisms and effects of neuroimmune interactions in the inner ear, this Research Topic yields a broad perspective on possible innovative therapeutic and diagnostic approaches to audiovestibular diseases and contributes to increasing visibility of this fascinating subject. We hope that in the next decade, the current research will elucidate biochemical pathways connecting immune responses in sensory circuits to functional changes at the cellular and systems levels. Further exploration of the inner ear's neuro-immuno-sensory axis might impact future therapy and monitoring of some otological diseases.

AUTHOR CONTRIBUTIONS

PP and AS drafted the manuscript. PP drew the figure. PP, FM, IV-N, and AS revised and approved the final version of this manuscript. All authors contributed to the article and approved the submitted version.

REFERENCES

1. Nutma E, Willison H, Martino G, Amor S. Neuroimmunology - the past, present and future. *Clin Exp Immunol.* (2019) 197:278–93. doi: 10.1111/cei.13279
2. Jahnke K. The blood-perilymph barrier. *Arch Otorhinolaryngol.* (1980) 228:29–34. doi: 10.1007/BF00455891
3. Juhn SK, Rybak LP, Fowlks WL. Transport characteristics of the blood–perilymph barrier. *Am J Otolaryngol.* (1982) 3:392–6. doi: 10.1016/S0196-0709(82)80016-1
4. Cohen-Salmon M, Regnault B, Cayet N, Caille D, Demuth K, Hardelin JP, et al. Connexin30 deficiency causes instrastrial fluid-blood barrier disruption within the cochlear stria vascularis. *Proc Natl Acad Sci USA*. (2007) 104:6229–34. doi: 10.1073/pnas.0605108104
5. Shi X. Pathophysiology of the cochlear intrastrial fluid-blood barrier (review). *Hear Res.* (2016) 338:52–63. doi: 10.1016/j.heares.2016.01.010
6. Quick CA. Antigenic causes of hearing loss. *Otolaryngol Clin North Am.* (1975) 8:385–94. doi: 10.1016/S0030-6665(20)32776-6
7. Tomiyama S, Harris JP. The endolymphatic sac: its importance in inner ear immune responses. *Laryngoscope.* (1986) 96:685–91. doi: 10.1288/00005537-198606000-00018
8. Hirose K, Discolo CM, Keasler JR, Ransohoff R. Mononuclear phagocytes migrate into the murine cochlea after acoustic trauma. *J Comp Neurol.* (2005) 489:180–94. doi: 10.1002/cne.20619
9. Sato E, Shick HE, Ransohoff RM, Hirose K. Repopulation of cochlear macrophages in murine hematopoietic progenitor cell chimeras: the role of CX3CR1. *J Comp Neurol.* (2008) 506:930–42. doi: 10.1002/cne.21583
10. Hirose K, Rutherford MA, Warchol ME. Two cell populations participate in clearance of damaged hair cells from the sensory epithelia of the inner ear. *Hear Res.* (2017) 352:70–81. doi: 10.1016/j.heares.2017.04.006
11. Warchol ME. Interactions between macrophages and the sensory cells of the inner ear. *Cold Spring Harb Perspect Med.* 9:a033555. doi: 10.1101/cshperspect.a033555
12. Szczepek AJ, Dudnik T, Karayay B, Sergeeva V, Olze H, Smorodchenko A. Mast cells in the auditory periphery of rodents. *Brain Sci.* (2020) 10:697. doi: 10.3390/brainsci10100697
13. Rai V, Wood MB, Feng H, Schabla NM, Tu S, Zuo J. The immune response after noise damage in the cochlea is characterized by a heterogeneous mix of adaptive and innate immune cells. *Sci Rep.* (2020) 10:15167. doi: 10.1038/s41598-020-72181-6
14. Hu BH, Zhang C, Frye MD. Immune cells and non-immune cells with immune function in mammalian cochleae. *Hear Res.* (2018) 362:14–24. doi: 10.1016/j.heares.2017.12.009
15. Dewyer NA, Kiringoda R, Mckenna MJ. Inner Ear Infections (Labyrinthitis). In: Durand M, Deschler D, editors. *Infections of the Ears, Nose, Throat, and Sinuses*. Cham: Springer (2018). p. 79–88. doi: 10.1007/978-3-319-74835-1_7
16. Buki B, Junger H, Zhang Y, Lundberg YW. The price of immune responses and the role of vitamin D in the inner ear. *Otol Neurotol.* (2019) 40:701–9. doi: 10.1097/MAO.0000000000002258

17. Oh GS, Kim HJ, Choi JH, Shen A, Kim CH, Kim SJ, et al. Activation of lipopolysaccharide-TLR4 signaling accelerates the ototoxic potential of cisplatin in mice. *J Immunol.* (2011) 186:1140–50. doi: 10.4049/jimmunol.1002183
18. Hirose K, Li SZ, Ohlemiller KK, Ransohoff RM. Systemic lipopolysaccharide induces cochlear inflammation and exacerbates the synergistic ototoxicity of kanamycin and furosemide. *J Assoc Res Otolaryngol.* (2014) 15:555–70. doi: 10.1007/s10162-014-0458-8
19. Koo JW., Quintanilla-Dieck L, Jiang M, Liu J, Urdang ZD, Allensworth JJ, et al. Endotoxemia-mediated inflammation potentiates aminoglycoside-induced ototoxicity. *Sci Transl Med.* (2015) 7:298ra118. doi: 10.1126/scitranslmed.aac5546
20. Kalinec GM, Lomberk G, Urrutia RA, Kalinec F. Resolution of cochlear inflammation: novel target for preventing or ameliorating drug-, noise- and age-related hearing loss. *Front Cell Neurosci.* (2017) 11:192. doi: 10.3389/fncel.2017.00192
21. Wood MB, Zuo J. The contribution of immune infiltrates to ototoxicity and cochlear hair cell loss. *Front Cell Neurosci.* (2017) 11:106. doi: 10.3389/fncel.2017.00106
22. Fayad JN, Makarem AO, Linthicum FHJr. Histopathologic assessment of fibrosis and new bone formation in implanted human temporal bones using 3D reconstruction. *Otolaryngol Head Neck Surg.* (2009) 141:247–52. doi: 10.1016/j.otohns.2009.03.031
23. Jia H, Wang J, Francois F, Uziel A, Puel JL, Venail F. Molecular and cellular mechanisms of loss of residual hearing after cochlear implantation. *Ann Otol Rhinol Laryngol.* (2013) 122:33–9. doi: 10.1177/000348941312200107
24. Astolfi L, Simoni E, Giarbini N, Giordano P, Pannella M, Hatzopoulos S, et al. Cochlear implant and inflammation reaction: Safety study of a new steroid-eluting electrode. *Hear Res.* (2016) 336:44–52. doi: 10.1016/j.heares.2016.04.005
25. Bas E, Bohorquez J, Goncalves S, Perez E, Dinh CT, Garnham C, et al. Electrode array-eluted dexamethasone protects against electrode insertion trauma induced hearing and hair cell losses, damage to neural elements, increases in impedance and fibrosis: a dose response study. *Hear Res.* (2016) 337:12–24. doi: 10.1016/j.heares.2016.02.003
26. Wilk M, Hessler R, Mugridge K, Jolly C, Fehr M, Lenarz T, et al. Impedance changes and fibrous tissue growth after cochlear implantation are correlated and can be reduced using a dexamethasone eluting electrode. *PLoS ONE.* (2016) 11:e0147552. doi: 10.1371/journal.pone.0147552
27. Bas E, Gupta C, Van De Water TR. A novel organ of corti explant model for the study of cochlear implantation trauma. *Anat Rec.* (2012) 295:1944–56. doi: 10.1002/ar.22585
28. Bas E, Goncalves S, Adams M, Dinh CT, Bas JM, Van De Water TR, et al. Spiral ganglion cells and macrophages initiate neuro-inflammation and scarring following cochlear implantation. *Front Cell Neurosci.* (2015) 9:303. doi: 10.3389/fncel.2015.00303
29. Okayasu T, O'Malley JT, Nadol JB Jr. Density of macrophages immunostained with anti-iba1 antibody in the vestibular endorgans after cochlear implantation in the human. *Otol Neurotol.* (2019) 40:e774–81. doi: 10.1097/MAO.0000000000002313
30. Noonan KY, Lopez IA, Ishiyama G, Ishiyama A. Immune response of macrophage population to cochlear implantation: cochlea immune cells. *Otol Neurotol.* (2020) 41:1288–95. doi: 10.1097/MAO.0000000000002764
31. Kaur T, Zamani D, Tong L, Rubel EW, Ohlemiller KK, Hirose K, et al. Fractalkine signaling regulates macrophage recruitment into the cochlea and promotes the survival of spiral ganglion neurons after selective hair cell lesion. *J Neurosci.* (2015) 35:15050–61. doi: 10.1523/JNEUROSCI.2325-15.2015
32. Barbeck M, Booms P, Unger R, Hoffmann V, Sader R, Kirkpatrick CJ, et al. Multinucleated giant cells in the implant bed of bone substitutes are foreign body giant cells-New insights into the material-mediated healing process. *J Biomed Mater Res A.* (2017) 105:1105–11. doi: 10.1002/jbm.a.36006
33. Nadol JB, O'Malley JT, Burgess BJ, Galler D. Cellular immunologic responses to cochlear implantation in the human. *Hear Res.* (2014) 318:11–17. doi: 10.1016/j.heares.2014.09.007
34. Magnan J, Ozgirgin ON, Trabalzini F, Lacour M, Escamez AL, Magnusson M, et al. European position statement on diagnosis, and treatment of Meniere's disease. *J Int Adv Otol.* (2018) 14:317–21. doi: 10.5152/iao.2018.140818
35. Basura GJ, Adams ME, Monfared A, Schwartz SR, Antonelli PJ, Burkard R, et al. Clinical Practice guideline: Meniere's disease. *Otolaryngol Head Neck Surg.* (2020) 162:S1–55. doi: 10.1177/0194599820909438
36. Ishiyama G, Lopez IA, Ishiyama P, Vinters HV, Ishiyama A. The blood labyrinthine barrier in the human normal and Meniere's disease macula utricle. *Sci Rep.* (2017) 7:253. doi: 10.1038/s41598-017-00330-5
37. Nakashima T, Naganawa S, Sugiura M, Teranishi M, Sone M, Hayashi H, et al. Visualization of endolymphatic hydrops in patients with Meniere's disease. *Laryngoscope.* (2007) 117:415–20. doi: 10.1097/MLG.0b013e31802c300c
38. Van Steekelenburg JM, Van Weijnen A, De Pont LMH, Vijlbrief OD, Bommeljé CC, Koopman JP, et al. Value of endolymphatic hydrops and perilymph signal intensity in suspected Ménière disease. *AJNR Am J Neuroradiol.* (2020) 41:529–34. doi: 10.3174/ajnr.A6410
39. Oberman BS, Patel VA, Cureoglu S, Isildak H. The aetiopathologies of Meniere's disease: a contemporary review. *Acta Otorhinolaryngol Ital.* (2017) 37:250–63. doi: 10.14639/0392-100X-793
40. Lopez-Escamez JA, Batuecas-Caletrio A, Bisdorff A. Towards personalized medicine in Meniere's disease. *F1000Res.* (2018) 7:F1000 Faculty Rev-1295. doi: 10.12688/f1000research.14417.1
41. Greco A, Gallo A, Fusconi M, Marinelli C, Macri G, De Vincentiis M. Meniere's disease might be an autoimmune condition? *Autoimmun Rev.* (2012) 11:731–8. doi: 10.1016/j.autrev.2012.01.004
42. Frejo L, Gallego-Martinez A, Requena T, Martin-Sanz E, Amor-Dorado JC, Soto-Varela A, et al. Proinflammatory cytokines and response to molds in mononuclear cells of patients with Meniere disease. *Sci Rep.* (2018) 8:5974. doi: 10.1038/s41598-018-23911-4
43. Bachinger D, Luu NN, Kempfle JS, Barber S, Zurrer D, Lee DJ, et al. Vestibular aqueduct morphology correlates with endolymphatic sac pathologies in meniere's disease-a correlative histology and computed tomography study. *Otol Neurotol.* (2019) 40:e548–55. doi: 10.1097/MAO.0000000000002198
44. Kampfe Nordstrom C, Danckwardt-Lilliestrom N, Laurell G, Liu W, Rask-Andersen H. The human endolymphatic sac and inner ear immunity: macrophage interaction and molecular expression. *Front Immunol.* (2018) 9:3181. doi: 10.3389/fimmu.2018.03181
45. Trune DR, Nguyen-Huynh A. Vascular pathophysiology in hearing disorders. *Semin Hear.* (2012) 33:242–50. doi: 10.1055/s-0032-1315723
46. Hao W, Yu H, Li H. Effects of intratympanic gentamicin and intratympanic glucocorticoids in Meniere's disease: a network meta-analysis. *J Neurol.* (2021). doi: 10.1007/s00415-020-10320-9. [Epub ahead of print].
47. Ren Y, Stankovic KM. The Role of Tumor Necrosis Factor Alpha (TNFalpha)in hearing loss and vestibular schwannomas. *Curr Otorhinolaryngol Rep.* (2018) 6:15–23. doi: 10.1007/s40136-018-0186-4

Conflict of Interest: The authors declare that the research was conducted in the absence of any commercial or financial relationships that could be construed as a potential conflict of interest.

frontiers in Immunology

ORIGINAL RESEARCH
published: 04 June 2019
doi: 10.3389/fimmu.2019.01229

Differential Proinflammatory Signature in Vestibular Migraine and Meniere Disease

*Marisa Flook[1], Lidia Frejo[1,2], Alvaro Gallego-Martinez[1], Eduardo Martin-Sanz[3], Marcos Rossi-Izquierdo[4], Juan Carlos Amor-Dorado[5], Andres Soto-Varela[6], Sofia Santos-Perez[6], Angel Batuecas-Caletrio[7], Juan Manuel Espinosa-Sanchez[1,8], Patricia Pérez-Carpena[1,9], Marta Martinez-Martinez[9], Ismael Aran[10] and Jose Antonio Lopez-Escamez[1,8]**

[1] Otology and Neurotology Group CTS495, Department of Genomic Medicine, Centre for Genomics and Oncological Research–Pfizer/Universidad de Granada/Junta de Andalucía (GENYO), Granada, Spain, [2] Department of Pediatric Otolaryngology and Department of Orthopedics, The Feinstein Institute for Medical Research, Northwell Health System, Manhasset, NY, United States, [3] Department of Otolaryngology, Hospital Universitario de Getafe, Getafe, Spain, [4] Department of Otolaryngology, Hospital Universitario Lucus Augusti, Lugo, Spain, [5] Department of Otolaryngology, Hospital Can Misses, Ibiza, Spain, [6] Division of Otoneurology, Department of Otorhinolaryngology, Complexo Hospitalario Universitario, Santiago de Compostela, Spain, [7] Department of Otolaryngology, Hospital Universitario Salamanca, Salamanca, Spain, [8] Department of Otolaryngology, Instituto de Investigación Biosanitaria ibs.GRANADA, Hospital Universitario Virgen de las Nieves, Granada, Spain, [9] Department of Otolaryngology, Hospital Universitario San Cecilio, Granada, Spain, [10] Department of Otolaryngology, Complexo Hospitalario de Pontevedra, Pontevedra, Spain

OPEN ACCESS

Edited by:
Isabel Varela-Nieto, Spanish National Research Council (CSIC), Spain

Reviewed by:
Ivan A. Lopez, University of California, Los Angeles, United States
Meenu Sharma, University of Texas MD Anderson Cancer Center, United States

***Correspondence:**
Jose Antonio Lopez-Escamez
antonio.lopezescamez@genyo.es

Specialty section:
This article was submitted to Molecular Innate Immunity, a section of the journal Frontiers in Immunology

Received: *26 March 2019*
Accepted: *14 May 2019*
Published: *04 June 2019*

Citation:
Flook M, Frejo L, Gallego-Martinez A, Martin-Sanz E, Rossi-Izquierdo M, Amor-Dorado JC, Soto-Varela A, Santos-Perez S, Batuecas-Caletrio A, Espinosa-Sanchez JM, Pérez-Carpena P, Martinez-Martinez M, Aran I and Lopez-Escamez JA (2019) Differential Proinflammatory Signature in Vestibular Migraine and Meniere Disease. Front. Immunol. 10:1229. doi: 10.3389/fimmu.2019.01229

Vestibular Migraine (VM) and Meniere's Disease (MD) are episodic vestibular syndromes defined by a set of associated symptoms such as tinnitus, hearing loss or migraine features during the attacks. Both conditions may show symptom overlap and there is no biological marker to distinguish them. Two subgroups of MD patients have been reported, according to their IL-1β profile. Therefore, considering the clinical similarity between VM and MD, we aimed to investigate the cytokine profile of MD and VM as a means to distinguish these patients. We have also carried out gene expression microarrays and measured the levels of 14 cytokines and 11 chemokines in 129 MD patients, 82 VM patients, and 66 healthy controls. Gene expression profile in peripheral blood mononuclear cells (PBMC) showed significant differences in MD patients with high and low basal levels of IL- 1β and VM patients. MD patients with high basal levels of IL- 1β (MDH) had overall higher levels of cytokines/chemokines when compared to the other subsets. CCL4 levels were significantly different between MDH, MD with low basal levels of IL- 1β (MDL), VM and controls. Logistic regression identified IL- 1β, CCL3, CCL22, and CXCL1 levels as capable of differentiating VM patients from MD patients (area under the curve = 0.995), suggesting a high diagnostic value in patients with symptoms overlap.

Keywords: Vestibular Migraine, Meniere Disease, differential diagnosis, IL-1β, CXCL1, CCL3, CCL22

INTRODUCTION

Meniere's Disease (MD) is a syndrome characterized by attacks of recurrent vertigo associated with ipsilateral cochlear symptoms, such as fluctuating sensorineural hearing loss (SNHL), tinnitus or aural pressure (1, 2).

Vestibular Migraine (VM) is defined by the occurrence of episodic vestibular symptoms and a history of migraine, with a temporal association in at least 50% of the attacks (3). VM

has an estimated population prevalence of about 1%, however with only medical history and symptomology it may be indistinguishable from MD at times (4–6).

It has been described that 8.4% of MD patients have headache compatible with migraine, during vertigo attacks (7). The major difference in the diagnosis criteria for these diseases are the auditory symptoms, which are necessary for the diagnosis of definite MD, however it has been reported that VM patients may have tinnitus during vertigo attacks, and also that 25% of migraine patients suffer from hearing loss (7, 8).

VM patients have a favorable response to anti-migraine drugs, which supports an underlying migraine mechanism. However, this evidence is insufficient as it is based on uncontrolled clinical case series, thus the apparent efficacy may be due to confounding factors, such as placebo response, spontaneous improvement and multiple drug effect (3). Moreover, a high prevalence of migraine in patients with MD has been previously described, suggesting a pathophysiological link between these diseases (8, 9).

Recently, the Meniere's disease Consortium identified five clinical subgroups in patients with unilateral and bilateral MD: Group 1 was defined by SNHL starting first in one ear and involving the second ear in the next months or years; Group 2 characterized by simultaneous hearing loss in both ears since the onset of the disease; Group 3 clustered familial MD; Group 4 associated with migraine in all cases and Group 5 was found in patients with an autoimmune disease in addition to MD (10, 11). Additionally, Frejo et al have observed two subgroups of MD patients, according to their IL-1β profile, patients with high levels of IL-1β (MDH) or patients with low levels of IL-1β (MDL), which may have different immune responses or functional states of the immune system (12).

Considering that the cytokine profile may allow to subgroup MD patients and the clinical similarity of MD and VM, we propose to investigate if the pro-inflammatory signature of these diseases may allow to distinguish these patients.

MATERIALS AND METHODS

Human Subjects

This study included a total of 129 patients with definite MD, 82 patients with VM, and 66 healthy controls. Patients were diagnosed according to the diagnostic criteria of the Barany Society for MD (1) and VM (3). The experimental protocols of this study were approved by the Institutional Review Board in all participating hospitals and every patient signed a written informed consent. The study was carried out according to the principles of the Declaration of Helsinki revised in 2013 for investigation with humans.

PBMC Isolation and Incubation

Peripheral blood was diluted 1:1 with 1 × PBS and disposed carefully onto the corresponding 25:15 volume of Lymphosep, Lymphocyte Separation Media (Biowest, Nuaillé, France). Samples were centrifuged for 20 min at 2,000 rpm to separate blood content. PBMC were collected and washed with 1 × PBS and cultured in RPMI 1640 supplemented with 10% (v/v) fetal bovine serum (Biowest, Nuaillé, France) and plated at 1.25×10^6 cells/mL in 6-well plates. PBMC were incubated during 16 h at 37°C in 7% CO_2. After the incubation, PBMC were centrifuged, RNA was harvested, and supernatants were collected and stored at −80°C.

RNA Extraction and Expression Array

RNA was isolated using the High Pure RNA Isolation Kit (Hoffmann-La Roche, Basel, Switzerland) following the manufacturer's protocol. RNA concentration was measured on Nanodrop (NanoDrop Technologies Inc.,Wilmington, DE, USA). RNA quality was checked using Agilent 2100 Bioanalyzer (Agilent Technologies, Waldbronn, Germany).

Expression levels were measured using the HumanHT-12 v4 Expression BeadChip (Illumina Inc., San Diego, CA, USA) with 500 ng of total RNA and processed with the high-resolution scanner iScan (Illumina Inc., San Diego, CA, USA).

The number of biological replicates for each condition was: 5 healthy controls, 4 MD patients with low cytokine basal levels, 3 MD patients with high cytokine basal levels and 6 VM patients.

Expression data analysis, normalization, differential expression analysis and Principal Component Analysis (PCA) was carried out as previously described by Frejo et al. (12). For pairwise comparisons fold-change>2 and adjusted *p*-value 0.05 cut-offs were used.

Core analysis was performed using Ingenuity Pathways Analysis (IPA®, Qiagen, Venlo, Netherlands, http://www.ingenuity.com/products/ipa) software, using the differentially expressed genes (DEG) with an adjusted *p*-value cut-off of 0.02.

Cytokine Measurement

Supernatants were collected and stored at −80°C until enough samples were acquired. Frozen samples were thawed immediately prior to analysis and none of the samples underwent more than two freeze-thaw cycles prior to analysis. Fourteen cytokines (IFNα-2, IFN-γ, IL-10, IL-1α, IL-1β, IL-1rα, IL-4, IL-6, IL-12p40, IL-12p70, IL-13, IL-17, IL-28A, and TNFα), and 11 chemokines (IL-8, CXCL10, CCL2, CCL3, CCL4, CCL5, CD40LG, CXCL1, CCL22, CXCL5, and CCL8) were measured using the commercially available Multiplex Bead-Based Kits (EMD Millipore, Billerica, MA, USA). The measurements were done in accordance with the kit-specific protocols provided by Millipore, using a Luminex 200 (Luminex Corp., Austin, TX, USA) and read with Luminex x PONENT 3.1 software (Luminex Corp.). The minimum detection limit for the assays can be found in **Table 1**. Samples with readings below or above these levels were assigned values of 0 pg/mL for the minimum value or 10,000 pg/mL for the maximum value. Two quality controls for each cytokine were run in duplicate. As the levels of IL-12p40, IL-12p70, IL-13, IL-17, and IL-28A were low or undetectable among all groups, they were excluded from the statistical analysis.

Statistical Analysis

A descriptive analysis was conducted using SPSS software v.22 (SPSS Inc., Chicago, IL, USA) for the clinical data and displayed

TABLE 1 | Assay sensitivity determined as Minimum Detection Concentration plus 2 Standard Deviations (MinDC+2SD) for the Milliplex® human cytokines/chemokines quantified.

Cytokine	MinDC+2SD (pg/mL)
IFNα2	4.8
INFγ	1.1
CXCL1	14.1
IL-10	1.6
IL-12p40	12.7
IL-12p70	1
CCL22	7.1
IL-13	1.9
IL-15	1.7
sCD40L	9.9
IL-17	1.2
IL-1RA	17.1
IL-1α	12.6
IL-1β	1
IL-4	7.1
IL-6	1.3
CXCL10	14
CCL2	3.4
CCL3	6.2
CCL4	4.8
TNFα	1.1
CCL5	1.9
CCL8	2.2
CXCL5	7.2
IL-28A	7.9

as mean ± standard error for the mean (SEM). Quantitative variables were compared using Mann-Whitney U test, Student's unpaired *T*-test and Krustal-Wallis H test. Qualitative variables were compared using Pearson Chi-square Test and Krustal-Wallis H test. The level of significance considered was *p*-value < 0.05.

Representative heatmaps of the cytokine levels were done using the gplots package for R.

Logistic Regression

We identified cytokines with differential production between MD and VM using Mann-Whitney test. Next, we performed logistic regressions, removing step-by-step the variables which had higher *p*-values, until we obtained a model for which all cytokines were significant. The coefficient of determination R^2, which summarizes the proportion of variance in the dependent variable associated with the predictor variables, was estimated by using Nagelkerke's R^2. A receiver operating characteristic (ROC) curve was generated to determine the ability to predict VM based on a model composed of cytokine production. Area under the curves (AUC) was calculated for the ROC curves.

RESULTS

VM Has an Earlier Onset Than MD

Table 2 compares the clinical features of 129 MD patients (26 MDH and 103 MDL) and 82 VM patients. Patients with VM were younger ($p = 1.20 \times 10^{-5}$) and had an earlier onset of the disease ($p = 4.41 \times 10^{-4}$) than MD patients. As expected, MD patients had worse hearing ($p = 5.32 \times 10^{-22}$), higher number of vertigo attacks ($p = 2.87 \times 10^{-3}$) and were more functionally affected by the disease ($p = 1.44 \times 10^{-11}$), when compared to VM patients. A significant difference was found in the prevalence autoimmune disease between VM and MD, namely MDL had the highest history of autoimmune disease ($p = 9.77 \times 10^{-3}$). On the other hand, VM patients suffered more from headaches ($p = 4.43 \times 10^{-16}$), and more specifically migraine episodes ($p = 1.89 \times 10^{-26}$) than MD patients. We also observed a higher number of drop attacks in patients with MDH (p-value $= 2.24 \times 10^{-14}$).

Gene Expression Profile on PBMCs can Differentiate MD, VM, and Healthy Controls

We compared gene expression profiles of PBMCs from 6 VM patients, 7 MD patients [4 with low basal levels of IL-1β and 3 with high basal levels of IL-1β (12)] and 5 healthy controls.

Using 1,894 genes, with 2 fold-change (FC) and an adjusted p-value $= 0.05$, the samples were clustered into 4 distinct groups by Principal Component Analysis (PCA), which corresponded to our 3 patient groups and healthy controls, as seen in **Figure 1**. Additionally, the hierarchical clustering of patients and controls according to the gene expression in PBMC, shows that MDL are more similar to healthy controls than to MDH.

Pairwise comparisons between groups were carried out due to inter-individual variability. We firstly compared the gene expression profile in PBMC from patients with VM and healthy controls and found 832 DEG (p-value < 0.02 and FC>2; **Supplementary Table 1**), being the most significant gene *CACNA2D2* (-5.3 FC and adjusted p-value $= 5.89 \times 10^{-6}$). The core analysis with IPA software gave us a list of 25 networks. The top ranked network had a score of 37 and 30 focus molecules (**Figure 2**).

Additionally, we compared the gene expression profile in PBMC from patients with VM to MDH and MDL separately (**Supplementary Tables 2**, **3**). We observed that 22 genes were differentially expressed in both comparisons, from which we retrieved a network with 10 focus molecules (score 23, **Figure 3A**). Of note, 286 genes were uniquely expressed when comparing PBMC from patients with VM to MDH, resulting in a top network with 22 focus molecules (score 32, **Figure 3B**). Moreover, 136 genes were uniquely expressed when comparing PBMC from patients with VM to MDL, resulting in a top network with 22 focus molecules (score 41, **Figure 3C**).

VM Patients Have Similar Cytokine Levels to MD Patients With Low Basal Levels of IL-1β

The expression array revealed significant differences in various cytokines and chemokines, therefore we decided to measure

TABLE 2 | Clinical and demographic variables assessed in patients with Meniere Disease with high levels of IL-1β (MDH), Meniere Disease with low levels of IL-1β (MDL), and Vestibular Migraine (VM).

Variable	MDH ($N = 26$)	MDL ($N = 103$)	VM ($N = 82$)	p-value
Age (mean ± SD)	60.6 ± 11.2	59.3 ± 13.7	48.6 ± 16.0	$\mathbf{1.20 \times 10^{-5}}$
Years of Evolution (mean ± SD)	12.0 ± 11.0	10.1 ± 8.5	10.9 ± 10.2	0.875
Age of onset (mean ± SD)	44.4 ± 10.5	47.3 ± 15.7	37.1 ± 17.2	$\mathbf{4.41 \times 10^{-4}}$
Sex (% female)	50	63.6	65.1	0.366
Laterality (% unilateral)	50.8	63	NA	0.264
Affected ear (% right ear)	26.9	27.6	NA	0.321
Hearing loss (% synchronic)	30.4	18	NA	0.342
Time until evolving to bilateral (months)	125.0 ± 118.6	55.8 ± 59.9	NA	0.106
MD type				0.736
1	69.6	64.4	NA	
2	0	4.4	NA	
3	8.7	7.8	NA	
4	13	10	NA	
5	8.7	13.3	NA	
Hearing stage (%)				$\mathbf{5.32 \times 10^{-22}}$
1	15.4	6.3	92.7	
2	26.9	29.2	7.3	
3	30.8	47.9	0	
4	26.9	15.6	0	
5	0	1	0	
Ear Family History (%)	12	29.4	34.9	0.130
Familial Meniere disease (%)	8.3	10.1	5,4	0.466
Headache (%)	38.5	37.6	98.6	**4.429 × 10–16**
Type of headache				$\mathbf{2.117 \times 10^{-7}}$
Migraine	50	51.4	94.6	
Tensional	50	48.6	5.4	
Migraine (%)	20	20.5	100	$\mathbf{1.887 \times 10^{-26}}$
Type of Migraine				0.569
Migraine with Aura	60	42.9	58.3	
Migraine without Aura	40	57.1	41.7	
History of autoimmune disease (%)	7.7	17.3	1.7	$\mathbf{9.77 \times 10^{-3}}$
Tumarkin crises (drop attacks)	1.9 ± 0.3	1.6 ± 0.7	NA	$\mathbf{2.241 \times 10^{-14}}$
Number of crisis in last 6 months	2.3 ± 3.0	2.0 ± 3.0	1.4 ± 2.1	$\mathbf{2.87 \times 10^{-3}}$
AAO-HNS Functional level (1–6)				0.241
1	8	17.9	70.9	$\mathbf{1.44 \times 10^{-11}}$
2	44	29.8	20	
3	16	27.4	9.1	
4	20	16.7	0	
5	12	6	0	
6	0	2.4	0	

Significant differences for p-value < 0.05 are highlighted in bold.

the levels of IFNα-2, IFN-γ, IL-10, IL-1α, IL-4, IL-8, CXCL10, CCL2, CCL3, CCL4, CCL5, CD40LG, CXCL1, CCL22, CXCL5, and CCL8 in a smaller cohort of patients, which included 24 MDH patients, 24 MDL patients, 20 VM patients and 10 healthy controls. Levels of IL-1β, IL-1RA, IL-6, and TNFα were measured in all cases and controls, in line with previous work carried out by our group (12).

The cytokines can be separated into 3 groups according to their levels: (a) high cytokine production in all groups, (b) cytokines which are higher in MDH than in the other groups and (c) cytokines that are higher in patients than in controls, as observed in **Figure 4**.

Also, we can observe that the cytokine levels of VM patients are very similar to MDL patients and that controls always have lower cytokine levels than the patients.

CCL4 Levels May Allow to Distinguish Between MD, VM and Healthy Controls

MDL had the lowest number of cytokines that were statistically different from healthy controls, as no differences were found

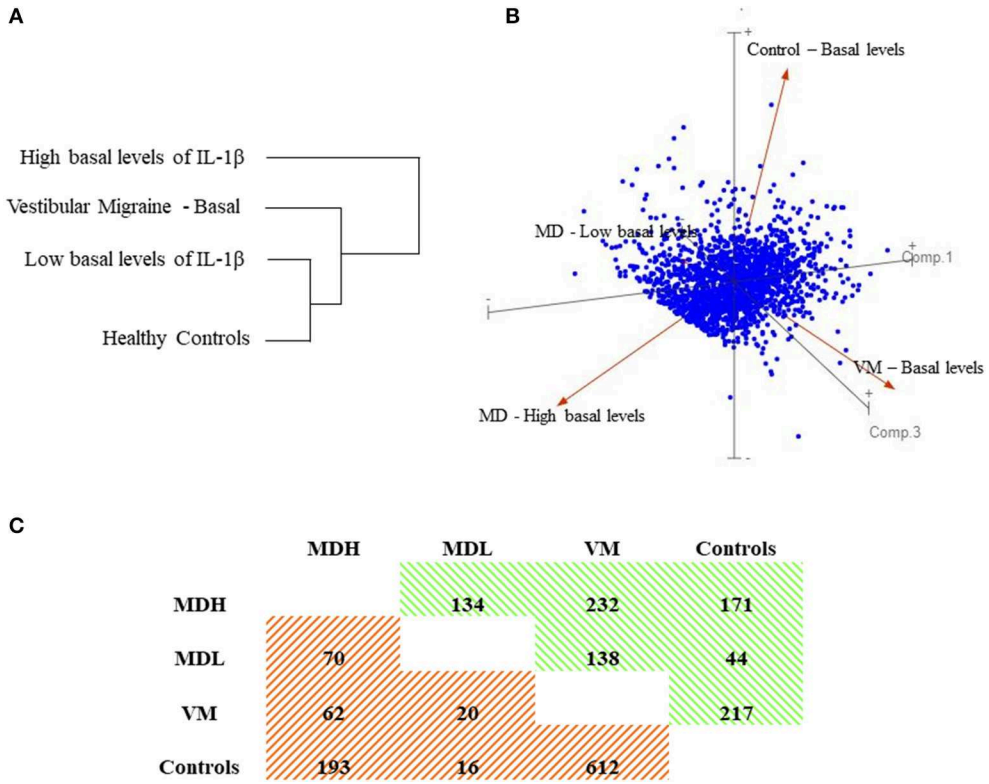

FIGURE 1 | Gene expression in PBMC. **(A)** Dendrogram showing hierarchical clustering of patients and controls according to the gene expression in PBMC. **(B)** Three-dimensional loading plot showing principal component analysis (PCA) using all datasets. **(C)** Matrix of up- and down- regulated genes for selected pairwise comparisons. Values indicate the number of up- or down- regulated genes with a fold-change (FC) >2 and *P*-value < 0.02. In green are the up-regulated genes (positive FC) and in orange are the down-regulated genes (negative FC).

in the levels of IL-10, IL-1β, IL-6, CCL5, CXCL1, IFNA2, and CXCL5 (all, $p > 0.1$) (**Supplementary Table 4**). On the other hand MDH had statistically different levels of all cytokines comparing to healthy controls ($p = 1.64 \times 10^{-12}$-4.61×10^{-2}].

Overall, MDH patients have higher levels of all cytokines, except for CCL22 ($p = [2.12 \times 10^{-4} - 3.01 \times 10^{-2}]$) and CXCL10 ($p = [2.18 \times 10^{-4}$-$2.10 \times 10^{-2}]$), for which VM patients hold the highest levels.

We observed that CCL4 allows to distinguish between all groups of patients and between patients and controls (by pairwise comparison $p = [6.30 \times 10^{-5}$-$1.04 \times 10^{-2}]$). Moreover, CXCL10 allows to distinguish most groups $p = [2.18 \times 10^{-4}$-$3.84 \times 10^{-2}]$), however it does not discriminate MDH from MDL ($p = 0.354$).

Despite the high similarity of cytokine levels of VM patients and MDL patients, the levels of IL-10 (p-value $= 9.84 \times 10^{-3}$), CXCL1 (p-value $= 1.42 \times 10^{-3}$), and IL-8 (p-value $= 9.79 \times 10^{-3}$) are significantly higher in PBMC from VM patients than in MDL patients.

IL-1β, CCL3, CCL22, and CXCL1 Levels May Allow to Distinguish Between MD and VM Patients

In order to discriminate VM patients from MD patients, we performed logistic regressions with the differentially released cytokines between MD and VM, for which we obtained a final regression model that included IL-1β, CCL3, CCL22, and CXCL1 levels as independent variables (**Table 3**). The ability of the model to predict patients with VM was assessed by plotting a ROC curve using the variables from the logistic regression, which has a 93.8% sensitivity, 95.8% specificity, 97.8% positive predictive value and 11.8% negative predictive value (**Figure 5**). Other regression models using three, two or one of the cytokines were also evaluated, but all showed a lower diagnostic accuracy (**Table 4**).

DISCUSSION

Our study shows that a small panel of cytokines and chemokines could be used for the differential diagnosis of VM and MD. Given that both conditions have a different therapeutic approach, our findings may contribute to improve the clinical management of VM and MD.

We observed that VM patients suffer more from migraine ($p = 1.87 \times 10^{-26}$) and have approximately a decade earlier onset than MD patients, ($p = 1.20 \times 10^{-5}$) and MD patients have more severe hearing loss ($p = 5.32 \times 10^{-22}$). Nevertheless, there is a symptom overlap which could be especially difficult to discriminate in earlier stages of the disease. Interestingly,

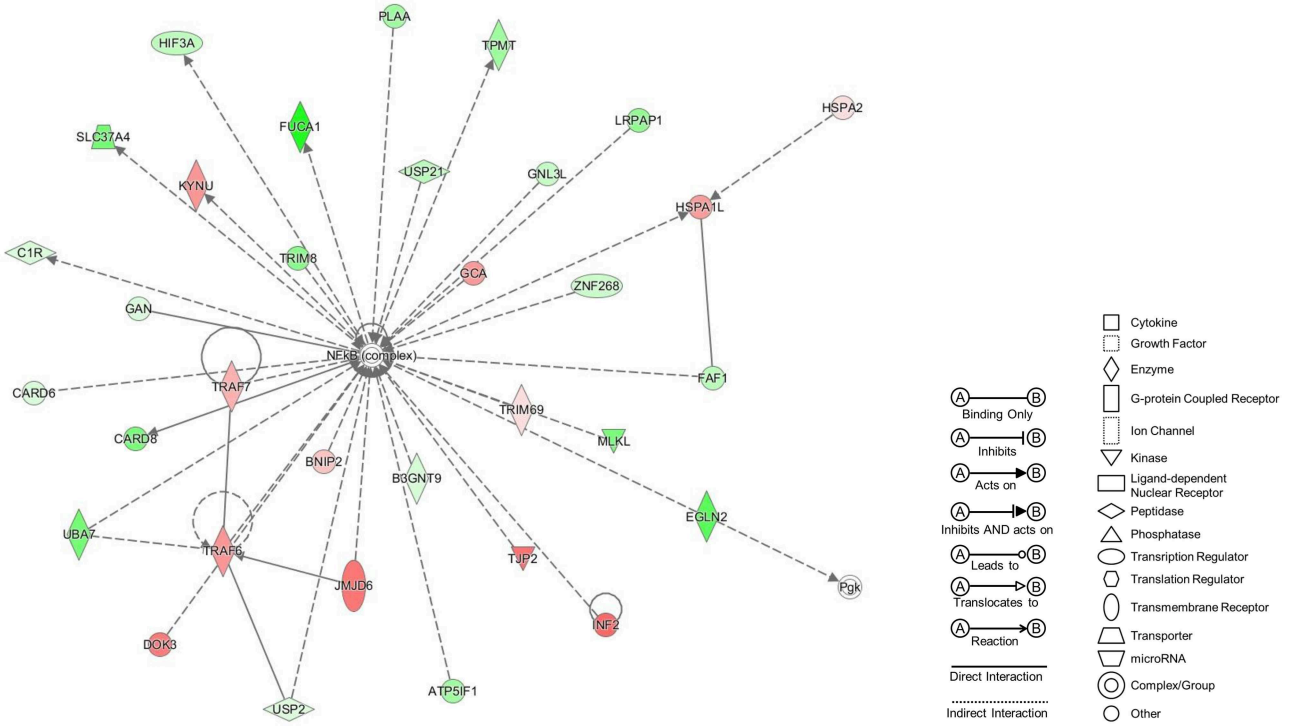

FIGURE 2 | Top Network from VM patients PBMCs at basal levels. Network retrieved after comparing by pairwise analysis gene expression data from VM patients to healthy controls. Genes in red were up-regulated, while genes in green were down-regulated.

MD type 4 patients, which are sporadic MD patients that suffer from migraine have been described to have a significantly earlier onset than the remaining MD patients (10, 11). These MD patients with comorbid migraine show migraine attacks that most of times are not associated with the episodic vertigo, but the temporal relationship between vertigo and migraine in MD needs to be investigated in a prospective longitudinal study. Specifically, bilateral MD type 4 (10) has the same mean age of onset (37 years old) as VM patients from our study, which further supports the necessity of a method to distinguish VM and MD patients that is not fully dependent of clinical information.

Our gene expression and cytokine results indicate that MDH and MDL are more similar between them than to VM. These results further support the hypothesis that MD is not a single disease or that it has various endophenotypes. Different MD subgroups have been already identified according to clinical manifestations and phenotype (10–12) and according to endolymphatic sac (ES) imaging (13).

Despite VM and MDL molecular similarity, these diseases seem to have distinct disease mechanisms, as there are 158 differentially expressed genes. When we compared the uniquely expressed genes between VM and MDL, we observe that the genes involved in the retrieved network are related to immune response, which seems to be upregulated in VM.

The presence of immunological activity in the inner ear has been previously described, both in animal models and humans. Immune responsiveness in the inner ear was firstly associated to the ES (14–16), however the presence of immune capacity in the cochlea has since been determined (17), namely due to the recent demonstration of IBA1 cells in the human ES and cochlea that express Major Histocompatibility Complex Type II (MHCII) (18). Nordström et al. (18) identified that the macrophage population of the stria vascularis, spiral ligament and spiral ganglion expressed MHCII, which is essential to initiate antigen-specific immune responses. Moreover, they propose that there might be an uptake and processing of antigens from the ES lumen, due to the co-expression of IBA1 and MHCII in epithelial cells and to trans-epithelial migration.

Here, we show that IL- 1β, CCL3, CCL22, and CXCL1 quantification could allow the differential diagnosis of VM and MD.

CXCL1, also known as GRO-α (Growth-related Oncogen-alpha) has an essential role in the recruitment and activation of neutrophils, mediating its function through CXCR2 signaling on neutrophils and by binding to glycosaminoglycans (GAG) on endothelial and epithelial cells and the extracellular matrix (19). CXCL1 is usually lower in patients with MD compared to VM.

CCL3 or MIP1- α (Macrophage Inflammatory Protein 1-alpha) is a macrophage secreted chemokine with inflammatory and chemokinetic properties, with CCR1, CCR4 and CCR5 binding. Recently, ES fibroblast cell lines, derived from MD

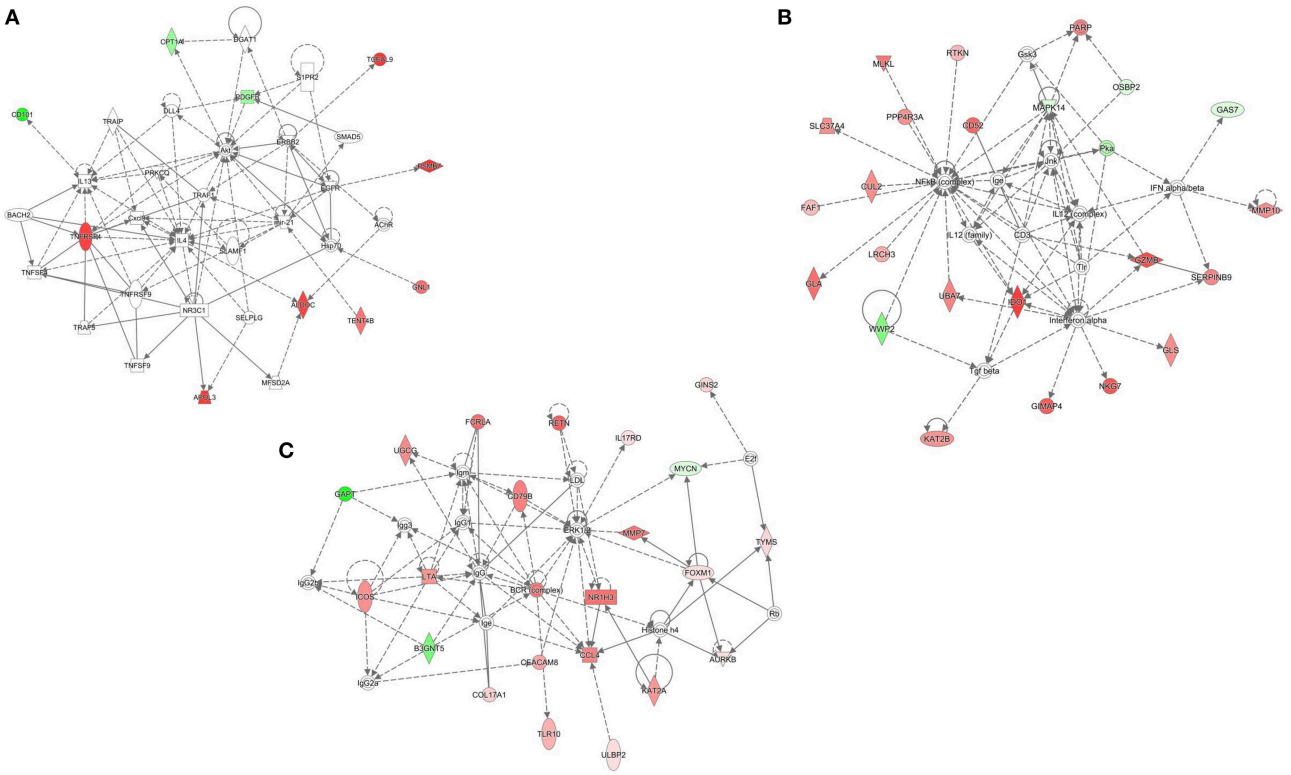

FIGURE 3 | Differentially expressed genes comparing VM to MDH and MDL. **(A)** Network obtained after taking common genes from pairwise comparison between MDH and VM and MDL and VM. **(B)** Network retrieved in MDH patients unique differentially expressed genes (DEG), after pairwise comparison to VM. **(C)** Network retrieved in MDL patients unique DEG, after pairwise comparison to VM. Genes in red were up-regulated, while genes in green were down- regulated.

patients have been established by Yamada et al. (20) and they observed that these cells produce CCL3 and that its production can be increased after Toll-like receptor (TLR) 3 and TLR4 stimulation. Moreover, they observed production of other cytokines, such as IL- 1β, CXCL10, thymic stromal lymphopoietin (TSLP), B lymphocyte stimulator (BLyS), IL-6 and IL-8. The levels of CCL3 are lower in patients with VM compared to MD, but higher than in healthy controls. Elevated levels of CCL3 have been reported in patients with migraine (21), which could support the hypothesis that VM shares migraine mechanisms (3).

CCL22 or MDC (Macrophage-derived chemokine) is a chemoattractant for monocytes, dendritic cells and natural killer cells and it binds to CCR4. IL-1β is a potent inflammatory mediator and is associated with various cellular mechanisms, such as cell activation, proliferation, and apoptosis (22). Yoshida et al cultured murine spiral ligament fibrocytes and verified that IL- 1β and TNFα stimulation resulted in production of various cytokines and chemokines, namely IL-6 and CCL2 (23).

The expression of CXCL1, CCL3, CCL22, and IL- 1β has been observed in mouse cochlear tissue (24), and CXCL1, CCL3, and IL-1β were also found in cells from the ES (25). Interestingly CXCL1 is the only chemokine which expression was also found in mouse vestibular cells (26) and of the four cytokines had the highest expression in all tissues.

Considering that we observed a cytokine increase in PBMCs extracted from peripheral blood, this could indicate that patients with MD and VM have a systemic proinflammatory response, which could explain some patients response to anti-inflammatory drugs (2, 27). On the other hand, this increased production of cytokines could also affect or represent activity that is occurring in the inner ear, thus the observed secretion of cytokines/chemokines may present a prolonged inflammatory response, leading to inner ear damage, through epithelial disruption.

Some studies have quantified cytokine levels in serum from migraine patients during the attack and non-attack periods. Fidan et al. (28) observed that IL-6 is higher in both periods when compared to healthy controls; CCL5, IL-10 and nitric oxide were only elevated during attack periods and TNFα, IL-1, IL-2, IFNγ, CCL2, CCL3, and CCL4 had no differences. On the other hand, Yucel et al. (29) saw an increase of CNDN5, ESM-1, IL-6, IL-1β, and TNFα during attacks. Additionally, Munno et al. (30) described an increase in TNFα, IL-4, and IL-5 in migraine patients, but no differences in IL-10 and IFNγ. In our work, we observed that VM patients had elevated levels of CCL5, IL-10, IL-1β, IFNγ, CCL2, CCL3, CCL4, and IL-4

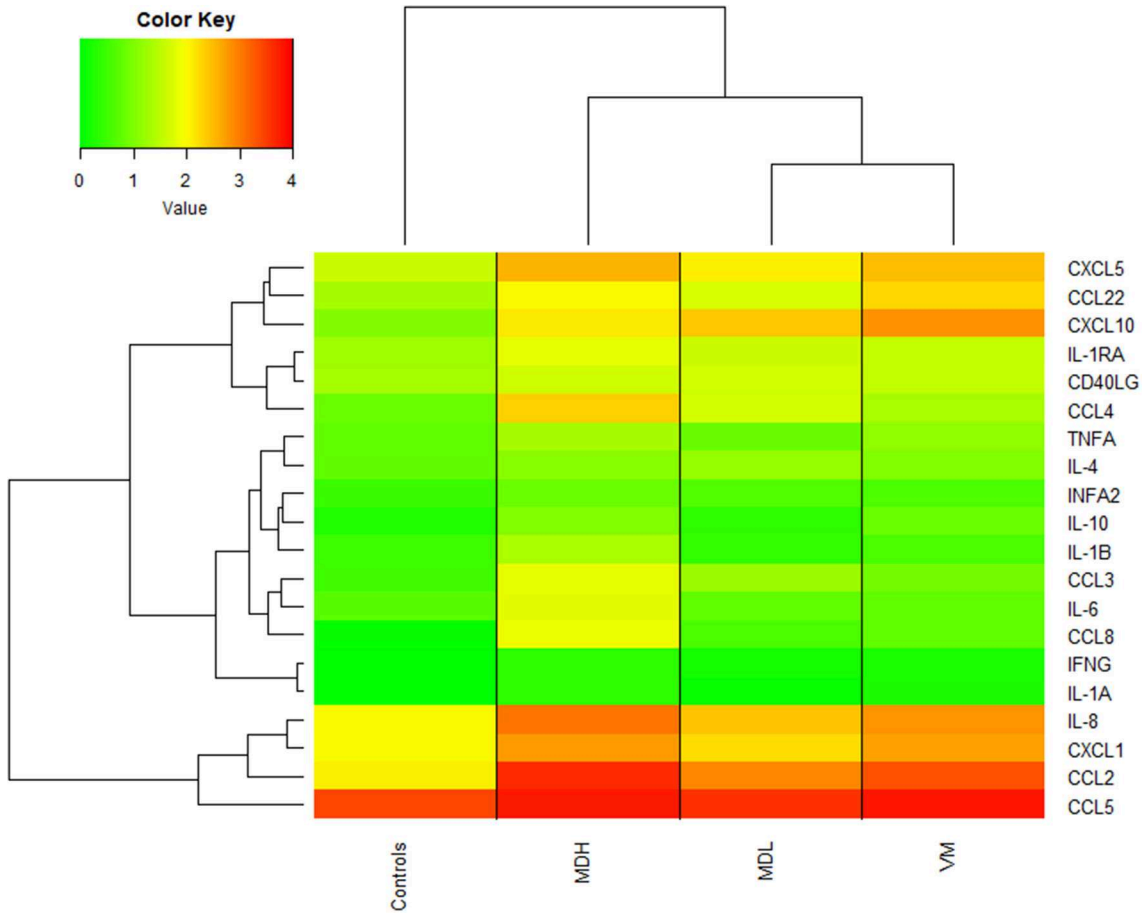

FIGURE 4 | Heatmap of cytokine/chemokine concentrations [$\log_{10}$(concentration (pg/mL) +1)] with dendrogram showing hierarchical clustering of patients and controls.

TABLE 3 | Logistic regression model to predict VM including IL-1β, CCL3, CXCL1, and CCL22 (Negelkerke's $R^2 = 0.909$).

	B	SE	Wald	Exp(B)	95% CI for EXP(B)	*p*-value
IL-1β	−1.99	0.94	4.50	0.14	0.02–0.86	0.03
CCL3	−1.07	0.45	5.68	0.34	0.14–0.83	0.02
CXCL1	0.02	0.01	5.22	1.02	1.00–1.04	0.02
CCL22	0.05	0.02	4.38	1.05	1.00–1.10	0.04

The total accuracy of the model was 95.2%.

(**Supplementary Table 4**) when compared to healthy controls, but no statistical differences in IL-6 and TNFα levels were found. Therefore, a comparison between VM patients and migraine patients, namely IL- 1β, CCL3, CCL22, and CXCL1 levels, could be beneficial to understand if there is a shared cytokine profile between migraine and VM or if this cytokine signature is specific to VM.

Autoinflammatory diseases are caused by a hyperactive inflammatory response, that leads to an immune deregulation, driven by IL-1, type I interferon, and NFκB (31). These diseases usually manifest themselves in the perinatal period, however milder and later-onset forms are being diagnosed in the adulthood (32). Some of these disorders have manifestations that mimic allergic and immunodeficiency disorders (31). Moreover, many of these diseases have sensorineural hearing loss as a symptom (31, 32). Autoimmune inner ear disease (AIED) is characterized by recurrent episodes of bilateral SNHL occurring over a period of several weeks or months (33). AIED has an overlapping audiovestibular phenotype with MD. Patients with AIED present elevated levels of proinflammatory cytokines, such as IL-1β and TNFα which resembles an autoinflammatory phenotype (33, 34). Recent efforts have been made to expand the immunological disease continuum to include monogenic and complex immune disorders that present both autoinflammatory or autoimmune manifestations, where diseases such as AIED would fall (33). Thus, considering the overall elevated levels of proinflammatory cytokines in patients with MDH and the similarity to AIED, we propose that MDH should be considered an autoinflammatory condition, yet longitudinal studies would be necessary to determine if these patients present continuously elevated proinflammatory cytokine levels or if it is a fluctuating condition.

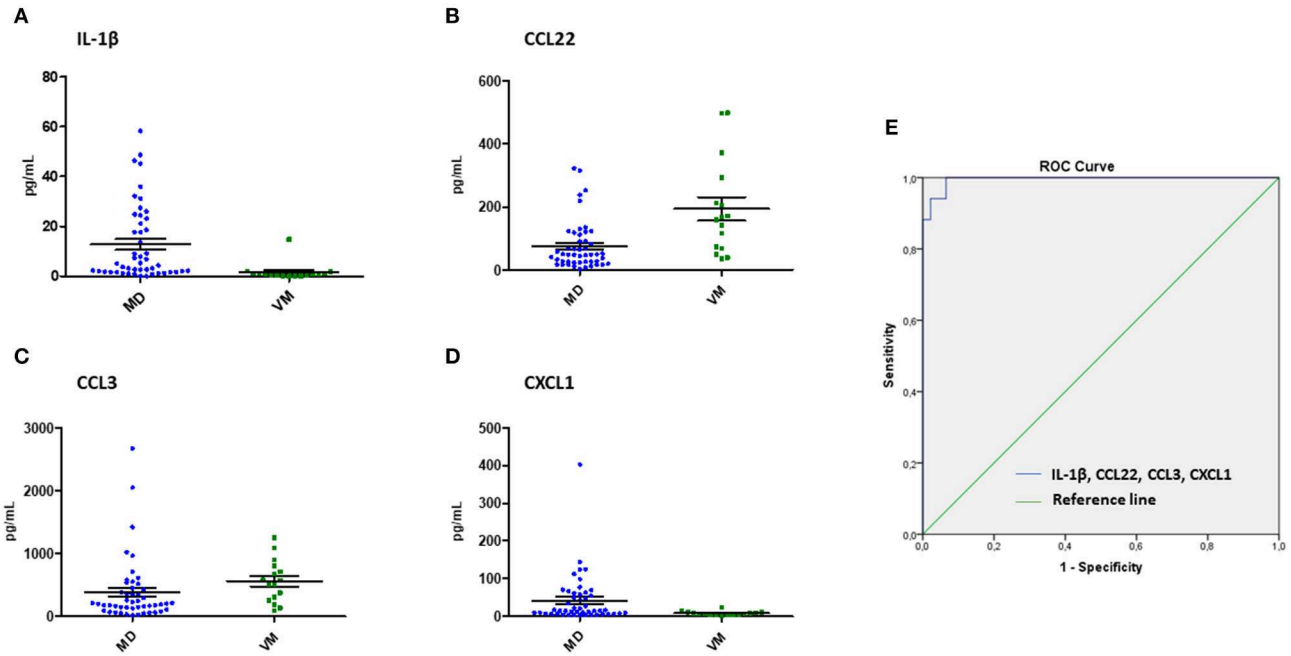

FIGURE 5 | Predictive biomarkers for Vestibular Migraine. Scatter dot plots showing the measured levels for IL-1β **(A)**, CCL22 **(B)**, CCL3 **(C),** and CXCL1 **(D)** in patients with VM and MD. **(E)** Receiver operating characteristic (ROC) curves to predict VM with IL-1β, CXCL1, CCL3, and CCL22. AUC (area under the curve) = 0.995.

TABLE 4 | Different multivariant or univariant models using IL-1β, CXCL1, CCL3, CCL22 as predictive variables.

Variables	AUC	% loss
IL-1β, CXCL1, CCL22, CCL3	0.993	
IL-1β, CXCL1, CCL22	0.962	3.1%
CXCL1, CCL22, CCL3	0.948	4.7%
CXCL1, CCL22	0.794	21.0%
IL-1β, CCL22, CCL3	0.945	6.0%
IL-1β, CCL22	0.921	7.6%
IL-1β, CXCL1, CCL3	0.957	3.9%
IL-1β	0.874	11.9%
CXCL1	0.720	27.3%
CCL3	0.795	19.8%
CCL22	0.794	19.9%

AUC–area under the curve.

In this study we were able to find a method that could allow a more accurate differential diagnosis between VM and MD. Since the cohort of patients for which we could measure all cytokines was limited (VM = 16 and MD = 48), these results should be replicated in a larger cohort of patients with VM, MD, and Migraine, also considering clinical variables to better characterize MD endophenotypes.

CONCLUSION

Patients with MD or VM have a different pro-inflammatory signature. A cytokine panel including IL- 1β, CCL3, CCL22, and CXCL1 could be used as biological markers for the differential diagnosis of VM and MD.

DATA AVAILABILITY

The datasets analyzed for this study can be found in the Gene Expression Omnibus with the accession number GSE109558: https://www.ncbi.nlm.nih.gov/geo/query/acc.cgi?acc=GSE109558.

ETHICS STATEMENT

This study was carried out in accordance with the recommendations of the Declaration of Helsinki with written informed consent from all subjects. The protocol number PI17/1644 was approved by the Granada Ethical Review Board on the 29/01/18.

AUTHOR CONTRIBUTIONS

MF and LF performed experimental work including, PBMC isolation and culture, RNA extraction and cytokine measurement. MF, LF, AG-M performed statistical and bioinformatic analysis. EM-S, MR-I, JA-D, AS-V, SS-P, AB-C, JE-S, PP-C, MM-M, IA and JL-E recruited patients and obtained informed consent from all individuals. JL-E designed the study. JL-E supervised all experiments and MF and JL-E drafted the manuscript. All authors revised and approved the final version of the manuscript.

FUNDING

This work was supported by PI13/1242 and PI17/1644 Grant from ISCIII by FEDER Funds from the EU. Marisa Flook is funded by FI18/00228 from ISCIII.

ACKNOWLEDGMENTS

MF is a Biomedicine Program Ph.D. student at the University of Granada. The authors would like to thank all patients and healthy controls participating in this study. We would also like to thank the Supercomputing and Bioinnovation Center (SCBI) from University of Málaga for sharing their resources (IPA®), Manuela Expósito Ruiz, for her advice in statistical approaches and Teresa Requena for the assistance in PBMC isolation.

SUPPLEMENTARY MATERIAL

The Supplementary Material for this article can be found online at: https://www.frontiersin.org/articles/10.3389/fimmu.2019.01229/full#supplementary-material

REFERENCES

1. Lopez-Escamez JA, Carey J, Chung WH, Goebel JA, Magnusson M, Mandalà M, et al. Diagnostic criteria for Menière's disease. *J Vestib Res.* (2015) 25:1–7. doi: 10.3233/VES-150549
2. Espinosa-Sanchez JM, Lopez-Escamez JA. Menière's disease. In: Furman J, Lempert T, editors. *Handbook of Clinical Neurology*. Amsterdam: Elsevier B.V. (2016). p. 257–77. doi: 10.1016/B978-0-444-63437-5.00019-4
3. Lempert T, Olesen J, Furman J, Waterston J, Seemungal B, Carey J, et al. Vestibular migraine: diagnostic criteria. *J Vestib Res*. (2012) 22:167–72. doi: 10.3233/VES-2012-0453
4. Sohn JH. Recent advances in the understanding of vestibular migraine. *Behav Neurol.* (2016) 2016:1–9. doi: 10.1155/2016/1801845
5. Liu YF, Xu H. The intimate relationship between vestibular migraine and meniere disease: a review of pathogenesis and presentation. *Behav Neurol.* (2016) 2016:3182735. doi: 10.1155/2016/3182735
6. Espinosa-Sanchez JM, Lopez-Escamez JA. New insights into pathophysiology of vestibular migraine. *Front Neurol*. (2015) 6:10–5. doi: 10.3389/fneur.2015.00012
7. Lopez-Escamez JA, Dlugaiczyk J, Jacobs J, Lempert T, Teggi R, von Brevern M, et al. Accompanying symptoms overlap during attacks in Menière's disease and vestibular migraine. *Front Neurol*. (2014) 5:1–5. doi: 10.3389/fneur.2014.00265
8. Ray J, Carr SD, Popli G, Gibson WP. An epidemiological study to investigate the relationship between Meniere's disease and migraine. *Clin Otolaryngol.* (2016) 41:707–10. doi: 10.1111/coa.12608
9. Ibekwe TS, Fasunla JA, Ibekwe PU, Obasikene GC, Onakoya PA, Nwaorgu OG. Migraine and Meniere's disease: two different phenomena with frequently observed concomitant occurrences. *J Natl Med Assoc*. (2008) 100:334–8. doi: 10.1016/S0027-9684(15)31246-3
10. Frejo L, Soto-Varela A, Santos-Perez S, Aran I, Batuecas-Caletrio A, Perez-Guillen V, et al. Clinical subgroups in bilateral Meniere disease. *Front Neurol.* (2016) 7:1–10. doi: 10.3389/fneur.2016.00182
11. Frejo L, Martin-Sanz E, Teggi R, Trinidad G, Soto-Varela A, Santos-Perez S, et al. Extended phenotype and clinical subgroups in unilateral Meniere disease: a cross-sectional study with cluster analysis. *Clin Otolaryngol*. (2017) 42:1172–80. doi: 10.1111/coa.12844
12. Frejo L, Gallego-Martinez A, Requena T, Martin-Sanz E, Amor-Dorado JC, Soto-Varela A, et al. Proinflammatory cytokines and response to molds in mononuclear cells of patients with Meniere disease. *Sci Rep*. (2018) 8:5974. doi: 10.1038/s41598-018-23911-4
13. Eckhard AH, Zhu MY, O'Malley JT, Williams GH, Loffing J, Rauch SD, et al. Inner ear pathologies impair sodium-regulated ion transport in Meniere's disease. *Acta Neuropathol*. (2018) 137:343–57. doi: 10.1007/s00401-018-1927-7
14. Rask-andersen H, Danckwardt-lilliestrom N, Friberg U, House W. Lymphocyte-macrophage activity in the human endolymphatic sac lymphocyte-macrophage activity in the human endolymphatic sac. *Acta Oto-Laryngologica Suppl*. (1991) 485:15–7. doi: 10.3109/00016489109128039
15. Okano T, Nakagawa T, Ito J. Distribution of bone marrow-derived cells in the vestibular end organs and the endolymphatic sac. *Acta Otolaryngol*. (2010) 130:88–94. doi: 10.3109/00016489.2010.486803
16. Moller MN, Kirkeby S, Vikesa J, Nielsen FC, Caye-Thomasen P. Gene expression in the human endolymphatic sac: the solute carrier molecules in endolymphatic fluid homeostasis. *Otol Neurotol*. (2015) 36:915–22. doi: 10.1097/MAO.0000000000000669
17. Hu BH, Zhang C, Frye MD. Immune cells and non-immune cells with immune function in mammalian cochleae. *Hear Res*. (2018) 362:14–24. doi: 10.1016/j.heares.2017.12.009
18. Nordström CK, Danckwardt-lilliestrom N, Laurell G, Liu W, Rask-andersen H. The human endolymphatic sac and inner ear immunity: macrophage interaction and molecular expression. *Front Immunol*. (2019) 9:3181. doi: 10.3389/fimmu.2018.03181
19. Sawant K V, Poluri KM, Dutta AK, Sepuru KM, Troshkina A, Garofalo RP, et al. Chemokine CXCL1 mediated neutrophil recruitment: role of glycosaminoglycan interactions. *Sci Rep*. (2016) 6:33123. doi: 10.1038/srep33123
20. Yamada T, Ogi K, Sakashita M, Kanno M, Kubo S, Ito Y, et al. Toll-like receptor ligands induce cytokine and chemokine production in human inner ear endolymphatic sac fibroblasts. *Auris Nasus Larynx*. (2017) 44:398–403. doi: 10.1016/j.anl.2016.10.007
21. Domingues RB, Duarte H, Senne C, Bruniera G, Brunale F, Rocha NP, et al. Serum levels of adiponectin, CCL3 MIP-1 α , and CCL5/RANTES discriminate migraine from tension-type headache patients. *Arq Neuropsiquiatr*. (2016) 74:626–31. doi: 10.1590/0004-282X20160096
22. Turner MD, Nedjai B, Hurst T, Pennington DJ. Cytokines and chemokines: at the crossroads of cell signalling and inflammatory disease. *Biochim Biophys Acta*. (2014) 1843:2563–82. doi: 10.1016/j.bbamcr.2014.05.014
23. Yoshida K, Ichimiya I, Suzuki M, Mogi G. Effect of proinflammatory cytokines on cultured spiral ligament fibrocytes. *Hear Res*. (1999) 137:155–9. doi: 10.1016/S0378-5955(99)00134-3
24. Cai T, Jen H, Kang H, Klisch TJ, Zoghbi HY, Groves AK. Characterization of the transcriptome of nascent hair cells and identification of direct targets of the atoh1 transcription factor. *J N*. (2015) 35:5870–83. doi: 10.1523/JNEUROSCI.5083-14.2015
25. Honda K, Kim SH, Kelly MC, Burns JC, Constance L, Li X, et al. Molecular architecture underlying fluid absorption by the developing inner ear. *Elife*. (2017) 6:e26851. doi: 10.7554/eLife.26851
26. Elkon R, Milon B, Morrison L, Shah M, Vijayakumar S, Racherla M, et al. RFX transcription factrs are essential for hearing in mice. *Nat Commun*. (2015) 6:8549. doi: 10.1038/ncomms9549
27. Strupp M, Thurtell MJ, Shaikh AG, Brandt T, Zee DS, Leigh RJ. Pharmacotherapy of vestibular and ocular motor disorders, including nystagmus. *J Neurol*. (2011) 258:1207–22. doi: 10.1007/s00415-011-5999-8
28. Fidan I, Yuksel S, Ýmir T, Irkeç C, Aksakal FN. The importance of cytokines, chemokines and nitric oxide in pathophysiology of migraine. *J Neuroimmunol.* (2006) 171:184–8. doi: 10.1016/j.jneuroim.2005.10.005
29. Yucel M, Kotan D, Gurol Çiftçi G, Çiftçi IH, Cikriklar HI. Serum levels of endocan, claudin-5 and cytokines in migraine. *Eur Rev Med Pharmacol Sci.* (2016) 20:930–6. Retrieved from: https://www.europeanreview.org/

30. Munno I, Centonze V, Marinaro M, Bassi A, Lacedra G, Causarano V, et al. Cytokines and migraine: increase of IL-5 and IL-4 plasma levels. *Headache*. (1998) 38:465–7. doi: 10.1046/j.1526-4610.1998.3806465.x
31. Broderick L. Hereditary autoinflammatory disorders: recognition and treatment. *Immunol Allergy Clin North Am*. (2019) 39:13–29. doi: 10.1016/j.iac.2018.08.004
32. Martinez-Quiles N, Goldbach-Mansky R. Updates on autoinflammatory diseases. *Curr Opin Immunol*. (2018) 55:97–105. doi: 10.1016/j.coi.2018.09.014
33. Vambutas A, Pathak S. AAO: Autoimmune and autoinflammatory (Disease) in otology: what is new in immune-mediated hearing loss. *Laryngoscope Investig Otolaryngol*. (2016) 1:110–5. doi: 10.1002/lio2.28
34. Pathak S, Goldofsky E, Vivas EX, Bonagura VR, Vambutas A. IL-1β is overexpressed and aberrantly regulated in corticosteroid nonresponders with autoimmune inner ear disease. *J Immunol*. (2011) 186:1870–9. doi: 10.4049/jimmunol.1002275

Conflict of Interest Statement: Cytokine/chemokine panel for the differential diagnosis of episodic vestibular syndrome. Patent P201930255, March 20, 2019, owned by the Servicio Andaluz de Salud (Andalusian Public Health System).

The authors declare that the research was conducted in the absence of any commercial or financial relationships that could be construed as a potential conflict of interest.

frontiers in Neurology

ORIGINAL RESEARCH
published: 10 June 2019
doi: 10.3389/fneur.2019.00570

Anti-inflammatory and Oto-Protective Effect of the Small Heat Shock Protein Alpha B-Crystallin (HspB5) in Experimental Pneumococcal Meningitis

Silvia T. Erni[1,2,3,4], *Gabriella Fernandes*[1,2,3], *Michelle Buri*[1,2], *Michael Perny*[1,2,3], *Rolf Jan Rutten*[5], *Johannes M. van Noort*[6], *Pascal Senn*[7], *Denis Grandgirard*[1,2], *Marta Roccio*[2,3,8*†] and *Stephen L. Leib*[1,2*†]

[1] Neuroinfection Laboratory, Institute for Infectious Diseases, University of Bern, Bern, Switzerland, [2] Cluster for Regenerative Neuroscience, DBMR, University of Bern, Bern, Switzerland, [3] Laboratory of Inner Ear Research, DBMR, University of Bern, Bern, Switzerland, [4] Graduate School for Cellular and Biomedical Sciences, University of Bern, Bern, Switzerland, [5] Audion Therapeutics, Amsterdam, Netherlands, [6] Delta Crystallon BV, Leiden, Netherlands, [7] Service d'oto-rhino-laryngologie (ORL) et de chirurgie cervico-faciale, Département des Neurosciences Cliniques, Hôpitaux Universitaires de Genève, Geneva, Switzerland, [8] Department of Otorhinolaryngology, Head & Neck Surgery, Inselspital, Bern, Switzerland

OPEN ACCESS

Edited by:
Paola Perin,
University of Pavia, Italy

Reviewed by:
Juan Carlos Amor-Dorado,
Hospital Can Misses, Spain
Moritz Gröschel,
Unfallkrankenhaus Berlin, Germany

***Correspondence:**
Marta Roccio
marta.roccio@dbmr.unibe.ch
Stephen L. Leib
stephen.leib@ifik.unibe.ch

[†] These authors have contributed equally to this work

Specialty section:
This article was submitted to Neuro-Otology, a section of the journal Frontiers in Neurology

Received: 29 March 2019
Accepted: 15 May 2019
Published: 10 June 2019

Citation:
Erni ST, Fernandes G, Buri M, Perny M, Rutten RJ, van Noort JM, Senn P, Grandgirard D, Roccio M and Leib SL (2019) Anti-inflammatory and Oto-Protective Effect of the Small Heat Shock Protein Alpha B-Crystallin (HspB5) in Experimental Pneumococcal Meningitis. Front. Neurol. 10:570. doi: 10.3389/fneur.2019.00570

Sensorineural hearing loss is the most common long-term deficit after pneumococcal meningitis (PM), occurring in up to 30% of surviving patients. The infection and the following overshooting inflammatory host response damage the vulnerable sensory cells of the inner ear, resulting in loss of hair cells and spiral ganglion neurons, ultimately leading to elevated hearing thresholds. Here, we tested the oto-protective properties of the small heat shock protein alpha B-crystallin (HspB5) with previously reported anti-inflammatory, anti-apoptotic and neuroprotective functions, in an experimental model of PM-induced hearing loss. We analyzed the effect of local and systemic delivery of HspB5 in an infant rat model of PM, as well as *ex vivo*, using whole mount cultures. Cytokine secretion profile, hearing thresholds and inner ear damage were assessed at predefined stages of the disease up to 1 month after infection. PM was accompanied by elevated pro-inflammatory cytokine concentrations in the cerebrospinal fluid (CSF), leukocyte and neutrophil infiltration in the perilymphatic spaces of the cochlea with neutrophils extracellular trap formation during the acute phase of the disease. Elevated hearing thresholds were measured after recovery from meningitis. Intracisternal but not intraperitoneal administration of HspB5 significantly reduced the levels of TNF-α, IL-6 IFN-γ and IL-10 in the acute phase of the disease. This resulted in a greater outer hair cell survival, as well as improved hearing thresholds at later stages. These results suggest that high local concentrations of HspB5 are needed to prevent inner ear damage in acute PM. HspB5 represents a promising therapeutic option to improve the auditory outcome and counteract hearing loss after PM.

Keywords: sensorineural hearing loss, *S.pneumoniae*, HspB5, inflammation, oto-protection, hair cells, neutrophil infiltration

INTRODUCTION

Worldwide around 460 million people suffer from disabling hearing loss (world health organization fact sheet 2019). This is caused by inherited genetic defects or acquired damage by ototoxic drugs, exposure to excessive noise, aging or certain infectious diseases such as meningitis. *Streptococcus pneumoniae* is the most common and simultaneously the most severe pathogen causing bacterial meningitis. Pneumococcal meningitis (PM) is associated with high mortality and risk for neurological sequelae, with sensorineural hearing loss representing the most frequent long term deficit (1) occurring in up to 30% of surviving patients (2).

Bacterial meningitis evokes a robust inflammatory response marked by recruitment of leukocytes, mostly polymorphonuclear neutrophils, to the cerebrospinal fluid (CSF) spaces, including the inner ear. For many years the cochlea was thought to be immune-privileged, but more recent studies have shown that resident macrophages are present in the lateral wall, in the spiral limbus and in the basal side of basilar membrane and are activated after insult (3–7).

Upon infection, pro-inflammatory cytokines such as TNFα, IL-1β, IL-6, IL-8 are secreted in the CSF (8, 9) and pneumococci and leukocytes infiltrate the perilymphatic space of the inner ear via the cochlear aqueduct (1, 6, 10). These processes, together with the release of the bacterial exotoxin pneumolysin, cause an accentuated inflammation of the inner ear, especially in the basal portion of the cochlea (11, 12). This results in histopathological changes of the sensory epithelium and associated structures, which are crucial for the hearing process. Spiral ganglion neuron loss and outer hair cell loss strongly correlate to the level of pneumococcal infection, with the most severe damage occurring in the basal part of the cochlea (8). Inner hair cells are not significantly lost but the number of presynaptic ribbons was shown to be decreased (8). Increased hearing thresholds are already observed during the acute phase of experimental pneumococcal meningitis and in most cases persist until later stages (8, 12–14).

Current treatment options for sensorineural hearing loss consist of hearing aids and cochlear implants, both relying for their effectiveness on remaining intact hair cells and/or spiral ganglion neurons (15). Novel therapeutics are highly needed to protect these cells in the first place or to induce a regenerative response.

Heat shock proteins have already been proposed as therapeutic targets in various diseases (16). Activation of heat shock proteins is the most ubiquitous and highly conserved stress response in biology (17, 18).

Specific to the inner ear, May et al. observed a protective effect of Hsp70 against aminoglycoside-induced hair cell death *in vitro* and *in vivo* (19). Additionally, expression of Hsp70 and induction of Hsp32 offered protection against cisplatin-induced hair cell death in utricle cultures (20).

Over the last decade, evidence has accumulated for the broad neuroprotective and anti-inflammatory activity of HspB5, also known as alpha B-crystallin or CRYAB (21, 22). Several studies demonstrated HspB5-mediated cell protection under various stress conditions (23) such as experimental autoimmune encephalomyelitis (24), stroke (25) and Alexander disease (26).

HspB5 is a member of the small heat shock family that is constitutively expressed in many tissues and especially abundant in eye, lens, heart, muscle and oligodendrocytes of the CNS (21, 23). In pathological conditions such as multiple sclerosis and brain ischemia it is also expressed in other glial cells (21, 27). HspB5 is stress-inducible (22) and has anti-apoptotic (28, 29), anti-inflammatory (21) and neuroprotective (30) functions.

Different mechanisms of action have been reported for HspB5 in the literature. The anti-inflammatory effect of HspB5 has been shown to be associated with activation of an immune-regulatory macrophage response via Toll-like receptors (TLR1/2) and the co-receptor CD14 (31, 32). Its chaperone activity, by binding to misfolded proteins also contributes to its anti-inflammatory activity (24, 26). Its anti-apoptotic effects have been instead attributed to direct interaction with pro-apoptotic molecules, such as Caspase-3, or by interfering with cytochrome C release from the mitochondria (33).

In a murine model of stroke, Cryab$^{-/-}$ mice had increased lesion size and diminished neurologic function compared with wild-type mice. Even 12 h after experimental stroke, systemic administration of HspB5 reduced both stroke volume and inflammatory cytokines associated with stroke pathology (25).

Furthermore, in a model of experimental autoimmune encephalomyelitis Cryab$^{-/-}$ mice showed worse scores in the acute and in the progressive phases, with higher Th1 and Th17 cytokine secretion and more intense CNS inflammation compared with their wild-type counterparts. Moreover, Cryab$^{-/-}$ astrocytes showed increased expression of cell death markers, such as cleaved caspase-3 and DNA breaks, detected by TUNEL staining, indicating an anti-apoptotic function of HspB5. Administration of recombinant HspB5 ameliorated experimental autoimmune encephalomyelitis (21).

A phase IIa randomized clinical trial with therapeutic application of HspB5 in relapsing-remitting multiple sclerosis patients, using intravenous doses of HspB5 was completed in 2015. Repeated administration of the lower doses of HspB5 resulted in a progressive decline in MS lesion activity, which was not seen in the placebo group (22).

Considering the abundance of HspB5 expression in peripheral tissues and its potential therapeutic value for counteracting inflammation and supporting neuroprotection, HspB5 is a promising candidate to test in the context of infection/inflammation-induced sensorineural hearing loss.

The aim of this study was to characterize the acute inflammatory phase of the disease upon infection and evaluate whether exogenous human recombinant HspB5 could be used to protect cochlear neurosensory cells in an infant rat model of *S. pneumoniae*-induced bacterial meningitis.

METHODS AND MATERIALS

All animal experiments were approved by the experimentation committee of the canton Bern, Switzerland (license to SSL

BE124/16 and BE1/18) and followed the Swiss national guidelines for the performance of animal experiments.

HspB5

For this study, GMP-grade sterile recombinant human HSPB5 (Delta Crystallon BV, Leiden, The Netherlands), was used. Previous analysis reported 5 ng/mg (0.0005 %) *E. Coli* proteins, <0.7 EU/mg endotoxins, and <75 pg/mg bacterial DNA.

Streptococcus pneumoniae Inoculum

A clinical isolate of *Streptococcus pneumoniae* (serotype 3) from a patient with bacterial meningitis had been adapted to rats through several *in vivo* passages and was prepared as previously reported (8, 34). Bacteria were cultured overnight in brain-heart infusion medium. Then the bacterial culture was diluted 1:10 in fresh medium and grown for another 5 h until the logarithmic phase was reached. The bacterial culture was centrifuged for 10 min at 3,100 g at 4°C. The pellet was re-suspended in 0.85 % NaCl followed by a second centrifugation and then diluted to the desired concentration by optical density measurements at 570 nm. Final inoculum concentration was later quantified by plating serial dilutions of the inoculum on Columbia sheep blood agar (CSBA) plates.

Infant Rat Model of Pneumococcal Meningitis With Therapeutic Intervention by HspB5

A well-established infant rat model of experimental pneumococcal meningitis was used as previously described (14, 35). A schematic is given in **Figure 3A**. Eleven-day old Wistar rats obtained from Charles River Laboratories (Sulzfeld, Germany) were infected by a single intracisternal injection of *S. pneumoniae* (10 µl of $8.20 \pm 1.8 \times 10^5$ cfu/ml). Control animals received same volume of saline (0.85 % NaCl). During the acute phase of meningitis, animals were weighted and clinically scored at 0, 18, 24, and 42 h post infection (hpi), as previously described (35). Disease symptoms were recorded and scored as follows: 1 = minimal or no spontaneous motor activity, coma; 2 = unable to turn upright within 30 s; 3 = turns upright within 30 s; 4 = signs of disease in terms of weight loss and/or appearance of fur, turns upright within 5 s; 5 = normal behavior, healthy. Spontaneous mortality was documented. Animals were sacrificed if scored 2 or lower.

Punctures of the cisterna magna were performed using a 30-gauge needle to collect CSF samples at 18 hpi, 24 hpi and 42 hpi to follow the inflammatory cytokine secretion pattern. A volume of about 15 µl was collected per animal per time point. CSF samples collected at 18 hpi, when animals developed symptomatic disease, were also used to confirm meningitis and quantify bacterial titer by means of serial dilution and plating on CSBA culture plates.

Antibiotic treatment with ceftriaxone (100 mg/kg, i.p. Rocephine, Roche) was initiated 18 hpi, given twice a day for up to 5 days in long term experiments.

To assess therapeutic effect of HspB5 in pneumococcal meningitis, animals were randomized for treatment with HspB5 or control. Recombinant human HspB5 was diluted in sterile saline and rats were injected intracisternally (i.c.) with 10 µg HspB5 in 10 µl saline or intraperitoneally (i.p.) with 50 µg HspB5 in 250 µl saline. These doses were chosen based on literature where they have been shown to be effective in a model of experimental stroke [50 µg i.p. daily for up to 1 week (25)], experimental autoimmune encephalomyelitis and spinal cord injury when delivered intravenously [10 µg i.v. every other day for 3 weeks; (21, 25, 36)]. For i.c. injections, HspB5 therapy was initiated shortly prior to infection (2 h before) to avoid excessive intracranial pressure by delivering inappropriate volumes of recombinant protein and bacteria concomitantly, followed by consecutive applications. This was done after CSF extraction at 18 hpi, and subsequently 3 days post infection (dpi) and 5 dpi. Control animals were injected with an equal volume of BSA in saline (10 µl of 1 mg/ml). For i.p. administration two different protocols were tested with animals receiving HspB5 or saline immediately prior to infection (2 h before), followed by consecutive applications at 18 hpi, 3 dpi and 5 dpi, or receiving HspB5 at 18 hpi, 3 dpi and 5 dpi. The examiner was blinded regarding treatment groups for the entire experiment as well as during data analyses.

Animals were sacrificed at two different time points for histological analyses. Namely at 42 hpi, to investigate the inflammatory response in the cochlea during the acute phase after infection or 4 weeks post infection, to assess hair cell and spiral ganglion survival. Animals were sacrificed with an overdose of pentobarbital (15 mg/100 g), and perfused via the left ventricle with 4 % paraformaldehyde (PFA) in phosphate-buffered saline (PBS).

Quantitative Analysis of Cytokine Expression on the CSF/Cytokine Analysis in CSF

A panel of PM-associated cytokines (TNF-α, IL-6, IL-1β, IFN-γ, and IL-10) was measured in the CSF at 18, 24 and 42 hpi by using a magnetic multiplex assay (Rat Magnetic Luminex® Assay, Rat Premixed Multi-Analyte Kit, R&D Systems, Bio-Techne) on a Bio-Plex 200 station (Bio-Rad Laboratories) as previously described (8, 37). Five microliters CSF were diluted to a final volume of 50 µl and at least 50 beads per analyte were measured. Calibration curves from recombinant standards were calculated with Bio-Plex Man-ager software (version 4.1.1) using a five-parameter logistic curve fitting. For samples below the detection limit, the value of detection limit provided by the manufacturer (TNF-α, 22.1 pg/ml; IL-6, 56.0 pg/ml; IL-1β, 26.7 pg/ml; IL-10, 18.6 pg/ml; IFN-γ, 70.5 pg/ml) was multiplied by the dilution factor.

Determination of Hearing Capacity by Auditory Brainstem Response

Hearing capacity was assessed by recording auditory brainstem responses (ABRs) to click and pure tone stimuli on both ears with the Smart EP system (Intelligent Hearing Systems, Miami, USA), as previously described (8, 34). Animals were anesthetized with isoflurane (5 % induction, 2 % maintenance) using the Combi-Vet Vaporizer System equipped with a digital flowmeter (Rothacher Medical, Switzerland). One hundred-microsecond

click stimuli and 5-ms pure tone pips (Blackman envelope; polarity alternating) were presented at a rate of 21.1 s^{-1}, ranging from 100 to 20 dB SPL in 10 dB decrements (5 dB decrements close to threshold). Responses were measured at 4, 8, 16 and 32 kHz. A total of 1,024 responses were averaged at each sound level and filtered between 100 and 1,500 Hz. The hearing threshold was defined as the lowest intensity that induced the appearance of a visually detectable first peak in the recording. Later peaks were not taken in consideration for the evaluation of the threshold as they were not reliable, especially in infected animals.

Histological Analyses

Cryosections

Cochleae were dissected immediately after perfusion of animals and placed for 4 h in 4 % PFA at 4°C and subsequently decalcified with Osteosoft (Merck, Germany) for at least 10 days.

Cochleae were dehydrated stepwise with 15 % for 2 h and 30 % sucrose overnight. Samples were embedded in optimal cutting temperature medium (O.C.T., Sakura, Netherlands) and cut with a cryostat (Leica CM3050 S) in 16 µm thick mid-modiolar sections, where every second section was mounted on Superfrost Plus microscopy slides (Thermo Fisher Scientific, USA) for quantification studies. To stain the samples, slides were put in a Shandon Sequenza staining rack (Thermo Fisher Scientific, USA). Sections were permeabilized for 10 min with 0.1 % Triton X-100 and blocked with blocking solution (2 % BSA, 0.01 % Triton X-100 in PBS) for 1 h at room temperature. Samples were incubated with primary antibodies (**Table 1**) overnight at 4°C. The next day slides were rinsed and incubated with the corresponding secondary antibody (**Table 1**) for 2 h at room temperature, rinsed again and mounted with a coverslip using Fluoroshield containing DAPI (Sigma).

Slides were visualized with a Nikon Eclipse Ti-E using a Nikon-PLAN Fluor 4x/0.13 NA, 10x/0.3 NA, 20x/0.50 NA or 40x/1.00 NA Oil objective and by a Zeiss 710 laser scanning microscope using a Zeiss Plan-Apochromat and 40x/1.3 NA oil objective for hair cell quantification.

SYTO9 Staining

SYTO9 (3.34 mM) and Propidium iodide (20 mM) of the LIVE/DEAD BactLight Bacterial Viability Kit (Molecular Probes) were mixed 1:1 and directly put on cochlear cryosections and incubated for 15 min at room temperature protected from light. Sections were washed once with PBS and mounted with Fluoroshied containing DAPI (Sigma) and visualized with a Nikon Eclipse Ti-E using a Nikon-PLAN Fluor 40x/1.00 NA Oil objective.

Sirius Red Staining

Cryosections of cochleae at 1 month post infection were immersed in xylene for 10 min at room temperature and transferred to ethanol (100, 100, 80, and 70%, all 10 s) before stained by using 0.1 % solution of Picro Sirius Red solution (Sigma) for 1 h at room temperature. Subsequently, sections were rinsed in 0.01 N HCl for 2 min. Sections were dehydrated in ascending concentrations of ethanol (70, 80, 100, and 100%, each 10 s) and cleared in two stages in xylene, 10 min each. Sections were mounted with Eukitt quick-hardening mounting medium (Fluka Analytical).

TABLE 1 | Antibodies used in the study.

	Species	Dilution	Company
PRIMARY ANTIBODY			
Anti-B-iII Tublin (TUJ)	Mouse	1:500	R & D Systems
Anti-Sox2	Mouse	1:200	RD Bioscience, USA
Anti-Sox10	Mouse	1:200	Santa Cruz Biotechnology,USA
Anti-myeloperoxidase (MPO)	Mouse	1:500	abcam
Anti-CD68	Mouse	1:500	Serotec
Anti-CD11b/OX42	Mouse	1:500	BD Bioscience, USA
Anti-Pou4f3/Brn-3c	Mouse	1:500	Santa Cruz Biotechnology,USA
Anti-alpha B-crystalline	Rabbit	1:500	Abcam, UK
Anti-iba1	Rabbit	1:500	Wako
Anti-CD206	Rabbit	1:500	Abcam, UK
Anti-Cleaved Caspase 3	Rabbit	1:500	Cell Signaling
Anti-Myo7a	Rabbit	1:500	Enzo Life Science
Anti-neutrophil elastase (M-18)	goat	1:500	Santa Cruz Biotechnology,USA
SECONDARY ANTIBODY			
Anti-goat AF488	Donkey	1:500	Molecular Probes
Anti-mouse Cy3	Donkey	1:500	Jackson (Milan, AG)
Anti-mouse Cy5	Goat	1:500	Jackson (Milan, AG)
Anti-mouse AF555	Goat	1:500	Invitrogen, USA
Anti-rabbit AF 647	Goat	1:500	Invitrogen, USA

TUNEL

TUNEL assay was performed by automated staining using Bond RX (Leica Biosystems) immunostainer. Paraffin slides were dewaxed in Bond dewax solution (product code AR9222, Leica Biosystems). Antigen retrieval was performed with Protease incubation for 25 min at 37°C. TdT enzyme incubation was performed for 20 min with antibody diluent (Leica AR9352), TdT Buffer (Promega M1893), DIG-11-dUTP (Roche, Ref 11570013910) and TdT Enzyme (Promega M1875) followed by incubation with mouse anti DIG-FITC (1:500) for 15 min and Rabbit anti FITC (1:1000) for 15 min. The reaction was visualized using AP (Alkaline phosphatase)-rabbit polymer for 15 min and fast red as red chromogen (Red polymer refine Detection, Leica Biosystems, Ref DS9390). Finally, the samples were counterstained with Haematoxylin and mounted with Aquatex (Merck). Stainings were performed by the translational research unit of the institute of Pathology, University of Bern.

Preparation of Organ of Corti Whole Mounts of Adult Rats and Immunofluorescent Staining

The fixed and decalcified cochleae were dissected with forceps (World Precision Instruments) and sapphire blades (World Precision Instruments) using a Nikon SMZ800 binocular microscope. The cochlea was cut in half, longitudinal from the apex to the oval window through the modiolus, the apical turn was left as one piece. Basal, middle and apical turns were separated and hook was cut off the lowest part of the basal turn

resulting in a total of five pieces per cochlea. The organ of Corti was isolated by removing the lateral wall and spiral ganglion.

The tissue pieces were permeabilized with 3 % Triton X-100 for 30 min, rinsed three times with PBS, and incubated in blocking solution for 2 h at room temperature. The hair cell-specific antibody against Myosin7a was incubated for at least 12 h at 4°C. The tissue was rinsed three times with PBS and incubated with the secondary antibodies and Phalloidin ATTO488 (Sigma) diluted 1:500 in blocking solution overnight at 4°C. Each tissue piece was rinsed with PBS and incubated for 15 min with 1:1000 DAPI at room temperature before being rinsed again and transfer to a 24 well glass bottom plate (Corning, USA) for confocal imaging.

Image acquisition was performed with a Zeiss 710 laser scanning microscope using a Zeiss Plan-Apochromat 10x/ 0.3 NA and 20x/0.8 NA objective for hair cell quantification.

Preparation of Organ of Corti Organotypic Cultures and Exposure to *S. pneumoniae*

Cochlear explants were isolated as previously reported (38). The organ of Corti from postnatal day 2 (p2) Wistar rats was plated on a Transwell insert (6-well format, Corning, USA) with a permeable polyester membrane (0.4 μm pore size). Membranes were pre-coated with Cell-Tak (Corning, USA) according to manufacturer's protocol. Explants were cultured on 1.5 ml DMEM/F12 (10 % FBS, 0.01 % Ampicillin) that was added to the lower compartment under the insert overnight at 37 °C with 5 % CO_2 before any treatment.

To mimic the *in vivo* conditions, *S. pneumoniae* were added to the medium in the lower compartment. The inoculum concentration was chosen according to the expected bacterial titers after bacterial proliferation in the CSF *in vivo* during the acute phase (18 hpi) of PM, i.e., 1.7×10^8 cfu/ml. Bacteria were prepared as described above and finally re-suspended in ampicillin- and FBS-free otic medium. Organ of Corti were exposed to bacteria for 2 h, washed and cultured for 4 more days in full otic medium (39). To assess the effect of HspB5, recombinant human HspB5 (50 μg/ml) was added to the cultures during exposure to bacteria and the following 4 days of cell culture.

Immunofluorescent Staining of Explants

At the end of the experiment explants were fixed with 4 % PFA for 10 min, washed and stored in PBS at 4°C until staining. The insert membrane was cut and explants were transferred to a 24 well plate. Explants were permeabilized for 30 min with 3 % Triton X-100 (Sigma-Aldrich, USA) and blocked for 1 h with blocking buffer (2 % BSA, 0.01 % Triton X-100 in PBS) at room temperature. Explants were incubated with the hair cell specific anti-Pou4f3 antibody, the supp-orting cell marker anti-Sox2 antibody and HspB5 specific antibody in blocking buffer overnight at 4°C. On the following day, tissue was rinsed three times and incubated with the secondary antibodies at room temperature for 2 h. Finally, samples were rinsed again three times with PBS and mounted on a glass slide with Fluoroshield containing DAPI (Sigma, USA). Image acquisition was performed with a Zeiss 710 laser scanning microscope using a Zeiss Plan-Apochromat and 20x/0.8 NA objective for hair cell quantification.

Data Analysis of Histological Samples

Image processing was performed with the open source image processing software FIJI, version 2.0.

Neutrophil extracellular traps (NETs) quantification: Five non-consecutive mid-modiolar cryosections per cochlea were used to quantify the area of the NETs (stained by MPO) in the scala tympani. The occluded area by NET formation was measured and calculated as percentage of the area of scala tympani.

Spiral ganglion neuron quantification: The density of spiral ganglion neurons was calculated on five non-consecutive mid-modiolar sections by counting βIII-Tubulin positive cells normalized to the area of the Rosenthal's canal.

Hair cell quantification: Pou4f3 or Myo7a positive cells of the organ of Corti were counted at three random microscopic fields for each cochlear region (basal, middle, apical) covering in total at least 1,200 μm. The number of hair cells (IHCs and OHCs) was expressed as unit per 100 μm.

Statistical Analysis

Statistical analysis was performed with GraphPad Prism software (Prism 7 for Windows; GraphPad Software Inc., San Diego, CA). Normal distribution of the datasets was tested by D'Agostino & Pearson and KS normality test. One-way ANOVA with Tukey's multiple comparison test was used to evaluate whether the means of more than two populations differ. Two-way ANOVA was used to determine the interaction of two independent variables (e.g., location in cochlea and treatment) on a dependent variable (e.g., hair cell count). Unpaired *t*-tests were used to compare parametric data sets of two groups. Welch's correction was applied if variances were not equal (F test).

If not stated otherwise, results are presented as mean values ± standard deviations. In box-plots, the horizontal line within the box represents the median, the cross indicates the mean, the top and the bottom of the box mark the 75th and 25th percentiles; the whiskers represent the range of the data (min-max). A two-tailed $p < 0.05$ was considered statistically significant, with $p < 0.05$ (*), $p < 0.01$ (**), $p < 0.001$ (***) and $p < 0.0001$ (****).

RESULTS

Pneumococcal Meningitis Induces Inflammatory Cell Infiltration to the Cochlea

We initially assessed the inflammatory response within the cochlea as a consequence of bacterial meningitis. We analyzed the presence of macrophages and neutrophils 42 h post infection, in the acute phase of the disease, using immunostaining of mid-modiolar sections.

In uninfected conditions, resident macrophages were present in various locations of the cochlea. CD68+ macrophages were most prominently found in the modiolus and the spiral ganglion (**Figure 1A**; **Figures S1A–C**). CD206+ macrophages were additionally seen in the spiral ligament (**Figures S1G–L**). Iba1+ macrophages were numerously present in the modiolus,

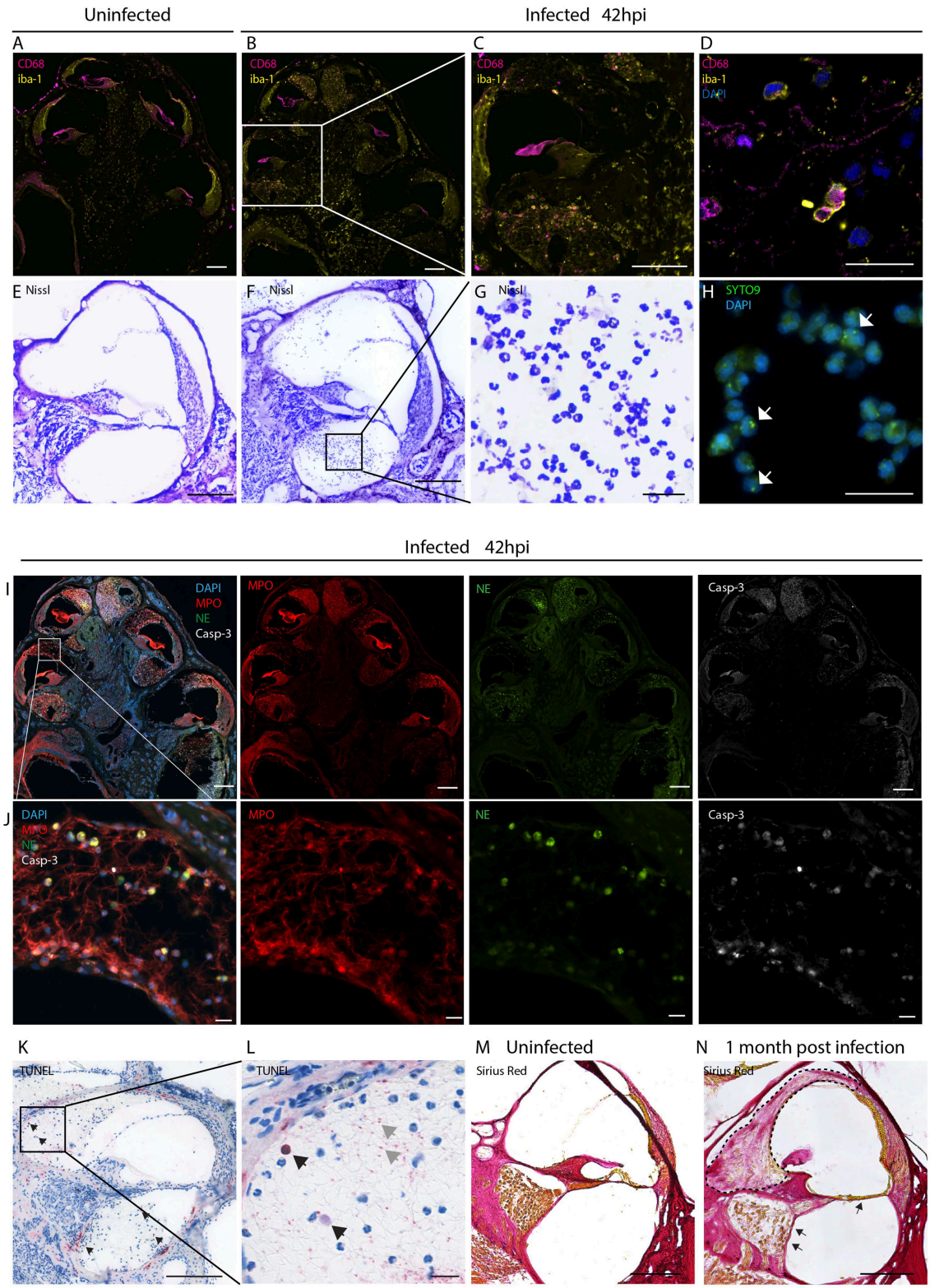

FIGURE 1 | Inflammatory infiltration of the perilymphatic spaces. Immunostainings for macrophages markers CD68 and iba1 on mid-modiolar sections of rat cochlea **(A)** uninfected and **(B)** 42 h post infection with *S. pneumonia.* **(C)** Close up of a middle turn and **(D)** of the perilymphatic space. **(E)** Nissl staining of a cochlear middle turn of an **(E)** uninfected animal and **(F)** 42 h post infection. **(G)** Higher magnification of cells infiltrating in the perilymphatic space showing the characteristic

(Continued)

FIGURE 1 | segmented nuclei morphology of neutrophils. **(H)** Presence of phagocytized *S. pneumoniae* stained with SYTO9 (white arrows) in infiltrating leukocytes. **(I)** Overview of mid-modiolar cryosections 42 h post infection stained for myeloperoxidase (MPO) and neutrophil elastase (NE) and cleaved Caspase-3 (Casp-3). Merge and single channels are shown **(J)** close-up view of the perilymphatic spaces (scala vestibuli) with reticular formed neutrophil extracellular traps (NETs). **(K)** TUNEL staining of a cochlear middle turn, 42 h post infection. **(L)** close-up of scala vestibuli. Black arrows indicate positive cells, gray arrows, extracellular DNA. **(M)** Collagen staining of an uninfected animal and **(N)** an animal 1 month post infection. Fibrosis, detected by sirius staining, is indicated by the dashed line. Arrows highlight loss of the organ of Corti structures and of the spiral ganglion neurons. Scale bars in overview images and middle turns indicate 200 μm while scale bars of **(D,G,H,J,L)** magnified perilymphatic spaces represent 20 μm.

the spiral ganglion, in the spiral ligament and in stria vascularis (**Figure 1A**; **Figures S1A-C**).

During the acute phase of the infection, macrophages infiltrated the perilymphatic spaces in the cochlea adopting round morphology (**Figures 1B–D**). Co-expression of Iba1 with CD68 and expression of CD11b (**Figures S1 D-F, M-O**), were indicative of cell activation.

Moreover, we observed infiltration of numerous granulocytes in the perilymphatic spaces (**Figures 1E–J**). Nissl staining showed that many of the infiltrating cells displayed segmented nuclei, typical of neutrophils (**Figures 1F,G**). 42 h post infection SYTO9 staining revealed the presence of phagocytized *S. pneumoniae* within the infiltrating leukocytes (**Figure 1H**).

Myeloperoxidase and neutrophil elastase staining confirmed presence of neutrophils releasing reticular-shaped neutrophil extracellular traps (NETs) (40) (**Figures 1I,J**). Concomitantly, we observed apoptotic cell death of the infiltrating cells, detected by cleaved caspase 3 (**Figures 1I,J**) and TUNEL staining (**Figures 1K,L**). The latter also revealed extracellular DNA in the perilymphatic spaces, possibly being NET-DNA (41, 42).

When cochlear histology was performed 4 weeks post infection, in 21 % of the cases (4/19), infiltrating granulocytes were replaced by fibrotic occlusions in the scalae vestibuli and tympani (**Figure 1N**, dashed line) ranging from slight occlusion to almost complete occlusion of the perilymphatic space (sc. vestibuli: 18.3 to 100 %, sc. tympani: 5.6 to 72.9 %). A representative image of fibrotic occlusion of the scala vestibuli is shown in **Figure 1N** next to an uninfected animal with clear cochlear ducts in **Figure 1M**. In severe cases the organ of Corti was degenerated and spiral ganglion neurons were lost (**Figure 1N**, arrows).

No inflammatory cells and no occlusions were found the endolymphatic space.

Local Administration of HspB5 to the CSF Space Showed Anti-inflammatory Effects

HspB5 is endogenously expressed in different cell types, including oligodendrocytes of the CNS (21, 23) and lack of this protein results in higher susceptibility to inflammatory damage (21, 25). We first analyzed the endogenous localization of HspB5 in the cochlea of uninfected rats. At 12 days of age, a clear expression of HspB5 was observed in a subset of Sox2+/Sox10+ Schwann cells in the Rosenthals' canal (**Figure 2A**) surrounding the TUJ+ spiral ganglion neurons, and also in some sparse cells in spiral ligament and Reissner's membrane (data not shown). In contrast, we could not detect HspB5 within the sensory epithelium, neither in 12 days old nor at 6 weeks of age (data not shown), while some supporting cells in the organ of Corti displayed positivity in very young postnatal animals at p2 (**Figure 2B**).

We then tested the effects of HspB5 administration on the inflammatory process caused by pneumococcal meningitis. In order to obtain high local concentrations of HspB5 in the CSF and perilymphatic spaces during the acute phase of inflammation, the recombinant protein was delivered directly to the cisterna magna immediately prior to the infection and subsequently at 18 h post infection (**Figure 3A**). The control group received an equivalent amount of bovine serum albumin (BSA). Intracisternal infection was performed by injection of 10 μl saline containing $8.20 \pm 1.8 \times 10^5$ cfu/ml living *S. pneumoniae*. This concentration of the inoculum was previously shown to cause moderate-to-severe damage to hair cells and spiral ganglion neurons (8).

The infection resulted in similar CSF bacterial concentration in the control ($8.98 \pm 6.38 \times 10^7$ cfu/ml, $n = 10$ animals) and the HspB5-treated group ($8.16 \pm 5.88 \times 10^7$ cfu/ml, $n = 8$) 18 h post infection (**Figure 3B**). Infected animals showed reduced weight gain (**Figure 3C**) and worsening of the clinical score compared to mock-infected animals ($p < 0.0001$) (**Figure 3D**). No significant difference in bacterial titer, weight change and clinical score was seen between the two treatment groups (BSA vs. HspB5). After repeated treatment with ceftriaxone, animals recovered from the infection. Clinical conditions improved and weight gain was normalized.

The CSF, collected at different time points after infection (18 hpi, 24 hpi, and 42 hpi), was analyzed for inflammatory cytokine secretion. Bacterial infection induced a rapid increase in cytokine production. HspB5-treated animals had significantly reduced levels of TNF-α ($p < 0.05$), IL-6 ($p < 0.05$), IL-10 ($p < 0.01$), and IFN-γ ($p < 0.05$) at the peak of the inflammatory process (24 hpi, **Figure 3E**).

When we assessed the presence of NETs at 42 hpi, we observed up to 90 % of the area of scala tympani occluded by NETs (**Figure 3F**) but we could not detect any differences as a result of HspB5 treatment (**Figure 3G**).

Intracisternal Administration of HspB5 Reduced Hearing Loss

Hearing tests were performed at 1 and 4 weeks post infection by assessing auditory brainstem responses (ABR) (**Figure 4A**). Representative click-ABR recordings are shown in **Figure 4B**. Rats were presented to a broadband click stimulus and pure tones at 4, 8, 16, and 32 kHz. Hearing thresholds for clicks were significantly elevated at 1 week post infection and persisted until

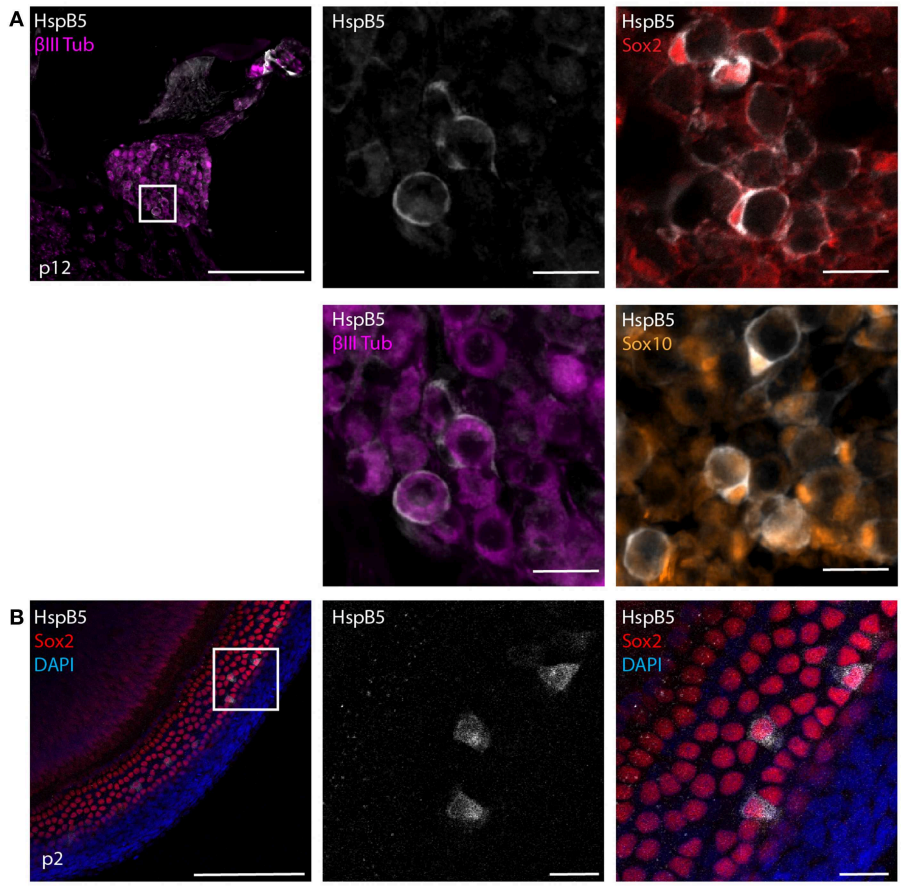

FIGURE 2 | Endogenous expression of HspB5. **(A)** Immunostaining of mid-modiolar cryosection stained for HspB5 (white) and the Schwann cells markers Sox2+ (red) and Sox10+ (orange) or the neuronal marker βIII Tubulin (magenta) in p12 rats. **(B)** Immunostaining of organ of Corti whole mounts of p2 animals for HspB5 (white) and the supporting cells marker Sox2 (red). Scale bars in overview images indicate 200 μm while scale bars of magnified areas represent 20 μm.

4 weeks post infection compared to the mock-infected controls ($p < 0.0001$) (**Figure 4C**).

Intracisternal HspB5-therapy significantly improved hearing thresholds. We saw a trend for improved hearing thresholds of broad band clicks compared to the untreated group already 1 week post infection (61.25 dB ± 18.63 vs. 73.5 dB ± 20.2, $p = 0.053$, unpaired *t*-test between the two infected groups, $n = 10$ animals per group; $p = 0.0978$ one-way ANOVA with Tukey's multiple comparison test, when including the control group.) and the difference was statistically significant at 4 weeks post infection (61.25 dB ± 61.25 vs. 76.5 dB ± 21.95, $p = 0.0230$, unpaired *t*-test, $n = 10$ animals per group; $p = 0.0406$, one-way ANOVA with Tukey's multiple comparison test) (**Figure 4C**). Pure tones ABR thresholds were lower at all frequencies tested in the HspB5-treated group, showing statistically significant differences at 1 week post infection (two-way ANOVA, $p = 0.0409$) (**Figure 4D**), while did not reach statistical significance at 4 weeks (**Figure 4E**).

Local HspB5 Delivery Protects Against Meningitis-Induced Sensory Cell Loss

Hair cell quantification was then performed on whole mount preparation of the organ of Corti at 4 weeks after infection (**Figure 5A**). We observed a moderate inner hair cell (IHC) loss, which was most pronounced in the hook, but no differences between the treatment groups were observed (**Figure 5B**). Outer hair cells (OHC) were instead strongly affected, especially in the basal and mid-basal part of the organ of Corti ($p<0.05$, t-test). A higher number of outer hair cells was still intact 4 weeks after infection in the HspB5-treated group (two-way ANOVA, $p = 0.0015$). Interestingly, we observed statistically significant differences in the basal and mid-basal portions (**Figure 5C**).

To further confirm the protective effect of HspB5 on the survival of hair cells to pathogen-induced damage, we performed *in vitro* experiments using organotypic cultures of the organ of Corti. Exposure of the organ of Corti explants to bacteria for 2 h caused OHC loss, more pronounced toward the base (**Figures 5D,F**). No significant changes were observed for IHC (**Figure 5E**). Outer hair cells were significantly lost at the base and middle turns compared to the unexposed samples (base: 12.94 OHC ± 10.83 vs. 37.31 OHC ± 5.23, middle: 24.08 OHC ± 7.95 vs. 38.39 OHC ± 3.375, $p<0.05$). When HspB5 (50 μg/ml) was added to the culture medium during exposure to the bacteria and for the following 4 days, OHCs loss in the base and middle portion was no

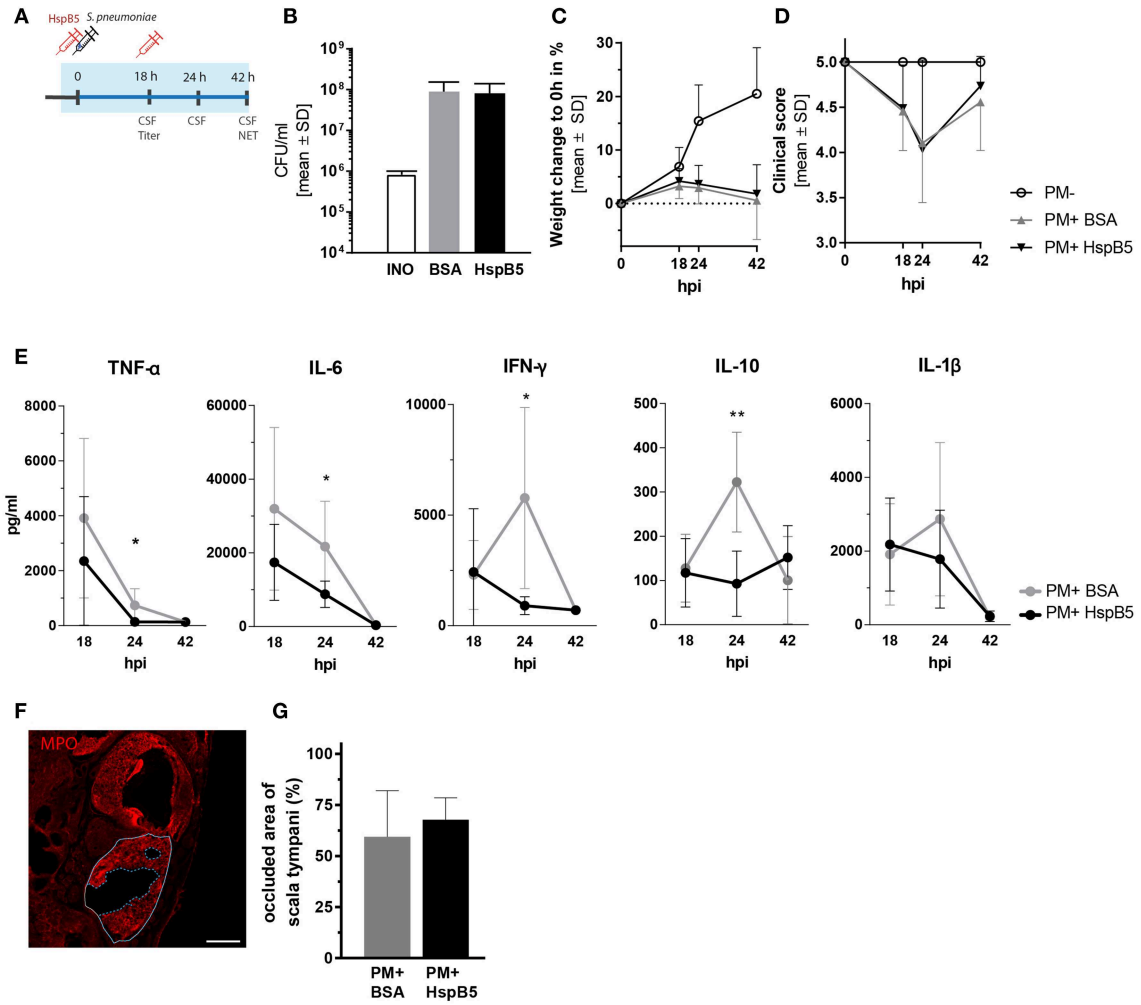

FIGURE 3 | Intracisternal administration of HspB5 and effects during the acute phase of pneumococcal meningitis. **(A)** Schematic representation of the experimental setup to study the acute phase outcomes. Intracisternal delivery of HspB5 (red syringe) is performed immediately prior to the infection and at 18hpi. Antibiotic treatment is initiated at 18 hpi and administered i.p. The acute phase (0–42 h) is indicated in blue. **(B)** Bacterial titer at 18 hpi indicates colony forming units in 1 ml of CSF **(C)** Relative weight change during acute infection showed a slight increase within the first 18 hpi and weight loss with the onset of clinical symptoms and antibiotic treatment. **(D)** Clinical scores deteriorated during the first 24 h after infection before sick animals recovered. **(E)** Quantification of inflammatory cytokines in the CSF at 18hpi, 24hpi, and 42hpi of untreated (gray, $n = 9$ animal) and treated animals (black, $n = 10$ animals) Statistical differences were assessed using unpaired *t*-test with Welch correction $^{*}p < 0.05$; $^{**}p < 0.01$. **(F)** Representative immunofluorescence of NET occlusion (basal turn) in infected animals with delineated areas of the scala tympani (white line) and NET occlusion (blue dashed line). Scale bar = 200 μm. **(G)** The ratio between the NET-occupied area and the area of scala tympani 42 h post infection, is plotted for untreated (gray, $n = 7$ animals) and HspB5-treated (black, $n = 4$ animals).

longer statistically significantly different from the untreated explants (**Figure 5F**).

Given the previously reported neuroprotective effect of HspB5 as well as its endogenous localization in the Rosenthals' canal, we also analyzed the survival of spiral ganglion neurons (**Figures 5G,H**). We focused specifically in the basal portion of the cochlea as we had previously reported a more significant damage (8). The large majority of animals tested in these experiments showed however only minimal loss of spiral ganglion neurons after meningitis in this region (**Figure 5I**), whereas middle and apical region appeared undamaged. This did not allow to assess the putative protective effects of HspB5 effectively.

Systemic Administration of HspB5 Had No Effect on Pro-inflammatory Cytokine Profile, Hair Cell Survival, and Hearing Threshold

We additionally assessed whether HspB5 exerted effects when administered systemically. Animals received either saline or HspB5 intraperitoneally. Moreover, we used a paradigm more close to clinical practice, where adjuvant treatment is initiated concomitant to antibiotic therapy starting 18 hpi, when first clinical signs appeared. Further HspB5 i.p. doses were applied at day 3 and 5, as previously described in **Figure 4A**. Animals were sacrificed either during the acute phase of the disease

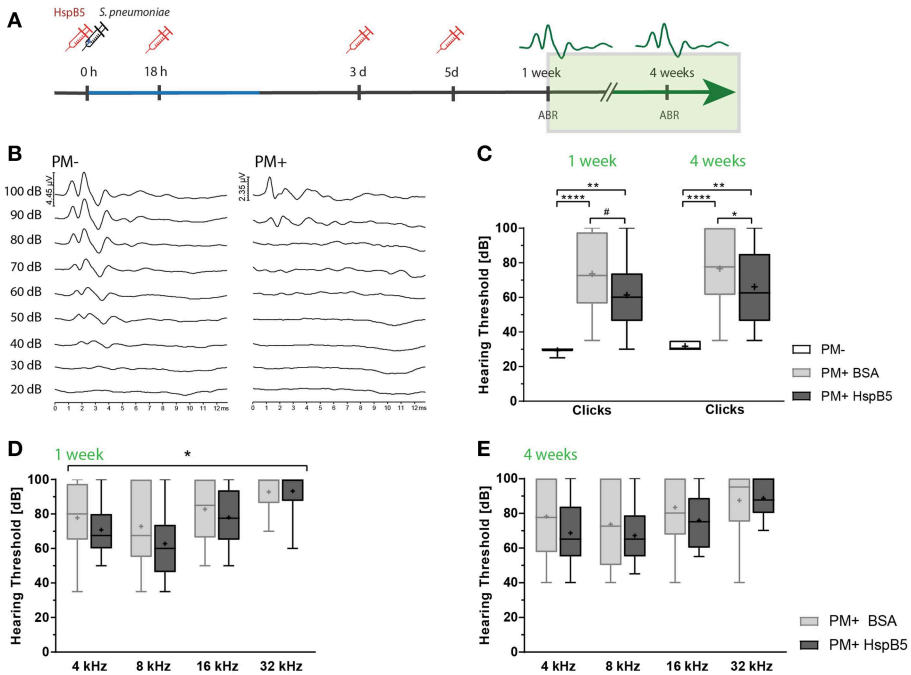

FIGURE 4 | Intracisternal administration of HspB5 results in improved hearing thresholds. **(A)** Schematic representation of the experimental setup to study late phase outcomes. Intracisternal delivery of HspB5 (red syringe) is performed immediately prior to the infection and at 18hpi, 3 days, and 5 days post infection. **(B)** Representative example of hearing thresholds of a control animal (PM-: 30 dB, left) and an infected animal (PM+: 90 dB, right). **(C)** ABR recording using broad band click stimuli 1 and 4 weeks post infection in uninfected ($n = 6$ ears of 3 animals) and infected animals [untreated: ($n = 20$ ears/10 animals) and HspB5 treated: ($n = 20$ ears/10 animals)]. **(D)** Pure tone ABR thresholds 1 and **(E)** 4 week post infection for untreated and HspB5 treated animals ($n = 20$ ears/10animals per group). Box and whisker plot quartiles from min-max. Statistical differences were assessed by one-way ANOVA with Tukey's multiple comparison test. $^{\#}p$ value for unpaired t-tests $p = 0.053$ (in **C**) and two-way ANOVA (in **D,E**). $^{*}p < 0.05$; $^{**}p < 0.01$ $^{****}p < 0.0001$.

(42 hpi), or 1 month after infection, after assessment of hearing thresholds.

In this paradigm, we did not see a difference between the treated and untreated animals, when animals were injected i.p., neither in pro-inflammatory cytokine secretion (**Figure 6A**), nor for hearing thresholds (**Figures 6B,C**). NET formation, spiral ganglion neuron density, hair cell number and presynaptic ribbons counts were also not significantly influenced by the treatment at 1 month after infection (data not shown).

We reasoned HspB5 may have reached the CSF and cochlear fluid too late compared to the inflammatory mediators using this treatment protocol, explaining its inefficacy. Therefore, we assessed HspB5- i.p. treatment in an additional cohort of animals, where administration started immediately prior to bacterial infection, and further delivered at 18 hpi, 3 dpi, and 5 dpi, as done for the i.c. administration. Also in this case however, we did not detect a difference in cytokine production (**Figure 6D**). A trend to improved ABR hearing thresholds was observed for broad-band clicks in the treated group at 4 weeks post infection, which however did not reach statistical significance (**Figure 6E**).

These results suggest that systemic delivery may not allow for reaching a sufficient concentration of HspB5 in the CSF and perilymphatic space to exert a protective effect in the acute phase of the disease.

DISCUSSION

The previously reported anti-inflammatory, anti-apoptotic and neuroprotective effect of the small heat shock protein HspB5 (21, 30, 36, 43, 44) prompted us to examine whether HspB5 could be used as a therapeutic agent to counteract bacterial meningitis-induced damage to the inner ear.

Our results demonstrate that intracisternal HspB5 therapy results in an increased outer hair cell survival and improved hearing thresholds after pneumococcal infection. This is the first report highlighting the use of HspB5 as a potential treatment option for bacterial meningitis-induced hearing loss.

We tested two routes of administration of the recombinant protein: local and systemic. Delivery to the inner ear via the round window niche was not feasible because animals suffering from pneumococcal meningitis are in too poor health conditions to support prolonged surgical procedures under anesthesia during the acute phase of the disease. We therefore decided to deliver the recombinant protein through i.c. injection, directly into the CSF, a procedure that does not require anesthesia and is performed very rapidly (less than a minute) in the present model. Intracisternal injection allows for direct access to the perilymphatic fluids, using similar routes as used by bacteria, though the cochlear aqueduct. While i.c. delivery allows direct access to the inner ear, the anti-inflammatory activity could also

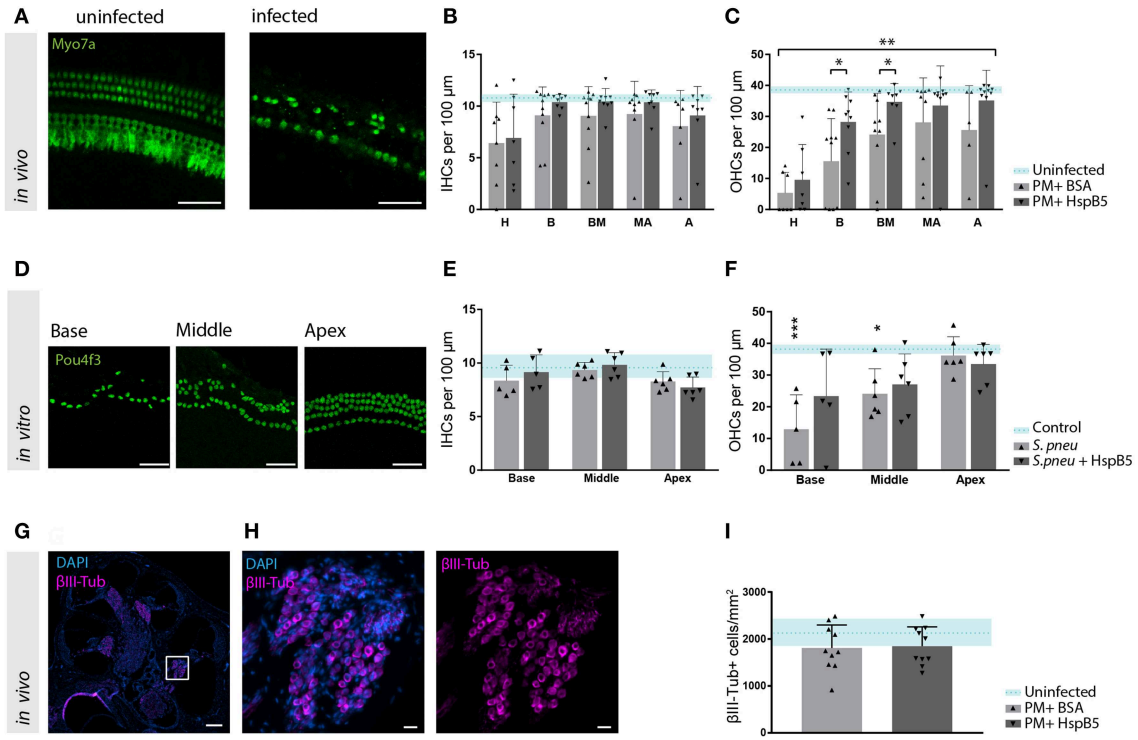

FIGURE 5 | HspB5 protects against *S. pneumonia* -induced sensory hair cell loss. **(A)** Representative example of a whole mount preparation of the organ of Corti stained with hair cells specific Myo7a (green), scale bar= 50 µm **(B)** Quantification of inner hair cells and **(C)** outer hair cells at 4 weeks post infection, uninfected animals ($n = 3$) indicated in blue as mean (blue dashed line) and standard deviations (blue shade), hair cell count of infected animals ($n = 10$/group) represented in bar graphs. 7–10 whole mount preparations were quantified per cochlea; H, hook; B, base; BM, base-middle; MA, middle-apex; A, apex. **(D)** Representative confocal images of the organ of Corti immunostained for hair cells (Pou4f3, green) 4 days after exposure to *S. pneumonia.* Basal, middle and apical turns are shown, scale bar= 50 µm **(E)** quantification of inner and **(F)** outer hair cells *in vitro* without bacteria $n = 4$ (light blue); untreated (gray) $n = 6$ and HspB5-treated (black) $n = 6$. **(G)** Mid-modiolar cross section of a control rat cochlea immunostained for the neuronal marker βIII-Tubulin (magenta) and cell nuclei (DAPI, blue), scale bar= 200 µm. **(H)** The Rosenthal's canal in the basal turn is shown at higher magnification, scale bar= 20 µm **(I)** Neuronal density quantification in the basal turn in uninfected ($n = 3$), infected untreated or HspB5-tretaed ($n = 10$ animals per group). Means with SD are indicted in the bar graphs. Dashed line with shade represents average count of uninfected cochlea with SD. A two-way ANOVA was used for determining interaction between variables and an unpaired *t*-test with Welch's correction was used for single comparison between untreated and HspB5 treated (in **B** and **C**) $^{*}p < 0.05$; $^{**}p < 0.01$. A one-way ANOVA with Tukey's multiple comparison test was used to evaluate whether the means of the population s differ in **(E,F)** $^{*}p < 0.05$; $^{***}p < 0.001$.

be the result of a modulation of the immune response exerted in the meningeal spaces and in the central nervous system, for example by binding to and modulating the activity of microglial cells in the brain parenchyma, as shown in other models (31). This would result consequently in less inflammatory products reaching the inner ear. Alternatively, or in combination with the above, local effects could be exerted through interaction with microglia and leukocytes in the cochlea and other inner ear compartments, or directly with cells within the sensory epithelium. This is also supported by the experiments conducted *in vitro*, where we have been able to detect hair cell protection against *S. pneumoniae*-induced damage, when applying HspB5 to the culture medium.

Local administration of HspB5 reduced inflammatory cytokine production, namely TNF-α, IL-6, and INF-γ, which are well-known to induce secondary inflammatory responses, including leukocyte infiltration and scar formation (45). It has already been reported that reduced inflammatory cytokine production in this model of pneumococcal meningitis is associated with reduced neuronal injury (34, 46, 47). Furthermore, inflammatory mediators are directly implicated in cochlear damage. For instance, TNF-α has been shown to trigger caspase expression or activation, leading to apoptosis (48). *In vitro*, excessive level of TNF-α increased the expression of apoptosis-related genes and induced cochlear cell death of outer hair cells in OC explant (49, 50). *In vivo*, anti-inflammatory strategies using for example TNFα-antibodies (51) or reducing the amount of TNF-α in the CSF via inhibition of the TNF-α-converting enzyme (TACE) with doxycycline (52), improved hearing function and reduced cochlear injury in the context of meningitis (51). In the present study, we detected reduced concentrations of TNF-α during bacterial meningitis in animals treated with HspB5 and observed attenuated hearing loss with better hair cell survival after recovery from infection in the these animals compared to the untreated cohort.

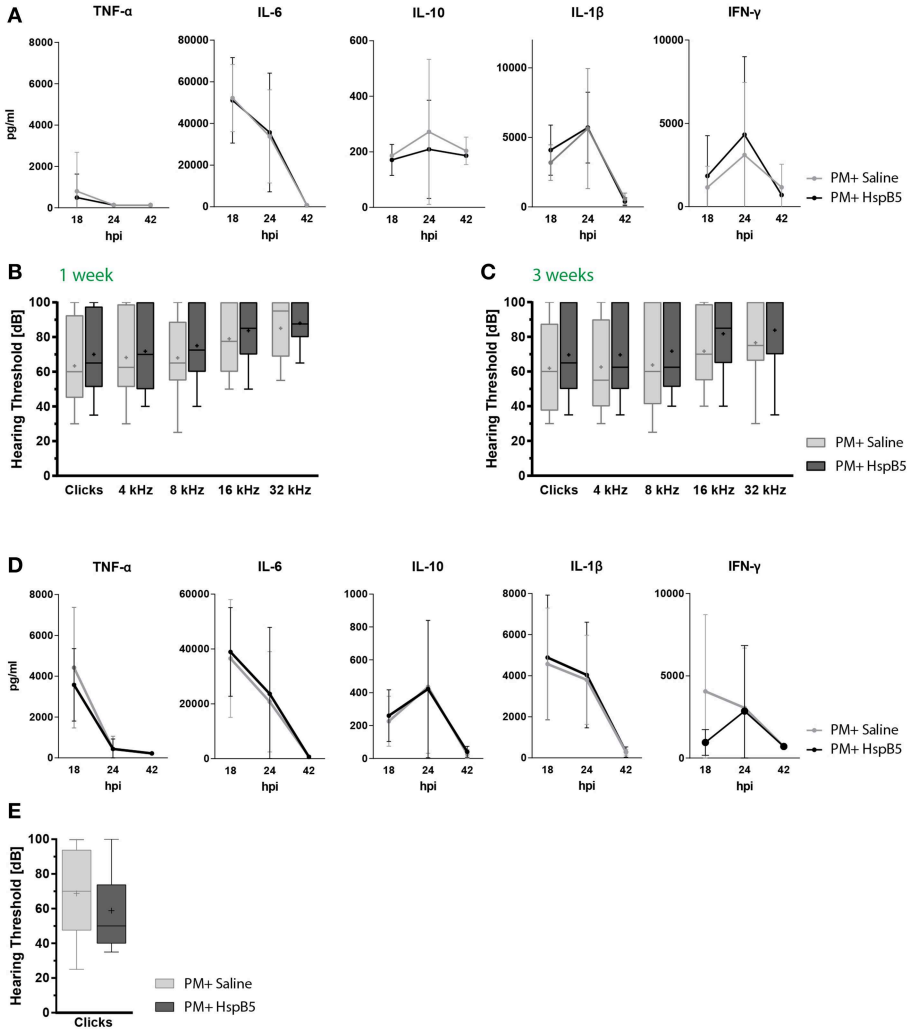

FIGURE 6 | Intraperitoneal administration of HspB5 does not change inflammatory cytokine profiles nor hearing thresholds. **(A)** Animals received a single HspB5 i.p. injection at 18hpi. Quantification of inflammatory cytokines in the CSF at 18, 24, and 42 h post infection; untreated ($n = 9$, gray) and HspB5-treated ($n = 10$, black) **(B)** Animals received a HspB5 i.p. injections at 18hpi, 3 days, and 5 days post infection. ABR hearing thresholds for clicks and pure tones 1 week and **(C)** 3 weeks post infection; untreated ($n = 26$ ears/13 animals, gray) and HspB5-treated ($n = 26$ ears/13 animals, black). **(D)** Animals received i.p. injections 2 h prior to infection, as well as at 18 hpi. Quantification of inflammatory cytokines in the CSF at 18, 24, and 42 h post infection; untreated ($n = 11$, gray) and HspB5-treated ($n = 10$, black) **(E)** Animals received i.p. injections 2 h prior to infection, as well as at 18 hpi, 3 days, and 5 days post infection. ABR hearing thresholds for clicks 4 weeks post infection; ($n = 28$ ears/14 animals, gray) and HspB5-treated ($n = 24$ ears/12 animals black). Box and whisker plot quartiles from min-max. Graphs show mean values with standard deviation. Statistical differences were assessed by single comparison using unpaired *t*-test and two-way ANOVA.

Interleukin-10 induction instead has been previously observed exclusively in severely infected animals (8), suggesting a secondary anti-inflammatory response. HspB5 dampening of IL-10 levels may correlate with an overall reduced inflammation.

Neutrophil activity, assessed here by NET formation in the perilymphatic space was however not sensitive to HspB5. The role of NETs, as well as all other inflammatory processes required for bacterial clearance and resolution of the infection, are nevertheless dual and while implicated in the development of the pathology, they are needed to protect against infections (53, 54). We have also attempted to quantify the numbers of macrophages infiltrating in the cochlea in response to meningitis and in the two treatment groups. We specifically focused on Iba1+ cells in the Rosenthal's canal. While we did not observe differences between the HspB5 and the saline-treated groups (data not shown), the branched morphology of the cells does not allow for a precise assessment using tissue sections. Alternative imaging modalities of entire cochlea whole mounts (7) would need to be optimized in order to adequately address this question.

In PM, where the damage is induced by an acute inflammatory reaction, limited to approximately 40 h, the time window for action of an effective anti-inflammatory therapy is limited. Reaching sufficiently high local concentration of the compound in a timely adequate manner is therefore technically challenging.

We tried to control for this aspect by delivering HspB5 therapy at the time of infection and further applied the at 18 h post infection. This should allow for a high local concentration at the time point when the cytokine burst occurs. While the i.c. delivery significantly reduced inflammatory cytokine production in this paradigm, i.p. injection using the same schedule was ineffective.

It has been reported that HspB5 is able to cross the blood brain barrier especially under inflammatory conditions (36, 55). Since pneumococcal meningitis causes increased permeability of the blood brain barrier, and the overshooting cochlear inflammation is accompanied by blood labyrinth barrier disruption, proven by increased Evans Blue extravasation (12, 56), we assumed HspB5 would cross both barriers also during pneumococcal meningitis. However, we did not observe any changes in the inflammatory reaction, cytokine production or sensorineural hearing loss phenotypes, when HspB5 was delivered systemically. The results of the systemic delivery paradigm therefore bring about the question of whether HspB5 did not reach, or did not reach in sufficient amount, or at the right time point, the inner ear and CSF since our effort to detect the i.p. delivered compound by classical immunostaining of the cochleae was unsuccessful.

In clinical practice, HspB5 could be applied directly in the CSF space, in a timely manner. Alternatively, intratympanic injection may be rather feasible in a human patient compared to infant rats. Testing the compounds in different models, involving less severe but chronic inflammation such chronic exposure to moderate levels of noise (57), may be alternatively used to better reveal the role of HspB5 in oto-protection.

In conclusion, our data provides evidence that HspB5, when administrated adequately, attenuates the inflammatory response and results in better outer hair cell survival with improved hearing thresholds. Since HspB5 was only beneficial when given directly to the CSF compartment at the time of infection, but not when delayed longer and delivered systemically, the early changes in cytokine expression observed upon HspB5 treatment may be crucial to conferring protection.

DATA AVAILABILITY

All datasets generated for this study are included in the manuscript and/or the **Supplementary Files**.

ETHICS STATEMENT

All animal experiments were approved by the experimentation committee of the canton Bern, Switzerland (license to SSL BE124/16 and BE1/18) and followed the Swiss national guidelines for the performance of animal experiments.

AUTHOR CONTRIBUTIONS

SE, MR, DG, SL, RR, and PS conceived and designed the study. SE, GF, MB, MR, and MP performed experiments. SE, GF, MR, DG, and SL analyzed the data. SE, MR, DG, JvN, and SL contributed to writing of the manuscript. All authors read and approved the final manuscript.

FUNDING

This work was supported by a Eurostars project (HEARit, Project ID: E!10491) through Innosuisse (Swiss Innovation Agency), and by the Swiss National Science Foundation (grant 162583).

ACKNOWLEDGMENTS

We acknowledge Delta Crystallon BV for providing human recombinant HspB5. We thank Franziska Simon and Robert Lukesch for excellent technical support. We are grateful to Alessio Balmelli and Nashwa Mustafa for help with the histological assessment. We thank the members of the Cluster of Regenerative Neurosciences (Department of BioMedical Research, University of Bern, Switzerland) and the ESCMID Study Group for Infectious Diseases of the Brain (ESGIB) for helpful discussion and suggestions. We thank Prof. Lawrence Steinman (Stanford University) and Shalina S. Ousman (University of Calgary) for providing Cryab KO tissue for antibody validation. We thank Dr. Amiq Gazdhar, Dr. Kleanthis Fytianos, Dr. José Galvan and Dr. Fauzy Nasher from the University of Bern for help with stainings.

SUPPLEMENTARY MATERIAL

The Supplementary Material for this article can be found online at: https://www.frontiersin.org/articles/10.3389/fneur.2019.00570/full#supplementary-material

Figure S1 | Macrophages in the cochlea. **(A–C)** Mid-modialar section of uninfected rat cochlea immunostained for CD68 (magenta) and iba1 (yellow), **(D–F)** Mid-modiloar sections of rat cochlea 42 hours post infection with *S. pneumoniae* immunostained for CD68 and iba1, **(G–I)** uninfected cochleae stained for CD68 (magenta) and CD206 (gray), **(J–L)** cochleae 42 hours post infection stained for CD68 and CD206, scale bars = 20 μm. **(M)** Representative example of CD11b (yellow) immunostaining and DAPI (blue) in uninfected animals and **(N)** 42hpi, scale bars = 200 μm **(O)** detail of the cells in the perilymphatic space, scale bar = 20 μm.

REFERENCES

1. van de Beek D, de Gans J, Spanjaard L, Weisfelt M, Reitsma JB, Vermeulen M. Clinical features and prognostic factors in adults with bacterial meningitis. *N Engl J Med.* (2004) 351:1849–59. doi: 10.1056/NEJMoa040845
2. Østergaard C, Konradsen HB, Samuelsson S. Clinical presentation and prognostic factors of Streptococcus pneumoniae meningitis according to the focus of infection. *BMC Infect Dis.* (2005) 5:93. doi: 10.1186/1471-2334-5-93
3. Hirose K, Rutherford MA, Warchol ME. Two cell populations participate in clearance of damaged hair cells from the sensory epithelia of the inner ear. *Hear Res.* (2017) 352:70–81. doi: 10.1016/J.HEARES.2017.04.006
4. Kalinec GM, Lomberk G, Urrutia RA, Kalinec F. Resolution of cochlear inflammation: novel target for preventing or ameliorating drug-, noise- and age-related hearing loss. *Front Cell Neurosci.* (2017) 11:192. doi: 10.3389/fncel.2017.00192

5. Liu W, Molnar M, Garnham C, Benav H, Rask-Andersen H. Macrophages in the human cochlea: saviors or predators—a study using super-resolution immunohistochemistry. *Front Immunol.* (2018) 9:223. doi: 10.3389/fimmu.2018.00223
6. Møller MN, Brandt C, Østergaard C, Caye-Thomasen P. Bacterial invasion of the inner ear in association with *Pneumococcal meningitis*. *Otol Neurotol.* (2014) 35:e178–e186. doi: 10.1097/MAO.0000000000000305
7. Perin P, Voigt FF, Bethge P, Helmchen F, Pizzala R. iDISCO+ for the Study of neuroimmune architecture of the rat auditory brainstem. *Front Neuroanat.* (2019) 13:15. doi: 10.3389/fnana.2019.00015
8. Perny M, Roccio M, Grandgirard D, Solyga M, Senn P, Leib SL. The severity of infection determines the localization of damage and extent of sensorineural hearing loss in experimental pneumococcal meningitis. *J Neurosci.* (2016) 36:7740–9. doi: 10.1523/JNEUROSCI.0554-16.2016
9. Täuber MG, Moser B. State-of-the-art clinical article cytokines and chemokines in meningeal inflammation : biology and clinical implications. *Clin Infect Dis.* (1999) 28:1–11.
10. Kesser BW, Hashisaki GT, Spindel JH, Ruth RA, Scheld WM. Time course of hearing loss in an animal model of pneumococcal meningitis. *Otolaryngol Neck Surg.* (1999) 120:628–37. doi: 10.1053/hn.1999.v120.a92772
11. Brandt CT, Cayé-Thomasen, P, Lund SP, Worsøe L, Østergaard C, Frimodt-Møller N, et al. Hearing loss and cochlear damage in experimental pneumococcal meningitis , with special reference to the role of neutrophil granulocytes. *Neurobiol Dis.* (2006) 23:300–311. doi: 10.1016/j.nbd.2006.03.006
12. Klein M, Koedel U, Pfister H-W, Kastenbauer S. Meningitis-associated hearing loss: protection by adjunctive antioxidant therapy. *Ann Neurol.* (2003) 54:451–8. doi: 10.1002/ana.10684
13. Coimbra RS, Loquet G, Leib SL. Limited efficacy of adjuvant therapy with dexamethasone in preventing hearing loss due to experimental pneumococcal meningitis in the infant rat. *Pediatr Res.* (2007) 62:291–4. doi: 10.1203/PDR.0b013e318123fb7c
14. Grandgirard D, Burri M, Agyeman P, Leib SL. Adjunctive daptomycin attenuates brain damage and hearing loss more efficiently than rifampin in infant rat pneumococcal. *Antimicrob Agents Chemother.* (2012) 56:4289–95. doi: 10.1128/AAC.00674-12
15. Rivolta MN. New strategies for the restoration of hearing loss: challenges and opportunities. *Br Med Bull.* (2013) 105:69–84. doi: 10.1093/bmb/lds035
16. Dubey A, Prajapati KS, Swamy M, Pachauri V. Heat shock proteins: a therapeutic target worth to consider. *Vet world.* (2015) 8:46–51. doi: 10.14202/vetworld.2015.46-51
17. Cunningham LL, Brandon CS. Heat shock inhibits both aminoglycoside- and cisplatin-induced sensory hair cell death. *J Assoc Res Otolaryngol.* (2006) 7:299–307. doi: 10.1007/s10162-006-0043-x
18. Martindale JL, Holbrook NJ. Cellular response to oxidative stress: Signaling for suicide and survival. *J Cell Physiol.* (2002) 192:1–15. doi: 10.1002/jcp.10119
19. May LA, Kramarenko II, Brandon CS, Voelkel-Johnson C, Roy S, Truong K, et al. Inner ear supporting cells protect hair cells by secreting HSP70. *J Clin Invest.* (2013) 123:3577–87. doi: 10.1172/JCI68480
20. Baker TG, Roy S, Brandon CS, Kramarenko IK, Francis SP, Taleb M, et al. Heat shock protein-mediated protection against cisplatin-induced hair cell death. *J Assoc Res Otolaryngol.* (2015) 16:67–80. doi: 10.1007/s10162-014-0491-7
21. Ousman SS, Tomooka BH, van Noort JM, Wawrousek EF, O'Conner K, Hafler DA, et al. Protective and therapeutic role for αB-crystallin in autoimmune demyelination. *Nature.* (2007) 448:474–9. doi: 10.1038/nature05935
22. Van Noort JM, Bsibsi M, Nacken PJ, Verbeek R, Venneker EHG. Therapeutic intervention in multiple sclerosis with alpha B-crystallin: A randomized controlled phase IIa trial. *PLoS ONE.* (2015) 10:1–19. doi: 10.1371/journal.pone.0143366
23. Arrigo A-P, Simon S, Gibert B, Kretz-Remy C, Nivon M, Czekalla A, et al. Hsp27 (HspB1) and αB-crystallin (HspB5) as therapeutic targets. *FEBS Lett.* (2007) 581:3665–74. doi: 10.1016/j.febslet.2007.04.033
24. Kurnellas MP, Brownell SE, Su L, Malkovskiy AV, Rajadas J, Dolganov G, et al. Chaperone activity of small heat shock proteins underlies therapeutic efficacy in experimental autoimmune encephalomyelitis. *J Biol Chem.* (2012) 287:36423–34. doi: 10.1074/jbc.M112.371229
25. Arac A, Brownell SE, Rothbard JB, Chen C, Ko RM, Pereira MP, et al. Systemic augmentation of αB-crystallin provides therapeutic benefit twelve hours post-stroke onset via immune modulation. *Proc Natl Acad Sci USA.* (2011) 108:13287–92. doi: 10.1073/pnas.1107368108
26. Hagemann TL, Boelens WC, Wawrousek EF, Messing A. Suppression of GFAP toxicity by αB-crystallin in mouse models of Alexander disease. *Hum Mol Genet.* (2009) 18:1190–9. doi: 10.1093/hmg/ddp013
27. Bsibsi M, Peferoen LAN, Holtman IR, Nacken PJ, Gerritsen WH, Witte ME, et al. Demyelination during multiple sclerosis is associated with combined activation of microglia/macrophages by IFN-γ and alpha B-crystallin. *Acta Neuropathol.* (2014) 128:215–29. doi: 10.1007/s00401-014-1317-8
28. Kamradt MC, Chen F, Cryns VL. The small heat shock protein alpha B-crystallin negatively regulates cytochrome c- and caspase-8-dependent activation of caspase-3 by inhibiting its autoproteolytic maturation. *J Biol Chem.* (2001) 276:16059–63. doi: 10.1074/jbc.C100107200
29. Mehlen P, Kretz-Remy C, Préville X, Arrigo AP. Human hsp27, Drosophila hsp27 and human alphaB-crystallin expression-mediated increase in glutathione is essential for the protective activity of these proteins against TNFalpha-induced cell death. *EMBO J.* (1996) 15:2695–706.
30. Masilamoni JG, Jesudason EP, Baben B, Jebaraj CE, Dhandayuthapani S, Jayakumar R. Molecular chaperone α-crystallin prevents detrimental effects of neuroinflammation. *Biochim Biophys Acta - Mol Basis Dis.* (2006) 1762:284–93. doi: 10.1016/j.bbadis.2005.11.007
31. Bsibsi M, Holtman IR, Gerritsen WH, Eggen BJL, Boddeke E, Valk P, et al. Alpha-B-crystallin induces an immune-regulatory and antiviral microglial response in preactive multiple sclerosis lesions. *J Neuropathol Exp Neurol.* (2013) 72:970–9. doi: 10.1097/NEN.0b013e3182a776bf
32. Noort JM, Van Bsibsi M, Nacken PJ, Gerritsen WH, Amor S, Holtman IR, et al. Biomaterials activation of an immune-regulatory macrophage response and inhibition of lung in fl ammation in a mouse model of COPD using heat-shock protein alpha B-crystallin-loaded PLGA microparticles. *Biomaterials.* (2013) 34:831–40. doi: 10.1016/j.biomaterials.2012.10.028
33. Bakthisaran R, Tangirala R, Rao CM. Biochimica et Biophysica Acta Small heat shock proteins : role in cellular functions and pathology. *BBA Proteins Proteom.* (2015) 1854:291–319. doi: 10.1016/j.bbapap.2014.12.019
34. Muri L, Grandgirard D, Buri M, Perny M, Leib SL. Combined effect of non-bacteriolytic antibiotic and inhibition of matrix metalloproteinases prevents brain injury and preserves learning, memory and hearing function in experimental paediatric pneumococcal meningitis. *J Neuroinflammation.* (2018) 15:233. doi: 10.1186/s12974-018-1272-8
35. Leib SL, Leppert D, Clements J, Täuber MG. Matrix metalloproteinases contribute to brain damage in experimental pneumococcal meningitis. *Infect Immun.* (2000) 68:615–20. doi: 10.1128/IAI.00073-14
36. Klopstein A, Santos-Nogueira E, Francos-Quijorna I, Redensek A, David S, Navarro X, et al.. Beneficial effects of B-crystallin in spinal cord contusion injury. *J Neurosci.* (2012) 32, 14478–88. doi: 10.1523/JNEUROSCI.0923-12.2012
37. Liechti FD, Grandgirard D, Leppert D, Leib SL. Matrix metalloproteinase inhibition lowers mortality and brain injury in experimental pneumococcal meningitis. *Infect Immun.* (2014) 82:1710–8. doi: 10.1128/IAI.00073-14
38. Perny M, Solyga M, Grandgirard D, Roccio M, Leib SL, Senn P. *Streptococcus pneumoniae* -induced ototoxicity in organ of Corti explant cultures. *Hear Res.* (2017) 350:100–9. doi: 10.1016/j.heares.2017.04.012
39. Kazuo O, Grimm CM, Corrales CE, Senn P, Monedero RM, Géléoc GSG, et al. Differential distribution of stem cells in the auditory and vestibular organs of the inner ear. *J Assoc Res Otolaryngol.* (2007) 8:18–31. doi: 10.1007/s10162-006-0058-3
40. Masuda S, Nakazawa D, Shida H, Miyoshi A, Kusunoki Y, Tomaru U, et al. NETosis markers: Quest for specific, objective, and quantitative markers. *Clin Chim Acta.* (2016) 459:89–93. doi: 10.1016/j.cca.2016.05.029
41. Boettcher M, Eschenburg G, Mietzsch S, Jiménez-Alcázar M, Klinke M, Vincent D, et al. Therapeutic targeting of extracellular DNA improves the outcome of intestinal ischemic reperfusion injury in neonatal rats. *Sci Rep.* (2017) 7:15377. doi: 10.1038/s41598-017-15807-6
42. Fuchs TA, Abed U, Goosmann C, Hurwitz R, Schulze I, Wahn V, et al. Novel cell death program leads to neutrophil extracellular traps. *J Cell Biol.* (2007) 176:231–41. doi: 10.1083/jcb.200606027
43. Masilamoni JG, Jesudason EP, Bharathi SN, Jayakumar R. The protective effect of α-crystallin against acute inflammation in mice. *Biochim Biophys Acta - Mol Basis Dis.* (2005a) 1740:411–20. doi: 10.1016/j.bbadis.2004.11.002

44. Masilamoni JG, Vignesh S, Kirubagaran R, Jesudason EP, Jayakumar R. The neuroprotective efficacy of α-crystallin against acute inflammation in mice. *Brain Res Bull.* (2005b) 67:235–41. doi: 10.1016/j.brainresbull.2005.07.002
45. Fujioka M, Okano H, Ogawa K. Inflammatory and immune responses in the cochlea: potential therapeutic targets for sensorineural hearing loss. *Front Pharmacol.* (2014) 5:287. doi: 10.3389/fphar.2014.00287
46. Grandgirard D, Schürch C, Cottagnoud P, Leib SL. Prevention of brain injury by the nonbacteriolytic antibiotic daptomycin in experimental pneumococcal meningitis. *Antimicrob Agents Chemother.* (2007) 51:2173–8. doi: 10.1128/AAC.01014-06
47. Grandgirard D, Oberson K, Bühlmann A, Gäumann R, Leib SL. Attenuation of cerebrospinal fluid inflammation by the nonbacteriolytic antibiotic daptomycin versus that by ceftriaxone in experimental pneumococcal meningitis. *Antimicrob Agents Chemother.* (2010) 54:1323–6. doi: 10.1128/AAC.00812-09
48. Baud V, Karin M. Signal transduction by tumor necrosis factor and its relatives. *Trends Cell Biol.* (2001) 11:372–7. doi: 10.1016/S0962-8924(01)02064-5
49. Haake SM, Dinh CT, Chen S, Eshraghi AA, Van De Water TR. Dexamethasone protects auditory hair cells against TNFα-initiated apoptosis via activation of PI3K/Akt and NFκB signaling. *Hear Res.* (2009) 255:22–32. doi: 10.1016/j.heares.2009.05.003
50. Wu Q, Wang GP, Xie J, Guo JY, Gong SS. Tumor necrosis factor-α-induced ototoxicity in mouse cochlear organotypic culture. *PLoS ONE.* (2015) 10:e0127703. doi: 10.1371/journal.pone.0127703
51. Aminpour S, Tinling SP, Brodie HA. Role of tumor necrosis factor-alpha in sensorineural hearing loss after bacterial meningitis. *Otol Neurotol.* (2005) 26:602–9. doi: 10.1097/00042871-200401001-00548
52. Meli DN, Coimbra RS, Erhart DG, Loquet G, Bellac CL, Täuber MG, et al. Doxycycline reduces mortality and injury to the brain and cochlea in experimental pneumococcal meningitis. *Infect Immun.* (2006) 74:3890–6. doi: 10.1128/IAI.01949-05
53. Delgado-Rizo V, Martínez-Guzmán MA, Iñiguez-Gutierrez L, García-Orozco A, Alvarado-Navarro A, Fafutis-Morris M. Neutrophil extracellular traps and its implications in inflammation: an overview. *Front Immunol.* (2017) 8:81. doi: 10.3389/fimmu.2017.00081
54. Hohlfeld R, Kerschensteiner M, Meinl E. Dual role of inflammation in CNS disease. *Neurology.* (2007) 68:S58–S63. doi: 10.1212/01.wnl.0000275234.43506.9b
55. Holtman IR, Bsibsi M, Gerritsen WH, Boddeke HWGM, Eggen BJL, van der Valk P, et al. Identification of highly connected hub genes in the protective response program of human macrophages and microglia activated by alpha B-crystallin. *Glia.* (2017) 65:460–73. doi: 10.1002/glia.23104
56. Kastenbauer S, Klein M, Koedel U, Pfister HW. Reactive nitrogen species contribute to blood-labyrinth barrier disruption in suppurative labyrinthitis complicating experimental pneumococcal meningitis in the rat. *Brain Res.* (2001) 904:208–17. doi: 10.1016/S0006-8993(01)02164-3
57. Tan WJT, Thorne PR, Vlajkovic SM. Characterisation of cochlear inflammation in mice following acute and chronic noise exposure. *Histochem Cell Biol.* (2016) 146:219–30. doi: 10.1007/s00418-016-1436-5

Conflict of Interest Statement: RR is the CEO of Audion Therapeutics, a biotech-company developing new strategies for hearing loss. JvN worked for Delta Crystallon BV but declares no conflict/financial interests.

The remaining authors declare that the research was conducted in the absence of any commercial or financial relationships that could be construed as a potential conflict of interest.

frontiers in Neuroscience

ORIGINAL RESEARCH
published: 13 June 2019
doi: 10.3389/fnins.2019.00620

Lack of Fractalkine Receptor on Macrophages Impairs Spontaneous Recovery of Ribbon Synapses After Moderate Noise Trauma in C57BL/6 Mice

Tejbeer Kaur[1], Anna C. Clayman[2], Andrew J. Nash[2], Angela D. Schrader[1], Mark E. Warchol[1] and Kevin K. Ohlemiller[1,2]*

[1] Department of Otolaryngology, Washington University School of Medicine, St. Louis, MO, United States, [2] Program in Audiology and Communication Sciences, Washington University School of Medicine, St. Louis, MO, United States

Noise trauma causes loss of synaptic connections between cochlear inner hair cells (IHCs) and the spiral ganglion neurons (SGNs). Such synaptic loss can trigger slow and progressive degeneration of SGNs. Macrophage fractalkine signaling is critical for neuron survival in the injured cochlea, but its role in cochlear synaptopathy is unknown. Fractalkine, a chemokine, is constitutively expressed by SGNs and signals via its receptor CX_3CR1 that is expressed on macrophages. The present study characterized the immune response and examined the function of fractalkine signaling in degeneration and repair of cochlear synapses following noise trauma. Adult mice wild type, heterozygous and knockout for CX_3CR1 on a C57BL/6 background were exposed for 2 h to an octave band noise at 90 dB SPL. Noise exposure caused temporary shifts in hearing thresholds without any evident loss of hair cells in CX_3CR1 heterozygous mice that have intact fractalkine signaling. Enhanced macrophage migration toward the IHC-synaptic region was observed immediately after exposure in all genotypes. Synaptic immunolabeling revealed a rapid loss of ribbon synapses throughout the basal turn of the cochlea of all genotypes. The damaged synapses spontaneously recovered in mice with intact CX_3CR1. However, CX_3CR1 knockout (KO) animals displayed enhanced synaptic degeneration that correlated with attenuated suprathreshold neural responses at higher frequencies. Exposed CX_3CR1 KO mice also exhibited increased loss of IHCs and SGN cell bodies compared to exposed heterozygous mice. These results indicate that macrophages can promote repair of damaged synapses after moderate noise trauma and that repair requires fractalkine signaling.

Keywords: cochlea, ribbon synapses, noise-induced hearing loss, macrophages, fractalkine, C57BL/6 mice

OPEN ACCESS

Edited by:
Isabel Varela-Nieto, Spanish National Research Council (CSIC), Spain

Reviewed by:
Laura Astolfi, University of Padua, Italy
Athanasia Warnecke, Hannover Medical School, Germany

****Correspondence:***
Tejbeer Kaur
tkaur@wustl.edu;
kaurt@ent.wustl.edu

Specialty section:
This article was submitted to Neurodegeneration, a section of the journal Frontiers in Neuroscience

Received: *02 April 2019*
Accepted: *29 May 2019*
Published: *13 June 2019*

Citation:
Kaur T, Clayman AC, Nash AJ, Schrader AD, Warchol ME and Ohlemiller KK (2019) Lack of Fractalkine Receptor on Macrophages Impairs Spontaneous Recovery of Ribbon Synapses After Moderate Noise Trauma in C57BL/6 Mice. Front. Neurosci. 13:620. doi: 10.3389/fnins.2019.00620

INTRODUCTION

The inner hair cell-spiral ganglion neuron (IHC-SGN) synaptic transmission is excitatory and glutamatergic (Puel, 1995). Glutamate is released from IHCs (Ruel et al., 2008; Seal et al., 2008) and both NMDA- and AMPA-type glutamate receptors are present on SGNs (Eybalin, 1993). The IHC-SGN synapses (a.k.a ribbon synapses) are vulnerable to degeneration due to noise trauma

(Puel et al., 1998). Such degeneration has been attributed to glutamate excitotoxicity. Excessive glutamate release due to acoustic trauma can overstimulate postsynaptic glutamate receptors on afferent nerve fiber (ANF) terminals resulting in their swelling, disruption of postsynaptic structures, degeneration of terminals and loss of function. Such synaptic damage can be blocked by glutamate receptor antagonists (Pujol et al., 1985, 1993; Gil-Loyzaga and Pujol, 1990; Puel et al., 1994, 1998; Ruel et al., 2007), while inhibiting glutamate reuptake exacerbates damage (Hakuba et al., 2000). Synaptic degeneration can precede both hair cell loss and threshold elevation and can trigger gradual loss of SGNs (Kujawa and Liberman, 2009). Such primary neural degeneration can affect sound localization and understanding of speech in noisy environments (Liberman, 2017). Moreover, lack of SGNs can limit the effectiveness of primary therapies for hearing loss such as hearing aids and cochlear implants. The denervated IHCs can be partially reinnervated by SGNs after excitotoxic or acoustic trauma; (Pujol et al., 1985; Puel et al., 1995, 1998; Pujol and Puel, 1999; Wang and Green, 2011) however, the underlying mechanisms remain unclear.

Excitotoxicity has been involved in many central nervous system (CNS) acute and chronic neurodegenerative diseases including epilepsy, Alzheimer's, Parkinson's, stroke, and multiple sclerosis. CNS excitotoxicity can activate and recruit microglia (brain macrophages) to the site of injury and these microglia can protect neurons and improve synaptic recovery following excitotoxic damage (Simard and Rivest, 2007; Lauro et al., 2010; Vinet et al., 2012; Eyo et al., 2014; Kato et al., 2016). Microglia-mediated protection against excitotoxicity has been attributed to fractalkine signaling (Meucci et al., 1998; Chapman et al., 2000; Deiva et al., 2004; Limatola et al., 2005; Ragozzino et al., 2006; Lauro et al., 2008, 2015; Cipriani et al., 2011; Catalano et al., 2013; Roseti et al., 2013). Fractalkine signaling represents a unique immune-neuron receptor-ligand pair, where fractalkine (CX_3CL1), a chemokine, is constitutively expressed on neurons in the CNS (Harrison et al., 1998; Kim et al., 2011) and by SGNs of mouse (Kaur et al., 2015) and human (Liu et al., 2018) cochlea. Fractalkine binds to its exclusive G-protein coupled receptor, CX_3CR1, which is expressed by cochlear macrophages, microglia and peripheral leukocytes (Jung et al., 2000; Hirose et al., 2005). Fractalkine occurs in two different forms: as a membrane-bound protein tethered to neuronal membranes by a mucin-like stalk, and as a soluble factor released upon cleavage of its N-terminal chemokine domain by metalloproteases (ADAM10/ADAM17) (Imai et al., 1997; Garton et al., 2001). The soluble chemokine domain of fractalkine, when cleaved, can act as chemoattractant, while the membrane-tethered mucin-stalk of fractalkine has been proposed to act as an adhesion molecule for leukocytes during inflammation (Haskell et al., 1999; Hermand et al., 2008).

We previously demonstrated that macrophages promote the survival of SGNs via fractalkine signaling after loss of their target hair cells (Kaur et al., 2015, 2018). Notably, the role of macrophages and fractalkine signaling in degeneration and repair of synapses are unknown. The present study characterized the immune response and examined the contribution of fractalkine signaling toward degeneration and repair of damaged synapses after synaptopathic noise trauma. We report that moderate noise trauma caused rapid degeneration of ribbon synapses and immediate macrophage migration into the damaged synaptic region without any evident hair cell loss. The damaged synapses undergo post-exposure spontaneous recovery in animals with intact fractalkine signaling. Notably, disruption of fractalkine signaling diminished synaptic recovery and increased neuronal loss after noise trauma. To our knowledge this is the first evidence of a protective role for macrophages and fractalkine signaling in noise-induced cochlear synaptopathy.

MATERIALS AND METHODS

Animals

The study used young adult (6 weeks of age) mice of both sexes on a C57BL/6 (B6) background. To define the role of fractalkine signaling in cochlear excitotoxicity $CX_3CR1^{+/+}$, $CX_3CR1^{GFP/+}$, and $CX_3CR1^{GFP/GFP}$ mice were employed (Jung et al., 2000). The mice were obtained from Dr. Hirose, Washington University in St. Louis, Missouri, originally obtained from Dan Littmann, New York University, New York. A targeted deletion of CX_3CR1 and replacement with the gene encoding green fluorescent protein (GFP) rendered all monocytes and macrophages endogenously fluorescent (Jung et al., 2000), which facilitates their visualization through confocal microscope. Cochlear macrophages express CX_3CR1 (Hirose et al., 2005). The $CX_3CR1^{GFP/+}$ mice (denoted as $CX_3CR1^{+/-}$ in the manuscript) with one copy of CX_3CR1 retain fractalkine signaling, while $CX_3CR1^{GFP/GFP}$ mice (denoted as $CX_3CR1^{-/-}$ in the manuscript) lack fractalkine signaling. Identification of $CX_3CR1^{+/-}$ and $CX_3CR1^{-/-}$ followed previously described methods (Jung et al., 2000). Mice were housed in the animal facility at the Central Institute for the Deaf (Washington University School of Medicine) and were maintained on a 12 h/day-night light cycle with open access to food and water. All experimental protocols were approved by the Animal Studies Committee of the Washington University School of Medicine (St. Louis, MO, United States).

Noise Exposures

The study employed mice on B6 background, which is a strain susceptible to noise- and age-related hearing loss (Henry and Chole, 1980; Hequembourg and Liberman, 2001). To induce cochlear synaptopathy, young mice (6 weeks of age) were exposed for 2 h to an octave 8–16 kHz band noise at 90 dB SPL. Noise exposures were performed in a foam-lined, single-walled soundproof room from Industrial Acoustics Company (IAC). Fully awake and unrestrained animals were placed singly or in pairs in modified cages (food, water, bedding removed) positioned up to two cages at once directly under an exponential horn. All noise was octave band (8–16 kHz), generated digitally using custom Labview routines (running on a PC) in conjunction with a Tucker-Davis Technologies Rz6

signal processor, and a Crown D-150A power amplifier that drove the speaker.

Auditory Brainstem Response

All auditory brainstem responses (ABRs) were performed by a "blinded" observer. ABRs were analyzed both prior to noise exposure (pre-NE, baseline) and after noise exposure (post-NE) at time 0 h (immediately after noise exposure), 2 and 8 weeks (2 months) recovery. Mice were anesthetized via i.p. injections of ketamine (100 mg/kg) and xylazine (20 mg/kg). Subcutaneous electrodes were placed behind the right pinna (inverting) and vertex (active). A ground electrode was placed near the trail of the mouse. Stimuli were 5-ms tone pips (0.5 ms cos2 rise-fall), delivered at 21/s with alternating stimulus polarity. Recorded electrical responses were amplified (∼10,000X), filtered (300 Hz to 3 kHz) and averaged using BioSig software (Tucker-Davis Technologies, Alachua, FL). The sound level was decreased in 5-dB steps from 99 dB SPL down to 15 dB SPL. At each sound level, 1,024 responses were averaged, and response waveforms were discarded as artifacts if the peak-to-peak voltage exceeded 15 μV. Thresholds at 5, 10, 20, 28.3, 40, and 56.6 kHz were determined by a single observer who noted the lowest sound level at which a recognizable waveform could be obtained. Waveforms were confirmed as auditory-evoked responses by their increasing latency and decreasing amplitude as the intensity of the stimulus was lowered. These threshold values (actual or assigned) were then used to calculate the mean ABR thresholds at each stimulus frequency.

Input/Output Function

For neural response, ABR wave 1 component was identified and the peak to trough amplitudes were computed by off-line analysis of stored ABR waveforms. ABR Wave I amplitude-versus-stimulus level (ABR I/O) data were obtained at 10 and 28.3 kHz. To minimize fatigue, repetition numbers varied from 100 at high sound levels to 1,000 near threshold. Stimuli were ordered from high to low sound levels [from max sound pressure available (∼100 dB) to 5 dB below visual detection of Wave I] in 5 dB steps. Wave I amplitude was measured from the estimated baseline prior to the response to the positive peak of Wave I. ABR wave 1 amplitudes were analyzed both prior to noise exposure (pre-NE, baseline), and after noise exposure (post-NE) at time 0 h (immediately after noise exposure), 2 and 8 weeks (2 months) recovery.

Distortion Product Otoacoustic Emissions

Mice were anesthetized as described above. Stimuli were presented at 5–40 kHz and delivered to the right ear by a custom-coupling insert. Distortion product (DP) grams were obtained for f2 ranging from 5 to 40 kHz, with a frequency ratio of f2/f1 of 1.2 and L1–L2 = 10 dB. Recordings were performed using EMAV software (Boys Town National Research Hospital). DPOAEs were performed by genotype-blinded person prior to noise exposure (pre-NE, baseline) and after noise exposure (post-NE) at time 0 h (immediately after noise exposure), 2 and 8 weeks (2 months) recovery.

Histology

Mice were sacrificed at time 0 h, 24 h (1 day), 2 and 8 weeks after noise exposure for histology unless specified. Mice were deeply anesthetized with Fatal Plus (Sodium Pentobarbital) and perfused (intra-cardiac) with phosphate-buffered 4% paraformaldehyde (PFA) (Electron Microscopy Sciences). Temporal bones were removed and post-fixed in 4% PFA for 15 min on ice (for synaptic immunolabeling) or 1 h at room temperature (for hair cells, macrophages and neuron labeling), rinsed in phosphate-buffered saline (PBS) twice, and placed in 0.1 M Ethylenediaminetetraacetic acid (EDTA), to allow decalcification for whole-mount dissections and for frozen mid-modiolar sectioning. Proteins were detected in both cochlear surface preparations and in cochlear mid-modiolar frozen sections using standard immunofluorescence methods. Briefly, tissue was rinsed with PBS (three times) and incubated at room temperature for 2 h in blocking solution (5% normal horse serum in 0.2% Triton X-100 in PBS). Cochleae were incubated overnight at room temperature with combinations of the primary antibodies. Hair cells were labeled with antibody against Myosin VIIa (Proteus Biosciences, Cat. No. 25-6790, 1:500). Neurons were labeled using Neurofilament 165 (NF165, Developmental Studies Hybridoma Bank, Cat. No. 2H3C, 2 μg/ml) and Beta III Tubulin (β-III tubulin, Tuj-1) antibodies (Covance, Cat. No. MMS435P, 1:500). Macrophages are endogenously GFP positive in both $CX_3CR1^{GFP/+}$ and $CX_3CR1^{GFP/GFP}$ mice, however, to enhance the fluorescence signal macrophages were immunolabeled with antibody against GFP (Invitrogen, Cat. No. A-11122,1:500). IHC ribbon synapses at the presynaptic zones were labeled with antibody against CtBP2 (BD Biosciences, Cat. No. 612044, 1:200) and postsynaptic densities with AMPA receptor GluA3 antibody (Santa Cruz Biotechnology, Cat. No. SC-7612, 1:50).

Cellular Imaging and Analyses

Fluorescence imaging was performed using an LSM 700 confocal microscope (Zeiss). For all cochleae, Z-series images were obtained at 10× (4.5-micron z-step-seize), 20× (1-micron z-step-size), or 63× (0.3-micron z-step-size) objectives. Image processing and quantitative analysis were performed using Volocity 3D image analysis software (version 6.1.1, PerkinElmer) and ImageJ (Fiji) 1.47b (National Institutes of Health).

Hair Cell Counts

Both inner and outer hair cells were identified by their immunoreactivity for Myosin VIIa. Hair cells were counted from the apical (5, 8, and 11 kHz), middle (16, 22, 28 kHz), basal (32 and 45 kHz) and hook (56 and 64 kHz) region of the cochlea unless otherwise stated. Data are expressed as percentage hair cell survival along the cochlear length.

Macrophage Counts

To assess macrophages per 100 μm of sensory epithelium, GFP-labeled macrophages were counted in the organ of Corti from maximum intensity projections taken from the apical (5, 8, and 11 kHz), middle (16, 22, 28 kHz) and basal (32 and 45 kHz) region of cochlear whole mounts. Macrophages were also counted in the IHC basal region above the habenula using yz optical sectioning and 3D slice features on Volocity 3D image analysis software (version 6.1.1, PerkinElmer) and reported as macrophages in the IHC-basal region per 100 μm of sensory epithelium. Macrophages in spiral ganglia were counted from at least 5–6 mid-modiolar sections per cochlea and normalized to the cross-sectional area of the Rosenthal's canal of the respective cochlear turn and averaged as number per 1,000 μm^2.

Spiral Ganglion Neuron Counts

Spiral ganglion counts were analyzed at 8 weeks (2 months), 16 weeks (4 months), and 24 weeks (6 months) after noise exposure. To assess the numbers of spiral ganglion cell bodies, NF165 and Tuj-1 labeled somata within Rosenthal's canal were counted from the maximum intensity projections of each section. Cell bodies counted from 5 to 6 sections per cochlea were normalized to the cross-sectional area of Rosenthal's canal per cochlear turn and averaged and reported as SGN density (per 1,000 μm^2).

Synaptic Counts

Confocal z-stacks were obtained using a high-resolution oil-immersion objective (63×) from 5, 8, 11, 16, 22, 28, 32, and 45 kHz regions in each case. Each stack spanned the entire synaptic pole of the hair cells in the z-dimensions, with z-step-size of 0.3 μm, from apical portion of the IHC to nerve terminal in the habenula perforata region. Maximum intensity projection images were exported to ImageJ (Fiji) 1.47b software and converted to black and white images. Juxtaposed pre- and post-synaptic punctae were counted manually from row of 10–12 IHCs along the lengths of the organ of Corti in the apical (5, 8, and 11 kHz), mid-apical and mid-basal (16, 22, 28 kHz), and basal (32 and 45 kHz) regions of each cochlea. Synaptic counts were divided by total number of surviving IHCs in the image and reported as synaptic ribbons per IHC.

Statistical Analyses

All the data analyses and statistics were performed using Prism version 7.0a (GraphPad). Data are presented as mean ± SD. *t*-test, one way or two-way ANOVA was applied as appropriate. Significance main effects or interactions were followed by appropriate *post hoc* tests. Details on error bars, statistical analysis, degree of freedom, number of animals, experimental replicates can be found in results and figure legends section of the manuscript. Results were considered statistically significant when probability (*p*-values) of the appropriate statistical test was less than or equal to the significance level, alpha (α) = 0.05. *F* values for ANOVAs are reported as $F_{(\text{degree of freedom numerator, degree of freedom denominator})}$.

RESULTS

Moderate Noise Trauma Induces Temporary Hearing Loss Without Any Hair Cell Death

$CX_3CR1^{+/-}$ mice (intact fractalkine signaling) were exposed for 2 h to moderate noise levels at 90 dB SPL. To verify whether such moderate noise exposure caused temporary or permanent hearing loss ABRs and DPOAEs were performed both prior to noise exposure (baseline) and after noise exposure (post-NE) at time 0 h (immediately after noise exposure), 2 and 8 weeks recovery. Noise exposure produced a ∼20–30 dB elevation of neural response thresholds at stimulus frequencies of 20, 28.3, 40, and 56.6 kHz at time 0 h recovery (**Figure 1A**). By 2 weeks post-exposure, response thresholds recovered to baseline thresholds and remained stable 8 weeks later (data not shown here). ABR thresholds at time 0 h recovery were significantly different at 20 and 28.3 kHz ($p < 0.0001$), and at 40 and 56.6 kHz ($p = 0.01$, $F_{(10,172)} = 4.89$, two-way ANOVA) when compared to thresholds at baseline and 2 weeks recovery. Elevation in ABR thresholds was coupled with attenuation of DPOAE levels at time 0 h recovery (**Figure 1B**) that nearly recovered to baseline DPOAE levels by 2 weeks recovery. DPOAE levels at time 0 h recovery were significantly different from baseline levels at frequencies above 6 kHz ($p < 0.0001$, $F_{(48,350)} = 2.60$, two-way ANOVA). DPOAE levels at 2 weeks were significantly different from baseline levels only at highest tested frequency (40 kHz) ($p = 0.0046$, two-way ANOVA). Moderate noise trauma did not result in loss of outer and IHCs throughout the cochlea at 0 h and 2 weeks after exposure, however, minimal degree of OHC loss was observed in the basal turn of the cochlea at 8 weeks after exposure (**Figure 1C**).

Moderate Noise Trauma Induces Rapid Degeneration and Spontaneous Recovery of Synapses

We next examined whether such moderate noise trauma induces cochlear synaptopathy in $CX_3CR1^{+/-}$ mice. Synaptic immunolabeling and quantification revealed a rapid loss of synaptic ribbons in $CX_3CR1^{+/-}$ mice exposed to noise at time 24 h recovery throughout the mid-basal and basal cochlear region when compared to unexposed $CX_3CR1^{+/-}$ mice (**Figures 1D,E,H**). Ribbon synapses per IHC of unexposed $CX_3CR1^{+/-}$ mice were 14.32 ± 1.7 (5.6 kHz), 16.57 ± 2.2 (11.3 kHz), 18.57 ± 3.3 (16.0 kHz), 16.62 ± 2.2 (22.6 kHz), 16.28 ± 1.9 (32.0 kHz), and 13.82 ± 3.7 (45.2 kHz). Synaptic loss was evident as early as 0 h (**Figure 1H**) but was more robust at 24 h post-exposure. Ribbon synapses per IHC of $CX_3CR1^{+/-}$ mice at 24 h post-exposure were 14.26 ± 3.4 (5.6 kHz), 14.9 ± 4.3 (11.3 kHz), 15.8 ± 2.4 (16.0 kHz),

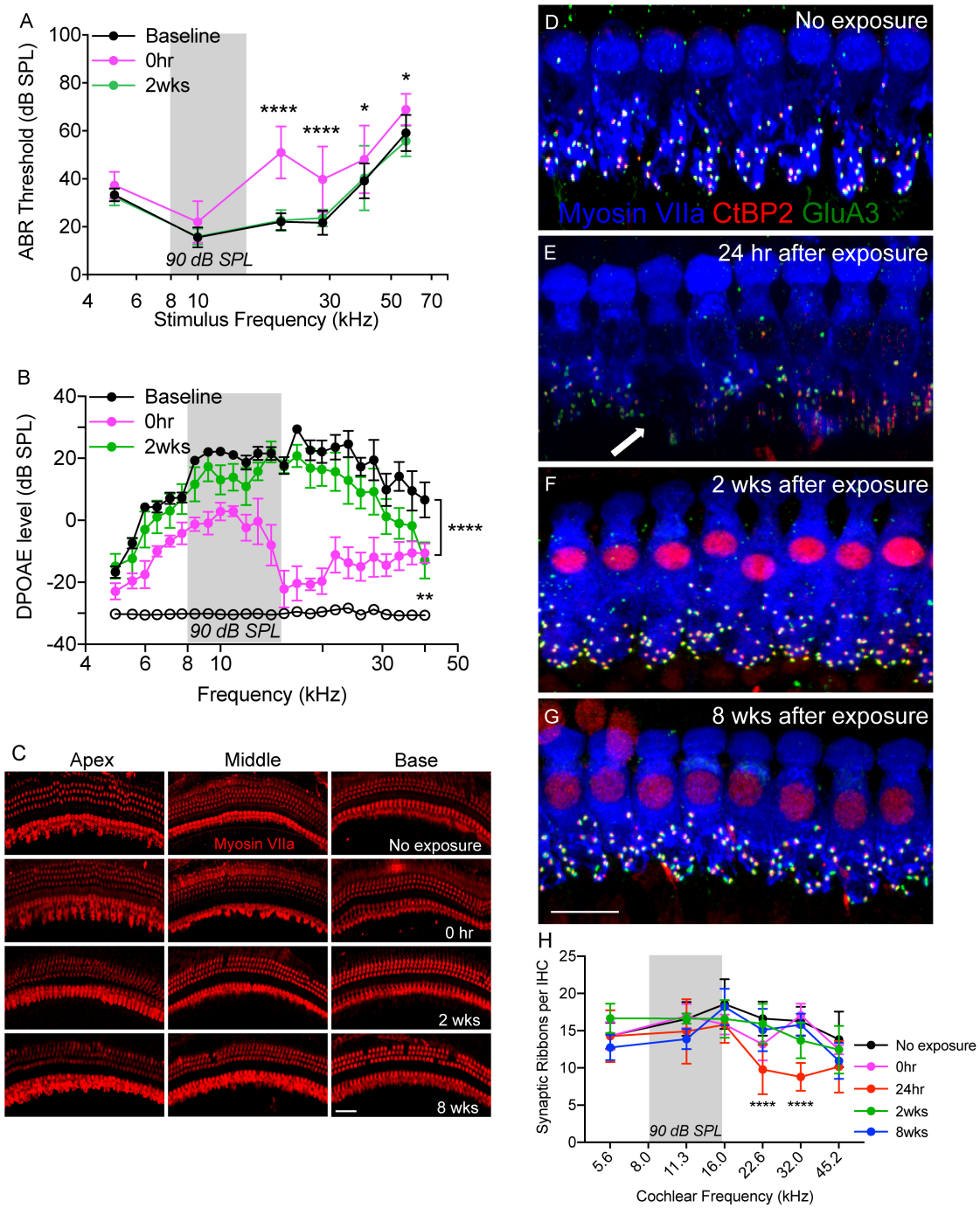

FIGURE 1 | Temporary noise-induced hearing loss causes synaptopathy. **(A)** Auditory brainstem response thresholds plotted as a function of stimulus frequencies obtained from $CX_3CR1^{+/-}$ mice prior to noise exposure (baseline), and at 0 h and 2 weeks after noise exposure. $n = 9$, $^*p < 0.05$ baseline vs. 0 h, $^{****}p < 0.0001$ baseline vs. 0 h and 2 weeks. **(B)** DPgrams obtained from $CX_3CR1^{+/-}$ mice prior to noise exposure (baseline), and at 0 h and 2 weeks after noise exposure. $n = 6$, $^{****}p < 0.0001$ baseline vs. 0 h, $^{**}p = 0.0046$ baseline vs. 2 weeks (at 40 kHz). Open black circles represents noise floor. **(C)** Representative micrographs of cochlear whole mounts from apical, middle and basal regions of $CX_3CR1^{+/-}$ mice not exposed to noise (no exposure) and at time 0 h, 2 and 8 weeks recovery after exposure immunolabeled for hair cell marker, Myosin VIIa (red). **(D)** Representative micrograph from unexposed $CX_3CR1^{+/-}$ mouse cochlea at 32 kHz region immunolabeled for pre-synaptic marker CtBP2 (red), post-synaptic marker GluA3 (green) and inner hair cell marker Myosin VIIa (blue) showing intact juxtaposed ribbon synapses. **(E)** Representative micrograph from $CX_3CR1^{+/-}$ mouse cochlea at 24 h after exposure from 32 kHz region showing disintegrated ribbon synapses indicated by white arrow. **(F)** Representative micrograph from $CX_3CR1^{+/-}$ mouse cochlea at 2 weeks after exposure from 32 kHz region showing synaptic repair. **(G)** Representative micrograph from $CX_3CR1^{+/-}$ mouse cochlea at 8 weeks after exposure from 32 kHz region showing stable synapses. Labeling colors in **(E–G)** are same as reported in **(D)**. **(H)** Ribbon synapses per IHC along the cochlear length, $n = 6$–9 mice per time point, $^{****}p < 0.0001$, 24 h vs. control. Gray bar in the graph represents the frequency band (8–16 kHz) of noise exposure. Scale bar, 63 μm **(C)** and 17 μm **(D–G)**.

9.78 ± 3.3 (22.6 kHz), 8.79 ± 1.8 (32.0 kHz), and 10.16 ± 3.4 (45.2 kHz). Two-way ANOVA followed by Tukey's multiple comparison tests revealed that synapses per IHC at 24 h post-exposure were statistically different from unexposed controls at 22.6 and 32.0 kHz ($p < 0.0001$, $F_{(20,149)} = 2.62$). The damaged synapses in exposed $CX_3CR1^{+/-}$ mice recovered by 2 weeks post-exposure and remained stable 8 weeks later (**Figures 1F–H**). Synapses per IHC of $CX_3CR1^{+/-}$ mice at time 2- and 8-weeks recovery were not different from that of unexposed $CX_3CR1^{+/-}$ mice ($p > 0.05$, Two-way ANOVA). Together, these results demonstrate that noise trauma at 90 dB SPL induces a temporary threshold shift (TTS) without any evident hair cell death and causes rapid synaptic degeneration that eventually repairs in young $CX_3CR1^{+/-}$ mice on B6 background.

Noise Trauma Induces Immediate Macrophage Recruitment Into the IHC-Synaptic Region Despite No Hair Cell Loss

To determine whether moderate noise exposure that does not cause hair cell death is able to activate and increase macrophage numbers in the damaged epithelium, we examined GFP positive macrophages in the sensory epithelium as well as in the inner

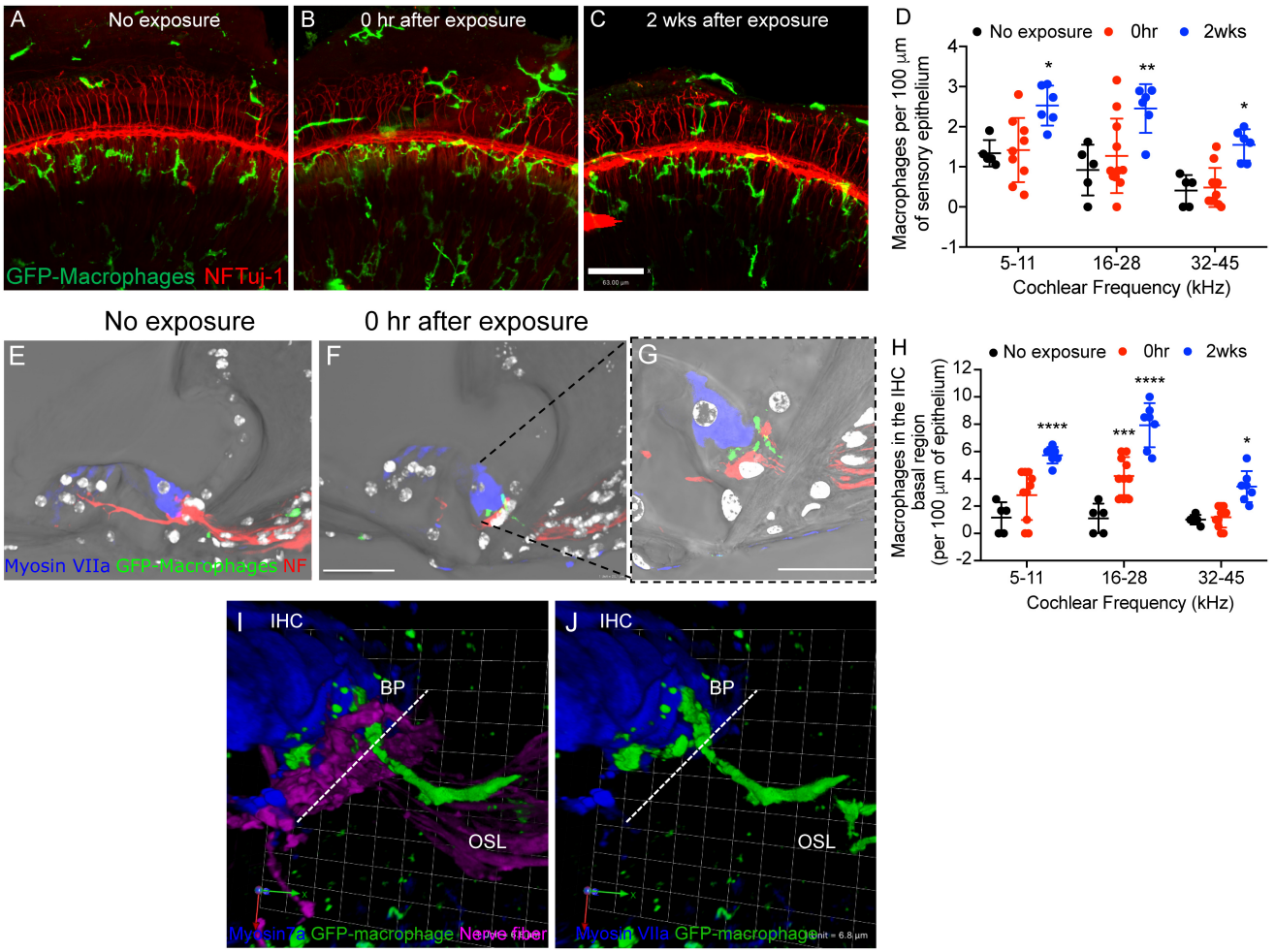

FIGURE 2 | Macrophage migrate into the epithelium after noise trauma. Representative cochlear whole mount micrographs from $CX_3CR1^{+/-}$ mice **(A)** not exposed to noise (no exposure), **(B)** at 0 h, and **(C)** 2 weeks after noise exposure immunolabeled for macrophages (green, GFP) and peripheral nerve fibers (red, NF165 and Tuj-1). **(D)** Macrophage numbers per 100 µm of sensory epithelium. No exposure ($n = 5$), 0 h ($n = 11$) and 2 weeks ($n = 7$). $^*p < 0.05$, $^{**}p < 0.01$, control vs. 2 weeks. **(E)** The organ of Corti from an unexposed mouse (no exposure) showing macrophages in the osseous spiral lamina away from the IHC-synaptic region. **(F)** GFP-macrophage observed in the basal region of an inner hair cell (Myosin VIIa, blue) at 0 h after noise exposure. **(G)** Higher magnification of **(F)** showing GFP-macrophage above the habenula and in the basal region of the IHC at 0 h after synaptopathic noise exposure. White color in E-G represents nuclei stained with DAPI. **(H)** Macrophage numbers in the IHC basal region per 100 µm of epithelium. No exposure ($n = 5$), 0 h ($n = 11$) and 2 weeks ($n = 7$).$^{***}p < 0.001$ (16–28 kHz), no exposure vs. 0 h, $^{****}p < 0.0001$ (5–11, 16–28 kHz), $^*p < 0.05$ (32–45 kHz), no exposure vs. 2 weeks. **(I,J)** 3D reconstruction of a confocal stack showing pseudopodia (cytoplasmic extension) of a GFP-macrophage above the habenula and under the basal pole (BP) of an inner hair cell (IHC, blue) and the cell body of the macrophage in the osseous spiral lamina (OSL). Dashed line represents demarcation of the organ of Corti from the OSL. Scale bar, 63 µm **(A–C)**, 20 µm **(E,F)**, 10 µm **(G)**, and 6.8 µm **(I,J)**.

spiral plexus of $CX_3CR1^{+/-}$ mice not exposed to noise (no exposure) and at time 0 h and 2 weeks after TTS-like noise trauma. In unexposed $CX_3CR1^{+/-}$ mice, GFP-macrophages are occasionally observed below or in the basilar membrane and also in the osseous spiral lamina away from the inner spiral plexus (**Figures 2A,D,E,H**). Moderate noise trauma led to an immediate (0 h) increase in macrophage numbers in the apical and middle region of the epithelium (**Figure 2B**) and also in the basal region of the IHCs above the habenula (**Figures 2F–J**). The numbers in the epithelium remained elevated at 2 weeks recovery and also increased in base of the cochlea (**Figures 2C,D,H**). The macrophage numbers in the epithelium at 0 h recovery were insignificant from no exposure control ($p > 0.05$, two-way ANOVA) but the numbers in the epithelium at 2 weeks recovery were significantly different from no exposure control in the apex ($p = 0.044$), middle ($p = 0.006$) and base ($p = 0.045$) cochlear region ($F_{(2,55)} = 21.93$, two-way ANOVA). Macrophage numbers counted in the apex (5–11 kHz), middle (16–28 kHz) and base (32 and 45 kHz) IHC-ANF synaptic region (above the habenula) per 100 μm of the epithelium at 0 h were 2.8 ± 1.8, 4.2 ± 1.3 and

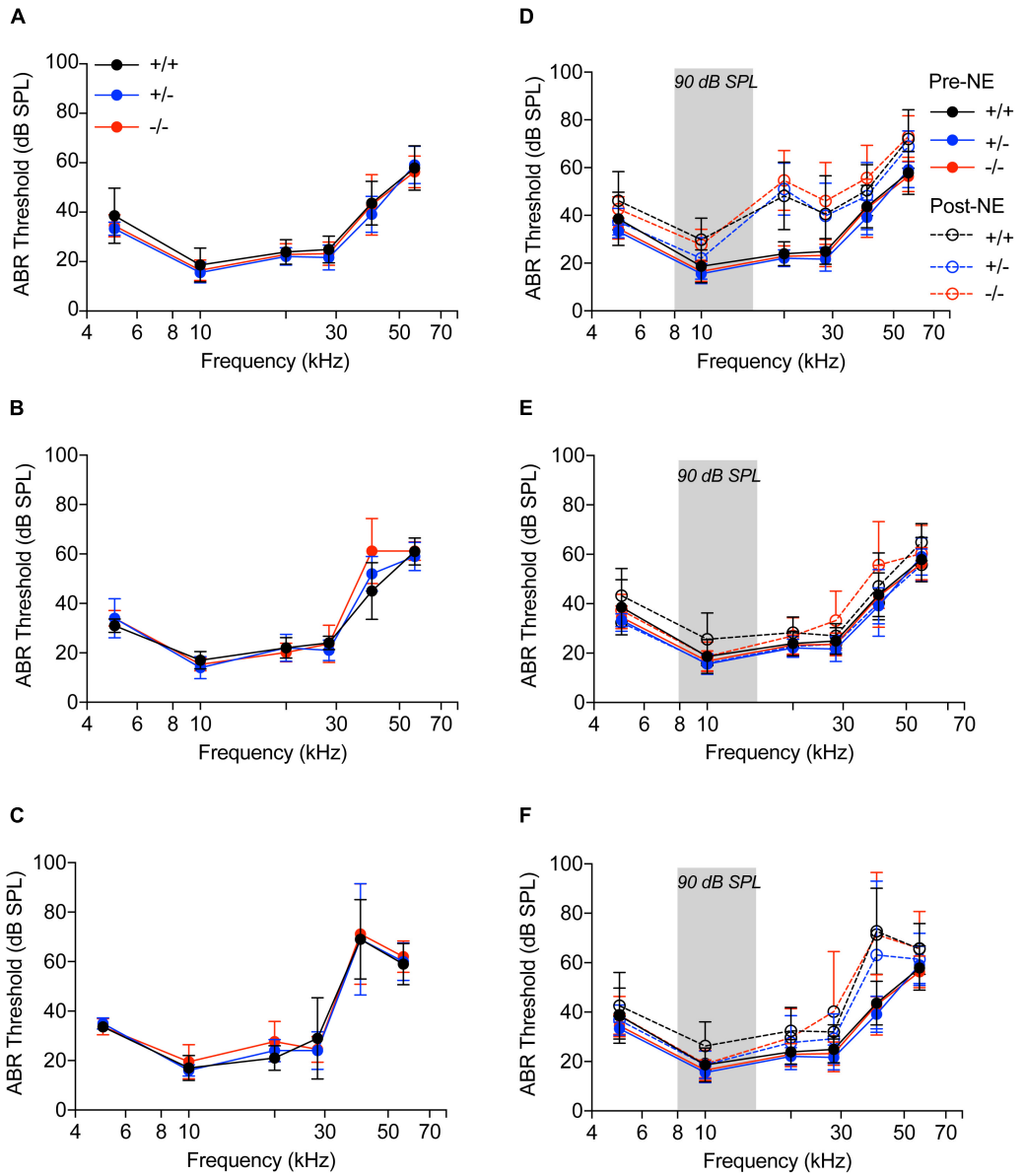

FIGURE 3 | Auditory brainstem responses. **(A–C)** Audiograms of $CX_3CR1^{+/+}$ (black), $CX_3CR1^{+/-}$ (blue) and $CX_3CR1^{-/-}$ (red) mice not exposed to noise at 6 weeks **(A)**, 8 weeks **(B)**, and 14 weeks **(C)** of age. n = 5–6 mice per genotype. **(D–F)** Audiograms of $CX_3CR1^{+/+}$ (black), $CX_3CR1^{+/-}$ (blue), and $CX_3CR1^{-/-}$ (red) mice exposed to noise at time 0 h **(D)**, 2 weeks **(E)**, and 8 weeks **(F)** recovery. Filled circles with solid lines represent thresholds prior to noise-exposure (Pre-NE) and unfilled circles with hyphenated lines represents thresholds post-noise exposure (Post-NE). $CX_3CR1^{+/+}$ (n = 7), $CX_3CR1^{+/-}$ (n = 9), $CX_3CR1^{-/-}$ (n = 15). Gray bar in the graph represents the frequency band (8–16 kHz) of noise exposure.

1.1 ± 0.75, respectively. Macrophage numbers in the IHC-ANF synaptic region at time 0 h recovery was significantly different from no exposure control only in the middle region ($p = 0.0002$, two-way ANOVA). By 2 weeks macrophage numbers in the apex, middle and base IHC synaptic region were 5.72 ± 0.6, 7.92 ± 1.6, and 3.42 ± 1.1, respectively. Those numbers were significantly different from no exposure control and 0 h recovery in all cochlear regions ($p < 0.0001$, $F_{(4,58)} = 4.67$, two-way ANOVA). These results indicate that moderate noise trauma that does not cause hair cell death is sufficient to induce a rapid and localized immune response into the vulnerable and damaged IHC synaptic region.

$CX_3CR1^{-/-}$ Mice Exhibit Nearly Complete Recovery of Hearing Thresholds and OHC Function Following Moderate Noise Trauma

We next sought to determine if cochlear macrophages influence auditory function, synaptic degeneration and repair after moderate noise trauma via fractalkine receptor, CX_3CR1. Unexposed $CX_3CR1^{+/+}$, $CX_3CR1^{+/-}$, and $CX_3CR1^{-/-}$ mice had normal hearing thresholds at 6 weeks of age (**Figure 3A**). ABR thresholds were elevated at stimulus frequencies of 40 and 56.6 kHz in all genotypes at 8 weeks (**Figure 3B**) and at 14 weeks of age (**Figure 3C**) which is likely due to presbycusis in B6 mice. Therefore, any functional or structural data analysis at and above 40 kHz was excluded from the present study. ABR measurements immediately after exposure demonstrated a significant ∼20–30 dB elevation in hearing thresholds at stimulus frequencies above 20 kHz when compared to baseline thresholds in all the three genotypes (**Figure 3D**, $p < 0.0001$, $F_{(25,431)} = 3.75$, two-way ANOVA). The thresholds at 0 h were not different between the genotypes. The elevated thresholds returned to baseline by 2 weeks post-exposure (**Figure 3E**) and remained stable at 8 weeks (**Figure 3F**) except at higher frequencies. $CX_3CR1^{-/-}$ mice exhibit incomplete recovery of thresholds at 28.3 kHz region (**Figures 3E,F**) and were significantly elevated from baseline thresholds ($p = 0.0056$ at 2 weeks post-NE, $p < 0.0001$ at 8 weeks post-exposure, two-way ANOVA, Tukey's *post hoc* multiple comparison test).

OHC function assessed by DPOAEs indicated no significant difference among the three genotypes prior to noise exposure (**Figure 4A**, filled circles with solid lines, $p > 0.999$, two-way ANOVA). Noise exposure immediately reduced DPOAE levels in all the genotypes (**Figure 4A**, unfilled circles with hyphenated lines, $p < 0.0001$, $F_{(120,1150)} = 1.649$, two-way ANOVA), when compared to baseline levels, with no significant difference among the genotypes. At 2 weeks after noise exposure, DPOAE levels returned to normal with no difference between the genotypes (**Figure 4B**). At 8 weeks, the DPOAE levels were reduced in all genotypes at frequencies above 20 kHz, however, the differences were not statistically significant (**Figure 4C**). These results demonstrate that lack of CX_3CR1 does not influence hearing thresholds and OHC function after moderate noise trauma.

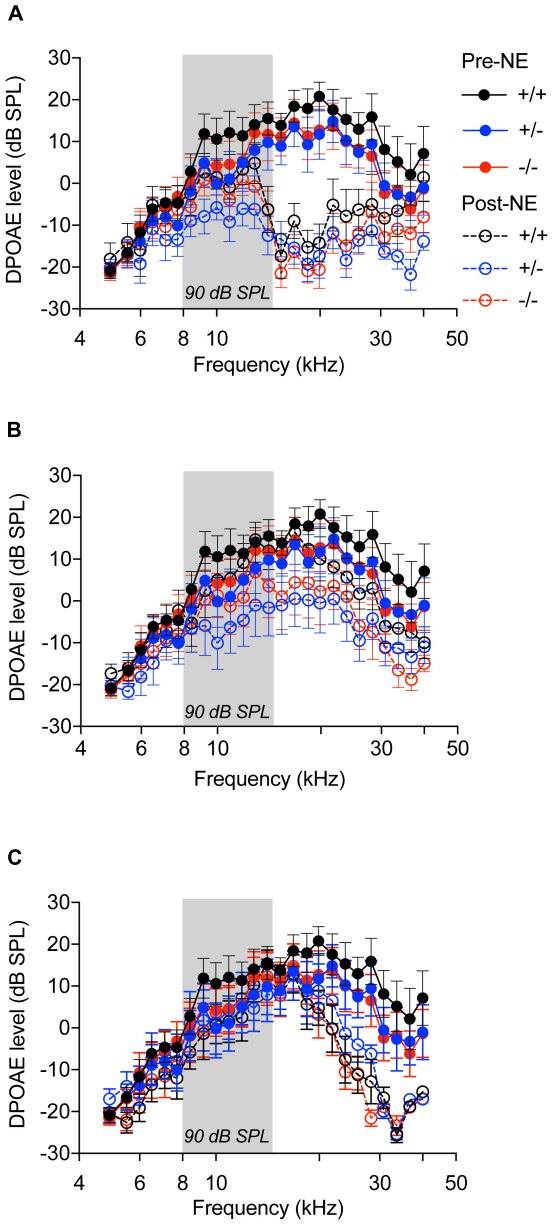

FIGURE 4 | Distortion product otoacoustic emissions. DP grams of $CX_3CR1^{+/+}$ (black), $CX_3CR1^{+/-}$ (blue), and $CX_3CR1^{-/-}$ (red) mice exposed to noise at time 0 h **(A)**, 2 weeks **(B)**, and 8 weeks **(C)** recovery. Filled circles with solid lines represent DP grams prior to noise-exposure (Pre-NE) and unfilled circles with hyphenated lines represents DP grams post-noise exposure (Post-NE). $CX_3CR1^{+/+}$ ($n = 8$), $CX_3CR1^{+/-}$ ($n = 9$), $CX_3CR1^{-/-}$ ($n = 9$). Gray bar in the graph represents the frequency band (8–16 kHz) of noise exposure.

$CX_3CR1^{-/-}$ Mice Display Attenuated ABR Wave 1 Amplitudes Following Noise Trauma

ABR wave 1 amplitudes-versus-stimulus level (ABR I/O) analysis at 28.3 kHz frequency region (**Figure 5A**) were significantly

attenuated in all three genotypes immediately after noise exposure (0 h) compared to genotype matched pre-noise amplitudes (**Figures 5B–B″**, $p < 0.01$, two-way ANOVA). The attenuated wave 1 amplitudes recovered in $CX_3CR1^{+/+}$ and $CX_3CR1^{+/-}$ animals by 2 weeks after exposure and remained stable at 8 weeks (**Figures 5C,C′,D,D′**). However, $CX_3CR1^{-/-}$ mice displayed persistent attenuation in amplitudes (53%) at both thresholds as well as suprathresholds levels (**Figures 5C″,D″**, $p = 0.015$ and $p = 0.0083$ at 2 and 8 weeks post-exposure, respectively, two-way ANOVA). The raw amplitudes in $CX_3CR1^{+/+}$, $CX_3CR1^{+/-}$, and $CX_3CR1^{-/-}$ mice at 28.3 kHz are provided in **Supplementary Table S1** (see **Supplementary Material**). ABR wave 1 amplitudes-versus-stimulus level (ABR I/O) analysis at 10 kHz frequency region revealed no difference in wave 1 amplitudes with respect to either genotype or recovery time post-noise exposure (data not shown). Together, the results show that exposed mice lacking CX_3CR1 have attenuated amplitudes of ABR wave 1 when compared to exposed mice with intact fractalkine signaling.

Lack of CX_3CR1 Impairs Synaptic Repair and Influences IHC Survival After Noise Trauma

To determine whether macrophages influence degeneration and repair of synapses via fractalkine signaling, $CX_3CR1^{+/-}$ and $CX_3CR1^{-/-}$ mice received a TTS-inducing noise exposure and temporal bones were collected at 24 h-, 2 weeks- and 8 weeks-recovery. Cochleae were fixed and processed for immunolabeling of presynaptic zones with an antibody against CtBP2, postsynaptic AMPA receptor subunit GluA3 antibody and for hair cells with anti-Myosin VIIa antibody (**Figures 6A–D**). There was no difference in ribbon synapses per surviving IHC across the cochlear length in unexposed (control) $CX_3CR1^{+/-}$ and $CX_3CR1^{-/-}$ mice (**Figure 6E**). At 24 h after exposure there was a rapid ∼50% loss of synaptic ribbons in both $CX_3CR1^{+/-}$ and $CX_3CR1^{-/-}$ mice throughout the basal turn of the cochlea (**Figures 6B,E**), compared to unexposed mice (**Figures 6A,E**). Two-way ANOVA followed by Tukey's *post hoc* test revealed that synaptic counts were significantly reduced in exposed mice at the 22.6, and 32.0 kHz regions compared to unexposed control mice ($p < 0.01$, $F_{(25,208)} = 1.79$). There was no difference in synaptic counts between $CX_3CR1^{+/-}$ and $CX_3CR1^{-/-}$ mice at 24 h after exposure (**Figure 6E**, $p = 0.99$, two-way ANOVA). In exposed $CX_3CR1^{+/-}$ mice, damaged synapses recovered by 2 weeks post-exposure (data not shown) and remained stable at 8 weeks (**Figures 6C,E**). However, $CX_3CR1^{-/-}$ mice displayed persistent synaptic degeneration at the 22–32 kHz region at 2 weeks (data not shown) and 8 weeks after exposure (**Figures 6D,E**). Synaptic counts per surviving IHCs in $CX_3CR1^{-/-}$ mice at 8 weeks post-exposure were significantly different from unexposed $CX_3CR1^{+/-}$ and $CX_3CR1^{-/-}$ mice ($p = 0.013$, two-way ANOVA) but not significant from $CX_3CR1^{+/-}$ mice at 8 weeks recovery ($p = 0.056$). Lack of CX_3CR1 did not affect macrophage numbers in the IHC-ANF synaptic region after exposure. The average macrophage numbers in the IHC synaptic region in exposed $CX_3CR1^{+/-}$ mice was 6.55 ± 0.88 and in exposed $CX_3CR1^{-/-}$ mice was 6.22 ± 1.98 (**Figure 6F**, $p = 0.654$, $t = 0.46$, Df = 11.4, two-tailed t-test). CX_3CR1 deficiency also resulted in damage and loss of IHCs from the base of the cochlea of 40% mice (**Figure 6H**). IHC loss in exposed $CX_3CR1^{-/-}$ mice was significantly different from exposed $CX_3CR1^{+/-}$ and unexposed control mice ($p = 0.0081$, $F_{(6,108)} = 3.08$, two-way ANOVA). Noise-exposed mice had OHC loss in the base and hook regions in all three genotypes (**Figure 6G**), however the loss was statistically insignificant when compared to unexposed mice ($p = 0.144$, $F_{(6,108)} = 1.67$, two-way ANOVA). These results demonstrate that disruption of fractalkine signaling impairs the spontaneous recovery of damaged synapses after moderate noise trauma.

CX_3CR1 Deficiency Leads to Diminished Survival of SGNs Following Moderate Noise Trauma

Immunolabeling for macrophages using anti-GFP antibody (to enhance the fluorescence signal) in mid-modiolar frozen sections demonstrate that such moderate noise exposure for 2 h to an octave band (8–16 kHz) noise at 90 dB SPL did not result in an increase in macrophage numbers in the spiral ganglion (SG) at any recovery time point (**Figures 7A–E**). Two-way ANOVA followed by Tukey's *post hoc* test revealed that macrophage density in the SG after noise exposure at any recovery time point was not significantly different from control or other recovery time points ($p = 0.46$, $F_{(8,78)} = 0.977$). To determine whether fractalkine signaling influenced SGN survival after synaptopathic TTS-like noise trauma, cochlear mid-modiolar frozen sections from $CX_3CR1^{+/-}$ and $CX_3CR1^{-/-}$ mice were immunolabeled for SGNs using NF165 and Tuj-1 antibodies. SGN density in exposed $CX_3CR1^{-/-}$ mice was indistinguishable to unexposed $CX_3CR1^{-/-}$ and exposed $CX_3CR1^{+/-}$ mice at 8 and 16 weeks post-exposure (data not shown). At 24 weeks after exposure, $CX_3CR1^{-/-}$ mice displayed increased loss of SGN cell bodies from the basal turn of the cochlea (**Figures 7I,J**) compared to unexposed $CX_3CR1^{+/-}$ and $CX_3CR1^{-/-}$ (**Figures 7F,G,J**) and exposed $CX_3CR1^{+/-}$ mice (**Figures 7H,J**). Two-way ANOVA followed by Tukey's *post hoc* test revealed that the SGN density in the basal cochlear region of $CX_3CR1^{-/-}$ mice was significantly different from unexposed age-matched control mice ($p = 0.0034$, $F_{(10,57)} = 6.22$). The SGN density in the exposed $CX_3CR1^{+/-}$ mice was not statistically significant from the unexposed age-matched controls ($p = 0.98$). The macrophage density in the SG of $CX_3CR1^{-/-}$ mice was not different from that of $CX_3CR1^{+/-}$ mice at all recovery time point including 24 weeks after noise trauma (**Figure 7K**, $p = 0.93$, two-way ANOVA). These results demonstrate that disruption of fractalkine signaling due to genetic loss of CX_3CR1 results in an increase in neuronal loss after moderate synaptopathic-noise trauma.

DISCUSSION

Cochlear synaptopathy can occur due to noise trauma (Kujawa and Liberman, 2009), ageing (Kujawa and Liberman, 2015),

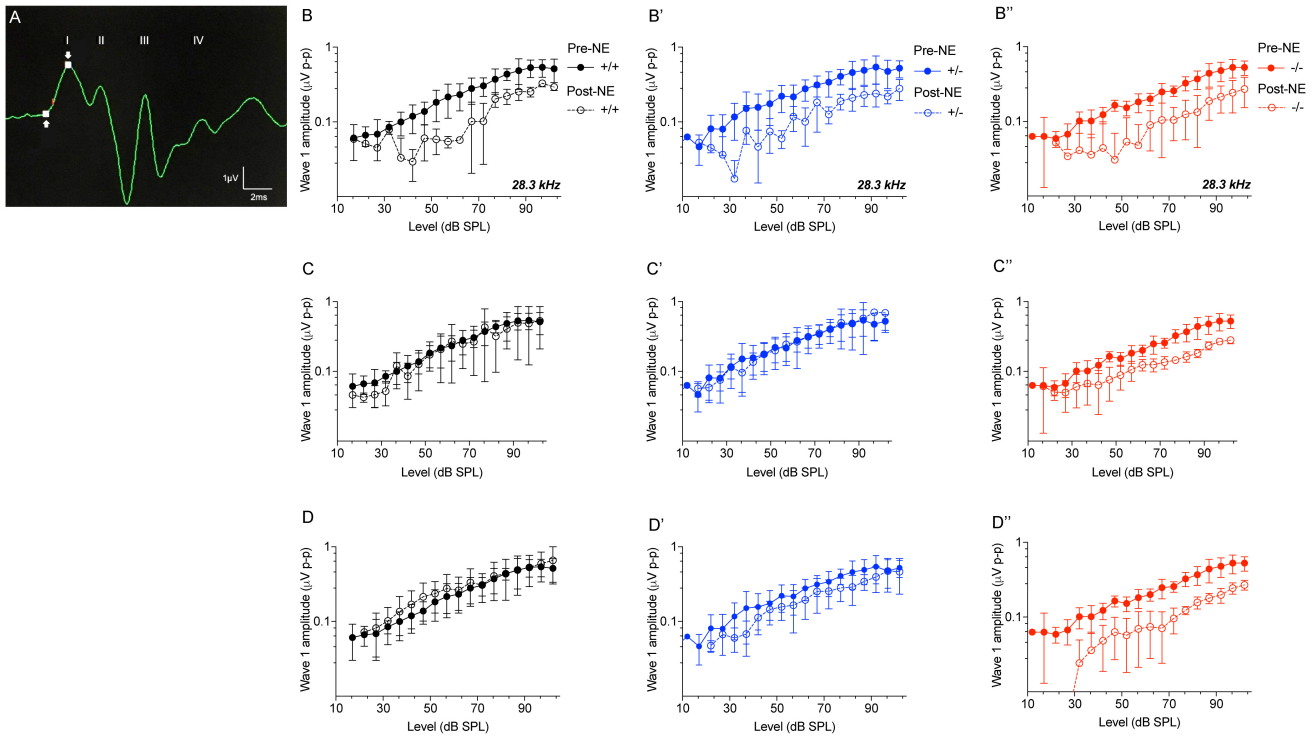

FIGURE 5 | ABR Wave 1 amplitudes against level series. **(A)** Representative ABR trace (28.3kHz, 80 dB SPL) showing placement of arrows at peak and trough of ABR wave 1 for amplitude measurements. ABR wave 1 amplitudes at 28.3 kHz from $CX_3CR1^{+/+}$ (black), $CX_3CR1^{+/-}$ (blue), and $CX_3CR1^{-/-}$ (red) mice exposed to noise at time 0 h **(B–B″)**, 2 weeks **(C–C″)**, and 8 weeks **(D–D″)** recovery. Filled circles with solid lines represent amplitudes prior to noise-exposure (Pre-NE) and unfilled circles with hyphenated lines represents amplitudes post-noise exposure (Post-NE). $CX_3CR1^{+/+}$ (n = 7), $CX_3CR1^{+/-}$ (n = 9), $CX_3CR1^{-/-}$ (n = 15).

and aminoglycoside-induced ototoxicity (Ruan et al., 2014). Synaptic loss can precede threshold elevation and can trigger gradual degeneration of SGNs (Kujawa and Liberman, 2009). The mechanisms underlying synaptic damage and subsequent neurodegeneration have not been elucidated beyond the studies of glutamate excitotoxicity (Pujol et al., 1985, 1993). It is notable, however, that the ANFs can undergo spontaneous regeneration and can partially recover their synaptic connections with IHCs after excitotoxic insults (Puel et al., 1995; Pujol and Puel, 1999) or following acoustic trauma (Puel et al., 1998). Whether this represents transient protein down- and up-regulation or actual degeneration and regeneration of synaptic elements remains unclear. The mechanisms of such spontaneous synaptic repair are also unclear. In the present study young B6 mice exposed to 90 dB SPL for 2 h produced a TTS. The elevated thresholds, incomplete recovery of DPOAE levels and some degree of loss of OHCs observed at higher cochlear frequencies at 2 months post-exposure recovery is attributed to the early onset of hearing loss in B6 mice (Henry and Chole, 1980; Hequembourg and Liberman, 2001). We report that young B6 mice exposed to 90 dB SPL produces a rapid loss of up to 50% of synapses at cochlear regions tuned to frequencies higher than the exposure band (8–16 kHz). At 2 weeks post-exposure recovery, the damaged synapses undergo nearly complete spontaneous repair. This is in contrast to previous studies that reported permanent loss of synapses following moderate noise trauma that causes reversible threshold elevation (Kujawa and Liberman, 2009). Those studies utilized mice of CBA/CaJ strain at 16 weeks of age. Previous studies in guinea pigs demonstrated post-exposure regeneration of cochlear nerve terminals in the IHC region at the ultrastructural level (Puel et al., 1998). On the contrary, Lin et al., 2011 reported the presence of the irreversible primary neural degeneration in noise-exposed guinea pigs by immunolabeling pre- and post-synaptic markers and applying high power confocal analysis. The spontaneous synaptic recovery that has been reported in the present study may be attributed to the different strain, and age of mice as well as to the noise levels. We have found that young B6 mice exposed to 100 dB SPL causes permanent threshold shifts (PTS) and partial synapse recovery (data not shown). Similar post-exposure synapse recovery in B6 mice have also been demonstrated by Shi et al. (2015) and Kim et al. (2019). Further understanding of the mechanisms of spontaneous synaptic repair in B6 mice would lead to the identification of novel targets to elicit synapse regeneration.

Moderate noise trauma induced a rapid and focal recruitment of macrophages into the damaged synaptic region despite any evident hair cell death. The source and phenotype of macrophages as well as the mechanisms that regulate their recruitment into the synaptic region remain unknown. Studies from the CNS have reported that excitotoxity and/or neuronal injury can lead to microglial activation and chemotaxis toward the site of injury, and various candidate signals that

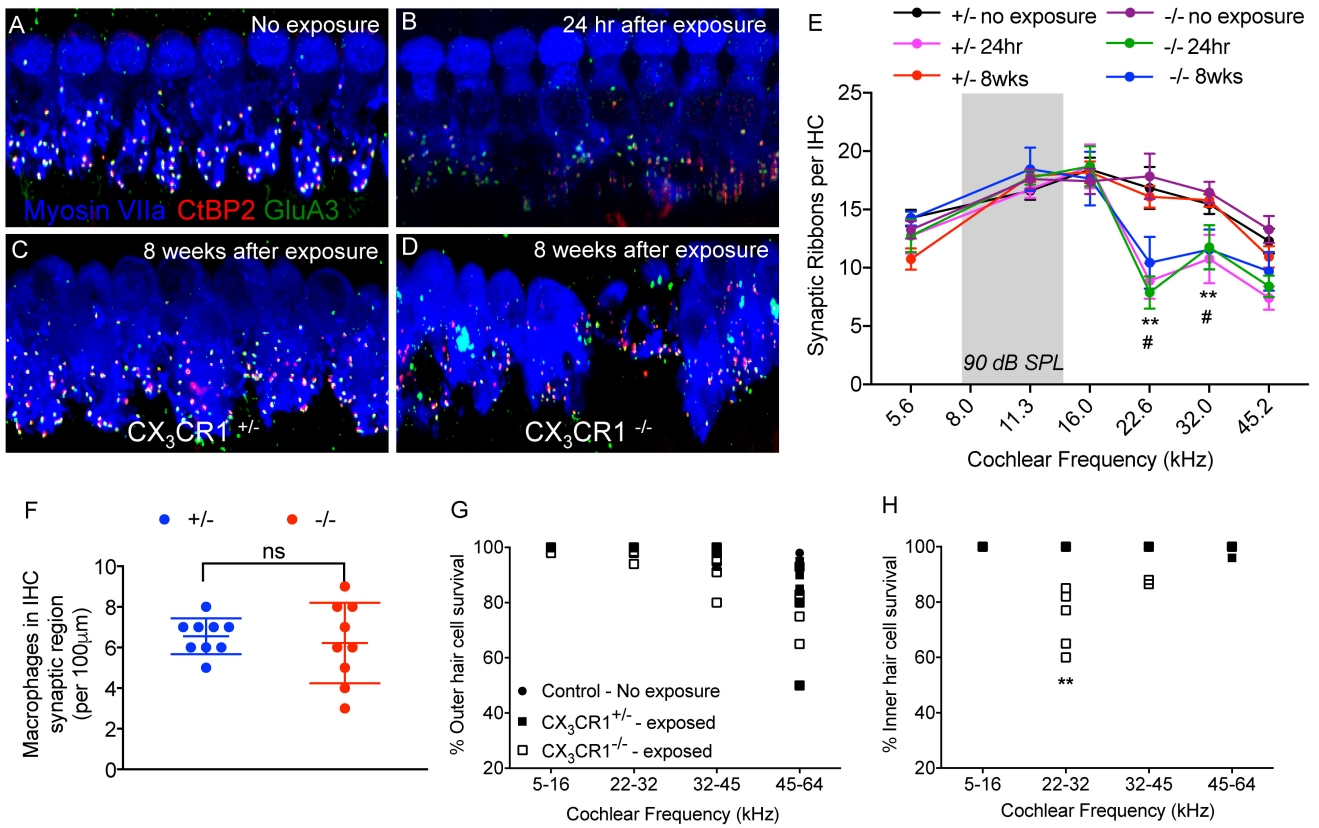

FIGURE 6 | Ribbon synapses, macrophages, and hair cell numbers in $CX_3CR1^{+/-}$ and $CX_3CR1^{-/-}$ mice after noise exposure. **(A)** Representative micrograph from $CX_3CR1^{+/-}$ mice not exposed to noise (no exposure) at 32 kHz region immunolabeled for pre-synaptic marker CtBP2 (red), post-synaptic marker GluA3 (green) and inner hair cell marker Myosin VIIa (blue) showing intact juxtaposed ribbon synapses. **(B)** Representative micrograph at 24 h after exposure from $CX_3CR1^{+/-}$ mice at 32 kHz region showing disintegrated ribbon synapses. **(C)** Representative micrograph at 8 weeks after exposure from $CX_3CR1^{+/-}$ mice at 32 kHz region showing stable repaired synapses. **(D)** Representative micrograph at 8 weeks after exposure from $CX_3CR1^{-/-}$ mice at 32 kHz region showing degenerated ribbon synapses. Labeling colors in panels (**B–D**) are same as reported in A. **(E)** Ribbon synapses per surviving IHC along the cochlear frequency regions. No exposure; n = 6–7 mice per genotype, 24 h after exposure; n = 5–6 mice per genotype, 8 weeks after exposure; n = 9–15 mice per genotype. $^{**}p < 0.01$ ($CX_3CR1^{+/-}$ and $CX_3CR1^{-/-}$, no exposure vs. 24 h), $\#p < 0.01$ ($CX_3CR1^{-/-}$, 8 weeks vs. no exposure). Gray bar in the graphs represents the frequency band (8–16 kHz) of noise exposure. **(F)** Average macrophage numbers in IHC synaptic region per 100 µm of sensory epithelium of exposed $CX_3CR1^{+/-}$ and $CX_3CR1^{-/-}$ mice, n = 9 per genotype, ns, not significant. Percentage outer hair cell survival **(G)** and inner hair cell survival **(H)**. Mice per genotype not exposed to noise (n = 6), $CX_3CR1^{+/-}$ (n = 9), $CX_3CR1^{-/-}$ (n = 15) at 8 weeks after exposure. $^{**}p < 0.01$. Scale, 17 µm (A-D).

could participate in microglial activation have been identified. Cytokines such as TNF-α, IL-1β, IFN-γ released from damaged neurons and from reactive astrocytes following excitotoxic events can activate the surrounding microglia (Zhang and Zhu, 2011). Lipid peroxidation (an oxidative stress indicator) plays an important role in neuronal degeneration. 4-hydroxynonenal, a product of lipid peroxidation, can activate and increase the phagocytic activity of microglia and peripheral macrophages through their association with scavenger receptors (Bruce-Keller, 1999). Molecules such as fractalkine have received much attention as microglial chemoattractants (Haskell et al., 1999; Hermand et al., 2008). CNS excitotoxicity can cause rapid cleavage of fractalkine from the neurons, increasing the levels of soluble fractalkine, which is a known chemoattractant (Chapman et al., 2000; Limatola et al., 2005). Nevertheless, our data show that the lack of CX_3CR1 did not influence macrophage density in the IHC-synaptic region or in the spiral ganglion following moderate noise trauma, suggesting that fractalkine may not be a necessary chemotactic factor. Other molecules such as adenosine triphosphate (ATP), are released from injured cells, and evoke microglial chemotaxis to the injured site, acting via microglia P2Y12 purinergic receptors (Honda et al., 2001; Haynes et al., 2006; Eyo et al., 2014; Kato et al., 2016). Noise is known to stimulate local ATP release in the cochlea (Telang et al., 2010), however, whether ATP evokes macrophage recruitment into the synaptic region is unknown. Macrophages expresses glutamate receptors (Biber et al., 1999), hence it is possible that the excessive glutamate released from the IHCs due to noise trauma can directly induce macrophage chemotaxis toward the synaptic region. Glutamate can directly induce microglial chemotaxis which is mediated by AMPA and metabotropic glutamate receptors on the microglia (Liu et al., 2009). Future studies investigating the source and phenotype of macrophages and mechanisms that regulate their migration

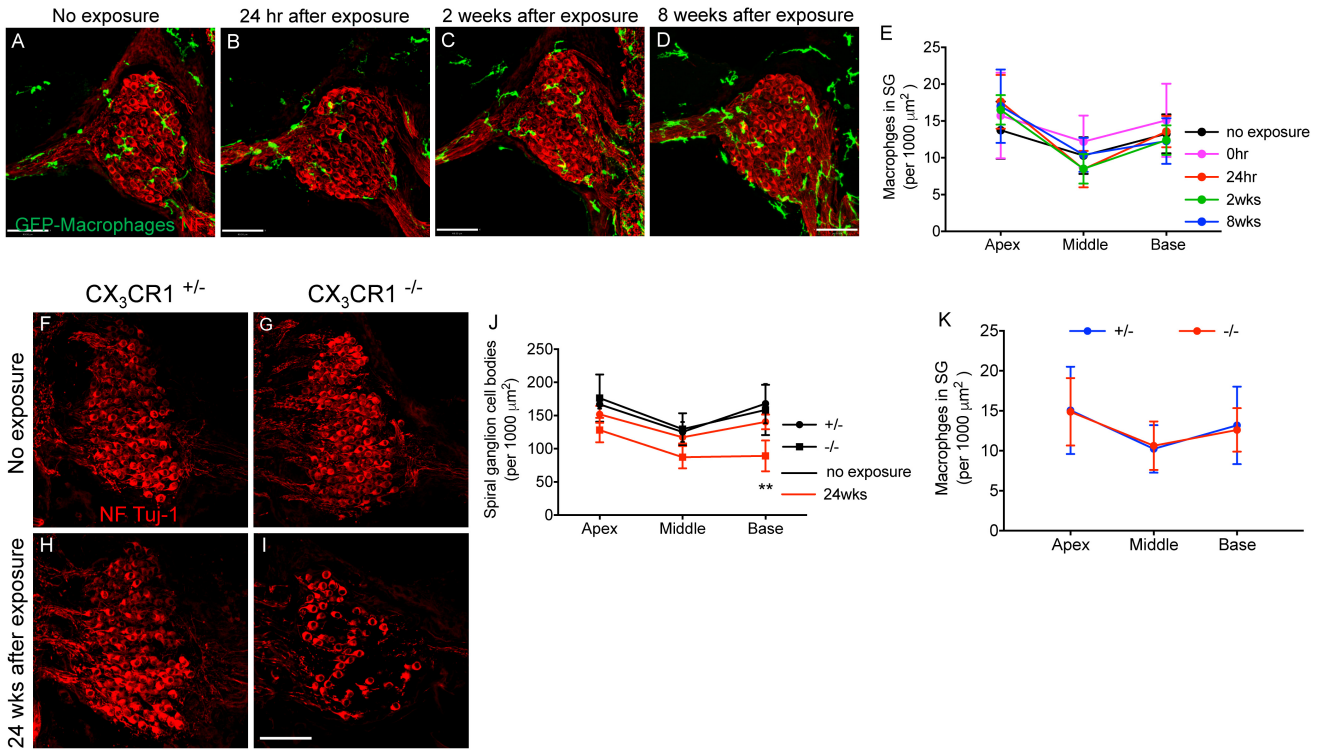

FIGURE 7 | Macrophage and Spiral ganglion neuron density in the spiral ganglion of $CX_3CR1^{+/-}$ and $CX_3CR1^{-/-}$ mice after exposure. Representative micrographs of cochlear mid-modiolar sections from $CX_3CR1^{+/-}$ mice not exposed to noise (no exposure) **(A)** and from $CX_3CR1^{+/-}$ mice at 24 h **(B)**, 2 weeks **(C)**, and 8 weeks **(D)** after exposure immunolabeled for macrophages (green, GFP) and spiral ganglion neurons (red, NF165 and Tuj-1). **(E)** Macrophage numbers in spiral ganglion (SG) (per 1,000 μm^2), n = 4–8 $CX_3CR1^{+/-}$ mice per recovery time point. Representative micrographs showing fewer SGN cell bodies immunolabeled for NF165 and Tuj-1 (red) in $CX_3CR1^{-/-}$ mice **(I)** compared to $CX_3CR1^{+/-}$ mice **(H)** at 24 weeks post-exposure and to unexposed age-matched control mice **(F,G)**. **(J)** Quantitative data on SGN density per 1,000 μm^2 from age-matched unexposed and exposed $CX_3CR1^{+/-}$ and $CX_3CR1^{-/-}$ mice at 24 weeks post-noise trauma. n = 4 mice per group, $^{**}p < 0.01$ $CX_3CR1^{-/-}$ mice 24 weeks post-NE vs. no exposure $CX_3CR1^{+/-}$ and $CX_3CR1^{-/-}$ mice. **(K)** Average macrophage density in SG of $CX_3CR1^{+/-}$ and $CX_3CR1^{-/-}$ mice at time 24 h, 2, 8, 16, and 24 weeks recovery after exposure. n = 4–9 per genotype per recovery time point. Scale bar, 63 μm.

into the damaged synaptic region after noise trauma would be valuable to better understand the inflammatory cells dynamics in cochlear pathology.

Our data demonstrate that the genetic disruption of fractalkine signaling impairs the spontaneous recovery of damaged synapses and leads to enhanced degeneration of auditory neurons following synaptopathic noise trauma. The enhanced neurodegeneration in the damaged cochlea of CX_3CR1 knockout animals corroborates our previous work (Kaur et al., 2015, 2018). The lack of synaptic recovery in the exposed $CX_3CR1^{-/-}$ mice is the first evidence for the role of macrophages and fractalkine in synaptic plasticity in the damaged cochlea. Increased synaptic degeneration in $CX_3CR1^{-/-}$ mice correlates with attenuated suprathreshold neural responses at higher frequencies without affecting hearing thresholds and DPOAE levels. Lack of CX_3CR1 did not affect macrophage density in the IHC-ANF synaptic region or in the ganglion after exposure suggesting that the increased synapse degeneration and neuronal loss in exposed $CX_3CR1^{-/-}$ mice is not due to reduced macrophage numbers. The underlying mechanisms of synaptopathy in the CX_3CR1 knockout animals is unclear, but could be driven, at least in part, by IHC pathology that is observed in a few (40%) $CX_3CR1^{-/-}$ mice. The exact contribution of macrophages in synaptic recovery is also not yet clear. An intriguing possibility is that macrophage migration into the damaged synaptic region is a protective mechanism designed to limit neurodegeneration and improve synaptic recovery following noise trauma. In support of this idea, serval studies in the CNS have suggested that microglial activation can attenuate excitotoxic injury and limit neurodegeneration (Simard and Rivest, 2007; Lauro et al., 2010; Vinet et al., 2012; Eyo et al., 2014; Kato et al., 2016) and improve synaptic recovery (Lazarov-Spiegler et al., 1996; Prewitt et al., 1997; Batchelor et al., 1999). Microglia-mediated protection against CNS excitotoxicity has been attributed to multiple mechanisms such as promoting neurite outgrowth (Prewitt et al., 1997; Batchelor et al., 1999), phagocytosing degenerating neurons and synapses (Abiega et al., 2016), and by promoting the release of neurotrophic factors such as basic fibroblast growth factor (bFGF) and nerve growth factor (NGF) (Heumann et al., 1987; Araujo and Cotman, 1993).

How might fractalkine signaling influence excitotoxicity and repair of cochlear synapses? One hypothesis is that fractalkine

signaling regulates macrophage inflammatory and toxic behavior in damaged cochlea. Studies in the CNS have shown that fractalkine signaling exert neuroprotective actions in many neuroinflammatory and neurodegenerative disease models and can also prevent neuronal damage during glutamate excitotoxity (Cardona et al., 2006; Limatola and Ransohoff, 2014). The protective effect of fractalkine against glutamate excitotoxicity appears to involve a reduction in NMDA- or glutamate-mediated rise in intracellular calcium levels (Deiva et al., 2004; Sheridan et al., 2014), reduced AMPA type mediated currents (Meucci et al., 1998; Limatola et al., 2005; Ragozzino et al., 2006), increased glutamate removal from synaptic cleft by enhancing the expression of function of glutamate transporter-1 (GLT-1) on astrocytes (Catalano et al., 2013), and increased microglial adenosine release (Lauro et al., 2008; Cipriani et al., 2011). In addition, CX_3CL1 can also modulate the clearance and phagocytic activity of microglia (Noda et al., 2011) that could be involved in the neuroprotective effects of CX_3CL1 in CNS disorders. Mice lacking CX_3CR1 develop increased disease severity in animal models of experimental autoimmune encephalomyelitis (EAE), low-endotoxemia, Parkinson's disease, Amyotrophic lateral sclerosis, and Diabetic retinopathy (Cardona et al., 2006, 2015; Mendiola et al., 2017). To a certain degree, such pathology is attributed to enhanced microglial expression of inflammatory cytokines like IL-1β, TNF-α, and IL-6. Our previous work reported an increased expression of IL-1β in the injured cochlea of mice lacking CX_3CR1 (Kaur et al., 2018). Future efforts toward understanding the mechanisms of fractalkine-mediated synaptic repair and neuroprotection may lead to therapeutic strategies for regeneration of synapses and neuroprotection in the injured cochlea.

Several animal studies have shown that neurotrophin therapies can partially regenerate damaged synapses and restore hearing after noise trauma (Wan et al., 2014; Suzuki et al., 2016; Chen et al., 2018). However, such partial effectiveness clearly demonstrates an additional need to understand the cellular and molecular mechanisms of neurite outgrowth and synapse regeneration to develop therapies to fully restore hearing. Our study has identified a novel endogenous immune pathway that may promote synaptic repair and neuron survival during hearing loss. Future studies investigating the contribution of activation of fractalkine signaling in degeneration and repair of cochlear synapses and determining the function of each fractalkine isoform (membrane or soluble) are necessary to completely understand the role of fractalkine in cochlear synaptopathy and neuropathy. Our research work also poses important clinical relevance for humans carrying the polymorphic variant $CX_3CR1^{I249/M280}$ that is estimated to be present in about 20–30% of the population. These changes in human CX_3CR1 decrease CX_3CL1 affinity (McDermott et al., 2001) and have been associated with multiple neurodegenerative disorders such as age-related macular degeneration (Chan et al., 2005; Schaumberg et al., 2014), Alzheimer's disease (Lopez-Lopez et al., 2017), and multiple sclerosis (Arli et al., 2013; Cardona et al., 2018). Based on the evidence of enhanced synaptic and neuronal damage in the injured cochlea of CX_3CR1-deficient mice, it would be of clinical relevance to dissect the effects of human $CX_3CR1^{V249/T280}$ receptor and its polymorphic variant $CX_3CR1^{I249/M280}$ in deaf ears. Such studies may merit evaluation as risk factors for susceptibility to sensorineural hearing loss. Together, our data suggest a pivotal role of CX_3CL1-CX_3CR1 signaling in repair of damaged synapses and neuron survival after noise trauma. Thus, modulating fractalkine signaling may be a relevant approach to mitigate cochlear synaptopathy and neuropathy.

DATA AVAILABILITY

The datasets generated for this study are available on request to the corresponding author.

ETHICS STATEMENT

This study was carried out in accordance with the recommendations of the Animal Welfare Act and Animal Welfare Regulations issued by the United States Department of Agriculture (USDA). All experimental protocols were approved by the Institutional Animal Care and Use Committee of the Washington University School of Medicine (St. Louis, MO, United States).

AUTHOR CONTRIBUTIONS

TK and KO designed and planned the study. TK, AC, AN, and KO performed the experiments and analyzed the data. AS performed the mouse genotyping. TK, MW, and KO contributed to the writing and editing of the manuscript. All authors read and approved the submitted version of the manuscript.

FUNDING

This work was supported by the National Institutes of Health and the National Institute on Deafness and Other Communication Disorders Grants R03DC015320 to TK and R01DC006283 to MW. This work was a part of the R03 grant funded to TK. Funds from R01DC006283 (MW) partly supported mouse breeding, maintenance, and genotyping.

ACKNOWLEDGMENTS

We thank Dr. Mark A. Rutherford (Assistant Professor, Department of Otolaryngology, Washington University St. Louis) for providing training with cochlear ribbon synapse immunolabeling.

SUPPLEMENTARY MATERIAL

The Supplementary Material for this article can be found online at: https://www.frontiersin.org/articles/10.3389/fnins.2019.00620/full#supplementary-material

TABLE S1 | Raw values of ABR wave 1 amplitudes against level series.

REFERENCES

Abiega, O., Beccari, S., Diaz-Aparicio, I., Nadjar, A., Layé, S., and Leyrolle, Q. (2016). Neuronal hyperactivity disturbs atp microgradients, impairs microglial motility, and reduces phagocytic receptor expression triggering apoptosis/microglial phagocytosis uncoupling. *PLoS Biol.* 14:e1002466. doi: 10.1371/journal.pbio.1002466

Araujo, D. M., and Cotman, C. W. (1993). Trophic effects of interleukin-4, -7 and -8 on hippocampal neuronal cultures: potential involvement of glial-derived factors. *Brain Res.* 600, 49–55. doi: 10.1016/0006-8993(93)90400-h

Arli, B., Irkec, C., Menevse, S., Yilmaz, A., and Alp, E. (2013). Fractalkine gene receptor polymorphism in patients with multiple sclerosis. *Int. J. Neurosci.* 123, 31–37. doi: 10.3109/00207454.2012.723079

Batchelor, P. E., Liberatore, G. T., Wong, J. Y., Porritt, M. J., Frerichs, F., Donnan, G. A., et al. (1999). Activated macrophages and microglia induce dopaminergic sprouting in the injured striatum and express brain derived neurotrophic factor and glial cell line-derived neurotrophic factor. *J. Neurosci.* 19, 1708–1716. doi: 10.1523/jneurosci.19-05-01708.1999

Biber, K., Laurie, D. J., Berthele, A., Sommer, B., Tölle, T. R., Gebicke-Härter, P. J., et al. (1999). Expression and signaling of group I metabotropic glutamate receptors in astrocytes and microglia. *J. Neurochem.* 72, 1671–1680. doi: 10.1046/j.1471-4159.1999.721671.x

Bruce-Keller, A. J. (1999). Microglial-neuronal interactions in synaptic damage and recovery. *J. Neurosci. Res.* 58, 191–201. doi: 10.1002/(sici)1097-4547(19991001)58:1<191::aid-jnr17>3.0.co;2-e

Cardona, A. E., Pioro, E. P., Sasse, M. E., Kostenko, V., Cardona, S. M., and Dijkstra, I. M. (2006). Control of microglial neurotoxicity by the fractalkine receptor. *Nat. Neurosci.* 9, 917–924. doi: 10.1038/nn1715

Cardona, S. M., Kim, S. V., Church, K. A., Torres, V. O., Cleary, I. A., and Mendiola, A. S. (2018). Role of the fractalkine receptor in CNS autoimmune inflammation: new approach utilizing a mouse model expressing the human CX3CR1I249/M280 variant. *Front. Cell. Neurosci.* 12:365. doi: 10.3389/fncel.2018.00365

Cardona, S. M., Mendiola, A. S., Yang, Y. C., Adkins, S. L., Torres, V., and Cardona, A. E. (2015). Disruption of fractalkine signaling leads to microglial activation and neuronal damage in the diabetic retina. *ASN Neuro.* 7, doi: 10.1177/1759091415608204

Catalano, M., Lauro, C., Cipriani, R., Chece, G., Ponzetta, A., Di Angelantonio, S., et al. (2013). CX3CL1 protects neurons against excitotoxicity enhancing GLT-1 activity on astrocytes. *J. Neuroimmunol.* 263, 75–82. doi: 10.1016/j.jneuroim.2013.07.020

Chan, C. C., Tuo, J., Bojanowski, C. M., Csaky, K. G., and Green, W. R. (2005). Detection of CX3CR1 single nucleotide polymorphism and expression on archived eyes with age-related macular degeneration. *Histol. Histopathol.* 20, 857–863. doi: 10.14670/HH-20.857

Chapman, G. A., Moores, K., Harrison, D., Campbell, C. A., Stewart, B. R., and Strijbos, P. J. (2000). Fractalkine cleavage from neuronal membranes represents an acute event in the inflammatory response to excitotoxic brain damage. *J. Neurosci.* 20:RC87.

Chen, H., Xing, Y., Xia, L., Chen, Z., Yin, S., and Wang, J. (2018). AAV-mediated NT-3 overexpression protects cochleae against noise-induced synaptopathy. *Gene Ther.* 25, 251–259. doi: 10.1038/s41434-018-0012-0

Cipriani, R., Villa, P., Chece, G., Lauro, C., Paladini, A., Micotti, E., et al. (2011). CX3CL1 is neuroprotective in permanent focal cerebral ischemia in rodents. *J. Neurosci.* 31, 16327–16335. doi: 10.1523/JNEUROSCI.3611-11.2011

Deiva, K., Geeraerts, T., Salim, H., Leclerc, P., Héry, C., Hugel, B., et al. (2004). Fractalkine reduces N-methyl-d-aspartate-induced calcium flux and apoptosis in human neurons through extracellular signal-regulated kinase activation. *Eur. J. Neurosci.* 20, 3222–3232. doi: 10.1111/j.1460-9568.2004.03800.x

Eybalin, M. (1993). Neurotransmitters and neuromodulators of the mammalian cochlea. *Physiol. Rev.* 73, 309–373. doi: 10.1152/physrev.1993.73.2.309

Eyo, U. B., Peng, J., Swiatkowski, P., Mukherjee, A., Bispo, A., and Wu, L. J. (2014). Neuronal hyperactivity recruits microglial processes via neuronal NMDA receptors and microglial P2Y12 receptors after status epilepticus. *J. Neurosci.* 34, 10528–10540. doi: 10.1523/JNEUROSCI.0416-14.2014

Garton, K. J., Gough, P. J., Blobel, C. P., Murphy, G., Greaves, D. R., Dempsey, P. J., et al. (2001). Tumor necrosis factor-alpha converting enzyme (ADAM17) mediates the cleavage and shedding of fractalkine (CX3CL1). *J. Biol. Chem.* 276, 37993–38001. doi: 10.1074/jbc.M106434200

Gil-Loyzaga, P., and Pujol, R. (1990). Neurotoxicity of kainic acid in the rat cochlea during early developmental stages. *Eur. Arch. Otorhinolaryngol.* 248, 40–48. doi: 10.1007/bf00634780

Hakuba, N., Koga, K., Gyo, K., Usami, S. I., and Tanaka, K. (2000). Exacerbation of noise-induced hearing loss in mice lacking the glutamate transporter GLAST. *J. Neurosci.* 20, 8750–8753. doi: 10.1523/jneurosci.20-23-08750.2000

Harrison, J. K., Jiang, Y., Chen, S., Xia, Y., Maciejewski, D., McNamara, R. K., et al. (1998). Role for neuronally derived fractalkine in mediating interactions between neurons and CX3CR1-expressing microglia. *Proc. Natl. Acad. Sci. U.S.A.* 95, 10896–10901. doi: 10.1073/pnas.95.18.10896

Haskell, C. A., Cleary, M. D., and Charo, I. F. (1999). Molecular uncoupling of fractalkine-mediated cell adhesion and signal transduction. Rapid flow arrest of CX3CR1-expressing cells is independent of G-protein activation. *J. Biol. Chem.* 274, 10053–10058. doi: 10.1074/jbc.274.15.10053

Haynes, S. E., Hollopeter, G., Yang, G., Kurpius, D., Dailey, M. E., Gan, W. B., et al. (2006). The P2Y12 receptor regulates microglial activation by extracellular nucleotides. *Nat. Neurosci.* 9, 1512–1519. doi: 10.1038/nn1805

Henry, K. R., and Chole, R. A. (1980). Genotypic differences in behavioral, physiological and anatomical expressions of age-related hearing loss in the laboratory mouse. *Audiology* 19, 369–383. doi: 10.3109/00206098009070071

Hequembourg, S., and Liberman, M. C. (2001). Spiral ligament pathology: a major aspect of age-related cochlear degeneration in C57BL/6 mice. *J. Assoc. Res. Otolaryngol.* 2, 118–129. doi: 10.1007/s101620010075

Hermand, P., Pincet, F., Carvalho, S., Ansanay, H., Trinquet, E., Daoudi, M., et al. (2008). Functional adhesiveness of the CX3CL1 chemokine requires its aggregation. Role of the transmembrane domain. *J. Biol. Chem.* 283, 30225–30234. doi: 10.1074/jbc.M802638200

Heumann, R., Lindholm, D., Bandtlow, C., Meyer, M., Radeke, M. J., Misko, T. P., et al. (1987). Differential regulation of mRNA encoding nerve growth factor and its receptor in rat sciatic nerve during development, degeneration, and regeneration: role of macrophages. *Proc. Natl. Acad. Sci. U.S.A.* 84, 8735–8739. doi: 10.1073/pnas.84.23.8735

Hirose, K., Discolo, C. M., Keasler, J. R., and Ransohoff, R. (2005). Mononuclear phagocytes migrate into the murine cochlea after acoustic trauma. *J. Comp. Neurol.* 489, 180–194. doi: 10.1002/cne.20619

Honda, S., Sasaki, Y., Ohsawa, K., Imai, Y., Nakamura, Y., Inoue, K., et al. (2001). Extracellular ATP or ADP induce chemotaxis of cultured microglia through Gi/o-coupled P2Y receptors. *J. Neurosci.* 21, 1975–1982. doi: 10.1523/jneurosci.21-06-01975.2001

Imai, T., Hieshima, K., Haskell, C., Baba, M., Nagira, M., Nishimura, M., et al. (1997). Identification and molecular characterization of fractalkine receptor CX3CR1, which mediates both leukocyte migration and adhesion. *Cell* 91, 521–530. doi: 10.1016/s0092-8674(00)80438-9

Jung, S., Aliberti, J., Graemmel, P., Sunshine, M. J., Kreutzberg, G. W., Sher, A., et al. (2000). Analysis of fractalkine receptor CX3CR1 function by targeted deletion and green fluorescent protein reporter gene insertion. *Mol. Cell. Biol.* 20, 4106–4114. doi: 10.1128/mcb.20.11.4106-4114.2000

Kato, G., Inada, H., Wake, H., Akiyoshi, R., Miyamoto, A., Eto, K., et al. (2016). Microglial Contact Prevents Excess Depolarization and Rescues Neurons from Excitotoxicity. *eNeuro* 3:ENEURO.0004–ENEURO.16. doi: 10.1523/ENEURO.0004-16.2016

Kaur, T., Ohlemiller, K. K., and Warchol, M. E. (2018). Genetic disruption of fractalkine signaling leads to enhanced loss of cochlear afferents following ototoxic or acoustic injury. *J. Comp. Neurol.* 526, 824–835. doi: 10.1002/cne.24369

Kaur, T., Zamani, D., Tong, L., Rubel, E. W., Ohlemiller, K. K., Hirose, K., et al. (2015). Fractalkine signaling regulates macrophage recruitment into the cochlea and promotes the survival of spiral ganglion neurons after selective hair cell lesion. *J. Neurosci.* 35, 15050–15061. doi: 10.1523/JNEUROSCI.2325-15.2015

Kim, K. W., Vallon-Eberhard, A., Zigmond, E., Farache, J., Shezen, E., Shakhar, G., et al. (2011). In vivo structure/function and expression analysis of the CX3C chemokine fractalkine. *Blood* 118, e156–e167. doi: 10.1182/blood-2011-04-348946

Kim, K. X., Payne, S., Yang-Hood, A., Li, S. Z., Davis, B., and Carlquist, J. (2019). Vesicular glutamatergic transmission in noise-induced loss and repair

of cochlear ribbon synapses. *J. Neurosci.* 2228–2218. doi: 10.1523/JNEUROSCI.2228-18.2019 [Epub ahead of Print].

Kujawa, S. G., and Liberman, M. C. (2009). Adding insult to injury: cochlear nerve degeneration after "temporary" noise-induced hearing loss. *J. Neurosci.* 29, 14077–14085. doi: 10.1523/JNEUROSCI.2845-09.2009

Kujawa, S. G., and Liberman, M. C. (2015). Synaptopathy in the noise-exposed and aging cochlea: Primary neural degeneration in acquired sensorineural hearing loss. *Hear. Res.* 330(Pt B), 191–199. doi: 10.1016/j.heares.2015.02.009

Lauro, C., Catalano, M., Di Paolo, E., Chece, G., de Costanzo, I., Trettel, F., et al. (2015). Fractalkine/CX3CL1 engages different neuroprotective responses upon selective glutamate receptor overactivation. *Front. Cell. Neurosci.* 8:472. doi: 10.3389/fncel.2014.00472

Lauro, C., Cipriani, R., Catalano, M., Trettel, F., Chece, G., Brusadin, V., et al. (2010). Adenosine A1 receptors and microglial cells mediate CX3CL1-induced protection of hippocampal neurons against Glu-induced death. *Neuropsychopharmacology* 35, 1550–1559. doi: 10.1038/npp.2010.26

Lauro, C., Di Angelantonio, S., Cipriani, R., Sobrero, F., Antonilli, L., Brusadin, V., et al. (2008). Activity of adenosine receptors type 1 is required for CX3CL1-mediated neuroprotection and neuromodulation in hippocampal neurons. *J. Immunol.* 180, 7590–7596. doi: 10.4049/jimmunol.180.11.7590

Lazarov-Spiegler, O., Solomon, A. S., Zeev-Brann, A. B., Hirschberg, D. L., Lavie, V., and Schwartz, M. (1996). Transplantation of activated macrophages overcomes central nervous system regrowth failure. *FASEB J.* 10, 1296–1302. doi: 10.1096/fasebj.10.11.8836043

Liberman, M. C. (2017). Noise-induced and age-related hearing loss: new perspectives and potential therapies. *F1000Res.* 6:927. doi: 10.12688/f1000research.113

Limatola, C., Lauro, C., Catalano, M., Ciotti, M. T., Bertollini, C., Di Angelantonio, S., et al. (2005). Chemokine CX3CL1 protects rat hippocampal neurons against glutamate mediated excitotoxicity. *J. Neuroimmunol.* 166, 19–28. doi: 10.1016/j.jneuroim.2005.03.023

Limatola, C., and Ransohoff, R. M. (2014). Modulating neurotoxicity through CX3CL1/CX3CR1 signaling. *Front. Cell. Neurosci.* 8:229. doi: 10.3389/fncel.2014.00229

Lin, H. W., Furman, A. C., Kujawa, S. G., and Liberman, M. C. (2011). Primary neural degeneration in the guinea pig cochlea after reversible noise-induced threshold shift. *J. Assoc. Res. Otolaryngol.* 12, 605–616. doi: 10.1007/s10162-011-0277-0

Liu, G. J., Nagarajah, R., Banati, R. B., and Bennett, M. R. (2009). Glutamate induces directed chemotaxis of microglia. *Euro. J. Neurosci.* 29, 1108–1118. doi: 10.1111/j.1460-9568.2009.06659.x

Liu, W., Molnar, M., Garnham, C., Benav, H., and Rask-Andersen, H. (2018). Macrophages in the human cochlea: saviors or predators-a study using super-resolution immunohistochemistry. *Front. Immunol.* 9:223. doi: 10.3389/fimmu.2018.00223

Lopez-Lopez, A., Gelpi, E., Lopategui, D. M., and Vidal-Taboada, J. M. (2017). Association of the CX3CR1-V249I variant with neurofibrillary pathology progression in late-onset Alzheimer's disease. *Mol. Neurobiol.* 55, 2340–2349. doi: 10.1007/s12035-017-0489-3

McDermott, D. H., Halcox, J. P., Schenke, W. H., Waclawiw, M. A., Merrell, M. N., Epstein, N., et al. (2001). Association between polymorphism in the chemokine receptor CX3CR1 and coronary vascular endothelial dysfunction and atherosclerosis. *Circ. Res.* 89, 401–407. doi: 10.1161/hh1701.095642

Mendiola, A. S., Garza, R., Cardona, S. M., Mythen, S. A., Lira, S. A., Akassoglou, K., et al. (2017). Fractalkine Signaling attenuates perivascular clustering of microglia and fibrinogen leakage during systemic inflammation in mouse models of diabetic retinopathy. *Front. Cell. Neurosci.* 10:303. doi: 10.3389/fncel.2016.00303

Meucci, O., Fatatis, A., Simen, A. A., Bushell, T. J., Gray, P. W., and Miller, R. J. (1998). Chemokines regulate hippocampal neuronal signaling and gp120 neurotoxicity. *Proc. Nat.l Acad. Sci. of U.S.A.* 95, 14500–14505. doi: 10.1073/pnas.95.24.14500

Noda, M., Doi, Y., Liang, J., Kawanokuchi, J., Sonobe, Y., Takeuchi, H., et al. (2011). Fractalkine attenuates excito-neurotoxicity via microglial clearance of damaged neurons and antioxidant enzyme heme oxygenase-1 expression. *J. Biol. Chem.* 286, 2308–2319. doi: 10.1074/jbc.m110.169839

Prewitt, C. M., Niesman, I. R., Kane, C. J., and Houlé, J. D. (1997). Activated macrophage/microglial cells can promote the regeneration of sensory axons into the injured spinal cord. *Exp. Neurol.* 148, 433–443. doi: 10.1006/exnr.1997.6694

Puel, J. L. (1995). Chemical synaptic transmission in the cochlea. *Prog. Neurobiol.* 47, 449–476. doi: 10.1016/0301-0082(95)00028-3

Puel, J. L., Pujol, R., Tribillac, F., Ladrech, S., and Eybalin, M. (1994). Excitatory amino acid antagonists protect cochlear auditory neurons from excitotoxicity. *J. Comparat. Neurol.* 341, 241–256. doi: 10.1002/cne.903410209

Puel, J. L., Ruel, J., Gervais d'Aldin, C., and Pujol, R. (1998). Excitotoxicity and repair of cochlear synapses after noise-trauma induced hearing loss. *Neuroreport* 9, 2109–2114. doi: 10.1097/00001756-199806220-00037

Puel, J. L., Saffiedine, S., Gervais d'Aldin, C., Eybalin, M., and Pujol, R. (1995). Synaptic regeneration and functional recovery after excitotoxic injury in the guinea pig cochlea. *C R Acad. Sci. III.* 318, 67–75.

Pujol, R., Lenoir, M., Robertson, D., Eybalin, M., and Johnstone, B. M. (1985). Kainic acid selectively alters auditory dendrites connected with cochlear inner hair cells. *Hear. Res.* 18, 145–151. doi: 10.1016/0378-5955(85)90006-1

Pujol, R., and Puel, J. L. (1999). Excitotoxicity, synaptic repair, and functional recovery in the mammalian cochlea: a review of recent findings. *Ann. N. Y. Acad. Sci.* 884, 249–254. doi: 10.1111/j.1749-6632.1999.tb08646.x

Pujol, R., Puel, J. L., Gervais d'Aldin, C., and Eybalin, M. (1993). Pathophysiology of the glutamatergic synapses in the cochlea. *Acta Otolaryngol.* 113, 330–334. doi: 10.3109/00016489309135819

Ragozzino, D., Di Angelantonio, S., Trettel, F., Bertollini, C., Maggi, L., Gross, C., et al. (2006). Chemokine fractalkine/CX3CL1 negatively modulates active glutamatergic synapses in rat hippocampal neurons. *J. Neurosci.* 26, 10488–10498. doi: 10.1523/JNEUROSCI.3192-06.2006

Roseti, C., Fucile, S., Lauro, C., Martinello, K., Bertollini, C., Esposito, V., et al. (2013). Fractalkine/CX3CL1 modulates GABAA currents in human temporal lobe epilepsy. *Epilepsia* 54, 1834–1844. doi: 10.1111/epi.12354

Ruan, Q., Ao, H., He, J., Chen, Z., Yu, Z., Zhang, R., et al. (2014). Topographic and quantitative evaluation of gentamicin-induced damage to peripheral innervation of mouse cochleae. *Neurotoxicology* 40, 86–96. doi: 10.1016/j.neuro.2013.11.002

Ruel, J., Emery, S., Nouvian, R., Bersot, T., Amilhon, B., Van Rybroek, J. M., et al. (2008). Impairment of SLC17A8 encoding vesicular glutamate transporter-3, vglut3, underlies nonsyndromic deafness dfna25 and inner hair cell dysfunction in null mice. *Am. J. Human Genetics* 83, 278–292. doi: 10.1016/j.ajhg.2008.07.008

Ruel, J., Wang, J., Rebillard, G., Eybalin, M., Lloyd, R., Pujol, R., et al. (2007). Physiology, pharmacology and plasticity at the inner hair cell synaptic complex. *Hear. Res.* 227, 19–27. doi: 10.1016/j.heares.2006.08.017

Schaumberg, D. A., Rose, L., DeAngelis, M. M., Semba, R. D., Hageman, G. S., and Chasman, D. I. (2014). Prospective study of common variants in CX3CR1 and risk of macular degeneration: pooled analysis from 5 long-term studies. *JAMA Ophthalmol.* 132, 84–95. doi: 10.1001/jamaophthalmol.2013.5506

Seal, R. P., Akil, O., Yi, E., Weber, C. M., Grant, L., Yoo, J., et al. (2008). Sensorineural Deafness and seizures in mice lacking vesicular glutamate transporter 3. *Neuron* 57, 263–275. doi: 10.1016/j.neuron.2007.11.032

Sheridan, G. K., Wdowicz, A., Pickering, M., Watters, O., Halley, P., O'Sullivan, N. C., et al. (2014). CX3CL1 is up-regulated in the rat hippocampus during memory-associated synaptic plasticity. *Front. Cell. Neurosci.* 12:233. doi: 10.3389/fncel.2014.00233

Shi, L., Liu, K., Wang, H., Zhang, Y., Hong, Z., Wang, M., et al. (2015). Noise induced reversible changes of cochlear ribbon synapses contribute to temporary hearing loss in mice. *Acta Otolaryngol.* 135, 1093–1102. doi: 10.3109/00016489.2015.1061699

Simard, A. R., and Rivest, S. (2007). Neuroprotective effects of resident microglia following acute brain injury. *J. Comparat. Neurol.* 504, 716–729. doi: 10.1002/cne.21469

Suzuki, J., Corfas, G., and Liberman, M. C. (2016). Round-window delivery of neurotrophin 3 regenerates cochlear synapses after acoustic overexposure. *Sci. Rep.* 6:24907. doi: 10.1038/srep24907

Telang, R. S., Paramananthasivam, V., Vlajkovic, S. M., Munoz, D. J., Housley, G. D., and Thorne, P. R. (2010). Reduced P2x(2) receptor-mediated regulation of endocochlear potential in the ageing mouse cochlea. *Purinergic Signal* 6, 263–272. doi: 10.1007/s11302-010-9195-6

Vinet, J., Weering, H. R., Heinrich, A., Kälin, R. E., Wegner, A., Brouwer, N., et al. (2012). Neuroprotective function for ramified microglia in hippocampal excitotoxicity. *J. Neuroinflammation* 9:27. doi: 10.1186/1742-2094-9-27

Wan, G., Gómez-Casati, M. E., Gigliello, A. R., Liberman, M. C., and Corfas, G. (2014). Neurotrophin-3 regulates ribbon synapse density in the cochlea and induces synapse regeneration after acoustic trauma. *eLife* 3:e03564. doi: 10.7554/eLife.03564

Wang, Q., and Green, S. H. (2011). Functional role of neurotrophin-3 in synapse regeneration by spiral ganglion neurons on inner hair cells after excitotoxic trauma in vitro. *J. Neurosci.* 31, 7938–7949. doi: 10.1523/JNEUROSCI.1434-10.2011

Zhang, X. M., and Zhu, J. (2011). Kainic Acid-induced neurotoxicity: targeting glial responses and glia-derived cytokines. *Curr. Neuropharmacol.* 9, 388–398. doi: 10.2174/157015911795596540

Conflict of Interest Statement: The authors declare that the research was conducted in the absence of any commercial or financial relationships that could be construed as a potential conflict of interest.

frontiers in Neurology

ORIGINAL RESEARCH
published: 25 June 2019
doi: 10.3389/fneur.2019.00665

Defining the Inflammatory Microenvironment in the Human Cochlea by Perilymph Analysis: Toward Liquid Biopsy of the Cochlea

Athanasia Warnecke[1,2*†], *Nils K. Prenzler*[1†], *Heike Schmitt*[1,2], *Kerstin Daemen*[3], *Jana Keil*[3], *Martin Dursin*[1], *Thomas Lenarz*[1,2†] *and Christine S. Falk*[3†]

[1] *Department of Otolaryngology, Hannover Medical School, Hanover, Germany,* [2] *Cluster of Excellence of the German Research Foundation (DFG; "Deutsche Forschungsgemeinschaft") "Hearing4all", Oldenburg, Germany,* [3] *Hannover Medical School, Institute of Transplant Immunology, Hanover, Germany*

OPEN ACCESS

Edited by:
Isabel Varela-Nieto, Spanish National Research Council (CSIC), Spain

Reviewed by:
Vincent Van Rompaey, University of Antwerp, Belgium
Daniel John Brown, Curtin University, Australia

***Correspondence:**
Athanasia Warnecke
warnecke.athanasia@mh-hannover.de

[†] *These authors have contributed equally to this work*

Specialty section:
This article was submitted to Neuro-Otology, a section of the journal Frontiers in Neurology

Received: *27 April 2019*
Accepted: *06 June 2019*
Published: *25 June 2019*

Citation:
Warnecke A, Prenzler NK, Schmitt H, Daemen K, Keil J, Dursin M, Lenarz T and Falk CS (2019) Defining the Inflammatory Microenvironment in the Human Cochlea by Perilymph Analysis: Toward Liquid Biopsy of the Cochlea. Front. Neurol. 10:665. doi: 10.3389/fneur.2019.00665

The molecular pathomechanisms in the majority of patients suffering from acute or progressive sensorineural hearing loss cannot be determined yet. The size and the complex architecture of the cochlea make biopsy and in-depth histological analyses impossible without severe damage of the organ. Thus, histopathology correlated to inner disease is only possible after death. The establishment of a technique for perilymph sampling during cochlear implantation may enable a liquid biopsy and characterization of the cochlear microenvironment. Inflammatory processes may not only participate in disease onset and progression in the inner ear, but may also control performance of the implant. However, little is known about cytokines and chemokines in the human inner ear as predictive markers for cochlear implant performance. First attempts to use multiplex protein arrays for inflammatory markers were successful for the identification of cytokines, chemokines, and endothelial markers present in the human perilymph. Moreover, unsupervised cluster and principal component analyses were used to group patients by lead cytokines and to correlate certain proteins to clinical data. Endothelial and epithelial factors were detected at higher concentrations than typical pro-inflammatory cytokines such as TNF-a or IL-6. Significant differences in VEGF family members have been observed comparing patients with deafness to patients with residual hearing with significantly reduced VEGF-D levels in patients with deafness. In addition, there is a trend toward higher IGFBP-1 levels in these patients. Hence, endothelial and epithelial factors in combination with cytokines may present robust biomarker candidates and will be investigated in future studies in more detail. Thus, multiplex protein arrays are feasible in very small perilymph samples allowing a qualitative and quantitative analysis of inflammatory markers. More results are required to advance this method for elucidating the development and course of specific inner ear diseases or for perioperative characterization of cochlear implant patients.

Keywords: hearing loss, neuroinflammation, cochlear implantation, cytokines, chemokines, endothelial factors, perilymph

INTRODUCTION

The inner ear harbors the sensory organs responsible for balance and hearing. For many decades, the inner ear was assumed to be an immune-privileged organ because the blood-labyrinth barrier largely excludes major systemic components of the inflammatory response from the cochlear microenvironment (1). Despite this tight junction blood-labyrinth barrier and the absence of a lymphatic drainage, classical local, and systemic inflammatory mechanisms have been identified in the cochlea. The responsiveness of some types of rapidly progressing hearing loss to steroids and immunosuppressive treatment (2) was the first discovery to challenge the idea of the cochlea as an immune-privileged organ. It was acknowledged that antibody- as well as T cell-mediated responses are involved in the onset or progression of some types of hearing loss (3). In addition, myeloid cells have been identified in several compartments of the murine inner ear, including the stria vascularis (4), the spiral ligament (5), and the spiral ganglion (5). Acute damage to the murine inner ear caused by noise or ototoxic medication was shown to induce inflammation (6, 7) and to increase cochlear macrophages and neutrophils in the stria vascularis and the spiral ganglion (4, 8). Live imaging of adult mouse utricles revealed a phagocytic removal of cellular debris initiated by supporting cells following structural and cellular damage (9). An up regulation of immune-related genes in the murine cochlea has been also reported after noise exposure (10).

In general, three types of immune responses can be differentiated based on the involvement of various immune cells and soluble immune mediators (SIM): the innate immune system, which may be involved rather early in the onset of inflammatory responses and the adaptive specific immune system at later stages associated with disease progression. In the absence of infection, a third type of immune response coined sterile inflammation may be initiated after cell damage leading to an inflammatory response of the tissue. Cells of the innate immune system can sense microorganisms and viruses by pattern-recognition receptors (PRRs) enabling the detection of bacterial and fungal cell-wall components and viral nucleic acids termed as conserved pathogen-associated molecular patterns (PAMPs) (11, 12). This leads to further recruitment of innate effector cells, i.e., neutrophils, monocytes/macrophages, dendritic cells, and natural killer cells, to the inflammatory site and this process is mainly mediated by inflammatory chemokines (13). In contrast, the adaptive T cell-mediated immune response is initiated after sensing of PAMPs by PRRs and antigen presentation, i.e., peptides in the context of major histocompatibility complex (MHC), particularly by dendritic cells (12). Migration of antigen presenting cells (APC) into the draining lymph node is important for activation of antigen (pathogen) -specific effector and helper T cells and antibody-producing B cells, respectively (13). However, in the absence of infection, it is currently unknown whether and how immune activation may be involved in the development of deafness.

One potential mechanism could be sensing of danger associated molecular pattern (DAMPs), which are mainly DNA, nuclear, and heat shock proteins released from damaged tissue cells by innate immune cells. Hence, sterile cell death or tissue injury can induce inflammation related to innate immune responses to pathogens (11). Usually, DAMPs are removed intracellularly under physiological conditions and remain undetected by the immune system. However, pathological conditions such as injury or oxidative stress lead to the release of DAMPs that might be extracellular in the first line such as fragments of the extracellular matrix that occur after severe damage or by proteases activated to promote tissue repair and remodeling (11).

In general, cochlear implantation causes trauma by opening of the cochlea and insertion of an electrode array. As a consequence, immunological and tissue repair mechanisms may occur and result in severe damage of the residual cochlear structural and ultrastructural components (14–17). Clinically, this results in loss of residual hearing after cochlear implantation (18–20). After damage, tumor necrosis factor alpha (TNF-α) was shown to be expressed and released by cells of the stria vascularis and the spiral ligament (8) and stimulate a cascade of cytokine and chemokine expression leading to recruitment of immune cells and further damage. Actually, anti-inflammatory therapeutics like glucocorticoids are administered alongside implantation to reduce trauma and rescue residual organ function, however, with minimal long-term efficacy (21). Suppression of inflammatory pathways may trigger compensatory responses by activation of alternative pathways (22) since inflammation is a necessary reaction protecting the organ from excessive damage (22). Also, there is increasing evidence that excessive activation of the glucocorticoid pathway can be neurotoxic (23–26). Alternative therapeutic interventions should, therefore, aim at stabilizing the local cochlear environment by balancing endogenous pro- and anti-inflammatory reactions, thus, allowing full resolution of inflammation and recovery of organ homeostasis that results in preservation of residual organ structures and improved speech perception (1).

Autologous bone marrow-derived mononuclear cells can release immunomodulative factors and have a highly protective effect on cochlear cells as shown in previous work (27). In order to advance such therapeutic approaches to daily clinical routine, information about the inflammatory microenvironment of the individual cochlea that is implanted would be helpful. Since tissue sampling from the inner ear is not possible without excessive damage and loss of the organ, we have developed a liquid biopsy by collecting human perilymphatic fluid from the inner ear (28). This can be easily performed since the round window membrane is the natural sealing of the cochlear perilymphatic space. Since the round window will be opened anyway to allow insertion of the electrode array during cochlear implantation, it is not critical to puncture the round window membrane just prior to the opening by a microcapillary allowing the atraumatic collection of the inner ear fluid by capillary forces.

In the present study, we used this approach to analyse perilymph samples with an array of inflammatory markers resembling SIM involved in innate and the adaptive immune responses or sterile tissue inflammation as well as epithelial and endothelial regulators and to correlate these with residual cochlear function prior to cochlear implantation.

TABLE 1 | Overview of demographic data of CI patients.

	All patients ($n = 44$)	Pts. with surditas (SDT) $n = 37$	Residual hearing (<80 db) $n = 7$	*P*-value
Age (mean; range)	45.2 (0.7–87.1)	43.12 ± 4.8	56.0 ± 6.4	0.27 (n.s.)
Sex (m/f) percentages	26/18 (59/41%)	15/12 (56/44%)	5/2 (71/29%)	

MATERIALS AND METHODS

The present study has been approved by the institutional ethical committee (approval no. 1883–2013). Perilymph was collected after written informed consent from the patients (in case of pediatric patients from their parents) receiving cochlear implantation between 09/17 and 05/18. A total of 43 patients (one being implanted bilaterally in two surgical sessions 3 weeks apart) resulting in a total of 44 perilymph samples were included. The collected sample volumes ranged from 1 to 4 μl. Demographic data of the patients are summarized in **Table 1**.

Perilymph Sampling

Human perilymph was collected with a customized glass microcapillary during cochlear implantation. For perilymph collection, the round window membrane was exposed by removal of its bony overhang and the intact membrane was punctured with the ultrathin and sharp tip of the glass capillary directly before the insertion of the electrode array. The collection was performed without any suctioning just by capillary forces. This resulted in different volumes of perilymph. The samples were left in the capillary and immediately transferred into a petri dish placed on ice. After transfer to the laboratory, the capillaries were connected to a pipette and the fluid was pipetted into small vials for freezing at −80°C until evaluation with a multiplex protein array.

Classification of Patients by Audiogram Data

All patients assigned to cochlear implantation were evaluated audiologically with a defined battery of tests according to our and international standards. Pure tone audiometry (PTA) was performed prior to surgery only in adults and kids at school age. Additionally, otoacoustic emissions, auditory brainstem responses, and electrocochleography were performed in each patient pre-operatively.

The pre-operative audiograms were used to classify patients into two groups: Patients with no residual hearing with averages in PTA of 80 dB or higher at three contiguous frequencies (250, 500, and 750 Hz). Patients with PTA threshold of <80 dB were considered as having residual hearing. In children, the responses in ABR were used for the classification and all small children included had no ABR responses. The etiology of hearing loss was unknown in the majority of the patients. Six patients had congenital severe hearing loss, eight patients congenital onset of hearing loss with progression over time and late onset hearing loss with progression was observed in 13 cases. Menière's disease ($n = 2$), meningitis ($n = 2$), vestibular schwannoma ($n = 1$), and otosclerosis were among the known etiologies. One patient suffered from congenital hearing loss and glucogen storage disease type 1, one from progressive hearing loss and myasthenia gravis. Repeated attacks of sudden sensorineural hearing loss were reported by six patients and two patients suffered from single sided deafness.

Quantification of Cytokine, Chemokine, and Tissue Factors Using Multiplex Protein Arrays

Concentrations of SIM and epithelial and endothelial factors were determined using Luminex-based multiplex arrays, i.e., human 27-Plex (M500KCAF0Y, BioRad, Hercules California, USA), and Cancer Panel 2 (171AC600M, BioRad) in a miniaturized variant of the manufacturer's instructions. As little as 1–2 μl of perilymph fluid were diluted with sample diluent (1:20) and incubated with multiplex beads for 45 min followed by two washings steps, cocktail of biotinylated secondary mAbs for 30 min and after final washing steps, streptavidin-PE was added. Greater than fifty beads per sample per analyte were detected using the BioPlex Manager 6.2 Software and concentrations were calculated according to individual standard curves for each analyte ranging from ∼20 ng/ml to the detection limit of ∼2 pg/ml.

Unsupervised Cluster and Principal Component Analyses

The complete dataset of 43 analytes from 44 perilymph samples was analyzed using Qlucore Omics Explorer (Version 3.3, Lund, Sweden). Data were log2 transformed, scaled to mean zero, variable one, and threshold of 0.01. Discriminating variables were determined using linear models and multigroup ANOVA comparisons.

Descriptive Statistical Analyses

D'Agostino-Pearson omnibus normality test was used to assess data distribution. Statistical analyses were performed as indicated in figure legends with $p < 0.05$ considered significant. All statistical analyses were calculated with GraphPad Prism (Version 6.07, La Jolla, USA).

RESULTS

Tissue factors and SIM were detectable in all perilymph samples of the 44 patients demonstrating the feasibility of the multiplex technology for small volumes below 5 μl perilymph fluid. A list of all proteins included in the human 27-plex and Cancer Panel 2 arrays is given in **Table 2**. Of note, a homogeneous concentration range was observed in all samples with the insulin-like growth factor binding protein 1 (IGFBP1) and the plasminogen activator inhibitor 1 (PAI-1) at very high concentrations (>1,000 pg/ml) followed by four proteins higher than 500 pg/ml, i.e., the cytokine IL-6, the granulocyte-macrophage colony stimulating factor (GM-CSF), the IL-1 receptor antagonist (IL-1RA), and

TABLE 2 | A list of all proteins included in the human 27-plex and cancer panel 2 arrays.

Human 27-plex	Cancer panel 2
FGF basic	Angiopoietin-2
Eotaxin	sCD40L
G-CSF	EGF
GM-CSF	Endoglin
IFN-γ	sFASL
IL-1β	HB-EGF
IL-1ra	IGFBP-1
L-2	IL-6
IL-4-IL10	IL-8
IL-12 (p70)	IL-18
IL-13	PAI-1
IL-15	PLGF
IL-17A	TGF-α
IP-10	TNF-α
MCP-1 (MCAF)	uPA
MIP-1α	VEGF-A
MIP-1β	VEGF-C
PDGF-BB	VEGF-D
RANTES	
TNF-α	
VEGF	

vascular endothelial growth factor A (VEGF-A) (**Figures 1A,B**). Together with high concentrations of the urokinase plasminogen activator (uPA), the ratio of PAI-1/uPA (mean ratio 20.3) showed a remarkably homogenous distribution (**Figure 1B**). Additional endothelial and epithelial factors were detected at high concentrations between 100 and 500 pg/ml of VEGF-D, -C, endoglin, epidermal growth factor (EGF), fibroblast-growth factor beta (FGF-β), and IL-18, a caspase-1 dependent indicator of cell damage. This pattern further supported a tissue-related microenvironment within perilymph fluid accompanied by several immune activation markers like the soluble Fas (CD95) ligand (sFasL), the chemokine CCL2 (MCP-1), responsible for recruitment of myeloid cells, and the granulocyte colony stimulating factor G-SCF in the same concentration range. Of note, the classical cytokine regulators of T cell function like IL-9, IL-10, IL-12p70, IL-15, IL-17, TNF-α, and the soluble CD40 ligand (sCD40L) were detectable at concentrations below 100 pg/ml along with typical inflammatory chemokines like CXCL8, CXCL10, and CCL4 indicating a low but detectable degree of both innate and adaptive immune activation. Within this intermediate group, the pro-inflammatory innate cytokine IL-1β was detected at remarkable concentrations (mean 51.5 pg/ml), which was balanced by a 10-fold excess of IL-1RA (mean concentration 566.3 pg/ml). The low concentration group (<100 pg/ml) comprised T cell cytokines like IL-2, IL-4, IL-7, IL-13, IFN-γ, chemokines (CCL3, CCL5) as well as endothelial factors (Ang-2, HB-EGF, TGF-a) arguing rather for a tightly regulated specific microenvironment composed by tissue factors and selected SIM in cochlear perilymph fluid than for an uncontrolled pro-inflammatory milieu. While most proteins showed a homogeneous, though not always gaussean distribution, a bimodal distribution could be observed for others like IGFBP-1, VEGF-D, IL-1β, and IL-6.

In order to exclude an impact of age on the composition of the cochlear microenvironment, a correlation matrix was calculated for all proteins vs. age with only minor negative correlations for sFasL (Spearman r −0.456), VEGF-C (Spearman r −0.3105), and FGF-b (Spearman r −0.34), and G-CSF (Spearman r −0.31, **Supplementary Table 1**). In addition, unsupervised hierarchical cluster and principal component analyses (PCA) revealed no correlation between age or gender and individual or particular groups of SIM or tissue factors within perilymph fluid (data not shown).

Unsupervised hierarchical clustering and PCA methods with $p < 0.05$ and $q < 0.1$ ANOVA settings were applied to group patients according to the lead cytokines IL-1β and IL-6 and the epithelial protein IGFBP-1, respectively (**Figures 2A,B**). With this approach, patients could be assigned to one of the following groups defined by significantly higher concentrations of IGFBP1, IL-1β, IL-6, or none of these (**Figure 2C**). Although these three proteins were clustered in the heat map shown in **Figure 2A**, they were not coregulated in the patients since they displayed elevated levels only in the IGFBP1, IL-1b, or IL-6 group, respectively. Therefore, the different patterns seem to be characteristic for patient subgroups, which indicates diverse pathways of inflammation and tissue repair/regeneration, finally leading to complete or progressive sensorineural hearing loss.

In order to uncover patterns related to residual hearing, CI patients were grouped into 37 individuals with no residual hearing as defined above as surditas (SDT) and seven patients with some residual hearing prior to implantation (RH, **Figure 3**). Among all tested proteins, significant differences were only detected for VEGF-D, IL-13, and IL-9 with lower VEGF-D levels in patients with no residual hearing compared to the group of patients with residual hearing ($^{**}p < 0.01$; **Figure 3A**). In contrast, IL-13 and IL-9 concentrations were higher in patients with complete deafness (surditas, SDT) compared to patients with residual hearing ($^{*}p < 0.05$; **Figure 3A**) although statistical significance was missed for IL-9 ($p = 0.058$). In contrast to VEGF-D, the other two ligands of VEGFR1/2, i.e., VEGF-A and -C did not differ between patients with complete or partial deafness (**Figure 3B**). Despite the broad concentration range of IGFBP1, a tendency was observed toward an increased concentration in patients with complete deafness, which was accompanied by a higher, though non-significantly, PAI-1/uPa ratio due to higher PAI-1 levels (data not shown). These patterns further support the idea of different pathways associated with progression of hearing loss and, hence, the possibility to identify biomarker candidates with relevance also for future treatment strategies in the course of implantation.

DISCUSSION

The approach of a multiplex-based protein analysis of human inner ear fluid was shown to be feasible and depicts a progress

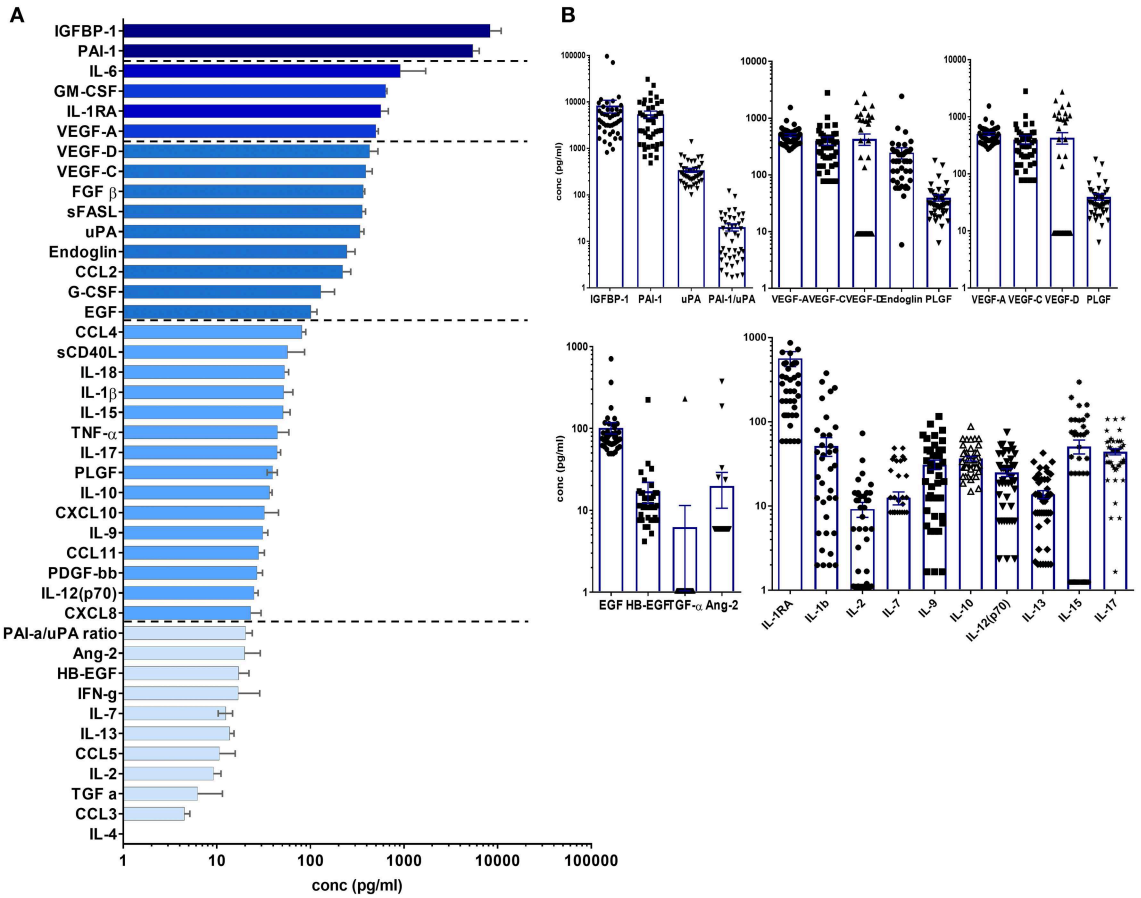

FIGURE 1 | Cytokine/chemokine and tissue factor composition of human perilymph fluid. **(A)** Human perilymph fluid comprises high concentrations of epithelial and endothelial proteins like IGFPB1, VEGF-A,-C,-D, some innate cytokines like IL-6, followed by chemokines and typical cytokines of the adaptive immune system like IFN-g, I-17, etc. Concentrations were determined from $n = 44$ perilymph samples, median concentrations ± SEM are displayed in a waterfall plot. **(B)** In order to show that most proteins were detected in all patient, the concentrations of individual proteins are shown for each sample using log scale graphs.

in hearing research where generally animal models were used. Here, we present an analytical method for the simultaneous detection and quantification of currently 43, but in the future up to 100 cytokines, chemokines, epithelial, and endothelial factors in tiny volumes of human perilymph. Surprisingly, the microenvironment in perilymph fluid was composed primarily by proteins regulating endothelial and epithelial functions followed by chemokines and cytokines (**Figure 1A**). With this strategy, we can characterize patterns of different immune responses allowing the definition of the cochlear inflammatory state in patients in which we can access the inner ear at the time of cochlear implantation. Some of the surgical approaches for the treatment of disorders affecting the inner ear enable collection of human perilymph and several centres use this technique for proteomics, metabolomics and microRNA detection (28–32). However, none of these previously reported techniques would allow the direct and simultaneous quantification of inflammatory and tissue markers.

Among the factors with the highest concentration, we identified regulators of tissue repair and angiogenesis along with inflammatory factors. The highly prevalent protein IGFBP1 regulates the action of insulin-like growth factor (IGF-1) by either enhancing or inhibiting its activity (33). IGF-1 plays a key role in embryonic and post-natal development of the cochlea (34) and has been identified as strong protective agent for hair cells (35). Indeed, local application of recombinant human IGF-1 was shown to be effective for the treatment and prevention of noise-induced hearing loss in guinea pigs (36) and in rats (37). Therefore, the broad range of IGFBP1 in CI patients indicates a tight regulation of the IGF receptor system. In addition, a synergy of the growth factors IGF-1 and EPO for acute neuroprotection by activation of the PI3-K-Akt pathway in cell culture experiments (33) has been described.

Plasminogen activator inhibitor-1 (PAI-1) is a pro-coagulant that is released by platelets and the endothelium in response to inflammation, damage, or ischemia and can be used as early marker for endothelial injury based on its inhibitory function of urokinase-like plasminogen activator (uPA) (38). Elevations of PAI-1 in bronchiolar lavage fluid is associated with experimentally-induced pulmonary fibrosis after thoracic

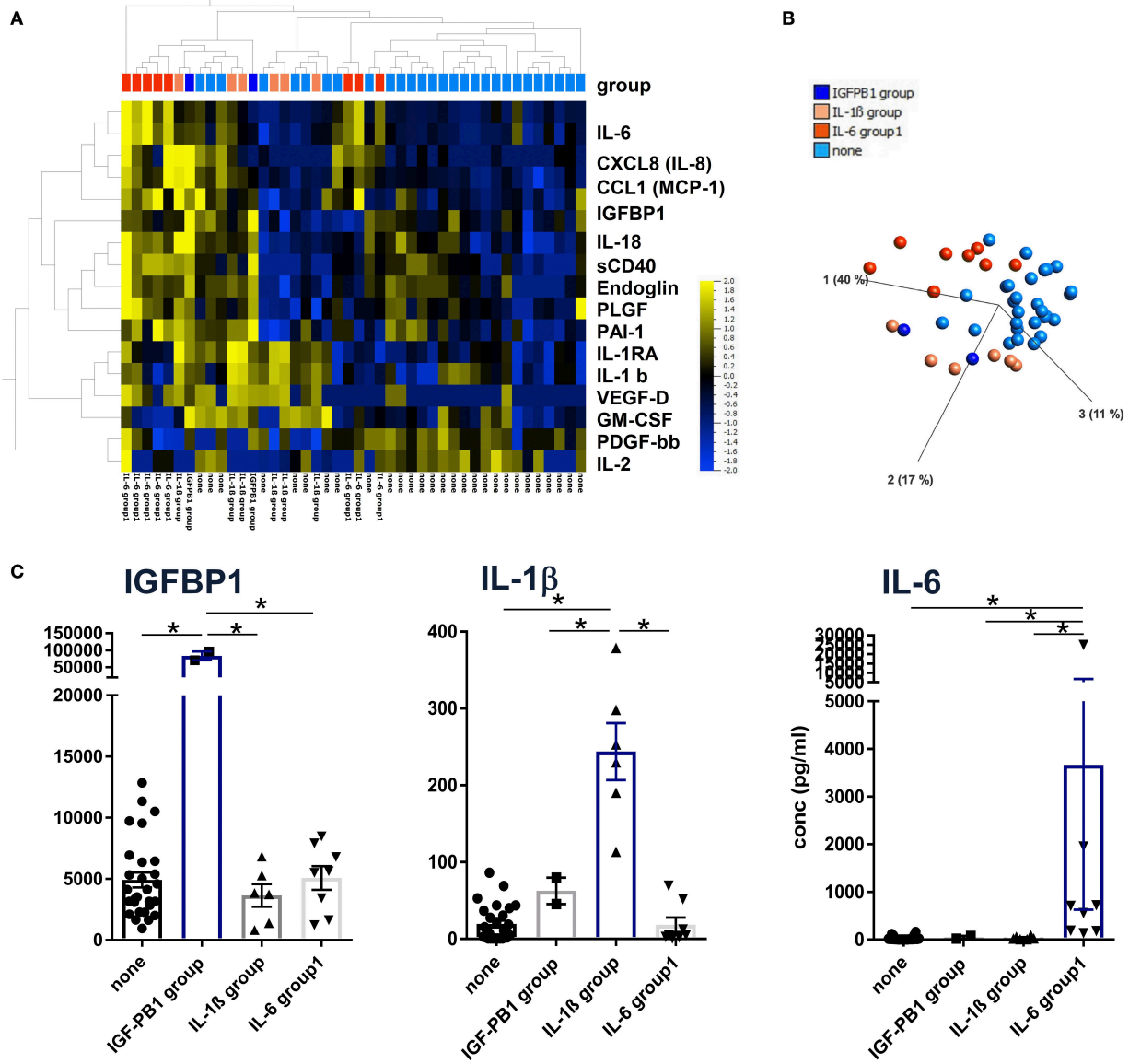

FIGURE 2 | Definition of patient subgroups according to hierarchical clustering, principal component analyses. **(A)** Concentrations of 43 proteins from 44 perilymph samples were log-normalized with a threshold of 0.01 and filtered to $p < 0.05$ with $q = 0.2$ and visualized using hierarchical cluster and **(B)** PCA algorithms (Qlucore Omics 3.6 Software). Patient subgroups were defined by significantly high IGFBP1, IL-1b, and IL-6 concentrations, respectively, indicated by the color code shown in **(B)**. **(C)** Descriptive statistics were applied to the four patient groups using raw protein concentrations and Kruskal-Wallis tests with $p < 0.05$ defined as significant and marked with an asterisk (*).

radiation exposure (39) and in patients with lethal acute respiratory distress syndrome (40). Thus, the presence of PAI-1, uPA, and the high PAI-1/uPA ratio (>10) in perilymph may be an indicator for cochlear distress and damage. In our prior study, PAI-1 was detected by mass spectrometry only in one perilymph sample of a patient with hepatitis C infection and otosclerosis (28) underlying the hypothesis for an inflammation indicator in perilymph. Tissue plasminogen activator (tPA) and uPA cleave plasminogen to the serine protease plasmin (41). Plasmin is the most significant protease that cleaves pro-neurotrophins to the active neurotrophins, thus providing trophic support to auditory neurons and stabilization of synapses (41). PAI-1 inhibits tPA and uPA and whether the increased presence of PAI-1 in perilymph might be an indicator of cochlear health needs further evaluation.

Interleukin1-receptor antagonist (IL-1RA) is a potent factor to reverse effects mediated by the pro-inflammatory cytokines interleukin 1α and β in many diseases. For example, in an animal model of tendinopathy, IL1-RA can reduce pathological changes (42). Increased levels of IL1-RA can be used as a predictor for cardiovascular mortality in patients with acute coronary syndrome or stable angina (43). Recombinant IL-1RA (Anakinra) is a useful treatment for several autoimmune diseases.

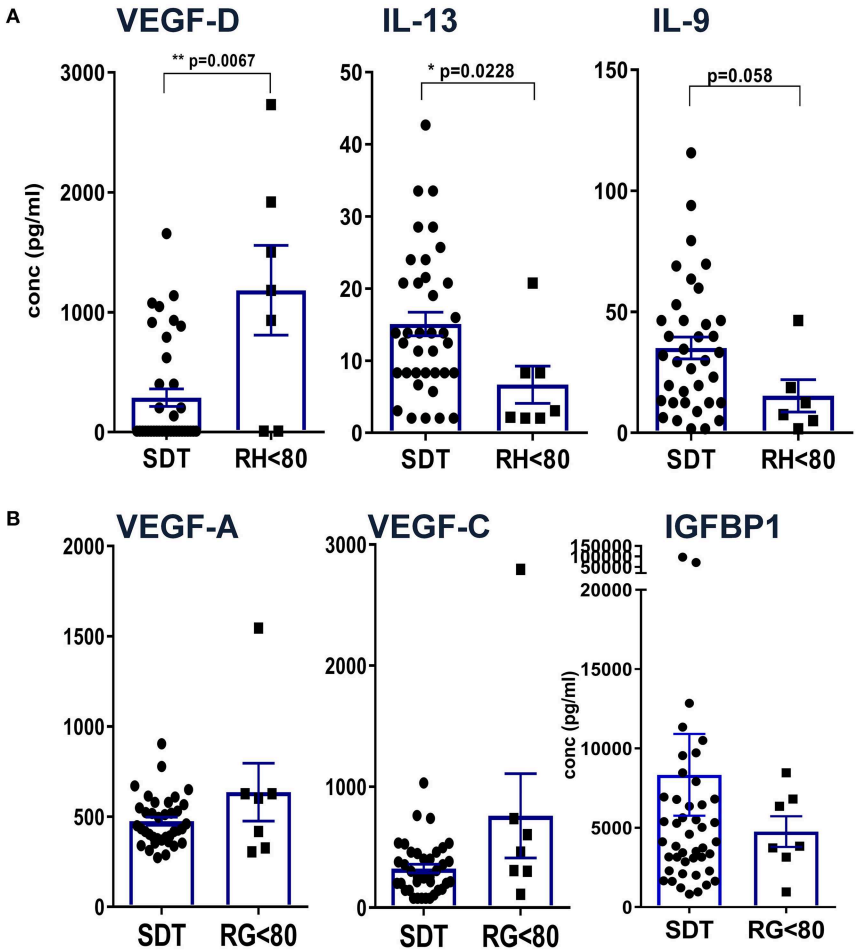

FIGURE 3 | Definition of differences between patients with complete hearing loss vs. residual hearing capacity. Patients were grouped according to their acoustical performance at the time of CI with a hearing cut-off of <80 for patients with residual hearing (RH) vs. complete deafness (surditas SDT). Mann-Whitney-*u*-tests were performed for **(A)** VEGF-D, IL-13, and IL-9 and **(B)** VEGF-A, -C, and IGFBP1, respectively, with differences $p < 0.05$ defined as significant and marked with (*) and $p < 0.001$ with (**).

However, the role of IL1-RA in the inner ear is unclear to date and in this specialized compartment it could act as anti-fibrotic agent in CI and the risk of consecutive fibrosis needs thorough investigation.

Interleukin 6 initiates classical innate inflammatory pathways and, furthermore, inhibits neuronal proliferation and differentiation, thus decreasing neurogenesis in the adult brain (44). In the course of infections, IL-6 is necessary for B cell development into plasma cells and their antibody production. Of note, IL-6 expression from inner ear fibrocytes can be triggered by TNFα (45, 46). In a mouse model, elevated IL-6 levels exacerbated CMV-related cytotoxic and inflammatory injury of the inner ear (47). Therefore, IL-6 levels in human perilymph fluid may be involved in causing hearing deficits associated with infections or other inflammatory cascades.

Adhesion molecules and endothelial factors are also involved in inner ear repair and regeneration. Especially VEGF family members induce vascular neogenesis and increases the permeability of the blood-brain-barrier (48). In our study, comparing patients with complete deafness to patients with residual hearing, there was no difference in the concentrations of VEGF-A and -C but VEGF-D was reduced in patients with deafness. VEGF-A was the first discovered form of the vascular endothelial growth factors and is a potent regulator of angiogenesis. It is secreted by a variety of cells upon oxygen deprivation (49) causing cell proliferation, apoptosis inhibition, increased vascular permeability, and recruitment of inflammatory cells (50–52). By contrast, VEGF-C and VEGF-D have a central role in lymphangiogenesis with little function in vasculogenesis via binding to VEFR2 and 3 (53). Interestingly, the expression of VEGF is increased after damage to the inner ear (54, 55). Reduced levels of VEGF-D in patients with complete deafness compared to patients with some residual hearing may be an indicator for on-going damage and reduced repair in the inner ear. It is also possible that the specific isoform VEGF-D may have protective effects on the inner ear although it has

been shown that VEGF without a distinction of its isoform has no protective effects on auditory hair cells (56). At present, we cannot define whether elevated VEGF-D levels may result from a compensatory mechanism that improves the capacity of the lymphatic vessels to remove fluid from the extravascular space (57).

Unexpectedly, higher IGFBP1 levels were measured in patients with complete loss of auditory function compared to patients with residual hearing. IGFBP1 represents an important regulator of insulin-like growth factors at the IGF receptor (58). Based on its general function for cell survival, the IGF pathway has been proposed as potential therapeutic target for the inner ear (59). Our previous finding of miRNAs involved in IGF signaling further supports the relevance of this pathway (32) along with this novel identification of another IGF regulator at the protein level.

The observation that classical Th1/Th2/Th17 cytokines were only detected at low concentrations compared to tissue factors and chemokines argues for a rather minor role of T cells for hearing loss at this late stage of cochlear implantation. Nevertheless, significantly higher concentrations of IL-13 and IL-9 were detected in perilymph of patients with complete loss compared to residual hearing, which would at least argue for an impact of Th2 and Th9 cytokines. Both cytokines can be induced by various stimuli including toxic substances via the aryl hydrocarbon receptor (AhR) that has recently been shown to act as transcription factor during development of the inner ear (60).

Taken together, our combined analysis of inflammatory and tissue regulatory proteins provides a more refined insight into the microenvironment of the inner ear. Several dysregulated pathways may lead to progressive sensorineural hearing loss and one possible scenario could be a combination of a toxic environment, sensed via AhR, further promoted under pro-inflammatory conditions and manifested by insufficient repair mechanisms that finally lead to complete deafness.

The following limitations of the presented study need to be taken into account. Contaminations with blood and cerebrospinal fluid (CSF) seem to be very unlike as discussed in our previous work (28). Surely, in the rare cases of a patent cochlear aqueduct, this may be different. Usually, such patients have a gusher and an increased yield of perilymph fluid during collection indicating the possibility of contamination with CSF. Among the patients included in this study, none had a gusher. Due to the small size of samples, the study is underpowered to analyse the association between cytokine networks and the degree of damage of the cochlea. Thus, this exploratory approach needs validation in large independent cohorts. In addition, only the baseline chemokine, cytokines, and growth factor profile can be assessed with the current perilymph sampling technology, not allowing for serial investigations. The study is also underpowered for any subgroup analyses due to the small size. Future studies will therefore, focus on the identification of cochlear inflammatory marker that are disease specific, represent the degree of the damage to the organ or may be even predictive for the performance that can be expected with a cochlear implant.

CONCLUSION

Multiplex protein analyses are feasible in very small samples (∼1 μl or less) of human perilymph fluid and is able to identify marker proteins of sterile inflammation as well as of the innate and adaptive immune system. Thus, this method may be advanced to a key perioperative characterization procedure for the inflammatory state of the cochlea in patients in need of cochlear implant. Knowledge about the state of the cochlea prior to implantation may offer an excellent tool for the deployment of novel adjuvant pharmacotherapies and may pave the avenue toward a new era of personalized medicine.

DATA AVAILABILITY

This manuscript contains previously unpublished data. The name of the repository and accession number are not available.

ETHICS STATEMENT

The present study has been approved by the institutional ethical committee (approval no. 1883–2013). Perilymph was collected after written informed consent from the patients (in case of pediatric patients from their parents) receiving cochlear implantation between 09/17 and 05/18.

AUTHOR CONTRIBUTIONS

AW and CF conception and design of the work, acquisition, analysis, interpretation of data for the work, drafting the work, and approval for publication of the content. NP and HS interpretation of data for the work, revising the manuscript critically for important intellectual content, and approval for publication of the content. KD and JK acquisition and analysis of data for the work and approval for publication of the content. MD and TL conception of the work, interpretation of data for the work, revising the manuscript critically for important intellectual content, and approval for publication of the content.

FUNDING

This work was funded by the Cluster of Excellence Hearing4all2.0 EXC 1077/2.

ACKNOWLEDGMENTS

The authors would like to thank Rolf Salcher and Kerstin Willenborg for the collection of perilymph samples in some of the patients.

SUPPLEMENTARY MATERIAL

The Supplementary Material for this article can be found online at: https://www.frontiersin.org/articles/10.3389/fneur.2019.00665/full#supplementary-material

REFERENCES

1. Fujioka M, Okano H, Ogawa K. Inflammatory and immune responses in the cochlea: potential therapeutic targets for sensorineural hearing loss. *Front. Pharmacol.* (2014) 5:287. doi: 10.3389/fphar.2014.00287
2. Brian F. Autoimmune sensorineural hearing loss. *Ann Otol Rhinol Laryngol.* (2004) 113:526–30. doi: 10.1177/000348940411300703
3. Okano T. Immune system of the inner ear as a novel therapeutic target for sensorineural hearing loss. *Front Pharmacol.* (2014) 5:205. doi: 10.3389/fphar.2014.00205
4. Zhang W, Dai M, Fridberger, A, Hassan A, Degagne J, Neng L, et al. Perivascular-resident macrophage-like melanocytes in the inner ear are essential for the integrity of the intrastrial fluid-blood barrier. *Proc Natl Acad Sci USA.* (2012) 109:10388–93. doi: 10.1073/pnas.1205210109
5. Sato E, Schick HE, Ransohoff RM, Hirose K. Repopulation of cochlear macrophages in murine hematopoietic progenitor cell chimeras: the role of CX3CR1. *J Comp Neurol.* (2008) 504:930–42. doi: 10.1002/cne.21583
6. Hirose K, Discolo CM, Keasler JR, Ransohoff R. Mononuclear phagocytes migrate into the murine cochlea after acoustic trauma. *J Comp Neurol.* (2005) 489:180–94. doi: 10.1002/cne.20619
7. Tornabene SV, Sato K, Pham L, Billings P, Keithley EM. Immune cell recruitment following acoustic trauma. *Hear Res.* (2006) 222:115–24. doi: 10.1016/j.heares.2006.09.004
8. Dinh CT, Goncalves S, Bas E, Van De Water TR, Zine A. Molecular regulation of auditory hair cell death and approaches to protect sensory receptor cells and/or stimulate repair following acoustic trauma. *Front Cell Neurosci.* (2015) 9:96. doi: 10.3389/fncel.2015.00096
9. Monzack EL, May LA, Roy S, Gale JE, Cunningham LL. Live imaging the phagocytic activity of inner ear supporting cells in response to hair cell death. *Cell Death Differ.* (2015) 22:1995–2005. doi: 10.1038/cdd.2015.48
10. Gratton MA, Eleftheriadou A, Garcia J, Verduzco E, Martin GK, Lonsbury–Martin BL, et al. Noise-induced changes in gene expression in the cochleae of mice differing in their susceptibility to noise damage. *Hear. Res.* (2011) 277:211–26. doi: 10.1016/j.heares.2010.12.014
11. Chen GY, Nuñez G. Sterile inflammation: sensing and reacting to damage. *Nat Rev Immunol.* (2010) 10:826–37. doi: 10.1038/nri2873
12. Iwasaki A, Medzhitov R. Control of adaptive immunity by the innate immune system. *Nat Immunol.* (2015) 16:343–53. doi: 10.1038/ni.3123
13. Esche C, Stellato C, Beck LA. Chemokines : key players in innate and adaptive immunity. *J Invest Dermatol.* (2005) 125:615–28. doi: 10.1111/j.0022-202X.2005.23841.x
14. Clark GM, Clark J, Cardamone T, Clarke M, Nielsen P, Jones R, et al. Biomedical studies on temporal bones of the first multi-channel cochlear implant patient at the University of Melbourne. *Cochlear Implants Int.* (2014) 15(Suppl 2):S1–15. doi: 10.1179/1754762814Y.0000000087
15. Ishai R, Herrmann BS, Nadol JB, Quesnel AM. The pattern and degree of capsular fibrous sheaths surrounding cochlear electrode arrays. *Hear Res.* (2017) 348:44–53. doi: 10.1016/j.heares.2017.02.012
16. Quesnel A, Nakajima H, Rosowski J, Hansen M, Gantz B, Nadol JB Jr. Delayed loss of hearing after hearing preservation cochlear implantation: Human temporal bone pathology and implications for etiology. *Hear Res.* (2015) 333:225–34. doi: 10.1016/j.heares.2015.08.018
17. Somdas MA, Li PM, Whiten DM, Eddington DK, Nadol JB Jr. Quantitative evaluation of new bone and fibrous tissue in the cochlea following cochlear implantation in the human. *Audiol Neurootol.* (2007) 12:277–84. doi: 10.1159/000103208
18. Astolfi L, Simoni E, Giarbini N, Giordano P, Pannella M, Hatzopoulos S, et al. Cochlear implant and inflammation reaction: safety study of a new steroid-eluting electrode. *Hear Res.* (2016) 336:44–52. doi: 10.1016/j.heares.2016.04.005
19. Bas E, Goncalves S, Adams M, Dinh CT, Bas JM, Van De Water TR, et al. Spiral ganglion cells and macrophages initiate neuro-inflammation and scarring following cochlear implantation. *Front Cell Neurosci.* (2015) 9:1–16. doi: 10.3389/fncel.2015.00303
20. Bas E, Gupta C, Van De Water TR. A novel organ of corti explant model for the study of cochlear implantation trauma. *Anat Rec (Hoboken).* (2012) 295:1944–56. doi: 10.1002/ar.22585
21. Kuthubutheen J, Joglekar S, Smith L, Friesen L, Smilsky K, Millman T, et al. The role of preoperative steroids for hearing preservation cochlear implantation: results of a randomized controlled trial. *Audiol Neurotol.* (2017) 22:292–302. doi: 10.1159/000485310
22. Kalinec GM, Lomberk G, Urrutia RA, Kalinec F. Resolution of cochlear inflammation: novel target for preventing or ameliorating drug-, noise- and age-related hearing loss. *Front Cell Neurosci.* (2017) 11:192. doi: 10.3389/fncel.2017.00192
23. Dumas TC, Gillette T, Ferguson D, Hamilton K, Sapolsky RM. Anti-glucocorticoid gene therapy reverses the impairing effects of elevated corticosterone on spatial memory, hippocampal neuronal excitability, and synaptic plasticity. *J Neurosci.* (2010) 30:1712–20. doi: 10.1523/JNEUROSCI.4402-09.2010
24. Pomara C, Neri M, Bello S, Fiore C, Riezzo I, Turillazzi E. Neurotoxicity by Synthetic androgen steroids: oxidative stress, apoptosis, and neuropathology: a review. *Curr Neuropharmacol.* (2015) 13:132–45. doi: 10.2174/1570159X13666141210221434
25. Roy M, Sapolsky RM. The exacerbation of hippocampal excitotoxicity by glucocorticoids is not mediated by apoptosis. *Neuroendocrinology.* (2003) 77:24–31. doi: 10.1159/000068337
26. Singer W, Kasini K, Manthey M, Eckert P, Armbruster P, Vogt MA, et al. The glucocorticoid antagonist mifepristone attenuates sound-induced long-term deficits in auditory nerve response and central auditory processing in female rats. *FASEB J.* (2018) 32:3005–19. doi: 10.1096/fj.201701041RRR
27. Roemer A, Köhl U, Majdani O, Klöß S, Falk C, Haumann S, et al. Biohybrid cochlear implants in human neurosensory restoration. *Stem Cell Res Ther.* (2016) 7:148. doi: 10.1186/s13287-016-0408-y
28. Schmitt HA, Pich A, Schröder A, Scheper V, Lilli G, Reuter G, et al. Proteome analysis of human perilymph using an intraoperative sampling method. *J. Proteome Res.* (2017) 16:1911–23. doi: 10.1021/acs.jproteome.6b00986
29. Mavel S, Emond P, Dufour-Rainfray D, Lefèvre A, Bakhos D, Blasco H. Validation of metabolomics analysis of human perilymph fluid using liquid chromatography-mass spectroscopy. *Hear Res.* (2018) 367:129–36. doi: 10.1016/j.heares.2018.05.016
30. Rasmussen JE, Laurell G, Rask-Andersen H, Bergquist J, Eriksson PO. The proteome of perilymph in patients with vestibular schwannoma. A possibility to identify biomarkers for tumor associated hearing loss? *PLoS ONE.* (2018) 13:1–16. doi: 10.1371/journal.pone.0198442
31. Schmitt H, Roemer A, Zeilinger C, Salcher R, Durisin M, Staecker H, et al. Heat shock proteins in human perilymph: implications for cochlear implantation. *Otol Neurotol.* (2018) 39:37–44. doi: 10.1097/MAO.0000000000001625
32. Shew M, Warnecke A, Lenarz T, Schmitt H, Gunewardena S, Staecker H. Feasibility of microRNA profiling in human inner ear perilymph. *Neuroreport.* (2018) 29:894–901. doi: 10.1097/WNR.0000000000001049
33. Digicaylioglu M, Garden G, Timberlake S, Fletcher L, Lipton SA. Acute neuroprotective synergy of erythropoietin and insulin-like growth factor I. *Proc Natl Acad Sci USA.* (2004) 101:9855–60. doi: 10.1073/pnas.0403172101
34. Camarero G, Avendano C, Fernandez-Moreno C, Villar A, Contreras J, de Pablo F, et al. Delayed inner ear maturation and neuronal loss in postnatal Igf-1-deficient mice. *J Neurosci.* (2001) 21:7630–41. doi: 10.1523/JNEUROSCI.21-19-07630.2001
35. Hayashi Y, Yamamoto N, Nakagawa T, Ito J. Insulin-like growth factor 1 induces the transcription of Gap43 and Ntn1 during hair cell protection in the neonatal murine cochlea. *Neurosci Lett.* (2014) 560:7–11. doi: 10.1016/j.neulet.2013.11.062
36. Lee KY, Nakagawa T, Okano T, Hori R, Ono K, Tabata Y, et al. Novel therapy for hearing loss: delivery of insulin-like growth factor 1 to the cochlea using gelatin hydrogel. *Otol Neurotol.* (2007) 28:976–81. doi: 10.1097/MAO.0b013e31811f40db
37. Iwai K, Nakagawa T, Endo T, Matsuoka Y, Kita T, Kim T-S, et al. Cochlear protection by local insulin-like growth factor-1 application using biodegradable hydrogel. *Laryngoscope.* (2006) 116:529–33. doi: 10.1097/01.mlg.0000200791.77819.eb
38. Farrell D, Rowell S, Hinson H, Dewey E, Condron M, Lealiiee L, et al. The procoagulant molecule plasminogen activator inhibitor-1 is associated with injury severity and shock in patients with and without

traumatic brain injury. *J Trauma Acute Care Surg*. (2018) 85:888–93. doi: 10.1097/ta.0000000000002040
39. Shioya S, Masuda T, Senoo T, Horimasu Y, Miyamoto S, Nakashima T, et al. Plasminogen activator inhibitor-1 serves an important role in radiation-induced pulmonary fibrosis. *Exp Ther Med*. (2018) 16:3070–6. doi: 10.3892/etm.2018.6550
40. Wang Y, Wang H, Zhang C, Zhang C, Yang H, Gao R, et al. Lung fluid biomarkers for acute respiratory distress syndrome: a systematic review and meta-analysis. *Crit Care*. (2019) 23:1–15. doi: 10.1186/s13054-019-2336-6
41. Lu B, Pang PT, Woo NH. The yin and yang of neurotrophin action. *Nat Rev Neurosci*. (2005) 6:603–14. doi: 10.1038/nrn1726
42. Eskildsen SM, Berkoff DJ, Kallianos SA, Weinhold PS. The use of an IL1-receptor antagonist to reverse the changes associated with established tendinopathy in a rat model. *Scand J Med Sci Sports*. (2019) 29:82–8. doi: 10.1111/sms.13310
43. Schofer N, Ludwig S, Rübsamen N, Schnabel R, Lackner KJ, Ruprecht HJ, et al. Prognostic impact of Interleukin-1 receptor antagonist in patients with documented coronary artery disease. *Int J Cardiol*. (2018) 257:24–9. doi: 10.1016/j.ijcard.2018.01.055
44. Kong X, Gong Z, Zhang L, Sun X, Ou Z, Xu B, et al. JAK2/STAT3 signaling mediates IL-6-inhibited neurogenesis of neural stem cells through DNA demethylation/methylation. *Brain Behav Immun*. (2019) 79, 159–173. doi: 10.1016/j.bbi.2019.01.027
45. Maeda K, Yoshida K, Ichimiya I, Suzuki M. Dexamethasone inhibits tumor necrosis factor-α-induced cytokine secretion from spiral ligament fibrocytes. *Hear Res*. (2005) 202:154–60. doi: 10.1016/j.heares.2004.08.022
46. Yoshida K, Ichimiya I, Suzuki M, Mogi G. Effect of proinflammatory cytokines on cultured spiral ligament fibrocytes. *Hear Res*. (1999) 137:155–9. doi: 10.1016/S0378-5955(99)00134-3
47. Yuehua Q, Longzhen Z, Kailin X, Lingyu Z, Lingjian M, Jun W, et al. Inflammatory lesions of cochlea in murine cytomegalovirus-infected mice with hearing loss. *Cell Biochem Biophys*. (2012) 62:281–7. doi: 10.1007/s12013-011-9292-3
48. John GR, Zameer A, Zhang Y, Gurfein BT, Argaw AT. VEGF-mediated disruption of endothelial CLN-5 promotes blood-brain barrier breakdown. *Proc Natl Acad Sci USA*. (2009) 106:1977–82. doi: 10.1073/pnas.0808698106
49. Jeong H-J, Kim J-B, Hong S-H, An N-H, Kim M-S, Park B-R, et al. Vascular endothelial growth factor is regulated by hypoxic stress via MAPK and HIF-1 alpha in the inner ear. *J Neuroimmunol*. (2005) 163:84–91. doi: 10.1016/j.jneuroim.2005.02.019
50. Ferrara N. Vascular endothelial growth factor: basic science and clinical progress. *Endocr Rev*. (2004) 25:581–611. doi: 10.1210/er.2003-0027
51. Takahashi H, Shibuya M. The vascular endothelial growth factor (VEGF)/VEGF receptor system and its role under physiological and pathological conditions. *Clin Sci (Lond)*. (2005) 109:227–41. doi: 10.1042/CS20040370
52. Tjwa M, Luttun A, Autiero M, Carmeliet P. VEGF and PlGF: two pleiotropic growth factors with distinct roles in development and homeostasis. *Cell Tissue Res*. (2003) 314:5–14. doi: 10.1007/s00441-003-0776-3
53. Melincovici CS, Boşca AB, Suşman S, Mărginean M, Mihu C, Istrate M, et al. Vascular endothelial growth factor (VEGF) – key factor in normal and pathological angiogenesis. *Rom J Morphol Embryol*. (2018) 59:455–67.
54. Picciotti PM, Fetoni AR, Paludetti G, Wolf FI, Torsello A, Troiani D, et al. Vascular endothelial growth factor (VEGF) expression in noise-induced hearing loss. *Hear Res*. (2006) 214:76–83. doi: 10.1016/j.heares.2006.02.004
55. Yang D, Zhou H, Zhang J, Liu L. Increased endothelial progenitor cell circulation and VEGF production in a rat model of noise-induced hearing loss. *Acta Otolaryngol*. (2015) 135:622–8. doi: 10.3109/00016489.2014.1003092
56. Monge Naldi A, Gassmann M, Bodmer D. Erythropoietin but not VEGF has a protective effect on auditory hair cells in the inner ear. *Cell Mol Life Sci*. (2009) 66:3595–9. doi: 10.1007/s00018-009-0144-x
57. Berntsson J, Smith JG, Johnson LSB, Söderholm M, Borné Y, Melander O, et al. Increased vascular endothelial growth factor D is associated with atrial fibrillation and ischaemic stroke. *Heart heartjnl*. (2018) 105:553–558. doi: 10.1136/heartjnl-2018-313684
58. Frost RA, Tseng L. Insulin-like growth factor-binding protein-1 is phosphorylated by cultured human endometrial stromal cells and multiple protein kinases *in vitro*. *J Biol Chem*. (1991) 266:18082–8.
59. Yamamoto N, Nakagawa T, Ito J. Application of insulin-like growth factor-1 in the treatment of inner ear disorders. *Front Pharmacol*. (2014) 5:208. doi: 10.3389/fphar.2014.00208
60. Perl K, Shamir R, Avraham KB. Computational analysis of mRNA expression profiling in the inner ear reveals candidate transcription factors associated with proliferation, differentiation, and deafness. *Hum Genomics*. (2018) 12:30. doi: 10.1186/s40246-018-0161-7

Conflict of Interest Statement: The authors declare that the research was conducted in the absence of any commercial or financial relationships that could be construed as a potential conflict of interest.

frontiers in Neurology

ORIGINAL RESEARCH
published: 10 July 2019
doi: 10.3389/fneur.2019.00728

Human Inner Ear Immune Activity: A Super-Resolution Immunohistochemistry Study

*Wei Liu, Charlotta Kämpfe Nordström, Niklas Danckwardt-Lilliestöm and Helge Rask-Andersen**

Section of Otolaryngology, Department of Surgical Sciences, Uppsala University Hospital, Uppsala, Sweden

Background: Like the brain, the human inner ear was long thought to be devoid of immune activity. Only the endolymphatic sac (ES) was known to be endowed with white blood cells that could process antigens and serve as an immunologic defense organ for the entire inner ear. Unexpectedly, the cochlear and vestibular organs, including the eighth cranial nerve, were recently shown to contain macrophages whose functions and implication in ear disease are somewhat undefined. Here, we review recent inner ear findings in man and extend the analyses to the vestibular nerve using super-resolution structured illumination microscopy (SR-SIM).

Materials and Methods: Human ESs and cochleae were collected during surgery to treat patients with vestibular schwannoma and life-threatening petro-clival meningioma compressing the brainstem. The ESs and cochleae were placed in fixative, decalcified, and rapidly frozen and cryostat sectioned. Antibodies against ionized calcium-binding adaptor molecule 1-expressing cells (IBA1 cells), laminin β2 and type IV collagen TUJ1, cytokine fractalkine (CX3CL1), toll-like receptor 4 (TLR4), CD68, CD11b, CD4, CD8, the major histocompatibility complex type II (MHCII), and the microglial marker TEME119 were used.

Results: IBA1-positive cells were present in the ESs, the cochlea, central and peripheral axons of the cochlear nerve, and the vestibular nerve trunk. IBA1 cells were found in the cochlear lateral wall, spiral limbus, and spiral ganglion. Notable variants of IBA1 cells adhered to neurons with "synapse-like" specializations and cytoplasmic projections. Slender IBA1 cells occasionally protracted into the basal lamina of the Schwann cells and had intimate contact with surrounding axons.

Discussion: The human eighth nerve may be under the control of a well-developed macrophage cell system. A small number of CD4+ and CD8+ cells were found in the ES and occasionally in the cochlea, mostly located in the peripheral region of Rosenthal's canal. A neuro-immunologic axis may exist in the human inner ear that could play a role in the protection of the auditory nerve. The implication of the macrophage system during disease, surgical interventions, and cell-based transplantation should be further explored.

Keywords: human, inner ear, IBA1, macrophages, structured illumination microscopy

OPEN ACCESS

Edited by:
Agnieszka J. Szczepek, Charité Medical University of Berlin, Germany

Reviewed by:
Takayuki Okano, Kyoto University, Japan
Martin Moller, Rigshospitalet, Denmark
Menachem Gross, Hebrew University Hadassah Medical School, Israel

****Correspondence:***
Helge Rask-Andersen
helge.rask-andersen@surgsci.uu.se

Specialty section:
This article was submitted to Neuro-Otology, a section of the journal Frontiers in Neurology

Received: *02 May 2019*
Accepted: *19 June 2019*
Published: *10 July 2019*

Citation:
Liu W, Kämpfe Nordström C, Danckwardt-Lilliestöm N and Rask-Andersen H (2019) Human Inner Ear Immune Activity: A Super-Resolution Immunohistochemistry Study. Front. Neurol. 10:728. doi: 10.3389/fneur.2019.00728

INTRODUCTION

The human inner ear and its immune activity are difficult to study because it is surrounded by the hardest bone in the body. In fact, the inner ear was long thought to lack immune activity. Immune cells were restricted to the so-called endolymphatic sac (ES), a membranous appendage situated on the posterior slope of the petrous pyramid at some distance from the sensory regions (**Figure 1A**). The ES contains white blood cells that populate the sub-epithelium and its lumen, and this was exquisitely described by Stacey Guild already in 1927 (1). He managed to maintain the integrity of the ES borders with luminal contents. Various types of leucocytes were observed and later analyses using ultrastructure showed signs of lymphocyte–macrophage interaction and mature plasma cells, suggesting an ongoing immune activity (2, 3). Hypothetically, antigens could reach this area from the respiratory mucosa of the middle ear, cochlear aqueduct, (4) or the vascular system (**Figure 1B**). A possible entry could be the round window that is enclosed by a thin membrane (<0.1 mm). The human inner ear tissue is extremely vulnerable and needs protection from pervasive infectious intrusions. Experimental results suggest that the ES may collect and neutralize noxious substances but can also exert secondary immune activity (5). Ablation of the ES has been shown to diminish this safeguard and to result in an increased vulnerability (6). Nevertheless, experiments suggested that immune responses are not entirely dependent on the ES. Specific immunity, after antigenic challenge, can be detected in the cochlea even after its ablation, but to a reduced extent (6). This indicates that antigen-presenting cells can also be present in the cochlea (7). Morphologic evidence of immune activity in the human ES was presented by Bui et al. (8). Recently, the immunological capacity of the ES was described through gene arrays (9).

New microscopic techniques have increased our concept of the molecular organization of the human inner ear. Immunohistochemistry was performed using super-resolution structured illumination microscopy (SR-SIM) of well-fixed specimens after mild decalcification (10–12). The ion channel machinery of the lateral wall ("cochlear battery") was recently analyzed (10, 13). Immune localization of IBA1-positive macrophages was made in the cochlea and ES (12, 14). This verified the existence of a multitude of macrophages in the human inner ear as previously demonstrated by light microscopy and immunostaining of celloidin sections of temporal bones (15). Here, we extended the analysis of the human ES, cochlea, and cochlear and vestibular nerves and ganglia (12, 14). We further analyzed CD4 and CD8 lymphocytes in the cochlea (16) and the ES. This study was a collaboration between neuro-otologists and cell biologists at the University Hospital of Uppsala, Sweden.

Abbreviations: CI, cochlear implant; E, endolymph; EDTA, ethylene-diamine-tetra-acetic acid; IBA1, ionized calcium-binding adaptor molecule 1; MHCII, major histocompatibility complex type II; SR-SIM, super-resolution structured illumination fluorescence microscopy; ST, scala tympani; StV, stria vascularis; SV, scala vestibuli; TEM, transmission electron microscopy; ES, endolymphatic sac; PBS, phosphate-buffered saline; BSA, bovine serum albumin; TLRA, toll-like receptor; TCL, tympanic covering layer; OC, organ of Corti; VGCs, vestibular ganglion cells; CI, cochlear implant; MVBs, multi-vesicular bodies; FN, facial nerve; IAM, internal acoustic meatus; Na-EDTA, sodium-ethylene-diamine-tetra-acetic acid; DAPI, 4′,6-diamidino-2-phenylindole dihydro-chloride; SG, spiral ganglion. SGCs, spiral ganglion cells; RC, Rosenthal's canal. CX3CL1, CX3C chemokine ligand 1; Sch, Schwann cells. Col. IV, collagen IV.

MATERIALS AND METHODS

Ethics Statement

Human cochleae were collected during trans-cochlear surgery to remove life-threatening petro-clival meningioma compressing the brainstem. To completely remove the tumors, a petrosectomy was performed that included a postero-inferior re-routing of the facial nerve. Instead of drilling the cochlea away, it was dissected out after approval from the ethical committee and the patient after written consent. The cochlea was immediately fixed according to the techniques described earlier (10, 17, 18). The study of human cochleae was approved by the local ethics committee (Etikprövningsnämnden Uppsala, no. 99398, 22/9 1999, cont. 2003, no. C254/4; no. C45/7 2007, Dnr. 2013/190) and the patients. Written information was given to patients operated for petro-clival meningioma. The patients ranged from 40 to 70 years of age. Their hearing thresholds (pure tone audiometry) were normal, except in a few cases where frequencies showed slightly increased thresholds. At vestibular schwannoma surgery, the ES is routinely drilled away and wasted. The ethical committee approved that such tissue could be collected and directly analyzed histologically without storing personal data.

Preparation of Human Tissue

Studies of the human cochlea are particularly challenging due to its vulnerability and fixation difficulties because of its encapsulation by hard bone. Five cochleae were dissected out using diamond drills of various sizes in standardized surgical procedures. An experienced surgeon with the assistance of instrumental nurses was allowed to handle the specimens and delivered them to the fixative. Unless stored according to the Swedish biobank law, no data on the age, gender, or audiometry of the patients can be retrieved. After the cochleae were dissected from the surrounding bones, they were diluted in 4% paraformaldehyde with 0.1 M phosphate-buffered saline (PBS) (pH 7.4). The cochleae, transferred from the operating room to the laboratory, were kept in ample fixative fluid for 24 h at 4°C. Next, the specimens were washed in 0.1 M PBS and then placed in 10% Na-ethylene-diamine-tetra-acetic acid (Na-EDTA) solution at pH 7.2 for decalcification. The Na-EDTA solution was renewed every 2 days until the decalcification process was complete, which took ∼3 weeks. The decalcified cochleae were rinsed with PBS and placed in 25% sucrose in PBS overnight (4°C). The cochleae were embedded in Tissue-Tek O.C.T. (Polysciences, Inc.), rapidly frozen in dry ice, and sectioned at 8–10 μm using a cryostat microtome (Leica, Tokyo, Japan). The cryo-sections were collected onto gelatin/chrome-alum-coated slides and stored in a freezer at −70°C before immunohistochemistry was conducted. The ESs were removed with a small rim of bone around the soft tissue. This tissue is normally drilled away during the routine trans-labyrinthine procedure to remove vestibular schwannomas.

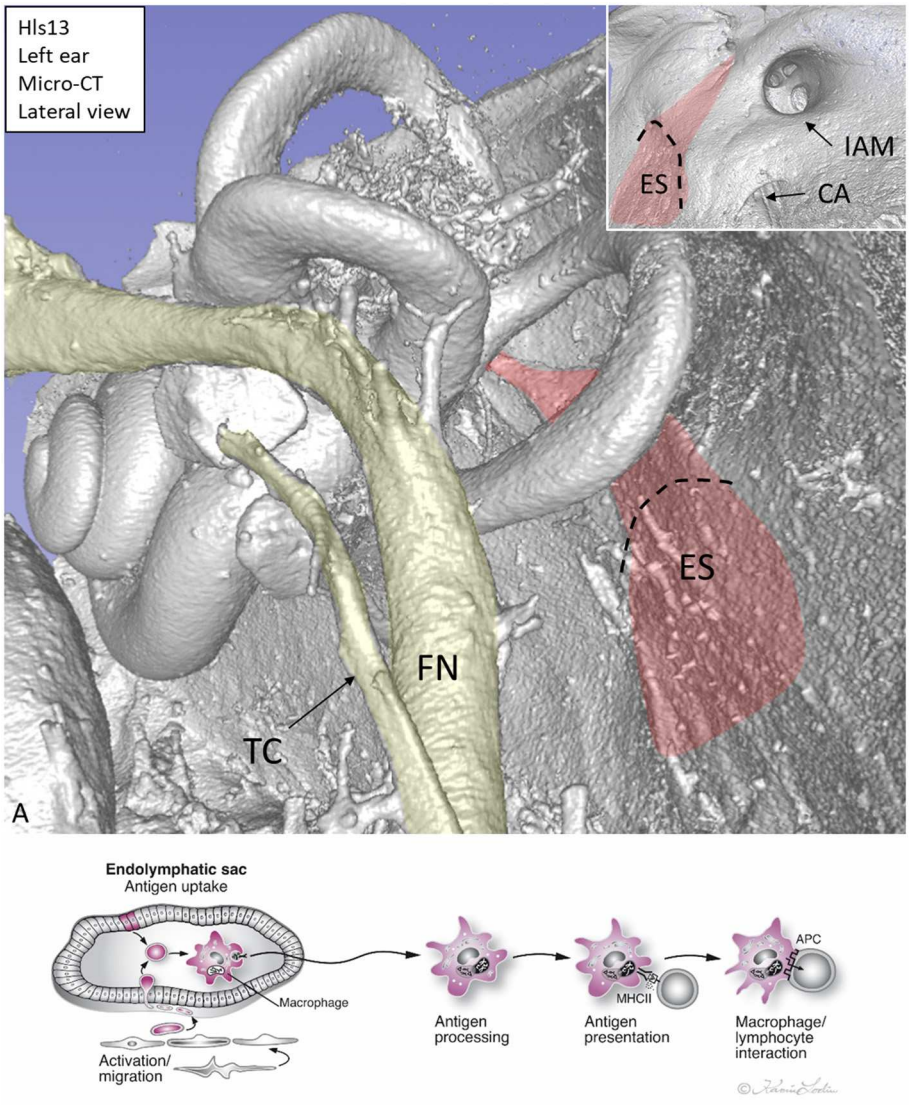

FIGURE 1 | (A) Micro-CT, 3D reconstruction of a left human inner ear silicone mold. The ES (red) is located on the posterior slope of the petrous pyramid. It is connected to the rest of the inner ear through the endolymphatic duct. Inset shows the intra-cranial view of the ES. **(B)** Hypothetical representation of scavenger and foreign substance uptake in the human ES. CA, cochlear aqueduct; IAM, internal acoustic meatus; FN, facial nerve; TC, tympanic chorda; MHCII, major histocompatibility complex class type II. APC, antigen-presenting cell.

Antibodies and Immunohistochemistry

Table 1 shows the antibodies used in the present study. The immunohistochemistry procedures performed on the sections have been described in previous publications (19–21). Briefly, the slide-mounted sections were incubated with an antibody solution under a humidified atmosphere at 4°C for 20 h. After rinsing with PBS three times for 5 min each, the sections were incubated with secondary antibodies conjugated to Alexa Fluor 488, 555, and 647 (Molecular Probes, Carlsbad, CA, USA), counter-stained with the nuclear stain 4′,6-diamidino-2-phenylindole dihydro-chloride (DAPI; Thermo Fisher Scientific, Waltham, MA, USA) for 5–7 min, rinsed with PBS (3 × 5 min), mounted with ProLong® Gold Antifade Mountant (Thermo Fisher Scientific), and covered with the specified cover glass required for optically matching the SIM objectives. Primary and secondary antibody controls and labeling controls were performed to exclude endogenous fluorescence or unspecific reaction products. As a routine control, sections were incubated with 2% bovine serum albumin (BSA), omitting the primary antibodies. The control experiment revealed no visible staining in any structure of the cochleae.

Imaging and Photography

To analyze sections, we used the methods earlier described by Liu et al. (14) The stained sections were first investigated with an inverted fluorescence microscope (Nikon TE2000; Nikon,

TABLE 1 | Antibodies used in this study.

Primary antibody	Type	Dilution	Host	Catalog number	Producer
IBA1	Polyclonal	1:100	Rabbit	PA5-27436	Thermo Fisher, Waltham, MA, USA
MHCII	Monoclonal	1:100	Mouse	MA5-11966	Thermo Fisher
Collagen IV	Polyclonal	1:10	Goat	AB769	Millipore, Burlington, VT, USA
CX3CL1	Monoclonal	1:50	Mouse	MAB3651-100	R&D Systems, Minneapolis, MN, USA
CD11b	Monoclonal	1:50	Rabbit	AB52478	Abcam, Cambridge, UK
CD4	Polyclonal	1:150	Goat	AF-379-NA	R&D Systems
CD8α	Monoclonal	1:100	Mouse	MAB1509	R&D Systems
CD68	Monoclonal	1:50	Mouse	NB100-683	Novus, Littleton, CO, USA
TLR 4	Oligoclonal	1:10	Rabbit	710185	Thermo Fisher
Tuj 1	Polyclonal	1:200	Rabbit	#04-1049	Millipore
Tuj 1	Monoclonal	1:200	Mouse	MAB1637	Millipore
TMEM119	Polyclonal	1:50	Rabbit	ab185337	Abcam

Secondary antibodies used were the following:
Anti-mouse IgG (H+L), Alexa Fluor 555 Polyclonal 1:400 Goat A21422, Invitrogen.
Anti-rabbit IgG (H+L), Alexa Fluor488 Polyclonal 1:400 Goat A11008, Invitrogen.
Anti-goat IgG (H+L), Alexa Fluor 488 Polyclonal 1:400 Donkey A21432, Invitrogen.
Anti-mouse IgG (H+L), Alexa Fluor 488 Polyclonal 1:400 Donkey A21202, Invitrogen.
Anti-rabbit IgG (H+L), Alexa Fluor 555 Polyclonal 1:400 Donkey A31572, Invitrogen.
Anti-goat IgG (H+L), Alexa Fluor 647 Polyclonal 1:400 Donkey A-21447, Thermo Fisher.

Tokyo, Japan) equipped with a spot digital camera with three filters (for emission spectra maxima at 358, 461, and 555 nm). Image-processing software (NIS Element BR-3.2; Nikon, Tokyo, Japan), including image merging and a fluorescence intensity analyzer, was installed on a computer system connected to the microscope. For laser confocal microscopy, we used the same microscope equipped with a three-channel laser emission system. The optical scanning and image-processing tasks were performed using Nikon EZ-C1 ver. 3.80 software (Nikon, Tokyo, Japan) and included the reconstruction of Z-stack images into projections and three-dimensional (3D) images. SR-SIM, using an Elyra S.1 SIM system with a 63×/1.4 Oil Plan-Apochromat objective (Zeiss, Oberkochen, Germany), a sCMOS camera (PCO Edge), and ZEN 2012 software (Zeiss), was performed to investigate the structures of interest. Multichannel SR-SIM imaging was achieved with the following laser and filter setup: 405 nm laser of excitation coupled with BP 420–480 + LP 750 filter, 488 nm laser of excitation with BP 495–550 + LP750 filter, 561 nm laser of excitation with BP 570–620 + LP 750 filter, and 647 nm laser of excitation with LP 655 filter. To maximize image quality, five grid rotations and five phases were used for each image plane and channel. The grid size was automatically adjusted by the ZEN software for each wavelength of excitation. SR-SIM images were processed with the ZEN software with theoretical point spread function (PSF).

From the SR-SIM dataset, 3D reconstruction was performed with an Imaris 8.2 (Bitplane, Zürich, Switzerland). A bright-field channel was merged with fluorescence to visualize the cell borders. The microscope is capable of achieving a lateral (X–Y) resolution of ≈100 nm and an axial (Z) resolution of ≈300 nm (11). The resolution of the SIM system in BioVis (Uppsala University) was measured with sub-resolution fluorescent beads (40 nm) (Zeiss) in the green channel (BP 495–550 + LP750). An average PSF value was obtained from multiple beads with the built-in experimental PSF algorithm of the ZEN software. The typical resolution of the system was 107 nm in the X–Y plane and 394 nm in the Z plane. Next, 3D reconstructions of TUJ1 and IBA1 protein expression were conducted. Both signals were reconstructed by a surface rendering mode using Imaris 8.2 software. SIM is a wide-field technique that is based on the Moire effect of interfering fine striped patterns of excitation with sub-diffraction features in the sample emission. This can be compared with the confocal technique where the fluorescence light is detected only at the focal plane. This results in doubling the resolution and offers better possibilities to demonstrate proteins at a subcellular level. Combined with confocal microscopy, these techniques allow overviews of protein distribution in the tissue, as well as a more detailed cellular localization.

RESULTS

SR-SIM of the Human ES (Figure 2)

Ionized calcium-binding adaptor molecule 1-expressing cells (IBA1 cells) resided in the surrounding connective tissue and epithelium of the human ES. Macrophages interacted with other cells, showed migrant behavior, and expressed markers that suggest their active role in the innate and adaptive inner ear defense and tolerance (12). Macrophages, as well as some epithelial cells in the human ES, expressed

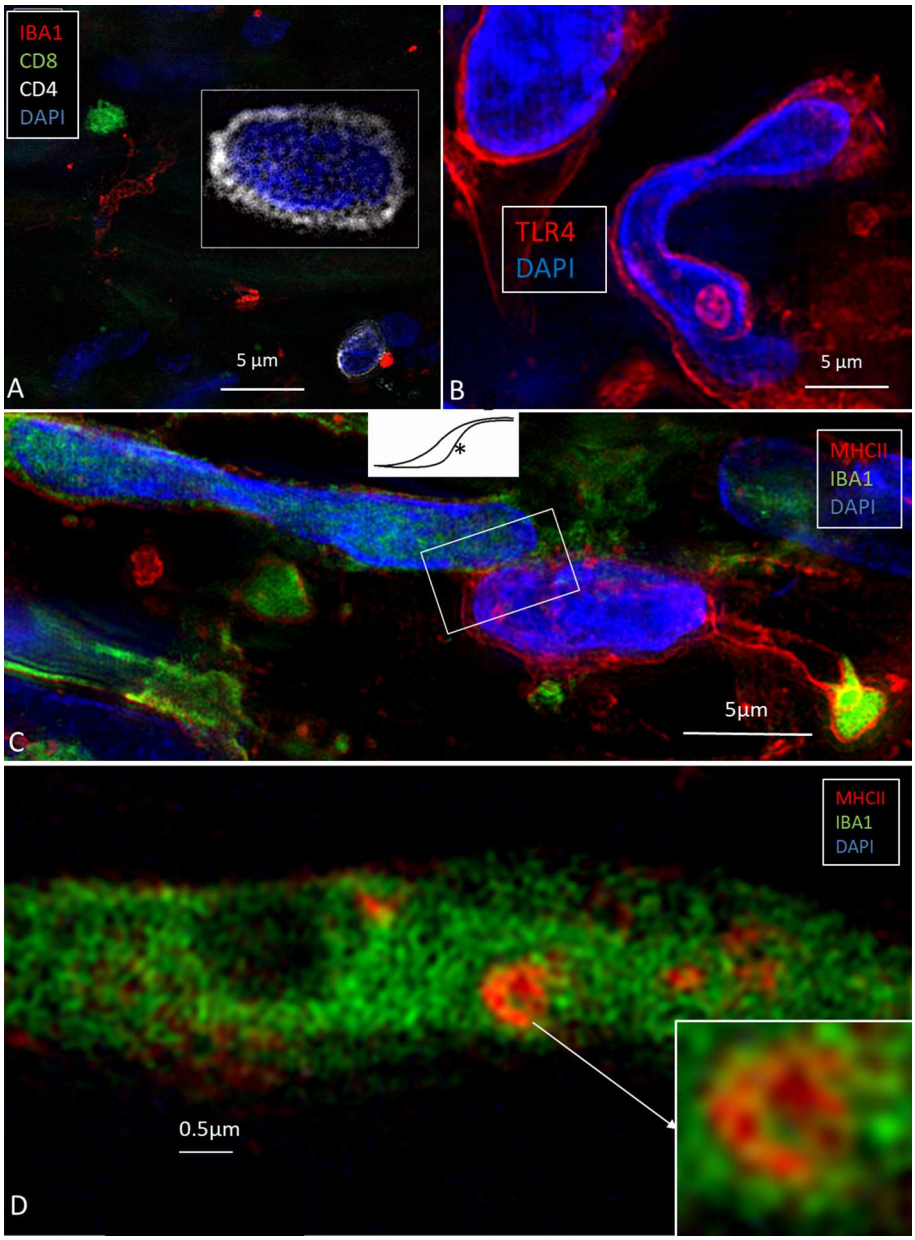

FIGURE 2 | (A) SR-SIM of CD4- and CD8-positive cells present in the perisaccular tissue. **(B)** Some cells express the toll-like receptor 4 (TLR4). **(C)** Sub-epithelial cell interaction near the external aperture of the vestibular aqueduct. IBA1 cells interact (framed area) with cells strongly expressing MHCII. Cell nuclei show different protein expression [from Kampfe-Nordstrom et al. (12) with permission]. **(D)** A sub-epithelial IBA1 cell contains a multi-vesicular body expressing MHCII.

major histocompatibility complex class type II (MHCII) mostly in the apical membrane. SR-SIM also revealed expression of toll-like receptor 4 (TLR4) in the cell membrane and in the cytoplasm among the sub-epithelial cells in the intermediate ES (**Figure 2B**). TLR4 was chosen since Møller et al. recently showed TLR4 and TLR7 expressed on the luminal side of the ES epithelium suggesting the ability to identify and trap bacterial antigens and virus RNA within the endolymphatic space (9). A few sub-epithelial cells expressed CD68, which was occasionally co-expressed with IBA1. The epithelium stained positive for the chemokine fractalkine. The expression was diffuse and intracellular, and occasionally, sub-epithelial fibrocytes also expressed fractalkine. Several migrating cells expressed CD68 and CD11b together with MHCII. Round cells expressing CD4 and CD8 were found in the ES, with more CD4+ than CD8+ cells (**Figure 2A**). Physical interaction between a CD4+ and an IBA1 cell was observed.

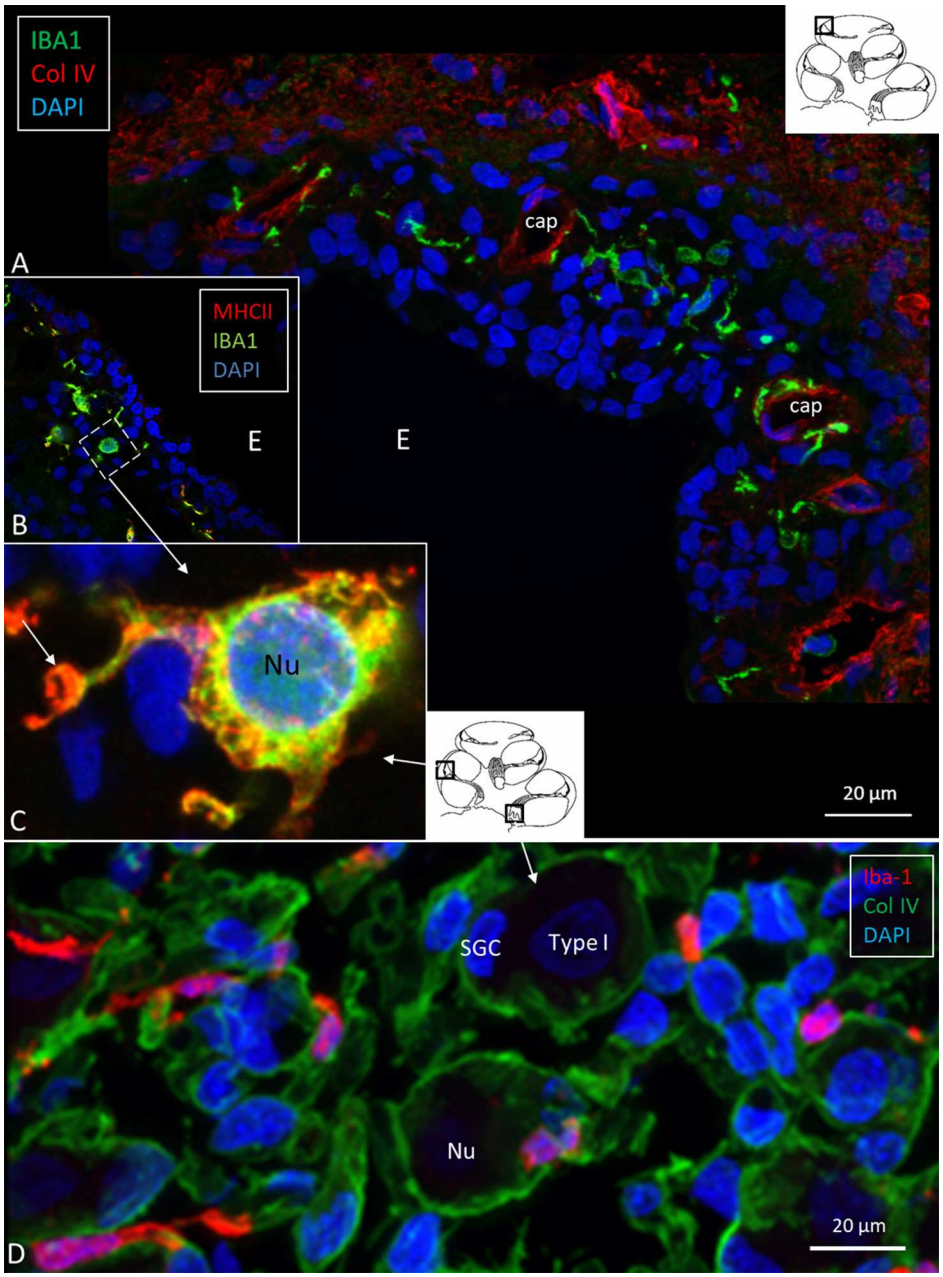

FIGURE 3 | (A) Immunofluorescence of IBA1 and collagen IV in the lateral wall of the apical turn of the human cochlea. Many perivascular IBA1 cells are seen in the StV and few in the spiral ligament. **(B)** Confocal microscopy of the human StV. Framed area is magnified in **(C)**. **(C)** SR-SIM of framed area in B. Cell co-express IBA1 and MHCII. The cell membrane expresses MHCII as well as cytoplasmic vesicles [**(B,C)** from Kampfe-Nordstrom et al. (12)]. **(D)** Confocal microscopy of spiral ganglion with several surrounding IBA1 cells. SGC, satellite glial cell; Nu, type I cell nucleus; Col. IV, collagen IV; cap, capillary; E, endolymph.

IBA1 Cells in the Human Cochlea

SR-SIM demonstrated IBA1-positive cells in the lateral cochlear wall, including the spiral ligament, scala vestibuli (SV) and tympani (ST), spiral limbus, endosteum, tympanic covering layer (TCL), and spiral lamina. Even the organ of Corti (OC) occasionally contained active macrophages (14). In the lateral wall, most IBA1 cells were found in the epithelium of the stria vascularis (StV) near and around the blood vessels (**Figure 3A**). The cells expressed MHCII (**Figures 3B,C**, insets). IBA1 cells were present in the modiolus and cochlear nerve. A substantial number of mesenchymal cells surrounding spiral ganglion (SG) cells were in fact macrophages (**Figure 3D**) (14). The cells did not express TMEM119. Many IBA1-positive macrophages expressed MHCII in the StV and SG. The cells contained cytoplasmic aggregates of MHCII, and their slender processes often embraced the vessels. Fewer but similarly stained cells were

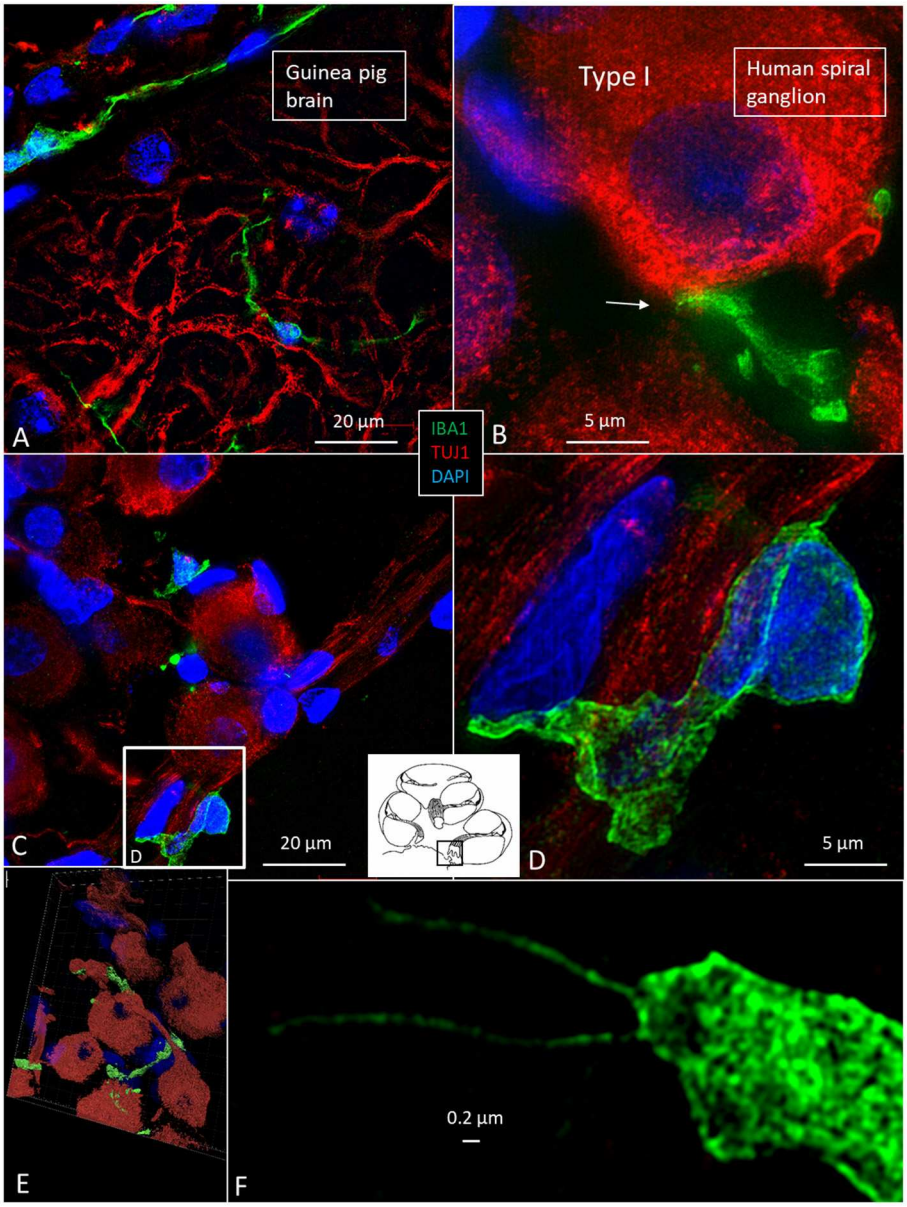

FIGURE 4 | (A) SR-SIM of guinea pig brain showing IBA1-positive cells within the parenchyma and in a surrounding tissue sheet. **(B)** SR-SIM of human SGC and a surrounding contacting IBA1 cell (arrow). **(C,D)** show IBA1-positive cells, of which some are closely associated with the axon initial segment. **(E)** SGCs and IBA1 cells (shown in **Video S1**). **(F)** Nanoscopy of a peri-ganglionic IBA1 cell. Its surface coat contains "antenna"-like processes [from Liu et al. (14)].

detected in the spiral ligament. TLR4 was expressed in the StV (not shown).

IBA1 Cells in the Human SG

The specificity of staining was compared to the guinea pig brain (**Figure 4A**). Several IBA1 cells were found in the human SG associated with the satellite cells (**Figures 4B–E**). IBA1 protein was expressed within the cytoplasm and in the cell nuclei (**Figure 4D**). The macrophages adhered to the basal lamina of the satellite cells located at the axonal and dendrite entry zones (**Figures 4C–E**; **Video S1**). At some places, the IBA1 cells seemed to perforate the basal lamina and reached the nerve cell membrane. "Synapse-like" endings faced the TUJ1-positive nerve soma (**Figure 4B**). Notable variants of IBA1 cells were found in Rosenthal's canal (RC). Free migrating cells were seen around and near the SGCs cells. They contained vesicles and thin (0.2 µm) remarkable processes projecting into the extracellular tissue (**Figure 4F**).

Macrophages in Central and Peripheral Axons

Macrophages were also physically related to axons and dendrites within RC and peripheral and central axons. IBA1 cells along the central axons were long and slender and

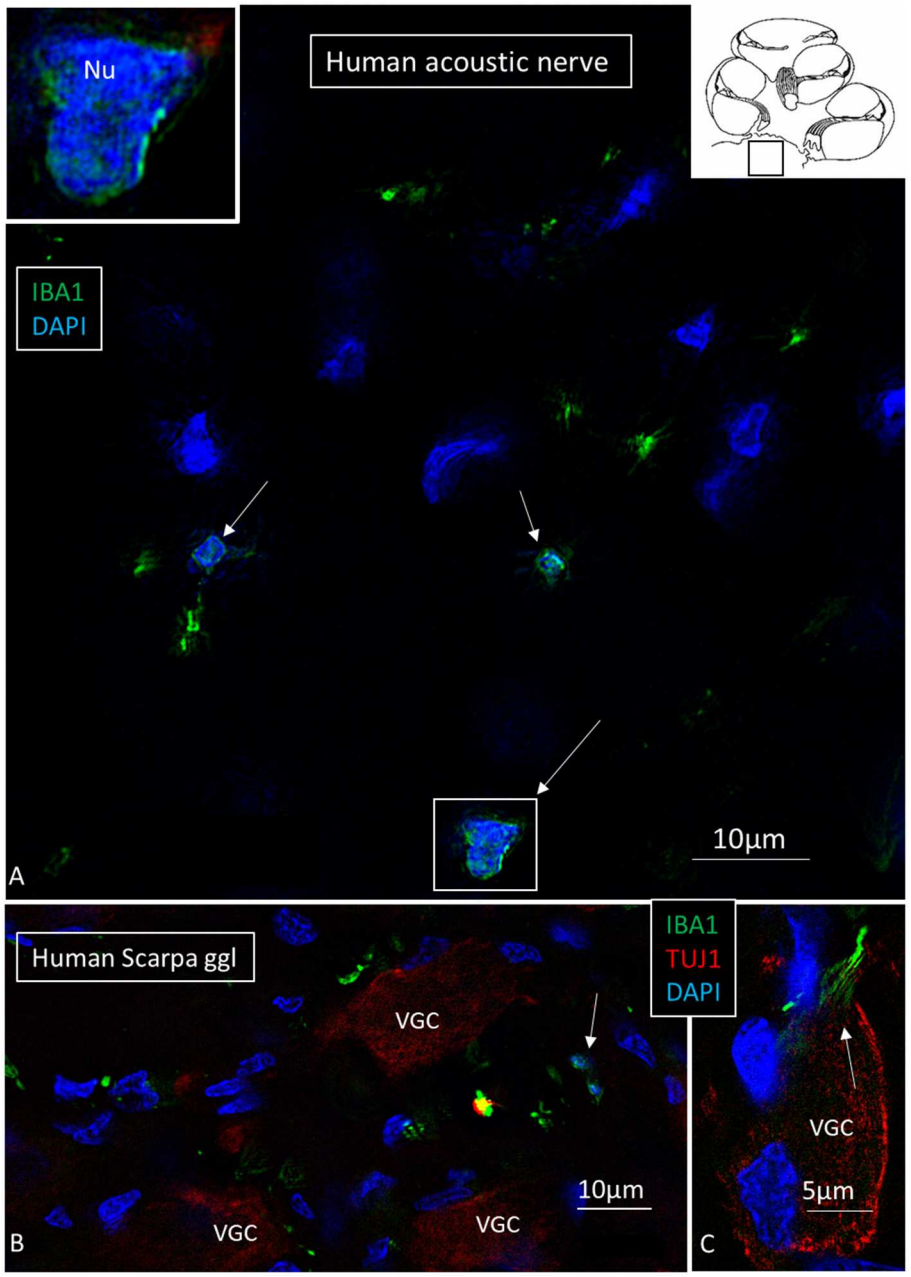

FIGURE 5 | (A) SR-SIM of a cross-sectioned human cochlear nerve. Transected IBA1-positive cell processes are seen (arrows). Framed area is shown with higher magnification in inset. Its cell nucleus expresses IBA1. **(B,C)** Sectioned vestibular nerve at the level of the vestibular ganglion cells (VGCs) demonstrates several IBA1-positive cells (arrows). TUJ1: nerve marker tubulin-1.

measured up to 50 µm with a diameter of ∼0.5 µm (**Figure 5**). Their nuclei expressed IBA1 (**Figure 5A**, left inset). The processes adhered to surrounding nerve fibers, and many had a terminal enlargement. Collagen IV and IBA1 co-staining showed that macrophage pseudopodia extended across the basal lamina of the Schwann cells in the osseous spiral lamina (**Figure 6**). The association with the myelin was uncertain. The IBA1 cells physically contacted Schwann cells' outer cell membrane (**Figures 6C,D**) (14). Whether or not the IBA1 branches directly adhered to the axonal cell membrane at the Ranvier nodes or intercellular clefts could not be determined with certainty. In several cells, IBA1 protein was associated with the nuclei pores (**Figures 6A,E**). At higher magnification, irregular stained areas (100–150 nm), representing cross-sectioned IBA1 branches, were noticed (**Figure 6B**). IBA1 cells ensued around the nerve fibers at the

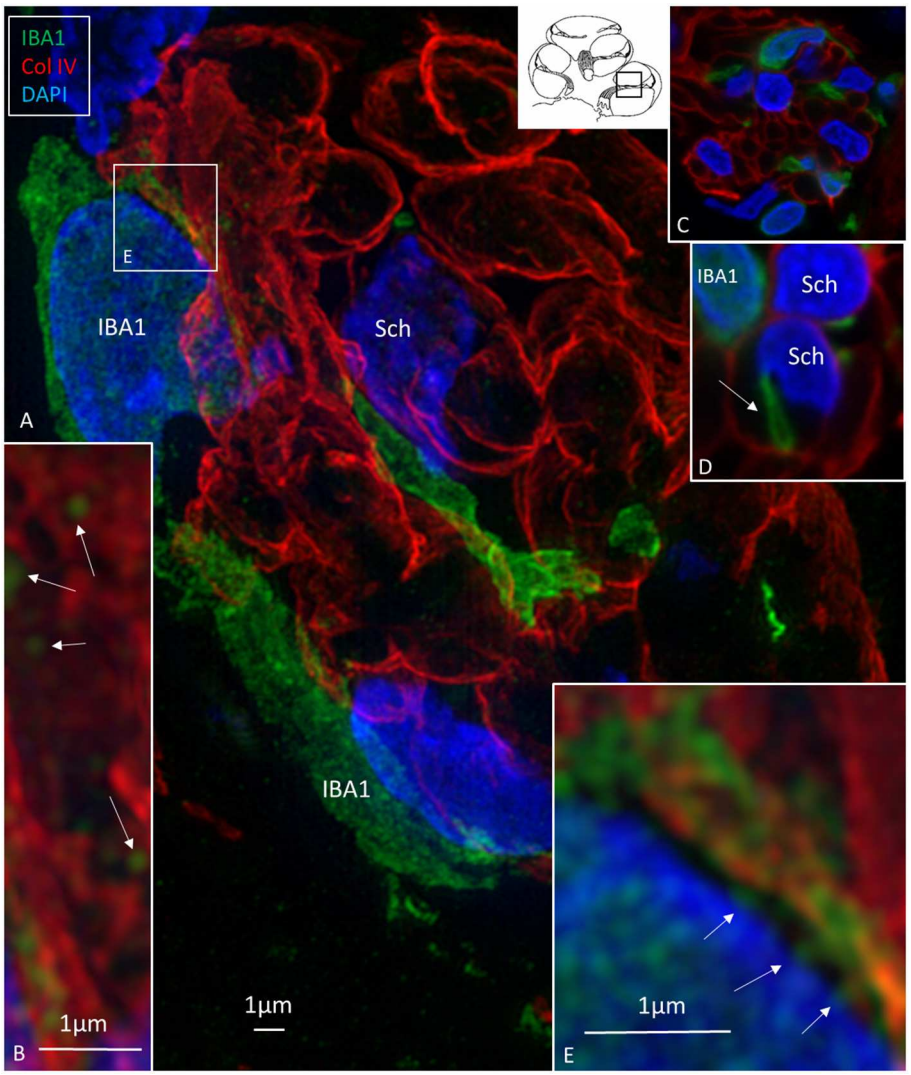

FIGURE 6 | (A) SR-SIM (maximal intensity projection) of the osseous spiral lamina (framed area in inset). Collagen IV stains the basal lamina of the Schwann cells (Sch) surrounding the axons. Several IBA1-immunoreactive cells intermingle with the axons. **(B)** Thin processes (~150 nm in diameter) run along the Schwann cells. **(C,D)** The processes sometimes penetrate the basal lamina of the Schwann cells. **(E)** IBA1 protein expressed in the cell nucleus and at the nuclear envelope (arrows).

habenula perforata where nerves fibers lacked myelin. These cells did not enter the nerve perforation or reached the OC. Some cells extended along the TCL. The vestibular ganglion cells (VGCs) and axons were also surrounded by many IBA1-positive cells (**Figures 5B,C**).

Expression of CX3C Chemokine Ligand 1 in the Cochlea

Cells within the OC showed moderate expression of fractalkine. There was no difference in staining between hair cells and supporting cells. Cells of the TCL showed some staining, but the inferior surface of the basilar membrane lacked expression. SG cells strongly expressed fractalkine with some irregular membrane densities (**Figure 7A**).

CD4+ and CD8+ Cells in the Human SG

A few CD4+ and CD8+ cells and their interactions with macrophages in the human cochleae were observed (**Figures 7B–E**). Some cells, together with occasional CD19-positive cell (**Figure 7F**), were located around modiolar blood vessels and along the border of RC (**Figure 7E**). The T cells were also seen in the medial wall between Rosenthal's canal and the ST. CD4+ and CD8+ cells were not found in the StV, or among the neurons in the Rosenthal's canal and the OC. A few isolated CD4+ and CD8+ cells were seen in the spiral ligament.

DISCUSSION

Our study confirms that the human inner ear and the eight cranial nerve contain a multitude of interacting IBA1-positive

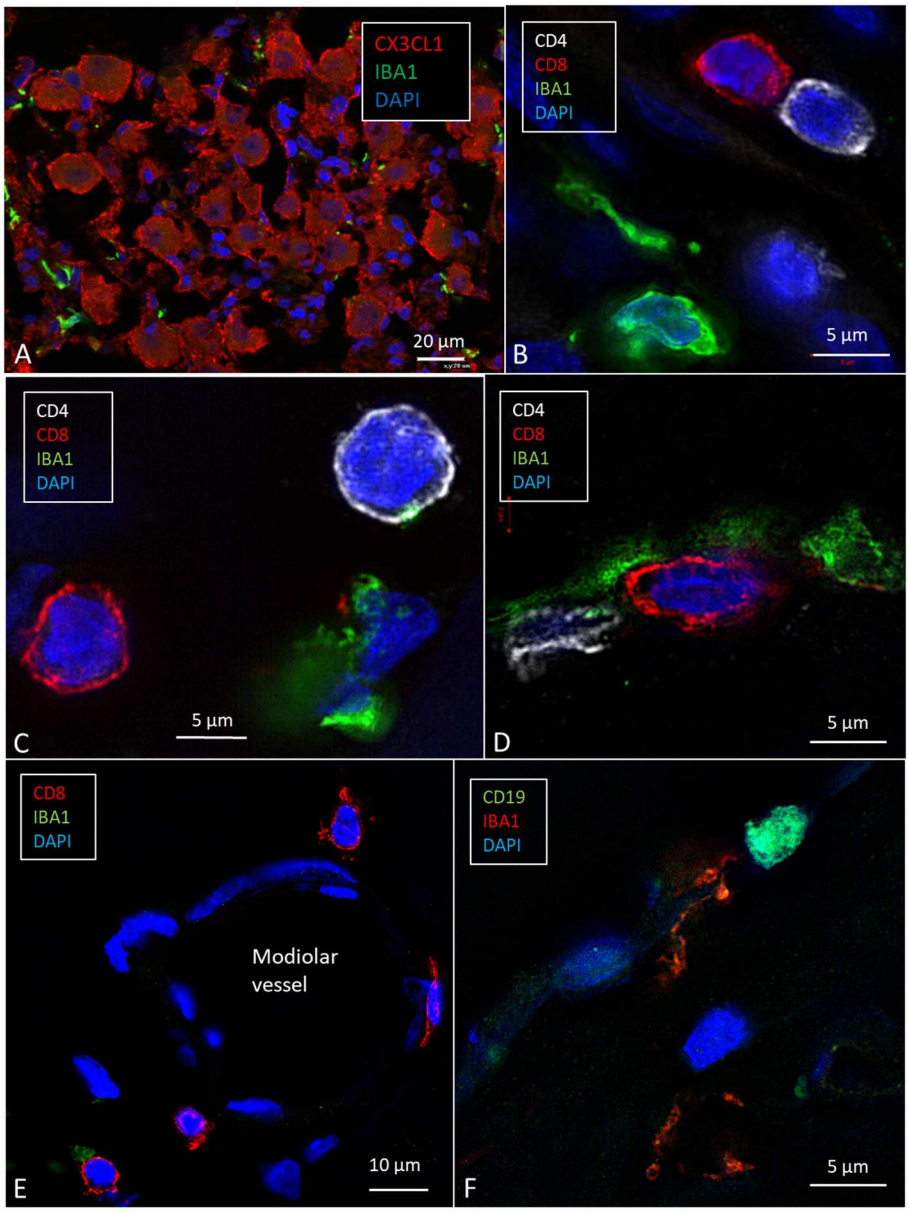

FIGURE 7 | SR-SIM (maximal intensity projection) of the human spiral ganglion. **(A)** Several IBA1-positive cells surround the SGCs that express CX3CL1. **(B–D)** CD4- and CD8-positive lymphocytes are seen in Rosenthal's canal and around a modiolar blood vessel **(E)** [after permission from Liu and Rask-Andersen (16)]. **(F)** A cell in the modiolus expresses CD19.

macrophages. O'Malley et al. (15) described cells expressing the macrophage markers CD163, IBA1, and CD68 in the connective tissue of the entire inner ear in normal human temporal bones. Some cells were even associated with neurons and the sensory epithelium. The location in the cochlear lateral wall suggests a function related to the "blood–labyrinth barrier" according to Zhang et al. (23) and Shi (24). Perivascular macrophages may control the exchange of agents across the vascular wall, but they have also been suggested to act as progenitors for postnatal vessels (24). In the brain and mouse spinal cord, these cells were shown to produce neurotrophic substances important for neuron survival (25, 26). Their highly variable morphology may reflect different functions and activation. We found no melanin in the cells, suggesting that they do not represent melanocytes or intermediate cells. According to Okano et al. (27), the cochlear macrophages appear to be monocyte-derived and do not represent microglia. We found no expression of TMEM119, a microglia marker in mouse and man (28), indicating that they were not microglia. The results support the findings by Hirose et al. (29, 30) and Sato et al. (31).

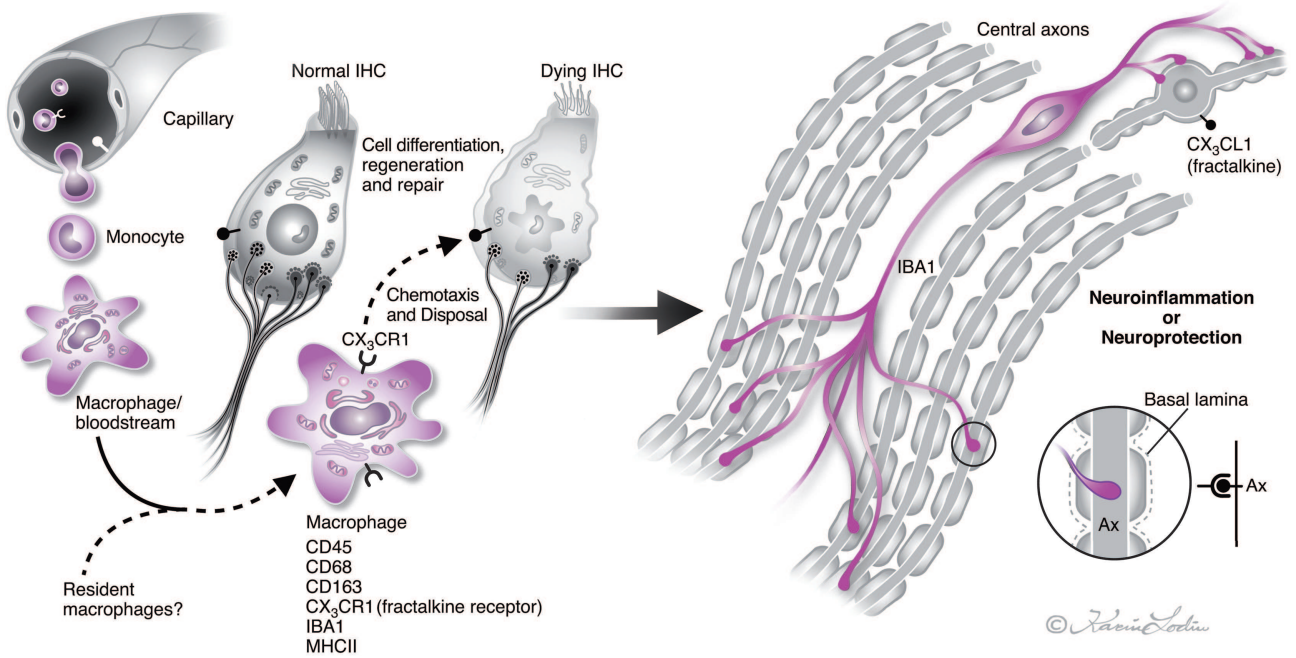

FIGURE 8 | Illustration of nerve/macrophage interaction in the human cochlea [modified after (14)]. Macrophages that are positive for ionized calcium-binding adaptor molecule 1 (IBA1) cells are located in the human cochlea in the spiral ganglion and less often in the OC. They may interact and form a protective link between hair cells and neurons *via* a CX3CL1/CX3CR1 signaling, as demonstrated experimentally by Kaur et al. (22). Macrophages are believed to derive from blood-borne monocytes (illustration by Karin Lodin).

Is There a Neuro-Immune Axis in the Human Cochlea?

Many elongated IBA1 cells had terminal podosomes that attached to adjacent neurons in the modiolar auditory nerve. Torres-Platas et al. (32) analyzed human microglia in gray and white matter of the dorsal anterior cingulate cortex, a region associated with neuro-inflammation. They found a similar pattern of cells running along myelinated nerve fibers. Kaur et al. (22) and Hirose et al. (30) showed that inner ear lesions elevate the number of macrophages in the auditory nerve, spiral ligament, and spiral limbus. Chemokine signaling (fractalkine/CX3CL1) increased macrophage invasion and survival of auditory neurons after induced hair cell damage (22). A link may therefore exist between hair cells and neurons with a macrophage/neuron interaction that protects the cochlear nerve under various conditions (**Figure 8**). Also, adverse signaling may cause cochlear disease. In the human brain, microglial chemokine receptors may possibly promote adult neurogenesis by inhibiting Sirt 1/p65 signaling (33) or increasing secretion of neuroprotective BDNF (34). As a result, macrophages may act both as saviors and foes inducing damaging inflammatory reactions (M1-like) or immunosuppression (M2-like) (35), thus restoring tissue (35–37) and stimulating cell regeneration (38). Our results show that IBA1 cells may establish direct physical contacts with both vestibular and cochlear axons and ganglion cell bodies. Several studies of the human SG conducted in our laboratory over the years have suggested that these cells represent un-specified mesenchymal cells. The present results may help to explain human auditory nerve response following hair cell degeneration caused either by noise or ototoxic drugs (39) or as a result of aging. Macrophages may physically interact with the nerve cell body since they lack a surrounding compact layer of myelin. This may explain why, in contrast to most animals, the acoustic nerve is preserved after loss of hair cells and peripheral axons, a requisite for cochlear implantation (CI), which is one of the greatest achievements in modern medicine.

Notably, IBA1 cells in the human cochlea and auditory nerve expressed MHCII that was not found in experimental studies, unless tissues were induced by inflammation or γ-interferon (40, 41). Okano et al. (42) found bone-marrow-derived cells in the vestibular end organs and ES expressing MHCII. This suggests that CD4+ and CD8+ T cells may initiate adaptive immune responses from interaction with antigen-presenting cochlear macrophages. Conversely, a T-cell-induced inflammation may lead to hair cell damage and neuronal death, *via* pro-inflammatory cytokines and chemokines (25). Such responses need to be avoided. Both innate and adaptive neuro-inflammation with invasion of B- and T-lymphocytes may be responsible for the neurodegenerative process in Alzheimer's disease and MS (43). Moreover, microglia may attract peripheral immune cells and provoke adverse immune processes (44). Conversely, microglia may be neuroprotective through the

production of neurotrophins (45, 46), and T cell autoimmunity has been found to even protect damaged neurons under certain conditions (47).

The ES—An Immunologic Key Player?

A way to avoid mounting destructive inflammation around the sensory cells could be to let the ES monitor primary and secondary immune responses (3, 40). Altermatt found a few lymphoid cells expressing MHCII in the human ES epithelium collected post-mortem (48). The co-expression of IBA1 and MHCII in cells and their migratory behavior across the epithelium suggest that antigens may be taken up from the ES lumen (12) and processed. The apical cell membranes of the ES epithelial cells and cytoplasmic vesicles strongly expressed MHCII molecules. This is notable in the intestine where MHCII plays a role in mucosal immunology, modulation, and disease (49–51). Spectacular associations of MHCII molecular aggregates were seen in the ES among organelles, plasma membrane endocytosis, and multi-vesicular bodies (MVBs). Studies show that MVBs are involved in antigen proteolysis and peptide coupling to the MHCII complex (52). Antigen-presenting cells express MHCII on their surface and give proper information to CD4+ T helper cells and B cells (52, 53) to initiate adaptive immune responses. Gloddek et al. (41) showed the role of the peripheral circulation in response to inner ear antigen stimulation. Our finding of occasional lymphocytes in the cochlea raises the possibility of a "homing" of lymphocytes processed in the ES as suggested by Gloddek et al. (41). Antigens could reach the ES as a first defense line, followed by programmed memory cells entering the cochlea and auditory nerve. Thus, the inner ear could be protected without initiating a full-scales and harmful immune cascade around the receptors. In earlier studies, lymphocytes were observed in the ST and around the spiral modiolar vein after immune challenges to the cochlea (41). This suggests that the vein is the initial site for lymphocytes entering the inner ear (54).

Cochlear Macrophages and Cell Renewal

In a recent study, we found migratory macrophages in the human cochlea near injured hair cells (14). These scavenger cells were thought to stimulate repair *via* supporting cells. Furthermore, active macrophages could be observed within the sensory epithelium after noise damage, suggesting that they are involved in tissue reconstruction (29, 55, 56). In the eye, macrophages, microglia, and T cells have been shown to enhance the survival of retinal ganglion cells and even regenerate damaged axons through the inflammatory response (57). Moreover, bone-marrow-derived cells, chiefly hematopoietic stem cells, were found to continuously populate the lateral wall in the adult cochlea (58). The authors believed that these cells can regenerate damaged fibrocytes and differentiate into macrophages in the adult auditory nerve. They even suggested that the cells may constitute a source for regeneration of the human acoustic nerve in the adult inner ear (59).

Stem-cell-based regeneration of sensorineural elements in the ear may be hindered by immune responses. The blood–labyrinth barrier may restrict cell migration and consists partly of endothelial tight junctions in the StV. The SG and ES contain fenestrated capillaries and lack a corresponding constricted barrier. In the central nervous system, monocyte-derived IBA1 cells expressing MHCII seem to respond to mesenchymal stem-cell grafting, even though resident microglia may also be involved (60). If similar restrictions prevail after inner ear nerve grafting remains to be elucidated.

In summary, our freshly fixed human specimens showed unique preservation and immunogenicity. The benign tumors could potentially influence the conditions. Tumor infiltration into the cochlea was not noticed, and we believe that the samples are physiologically representative. The results also affirm the findings by O'Malley et al. (15). However, a weakness of the study may be the age of the patients (∼40–60 years), as microglia of the aged brain can show an increased immune state (61).

DATA AVAILABILITY

All datasets generated for this study are included in the manuscript and/or the **Supplementary Files**.

AUTHOR CONTRIBUTIONS

WL and CK performed all the immunohistochemistry and processing of the human tissue, such as fixation, embedding, and cryo-sectioning. They also did confocal and SIM microscopy together with HR-A. HR-A is the main writer of the manuscript, and he also edited the figures, designed and supervised the research project, and participated in the research procedures and interpretation of the results and the photography. ND-L performed the surgery.

FUNDING

This study was supported by ALF funding from the Uppsala University and private funds from Börje Runögård, Sweden. This study was partly supported by Medel, Inc., Innsbruck, Austria.

ACKNOWLEDGMENTS

We are grateful to SciLyfe Laboratories and the BioVis Platform at Uppsala University for providing SR-SIM microscope equipment and for personal support throughout the study.

SUPPLEMENTARY MATERIAL

The Supplementary Material for this article can be found online at: https://www.frontiersin.org/articles/10.3389/fneur.2019.00728/full#supplementary-material

Video S1 | 3D reconstruction showing IBA-positive cells among TUJ1-positive neurons (red) in the human SG. Signals were remodeled using Imaris 8.2 software.

REFERENCES

1. Guild SR. Observations upon the structure and normal contents of the ductus and saccus endolymphaticus in the guinea pig (*Cavia cobaya*). *Am J Anat.* (1927) 39:102. doi: 10.1002/aja.1000390102
2. Rask-Andersen H, Stahle J. Lymphocyte–macrophage activity in the endolymphatic sac: an ultrastructural study of the rugose endolymphatic sac in the guinea pig. *ORL J Otorhinolaryngol Relat Spec.* (1979) 41:177–92. doi: 10.1159/000275458
3. Rask-Andersen H, Stahle J. Immunodefence of the inner ear? lymphocyte–macrophage interaction in the endolymphatic sac. *Acta Otolaryngol.* (1980) 89:283–94. doi: 10.3109/00016488009127140
4. Merchant SN, Gopen Q. A human temporal bone study of acute bacterial meningogenic labyrinthitis. *Am J Otol.* (1996) 17:375–85.
5. Tomiyama S, Harris JP. The endolymphatic sac: Its importance in inner ear immune responses. *Laryngoscope.* (1986) 96:685–91. doi: 10.1288/00005537-198606000-00018
6. Tomiyama S, Harris JP. The role of the endolymphatic sac in inner ear immunity. *Acta Otolaryngol.* (1987) 103:182–8. doi: 10.3109/00016488709107271
7. Gloddek B, Bodmer D, Brors D, Keithley EMM, Ryan AF. Induction of MHC class II antigens on cells of the inner ear. *Audiol Neurotol.* (2002) 7:317–23. doi: 10.1159/000066158
8. Wackym PA, Friberg U, Linthicum FH Jr, Bagger-Sjöbäck D, Bui HT, Hofman F, et al. Human endolymphatic sac: morphologic evidence of immunologic function. *Ann Otol Rhinol Laryngol.* (1987) 96:276–81. doi: 10.1177/000348948709600308
9. Møller MN, Kirkeby S, Vikesa J, Nielsen FC, Caye-Thomasen P. Gene expression demonstrates an immunological capacity of the human endolymphatic sac. *Laryngoscope.* (2015) 125:E269–75. doi: 10.1002/lary.25242
10. Liu W, Li H, Edin F, Brännström J, Glueckert R, Schrott-Fischer A, et al. Molecular composition and distribution of gap junctions in the sensory epithelium of the human cochlea—A super-resolution structured illumination microscopy (SR-SIM) study. *Ups J Med Sci.* (2017) 122:160–170. doi: 10.1080/03009734.2017.1322645
11. Gustafsson MGL, Shao L, Carlton PM, Rachel Wang CJ, Golubovskaya IN, Zacheus Cande W, et al. Three-dimensional resolution doubling in wide-field fluorescence microscopy by structured illumination. *Biophys J.* (2008) 94:4957–70. doi: 10.1529/biophysj.107.120345
12. Kampfe-Nordstrom C, Laurell G, Danckwardt-Lilliestrom N, Liu W, Rask-Andersen H. The human endolymphatic sac and inner ear immunity: macrophage interaction and molecular expression. *Front Immunol.* (2018) 9:3181. doi: 10.3389/fimmu.2018.03181
13. Liu W, Schrott-Fischer A, Glueckert R, Benav H, Rask-Andersen H. The human "cochlear battery"—Claudin-11 barrier and ion transport proteins in the lateral wall of the cochlea. *Front Mol Neurosci.* (2017) 10:239. doi: 10.3389/fnmol.2017.00239
14. Liu W, Molnar M, Garnham C, Benav H, Rask-Andersen H. Macrophages in the human cochlea: saviors or predators-A study using super-resolution immunohistochemistry. *Front Immunol.* (2018) 9:223. doi: 10.3389/fimmu.2018.00223
15. O'Malley JT, Nadol JB, Jr, McKenna MJ. Anti CD163+, Iba1+, and CD68+ Cells in the adult human inner ear: normal distribution of an unappreciated class of macrophages/microglia and implications for inflammatory otopathology in humans. *Otol Neurotol.* (2016) 37:99–108. doi: 10.1097/MAO.0000000000000879
16. Liu W, Rask-Andersen H. Super-resolution immunohistochemistry study on CD4 and CD8 cells and the relation to macrophages in human cochlea. *J Otol.* (2019) 14:1–5. doi: 10.1016/j.joto.2018.11.010
17. Rask-Andersen H, Liu W, Linthicum F. Ganglion cell and 'dendrite' populations in electric acoustic stimulation ears. *Adv Otorhinolaryngol.* (2010) 67:14–27. doi: 10.1159/000262593
18. Liu W, Edin F, Blom H, Magnusson P, Schrott-Fischer A, Glueckert R et al. Super-resolution structured illumination fluorescence microscopy of the lateral wall of the cochlea: the Connexin26/30 proteins are separately expressed in man. *Cell Tissue Res.* (2016) 365:13–27. doi: 10.1007/s00441-016-2359-0
19. Liu W, Boström M, Kinnefors A, Linthicum F, Rask-Andersen H. Expression of myelin basic protein in the human auditory nerve—An immunohistochemical and comparative study. *Auris Nasus Larynx.* (2012). 39:18–24. doi: 10.1016/j.anl.2011.04.007
20. Liu W, Edin F, Atturo F, Rieger G, Löwenheim H, Senn P, et al. The pre- and post-somatic segments of the human type I spiral ganglion neurons—Structural and functional considerations related to cochlear implantation. *Neuroscience.* (2015) 284:470–82. doi: 10.1016/j.neuroscience.2014.09.059
21. Liu W, Löwenheim H, Santi PA, Glueckert R, Schrott-Fischer A, Rask-Andersen H. Expression of trans-membrane serine protease 3 (TMPRSS3) in the human organ of Corti. *Cell Tissue Res.* (2018) 372:445–56. doi: 10.1007/s00441-018-2793-2
22. Kaur T, Zamani D, Tong L, Rubel EW, Ohlemiller KK, Hirose K, et al. Fractalkine signaling regulates macrophage recruitment into the cochlea and promotes the survival of spiral ganglion neurons after selective hair cell lesion. *J Neurosci.* (2015) 35:15050–61. doi: 10.1523/JNEUROSCI.2325-15.2015
23. Zhang W, Dai M, Fridberger A, Hassan A, Degagne J, Neng L, et al. Perivascular-resident macrophage-like melanocytes in the inner ear are essential for the integrity of the intrastrial fluid–blood barrier. *Proc Natl Acad Sci USA.* (2012) 109:10388–93. doi: 10.1073/pnas.1205210109
24. Shi X. Resident macrophages in the cochlear blood–labyrinth barrier and their renewal via migration of bone-marrow-derived cells. *Cell Tissue Res.* (2010) 342:21–30. doi: 10.1007/s00441-010-1040-2
25. Kraft AD, Mcpherson CA, Harry GJ. Heterogeneity of microglia and TNF signaling as determinants for neuronal death or survival. *Neurotoxicology.* (2009) 30:785–93. doi: 10.1016/j.neuro.2009.07.001
26. Kigerl KA, Gensel JC, Ankeny DP, Alexander JK, Donnelly DJ, Popovich PG. Identification of two distinct macrophage subsets with divergent effects causing either neurotoxicity or regeneration in the injured mouse spinal cord. *J Neurosci.* (2009) 29:13435–44. doi: 10.1523/JNEUROSCI.3257-09.2009
27. Okano T, Nakagawa T, Kita T, Kada S, Yoshimoto M, Nakahata T, et al. Bone marrow-derived cells expressing Iba1 are constitutively present as resident tissue macrophages in the mouse cochlea. *J Neurosci Res.* (2008) 86:1758–67. doi: 10.1002/jnr.21625
28. Bennett ML, Bennett FC, Liddelow SA, Ajami B, Zamanian JL, Fernhoff NB, et al. New tools for studying microglia in the mouse and human CNS. *Proc Natl Acad Sci USA.* (2016) 113:E1738–46. doi: 10.1073/pnas.1525528113
29. Hirose K, Discolo CM, Keasler JR, Ransohoff R. Mononuclear phagocytes migrate into the murine cochlea after acoustic trauma. *J Comp Neurol.* (2005) 489:180–94. doi: 10.1002/cne.20619
30. Hirose K, Rutherford MA, Warchol ME. Two cell populations participate in clearance of damaged hair cells from the sensory epithelia of the inner ear. *Hear Res.* (2017) 352:70–81. doi: 10.1016/j.heares.2017.04.006
31. Sato E, Shick HE, Ransohoff RM, Hirose K. Repopulation of cochlear macrophages in murine hematopoietic progenitor cell chimeras: the role of CX3CR1. *J Comp Neurol.* (2008) 506:930–42. doi: 10.1002/cne.21583
32. Torres-Platas SG, Comeau S, Rachalski A, Dal Bo G, Cruceanu C, Turecki G, et al. Morphometric characterization of microglial phenotypes in human cerebral cortex. *J Neuroinflammation.* (2014) 11:12. doi: 10.1186/1742-2094-11-12
33. Sellner S, Paricio-Montesinos R, Spieß A, Masuch A, Erny D, Harsan LA, et al. Microglial CX 3 CR1 promotes adult neurogenesis by inhibiting Sirt 1/p65 signaling independent of CX 3 CL1. *Acta Neuropathol Commun.* (2016) 4:102. doi: 10.1186/s40478-016-0374-8
34. Lauro C, Cipriani R, Catalano M, Trettel F, Chece G, Brusadin V, et al. Adenosine A1 receptors and microglial cells mediate CX3CL1-induced protection of hippocampal neurons against glu-induced death. *Neuropsychopharmacology.* (2010) 35:1550–9. doi: 10.1038/npp.2010.26
35. Loane DJ, Kumar A. Microglia in the TBI brain: the good, the bad, and the dysregulated. *Exp Neurol.* (2016) 275 (Pt 3):316–27. doi: 10.1016/j.expneurol.2015.08.018
36. David S, Kroner A. Repertoire of microglial and macrophage responses after spinal cord injury. *Nat Rev Neurosci.* (2011) 12:388–99. doi: 10.1038/nrn3053
37. Kumar A, Loane DJ. Neuroinflammation after traumatic brain injury: opportunities for therapeutic intervention. *Brain Behav Immun.* (2012) 26:1191–201. doi: 10.1016/j.bbi.2012.06.008

38. Saclier M, Yacoub-Youssef H, Mackey AL, Arnold L, Ardjoune H, Magnan M, et al. Differentially activated macrophages orchestrate myogenic precursor cell fate during human skeletal muscle regeneration. *Stem Cells.* (2013) 31:384–96. doi: 10.1002/stem.1288
39. Sato E, Shick HE, Ransohoff RM, Hirose K. Expression of fractalkine receptor CX3CR1 on cochlear macrophages influences survival of hair cells following ototoxic injury. *J Assoc Res Otolaryngol.* (2010) 11:223–34. doi: 10.1007/s10162-009-0198-3
40. Takahashi M, Harris JP. Analysis of immunocompetent cells following inner ear immunostimulation. *Laryngoscope.* (2006) 98:1133–8. doi: 10.1288/00005537-198810000-00018
41. Gloddek B, Ryan AF, Harris JP. Homing of lymphocytes to the inner ear. *Acta Otolaryngol.* (1991) 111:1051–9. doi: 10.3109/00016489109100755
42. Okano T, Nakagawa T, Ito J. Distribution of bone marrow-derived cells in the vestibular end organs and the endolymphatic sac. *Acta Otolaryngol.* (2010) 130:88–94. doi: 10.3109/00016489.2010.486803
43. Heppner FL, Ransohoff RM, Becher B. Immune attack: the role of inflammation in Alzheimer disease. *Nat Publ Gr.* (2015) 16:358–72. doi: 10.1038/nrn3880
44. Unger MS, Schernthaner P, Marschallinger J, Mrowetz H, Aigner L. Microglia prevent peripheral immune cell invasion and promote an anti-inflammatory environment in the brain of APP-PS1 transgenic mice. *J Neuroinflammation.* (2018) 15:274. doi: 10.1186/s12974-018-1304-4
45. Kerschensteiner M, Meinl E, Hohlfeld R. Neuro-immune crosstalk in CNS diseases. *Neuroscience.* (2009) 158:1122–32. doi: 10.1016/j.neuroscience.2008.09.009
46. Rapalino O, Lazarov-Spiegler O, Agranov E, Velan GJ, Yoles E, et al. Implantation of stimulated homologous macrophages results in partial recovery of paraplegic rats. *Nat Med.* (1998) 4:814–21. doi: 10.1038/nm0798-814
47. Moalem G, et al. Autoimmune T cells protect neurons from secondary degeneration after central nervous system axotomy. *Nat Med.* (1999) 5:49–55. doi: 10.1038/4734
48. Altermatt HJ, Gebbers J-O, Müller C, Arnold W, Laissue JA. Human endolymphatic sac: evidence for a role in inner ear immune defence (with 1 color plate). *ORL.* (1990) 52:143–8. doi: 10.1159/000276124
49. Peterson LW, Artis D. Intestinal epithelial cells: Regulators of barrier function and immune homeostasis. *Nat Rev Immunol.* (2014) 14:141–53. doi: 10.1038/nri3608
50. Yao C, Vanderpool KG, Delfiner M, Eddy V, Lucaci AG, Soto-Riveros C, et al. Electrical synaptic transmission in developing zebrafish: properties and molecular composition of gap junctions at a central auditory synapse. *J Neurophysiol.* (2014) 112:2102–13. doi: 10.1152/jn.00397.2014
51. Lin JT, Kitzmiller TJ, Cates JM, Gorham JD. MHC-independent genetic regulation of liver damage in a mouse model of autoimmune hepatocellular injury. *Lab Invest.* (2005) 85:550–61. doi: 10.1038/labinvest.3700246
52. Roche PA, Furuta K. The ins and outs of MHC class II-mediated antigen processing and presentation HHS public access. *Nat Rev Immunol.* (2015) 15:203–16. doi: 10.1038/nri3818
53. Blum JS, Wearsch PA, Cresswell P. Pathways of antigen processing. *Annu Rev Immunol.* (2013) 31:443–73. doi: 10.1146/annurev-immunol-032712-095910
54. Harris JP, Fukuda S, Keithley EM, Keithley EM. Spiral modiolar vein: Its importance in inner ear inflammation. *Acta Otolaryngol.* (1990) 110:357–65. doi: 10.3109/00016489009122560
55. Fredelius L, Rask-Andersen H, Johansson B, Urquiza R, Bagger-sjöbäck D, Wersäll J. Time sequence of degeneration pattern of the organ of Corti after acoustic overstimulation: a light microscopical and electrophysiological investigation in the Guinea pig. *Acta Otolaryngol.* (1988) 106:81–93. doi: 10.3109/00016488809107374
56. Fredelius L, Rask-Andersen H. The role of macrophages in the disposal of degeneration products within the organ of corti after acoustic overstimulation. *Acta Otolaryngol.* (1990) 109:76–82. doi: 10.3109/00016489009107417
57. Cui Q, Yin Y, Benowitz LI. The role of macrophages in optic nerve regeneration. *Neuroscience.* (2009) 158:1039–48. doi: 10.1016/j.neuroscience.2008.07.036
58. Lang H, Ebihara Y, Schmiedt RA, Minamiguchi H, Zhou D, Smythe N, et al. Contribution of bone marrow hematopoietic stem cells to adult mouse inner ear: Mesenchymal cells and fibrocytes. *J Comp Neurol.* (2006) 496:187–201. doi: 10.1002/cne.20929
59. Lang H, Nishimoto E, Xing Y, Brown LN, Noble KV, Barth JL, LaRue AC, et al. Contributions of mouse and human hematopoietic cells to remodeling of the adult auditory nerve after neuron loss. *Mol Ther.* (2016) 24:2000–11. doi: 10.1038/mt.2016.174
60. Le Blon D, Hoornaert C, Daans J, Santermans E, Hens N, Goossens H, et al. Distinct spatial distribution of microglia and macrophages following mesenchymal stem cell implantation in mouse brain. *Immunol Cell Biol.* (2014) 92:650–8. doi: 10.1038/icb.2014.49
61. Norden DM, Godbout JP. Review: microglia of the aged brain: Primed to be activated and resistant to regulation. *Neuropathol Appl Neurobiol.* (2013) 39:19–34. doi: 10.1111/j.1365-2990.2012.01306.x

Conflict of Interest Statement: Medel Inc., Innsbruck, Austria, generously contributed a portion of WL's salary.

The remaining authors declare that the research was conducted in the absence of any commercial or financial relationships that could be construed as a potential conflict of interest.

frontiers in Neurology

ORIGINAL RESEARCH
published: 16 July 2019
doi: 10.3389/fneur.2019.00749

Early Diagnosis of Hearing Loss in Patients Under Methadone Maintenance Treatment

Arash Bayat[1], *Nader Saki*[1], *Golshan Mirmomeni*[2] *and Ali Yadollahpour*[3]*

[1] Hearing Research Center, Imam Khomeini Hospital, Ahvaz Jundishapur University of Medical Sciences, Ahvaz, Iran, [2] Department of Biostatistics and Epidemiology, School of Health, Ahvaz Jundishapur University of Medical Sciences, Ahvaz, Iran, [3] Department of Medical Physics, School of Medicine, Ahvaz Jundishapur University of Medical Sciences, Ahvaz, Iran

Background and Objective: Methadone maintenance treatment (MMT) as the most effective treatment for opioid addictions could induce both reversible and permanent hearing loss. Therefore, early detection of methadone-induced hearing loss is necessary to prevent irreversible cochlear damage. The present study aims to identify the early onset of hearing loss in patients who underwent MMT and to compare them with the age and gender matched normal hearing peers.

Methods: This was an analytic cross-sectional study conducted on patients ($n = 27$ males; age range: 18–53 years old) who received 3 months MMT course (MMT group) and a control group consisting of age and gender matched healthy individuals ($n = 27$ males). Before MMT, all patients underwent conventional audiometry (250–8,000 Hz) and those with normal hearing threshold participated into the study. One month after MMT termination, the patients were assessed for possible hearing loss using conventional pure tone audiometry (PTA), extended high frequency (EHF) audiometry, and distortion product otoacoustic emissions (DPOAEs).

Results: Our results demonstrated that the mean EHF thresholds in the MMT patients were significantly greater than the age- and gender-matched healthy controls across all frequencies ($p < 0.001$). However, there was no statistically significant difference in conventional PTA thresholds between both groups ($p > 0.05$). DPOAE amplitudes significantly reduced at higher frequencies (3,000–8,000 Hz) in the MMT group, compared to the healthy control group. In contrast to the conventional PTA audiometry, the EHF and DPOAE assessments identified hearing impairments in 11 (40.74%), and 14 (51.85%) of the MMT patients, respectively. The main mechanisms proposed for methadone induced hearing loss are cochlear ischemia following vasospasm or vasculitis, direct effect of opioids on opioid receptors present in cochlear stria vascularis of inner ear, blood-labyrinth selective transport of opioidproteins and receptors, and genetic polymorphism and mutations.

Conclusion: The EHF and DPOAE tests have the potential to detect earlier changes in auditory function than conventional frequency audiometry in the MMT patients.

Keywords: hearing loss, methadone, pure tone audiometry, extended high frequency audiometry, otoacoustic emission

OPEN ACCESS

Edited by:
Agnieszka J. Szczepek, Charité Medical University of Berlin, Germany

Reviewed by:
Peter Thorne, The University of Auckland, New Zealand
Leonard Rybak, Southern Illinois University School of Medicine, United States

***Correspondence:**
Ali Yadollahpour
yadollahpour.a@gmail.com

Specialty section:
This article was submitted to Neuro-Otology, a section of the journal Frontiers in Neurology

Received: *07 April 2019*
Accepted: *26 June 2019*
Published: *16 July 2019*

Citation:
Bayat A, Saki N, Mirmomeni G and Yadollahpour A (2019) Early Diagnosis of Hearing Loss in Patients Under Methadone Maintenance Treatment. Front. Neurol. 10:749. doi: 10.3389/fneur.2019.00749

INTRODUCTION

Methadone has been used for many years in the clinical setting for detoxification treatment of opioid addiction, maintenance treatment of opioid addiction, and as a treatment option for moderate to severe pain (1). Methadone maintenance treatment (MMT) is among the most effective approaches for treatment of opioid addictions which is a maintenance-oriented, rather than abstinence-oriented approach. The common side effects of methadone are well-described and include sedation, constipation, respiratory depression, lightheadedness, dizziness, nausea, and vomiting. Other side effects include dysrhythmias, itching, sweating, and orthostatic hypotension (1–4).

Some studies have reported ototoxicity as a known but rare consequence of opioid medications (3–6). Moreover, it has been shown that opioid consumption could lead to dysfunction at the level of the cochlea or the neural pathways to the auditory cortex, which could either be of sudden or gradual onset (7, 8).

Pure-tone audiometry (PTA) is the most common procedure used to evaluate hearing sensitivity of an individual, which can determine the degree and type of hearing loss. During "conventional" auditory testing, PTA is used to identify hearing threshold in frequencies from 250 to 8,000 Hz. In addition to conventional PTA, extra high frequency (EHF) audiometry technique identifies hearing thresholds within the range of 9,000–18,000 Hz (9). The EHF assessment has been used for early detection of hearing loss attributable to lesions located in the base of the cochlear duct and may indicate alterations even before the characteristic effects appear in the conventional frequency range like noise induced hearing loss and ototoxicity (10).

Otoacoustic emissions (OAEs) are sounds measured in the external ear canal and a reflection of active processes in the cochlea. Initiation and physical characteristics of OAE depend on the physiological status of the outer hair cells (OHCs); thus, OAE testing could serve as an objective measure of ototoxic damage. OAEs can provide valuable information on the integrity of the OHCs within the cochlea and can be utilized for early identification of hearing impairments (11–13). Changes in the functions of OHC alter OAE responses and hearing thresholds. Distortion product OAE (DPOAE) is generated using two stimulating tones, f_1 and f_2 (where $f_1 < f_2$). The response is initiated in the overlapping region of the basilar membrane's response to the stimuli, somewhat nearer to the f_2 tonotopic place. A second component arises near the basilar membrane place that codes the distortion-product (DP) frequency ($2f_1 - f_2$). These two sources are combined within the ear canal and the resulting energy is measured as the clinical DPOAEs and may include generator sources basal to the primary tones. The presence of DPOAEs are generally associated with normal hearing and are reduced in individuals with mild to moderate hearing losses up to ∼50–60 dB HL. In subjects with hearing thresholds greater than about 60 dB HL, DPOAEs are not generated (14, 15).

Furthermore, studies conducted on the patients who had been treated with ototoxic medications have shown that EHF audiometry and DPOAE measurements can detect evidence of ototoxicity in the inner ear earlier than conventional audiometry, potentially serving as a predictor to ototoxic effects prior to damage occurs in frequencies that are critical for speech and language comprehension (10, 16, 17).

Several studies have reported the impacts of methadone as an ototoxic medication on auditory system but most of these studies were case reports (2–4, 8, 18). The clinical findings have suggested that methadone administration could lead to both reversible and irreversible hearing loss. Prospective monitoring of these ototoxic effects could reduce the hearing impairments. Early detection of hearing loss provides the necessary information to prevent or minimize the hearing loss progression. Moreover, early detection provides an opportunity to implement aural rehabilitation to impede the hearing impairments. To the best of our knowledge, all of the published reports on methadone associated hearing loss were case reports and there is no clinical trials conducted on a sample of patients with a control group. We could find six case reports published on hearing loss after methadone overdose or abuse (2–4, 18). Of them, four cases were reported to show speedy and fully recovery and only two case reports showed persistent hearing loss (4, 8). All of the cases were related to the patients with methadone overdose or abuse. Considering the wide spread administration of MMT for addiction treatments and the recently reported cases of methadone associated hearing loss, investigating the possible causality of methadone to the hearing loss through well-designed clinical trials is necessary.

The current study aims to investigate the diagnostic value of EHF audiometry and DPOAE methods in detecting early onset of hearing loss in the patients addicted to opioid who had underwent MMT. In this regard, the hearing thresholds of the patients were measured using PTA, EHF, and DPOAE techniques and compared against the age and gender matched normal peers.

METHODS

Study Population

This analytical cross-sectional study was conducted on 27 males (mean age: 35.64 ± 9.25; range: 18–53 years old) with opioid dependence who had been underwent an MMT course in a private clinic. The experiments of the study had lasted from March 2015 to July 2017. To reduce the bias and inter-individual variation we applied a robust inclusion and exclusion criteria. The inclusion criteria were patients who: (i) were at least 18 years of age; (ii) met the DSM-IV-TR or SM-5 criteria for opioid use disorder as assessed by an experienced psychiatrist; (iii) had positive test of opioid dependence in a urine examination before therapy; and (iv) continued to receive MMT for at least three months; (v) were not under any opioid or opioid treatment drugs. During MMT course, all patients were regularly monitored in a private addiction center and prescribed specific dose of methadone. The patients did not use any medication other than methadone for opioid treatment. The control group consisted of 27 healthy males with a similar age distribution (18–53 years of age; mean: 33.95 ± 8.64 years) of the MMT group. All control participants showed normal hearing thresholds (<20 dB HL at 250–8,000 Hz).

All subjects had bilaterally normal middle ear functions before the start of the MMT course. Individuals with a history of chronic exposure to intense noise, acoustic trauma,

ototoxic drug consumption, traumatic brain injuries and middle ear disorders were excluded from the study. Furthermore, we excluded those patients with a history of schizophrenia, neurocognitive disorders, neurodevelopmental disorders, major depressive disorders, bipolar disorders, and mental disorders due to medical conditions according to the definitions of DSM-IV-TR or DSM-5.

All the procedures of this study were in complete accordance with the Declaration of Helsinki on ethical principles for medical research involving human subjects (2014) (19). After the enrolment and before the start of the experiments, the researchers clearly explained the procedures, potential benefits and risks of the study to the participants. Written informed consent form was obtained from all participating subjects before the study.

MMT Course

The MMT course that consisted of daily 30 mg methadone 7 days per week and for 3 consecutive months.

The MMT course was continuous so that patients with interruption in methadone consumption (more than 2 days) were excluded from the study. During the MMT, patients just received methadone and consumption of any other medications was terminated at least 2 months before start of MMT course.

Hearing Assessment

Before starting MMT all patients underwent conventional audiometry (250–8,000 Hz) and those patients with normal hearing threshold were entered into the study. The audiological assessments (EHF and DPOAE) were conducted 1 month after termination of MMT course.

A clinical two-channel audiometer (Madsen Astera, GN Otometrics, Denmark) coupled with a standard (Telephonic TDH 39, Supra-aural) and extra high-frequency (Sennheiser HDA-200, Circumaural) headphones was used to record hearing thresholds. Conventional audiometry was determined for octave frequencies of 250–8,000 Hz, and EHF audiometry was determined for frequencies of 10,000, 12,000, 14,000, and 16,000 Hz. For EHF assessment, if the participants failed to respond to the maximum intensity produced by the audiometer, the instrument's highest output level was considered as their hearing threshold. All procedures for hearing assessment were carried out in an anechoic chamber according to ISO 8253-1.50 standards.

The DPOAE measurements were performed using a Madsen Capella system (GN Otometrics, Denmark) in an acoustically isolated chamber. Two primary pure tones at frequencies f1 and f2 were utilized, where f1 was set to 65 dB SPL and f2 to 55 dB SPL (f2/f1 ratio = 1.22). DPOAE amplitudes were recorded as a function of f2 frequency at 1,000–6,000 Hz. The acceptance criterion for DOPAE response was set to minimum level of 0 dB SPL and signal to noise ratio of $\geq$6 dB SPL at each f2 frequency (15).

Statistical Analysis

Statistical analysis was performed using SPSS version 18 software. Categorical variables were expressed as number and percentage and continuous variables were reported as mean $\pm$ standard deviation. Normality of the numerical data was verified using the Kolmogorov–Smirnov (K–S) test. Tests comparing paired data sets were conducted using paired-sample *t*-tests if K-S test indicated that the data were normally distributed. The Wilcoxon signed-rank test for related samples was used if the normality assumption was violated. For all statistical tests, the statistical significance level was set at $p = 0.05$.

RESULTS

The mean hearing thresholds of the both groups assessed by conventional PTA and EHF are presented in **Table 1**. The results showed that the mean thresholds at conventional frequencies (250–8,000 Hz) in the MMT group were slightly higher than control group, but these differences were not statistically significant (paired sample *t*-test, $p > 0.05$). In contrary, the mean thresholds for the EHF frequencies in the MMT group significantly increased from 10,000 to 16,000 Hz, compared to the healthy controls (paired sample *t*-test, $p < 0.001$) (**Table 1**). The mean DPOAE amplitudes for both groups are presented in **Table 2**. Although the mean DPOAE amplitudes did not differ significantly between the groups at the lower frequencies ($\leq$2,000 Hz), the mean amplitudes for frequencies 3,000–8,000 Hz were significantly reduced in the MMT subjects, compared to the controls in both ears.

EHF and DPOAE test, respectively, identified hearing loss in 11 (40.74%), and 14 (51.85%) of the patients who had previously received MMT. Ten (37.04%) patients exhibited abnormal hearing sensitivity in both EHF audiometry and DPOAE ranges in the MMT subjects.

DISCUSSION

The present study was aimed to identify the early onset of hearing loss in patients who underwent MMT and to compare them with the age matched normal hearing peers. Our findings showed a high prevalence of hearing impairment in patients who received MMT for at least 3 months. The standard method for ototoxicity monitoring is sequential measurement of pure-tone hearing thresholds within the conventional frequency range, 250–8,000 Hz. However, it seems that EHF audiometry and DPOAE technique are more sensitive procedures to detect early damage to auditory system.

All of the 27 enrolled patients who underwent MMT showed normal hearing at frequencies $\leq$8,000 Hz, whereas 11 (40.74%) subjects showed decreased hearing sensitivity at more than one of the four (10,000, 12,000, 14,000, or 16,000 Hz) EHFs. These findings show that methadone firstly damage the basal regions of the cochlea, leading to high frequency bilateral symmetrical sensorineural hearing loss (SNHL). In addition, hearing thresholds analysis in methadone group indicated a significant mild or moderate sloping hearing loss with high variability in EHF thresholds.

DPOAE test is non-invasive, fast and pre-neural procedure that provides frequency- and ear-specific information regarding the integrity of OHCs function of the cochlea. DPOAE assessments are commonly used for newborn hearing screening programs and differential diagnosis of auditory system disorders

TABLE 1 | Hearing thresholds in normal controls vs. patients underwent methadone maintenance treatment (MMT).

Group	Frequency (Hz)										
	250	**500**	**1,000**	**2,000**	**4,000**	**6,000**	**8,000**	**10,000**	**12,000**	**14,000**	**16,000**
RIGHT EAR											
MMT	7.54 (3.92)	11.09 (4.47)	11.45 (4.45)	12.89 (5.78)	13.66 (5.87)	13.30 (7.90)	15.45 (7.25)	26.95 (8.05)	33.90 (12.25)	42.25 (13.46)	54.05 (11.32)
Control	8.39 (3.68)	10.67 (4.95)	12.12 (3.89)	13.45 (5.19)	13.36 (6.34)	14.36 (4.94)	14.66 (6.95)	19.57 (8.58)	22.07 (9.25)	30.90 (10.69)	33.37 (8.90)
p-value	NS	NS	NS	NS	NS	NS	NS	<0.001	<0.001	<0.001	<0.001
LEFT EAR											
MMT	9.89 (3.17)	10.56 (4.78)	12.49 (4.52)	12.55 (6.23)	13.43 (4.54)	12.35 (7.81)	15.64 (3.12)	27.22 (11.34)	35.54 (8.07)	43.31 (9.25)	49.01 (11.92)
Control	8.54 (3.85)	10.66 (4.54)	11.94 (5.65)	12.28 (4.915)	13.09 (4.71)	11.63 (6.13)	14.31 (6.35)	21.74 (12.45)	25.78 (9.18)	29.45 (10.73)	36.22 (12.14)
p-value	NS	NS	NS	NS	NS	NS	NS	<0.001	<0.001	<0.001	<0.001

All data are expressed as mean (SD) dB HL; NS, Not significant.

TABLE 2 | The DPOAE amplitudes in normal controls vs. patients underwent methadone maintenance treatment (MMT).

Group	Frequency (Hz)					
	1,000	**2,000**	**3,000**	**4,000**	**60,000**	**8,000**
RIGHT EAR						
MMT	11.92 (5.62)	10.81 (3.28)	8.44 (5.31)	6.35 (7.08)	3.28 (5.54)	2.79 (3.64)
Control	11.35 (7.80)	11.07 (6.62)	12.75 (5.34)	10.06 (4.76)	8.47 (3.91)	7.38 (4.45)
p-value	NS	NS	<0.001	<0.001	<0.001	<0.001
LEFT EAR						
MMT	11.38 (5.74)	11.65 (3.90)	7.34 (5.76)	6.79 (4.13)	6.35 (7.08)	1.84 (3.77)
Control	12.06 (5.74)	12.58 (4.54)	10.45 (6.27)	11.23 (5.83)	10.02 (4.76)	6.12 (4.83)
p-value	NS	NS	0.031	<0.001	<0.001	<0.001

All data are expressed as mean (SD) dB SPL; DPOAE, Distortion-Product Otoacoustic Emission; NS, Not significant.

(14–16). During this study, we observed a significant decline in DPOAE amplitudes in 14 (51.85%) of the patients which was more pronounced in 3,000–8,000 Hz frequency ranges. These findings that the patients in our study who experienced a reduction in DPOAE amplitudes did not demonstrate clinically significant hearing impairment in the 250–8,000 Hz frequency range, implying that DPOAEs can detect subtle cochlear hair cell lesion before hearing loss is appeared in conventional frequency range in patients who underwent methadone therapy. Moreover, our findings indicated that decrements in DPOAE amplitudes occurred at a much faster rate for the higher frequencies than the lower frequencies.

Methadone is a synthetic opioid that is used as an analgesic and as a maintenance anti-addictive medication for patients with opioid dependency. There is a growing body of evidence that abuse of the synthetic opioid can lead to temporary or permanent SNHL (16). So far, six case reports have been published on hearing loss after methadone overdose (2–4, 18). Most of the cases (4 of 6) of hearing loss following methadone abuse have been reportedly shown fully and speedy recovery and only two case reports showed persistent SNHL (4, 8). The findings of these case reports suggested that the reversible or irreversible methadone induced SNHL depends on the duration and time of exposure as well as the health status of drug users (10). Christenson and Marjal (18) reported two patients of sudden SNHL after methadone abuse, though the hearing loss in both cases reversed completely within 24 h. However, none of our patients had history of taking an overdose of prescribed methadone. Most of the previously reported cases of opiate-induced SNHL seem to involve a retrocochlear process. However, there have been few cases of opioids induced SNHL that were improved only after cochlear implants indicating that the chronic opioid induced hearing loss is a cochlear process rather than retrocochlear process (20).

In all cases with speedy recovery the methadone was withheld but in the cases with persistent hearing loss, one case did not stop methadone and used it at prescribed dose (8) and on the other case the data is not available (4). In our study the patients received a fixed dose of methadone (30 mg per day) for three months continuously and then stopped the medication consumption one month before the audiometric assessments. Our findings contradicted the previous case reports in which the

patients showed speedy and full resolution following the stop of methadone consumption.

Opioid receptors function in neuronal systems and local networks involved in the initiation of drug action and the subsequent development of adaptations under repeated drug consumption. It has been shown that opioid neuropeptides participate in synaptic processing in inner hair cells of the cochlea (21). The expression of the four opioid receptors (morphine, deferens, ketocyclazocine, and nociceptin), endogenous opioid peptides, and the physiologic response in the cochlea of animal models and in humans suggest that synthetic opioids may influence the homeostasis of the inner ear (16).

Long term consumption of opioids could induce damage in the basal section of the cochlear that could subsequently lead to hearing loss. This damage could increase the hearing threshold especially in higher frequencies and reduce the DPOAE amplitude. This adverse effect of opioid on hearing threshold should be considered in interpretation of our findings. It is possible that the observed higher EHF thresholds and reduced DPOAE amplitudes in the patients with opioid dependency could be due to the basal turn cochlear damage induced by opioid consumptions rather than the effects of MMT.

The pathophysiology of methadone induced hearing loss is not fully understood yet. Different theories have been proposed to explain the effects of opioid drugs on hearing systems (2–4, 8, 16, 22). The most commonly proposed theories are cochlear ischemia, genetic polymorphism and mutations, blood-labyrinth selective transport of proteins and receptors, and direct effect of opioids on opioid receptors.

Cochlear ischemia is mainly occurred following vasospasm or vasculitis of the branch of the spiral modiolar artery. The cochlear structure is very susceptible to hypoxia. Different studies have shown that opioid drugs trigger the production and release of endothelin-1 as an endogenous vasoconstrictor (23). This factor binds to endothelin receptor (ET-A) located on smooth muscle cells of the spiral modiolar artery, and leads to vasospasm and then cochlear ischemia (4).

Genetic polymorphism has been reportedly a possible predisposing factor for opioid-induced hearing impairments particularly aminoglycosides induced hearing impairments. Different mutations and polymorphisms such as allelic variants in the liver metabolic enzymes and mutations induced by mu-opioid receptor (MOR), which are occurred in response to opioid drugs may contribute to different levels of hearing impairments (2).

Blood-labyrinth barrier plays pivotal role in regulating and establishing homeostasis of inner ear fluid mainly through selectively active transport of molecules based on the molecular weight. One hypothesis is based on the inter-person variation in the blood-labyrinth transport channels and differences in the molecular weight of opioid drugs so that in some opioid users opioid drugs are more likely to cross the barrier and induce hearing loss (4, 8).

Other hypothesis on the mechanism of action of opioids in inducing hearing loss is the effect of opioids on specific opioid receptors present in the inner ear. The main opioid receptors present in the central and peripheral nervous systems are mu (MOR), delta (DOR), and kappa (KOR) opioid receptor. The majority of opioids are MOR-agonist. Opioid receptors are present in different structures of the inner ear including inner and OHCs, spiral ganglion, supporting cells of the organ of Corti, and nerve fibers. The activation of MOR can inhibit calcium which in turn inhibits the basal adenylate cyclase activity. Endogenous opioid peptides such as endorphin and enkephalin have likely important role in auditory neuromodulation. These inhibitory effects are more pronounced in cochlear stria vascularis of inner ear, a structure which is rich in blood vessels, and could negatively affect mechanoelectrical transduction of the signal within the cochlea (16, 24, 25). It has been hypothesized that exogenous opioids could stimulate MOR which subsequently impairs endogenous auditory neuromodulation compounds that lead to hearing loss (26, 27). To understand the exact mechanisms of methadone induced hearing loss, further studies should be conducted.

Investigating the risk factors of methadone induced hearing loss, we should consider the mutual relationship between the substance abuse and prevalence of hearing loss. Several studies have suggested that individuals with hearing loss have higher susceptibility to substance abuse. McKee et al. compared the prevalence of substance use disorders among adults with and without self-reported hearing loss among a nationally representative sample ($n = 86{,}186$) of adults in the US. They reported that hearing loss was independently associated with an increased likelihood of substance abuse disorder. Moreover, hearing loss was independently associated with substance use disorders among age group of $\leq$49 years. Interestingly, these associations are particularly pronounced for prescription opioid use disorders in the group aged 18–34 years (28). However, in our study the subjects showed normal hearing threshold before the start of the MMT; thus, the observed hearing loss could be attributed to the 3 months MMT course. This should be noted that in our study we did not use EHF nor DPOAE for pre-MMT assessments of hearing threshold but we used the conventional PTA for hearing assessments. This limitation could decrease the certainty of the causal link between the MMT and the observed hearing loss.

In conclusion, our findings showed that EHF audiometry and DPOAE techniques have greater diagnostic values than the conventional PTA to detect early changes in auditory functions in patients undergoing MMT. However, opioid addictions could induce damage in the basal section of the cochlear which should be considered in interpretation of our findings. In this regard, it is possible that the observed higher EHF thresholds and reduced DPOAE amplitudes in the patients with opioid dependency may be due to the basal turn cochlear damage induced by opioid consumptions rather than the effects of MMT. Therefore, the effect of methadone treatment cannot be conclusively determined and further case control studies with large sample size with pre- and post-MMT assessments are necessary to shed more light on the effects of methadone on hearing functions.

DATA AVAILABILITY

The datasets generated for this study are available on request to the corresponding author.

ETHICS STATEMENT

All procedures of this study were approved by Ethics committee of Ahvaz Jundishapur University of Medical Sciences, Ahvaz, Iran.

AUTHOR CONTRIBUTIONS

AB, NS, GM, and AY contributed conception and design of the study. AB and NS collected the data and organized the database. GM and AY performed the statistical analysis. AB wrote the first draft of the manuscript. NS, GM, and AY wrote sections of the manuscript. All authors contributed to manuscript revision, read and approved the submitted version.

ACKNOWLEDGMENTS

Authors would like to thank the personnel of Khuzestan Cochlear Implant Center, Ahvaz, Iran for their support during this study.

REFERENCES

1. Manchikanti L, Singh A. Therapeutic opioids: a ten-year perspective on the complexities and complications of the escalating use, abuse, and nonmedical use of opioids. *Pain Phys.* (2008) 11:S63–88.
2. Shaw KA, Babu KM, Hack JB. Methadone, another cause of opioid-associated hearing loss: a case report. *J Emerg Med.* (2011) 41:635–9. doi: 10.1016/j.jemermed.2010.11.014
3. van Gaalen FA, Compier EA, Fogteloo AJ. Sudden hearing loss after a methadone overdose. *Eur Arch Oto Rhino Laryngol.* (2009) 266:773–4. doi: 10.1007/s00405-009-0935-6
4. Vorasubin N, Calzada AP, Ishiyama A. Methadone-induced bilateral severe sensorineural hearing loss. *Am J Otolaryngol.* (2013) 34:735–38. doi: 10.1016/j.amjoto.2013.08.011
5. Aulet RM, Flis D, Sillman J. A case of heroin induced sensorineural hearing loss. *Case Rep Otolaryngol.* (2014) 2014:962759. doi: 10.1155/2014/962759
6. Schrock A, Jakob M, Wirz S, Bootz F. Sudden sensorineural hearing loss after heroin injection. *Eur Arch Oto Rhino Laryngol.* (2008) 265:603–6. doi: 10.1007/s00405-007-0495-6
7. Kortequee S, Agada FO, Coatesworth AP. Sudden sensorineural hearing loss following intracarotid injection of heroin. *Int J Clin Pract Suppl.* (2005) 59:128–9. doi: 10.1111/j.1368-504X.2005.00359.x
8. Saifan C, Glass D, Barakat I, El-Sayegh S. Methadone induced sensorineural hearing loss. *Case Rep Med.* (2013) 2013:242730. doi: 10.1155/2013/242730
9. Katz J, Burkard R, Medwetsky L. *Handbook of Clinical Audiology*. Lippincott Williams & Wilkins (2002). Available online at: https://books.google.com/books/about/Handbook_of_Clinical_Audiology.html?id=Aj6nVIegE6AC (accessed August 7, 2018).
10. Vignesh SS, Jaya V, Moses A, Muraleedharan A. Identifying early onset of hearing loss in young adults with diabetes mellitus type 2 using high frequency audiometry. *Indian J Otolaryngol Head Neck Surg.* (2015) 67:234–7. doi: 10.1007/s12070-014-0779-2
11. Drexl M, Krause E, Gürkov R. A comparison of distortion product otoacoustic emission properties in Ménière's disease patients and normal-hearing participants. *Ear Hear.* (2017) 39:1. doi: 10.1097/AUD.0000000000000461
12. Katz J, Chasin M, English KM, Hood LJ, Tillery KL. *Handbook of Clinical Audiology*. Philadelphia, PA: Wolters Kluwer Health (2015).
13. Paglialonga A, Del Bo L, Ravazzani P, Tognola G. Quantitative analysis of cochlear active mechanisms in tinnitus subjects with normal hearing sensitivity: multiparametric recording of evoked otoacoustic emissions and contralateral suppression. *Auris Nasus Larynx.* (2010) 37:291–8. doi: 10.1016/j.anl.2009.09.009
14. Konrad-Martin D, Neely ST, Keefe DH, Dorn PA, Gorga MP. Sources of distortion product otoacoustic emissions revealed by suppression experiments and inverse fast Fourier transforms in normal ears. *J Acoust Soc Am.* (2001) 109:2862–79. doi: 10.1121/1.1370356
15. Reavis KM, McMillan G, Austin D, Gallun F, Fausti SA, Gordon JS, et al. Distortion-product otoacoustic emission test performance for ototoxicity monitoring. *Ear Hear.* (2011) 32:61–74. doi: 10.1097/AUD.0b013e3181e8b6a7
16. Lopez IA, Ishiyama A, Ishiyama G, Lopez A. Sudden sensorineural hearing loss due to drug abuse. *Semin Hear.* (2012) 33:251–60. doi: 10.1055/s-0032-1315724
17. Vasconcelos KA, de Frota SMMC, Ruffino-Netto A, Kritski AL. Sequential analysis as a tool for detection of amikacin ototoxicity in the treatment of multidrug-resistant tuberculosis. *J Bras Pneumol.* (2018) 44:85–92. doi: 10.1590/s1806-37562016000000312
18. Christenson BJ, Marjala AR. Two cases of sudden sensorineural hearing loss after methadone overdose. *Ann Pharmacother.* (2010) 44:207–10. doi: 10.1345/aph.1M250
19. General Assembly of the World Medical Association. World Medical Association Declaration of Helsinki: ethical principles for medical research involving human subjects. *J Am Coll Dent.* (2014) 81:14–8.
20. Oh AK, Ishiyama A, Baloh RW. Deafness associated with abuse of hydrocodone/acetaminophen. *Neurology.* (2000) 54:2345. doi: 10.1212/WNL.54.12.2345
21. Eybalin M. Neurotransmitters and neuromodulators of the mammalian cochlea. *Physiol Rev.* (1993) 73:309–73. doi: 10.1152/physrev.1993.73.2.309
22. MacDonald LE, Onsrud JE, Mullins-Hodgin R. Acute sensorineural hearing loss after abuse of an inhaled, crushed oxymorphone extended-release tablet. *Pharmacother J Hum Pharmacol Drug Ther.* (2015) 35:e118–21. doi: 10.1002/phar.1605
23. Ishiyama A, Lopez I, Ishiyama G, Ishiyama A. Review of opioid-associated hearing loss and possible mechanism of opioid-mediated endothelin-1-dependent cochlear vasoconstriction. *J Otol Rhinol.* (2014) 3. doi: 10.4172/2324-8785.1000145
24. Schweitzer VG, Darrat I, Stach BA, Gray E. Sudden bilateral sensorineural hearing loss following polysubstance narcotic overdose. *J Am Acad Audiol.* (2011) 22:208–14. doi: 10.3766/jaaa.22.4.3
25. Waldhoer M, Bartlett SE, Whistler JL. Opioid receptors. *Annu Rev Biochem.* (2004) 73:953–90. doi: 10.1146/annurev.biochem.73.011303.073940
26. Jongkamonwiwat N, Phansuwan-Pujito P, Sarapoke P, Chetsawang B, Casalotti SO, Forge A, et al. The presence of opioid receptors in rat inner ear. *Hear Res.* (2003) 181:85–93. doi: 10.1016/S0378-5955(03)00175-8
27. Nguyen KD, Mowlds D, Lopez IA, Hosokawa S, Ishiyama A, Ishiyama G. Mu-opioid receptor (MOR) expression in the human spiral ganglia. *Brain Res.* (2014) 1590:10–9. doi: 10.1016/j.brainres.2014.09.051
28. McKee MM, Meade MA, Zazove P, Stewart HJ, Jannausch ML, Ilgen MA. The relationship between hearing loss and substance use disorders among adults in the U.S. *Am J Prev Med.* (2019) 56:586–90. doi: 10.1016/j.amepre.2018.10.026

Conflict of Interest Statement: The authors declare that the research was conducted in the absence of any commercial or financial relationships that could be construed as a potential conflict of interest.

frontiers in Immunology

ORIGINAL RESEARCH
published: 17 July 2019
doi: 10.3389/fimmu.2019.01660

Nfatc4 Deficiency Attenuates Ototoxicity by Suppressing Tnf-Mediated Hair Cell Apoptosis in the Mouse Cochlea

Yanping Zhang[1,2†], *Diyan Chen*[1,2†], *Liping Zhao*[1,2], *Wen Li*[1,2], *Yusu Ni*[1,2*], *Yan Chen*[1,2*] and *Huawei Li*[1,2,3*]

[1] State Key Laboratory of Medical Neurobiology, Department of Affiliated Eye and ENT Hospital, ENT Institute and Otorhinolaryngology, Institutes of Biomedical Sciences and the Institutes of Brain Science and the Collaborative Innovation Center for Brain Science, Fudan University, Shanghai, China, [2] NHC Key Laboratory of Hearing Medicine, Fudan University, Shanghai, China, [3] Shanghai Engineering Research Centre of Cochlear Implant, Shanghai, China

OPEN ACCESS

Edited by:
Agnieszka J. Szczepek, Charité Medical University of Berlin, Germany

Reviewed by:
Tejbeer Kaur, Washington University in St. Louis, United States
Dalian Ding, University at Buffalo, United States

***Correspondence:**
Yusu Ni
niyusu@aliyun.com
Yan Chen
chenyan0528@fudan.edu.cn
Huawei Li
hwli@shmu.edu.cn

†*These authors have contributed equally to this work*

Specialty section:
This article was submitted to Multiple Sclerosis and Neuroimmunology, a section of the journal Frontiers in Immunology

Received: *19 March 2019*
Accepted: *03 July 2019*
Published: *17 July 2019*

Citation:
Zhang Y, Chen D, Zhao L, Li W, Ni Y, Chen Y and Li H (2019) Nfatc4 Deficiency Attenuates Ototoxicity by Suppressing Tnf-Mediated Hair Cell Apoptosis in the Mouse Cochlea. Front. Immunol. 10:1660. doi: 10.3389/fimmu.2019.01660

The loss of sensory hair cells in the cochlea is the major cause of sensorineural hearing loss, and inflammatory processes and immune factors in response to cochlear damage have been shown to induce hair cell apoptosis. The expression and function of Nfatc4 in the cochlea remains unclear. In this study, we investigated the expression of Nfatc4 in the mouse cochlea and explored its function using *Nfatc4*$^{-/-}$ mice. We first showed that *Nfatc4* was expressed in the cochlear hair cells. Cochlear hair cell development and hearing function were normal in *Nfatc4*$^{-/-}$ mice, suggesting that Nfatc4 is not critical for cochlear development. We then showed that when the hair cells were challenged by ototoxic drugs Nfatc4 was activated and translocated from the cytoplasm to the nucleus, and this was accompanied by increased expression of *Tnf* and its downstream targets and subsequent hair cell apoptosis. Finally, we demonstrated that Nfatc4-deficient hair cells showed lower sensitivity to damage induced by ototoxic drugs and noise exposure compared to wild type controls. The Tnf-mediated apoptosis pathway was attenuated in Nfatc4-deficient cochlear epithelium, and this might be the reason for the reduced sensitivity of Nfatc4-deficient hair cells to injury. These findings suggest that the amelioration of inflammation-mediated hair cell apoptosis by inhibition of Nfatc4 activation might have significant therapeutic value in preventing ototoxic drug or noise exposure-induced sensorineural hearing loss.

Keywords: Nfatc4, inflammation, inner ear, cochlear hair cells, cell apoptosis, hearing loss

INTRODUCTION

Hearing loss is one of the most common sensory disorders in humans, and around 466 million people worldwide have disabling hearing loss. Sensorineural hearing loss might result from genetic causes, the use of ototoxic drugs, excessive noise exposure, and aging. Sensory hair cells in the cochlea detect sound and are responsible for converting mechanical signals into electrical signals, and aminoglycosides and excessive noise exposure can induce caspase-mediated apoptosis in hair cells and thus lead to hearing loss (1, 2).

Increasing evidence suggests that inflammatory processes play significant roles in the response to cochlear injury. For example, the expression levels of pro-inflammatory cytokines, chemokines,

and cell adhesion molecules are increased in both acute and chronic noise-exposed mouse cochleae (3), and several clinical studies have shown that inflammation is a significant component of the mechanisms underlying presbycusis (4). Tumor necrosis factor (Tnf, also known as Tnf-α) is a central circulating factor that is essential for the systemic inflammatory mechanism. Tnf expression is increased in the mouse cochlea following acute and chronic noise exposure (3, 5), and exposure to Tnf can induce hair cell damage and apoptosis in cultured cochlear explants (6).

Nuclear factor of activated T cells 4 (*Nfatc4*), also known as *Nfat3*, encodes a member of the nuclear factor of activated T cells (NFAT) protein family, which are integral proteins in the development and function of the immune system. The activation of the NFAT family is controlled by calcineurin, a Ca^{2+}-dependent phosphatase. Originally identified in T cells as inducers of cytokine gene expression (7), NFAT proteins have been shown to play various roles in cells outside of the immune system, including functions in cell development, differentiation, and adaptation (8) and in neuronal excitability (9). Nfatc4 is also involved in cell apoptosis in many tissues and organs. Nfatc4 is anti-apoptotic and mediates cell survival in some tissues, such as neurons (10), and the NMDAR-Nfatc4-BDNF pathway contributes to cell survival during cortical development (11). However, in other tissues, such as glioma cells and renal tubular cells, Nfatc4 mediates cell apoptosis. In glioma cells, Nfatc4 activation is a prerequisite for the induction of DOX-mediated apoptosis (12). In renal tubular cells, a carboplatin-mediated increase in reactive oxygen species (ROS) leads to Nfatc4 activation and cell apoptosis, and treatment with N-acetylcysteine, an antioxidant, blocks Nfatc4 activation and thus prevents cell apoptosis (13).

However, the expression and function of Nfatc4 in the cochlea remains unclear. In this study, we found that Nfatc4 is expressed in the cochlear hair cells and that when the hair cells were challenged by neomycin (an ototoxic drug) Nfatc4 translocated to the nucleus, enhanced the expression of *Tnf* and its downstream targets, and led to hair cell apoptosis. Furthermore, Nfatc4-deficient hair cells showed reduced sensitivity to ototoxic drugs and noise exposure compared to wild type (WT) controls. The Tnf-mediated apoptosis pathway was attenuated in Nfatc4-deficient hair cells, and this might be the reason for the reduced sensitivity of Nfatc4-deficient hair cells to injury.

MATERIALS AND METHODS

Mice and Genotyping

Nfatc4 knockout mice were generated by Professor Gerald R. Crabtree (14) and provided by Dr. Yan-Ai Mei of Fudan University. As previously described (9, 14), *Nfatc4* knockout ($Nfatc4^{-/-}$) mice were backcrossed 10–12 times onto C57BL/6 mice to obtain homozygous *Nfatc4* mice. $Nfatc4^{-/-}$ and WT mice (littermates) were genotyped by PCR. The three primers used in genotyping were CCG GTG CAT CCC GGG TAA CCA ATC AGA GA; TCC TCA TCC TCG CAG CTT GCG GCC CC; and AGC GTT GGC TAC CCG TGA TAT TGC TGA AGA. The genotypes were identified by a 300 bp WT band and a 700 bp mutant band. Mice of both sexes were used. This study was carried out in strict accordance with the "Guiding Directive for Humane treatment of Laboratory Animals" issued by the Chinese National Ministry of Science and Technology in 2006. All experiments were approved by the Shanghai Medical Experimental Animal Administrative Committee (Permit Number: 2009-0082), and all efforts were made to minimize suffering and reduce the number of animals used.

Experimental Protocol (*In vivo* Studies)

Hearing thresholds were measured in anesthetized postnatal day (P)30 or P33 mice by auditory brainstem response (ABR) analysis as described previously (2). The hearing thresholds were assessed at four frequencies (8, 16, 24, and 32 kHz) using a TDT system (Tucker Davies Technologies).

To explore the effect of Nfatc4 deficiency on sensitivity to noise exposure in cochlear hair cells, the hearing function of P30 $Nfatc4^{-/-}$ and WT mice (littermates) was examined by ABR. Twenty-four hours after the ABR test, the mice were exposed to noise at 118 dB (8–16 kHz) for 2 h. At 2 days after noise exposure, hearing function was examined again by ABR, after which the mice were sacrificed and their cochleae were removed and fixed in 4% paraformaldehyde (PFA). After decalcification, the cochlear epithelium was prepared for morphological analysis.

Experimental Protocol (*In vitro* Studies)

Cochlear sensory epithelium was dissected from P2 mice and cultured as previously reported (15). Neomycin (1 mM, Sigma) was added to the medium for 6 h to kill hair cells. After neomycin was removed, the tissues were cultured in serum-free medium for an additional 24 h before fixation. For the Tnf inhibition experiment, lenalidomide (Len) or etanercept (ETA) and neomycin were added simultaneously. For the inhibition of calcineurin/NFAT signaling, cyclosporin A (CsA) or tacrolimus (FK506) and neomycin were added simultaneously.

Immunofluorescence and TUNEL Staining

Rabbit polyclonal anti-myosin VIIA (Myo7a) (Proteus Biosciences, 1:1,000 dilution), goat polyclonal anti-SRY (sex-determining region Y)-box 2 (Sox2) (Santa Cruz Biotechnology, 1:1,000 dilution), and mouse monoclonal anti-Nfatc4 (Santa Cruz Biotechnology, 1:200 dilution) were used. Corresponding donkey anti-rabbit, anti-goat, or anti-mouse secondary antibodies conjugated with Alexa Fluor 488, Alexa Fluor 568, or Alexa Fluor 647 (ThermoFisher Scientific, 1:500 dilution) were used. Immunofluorescence staining was

Abbreviations: Tnf, tumor necrosis factor; Nfatc4, Nuclear factor of activated T cells 4; NMDAR, N-methyl-D-aspartate receptor; BDNF, brain derived necrosis factor; ROS, reactive oxygen species; WT, wild type; ABR, auditory brainstem response; TDT system, Tucker Davies Technologies; PFA, 4% paraformaldehyde; Myo7a, myosin VIIA; IHCs, inner hair cells; OHCs, outer hair cells; Casp8, caspase 8; Casp9, caspase 9; Casp3, caspase 3; Len, Lenalidomide; ETA, Etanercept; Mif, migration inhibitory factor; TLR 4, Toll-like receptor 4; NOX3,NADPH oxidase 3; STAT1, signal transducers and activators of transcription 1; CsA, Cyclosporin A; FK506, Tacrolimus.

performed as previously reported (2). A TUNEL Kit (Roche) was used to detect apoptotic cells according to the manufacturer's instructions. Specimens were examined by confocal fluorescence microscopy (Leica SP8).

Real-Time PCR

Real-time PCR was performed on cochlear explants. A total of 2 μg total RNA was used for reverse transcription with Superscript III reverse transcriptase (Invitrogen), and real-time PCR was performed on an ABI 7500 real-time PCR system (Applied Biosystems) using the TB Green PrimeScript RT-PCR Kit (Takara). All primers were designed to flank individual exons and were tested by PCR. The optimized conditions were held constant for each sample to assure valid comparisons of the results. Primer sets were as follows: *Actb* (F) tct ttg cag ctc ctt cgt tg; (R) tcc ttc tga ccc att ccc ac; *Nfatc4* (F) tcg gag agg aaa agg agc c; (R) tgg tga gtg cat ccc tgg; *Tnf* (F) gcc tcc ctc tca tca gtt ct; (R) gca gcc ttg tcc ctt gaa g; *Casp8* (F) aac tgc gtt tcc tac cga ga; (R) cct tgt tcc tcc tgt cgt ct; *Casp3* (F) gag cag ctt tgt gtg tgt ga; (R) tgt ctc aat gcc aca gtc ca; *Casp9* (F) gga ccg tga caa act tga gc; *Casp9* (R) tct cca tca aag ccg tga cc. *Actb* was used as a housekeeping gene for control purposes. Each PCR reaction was carried out in triplicate, and the relative quantification of gene expression was analyzed using the $2^{-\Delta\Delta CT}$ method with *Actb* as the endogenous reference.

Cell Counting and Statistical Analysis

To quantify the immunostaining-positive cells, nine separate segments along the entire cochlea were selected from the apex to the base (corresponding to approximately 4.0, 5.6, and 8.0 kHz in the apical turn; 11.3, 16.0, and 22.6 kHz in the middle turn; and 32.0, 45.2, and 64.0 kHz in the basal turn). Data are presented as the mean ± SD. Student's 2-tailed *t*-test was used to analyze the differences between two groups in **Figures 4**, **5**. For the comparison of differences among three groups in **Figure 6E**, one-way ANOVA followed by Bonferroni *post-test* for multiple comparisons was used. For the comparison of differences among three or more groups in other figures, two-way ANOVA followed by Bonferroni *post-test* for multiple comparisons was used. $P < 0.05$ was considered significant, and the *p*-values are presented in the figures (*indicates $p < 0.05$, **indicates $p < 0.01$, and ***indicates $p < 0.001$).

RESULTS

Nfatc4 Was Expressed in the Cochlear Hair Cells

Immunofluorescence staining with the anti-Nfatc4 antibody was performed to determine the extent of Nfatc4 expression

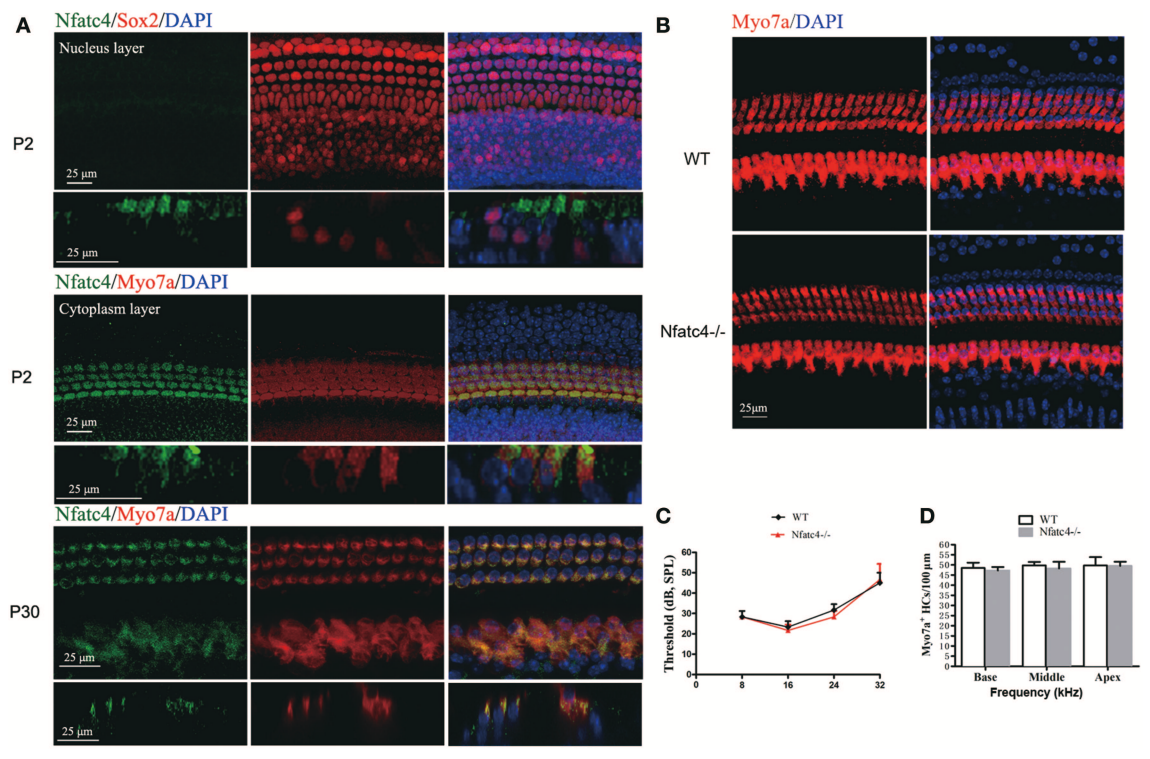

FIGURE 1 | Nfatc4 was expressed in the cochlear hair cells, and *Nfatc4*$^{-/-}$ mice showed normal cochlear development and hearing function. **(A)** Nfatc4 immunofluorescence staining in the cochlear hair cells (middle turns) of P2 and P30 WT mice. Myo7a and Sox2 were used as hair cell and supporting cell markers, respectively. **(B)** Myo7a immunofluorescence in cochlear hair cells (middle turn) of adult *Nfatc4*$^{-/-}$ and WT mice. **(C)** The hearing thresholds of ABR measurement in the adult *Nfatc4*$^{-/-}$ and WT mice. **(D)** The numbers of hair cells in *Nfatc4*$^{-/-}$ and WT mice. Scale bars: 25 μm. $n = 5$.

in the mouse cochlea. Myo7a and Sox2 were used as hair cell and supporting cell markers, respectively. Double staining of Nfatc4 and Myo7a showed that Nfatc4 was expressed in hair cells in all three turns of the cochlea in both the neonatal and adult mice (**Figure 1A**). Double immunofluorescence staining of Nfatc4 and Sox2 showed that Nfatc4 was not expressed in cochlear supporting cells (**Figure 1A**).

Nfatc4$^{-/-}$ Mice Showed Normal Cochlear Development and Hearing Function

To explore the role of Nfatc4 in the development of cochlear hair cells and in hearing function, we used *Nfatc4*$^{-/-}$ mice. In the adult stage, the morphological features and quantities of cochlear hair cells in the *Nfatc4*$^{-/-}$ mice were similar to the WT controls (**Figures 1B,D**). The hearing function of adult *Nfatc4*$^{-/-}$ mice was normal at 8, 16, 24, and 32 KHz as demonstrated by ABR measurement data (**Figure 1C**). These results suggested that *Nfatc4* is not a critical gene for cochlear development.

Cochlear Hair Cells in *Nfatc4*$^{-/-}$ Mice Showed Reduced Sensitivity to Aminoglycoside Antibiotic-Induced Ototoxicity

We next investigated the role of Nfatc4 in hair cell injury using an aminoglycoside antibiotic injury model. In this model, the sensitivity of hair cells to ototoxic drug injury increased from the apical turn to the basal turn. Cultured cochlear epithelium tissues from *Nfatc4*$^{-/-}$ and WT mice were treated with 1 mM neomycin for 6 h and harvested after an additional 24 h in culture (**Figure 2A**). Myo7a staining was then used to identify the remaining hair cells. In the WT control group with neomycin administration, the numbers of inner hair cells (IHCs) were 12.25 ± 0.5, 6.25 ± 1.71, and 4.75 ± 0.95 cells/100 μm in the apical, middle, and basal turns, respectively (**Figures 2B,D**), and the numbers of outer hair cells (OHCs) were 43.50 ± 3.11, 12.25 ± 1.71, and 1.00 ± 1.15 cells/100 μm in the apical, middle, and basal turns, respectively (**Figures 2B,C**). In the *Nfatc4*$^{-/-}$ cochlear epithelium with neomycin administration, more hair cells were observed, and

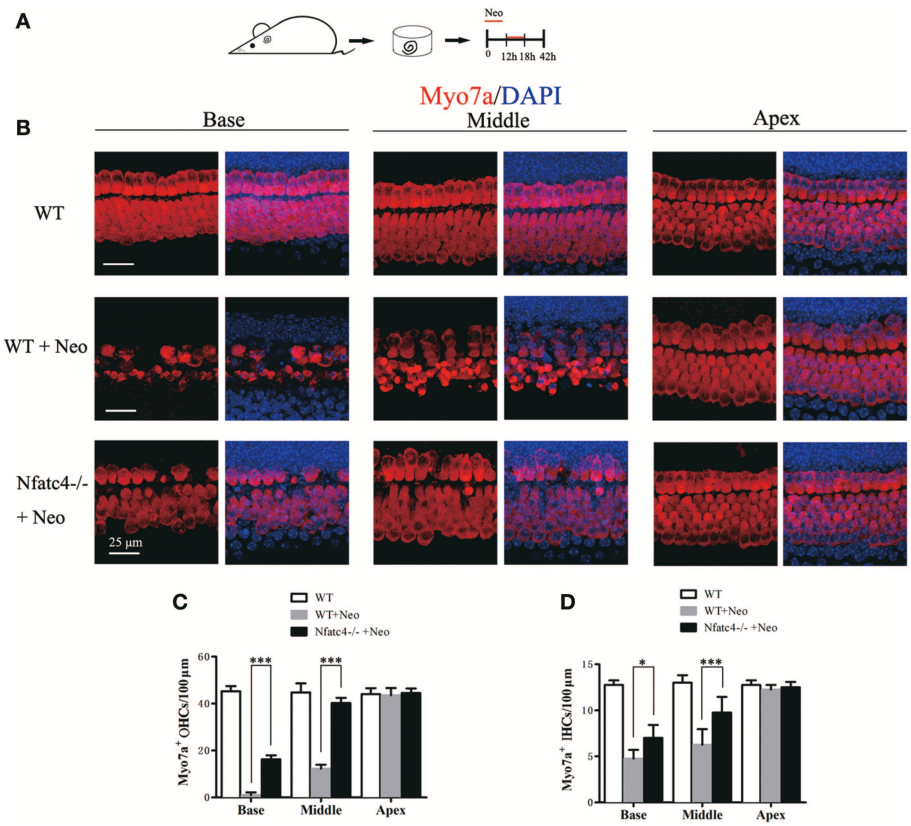

FIGURE 2 | Cochlear hair cells in *Nfatc4*$^{-/-}$ mice showed reduced sensitivity to aminoglycoside antibiotic-induced ototoxicity. **(A)** The diagram of the assay. Cochlear sensory epithelium samples from P2 *Nfatc4*$^{-/-}$ and WT mice were dissected out and allowed to recover for 12 h. The samples were treated with 1 mM neomycin for 6 h, allowed to recover for 24 h, and then used for immunostaining. **(B)** The representative Myo7a immunofluorescence staining of sensory epithelium from *Nfatc4*$^{-/-}$ and WT mice after neomycin treatment. **(C,D)** Quantification of inner hair cells (IHCs) and outer hair cells (OHCs). The numbers of IHCs and OHCs in the middle and basal turns were significantly greater in the cochlear epithelium from *Nfatc4*$^{-/-}$ mice than in WT mice after neomycin treatment. Scale bar = 25 μm. *indicates $p < 0.05$ and ***indicates $p < 0.001$. $n = 5$.

there were 12.5 ± 0.58, 9.75 ± 1.71, and 7.00 ± 1.41 cochlear IHCs/100 μm and 44.50 ± 1.91, 40.25 ± 2.22, and 16.25 ± 1.71 cochlear OHCs/100 μm in the apical, middle, and basal turns, respectively (**Figures 2B–D**). The numbers of hair cells in the middle and basal turns were significantly greater in the cochlear epithelium from *Nfatc4*$^{-/-}$ mice compared with control mice, indicating that *Nfatc4*$^{-/-}$ cochlear hair cells were less sensitive to aminoglycoside antibiotic-induced injury.

Nfatc4 Deficiency Protected Against Noise-Induced Hearing Loss and Hair Cell Loss

To further explore the role of Nfatc4 in the adult cochlea, we used a noise exposure hair cell injury model. In this model, the sensitivity of hair cells to noise injury depends on the noise frequency, intensity, and duration. In this experiment, adult mice were exposed to 118 dB noise (8–16 kHz) for 2 h, which leads to OHC loss in the apical-middle, middle, and basal turns and thus results in permanent hearing loss (16). Hearing function was examined by ABR at 2 days after noise exposure, and then the cochleae were harvested (**Figure 3A**). In the control group, noise exposure led to significant OHC loss in the cochlear turn at 11.3, 16.0, 22.6, 32.0, 45.2, and 64.0 kHz, which was consistent with results from a previous study (16). However, in *Nfatc4*$^{-/-}$ mice the noise-induced loss of OHCs was significantly decreased in the middle and basal turns (at 16.0, 22.6, 32.0, 45.2, and 64.0 kHz) compared with control mice (**Figures 3B,C**), indicating that adult *Nfatc4*-deficient cochlear hair cells were more tolerant of noise.

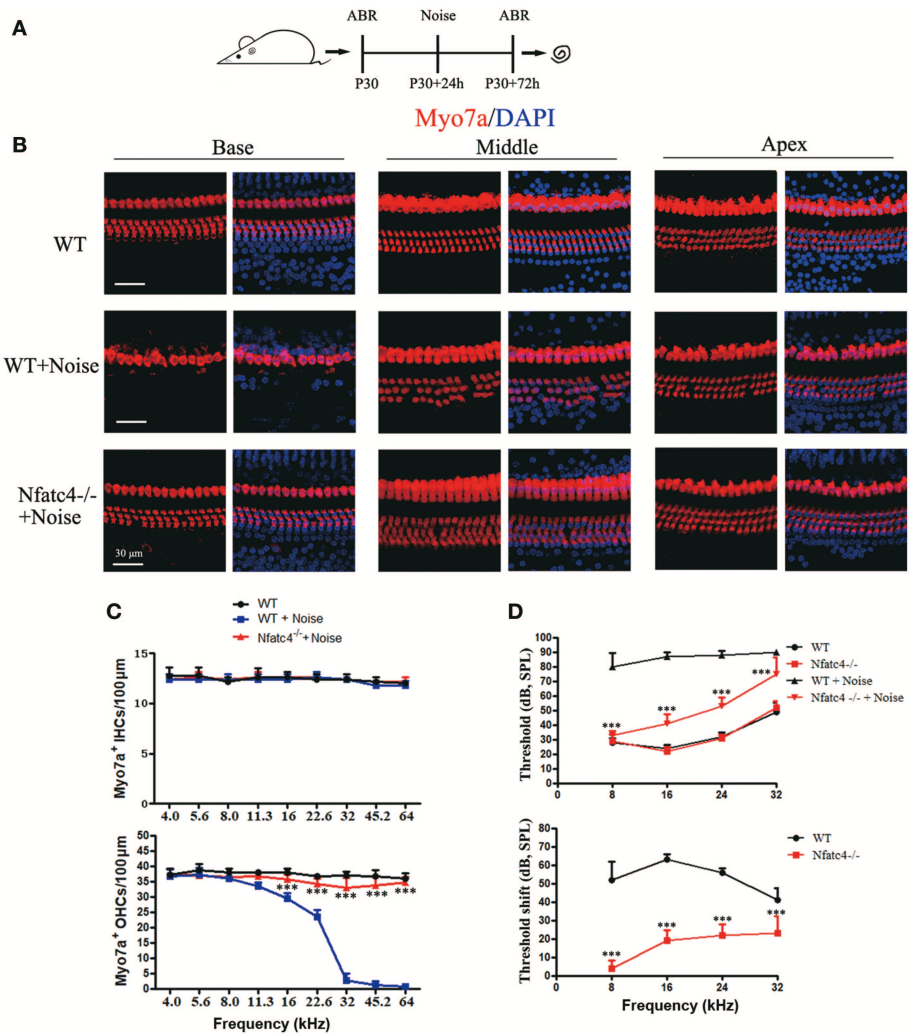

FIGURE 3 | Nfatc4-deficient mice displayed enhanced resistance to hearing loss induced by noise exposure. **(A)** The diagram of the assay for **(B–D)**. P30 *Nfatc4*$^{-/-}$ and WT mice (littermates) were examined by ABR, then 24 h later exposed to 118 dB noise (8–16 kHz) for 2 h. At 2 days after noise exposure, hearing function was examined again by ABR and the mouse cochleae were harvested. **(B)** The representative Myo7a immunofluorescence staining of sensory epithelium from *Nfatc4*$^{-/-}$ and WT mice after noise exposure. **(C)** Quantification of inner hair cells (IHCs) and outer hair cells (OHCs). The numbers of OHCs in the middle and basal turns were significantly greater in the cochlear epithelium from *Nfatc4*$^{-/-}$ mice than in WT mice after noise exposure. **(D)** Pure-tone ABR thresholds and threshold shift of *Nfatc4*$^{-/-}$ mice and WT mice after noise exposure. Scale bar = 30 μm. $n = 5$. ***$P < 0.001$ vs. the WT+Noise group.

At 2 days after noise exposure, the WT mice had significant hearing loss, as demonstrated by the increased ABR thresholds at 8, 16, 24, and 32 kHz (**Figure 3D**). In Nfatc4-deficient mice, the ABR threshold shifts were significantly lower at all frequencies compared with the control mice after noise exposure (**Figure 3D**), suggesting that Nfatc4 deficiency protects against noise-induced hearing loss *in vivo*.

Neomycin Treatment Triggered Nfatc4 Nuclear Translocation, Tnf Pathway Activation, and Hair Cell Apoptosis

Previous studies have reported Nfatc4 nuclear translocation in response to stress, such as methamphetamine-induced neuronal injury (17). In this study, we also observed Nfatc4 translocation from the cytoplasm to the nucleus when the hair cells were challenged by neomycin exposure. Under normal conditions, Nfatc4 was located in the cytoplasm of hair cells (**Figures 4A,B**). After the neomycin treatment, Nfatc4 was translocated to the hair cell nuclei (**Figure 4C**). Neomycin-induced Nfatc4 nuclear translocation occurred in nearly all the hair cells across the cochlear length as shown in **Figure 4D**. In previous studies, chromatin immunoprecipitation assays confirmed that the recruitment of Nfatc4 to the *Tnf* promoter was required in ultraviolet radiation-induced cell death (18), indicating that Tnf is a target of Nfatc4. In this study, we explored the expression of *Tnf* and its downstream signaling in cell apoptosis. As **Figure 4E** shows, after neomycin treatment the expression levels of *Tnf*, *Casp8*, and *Casp3* were significantly increased, suggesting that the Tnf pathway might play roles in neomycin-induced hair cell death. In addition, the mRNA expression of *Nfatc4* was increased after neomycin treatment (**Figure 4E**).

The Tnf-Mediated Cell Apoptosis Pathway Was Inhibited in Nfatc4-Deficient Cochleae After Exposure to Aminoglycoside Antibiotics

TUNEL staining was used to detect hair cell apoptosis (**Figure 5A**). In the WT control group, there were 13 ± 1.00 TUNEL+/Myo7a+ cells/100 μm in the middle turn of the cochlear epithelium after neomycin treatment. Consistent with the above results, the number of apoptotic hair cells was significantly decreased in the $Nfatc4^{-/-}$ cochlear epithelium to 3.2 ± 1.30 TUNEL+/Myo7a+ cells/100 μm in the middle turn ($p < 0.001$, **Figures 5B,C**). In the Nfatc4-deficient cochlear epithelium, the expression levels of *Tnf* and its downstream cascade (*Casp8* and *Casp3*) were significantly lower compared with the WT group after neomycin treatment (**Figure 5D**), indicating that the neomycin-induced and Tnf-mediated extrinsic apoptosis pathway was attenuated by Nfatc4 deficiency. However, the expression levels of *Casp9* were not significantly changed by Nfatc4 deficiency (**Figure 5D**), suggesting that the neomycin-induced intrinsic apoptosis pathway was not inhibited by Nfatc4 deficiency. These results indicated that Nfatc4 deficiency attenuates the hair cell apoptosis induced by neomycin injury, and this might be due to inhibition of the Tnf pathway.

Inhibition of Tnf Production Protected Cochlear Hair Cells Against Neomycin-Induced Damage

To further investigate the role of the Tnf pathway in hair cell damage, we used Len, an inhibitor of Tnf production (19, 20). Len (1 or 10 μM) and 1 mM neomycin were added simultaneously to the medium for 6 h, and cochlear epithelia were harvested after an additional 24 h (**Figure 6A**). qPCR was performed to confirm the inhibitory effect of Len on Tnf production, and the results showed that Len significantly decreased the mRNA expression of *Tnf* in neomycin-injured cochlear epithelium (**Figure 6E**). In the neomycin-treated group, there were 3.60 ± 1.14 and 1.00 ± 0.71 IHCs/100 μm and 7.80 ± 1.10 and 4.80 ± 0.83 OHCs/100 μm in the middle and basal turns, respectively (**Figures 6B–D**). In the neomycin combined with 1 μM Len-treated group, there were 3.20 ± 0.84 and 4.20 ± 0.84 IHCs/100 μm and 14.00 ± 0.71 and 8.20 ± 0.83 OHCs/100 μm in the middle and basal turns, respectively (**Figures 6B–D**). In the neomycin combined with 10 μM Len-treated group, there were 11.80 ± 0.83 and 7.20 ± 1.30 IHCs/100 μm and 47.20 ± 2.28 and 25.20 ± 1.48 OHCs/100 μm in the middle and basal turns, respectively (**Figures 6B–D**). The number of hair cells was significantly greater in the neomycin combined with Len-treated cochlear epithelium compared to the neomycin-treated group, indicating that inhibition of Tnf production significantly reduced neomycin-induced hair cell loss.

To further confirm the effect of inhibiting Tnf on neomycin-induced ototoxicity, etanercept (ETA, 1 or 10 μg/ml), a soluble Tnf decoy receptor drug that binds to Tnf and inhibits its interaction with endogenous Tnf receptors (21, 22), was used to block the Tnf pathway. Significantly more hair cells were observed in the neomycin combined with ETA (10 μg/ml)-treated cochlear epithelium compared to the neomycin-treated group in the middle and basal turns (**Figure S1**, $p < 0.05$), indicating that ETA administration significantly reduced neomycin-induced hair cell loss and further confirmed the protective role of Tnf inhibition in cochlear hair cells.

DISCUSSION

Some genes related to the immune system have been shown to play diverse roles in cochlear development, hearing function, and hearing protection. For example, macrophage migration inhibitory factor (Mif), an inflammatory cytokine, acts as a neurotrophin in the developing inner ear (23). *Mif* knockout mice are hearing impaired and demonstrate fewer sensory hair cells and altered innervation of the organ of Corti. A missense mutation of *NLRP3*, which encodes the NLRP3 inflammasome, causes autosomal-dominant sensorineural hearing loss accompanied by autoinflammatory signs and symptoms (24).

Aging (4, 25), cisplatin treatment (26–28), and noise injury (1) have all been shown to activate the immune system and to lead to the production of inflammatory mediators in the cochlea, and these factors can have diverse

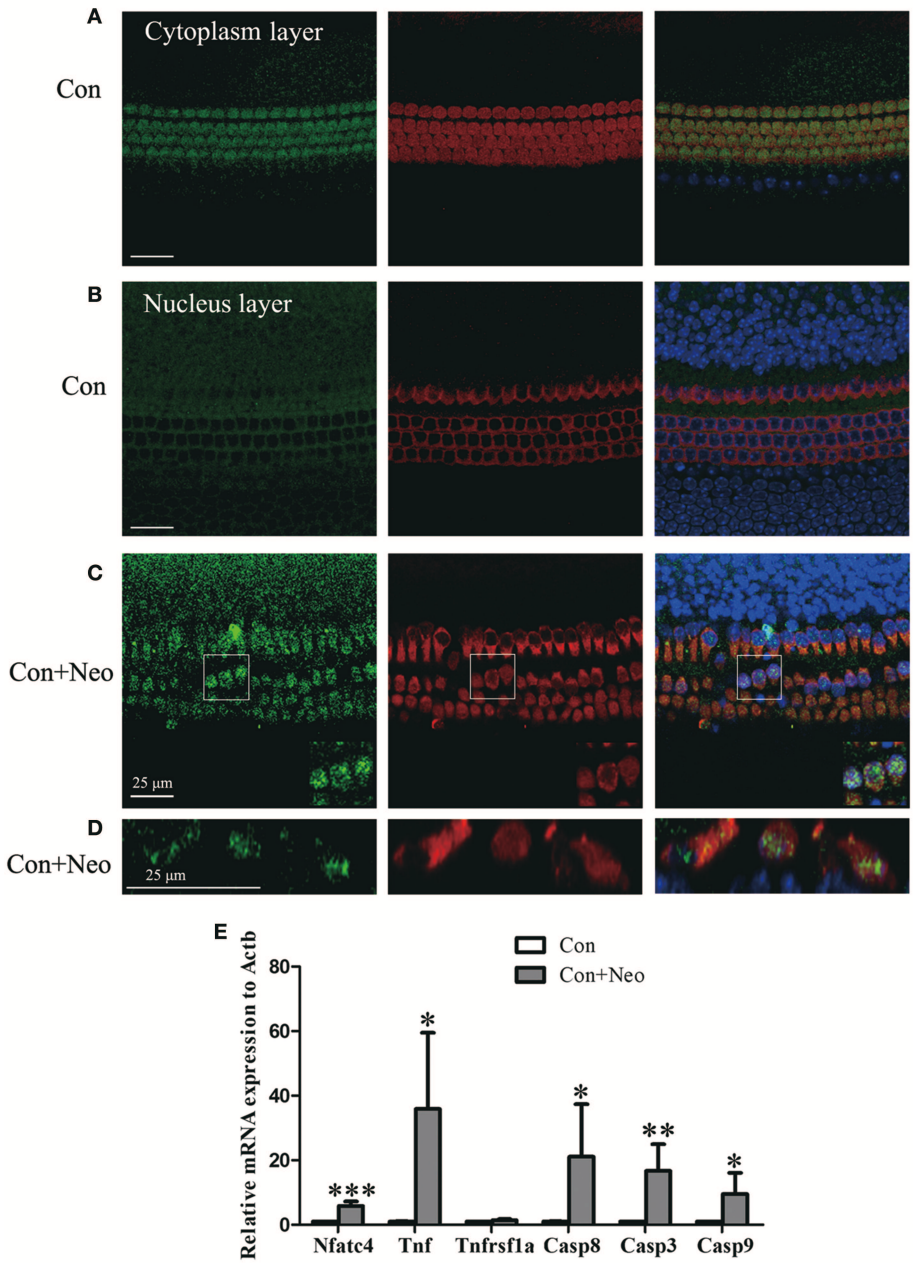

FIGURE 4 | Neomycin treatment triggered Nfatc4 nuclear translocation, Tnf pathway activation, and hair cell apoptosis. **(A–C)** Immunofluorescence staining showed the translocation of Nfatc4 from the cytoplasm to the nucleus. **(D)** The cross-sectional view of Nfatc4 staining in neomycin-treated cochlear epithelium. **(E)** qPCR analysis showed that *Nfatc4*, *Tnf*, *Casp3*, *Casp9*, and *Casp8* mRNA expression increased in the cochlear epithelium after neomycin damage. Scale bar = 25 μm. *indicates $p < 0.05$, **indicates $p < 0.01$, and ***indicates $p < 0.001$ vs. the Con group. $n = 5$.

actions in the inner ear. For example, activation of Toll-like receptor 4 activates the innate immune system and promotes sensory cell degeneration and cochlear dysfunction after acoustic injury (1), while activation of the adenosine A1 receptor protects against cisplatin ototoxicity in the cochlea by suppressing the NOX3/STAT1 inflammatory pathway (27). In addition, controlling inflammation by inhibition of STAT1 via siRNA protects against cisplatin-induced hair cell apoptosis (26).

In the embryonic brain, NFAT signaling is required to stimulate axon outgrowth (29), and Nfatc4 inhibits the expression of growth-associated protein 43 during neuronal maturation (30). In addition, the NMDAR-Nfatc4-BDNF pathway contributes to cell survival during the development

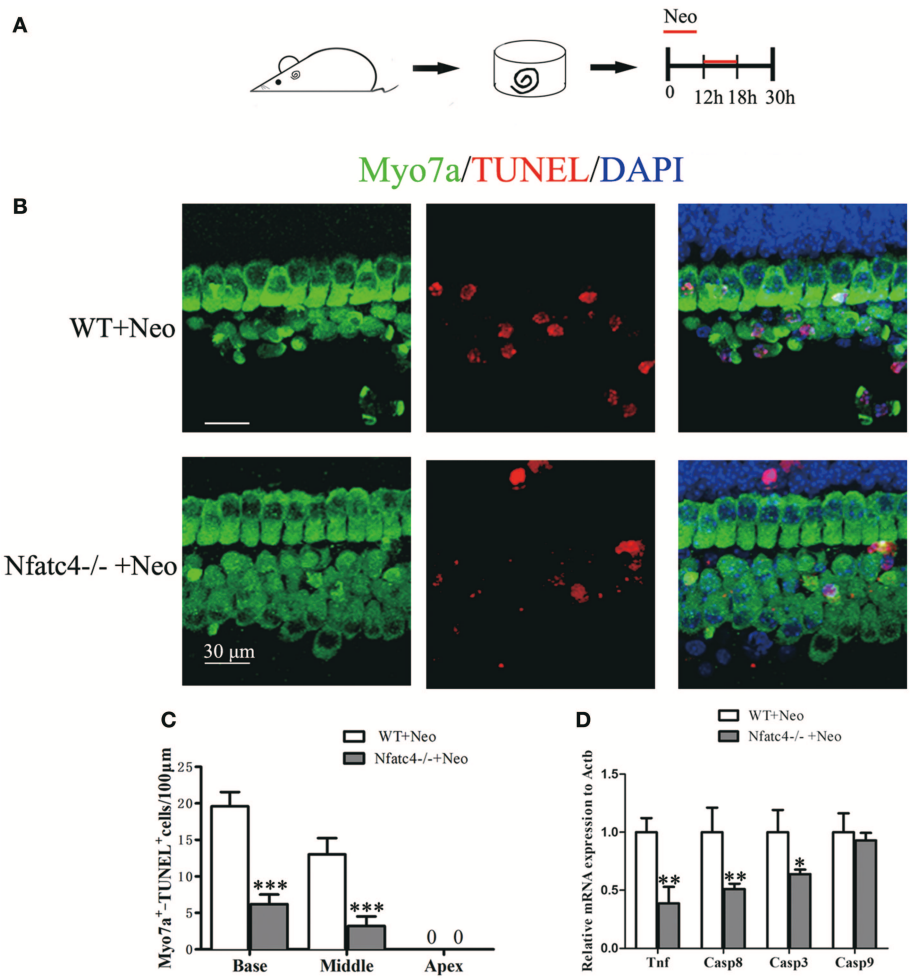

FIGURE 5 | The Tnf-mediated cell apoptosis pathway was inhibited and hair cell apoptosis was decreased in Nfatc4-deficient cochleae after neomycin exposure. **(A)** The diagram of the assay for **(B–D)**. Cochlear sensory epithelium samples from P2 *Nfatc4*$^{-/-}$ and WT mice were dissected out and allowed to recover for 12 h. The samples were treated with 1 mM neomycin for 6 h, allowed to recover for 12 h, and then used for TUNEL staining. **(B)** The representative Myo7a and TUNEL staining of sensory epithelium from *Nfatc4*$^{-/-}$ and WT mice after neomycin treatment. **(C)** The numbers of Myo7a^{+}/TUNEL^{+} cells in the middle and basal turns were significantly decreased in the cochlear epithelium from *Nfatc4*$^{-/-}$ mice compared to WT mice after neomycin treatment. **(D)** qPCR analysis showed that the expression levels of *Tnf*, *Casp3*, and *Casp8* were decreased in Nfatc4-deficient cochlear epithelium after neomycin damage. Scale bar = 30 μm. *indicates $p < 0.05$, **indicates $p < 0.01$, and ***indicates $p < 0.001$ vs. the WT+Neo group. $n = 5$.

of cortical neurons (11). In this study, we showed that Nfatc4 was expressed in mouse cochlear hair cells, but deficiency of Nfatc4 did not result in hair cell loss or in hearing malfunction (**Figure 1**), suggesting that Nfatc4 is not involved in the development of the auditory system.

The overproduction of ROS contributes to aminoglycoside-induced and noise exposure-induced hair cell death and associated hearing loss (2, 15, 31), and it has been reported that ROS activate Nfatc4 and lead to apoptosis in renal tubular cells (32). In this study, we showed that neomycin treatment activated Nfatc4 in cochlear hair cells, as demonstrated by the nuclear translocation of the Nfatc4 protein and the increased mRNA expression levels of *Nfatc4* (**Figure 4**), suggesting that Nfatc4 activation is involved in hair cell apoptosis. Nfatc4-deficient cochlear hair cells showed lower sensitivity to neomycin treatment and noise exposure (**Figures 2**, **3**), again indicating that Nfatc4 activation mediates hair cell death in response to injury.

It was previously reported that Nfatc4 works upstream of Tnf-induced apoptosis of glioma cells (12), and the recruitment of Nfatc4 to the *Tnf* promoter has been shown to be required in ultraviolet radiation-induced cell death in mouse embryonic fibroblasts (18). The noise exposure-mediated increase in Tnf expression has also been reported previously (3, 5). In this study, we found that neomycin treatment resulted in the activation of the Tnf-induced cell apoptosis pathway, as demonstrated by increased mRNA levels of *Tnf*, *Casp8*, and *Casp3* (**Figure 4**). In addition, the inhibition of Tnf production with Len or blocking Tnf with ETA significantly protected hair cells against neomycin-induced hair cell loss, suggesting that the Tnf pathway mediated hair cell death in response to neomycin injury (**Figure 6**

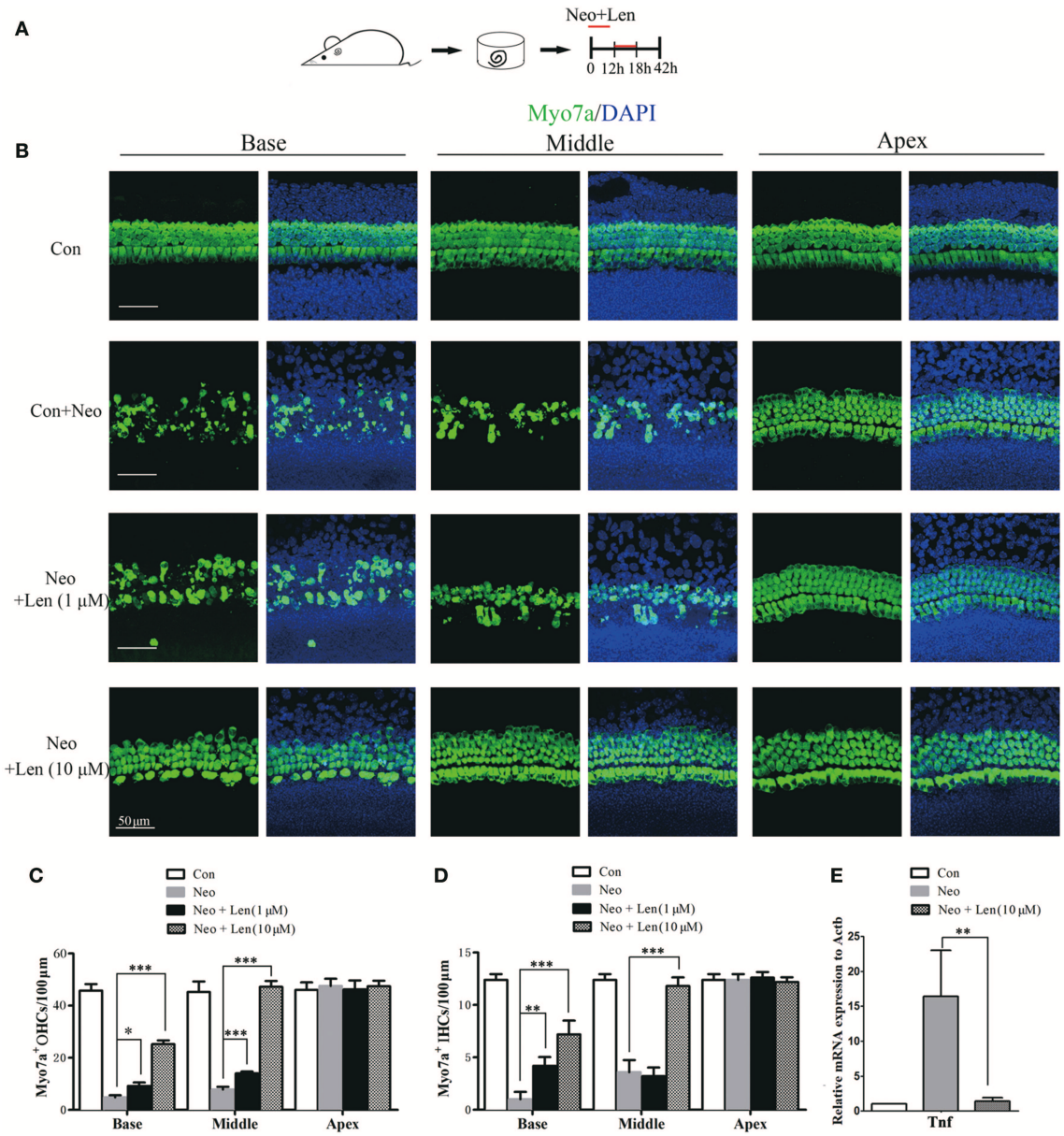

FIGURE 6 | Inhibition of Tnf production protected cochlear hair cells against neomycin-induced damage. **(A)** The diagram of the assay for **(B–D)**. Cochlear sensory epithelium samples from P2 WT mice were dissected out and allowed to recover for 12 h. The samples were treated with 1 mM neomycin and Len (1 or 10 μM) for 6 h, allowed to recover for 24 h, and then used for immunostaining. **(B)** Representative Myo7a immunofluorescence staining after drug treatment (neomycin alone or combined with Len). **(C,D)** Len treatment protected against neomycin-induced hair cell loss. **(E)** qPCR analysis showed that Len significantly decreased the mRNA expression of *Tnf* in neomycin-injured cochlear epithelium. Scale bar = 50 μm. *indicates $p < 0.05$, **indicates $p < 0.01$, and ***indicates $p < 0.001$. $n = 5$.

and **Figure S1**). Moreover, we found that the mRNA levels of *Tnf*, *Casp8*, and *Casp3* were significantly decreased in Nfatc4-deficient cochlear epithelium compared with controls (**Figure 5**), indicating that Nfatc4 deficiency inhibited the neomycin-induced activation of the Tnf pathway and subsequent apoptosis. Although a previous study reported that Tnf-α treatment results in NFAT nuclear translocation via activation of calcineurin in the neuroblastoma cells (33), in our experiments Nfatc4 nuclear translocation was not blocked by Tnf inhibition using Len (**Figure S3**), suggesting that Nfatc4 works upstream of Tnf in neomycin-induced hair cell apoptosis. Taken together, these results suggest that the protective role of Nfatc4 deficiency in cochlear hair cells might be attributed to the inhibition of Tnf-mediated apoptosis.

In other tissues, including the brain, the mechanism(s) of Nfatc4 activation after injury mainly focus on calcineurin/NFAT

signaling. The calcineurin/NFAT signaling inhibitors cyclosporin A (CsA) and tacrolimus (FK506) have been used in studies on the role of NFAT signaling in the survival of leukemia cells (34), T cell activation (35), and myeloid haematopoiesis (36). We used these two inhibitors to test whether they could protect cochlear hair cells against ototoxic drugs. We found that CsA administration had no obvious effect on the survival of cochlear hair cells (**Figure S2**). Neomycin-induced hair cell damage was only slightly attenuated by FK506 administration (**Figure S2**), and the protective effect of FK506 was far less than that of Nfatc4 deficiency or Len (a Tnf inhibitor). The possible role of calcineurin in the Nfatc4 activation in cochlear hair cells remains unclear.

In summary, this study reports the expression and function of Nfatc4 in cochlear hair cells. Although Nfatc4 does not appear to be involved in the development of cochlear hair cells or hearing function, Nfatc4 activation appears to mediate hair cell apoptosis induced by aminoglycoside drugs and noise exposure. Moreover, we have shown that Tnf-mediated apoptosis is involved in hair cell death and that Nfatc4 deficiency suppresses the activation of the Tnf pathway, thus protecting hair cells against caspase-mediated apoptosis after neomycin injury. These results suggest that Nfatc4 inhibition might be a new therapeutic target for the prevention of aminoglycoside and noise-induced hearing loss.

DATA AVAILABILITY

The raw data supporting the conclusions of this manuscript will be made available by the authors, without undue reservation, to any qualified researcher.

ETHICS STATEMENT

This study was carried out in strict accordance with the Guiding Directive for Humane treatment of Laboratory Animals issued by the Chinese National Ministry of Science and Technology in 2006. All experiments were approved by the Shanghai Medical Experimental Animal Administrative Committee (Permit Number: 2009-0082), and all efforts were made to minimize suffering and reduce the number of animals used.

AUTHOR CONTRIBUTIONS

HL, YC, and YN conceived and designed the experiments. YZ, DC, WL, and LZ performed and analyzed the experiments. YZ, YC, and HL wrote the paper.

FUNDING

This work was supported by the National Key R&D Program of China (2017YFA0103900, 2016YFC0905200), the National Natural Science Foundation of China (81620108005, 81830029, 81771010, 81570911, 81700906), and the Nature Science Foundation (No. 17ZR1404600) from Shanghai Science and Technology Committee.

ACKNOWLEDGMENTS

We wish to Dr. Ping-Jie Xiao and Dr. Yan-Ai Mei for providing the *Nfatc4* knockout mice and Jin Li and Yalin Huang of the Institutes of Biomedical Sciences of Fudan University for providing technical support with the confocal microscope.

SUPPLEMENTARY MATERIAL

The Supplementary Material for this article can be found online at: https://www.frontiersin.org/articles/10.3389/fimmu.2019.01660/full#supplementary-material

Figure S1 | Etanercept treatment protected cochlear hair cells against neomycin-induced damage. **(A)** The diagram of the assay for **(B–D)**. Cochlear sensory epithelium samples from P2 WT mice were dissected out and allowed to recover for 12 h. The samples were treated with 1 mM neomycin and etanercept (ETA, 1 μg/ml or 10 μg/ml) for 6 h, allowed to recover for 24 h, and then used for immunostaining. **(B)** The representative Myo7a immunofluorescence staining after drug treatment (neomycin alone or combined with ETA). **(C,D)** ETA treatment at 10 μg/ml protected against neomycin-induced hair cell loss. Scale bar = 20 μm. ***indicates $p < 0.001$. $n = 5$.

Figure S2 | The effects of calcineurin/NFAT signaling inhibitors on the survival of cochlear hair cells against neomycin-induced damage. **(A)** The diagram of the assay for **(B,C)**. Cochlear sensory epithelium samples from P2 WT mice were dissected out and allowed to recover for 12 h. The samples were treated with 1 mM neomycin and CsA/FK506 for 6 h, allowed to recover for 24 h, and then used for immunostaining. **(B)** The representative Myo7a immunofluorescence staining after drug treatment. **(C)** Quantification of the number of HCs. Scale bar = 20 μm. *indicates $p < 0.05$. $n = 5$.

Figure S3 | Immunofluorescence staining of Nfatc4 in neomycin combined with Len treated cochlear epithelium. Scale bar = 10 μm.

REFERENCES

1. Vethanayagam RR, Yang W, Dong Y, Hu BH. Toll-like receptor 4 modulates the cochlear immune response to acoustic injury. *Cell Death Dis.* (2016) 7:e2245. doi: 10.1038/cddis.2016.156
2. Chen Y, Li L, Ni W, Zhang Y, Sun S, Miao D, et al. Bmi1 regulates auditory hair cell survival by maintaining redox balance. *Cell Death Dis.* (2015) 6:e1605. doi: 10.1038/cddis.2014.549
3. Tan WJT, Thorne PR, Vlajkovic SM. Characterisation of cochlear inflammation in mice following acute and chronic noise exposure. *Histochem Cell Biol.* (2016) 146:219–30. doi: 10.1007/s00418-016-1436-5
4. Watson N, Ding B, Zhu X, Frisina RD. Chronic inflammation - inflammaging - in the ageing cochlea: a novel target for future presbycusis therapy. *Ageing Res Rev.* (2017) 40:142–8. doi: 10.1016/j.arr.2017.10.002
5. Fuentes-Santamaria V, Alvarado JC, Melgar-Rojas P, Gabaldon-Ull MC, Miller JM, Juiz JM. The role of glia in the peripheral and central auditory system following noise overexposure: contribution of TNF-alpha and IL-1beta to the pathogenesis of hearing loss. *Front Neuroanat.* (2017) 11:9. doi: 10.3389/fnana.2017.00009
6. Wu Q, Wang GP, Xie J, Guo JY, Gong SS. Tumor necrosis factor-alpha-induced ototoxicity in mouse cochlear organotypic culture. *PLoS ONE.* (2015) 10:e0127703. doi: 10.1371/journal.pone.0127703

7. Rao A, Luo C, Hogan PG. Transcription factors of the NFAT family: regulation and function. *Annu Rev Immunol.* (1997) 15:707–47. doi: 10.1146/annurev.immunol.15.1.707
8. Horsley V, Pavlath GK. NFAT: ubiquitous regulator of cell differentiation and adaptation. *J Cell Biol.* (2002) 156:771–4. doi: 10.1083/jcb.200111073
9. Yao JJ, Zhao QR, Liu DD, Chow CW, Mei YA. Neuritin up-regulates Kv4.2 alpha-subunit of potassium channel expression and affects neuronal excitability by regulating the calcium-calcineurin-NFATc4 signaling pathway. *J Biol Chem.* (2016) 291:17369–81. doi: 10.1074/jbc.M115.708883
10. Benedito AB, Lehtinen M, Massol R, Lopes UG, Kirchhausen T, Rao A, et al. The transcription factor NFAT3 mediates neuronal survival. *J Biol Chem.* (2005) 280:2818–25. doi: 10.1074/jbc.M408741200
11. Vashishta A, Habas A, Pruunsild P, Zheng JJ, Timmusk T, Hetman M. Nuclear factor of activated T-cells isoform c4 (NFATc4/NFAT3) as a mediator of antiapoptotic transcription in NMDA receptor-stimulated cortical neurons. *J Neurosci.* (2009) 29:15331–40. doi: 10.1523/Jneurosci.4873-09.2009
12. Gopinath S, Vanamala SK, Gujrati M, Klopfenstein JD, Dinh DH, Rao JS. Doxorubicin-mediated apoptosis in glioma cells requires NFAT3. *Cell Mol Life Sci.* (2009) 66:3967–78. doi: 10.1007/s00018-009-0157-5
13. Lin H, Sue YM, Chou Y, Cheng CF, Chang CC, Li HF, et al. Activation of a nuclear factor of activated T-lymphocyte-3 (NFAT3) by oxidative stress in carboplatin-mediated renal apoptosis. *Br J Pharmacol.* (2010) 161:1661–76. doi: 10.1111/j.1476-5381.2010.00989.x
14. Graef IA, Chen F, Chen L, Kuo A, Crabtree GR. Signals transduced by Ca^{2+}/calcineurin and NFATc3/c4 pattern the developing vasculature. *Cell.* (2001) 105:863–75. doi: 10.1016/s0092-8674(01)00396-8
15. Liu L, Chen Y, Qi J, Zhang Y, He Y, Ni W, et al. Wnt activation protects against neomycin-induced hair cell damage in the mouse cochlea. *Cell Death Dis.* (2016) 7:e2136. doi: 10.1038/cddis.2016.35
16. Hirose K, Liberman MC. Lateral wall histopathology and endocochlear potential in the noise-damaged mouse cochlea. *J Assoc Res Otolaryngol.* (2003) 4:339–52. doi: 10.1007/s10162-002-3036-4
17. Jayanthi S, Deng XL, Ladenheim B, McCoy MT, Cluster A, Cai NS, et al. Calcineurin/NFAT-induced up-regulation of the Fas ligand/Fas death pathway is involved in methamphetamine-induced neuronal apoptosis. *Proc Natl Acad Sci USA.* (2005) 102:868–73. doi: 10.1073/pnas.0404990102
18. Song L, Li J, Ye J, Yu G, Ding J, Zhang D, et al. p85alpha acts as a novel signal transducer for mediation of cellular apoptotic response to UV radiation. *Mol Cell Biol.* (2007) 27:2713–31. doi: 10.1128/MCB.00657-06
19. Wang Y, Xu J, Zhang X, Wang C, Huang Y, Dai K. TNF-alpha-induced LRG1 promotes angiogenesis and mesenchymal stem cell migration in the subchondral bone during osteoarthritis. *Cell Death Dis.* (2017) 8:e2715. doi: 10.1038/cddis.2017.129
20. Lapalombella R, Andritsos L, Liu Q, May SE, Browning R, Pham LV, et al. Lenalidomide treatment promotes CD154 expression on CLL cells and enhances production of antibodies by normal B cells through a PI3-kinase-dependent pathway. *Blood.* (2010) 115:2619–29. doi: 10.1182/blood-2009-09-242438
21. Lee JK, McCoy MK, Harms AS, Ruhn KA, Gold SJ, Tansey MG. Regulator of G-protein signaling 10 promotes dopaminergic neuron survival via regulation of the microglial inflammatory response. *J Neurosci.* (2008) 28:8517–28. doi: 10.1523/JNEUROSCI.1806-08.2008
22. Herrmann M, Anders S, Straub RH, Jenei-Lanzl Z. TNF inhibits catecholamine production from induced sympathetic neuron-like cells in rheumatoid arthritis and osteoarthritis *in vitro*. *Sci Rep.* (2018) 8:9645. doi: 10.1038/s41598-018-27927-8
23. Bank LM, Bianchi LM, Ebisu F, Lerman-Sinkoff D, Smiley EC, Shen YC, et al. Macrophage migration inhibitory factor acts as a neurotrophin in the developing inner ear. *Development.* (2012) 139:4666–74. doi: 10.1242/dev.066647
24. Nakanishi H, Kawashima Y, Kurima K, Chae JJ, Ross AM, Pinto-Patarroyo G, et al. NLRP3 mutation and cochlear autoinflammation cause syndromic and nonsyndromic hearing loss DFNA34 responsive to anakinra therapy. *Proc Natl Acad Sci USA.* (2017) 114:E7766–75. doi: 10.1073/pnas.1702946114
25. Kao SY, Soares VY, Kristiansen AG, Stankovic KM. Activation of TRAIL-DR5 pathway promotes sensorineural degeneration in the inner ear. *Aging Cell.* (2016) 15:301–8. doi: 10.1111/acel.12437
26. Kaur T, Mukherjea D, Sheehan K, Jajoo S, Rybak LP, Ramkumar V. Short interfering RNA against STAT1 attenuates cisplatin-induced ototoxicity in the rat by suppressing inflammation. *Cell Death Dis.* (2011) 2:63. doi: 10.1038/cddis.2011.63
27. Kaur T, Borse V, Sheth S, Sheehan K, Ghosh S, Tupal S, et al. Adenosine A1 receptor protects against cisplatin ototoxicity by suppressing the NOX3/STAT1 inflammatory pathway in the cochlea. *J Neurosci.* (2016) 36:3962–77. doi: 10.1523/JNEUROSCI.3111-15.2016
28. Borse V, Al Aameri RFH, Sheehan K, Sheth S, Kaur T, Mukherjea D, et al. Epigallocatechin-3-gallate, a prototypic chemopreventative agent for protection against cisplatin-based ototoxicity. *Cell Death Dis.* (2017) 8:e2921. doi: 10.1038/cddis.2017.314
29. Graef IA, Wang F, Charron F, Chen L, Neilson J, Tessier-Lavigne M, et al. Neurotrophins and netrins require calcineurin/NFAT signaling to stimulate outgrowth of embryonic axons. *Cell.* (2003) 113:657–70. doi: 10.1016/s0092-8674(03)00390-8
30. Nguyen T, Lindner R, Tedeschi A, Forsberg K, Green A, Wuttke A, et al. NFAT-3 is a transcriptional repressor of the growth-associated protein 43 during neuronal maturation. *J Biol Chem.* (2009) 284:18816–23. doi: 10.1074/jbc.M109.015719
31. Park JS, Jou I, Park SM. Attenuation of noise-induced hearing loss using methylene blue. *Cell Death Dis.* (2014) 5:170. doi: 10.1038/Cddis.2014.170
32. Sue YM, Chou HC, Chang CC, Yang NJ, Chou Y, Juan SH. L-Carnitine protects against carboplatin-mediated renal injury: AMPK- and PPAR alpha-dependent inactivation of NFAT3. *PLoS ONE.* (2014) 9:0104079. doi: 10.1371/journal.pone.0104079
33. Alvarez S, Blanco A, Fresno M, Munoz-Fernandez MA. TNF-alpha contributes to caspase-3 independent apoptosis in neuroblastoma cells: role of NFAT. *PLoS ONE.* (2011) 6:e16100. doi: 10.1371/journal.pone.0016100
34. Gregory MA, Phang TL, Neviani P, Alvarez-Calderon F, Eide CA, O'Hare T, et al. Wnt/Ca^{2+}/NFAT signaling maintains survival of Ph^{+} leukemia cells upon inhibition of Bcr-Abl. *Cancer Cell.* (2010) 18:74–87. doi: 10.1016/j.ccr.2010.04.025
35. Dutta D, Barr VA, Akpan I, Mittelstadt PR, Singha LI, Samelson LE, et al. Recruitment of calcineurin to the TCR positively regulates T cell activation. *Nat Immunol.* (2017) 18:196–204. doi: 10.1038/ni.3640
36. Fric J, Lim CXF, Koh EGL, Hofmann B, Chen JM, Tay HS, et al. Calcineurin/NFAT signalling inhibits myeloid haematopoiesis. *EMBO Mol Med.* (2012) 4:269–82. doi: 10.1002/emmm.201100207

Conflict of Interest Statement: The authors declare that the research was conducted in the absence of any commercial or financial relationships that could be construed as a potential conflict of interest.

frontiers in Neurology

REVIEW
published: 06 August 2019
doi: 10.3389/fneur.2019.00845

Main Aspects of Peripheral and Central Hearing System Involvement in Unexplained HIV-Related Hearing Complaints

Marrigje Aagje de Jong, Ari Luder and Menachem Gross*

Department of Otolaryngology—Head and Neck Surgery, Hadassah Hebrew-University Medical Center, Jerusalem, Israel

Objective: Hearing abnormalities frequently occur in Human Immunodeficiency Virus (HIV) infected individuals. Both conductive and uni- or bilateral sensorineural hearing loss (SNHL) have been described along with other audiological and vestibular symptoms such as tinnitus, vertigo and balance disturbances. While frequent middle ear infections may explain impairment of peripheral hearing abilities, the exact etiology of cochlear, and central auditory processing deficits still remains unclear. Direct effects of HIV, opportunistic infections, ototoxic side effects of antiretroviral therapy (ART), and immunologic responses to the central nervous system involving the auditory pathway have been proposed. We aim to review the audiological profile in HIV infected adults related to the effects of HIV and HAART on the inner ear structures.

Methods: We present a review of the literature on cases of HIV related SNHL in adult patients and studies conducted to investigate audiometric changes in such patients. Data on presentation, diagnosis and pathophysiology were reviewed.

Results: Sensorineural hearing loss in the higher frequencies is a common form of hearing loss in HIV infected individuals throughout disease progression, along with decreased otoacoustic emission (OAE) responses, increased PTA hearing thresholds and prolonged latencies for auditory brainstem responses (ABR).

Conclusion: HIV affects all stages of auditory perception in a way similar to accelerated aging of the auditory system. And we postulate that synaptic loss may be the first step, followed by cochlear damage and central pathology as the virus remains present in all the structures of the auditory pathway causing local inflammation and degeneration. Evaluation of hearing function among all patients diagnosed with HIV infection seems to be an accepted approach; it should include OAE testing, pure tone and speech audiometry, speech-in-noise tests and ABR measurements.

Keywords: inner ear, sensorineural hearing loss, HIV, audiometry, synaptopathy, ABR

OPEN ACCESS

Edited by:
Agnieszka J. Szczepek, Charité Medical University of Berlin, Germany

Reviewed by:
Jay C. Buckey, Dartmouth College, United States
Carla Gentile Matas, University of São Paulo, Brazil

****Correspondence:***
Marrigje Aagje de Jong
dejong.marije@gmail.com

Specialty section:
This article was submitted to Neuro-Otology, a section of the journal Frontiers in Neurology

Received: *14 May 2019*
Accepted: *22 July 2019*
Published: *06 August 2019*

Citation:
de Jong MA, Luder A and Gross M (2019) Main Aspects of Peripheral and Central Hearing System Involvement in Unexplained HIV-Related Hearing Complaints. Front. Neurol. 10:845. doi: 10.3389/fneur.2019.00845

INTRODUCTION

The Human Immunodeficiency Virus (HIV) is a single-stranded RNA virus, which is converted to double-stranded DNA after infection of the host cell and integrates into its cellular DNA. HIV can infect a variety of cell types but preferentially infects neurons and immune cells, such as $CD4^+$ T cells, macrophages, and microglial cells. Once integrated, the virus may become latent. This allows

the virus and its host cell to avoid detection by the immune system. In its dormant state the virus can remain in the human body for several years without causing symptoms. With time, disease progresses and the neuro- and lymphotrophic virus causes functional impairment and depletion of T-cells resulting in immunosuppression, possible development of opportunistic infections and malignancies in multiple organ systems. With regard to its manifestations in the temporal bone, common symptoms include tinnitus, dizziness, chronic otitis media, and hearing impairment (1, 2).

It has been shown that HIV has affinity for the central nervous system (CNS) and in 20% of HIV infections the first symptom is a neurological manifestation (3). The CNS can act as anatomical reservoir for the virus resulting in cognitive deficits and other central pathologies including the auditory processing pathways (4).

Several studies have investigated hearing loss among HIV infected children and adults as well as those who developed Acquired Immune Deficiency Syndrome (AIDS) presenting a broad spectrum of auditory and otologic pathologies, ranging from middle ear infections to conductive, mixed and sensorineural hearing loss (SNHL), vestibular symptoms, and subcortical and cortical pathologies. It is our aim to provide an overview of those studies investigating hearing function among the adult HIV infected population. In addition to the hearing performance, we discuss the different hypotheses about the responsible mechanism(s) with a specific focus on inner ear and central neural pathology—an attempt to answer the question whether HIV affects mostly peripheral or central auditory processes.

METHODS

Search Strategy and Selection

As a first step, a review of the literature was conducted using the databases of PubMed and the Cochrane Library on March, 2019. We searched for articles relating to patients with HIV infection (domain) with audiology testing (intervention) and subsequently, searched for articles limited to an adult population and published in the last 10 years. Articles were excluded if the main subject was not in relation to our domain in combination with determinant or in cases where the language was other than English. We screened references and related articles and conducted a general internet search to verify if all significant articles were included until day of admission of the manuscript.

We assessed and compared the hearing performances based on different audiology tests among patients with and without HIV infection in the selected studies. Due to heterogeneity in the study designs and the lack of standardized measurements, no meta-analysis was possible, and a critical conceptual review approach was chosen.

RESULTS

Based on our Pubmed and Cochrane search a total of nine articles were found and after subtracting the articles that did not meet the criteria of recent publication and/or adult population, only 4 remained. However, with articles found from references we selected a total of 13 relevant publications related to 11 different study populations from locations in Africa, Asia, South-America and the USA (2, 5–16).

In 6 articles the participants were asked to complete a questionnaire on self-reported hearing loss and/or otologic symptoms. Combined prevalence for each otovestibular complaint was as follows: aural fullness 30.5%, hearing loss 27.7%, tinnitus 20.9%, dizziness 24.9%, otalgia 15.8%, and aural pruritus 45% (2, 7, 9, 10, 13, 14). HIV infected patients receiving or not receiving antiretroviral therapy (ART) were not always analyzed separately. However, we noticed that for all otologic symptoms, except for aural fullness, the prevalence was slightly higher among those with ART and or longer disease process. Subjects receiving ART also reported greater difficulty understanding speech in noise (13).

Evaluation of Peripheral Dysfunction of the Middle and Inner Ear

The pneumatization and function of the middle ear can be assessed by otoscopic evaluation and tympanometry—a readily easy test to perform, also in endemic areas that are most affected by HIV. A total of 7 studies described tympanometry in their study protocol (2, 4, 9–11, 13, 16, 17). It should be stated that often acoustic immittance testing was only performed to exclude middle ear pathology before continuing hearing screening. Van der Westhuizen et al. documented otoscopic abnormalities in 55% of HIV infected participants, and in 8% they found tympanic membrane perforation and/or otorrhea. The tympanogram was of type B in 34% of cases (9). Similar results were found by Matas et al. with 33.3% of HIV infected participants showing abnormal tympanograms, and 40.7% of HIV infected participants that were receiving ART (10).

Measurements of hearing at the level of the inner ear include: otoacoustic emission (OAE) tests, pure tone audiometry (PTA) with speech reception threshold (SRT) and word recognition scores (WRS) in quiet. Except for one study focusing on central auditory processing (2), all included studies described distortion product OAE measurement (DPOAE) and or PTA in their research method.

DPOAE Measurements

OAE tests represent cochlear function and were evaluated in 4 studies (7, 9, 12, 13). A slight decrease in normal DPOAE functioning throughout disease progression was seen (7, 9). In contrast Torre et al. found no significant difference in the number of no responses (NR) between HIV seropositive and HIV seronegative subjects (15). In two studies it is not clear whether subjects with abnormal tympanograms (33–34%) were excluded from DPOAE measures (9, 13). Details and outcomes of those studies are summarized in **Table 1**.

PTA Measurements

Audiometry was done for air conduction in all studies, but only in half of those, bone conduction was performed. The frequency range varied from 0.125 to 20 kHz. In most cases 0.25–8 kHz were evaluated. The definition of hearing loss based on the pure tone

TABLE 1 | Overview of distortion product otoacoustic emission (DPOAE) testing results—prevalence and conclusion.

References	Year	Frequencies tested (Hz)	Definition abnormal or no response	HIV−group	HIV + group	ART/AIDS group
Khosa-Shangase (7)	2011	750–1,000–2,000–3,000–4,000–6,000–8,000	<7 dB difference = abnormal response or a change of >10 dB in consecutive measurements (three sessions were done over 6 months' time)	–	All normal in 3 sessions ($n = 16$)	Abnormal responses for 6–8 kHZ in session 3, but no change >10 dB ($n = 54$)
Van der Westhuizen et al. (9)	2013	1,818–2,542–3,616–5,083–7,206	6–10 dB difference = abnormal response <6 dB difference = no response Abnormal DPOAE in 3 frequencies is considered an abnormal test result.	–	39–44% abnormal response (18–24% bilateral) ($n = 112$)	45% abnormal response (28% bilateral) ($n = 78$)
Torre et al. (12)	2014	2,000–3,000–4,000–6,000	<6 dB difference = no response or absolute level <−15 dB SPL no DPOAE response in 4 frequencies is considered an abnormal cochlear function	Number of NR's increased across frequencies ($n = 220$)	Number of NR's increased across frequencies. "No responses" were more common in low frequen-cies for women ($n = 286$)	–
Maro et al. (13)	2014	1,500–1,700–2,000–2,200–3,000–3,200–4,000–4,200–6,000–6,200–7,800–8,000	No definition	DPOAE's were reduced in the HIV infected population compared to healthy individuals ($n = 302$) There were no differences for DPOAE measurements between HIV infected subjects receiving ART ($n = 319$) or not receiving ART ($n = 130$)		

average was either defined as a pure tone average threshold >20 or >25 dB HL. Van der Westhuizen et al. investigated a limited range of frequencies for two different criteria of hearing loss (9). **Table 2** presents an overview of the results regarding pure tone audiometry in the different studies. A total of 8 studies looked at variables such as gender, age, stage of disease, use of ART related to PTA hearing loss. The most prominent factor was increased age (5, 6, 11, 15, 16). Increased duration of disease, $CD4^+$ cell count, and advanced stage of disease seemed to increase the risk of hearing loss, but findings were not consistent in all studies (5, 9, 11, 14, 16). While Torre et al. found no association between treatment variables and PTA (15), Matas et al. described an increased odds ratio for hearing loss in HIV infected individuals receiving ART compared to treatment naïve individuals (2). Other studies noticed that patients receiving ART seemed to have worse hearing at initiation of treatment with improvement when continuing ART (6, 14).

Word Recognition Scores

As a measurement of retro-cochlear deficit, individuals can be asked to repeat word lists at comfortable hearing level. When done in quiet, the test can be too easy, not representing the daily listening environment leading to ceiling effects, even in those with hearing loss. Luque et al. and Torre et al. tested a 25-words list presented at 40–50 dB HL in quiet and found similar results (11, 15). The application of three-way ANOVA in the study of Luque et al. revealed higher WRS scores in HIV seronegative controls, and a significant difference compared to individuals with HIV infection at late stage disease (adjusted $P = 0.03$) (11). However, from a clinical perspective this difference seems inconsequential (16). There was also a significant effect of age on WRS regardless of HIV infection.

Evaluation of Central Auditory Pathways

The Central Auditory Pathway is a complex system that can be tested objectively through auditory brainstem evoked responses (ABR), EcoG, middle, and late latency evoked responses (MLR, LLR), P300 wave measurement and other specific tests. With our search criteria we found two articles looking at central auditory processing through ABR or gap detection thresholds (2, 13). Matas et al. compared controls with HIV infected subjects and AIDS patients (2). ABR measurements were done for clicks (80 dBnHL, 19 clicks/s) to measure latencies and interpeak intervals. MLR measurements (70 dBnHL monoaural click, 9.9 clicks/s) were performed to determine contra- and ipsilateral amplitudes. ABR latencies were prolonged for the HIV seropositive subjects and AIDS patients compared to controls, as well as the I-V interpeak latency (4.39 and 4.33 vs. 4.05 ms). MLR in HIV infected subjects showed prolonged latencies and decreased amplitudes when the electrode was placed at C3 compared to seronegative controls. The difference was most obvious for AIDS patients. P300 is an electric wave in the electric encephalogram that occurs at 300 ms after stimulus and is often measured at the posterior aspect of the skull. Matas et al. found also here significantly prolonged latencies for HIV infected and AIDS diseased participants (2). The Gap detection threshold

TABLE 2 | Overview of Pure Tone Audiometry results—prevalence and type of hearing impairment.

References	Year	Frequency range (kHz)	Definition HL (dBHL)	Prevalence HL HIV + (%)	Prevalence HL HIV + with AIDS /ART (%)	SNHL (%)	CHL (%)	Mixed HL (%)	HF SNHL (%)	Prevalence HL controls (%)
Ongulo and Oburra (5)	2010	0.25–8	>25	33.5 ($n = 194$)	–	74	22	4	–	8.1 ($n = 124$)
Makau et al. (6)	2010	? – 8	>25	31 ($n = 273$)	28 ($n = 271$)	Most common	–	–	–	–
Khosa-Shangase (7)	2011	0.25–8	>25	–	10 ($n = 150$)	73	27	0	33	–
Mathews et al. (8)	2012	0.5–8	>20	54 ($n = 30$)	54 ($n = 30$)	37–81	0–12.5	6.25–12.5	–	–
Van der Westhuizen et al. (9)	2013	0.5–4	>15 >25	32 ($n = 172$) 12 ($n = 172$)	44 ($n = 28$) 18 ($n = 28$)	21–31 –	12–13 –	–	17	–
Matas et al. (10)	2014	0.25–20	>20	27.8–58.8 ($n = 18$)	48.1–73.9 ($n = 27$)	38.5	20–30.8	–	15.4–80	0 ($n = 30$)
Luque et al. (11)	2014	0.25–8	>25	16.5 ($n = 127$)	18.9 ($n = 148$)	100	–	–	–	11.6 ($n = 137$)
Maro et al. (13)	2014	0.5–8	>25 (>30/>20 for specific freq.)*	0.8 ($n = 130$)	1.3–2.5 ($n = 319$)	–	–	–	–	0–3.5 ($n = 302$)
Fokouo et al. (14)	2015	0.125–8	>20	27.2 ($n = 90$)	–	61.7	18.3	20	–	5.6 ($n = 90$)
Torre et al. (15, 16)	2015/16	0.25–8	No definition**	–	–	6.25–16	18.75–20	0–8	–	–
Matas et al. (10)	2018	0.25–20	No definition***	–	–	–	–	–	–	–

HL, Hearing Loss; kHz, kilo Herz; dBHL, decibel Hearing Level; HIV +, HIV infected individuals with or without ART; AIDS, acquired immunodeficiency syndrome; ART, antiretroviral therapy; SNHL, sensorineural hearing loss; CHL, conductive hearing loss; HF SNHL, high frequency SNHL (among total SNHL); n, number of study participants for that group.

**PTA was not different for HIV infected individuals with or without ART, the HIV seronegative group had worse PTA outcomes.*

***High and low frequency PTA were significant higher for HIV infected participants (n = 222) compared to healthy controls (n = 174).*

****HIV infected participants (n = 41) had higher hearing thresholds in both conventional and high frequency audiometry when compared to the control group (n = 30).*

was evaluated in HIV infected subjects with or without ART (13). Measured at 65 dB, a slight increase in gap detection threshold was found among HIV infected participants compared to seronegative controls.

As some studies suggest, people with HIV can suffer from hearing complaints but show no objective abnormality in the audiometry (11, 18). ABR measurements are not clearly affected in all HIV patients with hearing complaints either. This makes it difficult to separate clearly between peripheral and central origins in HIV infected subjects with hearing complaints. A more recent hypothesis for a hidden form of hearing loss is synaptopathy. However, we found no study focusing on synaptopathy specifically in the HIV infected population.

DISCUSSION

It is known that HIV infected individuals who develop immunosuppression are more susceptible to several inflammatory and infectious processes affecting the temporal bone (1). This can result in conductive hearing loss, sensorineural damage or a mixed loss. However, auditory and vestibular complaints such as hearing loss and tinnitus are frequently mentioned in self-reports by adults, already in the early stages of symptomatic HIV infection (2, 6, 7, 9, 10, 14, 15). In particular, difficulty in understanding speech in noise is reported and data suggest a progression throughout disease stages (4). Our review summarizes the results from the most recent studies conducted to evaluate the middle ear, inner ear and central auditory pathways in adult patients with HIV infection and/or AIDS disease. Can we answer our question whether HIV impairs hearing function at a more peripheral or central etiology?

As stated before, it is not easy to discern, based on previous works, whether the main problem is peripheral or central. For simple reasons such as a wide variety in patients selected, differences in accessibility to auditory screening and HIV treatment, variable methods for hearing evaluation and the new developments and early initiation of ART possibly affecting their outcomes. Although no consistent pattern has been established, DPOAE's showed abnormal responses mainly in higher frequencies and decreased over time with disease progression (7). Decreased OAE's often precede alterations in normal audiograms and represent early cochlear damage, as occurs after noise exposure or ototoxic treatment (12, 17, 19). A variety of studies have hypothesized that some drugs used for ART (in particular the first line antiretroviral drugs known as NRTI's) cause such ototoxic damage or increase sensitivity to noise (20–23).

In 1995 Lewis described the phenomenon of ART related ototoxicity through damaged mitochondrial DNA causing oxidative stress leading to accelerated changes on the cochlea

or central auditory system similar to those described in aging humans (24). Increasing evidence now suggests that HIV infected individuals experience similar immunologic changes as seen in elderly persons with accelerated aging and related co-morbidities. It is thought that immune activation and inflammation translates into a general decline of the immune system resulting in those changes (25). This phenomenon is called immunosenescence or aging of the immune system and can very well play a role in HIV related hearing loss through damaged auditory pathways by HIV itself rather than through ART.

From the recent literature we selected, it is found that HIV individuals do not show poorer DPOAE test results after ART is initiated. While age was related to decreased responses, all variables related to HIV status (HIV viral load, $CD4^+$ cell count) and ART did not show significant correlation (7, 12, 13). A significant ototoxic effect from ART based on OAE testing is therefore unlikely.

Secondly, the presence of HIV in cochlear structures has been described by Pappas et al. (26). They found extracellular viral-like particles with morphologic characteristics of HIV-1 on the tectorial membrane in three cases. Numerous viral-like particles appearing essentially similar to identified HIV-1 particles in infected lymphocyte cultures were found within the cytoplasm of the connective tissue cells. These findings provide an insight into the cochlear pathogenesis of viral-induced hearing loss and vestibular impairment in HIV infected patients. Through possible persistent inflammation and immune activation.

When looking at PTA results, there is an undoubtedly higher prevalence of hearing loss among HIV infected individuals—mostly of the sensorineural type and in the higher frequencies. Although PTA changes were often documented as a mild to moderate loss, there is a trend toward progression with longer disease (5, 9, 14–16). When CD4+ cell counts drop to below 200 cells/μL immunological AIDS develops and is often indication to start ART. Some studies found an initial increase in PTA thresholds at this stage, but when ART was continued the prevalence of hearing loss decreased (14, 15). A possible explanation is the efficacy of ART on the immune system and a viral suppression leading to hearing improvement. However, contradictive results were found regarding the benefit of ART on hearing performance. Matas et al. and Van der Westhuizen et al. found a higher prevalence of SNHL among those receiving ART for advanced disease (9, 10). To differentiate between the effect from ART and from advanced disease is however difficult. It is known that second-line regimens are composed of newer and safer compounds than those used in first-line regimens (14). However, penetration of ART to the CNS is less optimal and can lead to incomplete recovery of the immune system. Even with good systemic control, HIV can persist in the CNS putting infected subjects at risk for cognitive impairment which continues to be prevalent in particular among those over 50 years old (11).

A variety of studies have hypothesized that HIV, while present in the CNS, has its direct effect on the vestibular and cochlear system as well as more central auditory processing pathways (13, 27, 28). As demonstrated by Matas et al. and Maro et al. MLR latencies and gap detection thresholds were prolonged as a measurement for central auditory processing (2, 13). Matas et al. also found prolonged wave I, III, and V latencies during ABR measurements similar to previous works (2, 29). Wave I represents the peripheral part of the auditory nerve at the spiral ganglion cells that connect the hair cells in the cochlea with the next neural processing unit, the cochlear nucleus, where wave III is generated (30). Wave III and V are delayed when more central conduction pathways are affected. Although the I-V interpeak latency was the only significant interpeak delay, the results by Matas et al. show that interpeak time I-III was more prolonged compared to interpeak III-V (2). This may correspond to the action potential conduction time from the hair cell to the cochlear nucleus and appears to be affected in HIV infected individuals from the study (30). Previously it was thought that hair cells were the most vulnerable elements to cochlear injury and aging. But recent work shows that loss of synapses and nerve fibers (known as synaptopathy) occur even before hair cell damage (18). The number of surviving cochlear synapses is represented by the amplitude of wave I in ABR testing. In this review we did not find recent data on the amplitudes in ABR among HIV infected adults. But with complaints of difficulty in understanding speech in noise, wave I abnormalities in ABR and a possible explanation of accelerated aging in HIV disease, it can be useful to conduct further research in this field among the HIV infected population. Since cochlear synaptic loss does not present itself in cochlear measurements such as OAE's and PTA (hidden hearing loss), it will be a challenging task.

In summary, auditory tests included in the present review showed overall decreased DPOAE's with disease progression, SNHL in the higher tones during PTA related to progression of disease and in particular to older age. Together with poorer word recognition scores in quiet, this is suggestive for cochlear damage. But central auditory measurements such as gap detection thresholds, ABR and MLR tests and the P300 also confirmed CNS involvement among HIV seropositive subjects. The affected processing of sound in HIV infected subjects is therefore not merely a peripheral or a central pathology. HIV affects all stages of auditory perception in a way similar to accelerated aging of the auditory system. And we postulate that synaptic loss may be involved, however further study is needed to evaluate this possible explanation. As well as cochlear damage and central pathology as the virus remains present in all the structures causing local inflammation and degeneration. Health care providers should be aware of the increased risk of hearing loss among HIV infected persons that are under their treatment. Early detection and the use of several auditory measurements is recommended. It should include OAE testing, pure tone and speech audiometry, speech in noise tests and ABR measurements.

AUTHOR CONTRIBUTIONS

MdJ, AL, and MG all contributed to the writing of this article.

REFERENCES

1. Cohen BE, Durstenfeld A, Roehm PC. Viral causes of hearing loss: a review for hearing health professionals. *Trends Hear*. (2014) 18:1–17. doi: 10.1177/2331216514541361
2. Matas CG, Samelli AG, Magliaro FC, Segurado, A. Audiological and electrophysiological alterations in HIV-infected individuals subjected or not to antiretroviral therapy. *Braz J Otorhinolaryngol.* (2018) 84:574–82. doi: 10.1016/j.bjorl.2017.07.003
3. Levy RM, Bredesen DE, Rosenblum ML. Neurological manifestations of the acquired immunodeficiency syndrome (AIDS): experience at UCSF and review of the literature. *J Neurosurg.* (2007) 107:1253–73. Discussion 1251. doi: 10.3171/JNS-07/12/1253
4. Zhan Y, Fellows AM, Qi T, Clavier OH, Soli SD, Shi X, et al. Speech in noise perception as a marker of cognitive impairment in HIV infection. *Ear Hear.* (2018) 39:548–54. doi: 10.1097/AUD.0000000000000508
5. Ongulo BA, Oburra HO. Hearing disorders in HIV positive adult patients not on anti-retroviral drugs at Kenyatta national hospital. *East Afr Med J.* (2010) 87:385–8. Available online at: https://www.ajol.info
6. Makau SM, Ongulo BA, Mugwe P. The pattern of hearing disorders in HIV positive patients on anti-retrovirals at Kenyatta national hospital. *East Afr Med J*. (2010) 87:425–9. Available online at: https://www.ajol.info
7. Khosa-Shangase K. An analysis of auditory manifestations in a group of adults with AIDS prior to antiretroviral therapy. *Afr J Infect Dis*. (2011) 5:11–22. doi: 10.4314/ajid.v5i1.66506
8. Matthews SS, Albert RR, Job A. Audio-vestibular function in human immunodeficiency virus infected patients in India. *Indian J Sex Transm Dis AIDS*. (2012) 33:98–101. doi: 10.4103/0253-7184.102115
9. Van der Westhuizen Y, Swanepoel DW, Heinze B, Hofmeyr LM. Auditory and otological manifestations in adults with HIV/AIDS. *Int J Audiol.* (2013) 52:37–43. doi: 10.3109/14992027.2012.721935
10. Matas CG, Angrisani RG, Magliaro FC, Segurado AA. Audiological manifestations in HIV-positive adults. *Clinics.* (2014) 69:469–75. doi: 10.6061/clinics/2014(07)05
11. Luque AE, Orlando MS, Leong U-C, Allen PD, Guido JJ, Yang H, et al. Hearing function in patients living with HIV/AIDS. *Ear Hear*. (2014) 35:e282–90. doi: 10.1097/AUD.0000000000000064
12. Torre P III, Hoffman HJ, Springer G, Cox C, Young M, Margolick JB, et al. Cochlear function among HIV-seropositive and HIV-seronegative men and women. *Ear Hear.* (2014) 35:56–62. doi: 10.1097/AUD.0b013e3182a021c8
13. Maro MPH II, Moshi N, Clavier OH, MacKenzie TA, Kline-Schoder RJ, Wilbur JC, et al. Auditory impairments in HIV-infected individuals in Tanzania. *Ear Hear.* (2014) 35:306–17. doi: 10.1097/01.aud.0000439101.07257.ed
14. Fokouo JV, Vokwely JE, Noubiap JJ, Nouthe BE, Zafack J, Minka Ngom ES, et al. Effect of HIV infection and highly active antiretroviral therapy on hearing function: a prospective case-control study from Cameroon. *JAMA Otolaryngol Head Neck Surg.* (2015) 141:436–41. doi: 10.1001/jamaoto.2015.125
15. Torre P III, Hoffman HJ, Springer G, Cox C, Young MA, Margolick JB, et al. Hearing loss among HIV-seropositive and HIV-seronegative men and women. *JAMA Otolaryngol Head Neck Surg.* (2015) 141:202–10. doi: 10.1001/jamaoto.2014.3302
16. Torre P III, Hoffman HJ, Springer G, Cox C, Young MA, Margolick JB, et al. Speech audiometry findings from HIV+ and HIV- adultsin the MACS and WIHS longitudinal cohort studies. *J Commun Disord.* (2016) 64:103–09. doi: 10.1016/j.jcomdis.2016.07.004
17. Khoza-Shangase K. Highly active antiretroviral therapy: does it sound toxic? *J Pharm Bioallied Sci.* (2011) 3:142–53. doi: 10.4103/0975-7406.76494
18. Parthasarathy A, Kujawa SG. Synaptopathy in the aging cochlea: characterizing early neural deficits in auditory temporal envelope processing. *J Neurosci.* (2018) 38:7108–19. doi: 10.1523/JNEUROSCI.3240-17.2018
19. Lucertini M, Moleti A, Sisto R. On the detection of early cochlear damage by otoacoustic emission analysis. *J Acoust Soc Am.* (2002) 111:972–8. doi: 10.1121/1.1432979
20. Rey D, L'Heritier A, Lang JM. Severe ototoxicity in a healthcare worker who received postexposure prophylaxis with stavudine, lamivudine, and nevirapine after occupational exposure to HIV. *Clin Infect Dis*. (2002) 34:417–8. doi: 10.1086/324368
21. Marra CM, Wechkin HA, Longstreth WT Jr, Rees TS, Syapin CL, Gates GA. Hearing loss and antiretroviral therapy in patients infected with HIV-1. *Arch Neurol.* (1997) 54:407–10. doi: 10.1001/archneur.1997.00550160049015
22. Simdon J, Watters D, Bartlett S, Connick E. Ototoxicity associated with use of nucleoside analog reverse transcriptase inhibitors: a report of 3 possible cases and review of the literature. *Clin Infect Dis*. (2001) 32:1623–7. doi: 10.1086/320522
23. Bektas D, Martin GK, Stagner BB, Lonsbury-Martin BL. Noise-induced hearing loss in mice treated with antiretroviral drugs. *Hear Res*. (2008) 239: 69–78. doi: 10.1016/j.heares.2008.01.016
24. Lewis W, Dalakas MC. Mitochondrial toxicity of antiviral drugs. *Nat. Med.* (1995) 1:417–22. doi: 10.1038/nm0595-417
25. Desai S, Landay A. Early immune senescence in HIV disease. *Curr HIV/AIDS Rep*. (2010) 7:4–10. doi: 10.1007/s11904-009-0038-4
26. Pappas DG Jr, Chandra HK, Lim J, Hillman DE. Ultrastructural findings in the cochlea of AIDS cases. *Am J Otol.* (1994) 15:456–65.
27. Minhas RS, Lyengar DA. Effect of HIV and antiretroviral treatment on auditory functions. *Int Arch Otorhinolaryngol.* (2018) 22:378–81. doi: 10.1055/s-0038-1639594
28. Buckey JC, Fellows AM, Albert Magohe MA, Maro I, Gui J, Clavier O, et al. Hearing complaints in HIV infection originate in the brain not the ear. *AIDS.* (2019) 33:1449–54. doi: 10.1097/QAD.0000000000002229
29. Palacios GC, Montalvo MS, Fraire MI, Leon E, Alvarez MT, Solorzano F. Audiologic and vestibular findings in a sample of human immunodeficiency virus type-1-infected Mexican children under highly active antiretroviral therapy. *Int J Pediatr Otorhinolaryngol.* (2008) 72:1671–81. doi: 10.1016/j.ijporl.2008.08.002
30. Rattay F, Danner SM. Peak I of the human auditory brainstem response results from the somatic regions of type I spiral ganglion cells: evidence from computer modeling. *Hear Res.* (2014) 315:67–79. doi: 10.1016/j.heares.2014.07.001

Conflict of Interest Statement: The authors declare that the research was conducted in the absence of any commercial or financial relationships that could be construed as a potential conflict of interest.

frontiers in Neurology

ORIGINAL RESEARCH
published: 16 August 2019
doi: 10.3389/fneur.2019.00895

Age-Related Changes in Immune Cells of the Human Cochlea

Kenyaria V. Noble[1], *Ting Liu*[1], *Lois J. Matthews*[2], *Bradley A. Schulte*[1,2] *and Hainan Lang*[1]*

[1] Department of Pathology and Laboratory Medicine, Medical University of South Carolina, Charleston, SC, United States,
[2] Department of Otolaryngology-Head and Neck Surgery, Medical University of South Carolina, Charleston, SC, United States

Age-related hearing loss is a chronic degenerative disorder affecting one in two individuals above the age of 75. Current population projections predict a steady climb in the number of older individuals making the search for interventions to prevent or reverse this disorder even more critical. There is growing acceptance that aberrant activity of resident or infiltrating immune cells, such as macrophages, is a major factor contributing to the onset and progression of age-related degenerative diseases. However, how macrophage populations and their functionally-driven morphological characteristics change with age in the human cochlea remains largely unknown. In this study, we employed immunohistochemical approaches along with confocal and super-resolution imaging, three-dimensional reconstructions, and quantitative analysis to determine age-related changes in macrophage numbers and morphology as well as interactions with other cell-types and structures of the auditory nerve and lateral wall in the human cochlea. In the cochlea of human ears from young and middle aged adults those macrophages in the auditory nerve assumed a worm-like structure in contrast to those in the spiral ligament or associated with the dense microvascular network in the stria vascularis which exhibited a highly ramified morphology. Macrophages in both the auditory nerve and cochlear lateral wall showed morphological alterations with age. The population of activated macrophages in the auditory nerve increased in cochleas obtained from older donors. Dual-immunohistochemical staining with macrophage, myelin, and neuronal markers revealed increased interactions of macrophages with the glial and neuronal components of the aged auditory nerve. These findings implicate the involvement of abnormal macrophage-glia interactions in age-related physiological and pathological alterations in the human cochlea. There is clearly a need to further investigate the contribution of macrophage-associated inflammatory dysregulation in human presbyacusis.

Keywords: hearing loss, macrophage, aging, human temporal bone, cochlea

OPEN ACCESS

Edited by:
Isabel Varela-Nieto, Spanish National Research Council (CSIC), Spain

Reviewed by:
Helge Rask-Andersen, Uppsala University, Sweden
Anneliese Schrott-Fischer, Innsbruck Medical University, Austria

***Correspondence:**
Hainan Lang
langh@musc.edu

Specialty section:
This article was submitted to Neurodegeneration, a section of the journal Frontiers in Neurology

Received: *04 May 2019*
Accepted: *02 August 2019*
Published: *16 August 2019*

Citation:
Noble KV, Liu T, Matthews LJ, Schulte BA and Lang H (2019) Age-Related Changes in Immune Cells of the Human Cochlea. Front. Neurol. 10:895. doi: 10.3389/fneur.2019.00895

INTRODUCTION

Age-related hearing loss (ARHL), or presbyacusis, is one of the most prevalent chronic disorders affecting the older adult population in the US, with one in three individuals over the age of 60 and one in two individuals over the age of 75 reporting moderate-to-severe hearing loss (1). ARHL is characterized by reduced hearing sensitivity as measured by pure-tone thresholds with individuals

often complaining of difficulties understanding speech, especially in noisy environments (2). This reduction in hearing may lead to quality of life changes such as social isolation and depression (3).

The most common treatment recommendation for ARHL is hearing aids. For those with moderate-to-profound hearing loss who no longer receive benefit from hearing aids, cochlear implants may be recommended. Cochlear implants are surgically placed devices which electrically stimulate the nerves of the inner ear directly. It has been shown that cochlear implantation may induce activation of both immune and non-immune cells, and thereby have a negative impact on the outcome of this therapeutic approach (4). Interrogation of the cochlear inflammatory response to implantation in a mouse model identified a significant up-regulation in the expression of pro-inflammatory cytokines such as IL-1β. A better understanding of the specific cellular and molecular mechanisms associated with ARHL, in particular the role of the immune system, is necessary to identify targetable cells and pathways for the development of new and novel approaches of remediation.

There is now growing acceptance that aberrant immune cell activity is a contributive factor in the onset and progression of age-related degenerative diseases (5, 6). This includes disorders such as cardiovascular disease, which has high prevalence among older individuals and is co-morbid with ARHL (7). Characterization of immune cell activity in cardiovascular disease pathology indicates atherosclerotic plaque formation is associated with the phagocytic uptake of lipid particles by macrophages (6, 8). Dementia, another chronic disorder which shows strong correlation with ARHL (9), is characterized by neurodegeneration in which the dysregulation of immune cell activity is a promising therapeutic target (5). For example, in Alzheimer's disease, reduced degradation activity by microglia has been shown to contribute to the accumulation of amyloid-beta plaques and neurofibrillary tangles (10), which can be ameliorated by the presence of young microglial cells (11).

Previous studies on the cellular and molecular processes which contribute to ARHL have focused primarily on degenerative changes in sensory hair cells (12–14) and the auditory nerve (15, 16). Immunohistochemical analysis of immune cell distribution in the mouse and human cochlea, indicates that macrophages are largely excluded from the healthy adult organ of Corti, the cochlear region housing the inner and outer hair cells (17). Other studies have provided evidence demonstrating not only the presence of resident macrophages in the cochlear lateral wall and auditory nerve but also their direct interaction with the strial microvessels and spiral ganglion neurons in the human ear (18–20). Furthermore, recent studies indicate that activated microglia play an important role in the disruption of the blood-brain barrier and demyelination in the central nervous system (21, 22).

Based on the above observations, we hypothesized that macrophage function and activity in the cochlea changes with age and these changes may be a contributive factor to pathophysiological alterations of cochlear structures in ARHL. Here we have addressed this hypothesis by evaluating changes in the number and morphology of macrophages, together with observations of interactions between activated macrophages and other cochlear cell types and structures in the lateral wall and auditory nerve in an age-graded series of human inner ears.

TABLE 1 | Human temporal bone donor metrics.

Group	ID	Age	Sex	Postmortem fixation interval (hours)
Younger ($n = 5$)	H41	20	M	23.5
	H98	31	M	7.0
	H109	42	M	8.7
	H87	55	F	5.8
	H107	65	M	5.3
Older ($n = 7$)	H38	68	F	6.5
	H94	69	F	5.4
	H114	75	F	3.5
	H55	86	M	4.8
	H33	87	F	3.6
	H51	89	F	35.0
	H34	>89	F	3.3

MATERIALS AND METHODS

Collection and Preparation of Cochlear Tissues

Human temporal bone samples were obtained from two sources; (1) the Medical University of South Carolina (MUSC) Hearing Research Program's temporal bone collection generated from a longitudinal study of ARHL and (2) the MUSC Carroll A. Campbell, Jr. Neuropathology Laboratory Brain Bank. In all cases of HTB collection, written and informed consent was obtained from the next-of-kin in accordance with South Carolina laws and regulations. Temporal bone research was approved by the MUSC Institutional Review Board as not human subject research (Pro0030845). **Table 1** lists the donors' age, sex, and the time between death and fixation for the 12 human temporal bones used in this study. After removal of the specimen (23), scalar perfusion was performed with a 4% solution of paraformaldehyde as previously described (24, 25) and fixation was continued by immersion for 48–72 h. The bones were then rinsed with phosphate-buffered saline (PBS) and decalcified in EDTA, for a period of 4–6 weeks as previously described (26, 27). Over this period, the specimens were trimmed to remove the hard bone covering the cochlea and vestibular apparatus of the inner ear. The inner ear portion of the trimmed temporal bones was processed for frozen sectioning and whole mount preparations as described previously (25, 28, 29).

For all analyses, the human cochlea samples were divided into two groups: younger group ranging in age from 20 to 65 years and older group ranging in age from 68 to >89 years (older).

Immunostaining and Quantitative Analysis of IBA1$^+$ Cells

The whole mounts and frozen sections of inner ear tissue were subjected to immunofluorescence staining as described briefly below. Whole mounts were washed with PBS and incubated in 4:1:1 (methanol: 30% hydrogen peroxide: dimethyl

TABLE 2 | Antibodies and other reagents used for immunohistochemistry.

Material	Company	Catalog no.	Dilution
Rabbit anti-IBA1	Wako	019-19741	1:200
Chicken anti-MBP	EMD Millipore	AB9348	1:100
Mouse anti-NF	Sigma	N0142	1:200
Mouse anti-CD163	Invitrogen	MA5-17716	1:200
Rabbit anti-Kir4.1	Alomone Labs	PC035AN0802	1:100
Biotinylated goat anti-Rabbit IgG	Vector	BA-1000	1:150
Biotinylated goat anti-Chicken IgY	Vector	BA-9010	1:150
Fluorescein Avidin D	Vector	A-2011	1:150
Texas Red Avidin D	Vector	A-2006	1:150
Propidium Iodide	Millipore Sigma	P4864	1:1,000
Hoechst 33342	Millipore Sigma	B2261	1:1,000

sulfoxide) solution for 1 h at room temperature prior to staining. The tissues/samples were incubated overnight at 4°C with a primary antibody (**Table 2**) diluted in 0.2% bovine serum albumin (BSA) in PBS. After rinsing with PBS, the appropriate biotinylated secondary antibody was applied to the sections followed by conjugation with Fluorescein-labeled (A-2011, Vector), Texas Red-labeled (A-2006, Vector) avidin, or a DAB immunoperoxidase secondary detection system (DAB150, Millipore). For dual-labeling, sections were processed using an avidin/biotin blocking kit (SP-2001, Vector) following the first staining reaction, according to the manufacturer's instructions. After a 30-min incubation in 0.2% BSA in PBS, staining was continued overnight by incubation with a second primary antibody. Nuclear counterstaining was performed with either propidium iodide (PI) or 4′,5-diamidino-2-phenylindole (DAPI).

The numbers of IBA1$^+$ cells located in the cochlear lateral wall and the auditory nerve within Rosenthal's Canal were quantified on randomized sections (2–4 sections per sample) by researchers blinded to specimen age. In this study, cell counting was performed on the frozen cochlear sections that were developed with a fluorescence staining approach, but not the DAB immunoperoxidase method. The use of the immunofluorescence staining, together with PI or DAPI nuclear counterstaining and confocal microscope, is the best approach to (1) identify the nuclear location of IBA1$^+$ macrophages, which is the crucial step of the macrophage count, and (2) to determine how macrophages interact with other cochlear cell types if needed. For the lateral wall, both the number of IBA1$^+$ cells and the number of processes per cell were quantified in the apical, middle, and basal turns of the cochlea at 40X magnification. For the auditory nerve, numbers of IBA1$^+$ cells were quantified only in the middle turn. Statistical analysis of the collected data was performed with SPSS Statistics (v25, IBM) using Shapiro-Wilk normality test to confirm the data was normally distributed. Younger vs. older adult group means were compared by Student's unpaired one-tailed *t*-test.

Confocal image stacks of frozen sections and whole mount tissues were acquired using a Zeiss LSM 880 NLO microscope with Zen acquisition software (Zeiss). Image stacks were composed of 1,024 pixels (x) by 1,024 pixels (y) taken at 0.5–1 μm intervals throughout the optical plane. For super-resolution imaging, confocal image stacks (0.2 μm intervals) of frozen sections were acquired using a Zeiss LSM 880 NLO microscope with Airyscan super-resolution detector and a 63x/1.4 Plan-Apochromat oil objective (Zeiss). Multi-color images were acquired using the following laser and filter combinations: Channel 1–561 nm laser excitation and BP 570–620 + LP 645; Channel 2–488 nm laser excitation and BP 420–480 + BP 495–550.

Image processing was performed using Zen Black or Zen 2012 Blue Edition (Carl Zeiss Microscopy), Adobe Photoshop CC (Adobe Systems), and GIMPshop (open source software).

RESULTS

Morphological Features of Macrophages Vary Between the Cochlear Lateral Wall and Auditory Nerve

To assess the morphology of resident macrophages in the human cochlea, we performed immunofluorescence staining using an antibody against the microglia/macrophage specific protein, ionized calcium binding adaptor molecule 1 (IBA1). In young and middle-aged ears, marked differences in morphological characteristics were seen between macrophages in the stria vascularis (SV; **Figures 1A,B**) and those associated with the auditory nerve both in the osseous spiral lamina (**Figures 1C,D**) and Rosenthal's canal (**Figures 1E,F**). Macrophages in the SV from 42- and a 55-year-old donor were characterized by cellular processes extending into the areas between marginal and basal cells, near the strial microvasculature (**Figures 1A′,B′**). This observation is in good agreement with a previous study showing strial macrophages interacting with the microvasculature (18). Observations of the auditory nerve in the same cochleas revealed macrophages in the osseous spiral lamina with a more bipolar architecture (**Figure 1D**, at this plane of view) and flat encroaching filopodia-like structures (**Figure 1D′**), suggesting interactions with peripheral neural projections. In Rosenthal's canal, IBA1$^+$ cells were observed with two distinct stellate forms, a less frequent form which was often oriented perpendicular to the axonal fibers (arrowhead, **Figure 1F**), and a more common "worm-like" cyto-architecture located near the neuronal soma (arrows, **Figure 1F′**). The differential characteristics of IBA1$^+$ macrophages located in the auditory nerve and cochlear lateral wall were also revealed by peroxidase DAB immunohistochemistry with frozen sections (**Figures 1G–J**). These differences in macrophage morphology among different cochlear regions may indicate a variety of macrophage functions since each cochlear compartment contributes uniquely to auditory physiology.

Super-resolution imaging was also applied to visualize the morphological differences of the macrophages in the auditory nerve and the lateral wall. **Figure 2** includes both the standard and super resolution confocal images of IBA1$^+$ macrophages taken from the same regions of the SV and auditory nerve in the middle-basal turn cochlea of a 55 year old donor. The enhancement in image quality and the power to resolve the

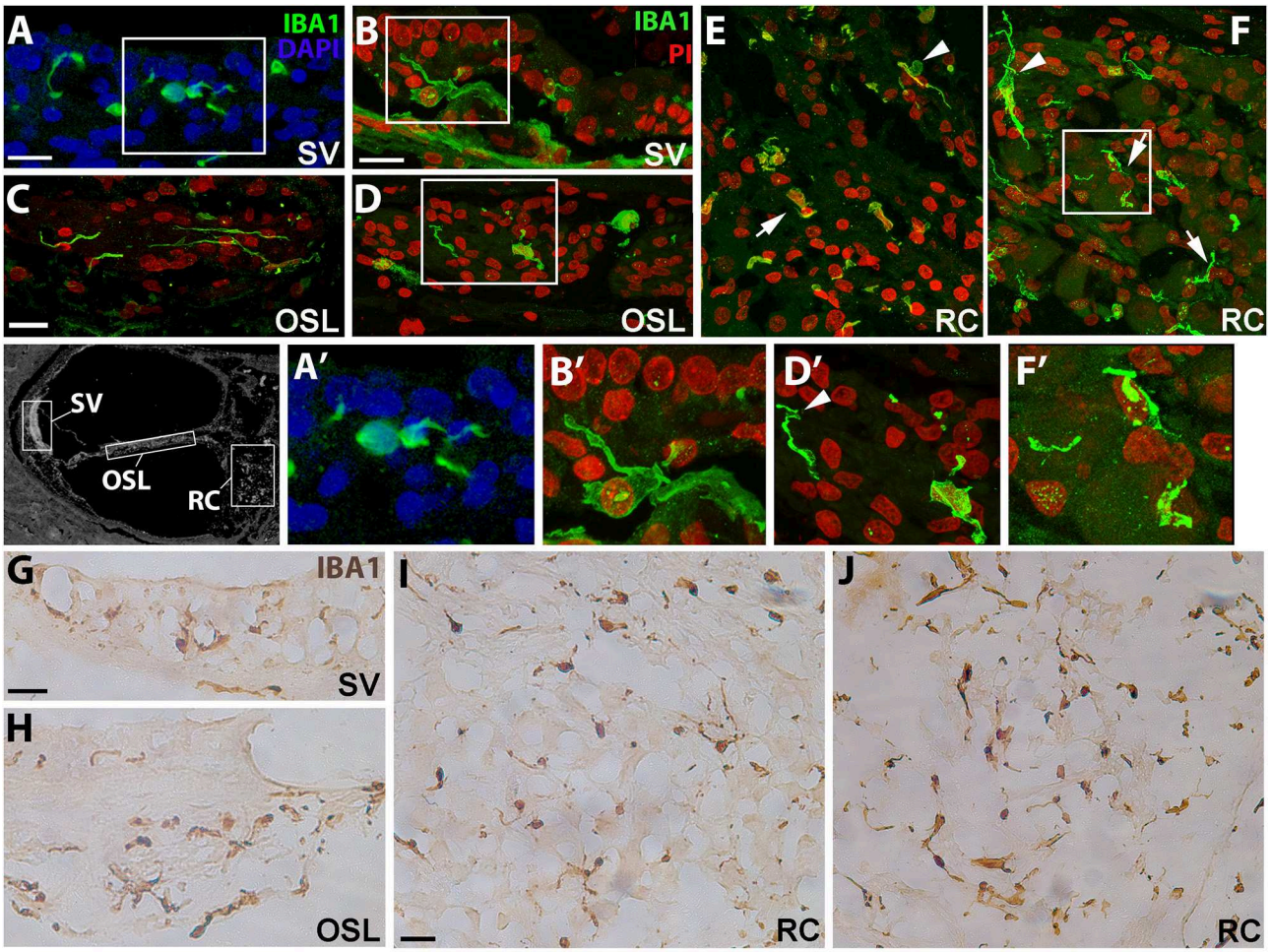

FIGURE 1 | Cochlear macrophages demonstrate unique morphologies in different regions of the human cochlea. Confocal imaging of immunofluorescence staining for ionized calcium-binding adaptor molecule-1 (IBA1$^+$, green) identifies resident macrophages in the stria vascularis (**A,B**—SV), osseous spiral lamina (**C,D**—OSL), and Rosenthal's canal (**E,F**—RC). Similar results were also revealed by peroxidase-DAB immunohistochemistry assay showing IBA1$^+$ macrophages in the SV **(G)**, OSL **(H)**, and RC **(I,J)**. Images in **(A′,B′,D′,F′)** are enlargements of the boxed areas in **(A,B,D,F)**, respectively. The black and white image in the left of **(A′)** was included to show different cochlear locations. The image was taken from a cochlear section that was stained for Kir4.1 antibody (30) and the section was obtained from an 86-year-old donor (H55). Strial macrophages **(A,B,G)** emit cellular processes that extend short distances from the cell body **(A′,B′)**. Macrophages in the OSL **(C,D,H)** are more worm-like in shape with thin cellular projections that sometimes wrap around structures (**D′**, arrowhead), most likely peripherally projecting axons, whereas macrophages in RC **(E,F,I,J)** typically have an elongated appearance (arrows); IBA1$^+$ macrophages with multiple processes are also seen (arrowheads). Images were obtained from a 42-year-old donor (H109; **A,C,E**), a 55-year-old donor (H87; **B,D,F,I**) and a 57-year-old donor (H122; **G,H,J**). Locations in the cochlea are indicated on the cochlear map by a black and white image at the middle left. Scale bars in **(A,B)** = 20 μm; in **(C)** applies to **(D–F)** = 20 μm; in **(G)** applies to **(H)** = 30 μm, in **(I)** applies to **(J)** = 30 μm.

nanoscopic filaments extending from the subcellular elements of the macrophage is clearly visualized in the super resolution images (**Figures 2A″,B″**).

A recent human temporal bone study characterized a number of macrophage/microglia markers, including CD163, on celloidin embedded sections of temporal bones from normal individuals (19). CD163 is a scavenger receptor expressed on the cell surface of monocytes and macrophages (31) demonstrated to be responsive to pro- and anti- inflammatory stimuli (32). In the present study, frozen sections were stained with an antibody against CD163, and we assessed immunoreactivity and distribution in different cochlear regions. CD163$^+$ macrophages were observed within the spiral ligament (SpL) of the cochlear lateral wall, osseous spiral lamina, and Rosenthal's canal, as demonstrated by representative images in **Figure 3**. Immunostaining for CD163 appears to be less illustrative of the macrophage morphological features compared to IBA1 staining (**Figure 1**), thus IBA1 antibody was selected as the marker to evaluate macrophage morphology and quantitative analysis in the study.

Diversity of Macrophages Within the Cochlear Lateral Wall

Cochlear macrophage morphology was further examined in the suprastrial, strial, and substrial regions of the cochlear

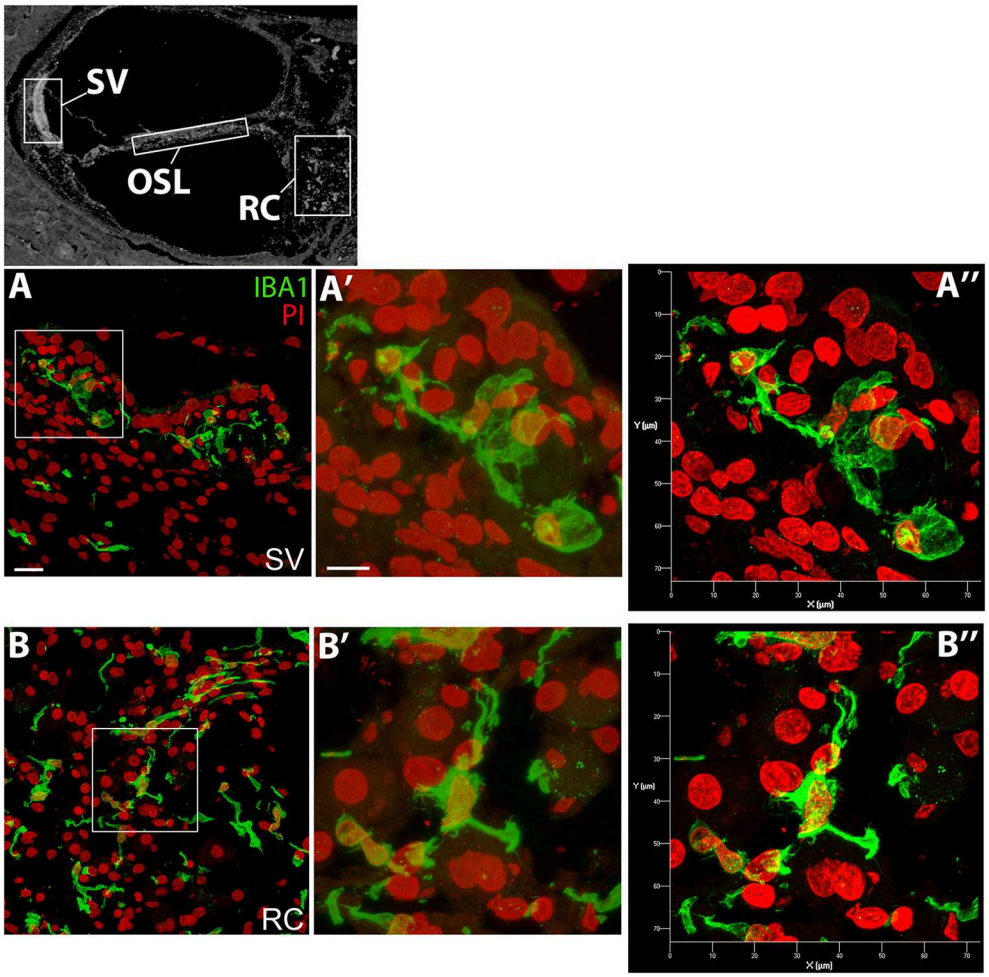

FIGURE 2 | Super-resolution confocal images obtained by ZEISS Airyscan detector showing differential morphology of the IBA1+ macrophages in the SV and RC. Confocal images **(A′,B′)** and super-resolution images **(A″,B″)** were taken from the same boxed areas outlined in A and B. The black and white image in the top panel was included to show different cochlear locations and it is the same image used in **Figure 1**. All images were taken from the SV and RC of a cochlea obtained from a 57-year-old donor (H122). Scale bar in **(A)** applies to **(B)** = 20 μm; in **(A′)** applies to **(B′)** = 10 μm.

lateral wall by immunostaining whole mounts for IBA1 (**Figure 4**). This procedure allows the three-dimensional features of individual macrophages to be clearly observed. The morphological characteristics of macrophages varied among different regions of the lateral wall. In the suprastrial region of the SpL, which is typically populated by type V fibrocytes, macrophages were observed with an elongated shape and extending a single filopodia-like structure (**Figure 4I**), or with a rounder shape and shorter flatter cellular process (**Figure 4I**). In the substrial region of the SpL, which typically contains type IV fibrocytes, the IBA1$^+$ cells displayed slightly extended cellular profiles in a polar morphology (**Figure 4III**). Macrophages in the SV exhibited a stellate appearance with numerous thin cellular extensions ("ramified" morphology; **Figure 4II**), a morphological profile typically associated with active surveillance of the biochemical activity in the local environment (33).

Age-Related Changes of Macrophages in the Cochlear Lateral Wall

Examination of the cochlear lateral wall from older donors revealed characteristic changes in IBA1$^+$ macrophage morphology in the SV and SpL using both immunofluorescence staining (**Figures 5A–D**) and peroxidase DAB immunohistochemistry (Data not shown). In the SV of the younger donors, macrophages had little cytoplasm surrounding the nucleus and numerous projecting processes (**Figure 5A**). In contrast, in older donors the number of processes projecting from macrophages was reduced while cytoplasmic volume around the nucleus appeared to increase (**Figure 5B**). Macrophages in the adjacent SpL exhibited similar morphological alterations of increased cytoplasmic volume and reduced cellular processes in older donors (**Figure 5D**).

In order to quantitatively assess changes in the cellular properties of macrophages in the SpL, IBA1$^+$ cells were counted

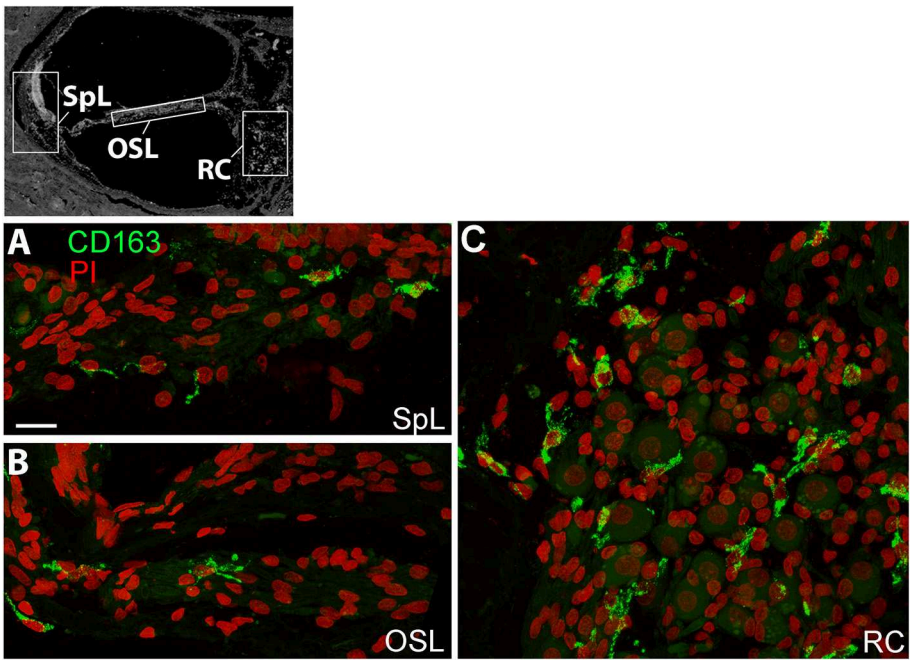

FIGURE 3 | CD163$^+$ macrophages are present in several regions of the human cochlea. The black and white image in the top panel was included to show different cochlear locations and it is the same image used in **Figures 1**, **2**. Confocal imaging of immunofluorescence staining for CD163 (IBA1$^+$, green) identifies resident macrophages in the spiral ligament (SpL, **A**), OSL **(B)**, and RC **(C)**. Images were obtained from a 57-year-old donor (H122). Scale bar in **(A)** applies to **(B,C)** = 20 μm.

in two age groups, younger vs. older donors (n = 5/group). The number of macrophages are reported as cell number per observed area, which included the entire cochlear turn. In the apical turn, the number of IBA1$^+$ macrophages was very similar in the younger and older groups (2.7 ± 1.0 vs. 2.9 ± 1.0 cells, respectively, $p = 0.34$). Quantification of macrophage numbers in the middle (7.8 ± 3.5 vs. 10.7 ± 3.8 cells) and basal turn (11.3 ± 6.5 vs. 14.5 ± 6.1 cells) of younger vs. older ears, respectively, indicates a trending increase in both of these regions in the older group, but this change failed to reach statistical significance (p-values = 0.12 and 0.23, respectively). The results of cell counting from individual donors, listed in **Table 3**, reveal a large amount of variability in the younger control group. Activated macrophages, defined as IBA1$^+$ cells with no or only a few cellular processes, were also quantified to determine if the number of activated macrophages changes with age. **Table 4** lists these results from individual donors. No statistically significant differences were found. In the apical turn, the presence of activated macrophages in the SpL was unchanged (1.0 ± 1 vs. 1.0 ± 0.5 cells, p = 0.50); though a trending increase in the number of activated macrophages was noted for the middle (4.0 ± 3.3 vs. 6.4 ± 2.4 cells, $p = 0.11$) and basal turns (4.9 ± 3.0 vs. 7.9 ± 3.5 cells, p = 0.09) of the older group.

Diverse Morphology of Macrophages in the Auditory Nerve

A recent study employing super-resolution imaging in the human cochlea demonstrated that resident macrophages in the auditory nerve make contact with spiral ganglion neurons (18). Here we assessed the cellular morphology of the IBA1$^+$ macrophages in the auditory nerve from an 87-year-old donor (**Figure 6**). In the middle turn (**Figure 6A**), the macrophages had thin cellular processes with little cytoplasm around the nucleus, an architecture possibly reflecting interactions with axons and neuronal cell soma. Macrophages in the basal turn from the same donor exhibit a markedly different appearance having amorphous or round shapes with less evidence of extended cellular projections (**Figure 6B**). Interestingly, no noticeable loss of β-Tubulin$^+$ spiral ganglion neurons was identified in the basal turn of the auditory nerve of this donor (**Figures 6C,D**). These observations suggest the morphology and activity of macrophages may be dependent on not only cell death, but also location and physiological and/or pathological activity along the cochlear axis.

Age-Related Changes in Number and Cellular Interactions of Macrophages in the Auditory Nerve

We have previously demonstrated the presence of myelination in the parikarya of some Type I spiral ganglion in the human auditory nerve (24) and provide further evidence of this phenomenon (**Figures 7A,B,D,E**) in the current study. To assess macrophage interactions with components of the human auditory nerve, we performed dual labeling immunohistochemistry. Antibodies against either neurofilament 200 (NF; **Figure 7C**) or myelin basic protein (MBP;

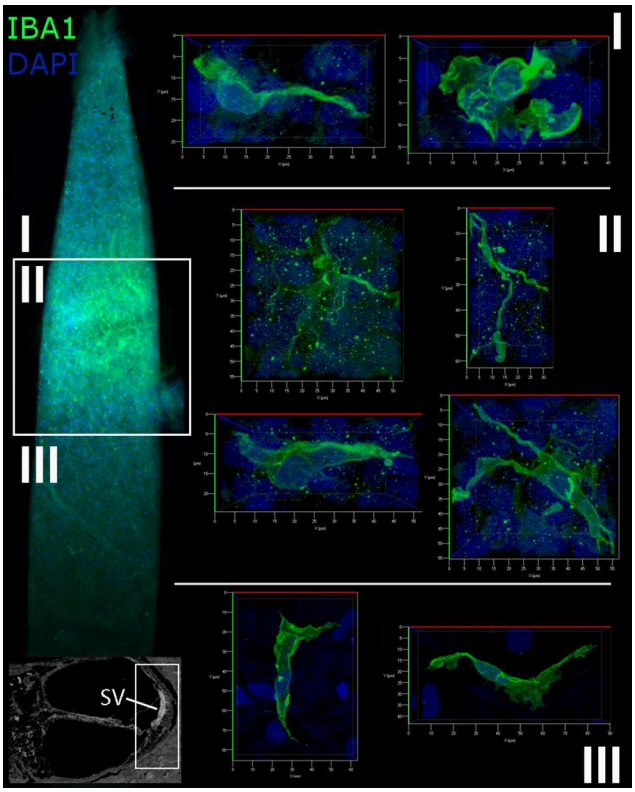

FIGURE 4 | Macrophages in the human cochlear lateral wall are morphologically diverse. A whole mount preparation of the SV and SpL in the basal turn of the cochlea from a 57-year old donor (H106) was stained for IBA1 (green). The low magnification image on the left maps the suprastrial **(I)**, strial **(II)**, and substrial **(III)** regions of the lateral wall where the images were acquired. Macrophages in the SV have a stellate appearance with thin processes, while the macrophages of the suprastrial **(I)** and substrial **(III)** regions of the SpL exhibit a bipolar morphology.

Figures 7B,D–F) were used in combination with an anti-IBA1 antibody to label auditory nerve components and macrophages, respectively. Macrophages with a variety of morphologies interact with myelin or axons of the auditory nerve. The filopodia-like structures of IBA1$^+$ macrophages are seen at discontinuities in the neurofilament bundles (**Figure 7C**I), running parallel to filamentous strands (**Figure 7C**II) as well as associated with the NF$^+$ neuronal cell elements (**Figure 7C**III). Analysis of IBA1$^+$ macrophage interactions with MBP$^+$ myelin (**Figure 7D**) revealed the encroachment of macrophage processes onto node of Ranvier-like structures (**Figure 7D**I) or spaces (**Figure 7D**III) in the ensheathing membrane. IBA1$^+$ macrophages with a rounded morphology were also observed interfacing directly with a myelinated axon (**Figure 7D**II). Three-dimensional reconstructions of confocal image stacks from dual labeling with MBP and IBA1 provided further evidence supporting macrophage interactions with the myelin around the spiral ganglion neuron soma (**Figure 7E**). These macrophage-myelin interactions are also observed in the osseous spiral lamina, where macrophage processes encircle MBP$^+$ myelin elements (shown in **Figure 7F**), as seen in the apical turn of a 42-year-old donor (H109).

To determine if age-associated alterations in morphology or cellular interactions occur in auditory nerve macrophages, dual labeling immunohistochemistry was applied using antibodies against IBA1 and MBP. Macrophages in the cochlea of a 31-year-old donor (**Figure 8A**) display an elongated shape, while those in the cochleas from 86- and 87-year-old donors (**Figures 8B,C**) have a more rounded or ovoid shape. Furthermore, macrophage processes in both older subjects demonstrated ensheathing behavior evidenced by IBA1$^+$ processes encompassing myelinated axonal fibers (**Figure 8B′**). Quantification of IBA1$^+$ cells in the middle turn of younger ($n = 5$) vs. older ($n = 7$) cochleas revealed a statistically significant increase in macrophage numbers in the auditory nerve with age (14.1 ± 4.0 vs. $= 19.0 \pm 3.3$ cells; $p = 0.021$). Results of the quantification for each donor sample are presented in **Table 3**.

DISCUSSION

Here for the first time we report observations of morphological diversity and age-related changes of macrophages in different regions of the human cochlea. Previous studies have characterized the expression of a number of key cellular markers—MHCII, CD11b, CD68, CD163, and IBA1—in macrophages of the human cochlea (18–20). Additionally, these reports described the morphological heterogeneity of macrophages within the human cochlea. However, none of these studies were able to conduct a quantitative analysis of age-related changes in either morphology or numbers of cochlear macrophages. The specimens used in the present study included 12 human donors from both sexes, with an age gradation of 20–>89-years old allowed analysis of age-related changes in macrophage morphology and numbers in the different cochlear compartments, together with observations of interactions between macrophages and other cell types.

Confocal analysis of frozen sections and whole mount samples from younger ears stained for the macrophage specific marker IBA1 provided evidence to support the morphological diversity of resident immune cells in the lateral wall, as well as in the auditory nerve. In the stria vascularis, macrophages were found to possess diverse cellular phenotypes, reflective of their close interaction with the microvascular network in both mice and humans (34, 35). Here we provide evidence from 12 human temporal bone samples showing that macrophages located in the lateral wall are morphologically distinct from those observed in the auditory nerve. Immune cells in the osseous spiral lamina and Rosenthal's canal were typically "worm-like" in appearance whereas the cyto-architecture of macrophages in the stria vascularis and spiral ligament was more variable and differed from that in the auditory nerve.

It has been well-established that the function of immune cells, especially the macrophage, has a significant impact on its morphology. Macrophages in "surveillance-mode" are typified by a highly branched morphology, while those en route to a location

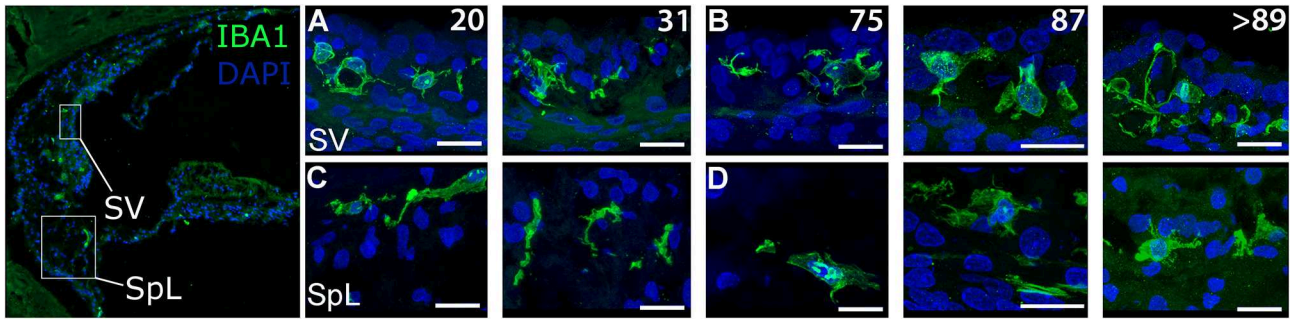

FIGURE 5 | Age-related alterations in IBA1$^+$ macrophage morphology and numbers in the human cochlear lateral wall. IBA1$^+$ resident macrophages are present in the SV and the SpL. Images from both regions document age-related changes in macrophage morphology. IBA1$^+$ cells from 20-, and a 31-year-old donar (H41 and H98, respectively) appeared to be in a "surveillance-mode" as defined by numerous processes extending from the central body **(A,C)**. In contrast, macrophages in a 75-, 87-, and >89-year-old donar (H114, H33, and H34, respectively) exhibited a rounded cellular morphology, increased cytoplasmic volume in the area surrounding the nucleus and reduced far-reaching cellular processes **(B,D)**. Scale bars in **(A–D)** = 20 μm.

TABLE 3 | Average number of macrophages in the human lateral wall and auditory nerve.

Group	ID	Age	Lateral wall			Auditory nerve
			Apical	Middle	Base	Middle
Younger ($n = 5$)	*H41	20	4.3 ± 1.5	11.3 ± 2.3	6.7 ± 2.5	20.0 ± 2.3
	H98	31	2.7 ± 0.6	11.7 ± 3.5	22.0 ± 3.6	16.0 ± 9.9
	H109	42	1.5 ± 0.7	4.5 ± 0.7	5.5 ± 0.7	12.0 ± 1.4
	H87	55	2.5 ± 1.3	4.8 ± 3.7	12.0 ± 4.1	13.0 ± 4.6
	H107	65	2.3 ± 1.2	7.0 ± 2.0	10.3 ± 2.5	9.5 ± 0.7
Older ($n = 7$)	H38	68	2.3 ± 2.3	4.7 ± 1.5	6.0 ± 1.0	17.5 ± 0.7
	H94	69	n.c.	n.c.	n.c.	20.0 ± 4.4
	H114	75	n.c.	n.c.	n.c.	13.0 ± 0.0
	*H55	86	4.0 ± 0.0	12.7 ± 3.1	19.3 ± 7.5	24.0 ± 4.0
	H33	87	3.7 ± 1.2	14.7 ± 2.1	19.3 ± 2.1	20.7 ± 6.4
	H51	89	1.7 ± 0.6	10.0 ± 3.6	10.0 ± 3.5	19.0 ± 1.4
	H34	>89	3.0 ± 1.0	11.7 ± 2.5	17.7 ± 2.5	19.3 ± 1.2

The data are presented as cell number per observed area which covered an intact cochlear turn.
**Post-mortem fixation time >20 h.*
n.c., not counted.

TABLE 4 | Average number of activated macrophages in the human lateral wall.

Group	ID	Age	Lateral wall		
			Apical	Middle	Base
Younger ($n = 5$)	H41	20	2.7 ± 1.2	9.0 ± 2.0	2.3 ± 2.3
	H98	31	1.0 ± 0.0	5.7 ± 4.0	9.3 ± 3.5
	H109	42	0.5 ± 0.7	2.0 ± 2.8	2.0 ± 1.4
	H87	55	1.0 ± 0.8	1.8 ± 3.4	6.3 ± 3.4
	H107	65	0.0 ± 0.0	1.7 ± 1.5	4.7 ± 2.1
Older ($n = 5$)	H38	68	0.7 ± 1.2	3.0 ± 1.0	4.0 ± 2.0
	H55	86	0.5 ± 0.7	6.3 ± 4.6	9.7 ± 3.5
	H33	87	1.7 ± 0.6	9.7 ± 0.6	12.7 ± 5.5
	H51	89	1.0 ± 1.0	6.0 ± 4.4	5.0 ± 1.7
	H34	>89	1.3 ± 1.1	7.0 ± 1.0	8.0 ± 2.6

The data are presented as cell number per observed area which covered an intact cochlear turn.

of injury or performing phagocytosis possess an amoeboid shape and the extension of no or only a few cellular processes (33, 36). In the lateral wall, the more prevalent highly ramified cellular morphology of macrophages may be a reflection of their need to receive external stimuli to guide activity, whereas, the "worm-like" structure of the macrophages found in the auditory nerve, is more conducive to motility within this particular cochlear compartment, as suggested by their direct contact with the plasmolemma of glial cells ensheathing axons and neurons which agrees with the direct interaction of macrophages with ganglion neuron cell bodies in mice and humans (29, 37). These differences in morphology likely relate to differences in functional activity in the separate regions of the cochlea.

The diversity in macrophage morphology identified in the different sub-regions of the lateral wall in a single ear may be directly related to the local tissue microenvironment. The suprastrial region (above Reissner's membrane) and the substrial region (below the basilar membrane) of the spiral ligament are largely occupied by type V and IV fibrocytes, respectively, that are bathed in perilymph (38). In these tissue spaces, resident immune cells were predominantly round or elongated in appearance with a few long processes extending from the cell body or, in some instances, more planar with the cytoplasm dispersed uniformly throughout the cell body. It is possible that variations in the architecture of the extracellular matrix or degree of spiral ligament involution could contribute to irregularities in macrophage cell shape (39). Interestingly, the expression pattern of ion transport enzymes by fibrocytes in the spiral ligament has been observed to change relative to the degree of strial atrophy in the aged gerbil cochlea (40).

The cells in the intrastrial space are exposed to an endolymph-like solution, where potassium is sequestered through an electrochemical gradient generated by the parenchymal cells of the stria vascularis and fibrocytes of the spiral ligament. Macrophages found in the intrastrial space are typically ramified

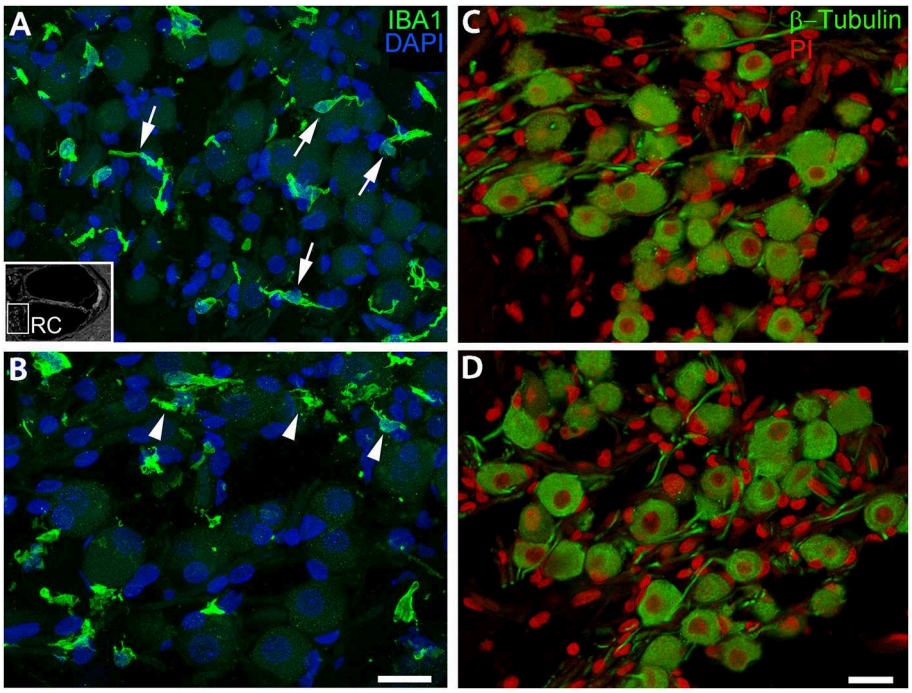

FIGURE 6 | IBA1$^+$ macrophages located in the auditory nerve demonstrate spatially-dependent alterations in morphology. These images from the auditory nerve (AN) of an 87-year-old donor (H33) demonstrate region-dependent changes in macrophage morphology. IBA1$^+$ macrophages in the middle turn **(A)** have an elongated spiral shape (arrows) whereas many cells in the basal turn **(B)** extend numerous short cellular projections (arrowheads), although there is no evidence supporting a robust loss of β-Tubulin$^+$ SGNs **(C,D)**, which appear in the same area of the AN. An inserted black and white image in the bottom-left of **(A)** shows the location of the AN in the cochlea. Scale bar in **(B)** applies to **(A)** = 20 μm; in **(D)** applies **(C)** = 20 μm.

in appearance with long cellular processes extending from a central body. In contrast macrophages in the spiral ligament, strial macrophages are typically observed interacting with the microvasculature. While macrophages found in the spiral ligament most likely execute canonical tissue macrophage functions, such as phagocytic uptake and degradation of dead cells and debris, the exact role of intrastrial macrophages remains unknown. The current literature provides conflicting reports regarding macrophage contributions to regulation of blood-labyrinth barrier permeability (34, 41). However, depletion of macrophages during cochlear development in the postnatal mouse results in severe abnormalities of the stria vascularis, implying a role for macrophages in the structural maturation of this specialized epithelium (29). Therefore, further study of changes in macrophage morphology and intercellular dynamics under steady state conditions are needed to understand how this process is regulated.

In this study, results from observations of cochleas from older donors indicated that alterations in macrophage morphology may differ in locations along the tonotopic axis. Interestingly, profiles characteristic of activation were typically observed in the basal turns of the aged cochleas. Quantitative analysis revealed a trending increase in the number of macrophages in the middle and basal turns of the spiral ligament. This increase was accompanied by an increase in the number of macrophages lacking or having very few cellular processes. This finding agrees with observations in mice, showing that a larger proportion of resident immune cells underlying the basilar membrane along the cochlear spiral become more amoeboid in shape with age, indicative of a more active vs. an inactive state (33, 42). To date, *in vitro* evidence of inflammatory cytokine secretion by spiral ligament fibrocytes (43) suggests a possible mechanism for the production of chemotactic factors with age that may induce recruitment of macrophages. Additionally, observations of intravascular monocyte-like cells in the human cochlear lateral wall implicates blood vessels as a likely site of immune cell extravasation (18). In light of these findings, future studies should aim to identify the molecular mediators of macrophage recruitment and infiltration in the aging cochlear lateral wall.

Here we present evidence of macrophage interactions with the glial cell-associated myelinated axonal projections of the type I spiral ganglion neurons and cell bodies in the human cochlea. The increasing frequency of these interactions with age suggests that macrophage activation and abnormal macrophage-glia interactions may be a contributing factor to age-related auditory nerve degeneration. Interestingly, work by Wu et al. (44) assessing cochlear neuropathy in a cohort of 20 human cochleas from "normal-hearing" individuals (0–89 years old), identified the loss of peripherally projecting axonal fibers, which are myelinated by Schwann cells, as a primary pathological process associated with hair cell and spiral ganglion neuron loss.

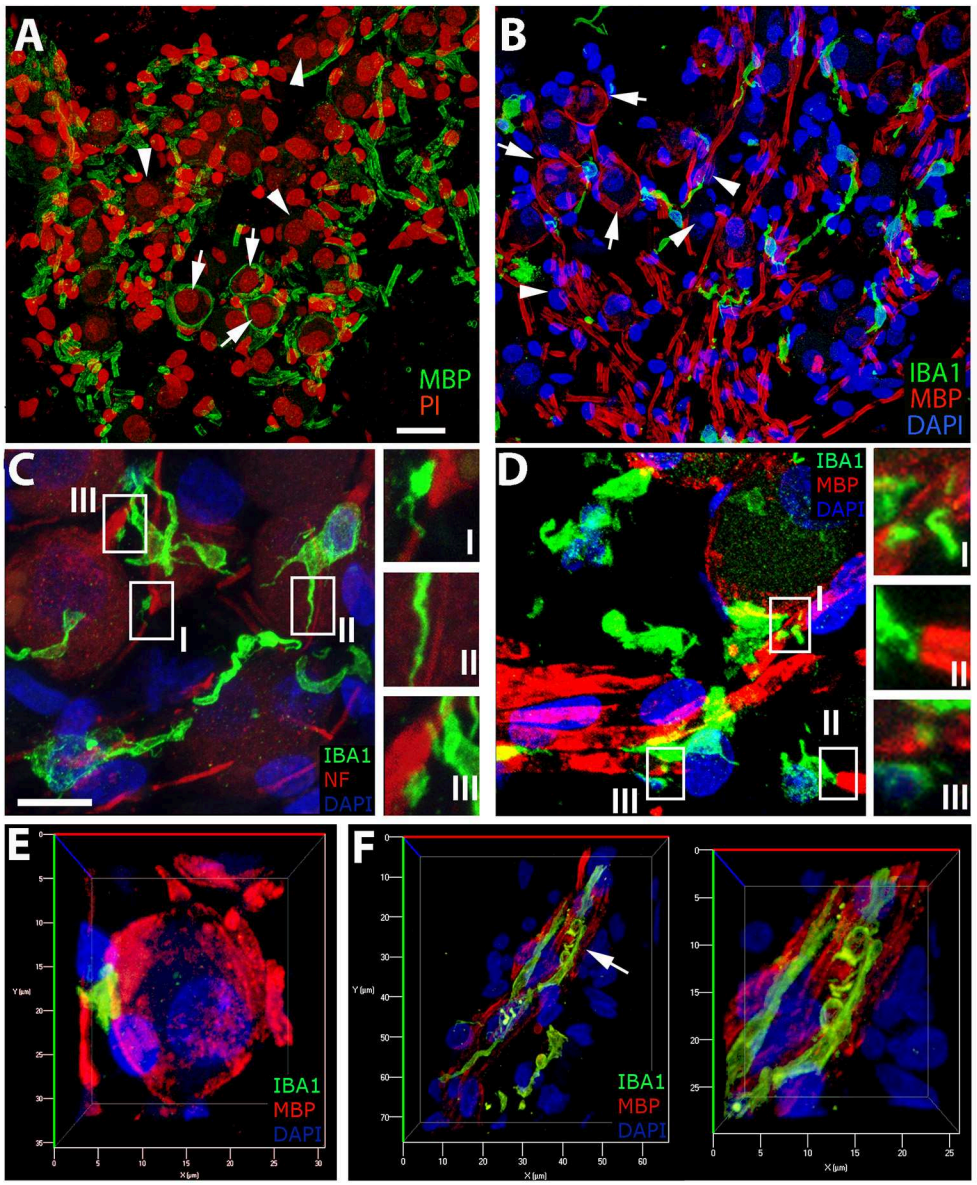

FIGURE 7 | IBA1$^+$cells in the auditory nerve demonstrate close contact with myelin and axons of the auditory nerve. **(A,B)** The presence of myelinated (MBP$^+$, arrows) and unmyelinated (arrowheads) spiral ganglion neurons (SGNs) in the human auditory nerve is demonstrated by representative images from the basal **(A)** and middle **(B)** turns of an 87-year-old donor (H33). IBA1$^+$ macrophages (green) are observed in close apposition with NF$^+$ axons (**C**, red) and MBP$^+$ myelin sheath (**B,D**, red) in sections from the middle turn of the same donor (H33). **(C)** Macrophages demonstrate a variety of interactions with the NF$^+$ components of spiral ganglion neurons (SGNs). Macrophage processes are observed interfacing with NF$^+$ axons in areas of discontinuities of the myelin sheath of SGNs (I), running parallel to the axon process (II), and in some cases directly interacting with the neural cell elements (III). **(D)** Macrophages are often observed with a "worm"-like morphology along myelinated neurons with processes terminating at areas with little or no myelin (I,III). **(E)** Three-dimensional reconstructions of confocal images from IBA1 and MBP dual-labeling provide further observations of macrophages interacting with the myelin of a Type I SGN soma in Rosenthal's canal of the cochlea obtained from the same donor (H33) shown in **(A–D)**. **(F)** Evidence of macrophage engulfment of MBP$^+$ myelin in the auditory nerve in the osseous spiral lamina in the apical turn of a 42-year-old donor (H109). The right panel is the enlarged image of the region identified by an arrow in the panel at left. Scale bar in **(A)** applies to **(B)** = 20 μm; in **(C)** applies to **(D)** = 10 μm.

We have shown previously in mice that cochlear macrophages in auditory nerves participate in modulation of glial cell numbers during postnatal development (29). In the present work, we provide evidence of direct interactions of macrophage with the myelinating glia of the auditory nerve in both Rosenthal's canal and the osseous spiral lamina. Quantitative analysis of an age-graded series of human cochleas as performed in this study indicated a statistically significant increase in macrophage numbers in the auditory nerve of the older group, suggesting macrophage activation occurs in the aged auditory nerve.

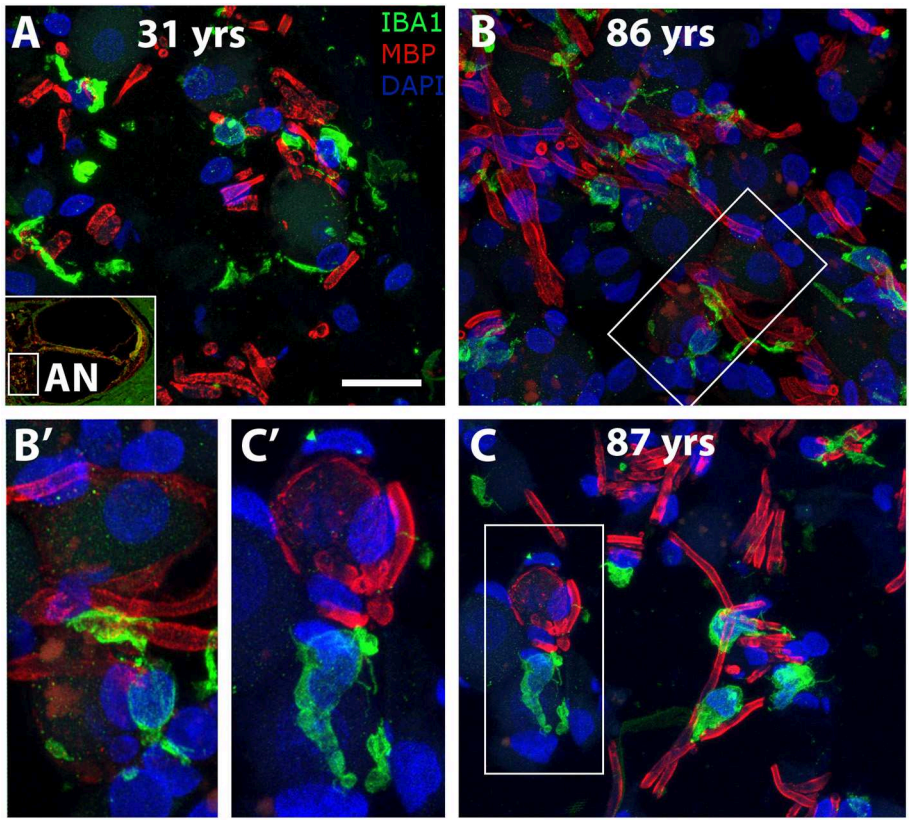

FIGURE 8 | Morphological alterations of macrophages suggest age-related changes in macrophage activity in the human auditory nerve. Dual immunofluorescent staining using antibodies against IBA1 (green) and MBP (red) revealed macrophage associations with the myelin component of axons in a young (**A**, H98) and two older (**B**, H55; **C**, H33) human cochleas. IBA1$^+$ immune cell processes appear to encircle the myelin of axonal projections (see enlarged images). Scale bar = 20 μm; 10 μm for enlarged images.

Recent immunohistochemical studies in mice have revealed the complex vascular network associated with the peripheral auditory nervous system, which may be the source of monocyte extravasation to the neural cochlear sub-compartment (45). Further work identifying the molecular components mediating macrophage-glia interactions and structural elements involved in immune cell infiltration are needed to better understand the role of resident and non-resident macrophages in the neural compartment.

"Inflammaging" describes the recently accepted phenomena by which human subjects, typically at the age of 65 and above, present with immune system dysregulation characterized by elevated levels of pro-inflammatory cytokines systemically and an impaired immune response (46–49). A limitation to the current study is the lack of evaluation for infiltration of other inflammatory cell types as lymphocyte infiltration is typically observed in neurodegenerative diseases (42, 50). The presence of CD4$^+$ and CD8$^+$ T-cells in the peripheral regions of Rosenthal's canal and the spiral ligament of freshly frozen temporal bones has recently been reported (20). Macrophages expressing antigen presentation proteins, such as MHCII, and their interaction with the aforementioned T lymphocytes suggests that adaptive immunity is amongst the cellular immune response processes initiated within the cochlea (20, 51). Nonetheless, the morphological changes and increased numbers of cochlear macrophages observed with age in the lateral wall and auditory nerve is in agreement with functional activation and structural changes of microglia in the central nervous system (52). Future work should address the age-related degenerative pathology occurring in the auditory nerve and the lateral wall focusing on factors which may initiate or exacerbate the potential cochlear inflammaging phenomenon.

DATA AVAILABILITY

All datasets generated for this study are included in the manuscript and/or the supplementary files.

AUTHOR CONTRIBUTIONS

KN, TL, BS, and HL contributed to the conception and design of the study. KN and TL performed the research. KN, HL, TL, BS, and LM analyzed the data. KN wrote the manuscript. All authors discussed the results and contributed to the final manuscript.

FUNDING

This work has been supported by National Institutes of Health Grants R01 DC012058 (HL), R56 DC012058 (HL), P50 DC00422 (HL), T32 DC014435 (KN), F31 DC017665 (KN), Glenn/AFAR scholarship (KN), and in part by the Cell & Molecular Imaging Shared Resource, Hollings Cancer Center, Medical University of South Carolina (P30 CA138313), the SC COBRE in Oxidants, Redox Balance, and Stress Signaling (P20 GM103542) and the Shared Instrumentation Grant (S10 OD018113). This investigation was conducted in a facility constructed with support from Research Facilities Improvement Program Grant No. C06 RR14516 from the NIH/NCRR.

ACKNOWLEDGMENTS

We thank Juhong Zhu, Gang Li, and Linda McCarson for their excellent technical assistance.

REFERENCES

1. Lin FR, Niparko JK, Ferrucci L. Hearing loss prevalence in the United States. *Arch Intern Med*. (2011) 171:1851–2. doi: 10.1001/archinternmed.2011.506
2. Dubno JR. Speech recognition across the lifespan: Longitudinal changes from middle age to older adults. *Am J Audiol*. (2015) 24:84–7. doi: 10.1044/2015_AJA-14-0052
3. Patel R, McKinnon BJ. Hearing loss in the elderly. *Clin Geriatr Med*. (2018) 34:163–74. doi: 10.1016/j.cger.2018.01.001
4. Bas E, Goncalves S, Adams M, Dinh CT, Bas JM, Van De Water TR, et al. Spiral ganglion cells and macrophages initiate neuro-inflammation and scarring following cochlear implantation. *Front Cell Neurosci*. (2015) 9:303. doi: 10.3389/fncel.2015.00303
5. Latta CH, Brothers HM, Wilcock DM. Neuroinflammation in Alzheimer's disease; A source of heterogeneity and target for personalized therapy. *Neuroscience*. (2015) 302:103–11. doi: 10.1016/j.neuroscience.2014.09.061
6. Park I, Kassiteridi C, Monaco C. Functional diversity of macrophages in vascular biology and disease. *Vascul Pharmacol*. (2017) 99:13–22. doi: 10.1016/j.vph.2017.10.005
7. Friedland DR, Cederberg C, Tarima S. Audiometric pattern as a predictor of cardiovascular status: development of a model for assessment of risk. *Laryngoscope*. (2009) 119:473–86. doi: 10.1002/lary.20130
8. Ball RY, Stowers EC, Burton JH, Cary NR, Skepper JN, Mitchinson MJ. Evidence that the death of macrophage foam cells contributes to the lipid core of atheroma. *Atherosclerosis*. (1995) 114:45–54. doi: 10.1016/0021-9150(94)05463-S
9. Loughrey DG, Kelly ME, Kelley GA, Brennan S, Lawlor BA. Association of age-related hearing loss with cognitive function, cognitive impairment, and dementia: a systematic review and meta-analysis. *JAMA Otolaryngol Head Neck Surg*. (2018) 144:115–26. doi: 10.1001/jamaoto.2017.2513
10. Frackowiak J, Wisniewski HM, Wegiel J, Merz GS, Iqbal K, Wang KC. Ultrastructure of the microglia that phagocytose amyloid and the microglia that produce beta-amyloid fibrils. *Acta Neuropathol*. (1992) 84:225–33. doi: 10.1007/BF00227813
11. Daria A, Colombo A, Llovera G, Hampel H, Willem M, Liesz A, et al. Young microglia restore amyloid plaque clearance of aged microglia. *EMBO J*. (2017) 36:583–603. doi: 10.15252/embj.201694591
12. Bredberg G, Lindeman HH, Ades HW, West R, Engström H. Scanning electron microscopy of the organ of Corti. *Science*. (1970) 170:861–3. doi: 10.1126/science.170.3960.861
13. Johnsson LG, Hawkins JE Jr. Sensory and neural degeneration with aging, as seen in microdissections of the human inner ear. *Ann Otol Rhinol Laryngol*. (1972) 81:179–93. doi: 10.1177/000348947208100203
14. Kusunoki T, Cureoglu S, Schachern PA, Baba K, Kariya S, Paparella MM. Age-related histopathologic changes in the human cochlea: a temporal bone study. *Otolaryngol. Head Neck Surg*. (2004) 131:897–903. doi: 10.1016/j.otohns.2004.05.022
15. Kidd AR III, Bao J. Recent advances in the study of age-related hearing loss: a mini-review. *Gerontology*. (2012) 58:490–6. doi: 10.1159/000338588
16. Makary CA, Shin J, Kujawa SG, Liberman MC, Merchant SN. Age-related primary cochlear neuronal degeneration in human temporal bones. *J Assoc Res Otolaryngol*. (2011) 12:711–7. doi: 10.1007/s10162-011-0283-2
17. Hirose K, Rutherford MA, Warchol ME. Two cell populations participate in clearance of damaged hair cells from the sensory epithelia of the inner ear. *Hear Res*. (2017) 352:70–81. doi: 10.1016/j.heares.2017.04.006
18. Liu W, Molnar M, Garnham C, Benav H, Rask-Andersen H. Macrophages in the human cochlea: saviors or predators-a study using super-resolution immunohistochemistry. *Front Immunol*. (2018) 9:223. doi: 10.3389/fimmu.2018.00223
19. O'Malley JT, Nadol JB Jr, McKenna MJ. Anti CD163+, Iba1+, and CD68+ cells in the adult human inner ear: normal distribution of an unappreciated class of macrophages/microglia and implications for inflammatory otopathology in humans. *Otol Neurotol*. (2016) 37:99–108. doi: 10.1097/MAO.0000000000000879
20. Liu W, Rask-Andersen H. Super-resolution immunohistochemistry study on CD4 and CD8 cells and the relation to macrophages in human cochlea. *J Otol*. (2019) 14:1–5. doi: 10.1016/j.joto.2018.11.010
21. Shigemoto-Mogami Y, Hoshikawa K, Sato K. Activated microglia disrupt the blood-brain barrier and induce chemokines and cytokines in a rat *in vitro* model. *Front Cell Neurosci*. (2018) 12:494. doi: 10.3389/fncel.2018.00494
22. Liddelow SA, Guttenplan KA, Clarke LE, Bennett FC, Bohlen CJ, Schirmer L, et al. Neurotoxic reactive astrocytes are induced by activated microglia. *Nature*. (2017) 541:481–7. doi: 10.1038/nature21029
23. Schuknecht H. Temporal bone removal at autopsy. Preparation and uses. *Arch Otolaryngol*. (1968) 87:129–37. doi: 10.1001/archotol.1968.00760060131007
24. Xing Y, Samuvel DJ, Stevens SM, Dubno JR, Schulte BA, Lang H. Age-related changes of myelin basic protein in mouse and human auditory nerve. *PLoS ONE*. (2012) 7:e34500. doi: 10.1371/journal.pone.0034500
25. Hao X, Xing Y, Moore MW, Zhang J, Han D, Schulte BA, et al. Sox10 expressing cells in the lateral wall of the aged mouse and human cochlea. *PLoS ONE*. (2014) 9:e97389. doi: 10.1371/journal.pone.0097389
26. Cunningham CD III, Weber PC, Spicer SS, Schulte BA. Canalicular reticulum in vestibular hair cells. *Hear Res*. (2000) 143:69–83. doi: 10.1016/S0378-5955(00)00022-8
27. Weber PC, Cunningham CD III, Schulte BA. Potassium recycling pathways in the human cochlea. *Laryngoscope*. (2001) 111:1156–65. doi: 10.1097/00005537-200107000-00006
28. Viana LM, O'Malley JT, Burgess BJ, Jones DD, Oliveira CA, Santos F, et al. Cochlear neuropathy in human presbycusis: confocal analysis of hidden hearing loss in post-mortem tissue. *Hear Res*. (2015) 327:78–88. doi: 10.1016/j.heares.2015.04.014
29. Brown LN, Xing Y, Noble KV, Barth JL, Panganiban CH, Smythe NM, et al. Macrophage-mediated glial cell elimination in the postnatal mouse cochlea. *Front Mol Neurosci*. (2017) 10:407. doi: 10.3389/fnmol.2017.00407
30. Liu T, Li G, Noble KV, Li Y, Barth JL, Schulte BA, et al. Age-dependent alterations of Kir4.1 expression in neural crest-derived cells of the mouse and human cochlea. *Neurobiol Aging*. (2019) 80:210–22. doi: 10.1016/j.neurobiolaging.2019.04.009
31. Van den Heuvel MM, Tensen CP, van As JH, Van den Berg TK, Fluitsma DM, Dijkstra CD, et al. Regulation of CD 163 on human macrophages: cross-linking of CD163 induces signaling and activation. *J Leukoc Biol*. (1999) 66:858–66. doi: 10.1002/jlb.66.5.858
32. Van Gorp H, Delputte PL, Nauwynck HJ. Scavenger receptor CD163, a Jack-of-all-trades and potential target for cell-directed therapy. *Mol Immunol*. (2010) 47:1650–60. doi: 10.1016/j.molimm.2010.02.008

33. Stence N, Waite M, Dailey ME. Dynamics of microglial activation: a confocal time-lapse analysis in hippocampal slices. *Glia*. (2001) 33:256–66. doi: 10.1002/1098-1136(200103)33:3<256::AID-GLIA1024>3.3.CO;2-A
34. Zhang W, Dai M, Fridberger A, Hassan A, Degagne J, Neng L, et al. Perivascular-resident macrophage-like melanocytes in the inner ear are essential for the integrity of the intrastrial fluid-blood barrier. *Proc Natl Acad Sci USA*. (2012) 109:10388–93. doi: 10.1073/pnas.1205210109
35. Shi X. Resident macrophages in the cochlear blood-labyrinth barrier and their renewal via migration of bone-marrow-derived cells. *Cell Tissue Res.* (2010) 342:21–30. doi: 10.1007/s00441-010-1040-2
36. Leone C, Le Pavec G, Même W, Porcheray F, Samah B, Dormont D, et al. Characterization of human monocyte-derived microglia-like cells. *Glia*. (2006) 54:183–92. doi: 10.1002/glia.20372
37. Szepesi Z, Manouchehrian O, Bachiller S, Deierborg T. Bidirectional microglia-neuron communication in health and disease. *Front Cell Neurosci.* (2018) 12:323. doi: 10.3389/fncel.2018.00323
38. Spicer SS, Schulte BA. Differentiation of inner ear fibrocytes according to their ion transport related activity. *Hear Res.* (1991) 56:53–64. doi: 10.1016/0378-5955(91)90153-Z
39. Spicer SS, Schulte BA. Spiral ligament pathology in quiet-aged gerbils. *Hear Res.* (2002) 172:172–85. doi: 10.1016/S0378-5955(02)00581-6
40. Spicer SS, Gratton MA, Schulte BA. Expression patterns of ion transport enzymes in spiral ligament fibrocytes change in relation to strial atrophy in the aged gerbil cochlea. *Hear Res.* (1997) 111:93–102. doi: 10.1016/S0378-5955(97)00097-X
41. Hirose K, Li SZ. The role of monocytes and macrophages in the dynamic permeability of the blood-perilymph barrier. *Hear Res.* (2019) 374:49–57. doi: 10.1016/j.heares.2019.01.006
42. Raivich G, Bohatschek M, Kloss CU, Werner A, Jones LL, Kreutzberg GW. Neuroglial activation repertoire in the injured brain: graded response, molecular mechanisms and cues to physiological function. *Brain Res Rev.* (1999) 30:77–105. doi: 10.1016/S0165-0173(99)00007-7
43. Ichimiya I, Yoshida K, Hirano T, Suzuki M, Mogi G. Significance of spiral ligament fibrocytes with cochlear inflammation. *Int J Pediatr Otorhinolaryngol.* (2000) 56:45–51. doi: 10.1016/S0165-5876(00)00408-0
44. Wu PZ, Liberman LD, Bennett K, de Gruttola V, O'Malley JT, Liberman MC. (2019). Primary neural degeneration in the human cochlea: evidence for hidden hearing loss in the aging ear. *Neuroscience*. 407:8–20. doi: 10.1016/j.neuroscience.2018.07.053
45. Jiang H, Wang X, Zhang J, Kachelmeier A, Lopez IA, Shi X. Microvascular networks in the area of the auditory peripheral nervous system. *Hear Res.* (2019) 371:105–16. doi: 10.1016/j.heares.2018.11.012
46. Bruunsgaard H, Andersen-Ranberg K, Jeune B, Pedersen AN, Skinhøj P, Pedersen BK. A high plasma concentration of TNF-alpha is associated with dementia in centenarians. *J Gerontol A Biol Sci Med Sci.* (1999) 54:M357–64. doi: 10.1093/gerona/54.7.M357
47. Fagiolo U, Cossarizza A, Scala E, Fanales-Belasio E, Ortolani C, Cozzi E, et al. Increased cytokine production in mononuclear cells of healthy elderly people. *Eur J Immunol.* (1993) 23:2375–8. doi: 10.1002/eji.1830230950
48. Mari D, Mannucci PM, Coppola R, Bottasso B, Bauer KA, Rosenberg RD. Hypercoagulability in centenarians: the paradox of successful aging. *Blood.* (1995) 85:3144–9.
49. Ferrucci L, Harris TB, Guralnik JM, Tracy RP, Corti MC, Cohen HJ, et al. Serum IL-6 level and the development of disability in older persons. *J Am Geriatr Soc.* (1999) 47:639–46. doi: 10.1111/j.1532-5415.1999.tb01583.x
50. Kawamata T, Akiyama H, Yamada T, McGeer PL. Immunologic reactions in amyotrophic lateral sclerosis brain and spinal cord tissue. *Am J Pathol.* (1992) 140:691–707.
51. Kämpfe Nordström C, Danckwardt-Lilliestöm N, Laurell G, Liu W, Rask-Andersen H. The human endolymphatic sac and inner ear immunity: macrophage interaction and molecular expression. *Front Immunol.* (2018) 9:3181. doi: 10.3389/fimmu.2018.03181
52. Davis EJ, Foster TD, Thomas WE. Cellular forms and functions of brain microglia. *Brain Res Bull.* (1994) 34:73–8. doi: 10.1016/0361-9230(94)90189-9

Conflict of Interest Statement: The authors declare that the research was conducted in the absence of any commercial or financial relationships that could be construed as a potential conflict of interest.

frontiers in Neurology

ORIGINAL RESEARCH
published: 06 September 2019
doi: 10.3389/fneur.2019.00948

Subcellular Abnormalities of Vestibular Nerve Morphology in Patients With Intractable Meniere's Disease

Pengjun Wang[1†], Huaming Zhu[1†], Wen Lu[1†], Qiang Song[1], Zhengnong Chen[1], Yaqin Wu[1], Hui Wang[1], Dongzhen Yu[1], Haibo Ye[1*], Haibo Shi[1,2*] and Shankai Yin[1,2]*

[1] Department of Otorhinolaryngology—Head and Neck Surgery, The Sixth People's Hospital affiliated to Shanghai Jiaotong University, Shanghai, China, [2] Shanghai Key Laboratory of Sleep Disordered Breathing, Shanghai, China

OPEN ACCESS

Edited by:
Jose Antonio Lopez-Escamez, Andalusian Autonomous Government of Genomics and Oncological Research (GENYO), Spain

Reviewed by:
Tadashi Kitahara, Nara Medical University, Japan
Ivan A. Lopez, University of California, Los Angeles, United States

***Correspondence:**
Dongzhen Yu
drdzyu@126.com
Haibo Ye
yehaibo_2012@163.com
Haibo Shi
hbshi@sjtu.edu.cn

[†]These authors have contributed equally to this work

Specialty section:
This article was submitted to Neuro-Otology, a section of the journal Frontiers in Neurology

Received: 10 April 2019
Accepted: 16 August 2019
Published: 06 September 2019

Citation:
Wang P, Zhu H, Lu W, Song Q, Chen Z, Wu Y, Wang H, Yu D, Ye H, Shi H and Yin S (2019) Subcellular Abnormalities of Vestibular Nerve Morphology in Patients With Intractable Meniere's Disease. Front. Neurol. 10:948. doi: 10.3389/fneur.2019.00948

Objective: Few studies so far have focused on the retrocochlear lesions in Meniere's disease (MD). This study aims to investigate pathological alterations in the central portion of the vestibular nerve (VN) in patients with intractable Meniere's disease (MD) and to explore retrocochlear lesions and their relationship with disease severity.

Methods: Eight MD patients with refractory vertigo received vestibular neurectomy via a retrosigmoid or translabyrinthine approach. Segments of VN were carefully removed and immediately fixed for histopathological examination. Five VN specimens were examined by light microscopy after hematoxylin/eosin staining; three specimens were extensively analyzed using transmission electron microscopy, to identify VN ultrastructural lesions. Correlations between lesions and patient clinical characteristics were examined.

Results: Histopathological examination revealed evidence of various types of chronic VN impairment, including the formation of corpora amylacea (CA), axon atrophy, and severe damage to the myelin sheath. Electron microscopy revealed membranous whorls within dilated Schmidt–Lanterman incisures, the formation of myeloid bodies, dysmyelination, and demyelination. Unexpectedly, we observed a positive correlation between the density of CA in VN tissue and the duration of disease, as well as the degree of hearing impairment, independent of age.

Conclusion: Our findings indicate that deformation of subcellular organelles in the central portion of the VN is one of the key pathological indicators for the progressive severity and intractability of vertigo and support a vestibular nerve degeneration.

Keywords: neurectomy, vestibular neuropathy, vertigo, Meniere's disease, ultrastructural deformation

INTRODUCTION

Meniere's disease (MD), first reported by Meniere (1), is a complex, multifactorial inner ear disease characterized by recurrent vertigo attacks, fluctuating, and progressive sensorineural hearing loss, tinnitus, and aural fullness in the affected ear. Given the heterogeneity of MD, its etiology and pathogenesis are complex. Proposed causes include endolymphatic hydrops, viral infection, genetic predisposition, and autoimmune involvement of the endolymphatic sac (2–5). However,

despite extensive research, the cause of MD, as well as its relationship to these etiological factors, remains unresolved.

Both hearing loss and vertigo are major symptoms of MD, indicating that lesions involve cochlear and vestibular components of the inner ear. Bixenstine et al. discovered spiral ganglion degeneration after surgery-induced endolymphatic hydrops in a guinea pig model showing larger damage in the apical that in the basal neurons (6). In addition, previous electron microscopic studies had systematically revealed the histopathology of the vestibular sensory epithelia in MD. Early studies predominantly focused on utricular maculae and confirmed degenerative alterations in the utricular sensory epithelium (7, 8). Later studies further investigated the semicircular canal cristae ampullares and otolithic organs from subjects with intractable MD. McCall et al. demonstrated varied degrees of neuroepithelial degeneration with severe pathological changes of the semicircular canal cristae ampullares and saccular maculae including monolayer epithelialization, basement membrane thickening, cellular vacuolization, stereocilia loss of hair cells, and increased stromal spaces (9). However, these studies have focused primarily on local lesions of the vestibular periphery, without considering impairment of the central portion of the vestibular nerve (VN).

Anatomical and physiological studies, however, have led to a fundamental understanding of the functional circuit of vestibular pathways. The structural integrity of VN is essential for vestibular sensory processing, particularly the conduction and projection of sensory input signals. Axons of the VN receive input from sensory receptors of the cristae ampullae and maculae, and project to the four ipsilateral vestibular nuclei. Of note, sensory information from the periphery must pass through the ganglion cells before reaching the central nervous nuclei (10). In rodent nociceptive neurons, the dorsal root ganglion acts as an electrical obstacle to spike propagation (11, 12). Rattay et al. demonstrated that spike conduction was delayed considerably in the soma regions of human type I spiral ganglions (13). Like the dorsal root and spiral ganglia, Scarpa's ganglion is a potential impediment that acts as a filter for action potential propagation. Peripheral sensory signals are modulated by Scarpa's ganglion and altered when reaching the central portion of the VN, which conducts the downstream sensory information toward the vestibular nuclei. The fidelity of post-ganglion action potential propagation between Scarpa's ganglion and the central processes relies on the integral structure and normal function of the central axon of the VN. Therefore, the central portion of the VN axon plays a key role in conveying the electrical information to the vestibular nuclei. Moreover, animal experiments have confirmed that vestibular neurectomy can compromise sensory inputs arising from the vestibular sensory end organs, resulting in vestibular symptoms including head tilt, asymmetry of muscular tone, and rotation of the body (14). Clinical evidence has also established that VN lesions, such as vestibular neuritis and vestibular schwannoma, lead to vertigo (15, 16). Therefore, investigating histopathological changes in the central portion of the VN in MD patients may provide significant insights into the cause and pathophysiology of the disease.

Unfortunately, little information on patients with MD is available from the few studies carried out to investigate pathological changes in the VN. Spencer et al. reported that VN axons exhibited extensive demyelination, indicating degenerative change, in patients with unilateral MD (17). However, Kitamura et al. found no morphological degeneration in VN surgical specimens from three MD patients (18). Such contradictory findings among the limited amount of research available mean that the issue of whether or not there are VN lesions in MD patients remains controversial. The clinical significance of identifying morphological lesions in the VN during MD relates to the implications for the therapeutic management of disease progression. In the present study, we discovered the presence of pathological changes in the central portion of the VN segments, and found that they were highly correlated with disease severity and found that they were highly correlated with disease severity.

MATERIALS AND METHODS

Patients

This study enrolled eight patients admitted to the Department of Otorhinolaryngology–Head and Neck Surgery who provided signed informed consent. In all patients, the diagnosis of MD was confirmed according to the 2015 criteria of the Classification Committee of the Bárány Society (19). The following data are shown in **Table 1**: patient age, gender, lesion side, symptoms, and symptomatic duration, data from the auditory functional evaluation, and the surgical approach. Pure tone audiometry was performed before the vestibular neurectomy. Electrocochleography (ECochG), which is considered as a complementary diagnostic measure for MD, demonstrated an elevated summating potential/action potential (SP/AP) ratio ($\geq$0.4) in all patients but one (case 3), whose affected ear was not responsive to the examination. All patients had intractable MD after comprehensive and prolonged therapy. Intractable MD was defined as failure to respond to various forms of medical management including diuretics, beta-histamine, antihistamines, oral prednisone, and intratympanic dexamethasone for at least 6 months. None of the patients underwent intratympanic gentamicin injection to avoid impairing their residual hearing. Three patients (cases 5, 6, and 8) had refractory vertigo despite endolymphatic sac decompression and one of them (case 5) underwent neurectomy via a translabyrinthine approach because of severe hearing loss. A patient with vestibular schwannoma was included as a control. This study was conducted in accordance with the Declaration of Helsinki (20). The study protocol was approved by the hospital ethics committee (Approval No. YS-2018-101).

Audiometry

Hearing levels were measured using a pure tone audiometer (Grason-Stadler GSI 61, USA) in a soundproof room with background noise lower than 18 dB. The audiometric thresholds for air and bone conduction were recorded at frequencies of 0.25, 0.5, 1, 2, 4, 6, and 8 kHz. The pure-tone average (PTA) of 0.5, 1, 2, and 4 kHz was used to evaluate the hearing level of the affected ear.

TABLE 1 | Patient information and clinical characteristics.

Case	Gender	Age (yr)	Side	Period (yr)	VA6m	EFAV	tinnitus	PTA (dBHL)	SP/AP	ESD	SA
1	F	59	R	10	20+	Yes	Yes	45	0.40	No	RS
2	F	56	L	11	20+	Yes	Yes	62	1.00	No	RS
3	F	67	L	3	3	Yes	Yes	47	No response	No	RS
4	M	57	L	8	3	Yes	Yes	52	0.61	No	RS
5	M	48	R	20	2	Yes	Yes	85	0.58	Yes	RL
6	M	41	L	5	3	Yes	Yes	30	0.53	Yes	RS
7	M	58	L	3	20+	Yes	Yes	71	0.49	No	RS
8	M	48	R	15	20+	Yes	Yes	54	0.52	Yes	RS

VA6m, numbers of vertigo attacks in 6 months; EFAV, ear fullness associated with vertigo attacks; PTA, pure-tone average; SP/AP, summating potential/action potential ratio; ESD, endolymphatic sac decompression; SA, surgery approach; RS, retrosigmoid approach; RL, translabyrinthine approach.

ECochG Recording

Electrocochleography (ECochG) was recorded using the evoked potential system (Neuropack M1 MEB-9200, Nihon Kohden, Japan). The tympanic membrane (TM) was identified at endoscopy and the electrode was placed on the posteroinferior quadrant of the TM. Reference and ground electrodes were placed on the ipsilateral earlobe and forehead, respectively. Stimuli consisting of alternating polarity clicks were delivered at 90 dB HL at a rate of 11.3/s. Then, 1,000 stimulus repetitions per recording were averaged over a 10-ms post-stimulus time frame. The SP amplitude was calculated from between pre-stimulation baseline and the first trough, while the AP amplitude was calculated from the onset of the SP deflection to its first negative peak. The SP/AP amplitude ratio was computed for the affected ear of each patient.

Vestibular Neurectomy

Surgery was performed on seven patients under the operating microscope via a retrosigmoid approach. After exposing the cerebellopontine angle, cranial nerve VIII was clearly identified. A fine vessel along the nerve denotes the cochleovestibular cleavage, which demarcates the vestibular and cochlear components (**Figure 1A**). The two components were bluntly separated from the cochleovestibular cleavage using a micro-dissector (**Figure 1B**). The central portion of VN was severed with micro-scissors, and an approximately 4-mm segment was carefully removed. Case 5 underwent a neurectomy via a translabyrinthine approach. With the mastoid cortex fully exposed, the semi-circular canals were removed. Then, the internal auditory canal was opened and the VN axons were identified and removed carefully. Special care was taken to protect the VN tissue from instrument trauma, compression, and desiccation intraoperatively. Specimens were immediately placed in fixative solutions. Specimens that obtained from healthy VN tissues adjacent to tumors and vestibular schwannoma were used as control.

Light Microscopic Examination

The VN specimens from five patients were immersed in 4% paraformaldehyde (diluted in sodium phosphate buffer, pH 7.4) and fixed for 12 h at 4°C. Tissues were embedded in paraffin blocks, and 4 μm cross-sections were obtained using a microtome (CV 5030; Leica, Germany). Sections were stained with hematoxylin/eosin (HE), observed under light microscopy (AZ100; Nikon, Japan), and imaged using NIS-Elements D software (Nikon). The corpora amylacea (CA) were identified based on their morphological features by two pathologists with more than 20 years of experience. The CA were counted manually using ImageJ (ver. 1.80) and 10∼12 high-magnification fields (×400) were analyzed per section. The same procedure was performed in examination of the healthy VN specimen and vestibular schwannoma.

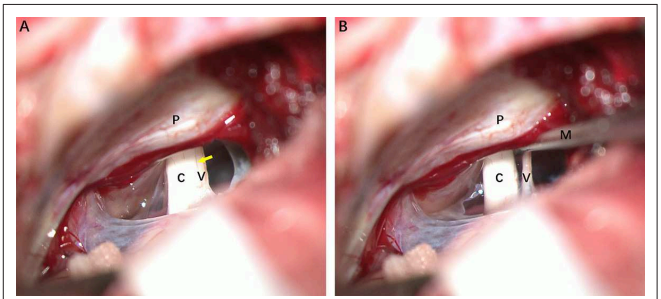

FIGURE 1 | Intraoperative photographs of a patient with left-sided Meniere's disease (MD), retrosigmoid approach. **(A)** Exposure of cranial nerve VIII. The fine vessel indicating the cochleovestibular cleavage (yellow arrow) is visible. **(B)** Separating cochlear and vestibular nerves with a micro dissector. C, cochlear nerve; V, vestibular nerve; M, micro dissector; P, petrous ridge of temporal bone.

Transmission Electron Microscopic Examination

Segments of VN obtained from three MD patients were fixed in phosphate-buffered 2% glutaraldehyde solution for 12 h at 4°C. Specimens were then post-fixed in 1% osmium tetroxide for 3 h, washed with phosphate buffer solution, dehydrated in increasing concentrations of ethanol, immersed in 100% propylene oxide, and embedded in EPON resin blocks (Shell Chemical, USA). Ultrathin sections (70 nm) were made from the blocks using a diamond knife on an ultramicrotome (EM UC7; Leica) and stained with uranyl acetate and lead citrate. Transverse tissue sections were viewed and imaged using a transmission electron

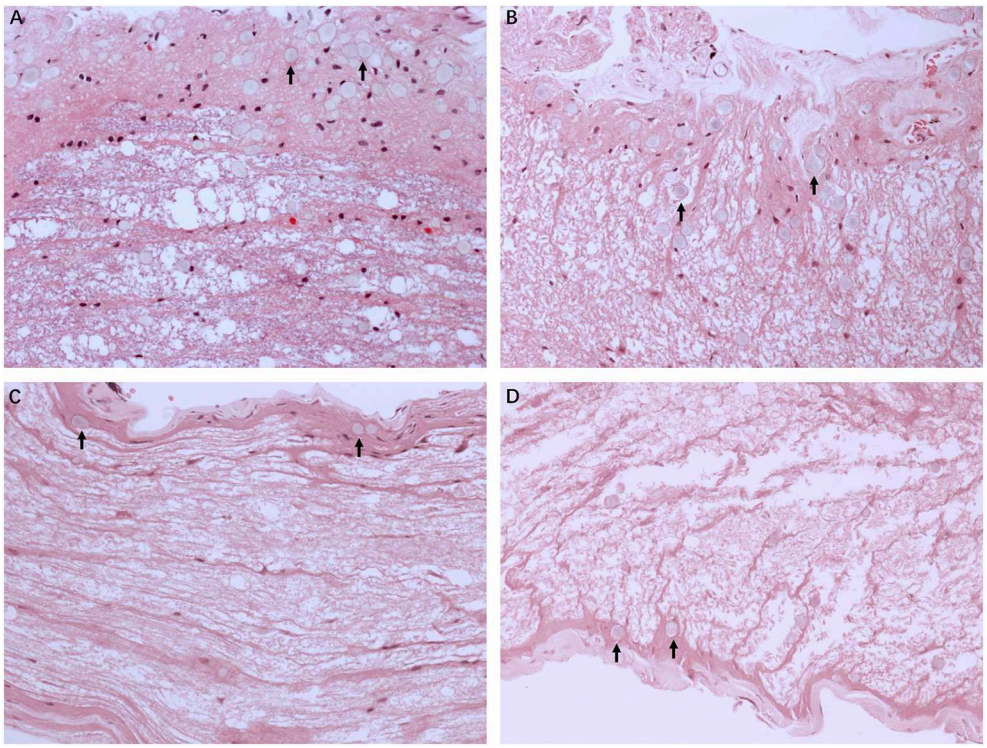

FIGURE 2 | Light microscopy images (×200) illustrating histological alteration in vestibular nerve (VN) tissues from various patients with intractable MD. **(A)** Case 5. Presence of numerous corpora amylacea (CA), a gray secretion-like structure (arrow). Edema of the nerve fibers and loose neuropil with vacuolar disintegration were present in the VN tissue. **(B)** Case 2. Edematous nerve fibers with numerous CA (arrow). **(C)** Case 3. Atrophic nerve fibers with sporadic CA (arrow). **(D)** Case 4. Mucous degenerative VN fibers, presenting a spongy appearance. Sporadic CA are visible (arrow).

microscope at 80 kV accelerating voltage (Tecnai G2 Spirit; FEI, USA) equipped with a digital camera (Gatan, USA).

Statistical Analysis

SPSS for Windows (ver. 22.0; IBM, USA) was used for the data analysis. Pearson's correlation and linear regression were utilized to examine relationships between the degree of pathological change and the age of MD patients, disease duration, and hearing level.

RESULTS

Morphological Changes in MD Affected Nerve Fibers

Figure 2 illustrates the gross light microscopic changes observed in sections of VN from patients with intractable MD. Decreased density and disorderly arrangement of nerve fibers was apparent on HE staining (**Figures 2A–D**). VN samples from all patients examined by light microscopy showed varying degrees of nerve fiber edema. The neuropil, i.e., the reticular structure comprised of axons, glial cell processes, and microvasculature, was loosely arranged and showed vacuolar disintegration (**Figure 2A**). Atrophy and mucous degeneration were observed in the affected VN fibers, which showed a spongy appearance (**Figure 2D**). A characteristic feature of the VN lesions was the presence of CA, which were typically seen in all sections as round or oval bodies ranging from 3.5 to 17 μm in diameter (**Figures 3A–D**). A low CA density was observed in the VN tissue from a patient with MD for 3 years (**Figure 3A**). Higher-magnification images showed that CA exhibited a concentric laminated appearance, with the center staining more deeply than the periphery (**Figure 3B**). The VN section obtained from a patient with a 20-year history of MD showed densely distributed CA (**Figure 3C**). Sporadically, fusion of two CA was observed in VN sections (**Figure 3D**). Noting that the density of CA varied among sections from different patients, CA were counted in every high-magnification field (×400). The distribution of CA density in the VN segments of patients is illustrated in **Figure 4A**. An inverse correlation was observed between density of CA and age ($r = -0.6955$; $p < 0.001$) (**Figure 4B**). However, we demonstrated that the density of CA was highly correlated with the duration of MD ($r = 0.7175$; $p < 0.0001$) (**Figure 4C**). Furthermore, the density of CA and PTA in the subjects was also found to be correlated ($r = 0.8509$; $p < 0.001$) (**Figure 4D**).

Morphological Features in Healthy Nerve Fibers and Vestibular Schwannoma

We analyzed the sections obtained from healthy VN tissue adjacent to tumors and vestibular schwannoma in order to determine whether the CA would be found in non-MD

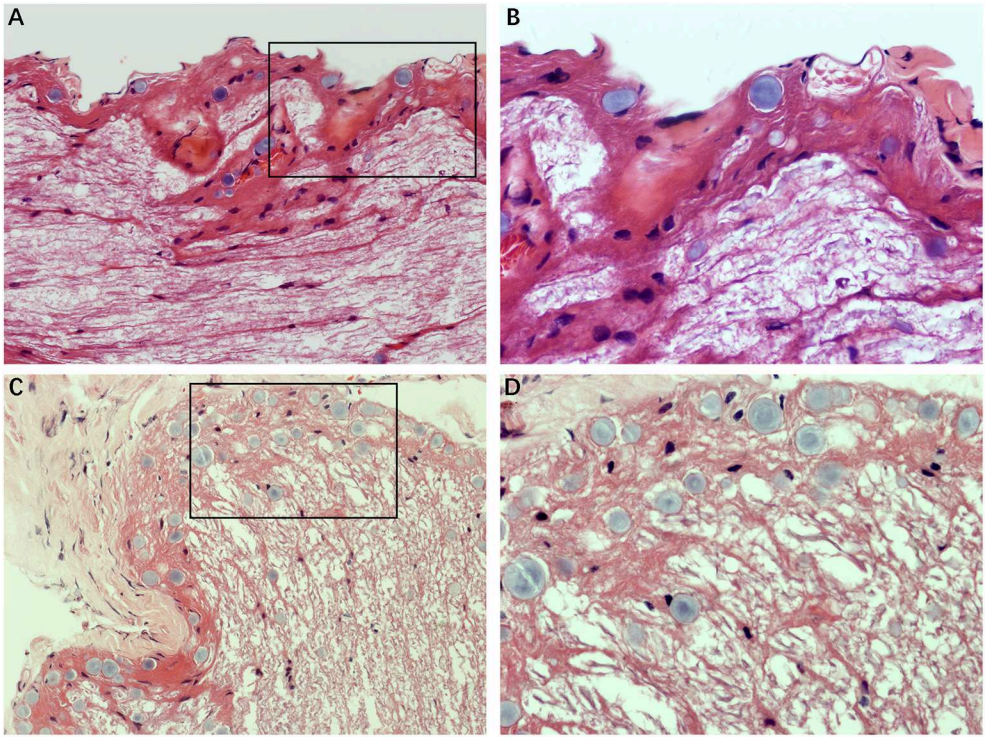

FIGURE 3 | The formation of CA. Images of VN sections from two patients with different durations of MD. **(A)** The distribution of CA scattering in the VN tissue from a patient with MD for 3 years (Case 3, ×200). **(B)** Higher magnification image (×400, framed in **A**) clearly showing the appearance of the lesion. **(C)** VN section from a patient with a longer history of MD (20 years) showing the presence of numerous CA (Case 2, ×200). **(D)** Higher magnification image (×400, framed in **C**) showing the pathological concentric laminated structure, with the center stained more deeply than the periphery.

conditions. Normal nerve fiber structures were clearly observed in healthy VN specimens, showing no appearance of edema, atrophy and spongy appearance. No evidence of CA was found in the healthy VN fibers (**Figure 5A**). Tissues form vestibular schwannoma showed the tumor and nerve fibers were encompassed by a connective tissue layer which was obviously thicker than normal outer thin connective tissue layer. The tumor cells were observed in fusiform shape, lacking of CA (**Figure 5B**). These results from control tissues provided direct evidence to ascertain that changes we observed in MD affected VN fiber deformation are of pathological origin.

Ultrastructural Lesions of Nuclei and Other Organelles

Detailed examination of transverse sections of VN tissue obtained from three patients with intractable MD was achieved using transmission electron microscopy. In all cases, micrographs providing representative views of the ultrastructural features of VN lesions were carefully chosen. Various pathological alterations indicating VN impairments were noted. Although the myelin sheaths of small axons had a normal appearance, ultrastructural changes in Schwann cells were apparent. Chromatin condensation, decomposition, and karyolysis were observed within the same VN sections. Fragmented chromatin was dispersed toward the edges of nuclei (**Figure 6A**). These morphological indications of Schwann cell apoptosis showed active disintegration in the VN of patients with intractable MD. Moreover, Schwann cell mitochondria in the VN fibers exhibited an altered vesicular appearance, with matrix distension. The deposition of lipofuscin, characterized by electron-dense bodies of varying shapes, was also noted in Schwann cells (**Figure 6B**). We found marked accumulation of lipofuscin in the central axons of VN fibers, with significant vesicular disintegration of axons devoid of axoplasm (**Figure 6C**). We also found evidence of lysosome-rich microglia, which act as macrophages in neural tissue, engulfing and scavenging apoptotic cell debris (**Figure 6D**).

Ultrastructural Alterations of Myelin Sheath

Fine structural alterations of myelin sheath were examined in ultrathin VN sections from three patients with intractable MD by transmission electron microscopy. The most extensive change noted was dysmyelination, with lamellar splitting and the formation of abnormal myelin. Delamination of myelin sheath, with the appearance of widened and disorderly myelin lamellae, was ubiquitous in the VN tissue. Axonal impairments were also observed to accompany dysmyelination or delamination (**Figure 7A**). The formation of myelin bodies due to myelin degradation was observed inside the myelin loop of Schwann cells. Axoplasm of fibers within the myelin

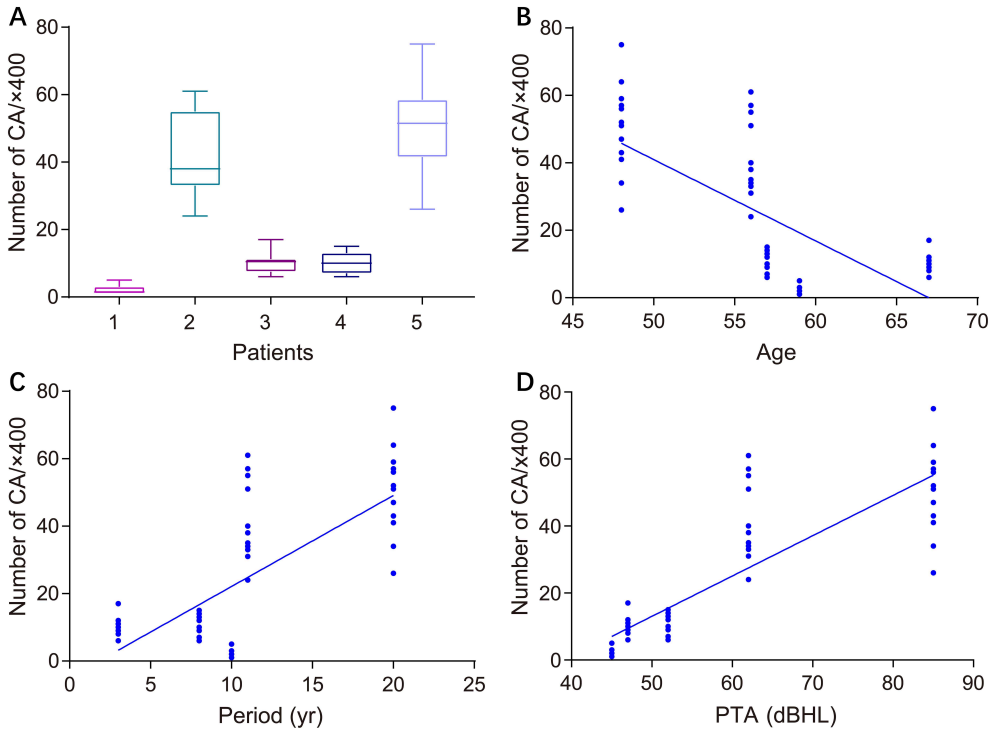

FIGURE 4 | Correlation between the density of CA in VN sections and clinical characteristics of patients with intractable MD. **(A)** Density of CA in all high-magnification fields (×400) for each patient. **(B)** Correlation of CA density with subject age (Pearson's correlation coefficient, $r = -0.6955$; $p < 0.001$). **(C)** Correlation of CA density with duration of MD (Pearson's correlation coefficient, $r = 0.7175$; $p < 0.0001$). **(D)** Correlation of CA density with subject hearing impairment category (HIC) (Spearman's rank correlation coefficient, $r = 0.5437$; $p < 0.0001$).

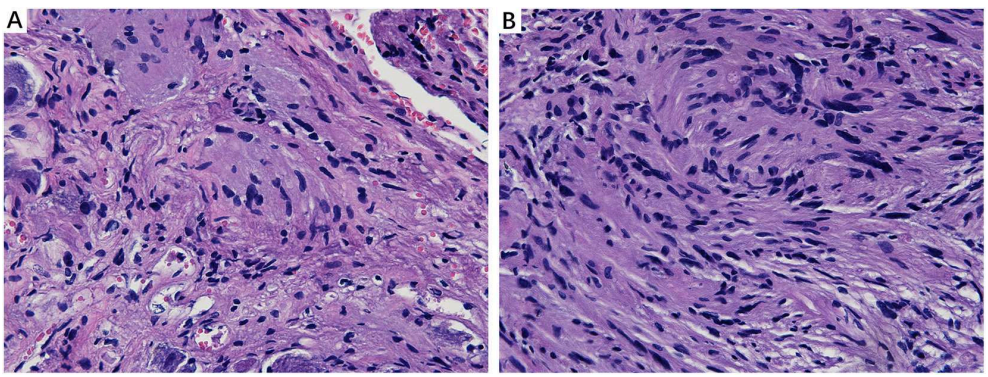

FIGURE 5 | Histological characteristics of nerve fibers in control tissues. **(A)** Healthy VN specimen showing clear nerve fiber structures with round or oval cells. No CA were found in the healthy never fibers (×400). **(B)** Tissue from a vestibular schwannoma showing the tumor and nerve fibers were surrounded by a thick connective tissue layer. The tumor cells were in fusiform shape, lacking of CA (×400).

loop appeared to have collapsed into several parts (**Figure 7B**). The most common pathological feature was morphological alterations to Schmidt–Lanterman incisures (SLI), which are cytoplasmic pockets that exist within compact myelin and connect the inner cell cytoplasm with the outer surface of the myelin sheath. SLI of the affected VN fibers exhibited membranous whorls, the size and electron density of which varied considerably. Projection of a focally distended SLI with an electron-dense substance was noted in the outer layer of the myelin sheath. Membrane whorls with volute-arranged and concentric lamellar-like structures occurred repeatedly within the myelin sheaths of Schwann cells (**Figure 7C**). SLI dilation with coarse granular components of medium electron density was detected inside the loose and degenerated myelin sheath. The axon appeared atrophic and without organelles (**Figure 7D**).

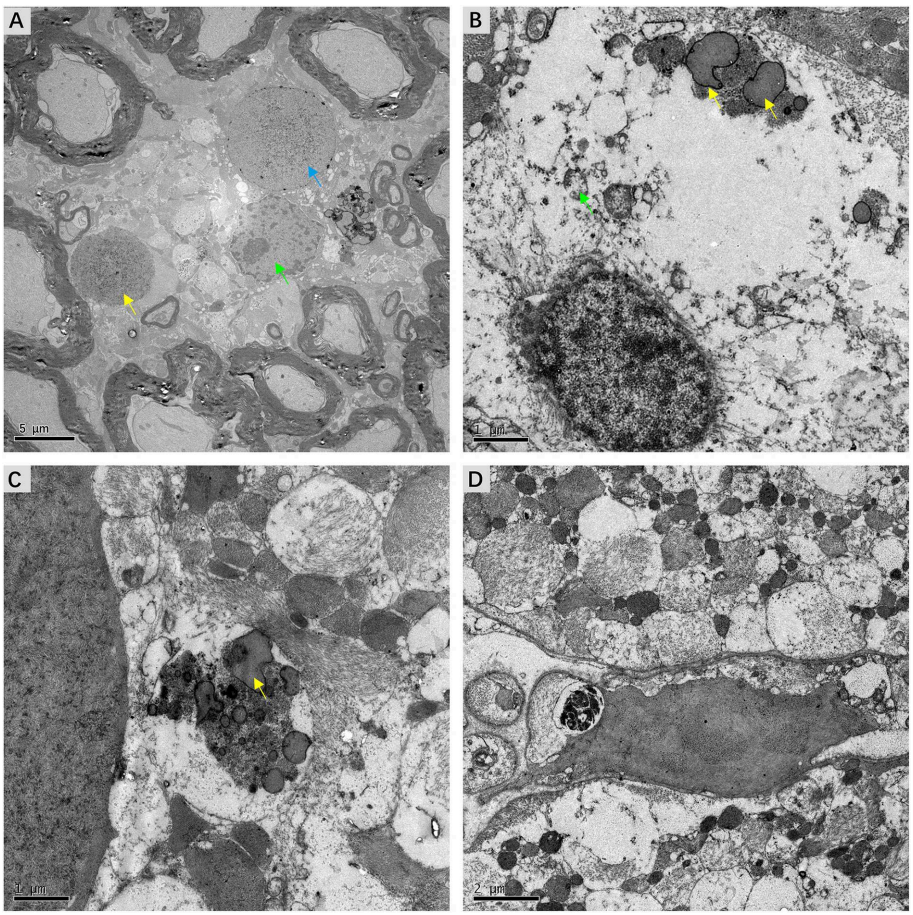

FIGURE 6 | Micrographs showing ultrastructural changes in affected VN tissues from patients with intractable MD. **(A)** Case 8. Degenerative processes in Schwann cells. The shrunken nucleus of a Schwann cell, with chromatin condensation (green arrow). Karyolysis with fragmented chromatin gathered toward the edge of the nucleus (blue arrow). The nucleus of an apoptotic Schwann cell with an electron-dense substance (yellow arrow). **(B)** Case 6. The deposition of lipofuscin within a Schwann cell (yellow arrow). Mitochondria with a swollen and vacuolar appearance (green arrow). **(C)** Same case, the axon of a nerve fiber undergoing significant vesicular disintegration, with apparent accumulation of lipofuscin (yellow arrow). **(D)** Case 7. A microglial cell engulfing fragmented cell debris. Scale bars: **(A)** = 2 µm, **(B,C)** = 1 µm, **(D)** = 2 µm.

DISCUSSION

Previous studies systematically investigated the vestibular sensory epithelia (7–9, 21, 22), which have been listed in **Table 2**. Pathological impairments within the central portion of the VN in refractory MD patients were demonstrated in this study. Morphological alterations were identified at several different subcellular sites in VN fibers, including nuclei and other organelles, and even axon components. The possibility that these morphological changes might result from fixation artifacts was excluded by the observation of apparently normal myelinated axons near abnormal ones (**Figure 6A**). Moreover, most of the microscopic alterations observed in this study appear to reflect chronic changes. Positive correlations between the presence of these lesions and the severity of MD were noted, which implies that therapeutic strategies aimed at neuroprotection could ameliorate the prognosis.

The current study confirmed that extensive CA, indicative of chronic impairment of peripheral nerves, is a microscopic feature of affected VN fibers in patients with intractable MD. Previous studies have assumed that CA are glycoproteinaceous structures that increase in the human brain during normal aging (23). However, new techniques have identified central nervous system CA in several neurodegenerative conditions, including Parkinson's disease, Huntington's disease, multiple sclerosis, temporal lobe epilepsy, and focal cortical dysplasia (24–27). The current investigation also found no positive correlation between the density of CA and aging, as VN sections from younger subjects also showed a higher level of CA. Although CA have even been considered as post-mortem artifacts, recent studies have confirmed that they contain complex components involved in waste elimination and neural protection (28, 29). Pisa et al. discovered that the external surface of CA contains fungal proteins in brain tissues from patients with Alzheimer's disease, amyotrophic lateral sclerosis, and Parkinson's disease, indicating

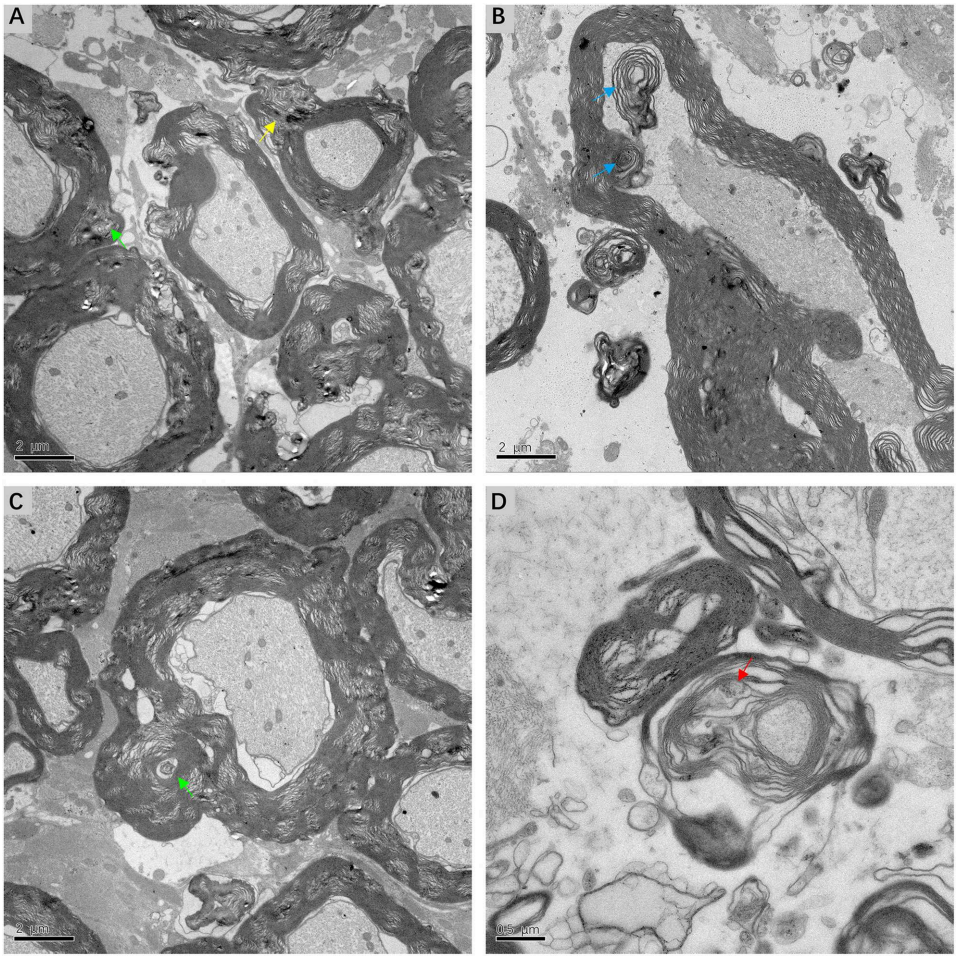

FIGURE 7 | Electron micrograph of myelin sheath, showing details of lesions in affected VN fibers in patients with intractable MD (**A,C,D** from case 8, **B** from case 7). **(A)** Extensive dysmyelination and delamination of myelin sheath showing clear degeneration of the involved VN fibers. Projection of focally distended Schmidt-Lanterman incisures (SLI) is seen within the myelin sheath (yellow arrow). **(B)** The formation of myelin bodies inside the myelin loop, indicating myelin degradation (blue arrow). Axoplasm of the fiber is collapsed into several parts. **(C)** Dilated SLI showing membranous whorls with a concentric lamellar-like structure (green arrow). These membranous whorls were frequently seen within widened SLI (**A**, green arrow). **(D)** Severe dilation of SLI with coarse granules of medium electron density (red arrow). The loose myelin sheath appears disintegrated. Scale bars: **(A–C)** = 2 μm, **(D)** = 0.5 μm.

that the formation of CA might associate with fungal infections (30). Stimulation with mold extracts triggered a significant release of TNF-α in MD patients who have higher basal levels of proinflammatory cytokines (31). These results suggested that fungal infection might be a potential etiology of MD, leading to accumulation of CA. The pathological changes noted in this study demonstrate that the formation of CA is highly correlated with the degree of central VN impairment, and that CA assist in the clean-up of abnormal materials, including cell debris or lipofuscin in VN fiber axons of advanced MD patients. This hypothesis is supported by our finding that CA level increased with disease duration.

This study also reveals the presence of myelin sheath deformation in the central portion of VN fibers at advanced stages of MD. Dysmyelination and delamination disintegrate the insulating myelin sheath, resulting in increased current leakage across the plasma membrane and deceleration or impedance of nerve conduction along internodes (32). The VN accepts sensory information regarding linear and angular acceleration, and projects to the brainstem vestibular nuclei and cerebellum (33). With a normal stimulus, the two sides of the peripheral vestibular system synergize with each other in a "pull-push" manner to maintain the balance of the body (34). Therefore, we speculate that lesions of the myelin sheath within the central VN axons affecting electrical conduction continuing on to the vestibular nuclei are likely to disturb the integrated processing of bilateral vestibular information, resulting in vertigo.

Unexpectedly, and unlike previous studies, we observed ultrastructural variations in SLI within the myelin sheath, including dilation and membranous whorls. SLI are thought to be pathways for transportation between Schwann cell bodies and axons, facilitating metabolism and maintaining the integrity of

TABLE 2 | Histopathological studies regarding the vestibular sensory epithelia in MD.

References	Utricular maculae	Saccular maculae	HSCC	SSCC	PSCC
Sanchez-Fernandez et al. (6)	Degenerative alterations	Not reported	Not reported	Not reported	Not reported
Rosenhall et al. (7)	Normal cytoarchitecture Cell cytoplasm vacuolation Cystic degeneration	Not reported	Not reported	Not reported	Not reported
Ylikoski et al. (21)	Sensory cell vacuolation Nuclear crescents No general degeneration	Not reported	Sensory cell vacuolation Nuclear crescents No general degeneration	Not reported	Not reported
Rizvi et al. (20)	Dilated utricle	Not shown	Ampullary distortion	Not reported	Not reported
McCall et al. (8)	Monolayer degeneration (24%) BM thickening (53%) Cellular vacuolization (82%) Stereocilia loss (94%) Increased stromal spaces (76%)	Monolayer degeneration (75%) BM thickening (75%) Cellular vacuolization (75%) Stereocilia loss (75%) Increased stromal spaces (50%)	Monolayer degeneration (92%) BM thickening (85%) Cellular vacuolization (69%) Stereocilia loss (100%) Increased stromal spaces (69%)	Monolayer degeneration (100%) BM thickening (100%) Cellular vacuolization (80%) Stereocilia loss (80%) Increased stromal spaces (80%)	Monolayer degeneration (100%) Stromal edema (100%) BM thickening (100%)

HSCC, horizontal semicircular canal crista ampullaris; SSCC, superior semicircular canal crista ampullaris; PSCC, posterior semicircular canal crista ampullaris; BM, basement membrane.

the myelin sheath (35, 36). Our study indicated that the altered shape and dimensions of SLI in the central portion of VN fibers, which affects the normal structure and function of myelin sheath, may cause aberrant nerve conduction and aggravate refractory vertigo. This hypothesis is coincident with our observation of atrophic axons in VN sections.

In addition, other microscopic features included the presence of microglia and the formation of lipofuscin in the affected VN. Lipofuscin, also known as age pigment, is produced when abnormal materials in the cytoplasm of cells are engulfed by autophagic vacuoles. The accumulation of lipofuscin is considered to indicate reduced function of lysosomes in these cells (37). Microglia act as endogenous macrophages in the nervous system, scavenging dying cells or cellular debris through phagocytosis and endocytosis (38). Therefore, the presence of lipofuscin and microglia indicate damage and decomposition of central VN fibers in patients with intractable MD.

The recognized limitation of this study was the small sample size. Multicenter studies with large sample sizes and studies using animal models are recommended in the future.

In summary, this study discovered subcellular lesions in the central portion of the VN in patients with intractable MD that were correlated with disease severity. The diverse pathological changes observed in the current study imply that intractable MD is likely to involve vestibular neuropathy. Histological abnormalities of the central portion of the affected VN may have the potential to explain the etiology of refractory vertigo. Neuroprotective agents like nerve growth factor are indicated in MD patients to prevent or relieve axonal impairment.

DATA AVAILABILITY

All datasets for this study are included in the manuscript and the supplementary files.

ETHICS STATEMENT

This study was carried out in accordance with the recommendations of ethical principles for 325 medical research involving human subjects (World Medical Association) with written informed consent from all subjects. All subjects gave written informed consent in accordance with the Declaration of Helsinki. The protocol was approved by the ethics committee of the Sixth People's Hospital affiliated to Shanghai Jiaotong University.

AUTHOR CONTRIBUTIONS

PW, HZ, and WL performed and analyzed pathological studies. PW wrote the manuscript draft. HS designed the study and corrected the manuscript. QS acquired electron microscope data. ZC, YW, HS, and SY performed operations and collected specimens. HW, HY, and DY evaluated hearing and vestibular function of patients and collected clinical data. SY critically reviewed the manuscript. All authors read and approved the final manuscript.

FUNDING

This work was supported by Shanghai Leadership Talent Training Plan (No. 2017062), the Key Project of Shanghai Jiao Tong University Medicine Science and Engineering Interdisciplinary Foundation (No. YG2016ZD02), and the Clinical Research Plan of Shanghai Shen Kang Hospital Development Center (16CR4022A, 16CR3041A).

ACKNOWLEDGMENTS

We thank Prof. Lu-Yang Wang (University of Toronto) for careful reading of the manuscript and language advice.

REFERENCES

1. Ménière P. Mémoire sur des lésions de l'oreille interne donnant lieu à des symptômes de congestion cérébrale apoplectiforme. *Gaz Med Paris*. (1861) 16:597–601.
2. Hallpike CS, Cairns H. Observations on the pathology of meniere's syndrome: (section of otology). *Proc R Soc Med*. (1938) 31:1317–36. doi: 10.1177/003591573803101112
3. Gallego-Martinez A, Espinosa-Sanchez JM, Lopez-Escamez JA. Genetic contribution to vestibular diseases. *J Neurol*. (2018) 265:29–34. doi: 10.1007/s00415-018-8842-7
4. Gazquez I, Soto-Varela A, Aran I, Santos S, Batuecas A, Trinidad G, et al. High prevalence of systemic autoimmune diseases in patients with Meniere's disease. *PLoS ONE*. (2011) 6:e26759. doi: 10.1371/journal.pone.0026759
5. Selmani Z, Marttila T, Pyykko I. Incidence of virus infection as a cause of Meniere's disease or endolymphatic hydrops assessed by electrocochleography. *Eur Arch Otorhinolaryngol*. (2005) 262:331–4. doi: 10.1007/s00405-004-0816-y
6. Bixenstine PJ, Maniglia MP, Vasanji A, Alagramam KN, Megerian CA. Spiral ganglion degeneration patterns in endolymphatic hydrops. *Laryngoscope*. (2008) 118:1217–23. doi: 10.1097/MLG.0b013e31816ba9cd
7. Sanchez-Fernandez JM, Marco J. Ultrastructural study of the human utricular macula and vestibular nerve in meniere's disease. *Acta Otolaryngol*. (1975) 79:180–8. doi: 10.3109/00016487509124673
8. Rosenhall U, Engstrom B, Stahle J. Macula utriculi in four cases with Meniere's disease. *Acta Otolaryngol*. (1977) 84:307–16. doi: 10.3109/00016487709123972
9. McCall AA, Ishiyama GP, Lopez IA, Bhuta S, Vetter S, Ishiyama A. Histopathological and ultrastructural analysis of vestibular endorgans in Meniere's disease reveals basement membrane pathology. *BMC Ear Nose Throat Disord*. (2009) 9:4. doi: 10.1186/1472-6815-9-4
10. Kent M, Platt SR, Schatzberg SJ. The neurology of balance: function and dysfunction of the vestibular system in dogs and cats. *Vet J*. (2010) 185:247–58. doi: 10.1016/j.tvjl.2009.10.029
11. Luscher C, Streit J, Quadroni R, Luscher HR. Action potential propagation through embryonic dorsal root ganglion cells in culture. I. Influence of the cell morphology on propagation properties. *J Neurophysiol*. (1994) 72:622–33. doi: 10.1152/jn.1994.72.2.622
12. Gemes G, Koopmeiners A, Rigaud M, Lirk P, Sapunar D, Bangaru ML, et al. Failure of action potential propagation in sensory neurons: mechanisms and loss of afferent filtering in C-type units after painful nerve injury. *J Physiol*. (2013) 591:1111–31. doi: 10.1113/jphysiol.2012.242750
13. Rattay F, Potrusil T, Wenger C, Wise A, K., Glueckert R, Schrott-Fischer A. Impact of morphometry, myelinization and synaptic current strength on spike conduction in human and cat spiral ganglion neurons. *PLoS ONE*. (2013) 8:e79256. doi: 10.1371/journal.pone.0079256
14. Pericat D, Farina A, Agavnian-Couquiaud E, Chabbert C, Tighilet B. Complete and irreversible unilateral vestibular loss: a novel rat model of vestibular pathology. *J Neurosci Methods*. (2017) 283:83–91. doi: 10.1016/j.jneumeth.2017.04.001
15. Nam GS, Jung CM, Kim JH, Son EJ. Relationship of vertigo and postural instability in patients with vestibular Schwannoma. *Clin Exp Otorhinolaryngol*. (2018) 11:102–8. doi: 10.21053/ceo.2017.01277
16. Jeong SH, Kim HJ, Kim JS. Vestibular neuritis. *Semin Neurol*. (2013) 33:185–94. doi: 10.1055/s-0033-1354598
17. Spencer RF, Sismanis A, Kilpatrick JK, Shaia WT. Demyelination of vestibular nerve axons in unilateral Meniere's disease. *Ear Nose Throat J*. (2002) 81:785–9. doi: 10.1177/014556130208101113
18. Kitamura K, Kaminaga C, Ishida T, Silverstein H. Ultrastructural analysis of the vestibular nerve in Meniere's disease. *Auris Nasus Larynx*. (1997) 24:27–30. doi: 10.1016/S0385-8146(96)00007-7
19. Lopez-Escamez JA, Carey J, Chung WH, Goebel JA, Magnusson M, Mandala M, et al. Diagnostic criteria for Meniere's disease. *J Vestib Res*. (2015) 25:1–7. doi: 10.3233/VES-150549
20. World Medical Association. World Medical Association Declaration of Helsinki: ethical principles for medical research involving human subjects. *JAMA*. (2013) 310:2191–4. doi: 10.1001/jama.2013.281053
21. Rizvi SS. Investigations into the cause of canal paresis in Meniere's disease. *Laryngoscope*. (1986) 96:1258–71. doi: 10.1002/lary.1986.96.11.1258
22. Ylikoski J, Collan Y, Palva T. Vestibular sensory epithelium in Meniere's disease. *Arch Otolaryngol*. (1979) 105:486–91. doi: 10.1001/archotol.1979.00790200048010
23. Cavanagh JB. Corpora-amylacea and the family of polyglucosan diseases. *Brain Res Brain Res Rev*. (1999) 29:265–95. doi: 10.1016/S0165-0173(99)00003-X
24. Rohn TT. Corpora amylacea in neurodegenerative diseases: cause or effect? *Int J Neurol Neurother*. (2015) 2:1031. doi: 10.23937/2378-3001/2/2/1031
25. Raine CS. The dale E. McFarlin memorial lecture: the immunology of the multiple sclerosis lesion. *Ann Neurol*. (1994) 36(Suppl.):S61–72. doi: 10.1002/ana.410360716
26. Wilhelmus MM, Verhaar R, Bol JG, van Dam AM, Hoozemans JJ, Rozemuller AJ, Drukarch B. Novel role of transglutaminase 1 in corpora amylacea formation? *Neurobiol Aging*. (2011) 32:845–56. doi: 10.1016/j.neurobiolaging.2009.04.
27. Singhrao SK, Morgan BP, Neal JW, Newman GR. A functional role for corpora amylacea based on evidence from complement studies. *Neurodegeneration*. (1995) 4:335–45. doi: 10.1016/1055-8330(95)90024-1
28. Auge E, Cabezon I, Pelegri C, Vilaplana J. New perspectives on corpora amylacea in the human brain. *Sci Rep*. (2017) 7:41807. doi: 10.1038/srep41807
29. Auge E, Duran J, Guinovart J, J., Pelegri C, Vilaplana J. Exploring the elusive composition of corpora amylacea of human brain. *Sci Rep*. (2018) 8:13525. doi: 10.1038/s41598-018-31766-y
30. Pisa D, Alonso R, Rabano A, Carrasco L. Corpora amylacea of brain tissue from neurodegenerative diseases are stained with specific antifungal antibodies. *Front Neurosci*. (2016) 10:86. doi: 10.3389/fnins.2016.00086
31. Frejo L, Gallego-Martinez A, Requena T, Martin-Sanz E, Amor-Dorado JC, Soto-Varela A, et al. Proinflammatory cytokines and response to molds in mononuclear cells of patients with Meniere disease. *Sci Rep*. (2018) 8:5974. doi: 10.1038/s41598-018-23911-4
32. Hamada MS, Popovic MA, Kole MH. Loss of saltation and presynaptic action potential failure in demyelinated axons. *Front Cell Neurosci*. (2017) 11:45. doi: 10.3389/fncel.2017.00045
33. Khan S, Chang R. Anatomy of the vestibular system: a review. *NeuroRehabilitation*. (2013) 32:437–43. doi: 10.3233/NRE-130866
34. Fetter M. Acute unilateral loss of vestibular function. *Handb Clin Neurol*. (2016) 137:219–29. doi: 10.1016/B978-0-444-63437-5.00015-7
35. Hoshi T, Suzuki A, Hayashi S, Tohyama K, Hayashi A, Yamaguchi Y, et al. Nodal protrusions, increased Schmidt-Lanterman incisures, and paranodal disorganization are characteristic features of sulfatide-deficient peripheral nerves. *Glia*. (2007) 55:584–94. doi: 10.1002/glia.20487
36. Berger BL, Gupta R. Demyelination secondary to chronic nerve compression injury alters Schmidt-Lanterman incisures. *J Anat*. (2006) 209:111–8. doi: 10.1111/j.1469-7580.2006.00561.x
37. Sulzer D, Mosharov E, Talloczy Z, Zucca FA, Simon JD, et al. Neuronal pigmented autophagic vacuoles: lipofuscin, neuromelanin, and ceroid as macroautophagic responses during aging and disease. *J Neurochem*. (2008) 106:24–36. doi: 10.1111/j.1471-4159.2008.05385.x
38. Prinz M, Erny D, Hagemeyer N. Ontogeny and homeostasis of CNS myeloid cells. *Nat Immunol*. (2017) 18:385–392. doi: 10.1038/ni.3703

Conflict of Interest Statement: The authors declare that the research was conducted in the absence of any commercial or financial relationships that could be construed as a potential conflict of interest.

frontiers in Neurology

ORIGINAL RESEARCH
published: 11 September 2019
doi: 10.3389/fneur.2019.00977

Cytokine Levels in Inner Ear Fluid of Young and Aged Mice as Molecular Biomarkers of Noise-Induced Hearing Loss

Lukas D. Landegger[1,2,3†], Sasa Vasilijic[1,2†], Takeshi Fujita[1,2], Vitor Y. Soares[1,2], Richard Seist[1,2], Lei Xu[4] and Konstantina M. Stankovic[1,2,5,6]*

[1] Eaton Peabody Laboratories, Department of Otolaryngology, Massachusetts Eye and Ear, Boston, MA, United States, [2] Department of Otolaryngology—Head and Neck Surgery, Harvard Medical School, Boston, MA, United States, [3] Department of Otolaryngology, Vienna General Hospital, Medical University of Vienna, Vienna, Austria, [4] Edwin L. Steele Laboratories, Department of Radiation Oncology, Harvard Medical School, Massachusetts General Hospital, Boston, MA, United States, [5] Program in Speech and Hearing Bioscience and Technology, Harvard Medical School, Boston, MA, United States, [6] Program in Therapeutic Science, Harvard Medical School, Boston, MA, United States

OPEN ACCESS

Edited by:
Agnieszka J. Szczepek, Charité Medical University of Berlin, Germany

Reviewed by:
Srdjan Vlajkovic, The University of Auckland, New Zealand
Bohua Hu, University at Buffalo, United States

***Correspondence:**
Konstantina M. Stankovic
konstantina_stankovic@meei.harvard.edu

[†]These authors have contributed equally to this work

Specialty section:
This article was submitted to Neuro-Otology, a section of the journal Frontiers in Neurology

Received: 17 July 2019
Accepted: 27 August 2019
Published: 11 September 2019

Citation:
Landegger LD, Vasilijic S, Fujita T, Soares VY, Seist R, Xu L and Stankovic KM (2019) Cytokine Levels in Inner Ear Fluid of Young and Aged Mice as Molecular Biomarkers of Noise-Induced Hearing Loss. Front. Neurol. 10:977. doi: 10.3389/fneur.2019.00977

Sensorineural hearing loss (SNHL) is the most common sensory deficit worldwide, frequently caused by noise trauma and aging, with inflammation being implicated in both pathologies. Here, we provide the first direct measurements of proinflammatory cytokines in inner ear fluid, perilymph, of adolescent and 2-year-old mice. The perilymph of adolescent mice exposed to the noise intensity resulting in permanent auditory threshold elevations had significantly increased levels of IL-6, TNF-α, and CXCL1 6 h after exposure, with CXCL1 levels being most elevated (19.3 ± 6.2 fold). We next provide the first immunohistochemical localization of CXCL1 in specific cochlear supporting cells, and its presumed receptor, Duffy antigen receptor for chemokines (DARC), in hair cells and spiral ganglion neurons. Our results demonstrate the feasibility of molecular diagnostics of SNHL using only 0.5 μL of perilymph, and motivate future sub-μL based diagnostics of human SNHL based on liquid biopsy of the inner ear to guide therapy, promote hearing protection, and monitor response to treatment.

Keywords: perilymph, noise-induced hearing loss, cytokines, CXCL1, DARC, age-related hearing loss

INTRODUCTION

Sensorineural hearing loss (SNHL) is the most common sensory deficit in the world. Disabling SNHL currently affects nearly half a billion people (1), and its incidence increases with age, affecting 16% of people aged 18 years and older, 34% of people aged 65–69 years, and 72% of people aged 85–90 years (2, 3). In addition to being economically costly to society, with the annual cost of unaddressed hearing loss being $750 billion globally (4), SNHL is physically and emotionally costly to individuals, as it is associated with cognitive dysfunction, dementia, and depression (5). Despite these staggering statistics, the cellular basis of human SNHL is typically unknown in living people because the inner ear cannot be biopsied today and its cells cannot be imaged clinically (6, 7). These barriers arise from the inner ear's small size, encasement in dense bone, and complex three-dimensional anatomy. There is a potential to overcome these barriers by performing liquid biopsy of the inner ear based on sampling of its fluid, perilymph, which bathes the vast majority of inner ear cells.

Noise exposure and aging are important causes of human SNHL, and noise exposure accelerates age-related hearing loss (8). According to the United States Department of Veteran Affairs, hearing loss and tinnitus are the most common disability claims of veterans (9). In addition to occupational noise exposure, recreational noise exposure is also threatening public health due to loud concerts, sporting events, and the increasing use of portable music players. The World Health Organization estimates that 1.1 billion young people are at risk of noise-induced hearing loss, primarily due to recreational exposure (4). Noise levels can cause permanent or temporary shifts in behavioral audiometric thresholds or physiologic metrics of hearing in both animals and humans (10). Permanent threshold shift (PTS) occur after exposure to high noise levels that cause irreversible structural damage in the cochlea, such as loss of hair cells, or their stereocilia and loss of cochlear neurons. Moderate noise exposure causes temporary threshold shift (TTS), characterized by a temporary elevation in physiologic or behavioral thresholds that recovers to pre-exposure levels within 1–2 weeks post exposure. A decade ago it was recognized that even TTS can cause permanent structural changes characterized by immediate loss of afferent synapses on inner hair cells, followed by a delayed loss of the associated neural somata (11). This neuropathic hearing loss is characterized by reduction in the amplitude of auditory brainstem response wave I, which reflects the activity of the cochlear nerve. However, not every TTS is associated with neuropathic hearing loss. Our laboratory has previously defined noise levels that differentiate neuropathic and non-neuropathic TTS in adolescent mice (12). In the current study we investigated how PTS, neuropathic TTS, and non-neuropathic TTS exposures are reflected in cytokine profiles in perilymph from young and old mice.

We focus on proinflammatory cytokines because they play an important role in a plethora of diseases (13), and are thought to be important mediators of numerous middle and inner ear maladies (14–17), including noise-induced hearing loss (18–21). However, past methods that have implicated cytokines in otologic disease are inappropriate for translation to living people, because they have required the destruction of sensorineural structures (e.g., for RT-PCR studies), post-mortem tissue processing (e.g., for immunohistochemistry), or pooling of samples from several animals to obtain an adequate volume of perilymph for analysis (22, 23).

While we (24, 25) and others (26–28) have demonstrated the feasibility of analyzing perilymph using proteomics or miRNA microarrays, cytokine levels in perilymph have never been directly measured before. Here we provide the first direct quantification of cytokine levels in perilymph and describe how these levels dynamically change after noise exposure and with aging. We demonstrate the feasibility of detecting molecular changes in as little as 0.5 μL of perilymph. We validate our findings by providing the first cellular distribution of CXCL1 and its putative receptor, DARC, in the cochlea. These results have important translational implications for future sub-μL based molecular diagnostics of human SNHL based on liquid biopsy of the inner ear to guide targeted therapy, promote hearing protection, and monitor patients' response to treatment.

RESULTS

Cytokine Levels Are Increased in Perilymph After Exposure to PTS-Inducing Noise Levels

Compared to the perilymph of unexposed animals ($N = 19$ ears), perilymph collected 6 h after exposing mice to noise levels that resulted in PTS (103 dB SPL at 8–16 kHz for 2 h) ($N = 17$ ears) demonstrated a statistically significant elevation of the levels of proinflammatory cytokines CXCL1 (vestibular perilymph = vPLF: 1,598.6 ± 509.0 *re* 83.0 ± 8.06 pg/mL, $p < 0.001$; cochlear perilymph = cPLF: 729.1 ± 178.6 *re* 75.8 ± 6.6 pg/mL, $p = 0.001$), IL-6 (vPLF: 1,258.9 ± 232.0 *re* 206.4 ± 19.6 pg/mL, $p < 0.001$; cPLF: 532.2 ± 72.2 *re* 254.8 ± 21.2 pg/mL, $p = 0.0042$), and TNF-α (vPLF: 56.2 ± 4.9 *re* 28.6 ± 2.7 pg/mL, $p < 0.0001$ (**Figure 1**). Of these 3 cytokines, CXCL1 exhibited the largest fold change: 19.3 ± 6.2 for vPLF and 9.6 ± 2.4 for cPLF (**Supplementary Figure 1**). Levels of IL-1β, IL-10, IL-12, IFN-γ, IL-4, and IL-5 did not significantly change 6 h after the same noise exposure. These results single out CXCL1 as the best candidate molecular biomarker of early PTS among the cytokines studied.

None of the tested cytokine levels demonstrated detectable changes 6 h after exposure to less intense noise that caused either non-neuropathic TTS (94 dB SPL at 8–16 kHz for 2 h) or neuropathic TTS (97 dB SPL at 8–16 kHz for 2 h) (**Figure 1**).

For cytokines with significant elevation after PTS-causing noise, the trends in cochlear and vestibular perilymph were generally similar, with vestibular perilymph showing higher inducible fluctuations than cochlear perilymph.

Measured Cytokine Levels Are Significantly Higher in Perilymph Than in CSF

The levels of all measured cytokines were higher in perilymph than in CSF (**Figures 1**, **2**; **Supplementary Figure 2**). CSF obtained through the cisterna magna, abbreviated cmCSF ($N = 10$ ears), did not show significant changes in any of the measured cytokines, confirming the specificity of the cytokine reaction to the inner ear (**Figure 1**). However, CSF collected through the posterior semicircular canal (PSC) ($N = 17$ ears) did demonstrate statistically significant elevations in the levels of the same three cytokines that were elevated in perilymph 6 h after PTS-causing noise exposure (**Figure 1**). This indicates that CSF collected through the labyrinth is not identical to the CSF collected through the cisterna magna, as the former reflects noise-induced changes in the tissues it flows by. Nonetheless, CSF collected through the labyrinth can serve as a rough proxy for the CSF collected through the cisterna magna because both demonstrate lower cytokine levels than in perilymph.

Levels of Proinflammatory Cytokines Demonstrate Dynamic Changes in Perilymph and Increase in Blood With Aging

The levels of proinflammatory cytokines IL-1β and TNF-α decreased significantly from age 8 weeks (corresponding to 2

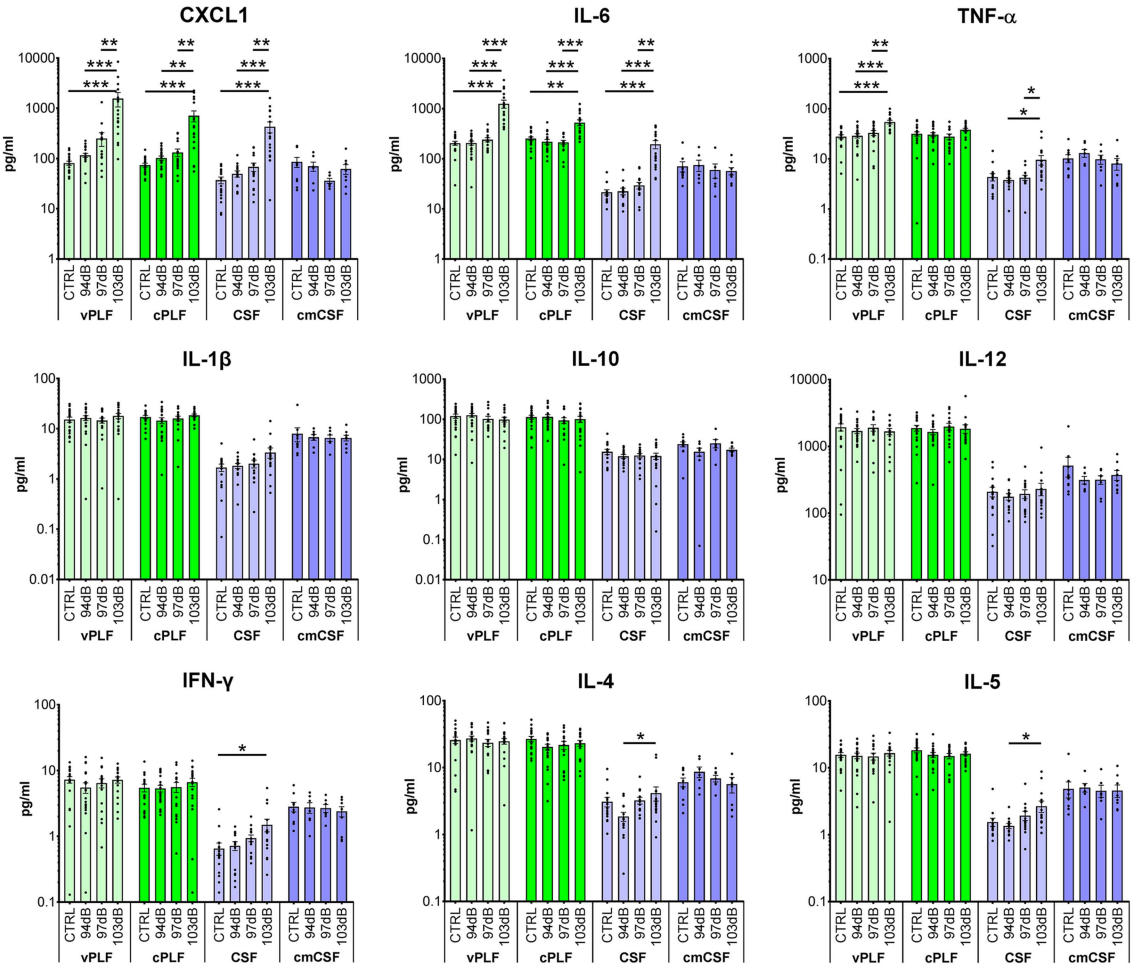

FIGURE 1 | Cytokine levels in murine perilymph and cerebrospinal fluid 6 h after noise exposure. Six-week-old mice were exposed to 8–16 kHz noise for 2 h at 94 dB SPL (non-neuropathic TTS), 97 dB SPL (neuropathic TTS), and 103 dB SPL (PTS). Unexposed mice served as controls (CTRL). Six hours post exposure, vestibular perilymph (vPLF), cochlear perilymph (cPLF), and cerebrospinal fluid (CSF) were collected through the posterior semicircular canal. In addition, CSF was collected via cisterna magna (cmCSF). Each dot represents measurements from one ear (vPLF, cPLF, and CSF) or animal (cmCSF). Data are shown as group means ± standard error of the mean. $N = 16$–20 ears for vPLF, cPLF, and CSF, each; $N = 14$–17 ears for cmCSF; $N = 7$–10 ears for control samples. $^{*}P < 0.05$, $^{**}P < 0.01$, or $^{***}P < 0.001$.

weeks after noise exposure) to 2 years in control unexposed animals (vPLF: 19.80 *re* 7.18 pg/mL, $p = 0.003$; cPLF: 18.46 *re* 8.13 pg/mL, $p = 0.0081$ for IL-1β; vPLF: 30.78 *re* 12.61 pg/mL, $p = 0.0010$; cPLF: 24.79 *re* 11.48 pg/mL, $p = 0.0009$ for TNF-α; **Figure 2**). Similar significant age-related changes in perilymph were observed after non-neuropathic and neuropathic TTS exposure (**Figure 2**). Moderate upregulation of IL-1β was only observed in vPLF 2 weeks after non-neuropathic TTS exposure ($p = 0.0420$).

In contrast to IL-1β and TNF-α, IL-6 levels increased significantly at 8 weeks of age in all analyzed samples regardless of noise exposure (**Figure 2**). The observed difference in control animals could be explained by age-related developmental kinetics of immune-competent cells. While the number of T lymphocytes in mice plateaus at about 2–4 months of age (29), T-cell response in mice matures around 8 weeks of age (30). Similar developmental kinetics may exist for innate immune cells such as macrophages, which are an important source of IL-6 in the cochlear microenvironment. While the number of inner ear macrophages or their cytokine producing capacity have not been quantified between 6- and 8-week-old mice, the total number of macrophages in the small intestine is significantly increased between 4 and 9 weeks of age (31). At 2 years of age, IL-6 levels in vPLF and cPLF were significantly lower than at 2 weeks or 6 h after neuropathic noise exposure (vPLF: 130.00 at 2 years *re* 504.90 pg/mL at 2 weeks, $p < 0.0001$, and 242.72 pg/mL at 6 h post noise exposure; cPLF: 141.29 at 2 years *re* 482.23 pg/mL at 2 weeks, $p = 0.0001$, and 215.05 pg/mL at 6 h post noise exposure). This stands in contrast to the control animals, where IL-6 levels in vPLF did not meet our criterion for change between 2 weeks and 2 years after noise exposure.

The level of CXCL1 decreased significantly at 2 years compared to 6 h after exposure to non-neuropathic TTS in cPLF

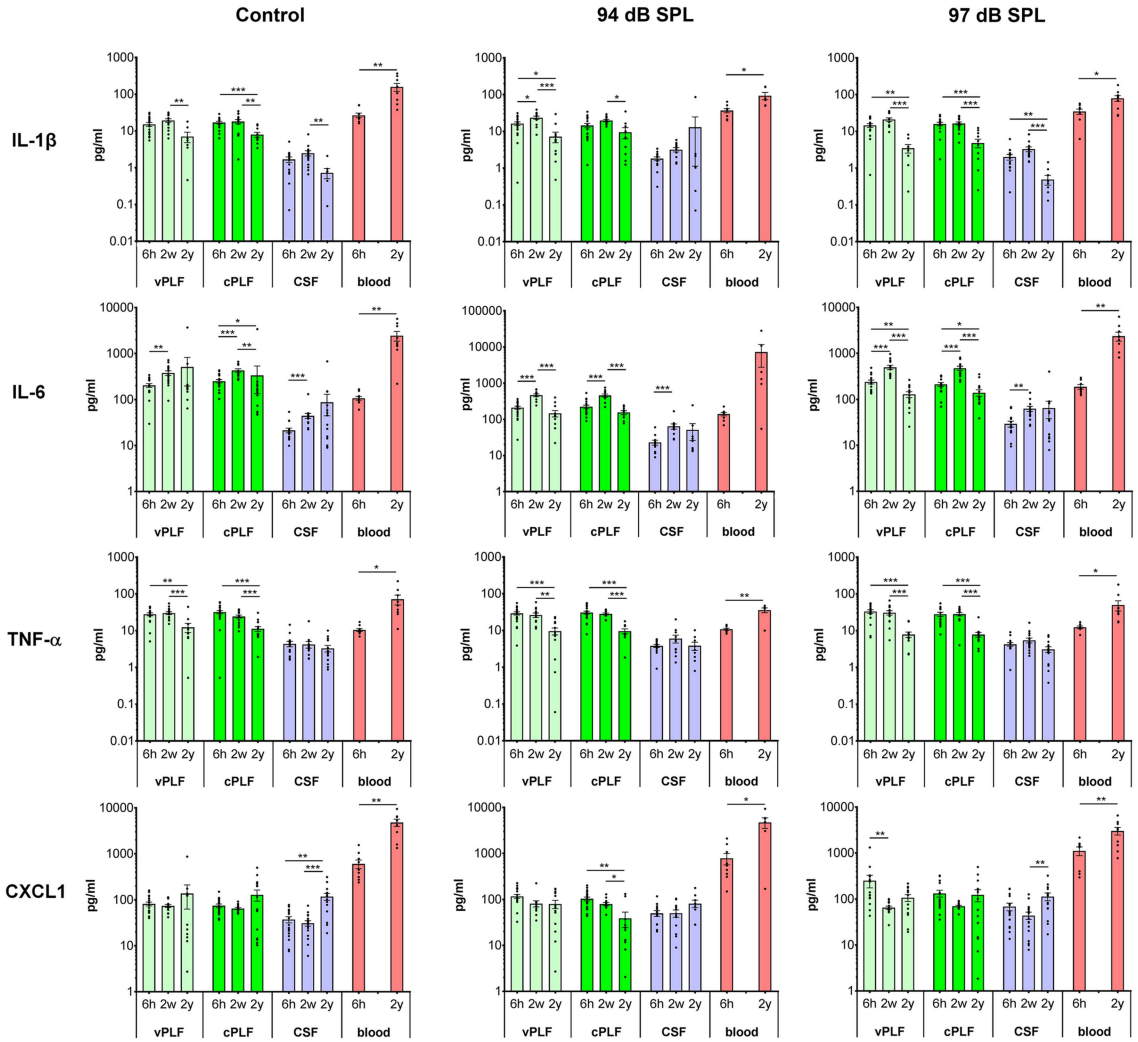

FIGURE 2 | Levels of proinflammatory cytokines IL-1β, IL-6, TNF-α, and CXCL1 in murine perilymph, cerebrospinal fluid and blood 6 h, 2 weeks, and 2 years after noise exposure. Six-week-old mice were exposed to 8–16 kHz noise for 2 h at 94 dB SPL and 97 dB SPL; unexposed mice served as controls. Samples were collected 6 h, 2 weeks, and 2 years post exposure. Vestibular perilymph (vPLF), cochlear perilymph (cPLF), and cerebrospinal fluid (CSF) were collected through the posterior semicircular canal. In addition, blood samples were obtained by cardiac puncture after thoracotomy. Each dot represents measurements from one ear (vPLF, cPLF, and CSF) or animal (blood). Data are shown as group means ± standard error of the mean. $N = 3$–20 ears for vPLF; $N = 3$–20 ears for cPLF; $N = 3$–17 ears for CSF; $N = 4$–10 animals for blood; $N = 7$–10 ears for control samples. $^{*}P < 0.05$, $^{**}P < 0.01$, or $^{***}P < 0.001$.

($p = 0.0033$), and at 2 weeks compared to 6 h after exposure to neuropathic TTS in vPLF ($p = 0.0147$). In contrast, CXCL1 levels increased significantly in the blood of 2-year-old mice compared to 6-week-old mice regardless of noise exposure (unexposed controls: 4,895.74 *re* 616.11 pg/mL, $p = 0.0039$; 94 dB group: 4,827.11 *re* 797.90 pg/mL, $p = 0.0256$; 97 dB group: 3,087.72 *re* 1,141.61 pg/mL, $p = 0.0093$).

Similar to proinflammatory cytokines, T-helper cell (Th)-related cytokines (IFN-γ, IL-2, IL-4, IL-5), and immunoregulatory (IL-10 and IL-12) cytokines in the perilymph and CSF of 2-year-old animals showed decreased values compared to young animals, regardless of noise exposure (**Supplementary Figure 2**). However, 2 weeks after noise exposure, an increase in cytokine levels was observed in CSF for IL-2 (94 dB SPL), IL-4 (97 dB SPL), and IL-12 (97 dB SPL) compared to 6 h after noise exposure.

In blood samples, all analyzed proinflammatory cytokines increased significantly from 6 weeks to 2 years of age regardless of noise exposure (control group: $p = 0.0092$ for IL-1β, $p = 0.0041$ for IL-6, $p < 0.0001$ for TNF-α, $p < 0.0001$ for CXCL1; 94 dB SPL group: $p = 0.0048$ for IL-1β, $p = 0.0360$ for IL-6, $p = 0.0076$ for TNF-α, $p = 0.0256$ for CXCL1; 97 dB SPL group: $p = 0.0127$ for IL-1β, $p < 0.0001$ for IL-6, $p < 0.0001$ for TNF-α, $p = 0.0093$ for CXCL1; **Figure 2**). In the Th-related group of cytokines, Th1 cytokines (IFN-γ and IL-2) trended toward age-related increase in levels, whereas Th2 cytokines (IL-4 and IL-5) demonstrated decreased or unchanged levels in old animals when compared to

young animals (**Supplementary Figure 2**). While IL-4 levels decreased significantly in old animals only in the control group ($p = 0.0385$), IL-5 levels were reduced in old animals of all groups ($p = 0.0041$ in the control group, $p = 0.0176$ in the 94 dB SPL group, $p < 0.0001$ in the 97 dB SPL group). The blood levels of immunoregulatory cytokine IL-10 were increased in old compared to young animals ($p = 0.0027$ in the control group, $p = 0.0330$ in the 94 dB SPL group, $p < 0.0001$ in the 97 dB SPL group). In contrast, blood IL-12 levels were similar between young and old animals, regardless of noise exposure (**Supplementary Figure 2**).

CXCL1 Localizes to Specific Cochlear Supporting Cells

While cellular expression of pro-inflammatory cytokines TNF-α and IL-6 has been previously reported in cochlear tissue (18), the cellular pattern of CXCL1 expression remains unknown. Therefore, we used immunohistochemistry applied to cochlear whole mounts of 6-week-old mice ($N = 4$ animals) to identify CXCL1-positive cells (**Figure 3**). The strongest immunoreactivity was observed in the cells adjacent to hair cells (**Figure 3Aa**). Co-staining for a hair-cell marker, Myo7A, revealed the strongest CXCL1-immunoreactivity between inner and outer hair cells, corresponding to the location of pillar cells (**Figure 3Ab–b'**). Further co-staining for a pillar cell marker, E-cadherin, as well as phalloidin, confirmed the pillar cells to be expressing CXCL1 at the highest level (**Figure 3Ba,b**). Using a comparative analysis of cochlear cross sections, whole mounts and 3D reconstructions, we observed that CXCL1 was differently expressed in the apical and basilar part of pillar cells, with predominant localization in the apical segment (**Figure 3Ac,d**). Basilar localization of CXCL1 in pillar cells was more prominent in the cochlear apex, suggesting a possible tonotopic distribution of CXCL1 (**Figure 4Ca,i**).

In addition to the dominant expression of CXCL1 in pillar cells, a marked CXCL1 positivity was found between outer hair cells. High magnification imaging (**Figure 3Ac'**) and Myo7A co-staining (**Figures 3Ab-b',Bh**) identified CXCL1 expression in the phalangeal processes of Deiters cells. Additionally, CXCL1 immunoreactivity was detected in interdental cells (**Figure 3Aa–a'**) and Claudius cells (**Figure 3Ab**). CXCL1 expression in these cells was also confirmed by the immunostaining of paraffin cross sections (**Figure 3Ad**). A semi-quantitative comparison of the staining intensity of CXCL1-positive cells is provided in **Supplementary Table 1**.

Noise Trauma Reduces CXCL1 Immunoreactivity in Pillar Cells

Considering the pivotal role of CXCL1 in the development of the inflammatory response, along with our finding that among the analyzed proinflammatory cytokines in perilymph CXCL1 experienced the largest noise-induced elevation, we studied the effect of acoustic trauma on CXCL1 immunoreactivity in pillar cells. Immunostaining of cochlear whole mounts from control ($N = 4$ animals) and noise-traumatized mice sacrificed 6 h after PTS-causing noise exposure ($N = 6$ animals) showed a noticeable decrease in CXCL1 immunoreactivity in pillar cells. The reduced CXCL1 expression was detectable in the cochlear base (**Figure 3Bm**) but not the apex (**Figure 3Bi**), as evident in the representative cochlear whole mounts. This noise exposure also caused the loss of outer hair cells (**Figure 3Bn,o,p**), consistent with previous reports (32). The number of outer hair cells was dramatically and significantly reduced at and above 31 kHz while the number of inner hair cells remained intact along the cochlear length (**Supplementary Figure 3**).

In order to identify other possible sources of CXCL1 in inflamed cochlear tissue, we compared the distribution of Iba-1 and CXCL1 positive cells in the cochlea because fibrocytes and Iba1-positive cochlear macrophages have the capacity to participate in the cochlear immune response after acoustic overstimulation (18, 33). Immunohistochemical analysis of cochlear sections ($N = 3$ control animals and $N = 3$ noise-exposed animals) revealed that the cochlear cells expressing Iba1 did not co-express CXCL1 (**Supplementary Figures 4B,C**). Instead, Iba1-negative pillar cells that were CXCL1-positive in control mice (**Supplementary Figure 4A**) continued to express CXCL1 6 h after exposure to PTS-causing noise that targets the cochlear base (8–16 kHz noise at 103 dB for 2 h, **Supplementary Figure 4B**).

DARC, a CXCL1 Receptor, Is Expressed in Cochlear Hair Cells, Supporting Cells and Spiral Ganglion Neurons

To identify the receptors through which CXCL1 may be exerting its effect in the inner ear, we studied expression of CXCR2 and DARC. We did not detect CXCR2 expression in the mature inner ear by qRT-PCR or immunostaining, consistent with a prior report (18).

In contrast to CXCR2, we saw specific immunostaining for DARC in the hair cells, outer pillar cells, a third row of Deiters cells, and spiral ganglion neurons ($N = 4$ animals) (**Figure 4A**). The analysis of DARC and Myo7A co-expression showed that DARC was more highly expressed in inner hair cells than in outer hair cells (**Figures 4A,Ba,d,Cb,f,j,n**). Considering the potential role of DARC in binding of CXCL1, we analyzed their co-expression and found that DARC was expressed in the columnar and basilar part of outer pillar cells, with CXCL1 co-localization only in the basilar part (**Figure 4Ba,a',d,d'**). In contrast to CXCL1, whose expression was reduced in the cochlear basal turn after exposure to noise targeting the base (**Figure 4Cm**), DARC immunoreactivity was not noticeably affected by noise exposure ($N = 4$ animals) (**Figure 4Cb,f,j,n**). A semi-quantitative comparison of the staining intensity of DARC-positive cells is provided in **Supplementary Table 2**.

Within the peripheral vestibular system, specific immunoreactivity for DARC was found within the crista ampullaris ($N = 4$ animals **Figure 5B**). Costaining for Myo7A, a hair cell marker (**Figure 5C**), and CXCL1 (**Figure 5A**) revealed that DARC was preferentially expressed in a subset of hair cells while CXCL1 was preferentially expressed in the surrounding supporting cells (**Figure 5D**).

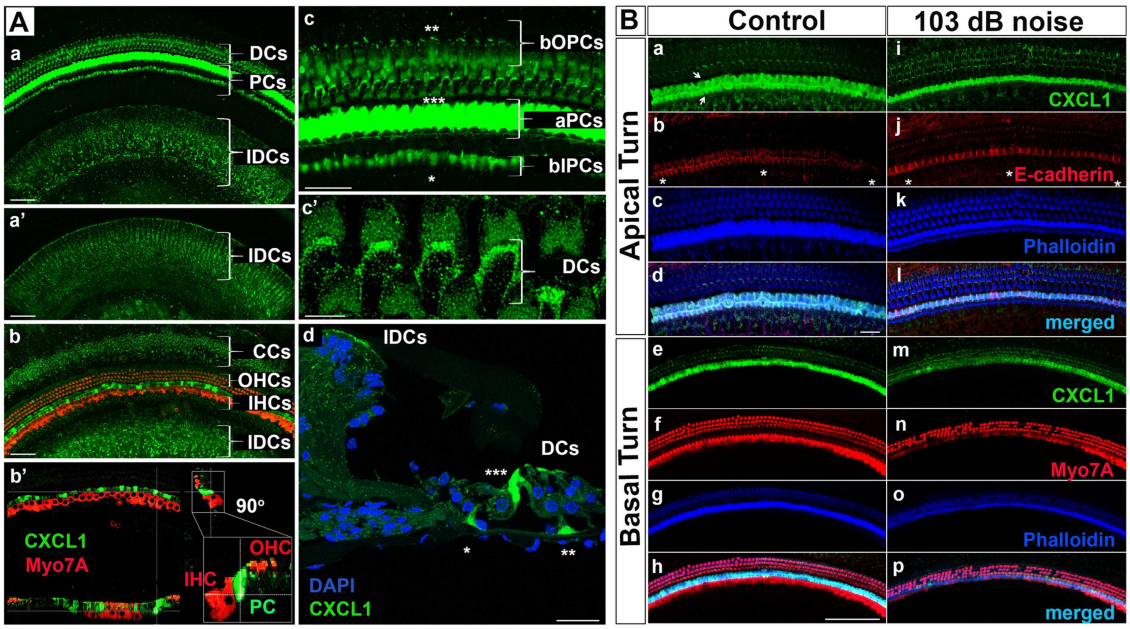

FIGURE 3 | CXCL1 immunoreactivity localizes to cochlear supporting cells and is reduced in pillar cells after noise exposure. **(A)** Cochlear whole mounts from 6-week-old control mice **(Aa–c'; Ba–h)** and age-matched mice exposed to noise causing PTS **(Ad; Bi–p)** revealed immunostaining for CXCL1 (green) in specific supporting cells but not Myo7A-expressing hair cells (red) **(Ab-b')**. **(Ad)** is a paraffin cross section. CXCL1 is expressed in Claudius cells (CCs) **(Ab)**, Deiters cells (DCs) **(Aa,c',d)**, pillar cells (PCs) **(Aa,b-b',c,d)**, and interdental cells (IDCs) **(Aa,b)**. CXCL1 is predominantly expressed in the apical part of PCs (aPCs) **(Ac,d)** and to a lesser extent in the basilar part of inner PCs (bIPCs) and outer PCs (bOPCs). Pillar cells are positioned between outer (OHCs) and inner hear cells (IHCs) **(Ab-b')**. Asterisks indicate bIPCs (*), bOPCs (**), and aPCs (***) **(Ac,d)**. A magnified view of DCs shows CXCL1 positivity in the phalangeal processes of DCs **(Ac')**. A selected section from a z-stack illustrates CXCL1 positivity in IDCs **(a')**. CXCL1 is also expressed in the apical surface of IDCs **(Aa,b,d)**. Slides represent maximum projections **(Aa,b,c-c')** and orthogonal sections **(Ab')** of confocal z-stacks through whole mounts of the organ of Corti in the cochlear basal region (~35 kHz). Scale bars: 5 μm **(Ac')**, 25 μm **(Ac,d)**, 50 μm **(Aa,b)**. **(B)** Cochlear whole mounts immunostained with anti-CXCL1 antibody (green) **(Ba,e,i,m)**, anti-E-cadherin antibody to identify pillar cells (red) **(Bb,j)**, anti-Myo7A to identify hair cells (red) **(Bf,n)**, and Phalloidin (blue) **(Bc,g,k,o)** revealed CXCL1 and E-cadherin co-expression in pillar cells **(Bb,j)**. The asterisk indicates the modiolar side of the organ of Corti **(Bb,j)**. Arrows indicate inner and outer pillar cells **(a)**. The number of CXCL1-positive cells was significantly reduced only in the cochlear base of noise-exposed animals **(Bm)** where OHC loss was noted. Scale bars: 20 μm (B-apical turn), 100 μm (B-basal turn). The slides represent maximum projections of confocal z-stacks through cochlear whole mounts in the apical and basal region of the cochlea (~8 and 32 kHz region, respectively). Representative images are based on biological replicates in 4 control and 6 noise-exposed animals.

DISCUSSION

First Direct Measurements of Cytokines in Perilymph

To the best of our knowledge, this study provides the first direct measurements of cytokines in murine perilymph. The finding that the cytokine profile of the first one μL of fluid collected through the murine inner ear is different than the cytokine profile of the rest of the fluid collected through the PSC is consistent with the first microliter representing perilymph and the other fluid being related to CSF. This difference is expected based on a widely patent cochlear aqueduct in rodents, which connects CSF space with the inner ear (34). While CSF collected through the inner ear is similar to the CSF collected through the cisterna magna, these fluids are not identical in their cytokine profiles. The elevated cytokine levels in CSF collected through the inner ear but not through the cisterna magna after PTS-inducing noise exposure are most likely due to contamination by secretions or shedding from inner ear cells. Taken together, labyrinthine CSF is a proxy for but is not identical to the CSF bathing the brain.

Our measurements of proinflammatory cytokine levels in perilymph following acoustic trauma are in line with the previous measurements of similar cytokines in cochlear tissues. Specifically, elevation in TNF-α and IL-6 mRNA expression was reported in the stria vascularis, spiral ganglion neurons, and spiral ligament in the early phase after PTS-inducing acoustic trauma (124 dB SPL) by RT-PCR in Sprague-Dawley rats (18). In a follow-up study using identical noise parameters, the same group reported IL-6 protein upregulation in cochlear tissue lysates using western blot 6 h after acoustic trauma in C57BL/6J mice (21). Treatment with an anti-IL-6 receptor antibody after noise trauma ameliorated hearing loss (21).

When comparing mouse strains with different susceptibility to noise-induced hearing loss, several immune-related genes were reported to be upregulated in the susceptible mice (35). In addition, *Tnip1*, a gene encoding the "tumor necrosis factor, alpha-induced protein 3" was expressed at higher levels in mice resistant to noise exposure. This protein is known to inhibit TNF-mediated apoptosis and NF-kappa B activation.

Furthermore, supporting our results, ELISA of bulk cochlear tissue lysates following middle ear inoculation with *Haemophilus*

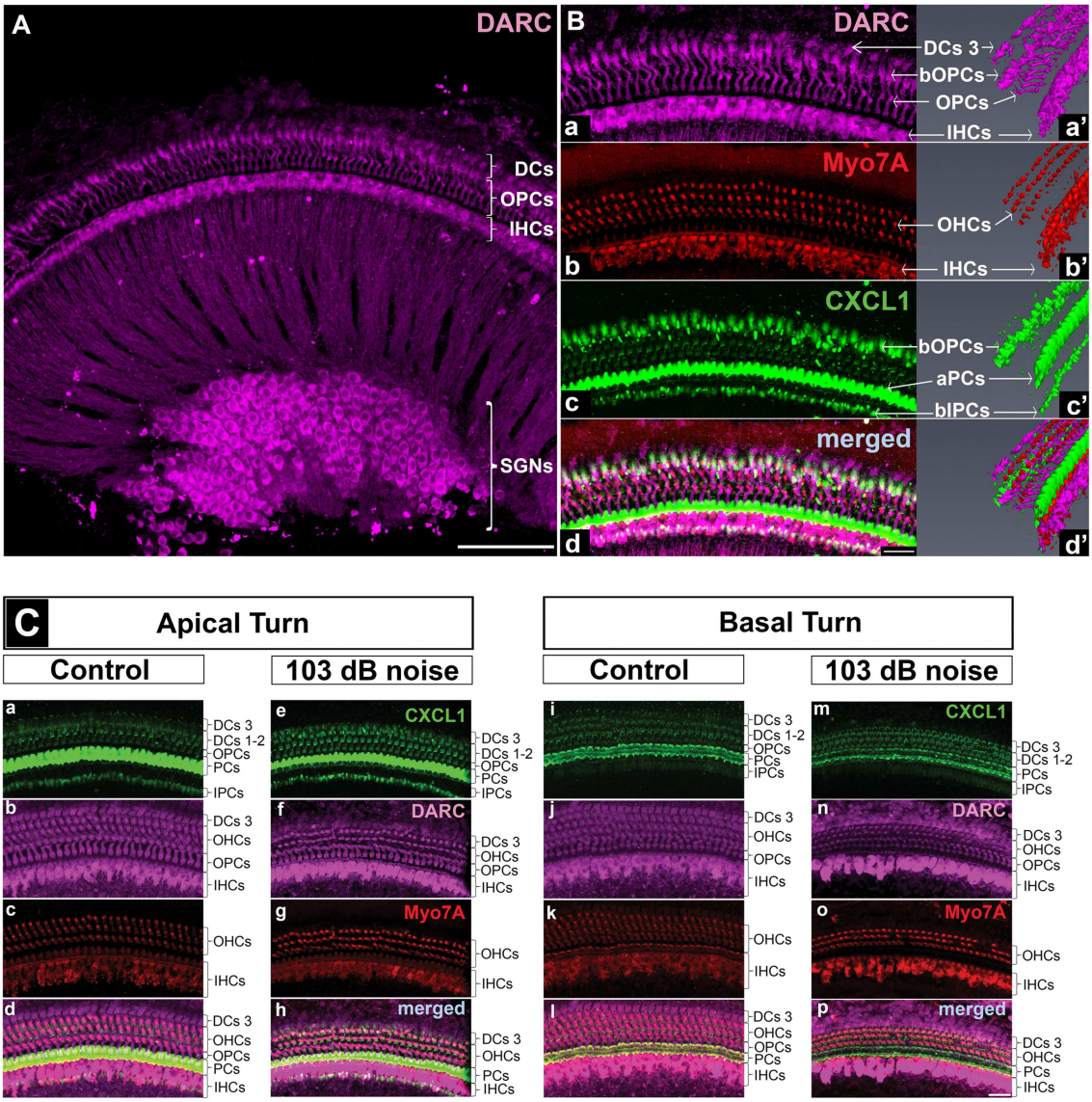

FIGURE 4 | DARC, atypical chemokine receptor, is expressed in cochlear hair cells, supporting cells, and spiral ganglion neurons. Cochlear whole mounts of control mice **(A,B,Ca-d,i-l)** and age-matched mice exposed to PTS-causing noise (103 dB SPL) **(Ce–h,m–p)** at 6 weeks of age and sacrificed 6 h later were stained with anti-DARC (magenta), anti-CXCL1 (green), and anti-Myo7A antibody (red). **(A)** DARC is brightly expressed in the outer pillar cells (OPCs), inner hair cells (IHCs) and spiral ganglion neurons (SGNs), and moderately expressed in outer hair cells (OHCs) and Deiters cells (DCs). Scale bar, 100 μm. **(B)** A high magnification view of the whole mount shown in A and a corresponding 3D reconstruction illustrate DARC expression in the columnar part of OPCs and DARC coexpression with CXCL1 in the basilar part of OPCs (bOPCs) **(Ba–d,a'–d')**. Three-dimensional reconstruction of CXCL1 expression confirms the finding illustrated in the **Figure 5**, highlighting the main localization of CXCL1 in the apical part of PCs (aPCs) followed by the basilar parts of inner PCs (bIPCs) and outer PCs (bOPCs) **(Bc')**. Scale bar, 25 μm. **(C)** PTS-causing acoustic trauma did not appreciably affect DARC positivity while causing reduction in CXCL1 positivity in the basal turn of PCs. Scale bar, 25 μm. The slides represent maximum projections of confocal z-stacks through whole mounts in the apical and basal region of the cochlea (~8 and 32 kHz region, respectively). Representative images are based on biological replicates in 4 control and 3 noise-exposed animals.

influenzae to model acute otitis media (16) revealed cytokine levels in cochlear tissue that were generally within the same order of magnitude as the cytokine levels that we measured in cochlear fluid. However, the precise absolute values differed, at least in part due to differences in techniques, mouse strains, animal age and experimental models. Notably, IL-1β, IL-6, and CXCL1 levels were elevated in both studies while the levels of several cytokines analyzed in our study were below the detection limits of the assay used by Trune et al. (15) (e.g., IL-4, IL-5, IL-12, IFN-γ) (16). Together, these studies highlight the importance of proinflammatory cytokines in mediating different cochlear pathologies.

Complementing our results in the auditory periphery, a recent study demonstrated that neuroinflammation in the

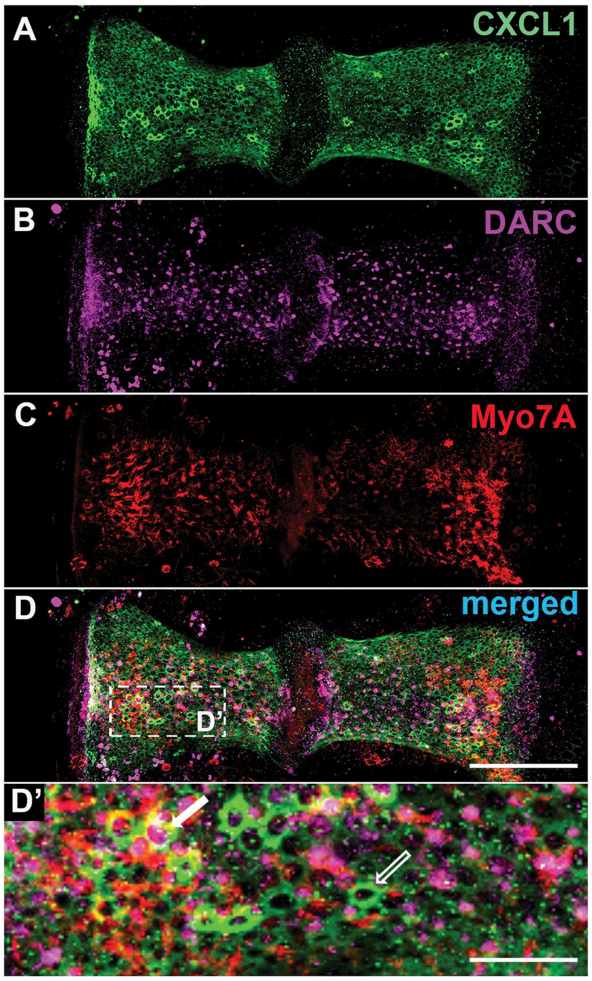

FIGURE 5 | Within the crista ampullaris, CXCL1 localizes to supporting cells while DARC preferentially localizes to a subset of hair cells. Whole mounts of the crista ampullaris of control mice stained with anti-CXCL1 (green) **(A)**, anti-DARC (magenta) **(B)**, and anti-Myo7A (red) **(C)** antibodies. CXCL1 is expressed in the polygonally-shaped supporting cells of the crista ampullaris (**A, D'**- an empty white arrow). Myo7A-positive hair cells are separated by intervening CXCL1-positive supporting cells. DARC-positive cells are scattered within the crista's epithelium, with predominant localization in the central zone of each hemicrista **(B)**, sometimes surrounded by CXCL1-positive supporting cells (a solid white arrow) **(D')**. Scale bars, 100 μm **(A–D)**, 25 μm **(D')**. The pictures represent maximum projections of confocal z-stacks through whole mounts, based on biological replicates in 4 control cochleae.

rodent auditory cortex following noise-induced hearing loss is associated with elevated tissue expression of proinflammatory cytokines, including TNF-α (36). Using genetic knockout and pharmacologic blockade of TNF-α, the authors conclude that targeting neuroinflammation may be a therapeutic strategy for tinnitus and other hearing loss-related disorders.

CXCL1 and DARC in Cochlear Physiology and Pathology

While this is the first detailed description of the cellular localization of CXCL1 (formerly known as KC or Gro-α) within the mammalian cochlea, prior studies that analyzed pooled inner ear tissue noted upregulation of CXCL1 mRNA during cochlear inflammation and development. Specifically, CXCL1 mRNA was upregulated in the inner ear tissue of mice with chronic otitis media, based on qRT-PCR analysis (37). Further, CXCL1 and IL-6 mRNA expression was upregulated, based on qRT-PCR, in the cochlear lateral wall during inflammation following the pharmacological inhibition of the cochlear mitochondrial respiratory chain in a rat model (19). Together with TNF-α, CXCL1 mRNA expression was also upregulated in inner ear tissue after cochlear implantation in guinea pigs (38). Finally, the bulk RNA-Seq data from the developing organ of Corti revealed CXCL1 gene expression in "surrounding cells" (i.e., the collectively analyzed non-hair cells) (39). In other tissues, CXCL1 expression was reported in neutrophils, macrophages, and epithelial cells (40, 41).

Our finding of CXCL1 expression in the pillar cells, Deiters cells, interdental cells, and vestibular supporting cells of control animals suggests constitutive CXCL1 expression in the inner ear under physiologic conditions, and implicates these cell types in immune and inflammatory regulation in the inner ear. Our finding of reduced CXCL1 expression in pillar cells coupled with the elevated CXCL1 levels in perilymph after acoustic trauma suggests CXCL1 release into perilymph after pathologic noise exposure that damages pillar cells. The noise-induced elevation of CXCL1 levels in perilymph could also reflect higher production in the cochlear microenvironment. Since macrophages did not express CXCL1 6 h after acoustic trauma, the CXCL1-positive supporting cells appear to be the main producers of CXCL1. Relevantly, both pillar and Deiters cells express transforming growth factor-β-activated kinase-1 (TAK1) (42), a potent activator of proinflammatory signaling pathways including p38 (43), which is necessary for the activation of CXCL1 gene expression (44). Because the main activators of TAK1 are IL-1β and TNF-α (45), it is possible that these cytokines, in part produced by activated macrophages after noise trauma, can initiate TAK1-mediated activation of p38 and the consequent upregulation of CXCL1 gene expression in supporting cells. This process could take place very early after noise-induced trauma, since we found upregulation on CXCL1 gene expression as early as 2 h after PTS-inducing acoustic trauma (**Supplementary Figure 5**).

Apart from its proinflammatory activity, CXCL1 may play a neuromodulatory role in the inner ear given the close proximity of nerve fibers within the organ of Corti and CXCL1-expressing supporting cells (**Figure 6**). This hypothesis is inspired by studies in the central nervous system where CXCL1 has been implicated in the development and maintenance of neuropathic pain (46), as well as in promoting axon myelination (47) and triggering the resolution of tissue injury (48). By binding to chemokine receptor CXCR2 (49) expressed by neurons, CXCL1 may change neuronal membrane properties by modulating the expression and activity of ion channels.

While we did not detect CXCR2 expression in the cochlea, we describe for the first time cell-specific expression of another CXCL1 receptor, DARC, in the inner ear. Though DARC is well-known as an erythrocyte antigen, acting as a receptor for

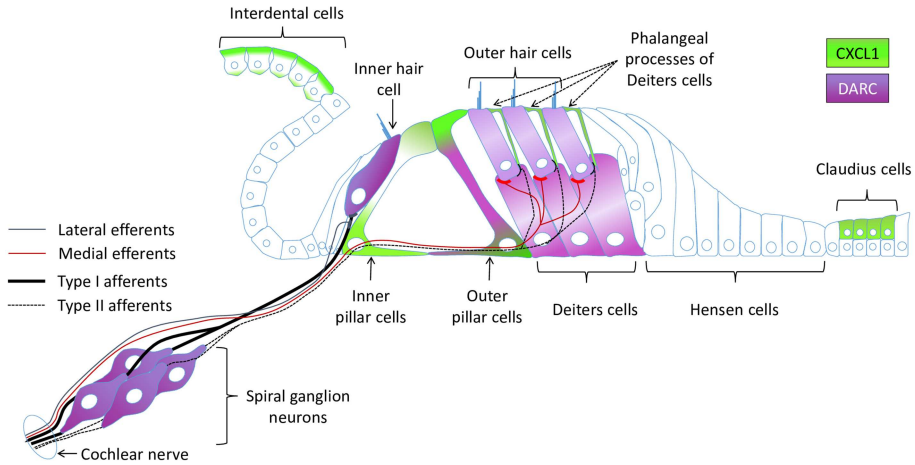

FIGURE 6 | A schematic of the cochlear epithelium summarizing expression of CXCL1 and DARC within the organ of Corti and surrounding cells.

malarial parasites (*Plasmodium vivax* and *Plasmodium knowlesi*), its primary function is the sequestration and transcytosis of chemokines (50). Together with other atypical chemokine receptors (ACKRs), DARC (ACKR1) has the ability to bind different CC, and CXC chemokines, including CXCL1, which DARC binds with the highest affinity (51). In addition to erythrocytes, DARC is predominantly expressed on venular endothelial cells of various tissues (52), and on some specialized cell types such as renal epithelial cells (53), Purkinje cells (54), and bone marrow macrophages (55). Here we report that DARC is expressed in the SGNs and inner ear sensorineural epithelium, primarily in the inner hair cells, outer pillar cells, and the third row of Deiters cells. While the precise physiological role of DARC in the inner ear remains to be determined, a recent study of *Darc* knockout mice reported that DARC deficiency affords improved hearing recovery after intense noise exposure when compared to wild type mice (56). However, we did not detect a striking difference in the immunostaining intensity for cellular distribution of DARC in unexposed vs. noise-exposed animals. Moreover, our finding that CXCL1 and DARC are expressed in the sensorineural epithelium and spiral ganglion neurons under steady state conditions suggests a non-inflammatory role of CXCL1 and DARC in cochlear physiology. Furthermore, the juxtaposition of the pillar cells and the inner hair cells as the two cell types brightly positive for CXCL1 and DARC, respectively, suggests that CXCL1/DARC interaction may be involved in their communication. Although DARC has been assumed not to mediate G protein-coupled receptor (GPCR) signaling upon chemokine binding (50), GPCR-independent activation of the ERK1/2 MAPK pathway was reported in airway smooth muscle cells after CXCL1/DARC interaction (57). It is interesting that the viability of outer hair cells is tightly influenced by ERK1/2 phosphorylation status in Deiters cells (58), which we find to express CXCL1 and DARC. Additionally, the expression of DARC in outer pillar cells, which abundantly express CXCL1 in their apical and basilar segments, implicates the transcytosis and sequestration of CXCL1 in pillar cells as a possible role of DARC.

CXCL1 as a Candidate Molecular Biomarker of Acute PTS

Our data suggest that CXCL1, potentially together with IL-6 and TNF-α, is a candidate molecular biomarker of acute PTS. The interplay between CXCL1 and IL-6 is known in other areas of the body, including upregulation of CXCL1 by IL-6 in the CNS (59), pancreatic acinar cells (60), and lung endothelium (61). TNF-α is also known to induce a marked release of CXCL1 in various cell types, including human vascular endothelial cells (62). Correspondingly, intraperitoneal injection of CXCL1 in mice induces TNF-α production (63). Moreover, TNF-α usually acts synergistically with IL-6 to enhance IL-6 secretion in human airway smooth muscle cells (64). However, IL-6 can elicit not only pro-, but also anti-inflammatory responses (65) and can increase the release of soluble TNF-α receptors (66).

Inflammaging

Our studies in young compared to old animals revealed different patterns of age-related cytokine changes in perilymph and blood. In contrast to blood, where almost all tested proinflammatory cytokines were upregulated in old animals, IL-1β and TNF-α levels were significantly decreased in the perilymph of control animals. The detected elevation of IL-1β, IL-6, and TNF-α in the blood of older animals is in line with "inflammaging," a phenomenon describing an age-related low-grade persistent increase in inflammatory molecules (67). However, the reduced levels of IL-1β and TNF-α in the perilymph of 2-year-old mice compared to adolescent mice suggests specialized mechanisms that regulate cytokine homeostasis in the inner ear with age. While Shi et al. (68) reported increased levels of IL-1β, IL-6, TNF-α, and IL-18 in the cochlear tissue of 1-year old mice compared to "young mice," the age of "young mice" is not specified and their "old" mice were half the age of our old mice. Moreover, Shi et al. (68) did not specify mouse strain, making it difficult to directly compare the two studies (68). Another explanation for our findings is that there is loss of sensorineural and other cells

in aging cochleae, resulting in fewer cells capable of releasing the detected cytokines.

Importantly, there is a correlation between cytokines and age-related hearing loss. A cohort study of 8,675 Japanese subjects revealed an association between hearing impairment and polymorphisms of genes encoding inflammatory mediators TNF-α and TNF receptor super family 1B (15). In mice, when comparing animals at 3 weeks and 3 months of age, increased expression of genes involved in the immune response (e.g., complement component 4, parts of immunoglobulins or *Ifit1*, interferon-induced protein with tetratricopeptide repeats) was noted at 3 months (69).

Translational Implications

Our data lend further support to the idea that cytokines represent potential therapeutic targets for several inner ear maladies, including noise-induced hearing loss (19). Small molecules targeting TNF-α have already been used in clinical trials to ameliorate different types of (SNHL) [reviewed by (70)]. Similarly, small molecules targeting IL-6 and CXCL1 pathways are currently being used in clinical trials for non-otologic diseases. Our data strongly motivate future studies to test the repurposing of these small molecules to combat noise-induced hearing loss. Clearly, those repurposing studies will have to be carefully designed to consider the complexities of cytokine hemostasis, as illustrated by a recent clinical observation that a TNF-α reduction and an IL-6 increase in serum strongly correlated with a good therapeutic response after corticosteroid therapy for idiopathic sudden SNHL (71). Interestingly, noise induces not only changes in levels of perilymphatic molecules but also in perilymphatic volume (72), suggesting additional targets for future clinical therapies.

Our demonstration of the feasibility of detecting noise-induced and age-related changes in protein profiles in as little as 0.5 μL of perilymph opens future possibilities for liquid biopsy of the human inner ear based on perilymph sampling. Given that the volume of human perilymph is about 150-fold larger than the volume of mouse perilymph, clinical translation of our approach is within reach, with a negligible risk of hearing loss due to sampling of sub-μL volume of perilymph. Eventual routine liquid biopsy of inner ear fluid would address a major unmet medical need, and usher in an era of accurate molecular diagnosis of SNHL to guide precise, personalized therapies.

MATERIALS AND METHODS

Mice

Wild-type CBA/CaJ mice were used because they have good cochlear sensitivity through most of their life. Mice (purchased from Jackson Laboratory, Bar Harbor, ME) of either sex were used in an estimated 50/50 ratio. They were randomly assigned to different noise exposure groups or to the control group at 6 weeks of age. Animal weight was comparable in all groups. Experiments were designed to typically have one mouse from each group housed in any given cage. When animals were not used for one of the interventions, they were kept in our animal care facility with *ad libitum* access to food and water. Ambient sound pressure levels in our animal care facility are in general under 40 dB SPL and peak noise levels do not exceed 70 dB SPL (73). A total of 100 mice were used to study the short- and long-term effects of noise exposure on cytokine levels in perilymph. Immunohistochemistry was performed on 4 control mice and 6 mice exposed to PTS-causing noise. All experiments were approved by the Institutional Animal Care and Use Committee at Massachusetts Eye and Ear.

Noise Exposures (94, 97, and 103 dB Sound Pressure Level)

Experiments were carried out as described in the publication from our laboratory that established the noise levels that cause neuropathic TTS, non-neuropathic TTS and PTS in the cochlear base, specifically the areas where tones with frequencies of ∼25 kHz and higher are processed (12). Briefly, mice were exposed for 2 h to an octave-band noise (8–16 kHz) at 94, 97, or 103 dB sound pressure level (SPL). Audio trauma was induced in the morning and the noise levels were calibrated with a microphone at the beginning of each session. The rodents were awake and could move freely in small cages under a horn in the exposure booth. Jensen et al. and other studies (12, 74) robustly and reproducibly documented the short and long-term effects of these noise levels on cochlear physiology and histology using the same equipment and mice of the same age and strain that we used here. Therefore, we did not replicate measurements of auditory function in the current study to avoid the potentially unfavorable effects of prolonged anesthesia (especially for the oldest animals) required to complete hearing tests prior to perilymph sampling.

Perilymph Collection

For perilymph sampling we used the approach developed by Salt's and Hirose's laboratories (34). Briefly, mice were anesthetized with ketamine (100 mg/kg i.p.) and xylazine (10 mg/kg i.p.); half of the initial dose was given as booster. After fixing the head in a stereotaxic frame (David Kopf Instruments, Tujunga, CA), a retroauricular incision was made. Using blunt dissection of the subcutaneous tissue and underlying muscles, the PSC was exposed. The area was dried with absorbent points (Kerr, Orange, CA) and a layer of cyanoacrylate glue (Permabond 101, Permabond, Pottstown, PA) was applied to seal the area to obtain an uncontaminated sample. After the glue had dried, a 30° House oval window pick (Bausch+Lomb, Rochester, NY) was used to perforate the layer of glue and then make a canalostomy into the PSC. As soon as perilymph started to flow through the canalostomy, a calibrated (5 μL) disposable micropipette (VWR, Radnor, PA) was placed on top of it (**Supplementary Figure 6** shows a schematic of perilymph sampling). The micropipettes had previously been marked to macroscopically indicate an estimate of the required sampling volume (0.5 μL for vestibular perilymph; 0.5 μL for cochlear perilymph; up to 5 μL for both types of CSF). Once the mark on the micropipette was reached, a 1 cm reticle with micrometer resolution (Carl Zeiss, Oberkochen, Germany) was used to quantify the exact volume of sampled perilymph under microscopic guidance. Because there is no physical separation of these types of liquid in the inner ear, the distinction between them is based on meticulous collection

and previous calculations by the Salt and Hirose laboratories. Only clear specimens were processed further; samples that were contaminated with blood were discarded. Using a tube with a syringe (included when buying the microcapillary pipettes) the sample was transferred into an Eppendorf tube (Eppendorf, Hamburg, Germany) that had been prefilled with 10 μL of double-filtered PBS (Millipore Sigma, Burlington, MA). The tube was sealed with parafilm (Bemis Company, Neenah, WI), immediately placed on ice and transferred into a −80°C freezer until further use. Usually, the left ear was processed first. Once finished, the canalostomy in the PSC was covered with glue, and the right ear was sampled next.

Cerebrospinal Fluid Collection

After bilateral specimen collection from the PSCs, CSF was collected from the cisterna magna as previously described (75). Briefly, the same disposable micropipettes as for perilymph sampling were pulled on a Sutter P-87 micropipette puller (Sutter instrument, Novato, CA) and trimmed with scissors to obtain a tip with an inner diameter of about 0.5 mm. A sagittal skin incision inferior to the occiput was made and subcutaneous tissue and muscles were separated. The skull over the dura magna was dried and the dura was penetrated with the microcapillary tube, which resulted in CSF filling the tube. The CSF specimen was then processed like the perilymph samples described above and stored in the −80°C freezer.

Blood Collection

As the final procedure for every animal, a blood sample was obtained by cardiac puncture after thoracotomy. The sample was transferred into a serum gel with a clotting activator tube (Sarstedt, Nümbrecht, Germany) and left standing upright at room temperature for 30 min. It was then spun down (10,000 g for 5 min) and the supernatant was transferred into an Eppendorf tube that was sealed with parafilm and stored at −80°C.

Immunoassay Based on Electrochemiluminescence

The V-PLEX Proinflammatory Panel 1 Mouse Kit (#K15048D, Meso Scale Discovery = MSD, Rockville, MD) was used to analyze the perilymph, CSF, and blood samples. It is an immunoassay based on electrochemiluminescence that quantifies the levels of the following cytokines: IFN-γ, IL-1β, IL-2, IL-4, IL-5, IL-6, CXCL1, IL-10, IL-12p70, and TNF-α. Briefly, samples and corresponding standards (calibrators) were added into wells of MSD MULTI-SPOT 96-well plates, pre-coated with capture antibodies, and incubated for 2 h at room temperature. Plates were washed three times with 150 μL/well of washing buffer, and 25 μL of detection antibody solution containing antibody conjugated with electrochemiluminescent labels (MSD SULFO-TAG) was applied into each well. Samples were incubated for an additional two h, then washed as described before, and treated with 2X Read Buffer T. Electrochemiluminescence was measured on the matching MSD SI2400 instrument. Concentration of cytokines was determined from electrochemiluminescence signals fitted to the calibration curve.

Whole Mount Preparation and Confocal Immunohistochemistry

Cochlear whole mounts were dissected and mounted as described previously (76). Immunofluorescent staining was carried out as reported (77). The following antibodies/stains at the specified concentrations were used: rabbit anti-Myosin 7A (Myo7A, #25-6790 Proteus Biosciences, Ramona, CA, 1:400), mouse anti-Myosin 7A (Myo7A, #138-1-S, Developmental Studies Hybridoma Bank, Iowa City, IA, 1:10), rabbit anti-GRO alpha (CXCL1) biotin (#NBP1-51188B, Novus Biologicals, Littleton, CO, 1:150), mouse anti-E-Cadherin (#610181 BD Biosciences, San Jose, CA, 1:200), sheep-anti DARC (#PA5-47861 Thermo Fisher Scientific, Waltham, MA, 1:25) Phalloidin (#A22283 Thermo Fisher Scientific, Waltham, MA, 1:200), Alexa Fluor 555 anti-mouse and Alexa Fluor 647 anti-rabbit (#A21422 and #A21245 Thermo Fisher Scientific, Waltham, MA, 1:1,000), Alexa Fluor 488 anti-sheep (#A-11015 Thermo Fisher Scientific, Waltham, MA, 1:400), Streptavidin, Alexa Fluor 488 (#S11223, Thermo Fisher Scientific, Waltham, MA, 1:200). For the quantification of inner and outer hair cell numbers before and after noise exposure, the same confocal microscopy settings were used (Leica SP5, Wetzlar, Germany). Images were obtained with 20x, 40x, and 63x objectives. The z-step size was 1.5–2 μm, and cells were counted over a distance of 300 μm.

Statistical Analysis

GraphPad PRISM (GraphPad Software Inc., La Jolla, CA) was used for all statistical analyses. For cytokine measurements, Bartlett's test was used to check for homoscedasticity. When variances among the groups were equal, one-way ANOVA was used to compare the groups. If ANOVA was significant ($p < 0.05$), pair-wise comparison was performed and Bonferroni correction was applied for multiple comparisons. When variances were not equal, Kruskal-Wallis test was used. If the test was significant ($p < 0.05$), Wilcoxon rank-sum test was applied, followed by Bonferroni correction. Composite graphs showing individual and average values were constructed using GraphPad PRISM.

DATA AVAILABILITY

All datasets generated for this study are included in the manuscript/**Supplementary Files**.

ETHICS STATEMENT

The animal study was reviewed and approved by Institutional Animal Care and Use Committee at Massachusetts Eye and Ear.

AUTHOR CONTRIBUTIONS

KMS conceived the project, designed experiments, and supervised all aspects of research. Perilymph samples were collected by LDL, TF, and VYS. Noise exposures were carried out by LDL and RS. Dissection of whole mounts was performed by LDL, SV, and RS. Immunohistochemical staining, confocal

microscopy, and image analysis was performed by SV. Perilymph samples were processed by LDL, SV, and LX. TF performed statistical analyses of perilymph samples. LDL, SV, and KMS wrote the manuscript with editorial input from all other authors.

FUNDING

This work was supported by the Department of Defense grant W81XWH-15-1-0472, National Institute on Deafness and Other Communication Disorders grant R01 DC015824, Nancy Sayles Day Foundation, Lauer Tinnitus Research Center, the Barnes Foundation, the Zwanziger Foundation, and by Sheldon and Dorothea Buckler (KMS).

SUPPLEMENTARY MATERIAL

The Supplementary Material for this article can be found online at: https://www.frontiersin.org/articles/10.3389/fneur.2019.00977/full#supplementary-material

REFERENCES

1. Wilson BS, Tucci DL, Merson MH, O'Donoghue GM. Global hearing health care: new findings and perspectives. *Lancet*. (2017) 390:2503–15. doi: 10.1016/S0140-6736(17)31073-5
2. Schiller JS, Lucas JW, Peregoy JA. Summary health statistics for U.S. Adults: national health interview survey, 2011. *Vital Health Stat*. (2012) 10:1–218. Available online at: https://www.cdc.gov/nchs/data/series/sr_10/sr10_256.pdf
3. Gates GA, Cooper JC Jr, Kannel WB, Miller NJ. Hearing in the elderly: the Framingham cohort, 1983–1985. Part I. Basic audiometric test results. *Ear Hear*. (1990) 11:247–56. doi: 10.1097/00003446-199008000-00001
4. WHO. *Hearing Loss Due to Recreational Exposure to Loud Sounds*. (2015). Available online at: https://apps.who.int/iris/bitstream/handle/10665/154589/9789241508513_eng.pdf?sequence=1&isAllowed=y (accessed August 25, 2019).
5. West JS, Low JC, Stankovic KM. Revealing hearing loss: a survey of how people verbally disclose their hearing loss. *Ear Hear*. (2016) 37:194–205. doi: 10.1097/AUD.0000000000000238
6. Iyer JS, Zhu N, Gasilov S, Ladak HM, Agrawal SK, Stankovic KM. Visualizing the 3D cytoarchitecture of the human cochlea in an intact temporal bone using synchrotron radiation phase contrast imaging. *Biomed Opt Express*. (2018) 9:3757–67. doi: 10.1364/BOE.9.003757
7. Iyer JS, Batts SA, Chu KK, Sahin MI, Leung HM, Tearney GJ, et al. Micro-optical coherence tomography of the mammalian cochlea. *Sci Rep*. (2016) 6:33288. doi: 10.1038/srep33288
8. Kujawa SG, Liberman MC. Acceleration of age-related hearing loss by early noise exposure: evidence of a misspent youth. *J Neurosci*. (2006) 26:2115–23. doi: 10.1523/JNEUROSCI.4985-05.2006
9. VA. *VA Research on HEARING LOSS*. (2016). Available online at: https://www.research.va.gov/pubs/docs/va_factsheets/HearingLoss.pdf (accessed August 25, 2019).
10. Ryan AF, Kujawa SG, Hammill T, Le Prell C, Kil J. Temporary and permanent noise-induced threshold shifts: a review of basic and clinical observations. *Otol Neurotol*. (2016) 37:e271–5. doi: 10.1097/MAO.0000000000001071
11. Kujawa SG, Liberman MC. Adding insult to injury: cochlear nerve degeneration after "temporary" noise-induced hearing loss. *J Neurosci*. (2009) 29:14077–85. doi: 10.1523/JNEUROSCI.2845-09.2009
12. Jensen JB, Lysaght AC, Liberman MC, Qvortrup K, Stankovic KM. Immediate and delayed cochlear neuropathy after noise exposure in pubescent mice. *PLoS ONE*. (2015) 10:e0125160. doi: 10.1371/journal.pone.0125160
13. Dinarello CA. Proinflammatory cytokines. *Chest*. (2000) 118:503–8. doi: 10.1378/chest.118.2.503
14. Satoh H, Firestein GS, Billings PB, Harris JP, Keithley EM. Proinflammatory cytokine expression in the endolymphatic sac during inner ear inflammation. *J Assoc Res Otolaryngol*. (2003) 4:139–47. doi: 10.1007/s10162-002-3025-7
15. Uchida Y, Sugiura S, Ueda H, Nakashima T, Ando F, Shimokata H. The association between hearing impairment and polymorphisms of genes encoding inflammatory mediators in Japanese aged population. *Immun Ageing*. (2014) 11:18. doi: 10.1186/s12979-014-0018-4
16. Trune DR, Kempton B, Hausman FA, Larrain BE, MacArthur CJ. Correlative mRNA and protein expression of middle and inner ear inflammatory cytokines during mouse acute otitis media. *Hear Res*. (2015) 326:49–58. doi: 10.1016/j.heares.2015.04.006
17. MacArthur CJ, Pillers DA, Pang J, Kempton JB, Trune DR. Altered expression of middle and inner ear cytokines in mouse otitis media. *Laryngoscope*. (2011) 121:365–71. doi: 10.1002/lary.21349
18. Fujioka M, Kanzaki S, Okano HJ, Masuda M, Ogawa K, Okano H. Proinflammatory cytokines expression in noise-induced damaged cochlea. *J Neurosci Res*. (2006) 83:575–83. doi: 10.1002/jnr.20764
19. Fujioka M, Okano H, Ogawa K. Inflammatory and immune responses in the cochlea: potential therapeutic targets for sensorineural hearing loss. *Front Pharmacol*. (2014) 5:287. doi: 10.3389/fphar.2014.00287
20. Kurabi A, Keithley EM, Housley GD, Ryan AF, Wong AC. Cellular mechanisms of noise-induced hearing loss. *Hear Res*. (2017) 349:129–37. doi: 10.1016/j.heares.2016.11.013
21. Wakabayashi K, Fujioka M, Kanzaki S, Okano HJ, Shibata S, Yamashita D, et al. Blockade of interleukin-6 signaling suppressed cochlear inflammatory response and improved hearing impairment in noise-damaged mice cochlea. *Neurosci Res*. (2010) 66:345–52. doi: 10.1016/j.neures.2009.12.008
22. Hu Y, Malone JP, Fagan AM, Townsend RR, Holtzman DM. Comparative proteomic analysis of intra- and interindividual variation in human cerebrospinal fluid. *Mol Cell Proteomics*. (2005) 4:2000–9. doi: 10.1074/mcp.M500207-MCP200
23. Nagaraj N, Mann M. Quantitative analysis of the intra- and inter-individual variability of the normal urinary proteome. *J Proteome Res*. (2011) 10:637–45. doi: 10.1021/pr100835s
24. Lysaght AC, Kao SY, Paulo JA, Merchant SN, Steen H, Stankovic KM. Proteome of human perilymph. *J Proteome Res*. (2011) 10:3845–51. doi: 10.1021/pr200346q
25. Lin H-C, Ren Y, Lysaght AC, Kao S-Y, Stankovic KM. Proteome of normal human perilymph and perilymph from people with disabling vertigo. *PLoS One*. (2019) 14:e0218292. doi: 10.1371/journal.pone.0218292
26. Shew M, Warnecke A, Lenarz T, Schmitt H, Gunewardena S, Staecker H. Feasibility of microRNA profiling in human inner ear perilymph. *Neuroreport*. (2018) 29:894–901. doi: 10.1097/WNR.0000000000001049
27. Schmitt H, Roemer A, Zeilinger C, Salcher R, Durisin M, Staecker H, et al. Heat shock proteins in human perilymph: implications for cochlear implantation. *Otol Neurotol*. (2018) 39:37–44. doi: 10.1097/MAO.0000000000001625
28. Schmitt HA, Pich A, Schroder A, Scheper V, Lilli G, Reuter G, et al. Proteome analysis of human perilymph using an intraoperative sampling method. *J Proteome Res*. (2017) 16:1911–23. doi: 10.1021/acs.jproteome.6b00986
29. Velardi A, Cooper MD. An immunofluorescence analysis of the ontogeny of myeloid, T, and B lineage cells in mouse hemopoietic tissues. *J Immunol*. (1984) 133:672–7.
30. Jackson SJ, Andrews N, Ball D, Bellantuono I, Gray J, Hachoumi L, et al. Does age matter? The impact of rodent age on study outcomes. *Lab Anim*. (2017) 51:160–9. doi: 10.1177/0023677216653984
31. Shaw TN, Houston SA, Wemyss K, Bridgeman HM, Barbera TA, Zangerle-Murray T, et al. Tissue-resident macrophages in the intestine are long lived and defined by Tim-4 and CD4 expression. *J Exp Med*. (2018) 215:1507–18. doi: 10.1084/jem.20180019
32. Bohne BA, Kimlinger M, Harding GW. Time course of organ of Corti degeneration after noise exposure. *Hear Res*. (2017) 344:158–69. doi: 10.1016/j.heares.2016.11.009

33. Frye MD, Zhang C, Hu BH. Lower level noise exposure that produces only TTS modulates the immune homeostasis of cochlear macrophages. *J Neuroimmunol*. (2018) 323:152–66. doi: 10.1016/j.jneuroim.2018.06.019
34. Hirose K, Hartsock JJ, Johnson S, Santi P, Salt AN. Systemic lipopolysaccharide compromises the blood-labyrinth barrier and increases entry of serum fluorescein into the perilymph. *J Assoc Res Otolaryngol*. (2014) 15:707–19. doi: 10.1007/s10162-014-0476-6
35. Gratton MA, Eleftheriadou A, Garcia J, Verduzco E, Martin GK, Lonsbury-Martin BL, et al. Noise-induced changes in gene expression in the cochleae of mice differing in their susceptibility to noise damage. *Hear Res*. (2011) 277:211–26. doi: 10.1016/j.heares.2010.12.014
36. Wang W, Zhang LS, Zinsmaier AK, Patterson G, Leptich EJ, Shoemaker SL, et al. Neuroinflammation mediates noise-induced synaptic imbalance and tinnitus in rodent models. *PLoS Biol*. (2019) 17:e3000307. doi: 10.1371/journal.pbio.3000307
37. MacArthur CJ, Hausman F, Kempton JB, Sautter N, Trune DR. Inner ear tissue remodeling and ion homeostasis gene alteration in murine chronic otitis media. *Otol Neurotol*. (2013) 34:338–46. doi: 10.1097/MAO.0b013e31827b4d0a
38. Zhang H, Stark G, Reiss L. Changes in gene expression and hearing thresholds after cochlear implantation. *Otol Neurotol*. (2015) 36:1157–65. doi: 10.1097/MAO.0000000000000787
39. Scheffer DI, Shen J, Corey DP, Chen ZY. Gene expression by mouse inner ear hair cells during development. *J Neurosci*. (2015) 35:6366–80. doi: 10.1523/JNEUROSCI.5126-14.2015
40. Becker S, Quay J, Koren HS, Haskill JS. Constitutive and stimulated MCP-1, GRO alpha, beta, and gamma expression in human airway epithelium and bronchoalveolar macrophages. *Am J Physiol*. (1994) 266:L278–86. doi: 10.1152/ajplung.1994.266.3.L278
41. Iida N, Grotendorst GR. Cloning and sequencing of a new gro transcript from activated human monocytes: expression in leukocytes and wound tissue. *Mol Cell Biol*. (1990) 10:5596–9. doi: 10.1128/MCB.10.10.5596
42. Parker MA, Jiang K, Kempfle JS, Mizutari K, Simmons CL, Bieber R, et al. TAK1 expression in the cochlea: a specific marker for adult supporting cells. *J Assoc Res Otolaryngol*. (2011) 12:471–83. doi: 10.1007/s10162-011-0265-4
43. Ninomiya-Tsuji J, Kishimoto K, Hiyama A, Inoue J, Cao Z, Matsumoto K. The kinase TAK1 can activate the NIK-I kappaB as well as the MAP kinase cascade in the IL-1 signalling pathway. *Nature*. (1999) 398:252–6. doi: 10.1038/18465
44. Kim C, Sano Y, Todorova K, Carlson BA, Arpa L, Celada A, et al. The kinase p38 alpha serves cell type-specific inflammatory functions in skin injury and coordinates pro- and anti-inflammatory gene expression. *Nat Immunol*. (2008) 9:1019–27. doi: 10.1038/ni.1640
45. Sakurai H. Targeting of TAK1 in inflammatory disorders and cancer. *Trends Pharmacol Sci*. (2012) 33:522–30. doi: 10.1016/j.tips.2012.06.007
46. Silva RL, Lopes AH, Guimaraes RM, Cunha TM. CXCL1/CXCR2 signaling in pathological pain: role in peripheral and central sensitization. *Neurobiol Dis*. (2017) 105:109–16. doi: 10.1016/j.nbd.2017.06.001
47. Karim H, Kim SH, Lapato AS, Yasui N, Katzenellenbogen JA, Tiwari-Woodruff SK. Increase in chemokine CXCL1 by ERbeta ligand treatment is a key mediator in promoting axon myelination. *Proc Natl Acad Sci USA*. (2018) 115:6291–6. doi: 10.1073/pnas.1721732115
48. Sawant KV, Poluri KM, Dutta AK, Sepuru KM, Troshkina A, Garofalo RP, et al. Chemokine CXCL1 mediated neutrophil recruitment: role of glycosaminoglycan interactions. *Sci Rep*. (2016) 6:33123. doi: 10.1038/srep33123
49. Tsai HH, Frost E, To V, Robinson S, Ffrench-Constant C, Geertman R, et al. The chemokine receptor CXCR2 controls positioning of oligodendrocyte precursors in developing spinal cord by arresting their migration. *Cell*. (2002) 110:373–83. doi: 10.1016/S0092-8674(02)00838-3
50. Nibbs RJ, Graham GJ. Immune regulation by atypical chemokine receptors. *Nat Rev Immunol*. (2013) 13:815–29. doi: 10.1038/nri3544
51. Chaudhuri A, Zbrzezna V, Polyakova J, Pogo AO, Hesselgesser J, Horuk R. Expression of the Duffy antigen in K562 cells. Evidence that it is the human erythrocyte chemokine receptor. *J Biol Chem*. (1994) 269:7835–8.
52. Thiriot A, Perdomo C, Cheng G, Novitzky-Basso I, McArdle S, Kishimoto JK, et al. Differential DARC/ACKR1 expression distinguishes venular from non-venular endothelial cells in murine tissues. *BMC Biol*. (2017) 15:45. doi: 10.1186/s12915-017-0381-7
53. Chaudhuri A, Nielsen S, Elkjaer ML, Zbrzezna V, Fang F, Pogo AO. Detection of Duffy antigen in the plasma membranes and caveolae of vascular endothelial and epithelial cells of non-erythroid organs. *Blood*. (1997) 89:701–12.
54. Horuk R, Martin AW, Wang Z, Schweitzer L, Gerassimides A, Guo H, et al. Expression of chemokine receptors by subsets of neurons in the central nervous system. *J Immunol*. (1997) 158:2882–90.
55. Hur J, Choi JI, Lee H, Nham P, Kim TW, Chae CW, et al. CD82/KAI1 maintains the dormancy of long-term hematopoietic stem cells through interaction with DARC-expressing macrophages. *Cell Stem Cell*. (2016) 18:508–21. doi: 10.1016/j.stem.2016.01.013
56. Edderkaoui B, Sargsyan L, Hetrick A, Li H. Deficiency of duffy antigen receptor for chemokines ameliorated cochlear damage from noise exposure. *Front Mol Neurosci*. (2018) 11:173. doi: 10.3389/fnmol.2018.00173
57. Al-Alwan LA, Chang Y, Rousseau S, Martin JG, Eidelman DH, Hamid Q. CXCL1 inhibits airway smooth muscle cell migration through the decoy receptor Duffy antigen receptor for chemokines. *J Immunol*. (2014) 193:1416–26. doi: 10.4049/jimmunol.1302860
58. Lahne M, Gale JE. Damage-induced activation of ERK1/2 in cochlear supporting cells is a hair cell death-promoting signal that depends on extracellular ATP and calcium. *J Neurosci*. (2008) 28:4918–28. doi: 10.1523/JNEUROSCI.4914-07.2008
59. Roy M, Richard JF, Dumas A, Vallieres L. CXCL1 can be regulated by IL-6 and promotes granulocyte adhesion to brain capillaries during bacterial toxin exposure and encephalomyelitis. *J Neuroinflammation*. (2012) 9:18. doi: 10.1186/1742-2094-9-18
60. Zhang H, Neuhofer P, Song L, Rabe B, Lesina M, Kurkowski MU, et al. IL-6 trans-signaling promotes pancreatitis-associated lung injury and lethality. *J Clin Invest*. (2013) 123:1019–31. doi: 10.1172/JCI64931
61. Ahuja N, Andres-Hernando A, Altmann C, Bhargava R, Bacalja J, Webb RG, et al. Circulating IL-6 mediates lung injury via CXCL1 production after acute kidney injury in mice. *Am J Physiol Renal Physiol*. (2012) 303:F864–72. doi: 10.1152/ajprenal.00025.2012
62. Lo HM, Lai TH, Li CH, Wu WB. TNF-alpha induces CXCL1 chemokine expression and release in human vascular endothelial cells *in vitro* via two distinct signaling pathways. *Acta Pharmacol Sin*. (2014) 35:339–50. doi: 10.1038/aps.2013.182
63. Vieira SM, Lemos HP, Grespan R, Napimoga MH, Dal-Secco D, Freitas A, et al. A crucial role for TNF-alpha in mediating neutrophil influx induced by endogenously generated or exogenous chemokines, KC/CXCL1, and LIX/CXCL5. *Br J Pharmacol*. (2009) 158:779–89. doi: 10.1111/j.1476-5381.2009.00367.x
64. McKay S, Hirst SJ, Haas MB, de Jongste JC, Hoogsteden HC, Saxena PR, et al. Tumor necrosis factor-alpha enhances mRNA expression and secretion of interleukin-6 in cultured human airway smooth muscle cells. *Am J Respir Cell Mol Biol*. (2000) 23:103–11. doi: 10.1165/ajrcmb.23.1.3765
65. Scheller J, Chalaris A, Schmidt-Arras D, Rose-John S. The pro- and anti-inflammatory properties of the cytokine interleukin-6. *Biochim Biophys Acta*. (2011) 1813:878–88. doi: 10.1016/j.bbamcr.2011.01.034
66. Tilg H, Trehu E, Atkins MB, Dinarello CA, Mier JW. Interleukin-6 (IL-6) as an anti-inflammatory cytokine: induction of circulating IL-1 receptor antagonist and soluble tumor necrosis factor receptor p55. *Blood*. (1994) 83:113–8. doi: 10.1016/1043-4666(94)90044-2
67. Nikolich-Zugich J. The twilight of immunity: emerging concepts in aging of the immune system. *Nat Immunol*. (2018) 19:10–19. doi: 10.1038/s41590-017-0006-x
68. Shi X, Qiu S, Zhuang W, Yuan N, Wang C, Zhang S, et al. NLRP3-inflammasomes are triggered by age-related hearing loss in the inner ear of mice. *Am J Transl Res*. (2017) 9:5611–8.
69. Gong TW, Karolyi IJ, Macdonald J, Beyer L, Raphael Y, Kohrman DC, et al. Age-related changes in cochlear gene expression in normal and shaker 2 mice. *J Assoc Res Otolaryngol*. (2006) 7:317–28. doi: 10.1007/s10162-006-0046-7
70. Ren Y, Stankovic KM. The role of tumor necrosis factor alpha (TNFα) in hearing loss and vestibular schwannomas. *Curr Otorhinolaryngol Rep*. (2018) 6:15–23. doi: 10.1007/s40136-018-0186-4
71. Tsinaslanidou Z, Tsaligopoulos M, Angouridakis N, Vital V, Kekes G, Constantinidis J. The expression of TNFα, IL-6, IL-2, and IL-8 in the

serum of patients with idiopathic sudden sensorineural hearing loss: possible prognostic factors of response to corticosteroid treatment. *Audiology and Neurotology Extra*. (2016) 6:9–19. doi: 10.1159/000442016

72. Kim J, Xia A, Grillet N, Applegate BE, Oghalai JS. Osmotic stabilization prevents cochlear synaptopathy after blast trauma. *Proc Natl Acad Sci USA*. (2018) 115:E4853–60. doi: 10.1073/pnas.1720121115
73. Liberman MC, Liberman LD, Maison SF. Efferent feedback slows cochlear aging. *J Neurosci*. (2014) 34:4599–607. doi: 10.1523/JNEUROSCI.4923-13.2014
74. Suzuki J, Corfas G, Liberman MC. Round-window delivery of neurotrophin 3 regenerates cochlear synapses after acoustic overexposure. *Sci Rep*. (2016) 6:24907. doi: 10.1038/srep24907
75. Liu L, Duff K. A technique for serial collection of cerebrospinal fluid from the cisterna magna in mouse. *J Vis Exp*. (2008) e960. doi: 10.3791/960
76. Landegger LD, Pan B, Askew C, Wassmer SJ, Gluck SD, Galvin A, et al. A synthetic AAV vector enables safe and efficient gene transfer to the mammalian inner ear. *Nat Biotechnol*. (2017) 35:280–4. doi: 10.1038/nbt.3781
77. Landegger LD, Dilwali S, Stankovic KM. Neonatal murine cochlear explant technique as an *in vitro* screening tool in hearing research. *J Vis Exp*. (2017) e55704. doi: 10.3791/55704

Conflict of Interest Statement: The authors declare that the research was conducted in the absence of any commercial or financial relationships that could be construed as a potential conflict of interest.

frontiers in Neurology

MINI REVIEW
published: 18 September 2019
doi: 10.3389/fneur.2019.00978

Biomarkers in Vestibular Schwannoma–Associated Hearing Loss

Luis Lassaletta[1,2,3]*, *Miryam Calvino*[1,2], *Jose Manuel Morales-Puebla*[1], *Pablo Lapunzina*[2,3,4], *Lourdes Rodriguez-de la Rosa*[2,3,5], *Isabel Varela-Nieto*[2,3,5] and *Victor Martinez-Glez*[2,3,4]

[1] Department of Otorhinolaryngology, La Paz University Hospital, Madrid, Spain, [2] IdiPAZ Research Institute, Madrid, Spain, [3] Centre for Biomedical Network Research on Rare Diseases (CIBERER), CIBER, Institute of Health Carlos III, Madrid, Spain, [4] Institute of Medical and Molecular Genetics (INGEMM), La Paz University Hospital, Madrid, Spain, [5] Institute for Biomedical Research "Alberto Sols" (IIBM), Spanish National Research Council-Autonomous University of Madrid (CSIC-UAM), Madrid, Spain

Vestibular schwannomas (VSs) are benign tumors composed of differentiated neoplastic Schwann cells. They can be classified into two groups: sporadic VS and those associated with neurofibromatosis type 2 (NF2). VSs usually grow slowly, initially causing unilateral sensorineural hearing loss (HL) and tinnitus. These tumors cause HL both due to compression of the auditory nerve or the labyrinthine artery and due to the secretion of different substances potentially toxic to the inner ear or the cochlear nerve. As more and more patients are diagnosed and need to be managed, we are more than ever in need of searching for biomarkers associated with these tumors. Owing to an unknown toxic substance generated by the tumor, HL in VS may be linked to a high protein amount of perilymph. Previous studies have identified perilymph proteins correlated with tumor-associated HL, including μ-Crystallin (CRYM), low density lipoprotein receptor-related protein 2 (LRP2), immunoglobulin (Ig) γ-4 chain C region, Ig κ-chain C region, complement C3, and immunoglobulin heavy constant γ 3. Besides, the presence of specific subtypes of heat shock protein 70 has been suggested to be associated with preservation of residual hearing. It has been recently demonstrated that chemokine receptor-4 (CXCR4) is overexpressed in sporadic VS as well as in NF2 tumors and that hearing disability and CXCR4 expression may be correlated. Further, the genetic profile of VS and its relationship with poor hearing has also been studied, including DNA methylation, deregulated genes, growth factors, and *NF2* gene mutations. The knowledge of biomarkers associated with VS would be of significant value to maximize outcomes of hearing preservation in these patients.

Keywords: vestibular schwannoma, neurofibromatosis type 2, biomarkers, hearing loss, perilymph, chemokine, heat shock protein, genotype

OPEN ACCESS

Edited by:
Toshihisa Murofushi, Teikyo University, Japan

Reviewed by:
Angel Batuecas-Caletrio, University of Salamanca Health Care Complex, Spain
Takeshi Tsutsumi, Tokyo Medical and Dental University, Japan

***Correspondence:**
Luis Lassaletta
lassalettaluis@gmail.com

Specialty section:
This article was submitted to Neuro-Otology, a section of the journal Frontiers in Neurology

Received: *11 June 2019*
Accepted: *27 August 2019*
Published: *18 September 2019*

Citation:
Lassaletta L, Calvino M, Morales-Puebla JM, Lapunzina P, Rodriguez-de la Rosa L, Varela-Nieto I and Martinez-Glez V (2019) Biomarkers in Vestibular Schwannoma–Associated Hearing Loss. Front. Neurol. 10:978. doi: 10.3389/fneur.2019.00978

INTRODUCTION

Vestibular schwannomas (VSs), previously termed acoustic neuromas, are non-malignant tumors composed of Schwann cells of the vestibulocochlear nerve (VIII cranial nerve), arising from either the internal auditory canal (IAC) or the cerebellopontine angle (CPA). They can be classified into two groups: sporadic VS and those associated with neurofibromatosis type 2 (NF2) (1). Most VSs

are sporadic (90%), with a combined lifetime risk of 1:1,000 for developing a unilateral tumor (1, 2). Nowadays, a higher rate of VS diagnosis has been described, due to incidental findings from magnetic resonance imaging (MRI) performed due to unrelated complaints (3).

The mortality rate of VS ranges from 0.2 to 1% (4). Due to their anatomic position, patients suffer from progressive hearing loss (90%) and tinnitus (>60%), with facial numbness (12%) and facial paralysis (6%) occurring mainly among patients with larger lesions. Balance dysfunction is often present, although <20% of patients manifest with vertigo symptoms (1, 2). VSs usually grow slowly, leading to unilateral sensorineural hearing loss (SNHL) and tinnitus, theoretically caused by compression of the auditory nerve (3) or by spasm or occlusion of the labyrinthine artery (5). Sudden SNHL may also be the clinical presentation in up to 22% of the cases (6). These tumors may cause hearing loss also due to the secretion of substances potentially toxic to the inner ear or the cochlear nerve (1, 7, 8).

Diagnosis of VS may be either from cranial MRI performed for unrelated complaints or, usually, due to unilateral hearing loss or tinnitus (1, 9).

Audiological tests including audiometry and auditory brainstem response are not reliable predictors of CPA pathology (10). As most patients with CPA tumors have a comparable set of symptoms and audiometric results, the diagnosis relies mainly on imaging. The gold standard for the diagnosis of VS is MRI with gadolinium (1). In the last years, improvements in technology and a higher accessibility to MRI have increased the number of diagnosed VSs (11).

Approximately three of each of the four VSs exhibit no growth, leading to an observation strategy (wait and scan). Mean growth is about 2–4 mm/year in growing tumors (12). The hearing status, the growth rate, the subject's age, and the surgeon's experience are the main factors when deciding between surgery (destructive or conservative) and gamma knife therapy (13). In recent years, gamma knife radiosurgery is becoming a more popular choice for subjects with growing small or medium tumors and useful hearing, while patients with large-size tumors usually undergo surgery (14).

As more and more patients are diagnosed and need to be managed, we are more than ever in need of searching for biomarkers associated with these tumors, in order to help with the choice of selecting between a "wait-and-scan" approach and surgery (15) aimed at reducing morbidity and increasing the hearing outcomes (4).

TABLE 1 | Proposed biomarkers of human VSs related to worse hearing.

CRYM	μ-Crystallin
FN1	Fibronectin 1
KRT10	Keratin 10
APOC3	Apolipoprotein C-III
VCAN	Versican
DCD	Dermcidin
SERPINB12	Serpin family B member 12
CTSD	Cathepsin D
SERPINB3	Serpin family B member 3
SERPINA5	Serpin family A member 5
SOD3	Superoxide dismutase 3, extracellular
PARK7	Parkinson disease protein 7
SERPINF1	Serpin family F member 1
CHI3L1	Cartilage glycoprotein 39
LRP2	Low-density lipoprotein receptor-related protein 2

Modified from Lysaght et al. (20).

BIOLOGICAL MARKERS

Due to the lack of biopsy sampling without the destruction of the organ, little is known about the cellular and molecular correlates in inner ear pathology (16).

In recent years, considerable progress in proteomics has been enabled by modern technology. By a shotgun proteomics approach, the identification of proteins with high sensitivity is enabled (17). Mass spectrometric (MS) analyses have been successfully used for auditory proteomics and require a more concerted effort for biomarker identification (18). In addition, sophisticated methods for perilymph sampling (19) have revolutionized the field of otology, offering precious biofluid samples for analysis.

Perilymph Proteome

Perilymph, an extracellular fluid of the inner ear, is found within the scala tympani and vestibuli of the cochlea. During an apoptotic or necrotic episode inside the inner ear, the proteins that are secreted can be found at high concentrations in this fluid (20). The knowledge of the perilymph proteome may shed some light on the mechanisms of tumor-associated hearing loss, which are mostly unknown to date (15). Stankovic et al. speculated that because of an unknown toxic substance generated by the VS, hearing loss in VS could be linked to a high protein concentration in the perilymph (7).

Perilymph Proteins Related to Hearing Loss

In 2011, Lysaght et al. identified 15 proteins from perilymph specimens (selected by comparing VS and cochlear implant samples) with differential expression and biological function. They suggested the use of this list in future research focused on distinguishing between better vs. worse hearing in patients with VS (see **Table 1**) (20).

μ-Crystallin (CRYM) or nicotinamide adenine dinucleotide phosphate (NADPH)-regulated thyroid hormone binding protein is located within the cytoplasm, where it promotes transcription of the thyroid hormone triiodothyronine (T3) (20, 21). *CRYM* gene mutations cause autosomal-dominant hearing loss due to changes in the intracellular localization and the inability to bind to T3, which may lead to an altered K+ recycling (20, 22).

Low density lipoprotein receptor-related protein 2 (LRP2) or megalin is a trans-membrane receptor protein, which can be found in certain epithelial cells such as those of the ear. LRP2 has the ability to bind several ligands, being essential in the

process of endocytosis of different elements such as sterols, lipoproteins, hormones, and vitamin binding proteins. Two well-known conditions, Donnai-Barrow and facio-oculo-acoustico-renal (FOAR) syndromes (23), both associated with SNHL, are the result of mutations in the *LRP2* gene (20).

On the other hand, of the 91 commonly identified perilymph proteins of patients with VS on an individual level, Rasmussen et al. described four proteins that were significantly associated with tumor-related deafness: Immunoglobulin (Ig) γ-4 chain C region, Ig κ chain C region, complement C3, and immunoglobulin heavy constant γ 3. These 91 proteins were identified in 12 out of 15 samples they used in the study (15), which was confirmed by analogy with data from previous MS research on perilymph (20, 24).

Moreover, alpha-2-HS-glycoprotein, a suggested inflammatory and immunological intermediary in perilymph, was suggested to be associated with deafness in patients with SVs. It was also discovered in samples from VS patients in 2017 (24), and although its concentration was not directly linked to the hearing outcomes, the authors attempted to further investigate this potential association. Rasmussen et al. hypothesized that VS may excrete alpha-2-HS-glycoprotein to the perilymph, where its inflammatory activity may lead to SNHL. Factors elicited from the VS may also affect the inner ear, inducing an upregulation of alpha-2-HS-glycoprotein within the perilymph (15).

Heat Shock Proteins and Hearing Loss

Heat shock proteins (HSPs) are stress proteins, which mediate cell survival under critical environmental conditions (25). Increased perilymph levels of 10 different subgroups of HSP were detected in subjects undergoing cochlear implantation that preserved hearing when compared with those without hearing preservation, and cochlear transcriptome data suggest that there is a baseline protective expression of HSP70 1A, 1B, 2, 4, 5, 6, 8, 9, and 12A mRNA (16).

HSP90 is the most important chaperone for cellular stress. It is involved in pathological processes, such as cancer development (26), and its increased expression as a stress responsive biomarker is present in multiple types of tissue inflammation (27).

Recently, Schmitt et al. found that HSP90 was determined in the perilymph of half of the patients ($n = 18$) experiencing complete loss of residual hearing loss after cochlear implantation, whereas only one of the patients with preserved residual hearing showed HSP90 in perilymph. The upregulation of HSP90 in the perilymph may therefore induce the migration of macrophages and leukocytes, resulting in cochlear inflammation. However, despite the cellular changes observed, the authors could not detect a significant difference in HSP90 expression in patients with VS compared with patients without tumor (16).

On the other hand, HSP70 has been identified as an otoprotective agent and protects hair cells from stress-induced apoptosis (28). Interestingly, the presence of some subtypes of HSP70 seemed to correlate with preservation of residual hearing in cochlear implantation (16). It has been associated with an increase in the cell proliferation rate (29) and, according to Schmitt et al., could take part in the development of VS, despite the authors not finding any correlation between HSP70 expression and VS when comparing with subjects without tumor (16). One explanation could be the low proliferation rate of these tumors; by contrast, medulloblastomas, fast-proliferating intracranial tumors with poor prognosis, showed an increased expression of HSP70 (29).

According to these findings, more data on the regulation of these proteins and perilymph proteomics are mandatory to demonstrate the role of these HSPs in patients with VS and hearing loss.

Increased Concentration of Perilymphatic Proteins and MRI Findings

Increased signal intensity of the fluid on three-dimensional fluid-attenuated inversion recovery (3D-FLAIR) MRI has been reported in various diseases, including SNHL, and VS (30–33). An increased concentration of proteins in the perilymphatic space has been proposed to explain the enhanced cochlear signal on FLAIR images in subjects with VS (34–37).

Kim et al. demonstrated a correlation between a higher cochlear signal on 3D FLAIR images and hearing loss in patients with VS (38). The correlation was stronger in intrameatal tumors when compared to all subjects, and no correlation was found when considering only CPA tumors. Interestingly, the cochlear signal intensity on MRI was significantly higher in tumors confined to the IAC.

Endolymphatic Hydrops

Ipsilateral inner ear alterations, including endolymphatic hydrops (EH) and acidophilic-staining precipitate, have been observed in temporal bone histopathological studies from patients with VS (5, 39). In the past years, intratympanic gadolinium injection has arisen as a new tool in the diagnosis of EH (40). Recently, delayed intravenous gadolinium-enhanced high-resolution MRI of the inner ear has been shown to provide resolution adequate for accurate detection of EH (41, 42). In addition, heavily weighted T2 sequences are useful to evaluate the cochlear fluids in patients with VS. In patients with a tumor entirely blocking the IAC, the volume of the vestibular endolymphatic space can be determined with great certainty. Venkatasamy et al. described a difference in the perilymphatic signal on a T2-weighted steady state free precession acquisition at 3T, providing a new tool for differentiating schwannomas and meningiomas (43). In patients with VS, a correlation between the endolymphatic space volume and the level of hearing loss has been described. Eliezer et al., using a 3D non-contrast T2 heavily weighted sequence at 3T, showed that the utricle volume was correlated with the patient's hearing loss in a series of 23 VSs. As most subjects with VS benefit from a wait-and-scan strategy, based on these MRI results, they suggest that a treatment leading to decreased EH could be administrated to achieve better hearing outcomes (44). In a recent paper (45), a saccular dilatation on the ipsilateral side was demonstrated in 30% of VSs (53 out of 183 patients with typical VS). In this study, a 3D non-contrast high-resolution T2-weighted sequence was used.

Tissue Sample Proteins

Cytokines and Hearing Loss

A large number of cytokines are produced by tumors (46) including VSs. To maintain the homeostasis in the cochlea, the cytokine balance is of vital importance (47). Like other substances, cytokines have been suggested to play a role in the labyrinth of degenerative changes (5). However, few studies have examined the role of these proteins in VS (48, 49).

Chemokine receptor-4 (CXCR4) is implicated in several pathological processes, including autoimmune disease, infection, and tumor development (50, 51). CXCR4 is overexpressed in many neoplasms, being capable of increasing tumor growth and invasiveness (52, 53).

C-X-C Motif Chemokine Ligand 12 (CXCL12), a ligand for CXCR4, cooperates with metastatic cells to CXCL12-expressing organs. The Ras/Raf/MEK and the PI3K/Akt/mTOR pathways can be activated by CXCL12 binding to the CXCR4 receptor. In a similar way, the loss of Merlin (52, 53), a tumor suppressor protein encoded by the *NF2* gene in VS (54), leads to activation of these two primary pathways.

Recently, Breun et al. have described that CXCR4 could play a role in the pathogenesis of both sporadic and NF2-associated VS. In their study CXCR4 was overexpressed in these tumors, with no significant differences found between the two groups. CXCR4 mRNA expression increased with the degree of hearing loss when compared with the control group, with the results lacking statistical difference (53).

Although tumor extension may be related to hearing impairment in VS (55), there is usually a discrepancy between tumor size and hearing disability (9). A reason why hearing disability is not always correlated with tumor dimensions could be an invasive growth pattern caused by CXCR4 overexpression in certain tumors. Indeed, Breun et al. detected no correlation between CXCR4 expression and tumor extension; therefore, this chemokine receptor may be significant for tumor invasiveness, as exhibited by hearing disability (53).

Molecular Biology

According to Celis-Aguilar et al.'s review (8), the molecular biology of VS could been explained by several pathogenic mechanisms including chromosome 22 loss, *NF2* gene mitotic recombination (56), DNA methylation (57), deregulation of genes (58), immunogenic factors (59), cytokines, and growth factors (60–62), and *NF2* gene mutation (63).

DNA Methylation

Epigenetic alterations are found across many solid cancers, and although most efforts in VS are limited to the controversial DNA methylation of the *NF2* gene, other changes have shown to play an important role in VS. Lassaletta et al. investigated the methylation status of 16 genes in 22 sporadic VSs and related it to clinical and radiological findings (57), the connection observed between *TP73* aberrant methylation and deafness being important [Pure Tone Average (PTA) = 43 and 17 dB for patients with methylated and unmethylated *TP73* genes, respectively]. A genome-wide methylation analysis in VS also showed a trend toward hypomethylation in several miRNAs and coding genes, including alternative transcripts, opening a window to possible therapeutic targets (64).

Deregulated Genes

In a study searching for associations between the molecular basis of VS and hearing loss (7), surgical specimens of these tumors from 13 patients were classified into two groups based on gene expression, one with good hearing (word recognition >70% and PTA $\leq$ 30 dB) and another with poor hearing. *PEX5L*, *RAD54B,* the prostate-specific membrane antigen-like gene, and *PSMAL* had low expression in VS patients with bad hearing outcomes. Besides, the *CEA-CAM7* gene and Carcinoembryonic Antigen (CEA) protein were overexpressed in VS patients with poor hearing (8).

Growth Factors

The development of VS has also been associated with abnormal expression of growth factors. In a study of tumor samples from 11 subjects with VS, Lassaletta et al. described an inverse correlation between the expression of platelet-derived growth factor A and deafness (65). On the other hand, vascular endothelial growth factors (VEGFs) have been associated with the hearing status of patients with VSs (66, 67). Most VSs express VEGF, and it has been suggested that this growth factor may play a role in both tumor growth and hearing status (68, 69). Bevacizumab, a VEGF neutralizing antibody, was used by Plotkin et al. to treat patients with VS, an increase in hearing reported in four out of seven subjects treated with this drug (67). In recent years, bevacizumab has been reported to increase speech understanding and hearing quality in several NF2 patients (68, 70).

NF2 Gene Mutation

NF2 gene mutations have been associated with the hearing level of patients with VS. In the study of Lassaletta et al., 51 cases undergoing surgery for VS were analyzed. Patients with *NF2* gene mutations presented lower PTA thresholds compared with nonmutated cases (71).

Selvanathan et a1. analyzed the impact of age of onset on the existence of several NF2-related symptoms, including hearing impairment or tinnitus, and found that there was a significantly younger age of onset of symptoms in patients with nonsense or frameshift mutation (i.e., mutations that produce protein truncation). They hypothesized that a younger age of onset of VS could explain the younger age of onset of hearing loss (and tinnitus) (72).

Halliday et al. proposed a genetic severity score (1, tissue mosaic; 2A, mild classic; 2B, moderate classic; and 3, severe) in order to predict morbidity for NF2 subjects in certain dimensions including hearing status (73). According to Emmanouil et al., if subjects were stratified according to genetic severity, it could help to obtain a better prognostication of the hearing decline. In their study, they described a significant difference in terms of hearing decline according to the genetic severity: the median age for subjects rated as "severe" was 32 years, compared to a median of 80 years for patients classified as "tissue mosaic" (74).

CONCLUSION

So far, no reliable methods are able to predict the evolution of hearing loss in subjects with VS. Several markers such as perilymph proteins have been associated with tumor hearing loss. Also, specific subtypes of HSP70 have been correlated with hearing outcomes. Cytokines produced by VS, especially CXCR4 expression, have been related to hearing impairment. DNA methylation, deregulated genes, growth factors, and *NF2* gene mutation have also been related to hearing loss in subjects with VS. Most of these potential markers of hearing loss are not routinely available for the clinician. On the other hand, recent findings on imaging, especially delayed intravenous gadolinium-enhanced high-resolution MRI, and 3D non-contrast heavily T2-weighted sequences are promising in terms of therapeutic management of patients with VS showing signs of EH. The precise knowledge of biomarkers associated with hearing loss in patients with VS would be useful to minimize morbidity and to maximize outcomes of hearing in these patients.

AUTHOR CONTRIBUTIONS

All authors listed have made a substantial, direct and intellectual contribution to the work, and approved it for publication.

FUNDING

This work was supported by a FEDER/Ministerio de Economía y Competitividad grant (SAF2017-86107-R) and by a Comunidad Autónoma de Madrid grant (B2017/BMD-3688).

REFERENCES

1. Kaul V, Cosetti MK. Management of vestibular schwannoma (including NF2): facial nerve considerations. *Otolaryngol Clin North Am.* (2018) 51:1193–212. doi: 10.1016/j.otc.2018.07.015
2. Schmidt RF, Boghani Z, Choudhry OJ, Eloy JA, Jyung RW, Liu JK. Incidental vestibular schwannomas: a review of prevalence, growth rate, and management challenges. *Neurosurg Focus.* (2012) 33:E4. doi: 10.3171/2012.7.Focus12186
3. Halliday J, Rutherford SA, McCabe MG, Evans DG. An update on the diagnosis and treatment of vestibular schwannoma. *Expert Rev Neurother.* (2018) 18:29–39. doi: 10.1080/14737175.2018.1399795
4. Sughrue ME, Yang I, Aranda D, Rutkowski MJ, Fang S, Cheung SW, et al. Beyond audiofacial morbidity after vestibular schwannoma surgery. *J Neurosurg.* (2011) 114:367–74. doi: 10.3171/2009.10.Jns091203
5. Roosli C, Linthicum FH Jr, Cureoglu S, Merchant SN. Dysfunction of the cochlea contributing to hearing loss in acoustic neuromas: an underappreciated entity. *Otol Neurotol.* (2012) 33:473–80. doi: 10.1097/MAO.0b013e318248ee02
6. Fujita T, Saito K, Kashiwagi N, Sato M, Seo T, Doi K. The prevalence of vestibular schwannoma among patients treated as sudden sensorineural hearing loss. *Auris Nasus Larynx.* (2018) 46:78–82. doi: 10.1016/j.anl.2018.06.008
7. Stankovic KM, Mrugala MM, Martuza RL, Silver M, Betensky RA, Nadol JB Jr, et al. Genetic determinants of hearing loss associated with vestibular schwannomas. *Otol Neurotol.* (2009) 30:661–7. doi: 10.1097/MAO.0b013e3181a66ece
8. Celis-Aguilar E, Lassaletta L, Torres-Martin M, Rodrigues FY, Nistal M, Castresana JS, et al. The molecular biology of vestibular schwannomas and its association with hearing loss: a review. *Genet Res Int.* (2012) 2012:856157. doi: 10.1155/2012/856157
9. Lassaletta L, Gavilan J. An update on the treatment of vestibular schwannoma. *Acta Otorrinolaringol Esp.* (2009) 60:131–40. doi: 10.1016/S2173-5735(09)70116-4
10. Tutar H, Duzlu M, Goksu N, Ustun S, Bayazit Y. Audiological correlates of tumor parameters in acoustic neuromas. *Eur Arch Otorhinolaryngol.* (2013) 270:437–41. doi: 10.1007/s00405-012-1954-2
11. Stangerup SE, Caye-Thomasen P. Epidemiology and natural history of vestibular schwannomas. *Otolaryngol Clin North Am.* (2012) 45:257–68, vii. doi: 10.1016/j.otc.2011.12.008
12. Nikolopoulos TP, Fortnum H, O'Donoghue G, Baguley D. Acoustic neuroma growth: a systematic review of the evidence. *Otol Neurotol.* (2010) 31:478–85. doi: 10.1097/MAO.0b013e3181d279a3
13. Pinna MH, Bento RF, Neto RV. Vestibular schwannoma: 825 cases from a 25-year experience. *Int Arch Otorhinolaryngol.* (2012) 16:466–75. doi: 10.7162/s1809-97772012000400007
14. Boari N, Bailo M, Gagliardi F, Franzin A, Gemma M, del Vecchio A, et al. Gamma Knife radiosurgery for vestibular schwannoma: clinical results at long-term follow-up in a series of 379 patients. *J Neurosurg.* (2014) 121(Suppl):123–42. doi: 10.3171/2014.8.Gks141506
15. Rasmussen JE, Laurell G, Rask-Andersen H, Bergquist J, Eriksson PO. The proteome of perilymph in patients with vestibular schwannoma. A possibility to identify biomarkers for tumor associated hearing loss? *PLoS ONE.* (2018) 13:e0198442. doi: 10.1371/journal.pone.0198442
16. Schmitt H, Roemer A, Zeilinger C, Salcher R, Durisin M, Staecker H, et al. Heat shock proteins in human perilymph: implications for cochlear implantation. *Otol Neurotol.* (2018) 39:37–44. doi: 10.1097/mao.0000000000001625
17. Darville LN, Sokolowski BH. In-depth proteomic analysis of mouse cochlear sensory epithelium by mass spectrometry. *J Proteome Res.* (2013) 12:3620–30. doi: 10.1021/pr4001338
18. Alawieh A, Mondello S, Kobeissy F, Shibbani K, Bassim M. Proteomics studies in inner ear disorders: pathophysiology and biomarkers. *Expert Rev Proteomics.* (2015) 12:185–96. doi: 10.1586/14789450.2015.1024228
19. Salt AN, Hale SA, Plonkte SK. Perilymph sampling from the cochlear apex: a reliable method to obtain higher purity perilymph samples from scala tympani. *J Neurosci Methods.* (2006) 153:121–9. doi: 10.1016/j.jneumeth.2005.10.008
20. Lysaght AC, Kao SY, Paulo JA, Merchant SN, Steen H, Stankovic KM. Proteome of human perilymph. *J Proteome Res.* (2011) 10:3845–51. doi: 10.1021/pr200346q
21. Mori J, Suzuki S, Kobayashi M, Inagaki T, Komatsu A, Takeda T, et al. Nicotinamide adenine dinucleotide phosphate–dependent cytosolic T(3) binding protein as a regulator for T(3)-mediated transactivation. *Endocrinology.* (2002) 143:1538–44. doi: 10.1210/endo.143.4.8736
22. Oshima A, Suzuki S, Takumi Y, Hashizume K, Abe S, Usami S. CRYM mutations cause deafness through thyroid hormone binding properties in the fibrocytes of the cochlea. *J Med Genet.* (2006) 43:e25. doi: 10.1136/jmg.2005.034397
23. Kantarci S, Al-Gazali L, Hill RS, Donnai D, Black GC, Bieth E, et al. Mutations in LRP2, which encodes the multiligand receptor megalin, cause Donnai-Barrow and facio-oculo-acoustico-renal syndromes. *Nat Genet.* (2007) 39:957–9. doi: 10.1038/ng2063
24. Schmitt HA, Pich A, Schroder A, Scheper V, Lilli G, Reuter G, et al. Proteome analysis of human perilymph using an intraoperative sampling method. *J Proteome Res.* (2017) 16:1911–23. doi: 10.1021/acs.jproteome.6b00986
25. Taldone T, Ochiana SO, Patel PD, Chiosis G. Selective targeting of the stress chaperome as a therapeutic strategy. *Trends Pharmacol Sci.* (2014) 35:592–603. doi: 10.1016/j.tips.2014.09.001
26. Haase M, Fitze G. HSP90AB1: helping the good and the bad. *Gene.* (2016) 575:171–86. doi: 10.1016/j.gene.2015.08.063

27. Poulaki V, Iliaki E, Mitsiades N, Mitsiades CS, Paulus YN, Bula DV, et al. Inhibition of Hsp90 attenuates inflammation in endotoxin-induced uveitis. *Faseb J.* (2007) 21:2113–23. doi: 10.1096/fj.06-7637com
28. Takada Y, Takada T, Lee MY, Swiderski DL, Kabara LL, Dolan DF, et al. Ototoxicity-induced loss of hearing and inner hair cells is attenuated by HSP70 gene transfer. *Mol Ther Methods Clin Dev.* (2015) 2:15019. doi: 10.1038/mtm.2015.19
29. Alexiou GA, Vartholomatos G, Stefanaki K, Patereli A, Dova L, Karamoutsios A, et al. Expression of heat shock proteins in medulloblastoma. *J Neurosurg Pediatr.* (2013) 12:452–7. doi: 10.3171/2013.7.Peds1376
30. Bhadelia RA, Tedesco KL, Hwang S, Erbay SH, Lee PH, Shao W, et al. Increased cochlear fluid-attenuated inversion recovery signal in patients with vestibular schwannoma. *AJNR Am J Neuroradiol.* (2008) 29:720–3. doi: 10.3174/ajnr.A0968
31. Lee IH, Kim HJ, Chung WH, Kim E, Moon JW, Kim ST, et al. Signal intensity change of the labyrinth in patients with surgically confirmed or radiologically diagnosed vestibular schwannoma on isotropic 3D fluid-attenuated inversion recovery MR imaging at 3 T. *Eur Radiol.* (2010) 20:949–57. doi: 10.1007/s00330-009-1626-9
32. Yamazaki M, Naganawa S, Kawai H, Nihashi T, Fukatsu H, Nakashima T. Increased signal intensity of the cochlea on pre- and post-contrast enhanced 3D-FLAIR in patients with vestibular schwannoma. *Neuroradiology.* (2009) 51:855–63. doi: 10.1007/s00234-009-0588-6
33. Yoshida T, Sugiura M, Naganawa S, Teranishi M, Nakata S, Nakashima T. Three-dimensional fluid-attenuated inversion recovery magnetic resonance imaging findings and prognosis in sudden sensorineural hearing loss. *Laryngoscope.* (2008) 118:1433–7. doi: 10.1097/MLG.0b013e318172ef85
34. Palva T, Raunio V. Cerebrospinal fluid and acoustic neurinoma specific proteins in perilymph93:201-3. *Acta Otolaryngol.* (1982) 93:201–3.
35. Rasmussen N, Bendtzen K, Thomsen J, Tos M. Antigenicity and protein content of perilymph in acoustic neuroma patients. *Acta Otolaryngol.* (1984) 97:502–8.
36. Silverstein H. Labyrinthine tap as a diagnostic test for acoustic neurinoma. *Otolaryngol Clin North Am.* (1973) 6:229–44.
37. Thomsen J, Saxtrup O, Tos M. Quantitated determination of proteins in perilymph in patients with acoustic neuromas. *ORL J Otorhinolaryngol Relat Spec.* (1982) 44:61–5. doi: 10.1159/000275574
38. Kim DY, Lee JH, Goh MJ, Sung YS, Choi YJ, Yoon RG, et al. Clinical significance of an increased cochlear 3D fluid-attenuated inversion recovery signal intensity on an MR imaging examination in patients with acoustic neuroma. *AJNR Am J Neuroradiol.* (2014) 35:1825–9. doi: 10.3174/ajnr.A3936
39. Hizli O, Cureoglu S, Kaya S, Schachern PA, Paparella MM, Adams ME. Quantitative vestibular labyrinthine otopathology in temporal bones with vestibular schwannoma. *Otolaryngol Head Neck Surg.* (2016) 154:150–6. doi: 10.1177/0194599815601070
40. Le CH, Truong AQ, Diaz RC. Novel techniques for the diagnosis of Meniere's disease. *Curr Opin Otolaryngol Head Neck Surg.* (2013) 21:492–6. doi: 10.1097/MOO.0b013e328364869b
41. Bernaerts A, Vanspauwen R, Blaivie C, van Dinther J, Zarowski A, Wuyts FL, et al. The value of four stage vestibular hydrops grading and asymmetric perilymphatic enhancement in the diagnosis of Meniere's disease on MRI. Neuroradiology. (2019) 61:421–9. doi: 10.1007/s00234-019-02155-7
42. Moayer R, Ishiyama GP, Karnezis S, Sepahdari AR, Ishiyama A. High resolution three-dimensional delayed contrast MRI detects endolymphatic hydrops in patients with vertigo and vestibular schwannoma. *Otol Neurotol.* (2018) 39:e39–44. doi: 10.1097/mao.0000000000001627
43. Venkatasamy A, Le Foll D, Karol A, Lhermitte B, Charpiot A, Debry C, et al. Differentiation of vestibular schwannomas from meningiomas of the internal auditory canal using perilymphatic signal evaluation on T2-weighted gradient-echo fast imaging employing steady state acquisition at 3T. *Eur Radiol Exp.* (2017) 1:8. doi: 10.1186/s41747-017-0012-7
44. Eliezer M, Poillon G, Maquet C, Gillibert A, Horion J, Marie JP, et al. Sensorineural hearing loss in patients with vestibular schwannoma correlates with the presence of utricular hydrops as diagnosed on heavily T2-weighted MRI. *Diagn Interv Imaging.* (2019) 100:259–68. doi: 10.1016/j.diii.2019.01.006
45. Karch-Georges A, Veillon F, Vuong H, Rohmer D, Karol A, Charpiot A, et al. MRI of endolymphatic hydrops in patients with vestibular schwannomas: a case-controlled study using non-enhanced T2-weighted images at 3 Teslas. *Eur Arch Otorhinolaryngol.* (2019) 276:1591–9. doi: 10.1007/s00405-019-05395-8
46. Lin WW, Karin M. A cytokine-mediated link between innate immunity, inflammation, and cancer. *J Clin Invest.* (2007) 117:1175–83. doi: 10.1172/jci31537
47. Adams JC. Clinical implications of inflammatory cytokines in the cochlea: a technical note. *Otol Neurotol.* (2002) 23:316–22. doi: 10.1097/00129492-200205000-00015
48. Hattermann K, Li G, Hugo HH, Mentlein R, Mehdorn HM, Held-Feindt J. Expression of the chemokines CXCL12 and CX3CL1 and their receptors in human nerve sheath tumors. *Histol Histopathol.* (2013) 28:1337–49. doi: 10.14670/hh-28.1337
49. Held-Feindt J, Rehmke B, Mentlein R, Hattermann K, Knerlich F, Hugo HH, et al. Overexpression of CXCL16 and its receptor CXCR6/Bonzo promotes growth of human schwannomas. *Glia.* (2008) 56:764–74. doi: 10.1002/glia.20651
50. Pozzobon T, Goldoni G, Viola A, Molon B. CXCR4 signaling in health and disease. *Immunol Lett.* (2016) 177:6–15. doi: 10.1016/j.imlet.2016.06.006
51. Bar-Shavit R, Maoz M, Kancharla A, Nag JK, Agranovich D, Grisaru-Granovsky S, et al. G protein–coupled receptors in cancer. *Int J Mol Sci.* (2016) 17:1320. doi: 10.3390/ijms17081320
52. Domanska UM, Kruizinga RC, Nagengast WB, Timmer-Bosscha H, Huls G, de Vries EG, et al. A review on CXCR4/CXCL12 axis in oncology: no place to hide. *Eur J Cancer.* (2013) 49:219–30. doi: 10.1016/j.ejca.2012.05.005
53. Breun M, Schwerdtfeger A, Martellotta DD, Kessler AF, Perez JM, Monoranu CM, et al. CXCR4: a new player in vestibular schwannoma pathogenesis. *Oncotarget.* (2018) 9:9940–50. doi: 10.18632/oncotarget.24119
54. Lim SH, Ardern-Holmes S, McCowage G, de Souza P. Systemic therapy in neurofibromatosis type 2. *Cancer Treat Rev.* (2014) 40:857–61. doi: 10.1016/j.ctrv.2014.05.004
55. Samii M, Matthies C. Management of 1000 vestibular schwannomas (acoustic neuromas): hearing function in 1000 tumor resections. *Neurosurgery.* (1997) 40:248–60; discussion 60–2.
56. Hadfield KD, Smith MJ, Urquhart JE, Wallace AJ, Bowers NL, King AT, et al. Rates of loss of heterozygosity and mitotic recombination in NF2 schwannomas, sporadic vestibular schwannomas and schwannomatosis schwannomas. *Oncogene.* (2010) 29:6216–21. doi: 10.1038/onc.2010.363
57. Lassaletta L, Bello MJ, Del Rio L, Alfonso C, Roda JM, Rey JA, et al. DNA methylation of multiple genes in vestibular schwannoma: relationship with clinical and radiological findings. *Otol Neurotol.* (2006) 27:1180–5. doi: 10.1097/01.mao.0000226291.42165.22
58. Caye-Thomasen P, Borup R, Stangerup SE, Thomsen J, Nielsen FC. Deregulated genes in sporadic vestibular schwannomas. *Otol Neurotol.* (2010) 31:256–66. doi: 10.1097/MAO.0b013e3181be6478
59. Archibald DJ, Neff BA, Voss SG, Splinter PL, Driscoll CL, Link MJ, et al. B7-H1 expression in vestibular schwannomas. *Otol Neurotol.* (2010) 31:991–7. doi: 10.1097/MAO.0b013e3181e40e4f
60. Niemczyk K, Vaneecloo FM, Lecomte MH, Lejeune JP, Lemaitre L, Skarzynski H, et al. Correlation between Ki-67 index and some clinical aspects of acoustic neuromas (vestibular schwannomas). *Otolaryngol Head Neck Surg.* (2000) 123:779–83. doi: 10.1067/mhn.2000.111356
61. Blair KJ, Kiang A, Wang-Rodriguez J, Yu MA, Doherty JK, Ongkeko WM. EGF and bFGF promote invasion that is modulated by PI3/Akt kinase and Erk in vestibular schwannoma. *Otol Neurotol.* (2011) 32:308–14. doi: 10.1097/MAO.0b013e318206fc3d
62. O'Reilly BF, Kishore A, Crowther JA, Smith C. Correlation of growth factor receptor expression with clinical growth in vestibular schwannomas. *Otol Neurotol.* (2004) 25:791–6. doi: 10.1097/00129492-200409000-00024
63. Martinez-Glez V, Franco-Hernandez C, Alvarez L, De Campos JM, Isla A, Vaquero J, et al. Meningiomas and schwannomas: molecular subgroup classification found by expression arrays. *Int J Oncol.* (2009) 34:493–504. doi: 10.3892/ijo_00000174
64. Torres-Martin M, Lassaletta L, de Campos JM, Isla A, Pinto GR, Burbano RR, et al. Genome-wide methylation analysis in vestibular schwannomas shows putative mechanisms of gene expression modulation and global hypomethylation at the HOX gene cluster. *Genes Chromosomes Cancer.* (2015) 54:197–209. doi: 10.1002/gcc.22232

65. Lassaletta L, Martinez-Glez V, Torres-Martin M, Rey JA, Gavilan J. cDNA microarray expression profile in vestibular schwannoma: correlation with clinical and radiological features. *Cancer Genet Cytogenet.* (2009) 194:125–7. doi: 10.1016/j.cancergencyto.2009.06.016
66. Koutsimpelas D, Stripf T, Heinrich UR, Mann WJ, Brieger J. Expression of vascular endothelial growth factor and basic fibroblast growth factor in sporadic vestibular schwannomas correlates to growth characteristics. *Otol Neurotol.* (2007) 28:1094–9. doi: 10.1097/MAO.0b013e31814b2787
67. Plotkin SR, Stemmer-Rachamimov AO, Barker FG 2nd, Halpin C, Padera TP, Tyrrell A, et al. Hearing improvement after bevacizumab in patients with neurofibromatosis type 2. *N Engl J Med.* (2009) 361:358–67. doi: 10.1056/NEJMoa0902579
68. Blakeley JO, Ye X, Duda DG, Halpin CF, Bergner AL, Muzikansky A, et al. Efficacy and biomarker study of bevacizumab for hearing loss resulting from neurofibromatosis type 2–associated vestibular schwannomas. *J Clin Oncol.* (2016) 34:1669–75. doi: 10.1200/jco.2015.64.3817
69. Wong HK, Lahdenranta J, Kamoun WS, Chan AW, McClatchey AI, Plotkin SR, et al. Anti–vascular endothelial growth factor therapies as a novel therapeutic approach to treating neurofibromatosis-related tumors. *Cancer Res.* (2010) 70:3483–93. doi: 10.1158/0008-5472.Can-09-3107
70. Huang V, Bergner AL, Halpin C, Merker VL, Sheridan MR, Widemann BC, et al. Improvement in patient-reported hearing after treatment with bevacizumab in people with neurofibromatosis type 2. *Otol Neurotol.* (2018) 39:632–8. doi: 10.1097/mao.0000000000001781
71. Lassaletta L, Torres-Martin M, Pena-Granero C, Roda JM, Santa-Cruz-Ruiz S, Castresana JS, et al. NF2 genetic alterations in sporadic vestibular schwannomas: clinical implications. *Otol Neurotol.* (2013) 34:1355–61. doi: 10.1097/MAO.0b013e318298ac79
72. Selvanathan SK, Shenton A, Ferner R, Wallace AJ, Huson SM, Ramsden RT, et al. Further genotype—phenotype correlations in neurofibromatosis 2. *Clin Genet.* (2010) 77:163–70. doi: 10.1111/j.1399-0004.2009.01315.x
73. Halliday D, Emmanouil B, Pretorius P, MacKeith S, Painter S, Tomkins H, et al. Genetic Severity Score predicts clinical phenotype in NF2. *J Med Genet.* (2017) 54:657–64. doi: 10.1136/jmedgenet-2017-104519
74. Emmanouil B, Houston R, May A, Ramsden JD, Hanemann CO, Halliday D, et al. Progression of hearing loss in neurofibromatosis type 2 according to genetic severity. *Laryngoscope.* (2019) 129:974–80. doi: 10.1002/lary.27586

Conflict of Interest Statement: The authors declare that the research was conducted in the absence of any commercial or financial relationships that could be construed as a potential conflict of interest.

frontiers in Neurology

ORIGINAL RESEARCH
published: 22 October 2019
doi: 10.3389/fneur.2019.01115

Early Development of Resident Macrophages in the Mouse Cochlea Depends on Yolk Sac Hematopoiesis

Ippei Kishimoto[1], *Takayuki Okano*[1]*, *Koji Nishimura*[1], *Tsutomu Motohashi*[2] and *Koichi Omori*[1]

[1] Department of Otolaryngology, Head and Neck Surgery, Graduate School of Medicine, Kyoto University, Kyoto, Japan, [2] Department of Tissue and Organ Development, Regeneration, and Advanced Medical Science, Graduate School of Medicine, Gifu University, Gifu, Japan

Resident macrophages reside in all tissues throughout the body and play a central role in both tissue homeostasis and inflammation. Although the inner ear was once believed to be "immune-privileged," recent studies have shown that macrophages are distributed in the cochlea and may play important roles in the immune system thereof. Resident macrophages have heterogeneous origins among tissues and throughout developmental stages. However, the origins of embryonic cochlear macrophages remain unknown. Here, we show that the early development of resident macrophages in the mouse cochlea depends on yolk sac hematopoiesis. Accordingly, our results found that macrophages emerging around the developing otocyst at E10.5 exhibited dynamic changes in distribution and *in situ* proliferative capacity during embryonic and neonatal stages. Cochlear examination in *Csf1r*-null mice revealed a substantial decrease in the number of Iba1-positive macrophages in the spiral ganglion and spiral ligament, whereas they were still observed in the cochlear mesenchyme or on the intraluminal surface of the perilymphatic space. Our results demonstrated that two subtypes of resident macrophages are present in the embryonic cochlea, one being Csf1r-dependent macrophages that originate from the yolk sac and the other being Csf1r-independent macrophages that appear to be derived from the fetal liver via systemic circulation. We consider the present study to be a starting point for elucidating the roles of embryonic cochlear resident macrophages. Furthermore, resident macrophages in the embryonic cochlea could be a novel target for the treatment of various inner ear disorders.

Keywords: resident macrophage, embryonic cochlea, Csf1r, Iba1, yolk sac, fetal liver, *in situ* proliferative capacity, immunohistochemistry

OPEN ACCESS

Edited by:
Isabel Varela-Nieto, Spanish National Research Council (CSIC), Spain

Reviewed by:
Masato Fujioka, Keio University, Japan
Florent Ginhoux, Singapore Immunology Network (Agency for Science, Technology and Research), Singapore

***Correspondence:**
Takayuki Okano
tokano@ent.kuhp.kyoto-u.ac.jp

Specialty section:
This article was submitted to Neuro-Otology, a section of the journal Frontiers in Neurology

Received: *30 July 2019*
Accepted: *07 October 2019*
Published: *22 October 2019*

Citation:
Kishimoto I, Okano T, Nishimura K, Motohashi T and Omori K (2019) Early Development of Resident Macrophages in the Mouse Cochlea Depends on Yolk Sac Hematopoiesis. Front. Neurol. 10:1115. doi: 10.3389/fneur.2019.01115

INTRODUCTION

Congenital hearing loss, which occurs in approximately one in one thousand newborns, is one of the many burdensome congenital anomalies or disabilities (1). In particular, cytomegalovirus (CMV) infection during the gestational period accounts for 15–21% of all congenital hearing loss cases (2). Although a large number of children develop hearing loss via congenital CMV infection every year, the detailed pathophysiology of CMV infection in the auditory pathway, including the cochlea, has not been fully understood. Moreover, no therapeutic treatment for congenital hearing loss due to prenatal viral infections, such as CMV or rubella virus, is currently present.

To elucidate the pathophysiological mechanisms and develop effective methods for treating cochlear damage due to intrauterine infection, understanding the immune system of the inner ear, especially during the embryonic period, is essential. The inner ear was once believed to be "immune-privileged" given that IgG concentrations in the perilymph was as low as that in the cerebrospinal fluid and no lymphatic drainage or lymphoid tissue was present inside the inner ear (3, 4). However, recent studies have revealed the presence of immune-competent cells in the cochlea, which are referred to as resident macrophages in the cochlea (5, 6). Tissue resident macrophages are distributed in virtually all tissues throughout the body and play a central role in both tissue homeostasis and inflammation, completing tissue-specific functions, and protecting the organs and tissue from infection (7, 8).

Regarding ontogeny of tissue resident macrophages, researchers have debated for decades whether resident macrophages were continuously and predominantly repopulated by blood-circulating monocytes, which arise from progenitors in the adult bone marrow (BM) (8). However, several studies have recently revealed that resident macrophages in the steady state have heterogeneous origin among tissues. The homeostatic contribution of circulating monocytes to macrophage populations seems to be restricted to a few specific tissues, including the gut, dermis, and heart, with a turnover rate unique to each tissue in the steady state (8–11). Alternatively, many resident macrophage populations arise from embryonic precursors that reside in these tissues prior to birth and maintain themselves locally throughout adulthood, independent of a major contribution from BM-derived precursors (8). In the steady state, resident macrophages in adult tissues have three major origins, including the yolk sac macrophage, fetal liver monocytes, and BM monocytes (8). As for the functional differences among macrophages derived from the three different origins, it is suggested that there might be some difference in gene expression of macrophages depending on their origins according to the study comparing the gene expression profiles in repopulated bone marrow-derived macrophages after genotoxic irradiation (12) or conditional depletion of macrophages (13). It is also reported that the capacity for self-maintenance (8) or the involvement to pancreatic tumor growth (14) is dominant in macrophages of embryonic origin, whereas the capacity to produce TNF during DSS-induced colitis (15) or Toxoplasma infection (16) is limited to macrophages derived from BM monocyte. However, difference in the role of macrophages of each origin are yet to be elucidated. The proportion of resident macrophages according to each origin differs depending on developmental stages and tissues. For example, most of the microglia in the brain come from the yolk sac macrophage, whereas macrophages from the other two origins contribute little in any stage of life (17). In contrast, although resident macrophages in the gut are derived from the yolk sac during the early embryonic stage, monocytes derived from the fetal liver subsequently comprise most of the resident macrophages in the gut at birth, with most of the resident macrophages ultimately being supplied by the BM during adulthood (8, 10). Regarding resident macrophages in the cochlea, previous reports have shown that at least part of the macrophages in the cochlea are recruited from BM precursors in the steady state (6, 18, 19), in local surgical stress (6), and after noise exposure (18) in adult mice. However, no studies have report the origins of embryonic cochlear macrophages.

The present study examined the development and distribution of resident macrophages in the developing mouse cochlea to elucidate the early spatial and temporal development of cochlear resident macrophages. Colony stimulating factor-1 (Csf1) signaling regulates the survival, proliferation, and differentiation of resident macrophages (20), while its receptor (Csf1 receptor, Csf1r) has been reported to be indispensable for macrophage development from fetal monocytes (17, 21). We therefore took advantage of *Csf1r-null* mice, focusing particularly on the origin and settlement of resident macrophages in the early stages of cochlear development.

MATERIALS AND METHODS

Animals

Pregnant female ICR mice at gestational day 9–19 and pups at postnatal day (P) 1–21 were purchased from Japan SLC, Inc. (Hamamatsu, Japan). *Csf1r*-null mice (22) were kindly provided by Dr. Issay Kitabayashi, National Cancer Center Japan, Tokyo, Japan. Genotyping for *Csf1r*-null allele was performed as previously reported (18). Transgenic mice carrying the Sox10-IRES-Venus allele were also bred as previously reported (23). All animals were maintained under conventional conditions at the Institute of Laboratory Animals, Kyoto University Graduate School of Medicine. All experimental protocols were approved by the Animal Research Committee, Kyoto University Graduate School of Medicine and conducted in accordance with the National Institutes of Health Guide for the Care and Use of Laboratory Animals.

Preparation of Frozen Sections

Fetal Mice

Under general anesthesia using medetomidine, midazolam, and medetomidine butorphanol, fetal mice from E9.5 to E17.5 were extracted from the uterus and immediately decapitated. Whole heads were immersed in 4% paraformaldehyde in phosphate buffer overnight at 4°C and then cryoprotected with 30% sucrose in phosphate buffered saline (PBS) overnight. Specimens were prepared as cryostat sections (10 μm in thickness). Midmodiolar sections were provided for histological analyses.

Neonatal Mice

Neonatal mice from P0 to P6 were decapitated soon after euthanization, and whole heads were immersed in 4% paraformaldehyde in phosphate buffer overnight at 4°C and then cryoprotected with 30% sucrose in PBS overnight. Specimens were prepared as cryostat sections (10 μm in thickness). Midmodiolar sections were provided for histological analyses.

Mice at P21

Under general anesthesia using medetomidine, midazolam, and medetomidine butorphanol, mice were perfused intracardially

with ice-cooled phosphate-buffered saline (PBS), followed by 4% paraformaldehyde in phosphate buffer. Temporal bones were collected and immersed in the same fixative for 4 h at 4°C. Samples were decalcified with 10% ethylenediaminetetraacetic acid in phosphate buffer and cryoprotected with 30% sucrose in PBS. Specimens were prepared as cryostat sections (10 μm in thickness). Midmodiolar sections were provided for histological analyses.

Immunohistochemistry

Cryostat sections were immersed in blocking solution containing 10% goat serum for 30 min and incubated with a primary antibody at 4°C overnight. Macrophages were labeled according to antibodies for ionized calcium-binding adapter molecule 1 (Iba1), which is specific for microglia/macrophages (24), CD11b, which is a monocyte/macrophage-specific glycoprotein, F4/80, which is a marker for resident macrophages (25), and macrosialin CD68, which is highly expressed in macrophages and other mononuclear phagocytes (26). Ki67 and Phosphohistone H3 (PHH3) were used as cell proliferation markers. The primary antibodies used herein included rabbit anti-Iba1 (1:1,000; Wako Pure Chemicals, Osaka, Japan), rat anti-F4/80 (1:2,000; A3-1; Bio-Rad Laboratories, Inc., Hercules, CA), rat anti-CD68 (1:1,000; FA-11; Serotec, Oxford, United Kingdom), rat anti-CD11b (1:500; M1/70; BD Biosciences, San Jose, CA, USA), rabbit anti-Ki67 (1:500; SP6; Thermo Fisher Scientific K.K., Tokyo, Japan), and mouse anti-pHH3 (1:200; 6G3; Cell Signaling Technology Japan, K.K., Tokyo, Japan) antibodies. Localization of primary antibodies was visualized using secondary antibodies conjugated with Alexa Fluor 488, 546, 633, or 647 (1:500; Molecular Probes, Invitrogen, Carlsbad, CA, USA). Cell nuclei and actin filaments were counterstained with 4′,6-diamidino-2-phenylindole dihydrochloride (DAPI; Invitrogen) and Alexa 633-labeled phalloidin (Invitrogen), respectively. Negative controls lacked primary antibody labeling. Fluorescent images were acquired using a Leica TCS SPE (Leica Microsystems, Wetzlar, Germany).

Data Analysis of Histological Samples

Quantification of Macrophage Subtypes and Proliferating Cells

After quantifying Iba1-, CD11b-, pHH3-, and Ki67-positive cells, each cell type was defined as follows. An Iba1-positive cell had both a nucleus and cell body that were positive for DAPI and Iba1 immunohistostaining, respectively. A CD11b-positive cell had both a nucleus and cell membrane that were positive for DAPI and CD11b immunohistostaining, respectively. A pHH3- or Ki67-positive cell had a nucleus that was positive for both DAPI and pHH3 or Ki67, respectively.

The proportion of pHH3 -positive cells in Iba1-positive cells and the proportion of Ki67-positive cells in F4/80-positive cells were defined as the number of cells double positive for pHH3 and Iba1 staining divided by the number of Iba1-positive cells and as the number of cells double positive for Ki67 and F4/80 staining divided by the number of F4/80-positive cells, respectively.

Cell Density of Iba1- or CD11b-Positive Cells

Cell density of Iba1- or CD11b-positive cells was defined as the number of Iba1- or CD11b-positive cells per square millimeter of the specimen. The whole area of the cochlea was defined as the inside area of the bony cochlea. The area of the bony cochlea, spiral ganglion, spiral ligament, and stria vascularis was determined through phalloidin and DAPI staining.

Cell density data of Iba1- or CD11b-positive cells from one mouse consisted of at least five inconsecutive specimen sections. Cell density in the spiral ganglion, spiral ligament, and stria vascularis was defined as the number of cells per 1 mm-square of the spiral ganglion, spiral ligament, or stria vascularis, whereas that in the cochlear mesenchyme and on the intraluminal surface of the perilymphatic space was defined as the number of cells per 1 mm-square of bony cochlea.

Statistical Analysis

Statistical analysis was performed using GraphPad Prism software (Prism 8 for Windows; GraphPad Software Inc., San Diego, CA). One-way analysis of variance (ANOVA) with Tukey's multiple comparisons test, Sidak's multiple comparisons test, or unpaired *t*-tests was used for parametric analyses. Results are presented as mean values ± standard errors. A two-tailed $p < 0.05$ was considered statistically significant.

RESULTS

Tissue Macrophage Emergence in the Mesenchyme Around the Developing Otocyst Between E9.5 and E10.5

Initially, emergence distribution of macrophages in the embryonic mouse cochlea was examined using immunohistochemistry for Iba1, CD68, and F4/80. In embryonic mice, resident macrophages appear at E10.5 in various tissues, including the brain (17) and skin (27). At E9.5, neither Iba1-, CD68-, nor F4/80-positive macrophages were observed around the otocyst (**Figures 1A,D,G**), whereas macrophage precursors labeled with Iba1, CD68, or F4/80 were observed in the yolk sac at E9.5 (**Figures 1B,E,H**). At E10.5, however, macrophages were observed around the otocyst labeled with either anti-Iba1, CD68, or F4/80 antibodies (**Figures 1C,F,I**). The aforementioned data indicate that resident macrophages migrate and settle in the mesenchyme surrounding the otocyst as early as E10.5. Moreover, hematopoiesis at E9.5 or E10.5 is thought to be mainly provided by yolk sac. Therefore, these results suggest that progenitors of cochlear resident macrophages could be supplied by the yolk sac given that primitive macrophages first appear in the blood islands of the mouse yolk sac at E9 and hematopoiesis in the fetal liver or aorta-gonad-mesonephron area starts from E10.5 onward (28).

Dynamic Changes in the Distribution of Resident Macrophages in the Developing Cochlea

We next examined the distribution of Iba1-positive macrophages in the developing cochlea following their emergence around

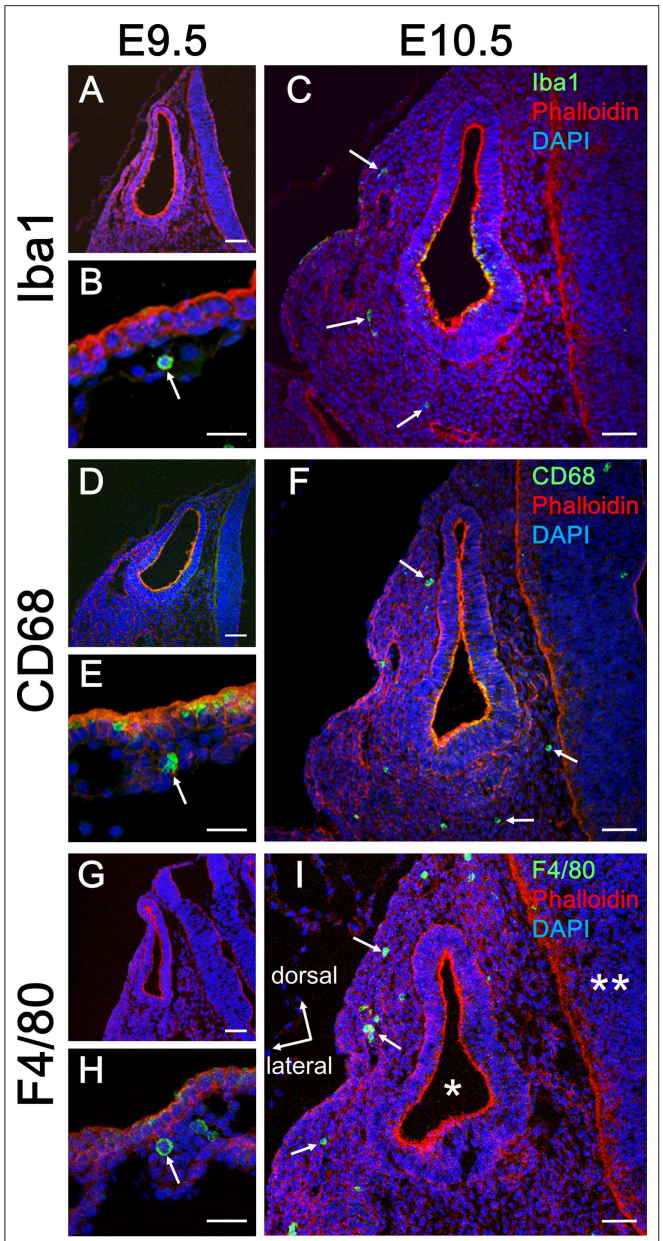

FIGURE 1 | Emergence of macrophages around the otocyst at E10.5. At E9.5, although no macrophages were observed around the otocyst, which were labeled according to macrophage marker, Iba1, CD68, or F4/80 **(A,D,G)**, they were observed in the yolk sac at the same period **(B,E,H)**. At E10.5, however, macrophages resided around the otocyst, which were labeled according to macrophage marker, Iba1, CD68, or F4/80 **(C,F,I**, arrows). Asterisk = otocyst; double asterisk = neural tube. Scale bars = 50 μm in **(A,C,D,F,G,I)** and 20 μm in **(B,E,H)**.

the otocyst at E10.5. In the developing embryonic cochlea from the period E13.5 to E15.5, Iba1-positive macrophages were observed in the cochlear mesenchyme (**Figures 2A,B**). During the perinatal, neonatal, and adult stages, Iba1-positive macrophages were widely distributed in the cochlea, particularly in the spiral ganglion, spiral ligament, and stria vascularis, as well as on the intraluminal surface of perilymphatic space or the mesenchyme (**Figures 2C,D**). Cell density of Iba1-positive macrophages varied depending on the region and embryonic stages (**Figures 2E–G**). It was 5.29 ± 5.29 at E14.5, 162 ± 23.6 at E15.5, 77.5 ± 16.7 at E17.5, 105 ± 50.8 at P0, 411 ± 36.6 at P3, 492 ± 49.9 at P6, and 513 ± 17.8 at P21 in the spiral ganglion (/mm^2, mean ± SEM), 550 ± 57.2 at E17.5, 628 ± 61.9 at P0, 666 ± 47.3 at P3, 438 ± 58.8 at P6, and 270 ± 37.3 at P21 in the spiral ligament (/mm^2, mean ± SEM), and 0 ± 0 at E17.5, 0 ± 0 at P0, 430 ± 41.5 at P3, 583 ± 96 at P6, and 356 ± 32 in the stria vascularis (/mm^2, mean ± SEM). The density of Iba1-positive cells in the spiral ganglion increased as developmental stages progressed, whereas the density of Iba1-positive macrophages in the spiral ligament achieved a peak at P3 and subsequently decreased during the neonatal stages (from P3 onward). On the other hand, Iba1-positive macrophages in the stria vascularis were observed only after birth and its peak was observed at neonatal stages. Statistical analyses demonstrated significant differences in Iba1-positive macrophage density among the developmental stages in each part of the cochlea, such as the spiral ganglion, spiral ligament, and stria vascularis (one-way ANOVA, $p < 0.0001$, $p = 0.0028$, and $p < 0.0001$, respectively). *Post-hoc* analysis using Sidak's multiple comparisons test between two sequential developmental stages showed significant changes in Iba1-positive macrophage density between E14.5 and E15.5 and between P0 and P3 in the spiral ganglion ($p = 0.0128$ and $p < 0.0001$, respectively) and between P0 and P3 and between P6 and P21 in the stria vascularis ($p = 0.0001$ and 0.0378, respectively). Taken together, the aforementioned data indicated dynamic changes in the distribution of cochlear resident macrophages depending on cochlear tissue area or developmental stages.

In situ Proliferation Capacity of Cochlear Resident Macrophages

Recent studies have shown that resident macrophages proliferate *in situ* and self-maintain locally (29, 30) in organs, such as the brain (31), lungs (29), and heart (7). However, studies have yet to determine whether cochlear resident macrophages proliferate *in situ*. Thus, we assessed the *in situ* proliferation capacity of cochlear resident macrophages. Accordingly, pHH3- and Ki67-positive macrophages were found in the developing cochlea at the embryonic and neonatal stages (**Figures 3A–H**). The percentage of pHH3-positive cells among Iba1-positive cells was <1% in the spiral ligament (**Figure 3I**), while no pHH3-positive cells among Iba1-positive cells were found in the spiral ganglion at any developmental stage (from E14.5 to P21). The percentage of pHH3-positive cells among Iba1-positive cells was 0.329 ± 0.329 at E17.5, 0.604 ± 0.361 at P0, 0.516 ± 0.284 at P3, and 0.00 ± 0.00 at P6 in the spiral ligament (%, mean ± SEM). The percentage of Ki67-positive cells among F4/80-positive cells achieved a peak at P0 in the spiral ganglion and at P3 in the spiral ligament (**Figures 3J,K**). It was 30.2 ± 6.99 at E17.5, 37.1 ± 5.92 at P0, 25.0 ± 5.01 at P3, 5.85 ± 1.52 at P6, and 3.84 ± 2.29 at P21 in the spiral ligament (%, mean ± SEM), and 20.7 ± 7.44 at E17.5, 26.0 ± 2.84 at P0, 41.3 ± 2.67 at P3, 16.6 ± 1.37 at P6, and 0.472 ± 0.472 at P21 in the spiral ganglion (%, mean ± SEM). Statistical analyses

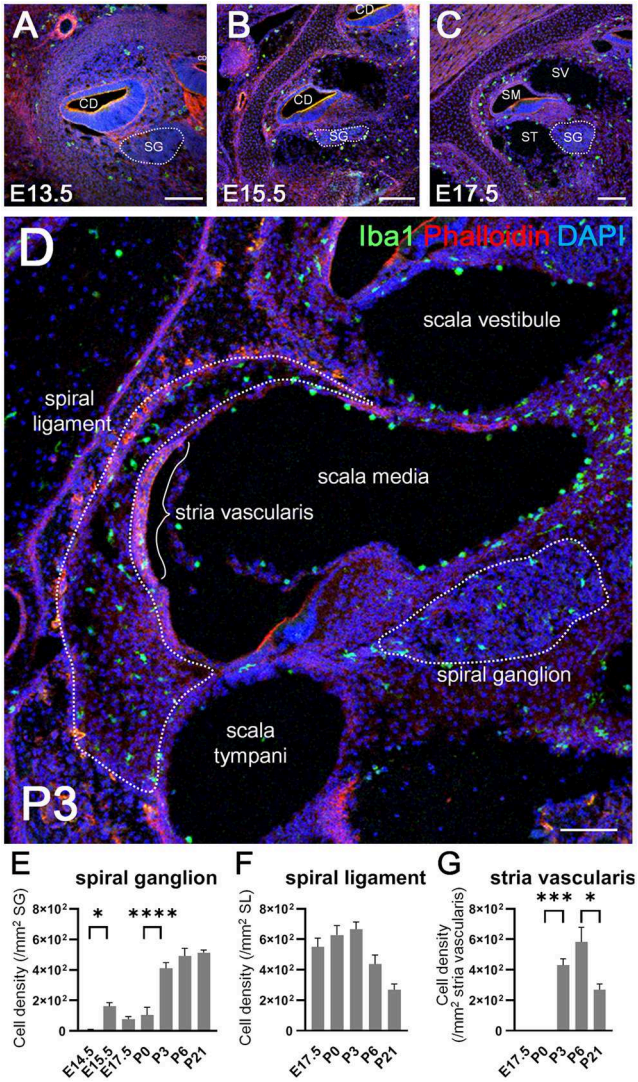

FIGURE 2 | Distribution and cell density of Iba1-positive macrophages in the cochlea at embryonic, neonatal, and adult stages. **(A–D)** Immunohistochemistry findings of the cochlea at E13.5 **(A)**, E15.5 **(B)**, E17.5 **(C)**, and P3 **(D)** using anti-Iba1 antibody. During the embryonic stages, Iba1-positive macrophages were distributed in the cochlear mesenchyme **(A,B)**. At E17.5 or P3, Iba1-positive macrophages were distributed widely in the cochlea, especially in the spiral ligament, spiral ganglion, and stria vascularis **(C,D)**. **(E–G)** Iba1-positive cell density in the spiral ganglion, spiral ligament, and stria vascularis at various developmental stages. In the spiral ganglion, Iba1-positive cell density increased as developmental stages progressed, whereas in the spiral ligament, the same achieved a peak at P3 and subsequently decreased during the neonatal stages (from P3 onward). On the other hand, Iba1-positive cell in the stria vascularis were observed only after birth and its peak was observed at neonatal stages. CD, cochlear duct; SG, spiral ganglion; SM, scala media; ST, scala tympani; SV, scala vestibuli. Scale bars = 100 μm. Statistical differences were assessed using one-way ANOVA with Sidak's multiple comparisons test. $^{*}p < 0.05$; $^{***}p = 0.001$; $^{****}p < 0.0001$.

showed no significant difference in the proportion of pHH3-positive cells among Iba1-positive macrophages across different developmental stages in the spiral ligament (one-way ANOVA, $p = 0.467$). In contrast, significant differences were observed in the proportion of Ki67-positive cells among F4/80-positive cells across developmental stages in both the spiral ligament and spiral ganglion (one-way ANOVA, $p = 0.0005$ and $p < 0.0001$, respectively). In the spiral ligament, significant differences were demonstrated in the proportion of Ki67-positive macrophages between E17.5 and P6 or P21 (Tukey's multiple comparisons test, $p = 0.0199$ or 0.0113, respectively), between P0 and P6 or P21 ($p = 0.0028$ or 0.0016, respectively) and between P3 and P21 ($p = 0.049$). In the spiral ganglion, significant differences in the proportion of Ki67-positive macrophages were observed between E17.5 and P3 or P21 (Tukey's multiple comparisons test, $p = 0.0124$ or 0.0142, respectively), between P0 and P21 ($p = 0.0021$), between P3 and P6 ($p = 0.0029$), and between P3 and P21 ($p < 0.0001$). The aforementioned data suggest that resident macrophages in the spiral ligament or spiral ganglion of developing cochlea have capacity for *in situ* proliferation and self-renewal.

Distinction Between Macrophages in the Embryonic Cochlea and Cell Population of Neural Crest Origin

A large population of perivascular cells has been reported to be present in the area around the blood-labyrinth barrier in the stria vascularis of the lateral cochlear wall in adult mice. The cells are identified as perivascular resident macrophages or perivascular-resident macrophage-like melanocytes given their positivity for several macrophage markers, including F4/80, CD68, and CD11b (19, 32). Considering that melanocytes are generally thought to originate from the neural crest, we examined whether macrophages that reside in the spiral ligament or spiral ganglion of the embryonic cochlea were derived from the neural crest. We took advantage of transgenic mice carrying the Sox10-IRES-Venus cassette to visualize the cell population of neural crest origin and compare it to CD68-positive macrophages. At E12.5 and E17.5, macrophages expressing CD68 in the embryonic cochlea were distinct from Sox10-Venus positive cells (**Figures 4A,B**). Although Sox10 not only marks neural crest-derived cells but also delaminating neuroblasts and otic placode-derived prosensory cells (23, 33), such data indicate that resident macrophages in the embryonic cochlea do not originate from the neural crest, while presumably cochlear resident macrophages expressing macrophage markers, including F4/80, CD68, or Iba1, observed in the spiral ligament and spiral ganglion were distinct from perivascular resident macrophages or perivascular-resident macrophage-like melanocytes.

Fetal Liver Hematopoiesis as an Alternative Source of Cochlear Macrophage Precursors

As mentioned previously, embryonic hematopoiesis is first established in yolk sac at E9 followed by migration of hematopoietic progenitors into the fetal liver from E10.5 onward. Therefore, the distribution of CD11b-positive cells in the developing cochlea were subsequently examined to determine

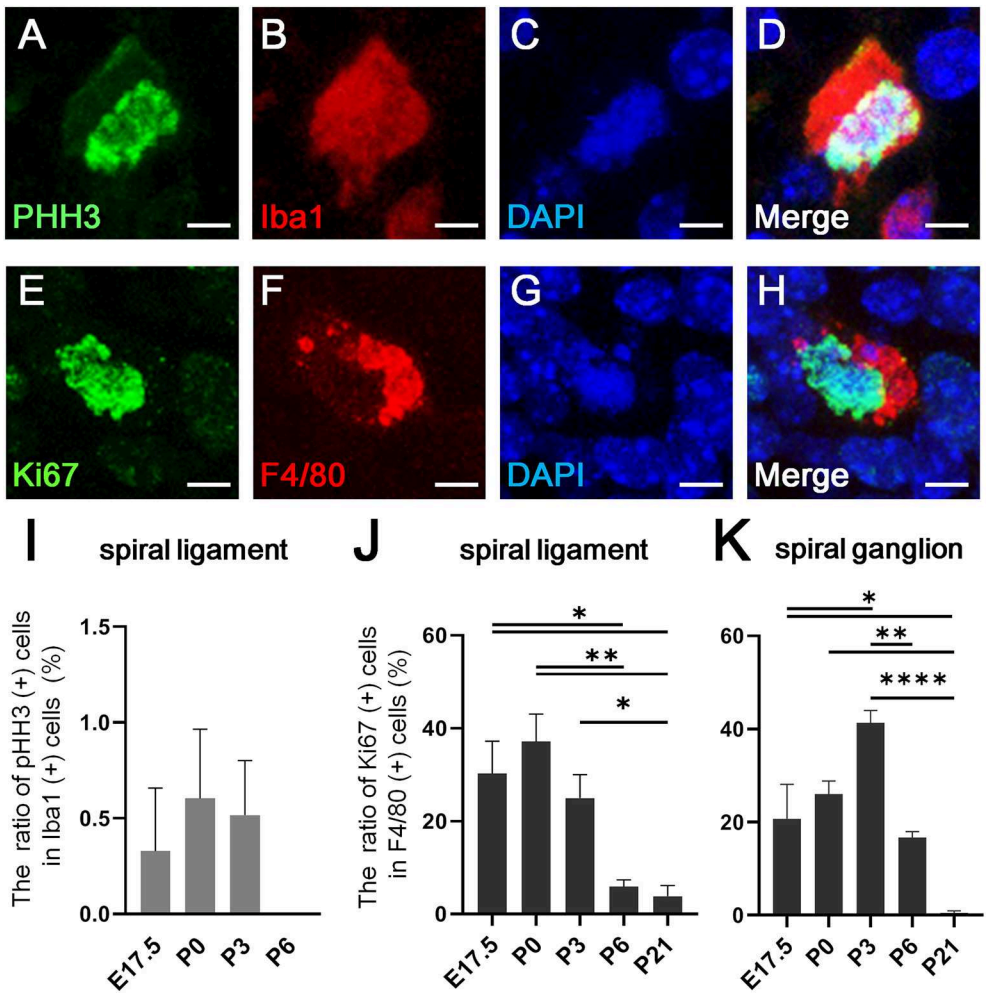

FIGURE 3 | *In situ* proliferative capacity of resident macrophages in the cochlea. **(A–D)** A typical cell double-positive for pHH3 and Iba1, which was found in the cochlear mesenchyme at E13.5, is shown by immunostaining for pHH3 **(A)**, Iba1 **(B)**, DAPI **(C)**, and Merge **(D)**. **(E–H)** A typical cell double-positive for Ki67 and F4/80, which was also found in the cochlear mesenchyme at E13.5, is shown by immunostaining for Ki67 **(E)**, F4/80 **(F)**, DAPI **(G)**, and Merge **(H)**. **(I)** The proportion of pHH3 and Iba1 double-positive cells among Iba1-positive cells in the spiral ligament. **(J,K)** The proportion of Ki67 and F4/80 double-positive cells among F4/80-positive cells in the spiral ligament **(J)** and spiral ganglion **(K)**. SL, spiral ligament; SG; spiral ganglion. Scale bars = 10 μm in **(A–H)**. Statistical differences were assessed using one-way ANOVA with Tukey's multiple comparisons test. $^{*}p < 0.05$; $^{**}p < 0.01$; $^{****}p < 0.0001$.

whether fetal liver hematopoiesis could serve as a source of resident macrophage precursors (34). Unlike Iba1-, CD68-, or F4/80-positive cells, CD11b-positive cells were rarely found around the otocyst or the cochlea by E13.5. Moreover, a few CD11b-positive cells were observed in the cochlear mesenchyme from E14.5 onward (**Figure 5A**). At E17.5, the embryonic stage at which the perilymphatic space was clearly formed, CD11b-positive cells were found in the cochlear mesenchyme around the cochlear modiolus, especially in the apical turn, or on the intraluminal surface of the scala tympani and scala vestibuli (**Figures 5B,C**). At P21, CD11b-positive cells were mainly observed on the intraluminal surface of the scala tympani and scala vestibuli (**Figure 5D**). The distribution of CD11b-positive cells demonstrated a unique pattern distinct from that of Iba1-, CD68-, or F4/80-positive cells. Thus, the aforementioned data suggest that fetal liver homeostasis could serve as an alternative source of cochlear macrophage precursors.

Transition of Cochlear Macrophage Phenotype From Fetal Liver-Derived Circulating Monocyte Precursors to Tissue Resident Macrophages

The findings regarding the distribution of CD11b-positive cells in the developing cochlea led us to hypothesize that CD11b-positive precursors derived from fetal liver also settle and differentiate as tissue resident macrophages in the cochlea. To assess distribution differences between cochlear resident macrophages and precursors derived from the fetal liver, we next performed double immunostaining for Iba1 and CD11b using developing cochleae. As expected from the results presented in **Figures 2**,

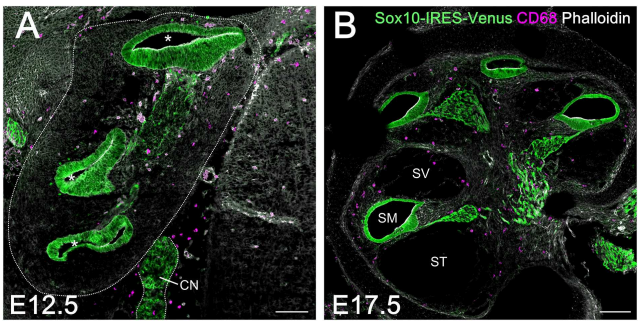

FIGURE 4 | Comparison between resident macrophages and cell population of neural crest origin in the embryonic cochlea using Sox10-IRES-Venus mice. Macrophages expressing CD68 in the embryonic cochlea were distinct from Sox10-Venus positive cells at E12.5 **(A)** and E17.5 **(B)**, indicating that resident macrophages in the embryonic cochlea did not originate from the neural crest. A dotted line shows the lateral edge of the cochlea. Asterisks, cochlear duct; CN, cochlear nerve; SM, scala media; ST, scala tympani; SV, scala vestibuli. Scale bars = 100 μm.

5, the spatial distribution patterns of Iba1- and CD11b-positive cells were totally distinct from each other (**Figure 6A**). However, some cochlear macrophages expressed both Iba1 and CD11b (**Figures 6A,F–I**). The aforementioned data suggest that at least three types of monocytes/macrophage linage cells are present in the cochlea: Iba1 or CD11b single-positive cells (**Figures 6A–E**), Iba1, and CD11b double-positive cells (**Figures 6A,F–I**). Our data also imply the possibility for direct transition of macrophage phenotype from CD11b-positive macrophage precursors to Iba1-positive macrophages. Moreover, Iba1, and CD11b double-positive cells were exclusively observed in the mesenchyme of the cochlear modiolus or on the intraluminal surface of perilymphatic space at any developmental stage between E14.5 and P21 (**Figures 6A,J–L**).

Essential Role of Csf1 Signaling in Cochlear Resident Macrophage Development and the Independent Contribution of Fetal Liver Hematopoiesis to Monocyte Precursors in the Cochlear Modiolus

According to the results of previous studies, the development of macrophages originating from the yolk sac largely depend on Csf1 signaling, whereas the development of fetal liver monocytes is independent of Csf1 signaling (17, 21, 34). To study the role of Csf1 signaling or yolk sac hematopoiesis in the development of cochlear resident macrophages and their precursors, we took advantage of *Csf1r*-null mice (22) and assessed the distribution of Iba1- and CD11b-positive cells in the cochlea at E17.5. While Iba1-positive macrophages were widely distributed over the entire cochlea of wildtype mice (**Figure 7A**), fewer Iba1-positive macrophages were observed in the mesenchyme of cochlear modiolus or the intraluminal surface of perilymphatic space in *Csf1r*-null mice (**Figure 7B,J,K,M,N**). Particularly in the spiral ganglion and spiral ligament, no Iba1-positive macrophages were found in the cochlea of *Csf1r*-null mice (**Figures 7D,E,G,H**). Cell density of Iba1-positive macrophages at E17.5, in wildtype and *Csf1r*-null mice, respectively, was 146 ± 11.3 and 5.13 ± 0.516 in the entire cochlea (/mm2, mean ± SEM), 49.3 ± 4.17 and 0.00 ± 0.00 in the spiral ganglion (/mm2, mean ± SEM), 594 ± 65.6 and 0.00 ± 0.00 in the spiral ligament (/mm2, mean ± SEM), 52.3 ± 7.26 and 4.20 ± 0.428 in mesenchyme cochlear modiolus (/mm2, mean ± SEM), and 11.6 ± 0.559 and 1.60 ± 0.769 on the intraluminal surface of perilymphatic space (/mm2, mean ± SEM). Statistical analysis showed that *Csf1r*-null mice had significantly lower Iba1-positive cell density than wildtype mice in the entire cochlea (unpaired *t*-test, $p < 0.0001$) (**Figure 7C**) and in any region, including the spiral ganglion, spiral ligament, mesenchyme of cochlear modiolus, and intraluminal surface of perilymphatic space ($p < 0.0001$, $p = 0.0001$, $p = 0.0006$, and $p < 0.0001$, respectively) (**Figures 7F,I,L,O**). In contrast, the distribution of cochlear CD11b-positive cells in *Csf1r*-null mice demonstrated a spatial pattern identical to that in wildtype mice. In both wildtype and *Csf1r*-null mice, CD11b-positive cells were observed on the intraluminal surface of the perilymphatic space or in the mesenchyme of the cochlear modiolus (**Figures 8A–D**). Cell density of CD11b-positive cells at E17.5, in wildtype and *Csf1r*-null mice, respectively, was 7.44 ± 1.81 and 6.54 ± 1.68 in the mesenchyme of cochlear modiolus (/mm2, mean ± SEM), 1.68 ± 0.300 and 0.845 ± 0.201 on the intraluminal surface of the perilymphatic space (/mm2, mean ± SEM), and 9.12 ± 1.98 and 7.38 ± 1.53 in the entire cochlea (/mm2, mean ± SEM). Statistical analysis showed that no significant difference in the density of CD11b-positive cells between wildtype and *Csf1r*-null mice in the mesenchyme of the cochlear modiolus, intraluminal surface of the perilymphatic space, and entire cochlea (unpaired *t*-test, $p = 0.731$, 0.066, and 0.5281, respectively) (**Figure 8E**). Taken together, Csf1 signaling plays an essential role in the development of cochlear resident macrophages originating from the yolk sac. Meanwhile, fetal liver hematopoiesis seems to contribute to monocyte precursors in the cochlear modiolus independent of Csf1 signaling.

DISCUSSION

The present study revealed that resident macrophages in mice emerge around the otocyst at as early as E10.5. Resident macrophages were distributed in the cochlear mesenchyme during the embryonic stages and subsequently located particularly in the spiral ligament, spiral ganglion, and stria vascularis in the postnatal cochlea. The density of the cochlear macrophages increased as mice grew, peaked around the neonatal stages, and decreased from P3 onward. In addition, cochlear macrophages have *in situ* proliferative capacity especially during the perinatal period. We also identified CD11b-positive monocytes that seemed to be derived from the fetal liver as an alternative cell source of macrophage precursors and are distributed in the mesenchyme of cochlear modiolus or on the intraluminal surface of the perilymphatic space. Although the use of an adequate fate mapping model should be desirable to ascribe a hematopoietic lineage to a type of macrophage, our

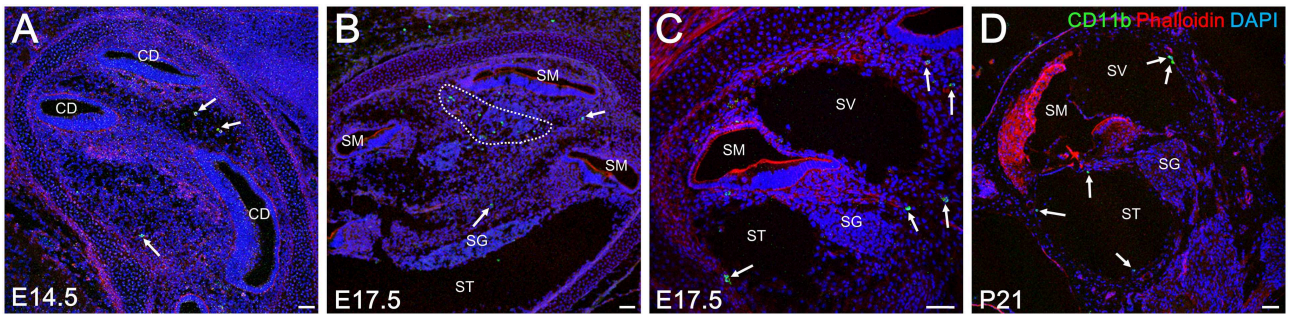

FIGURE 5 | Distribution of CD11b-positive cells in the cochlea at embryonic, neonatal, and adult stages. From E14.5 onward, CD11b-positive cells were observed in the cochlear mesenchyme (**A**, arrows). At E 17.5, CD11b-positive cells were observed in the mesenchyme around the cochlear modiolus (**B**, arrows) or on the intraluminal surface of the scala tympani and scala vestibuli (**C**, arrows). At P21, CD11b-positive cells were found mainly on the intraluminal surface of the scala tympani and scala vestibuli (**D**, arrows). CD, cochlear duct; SG, spiral ganglion; SM, scala media; ST, scala tympani; SV, scala vestibuli. Scale bars = 50 μm.

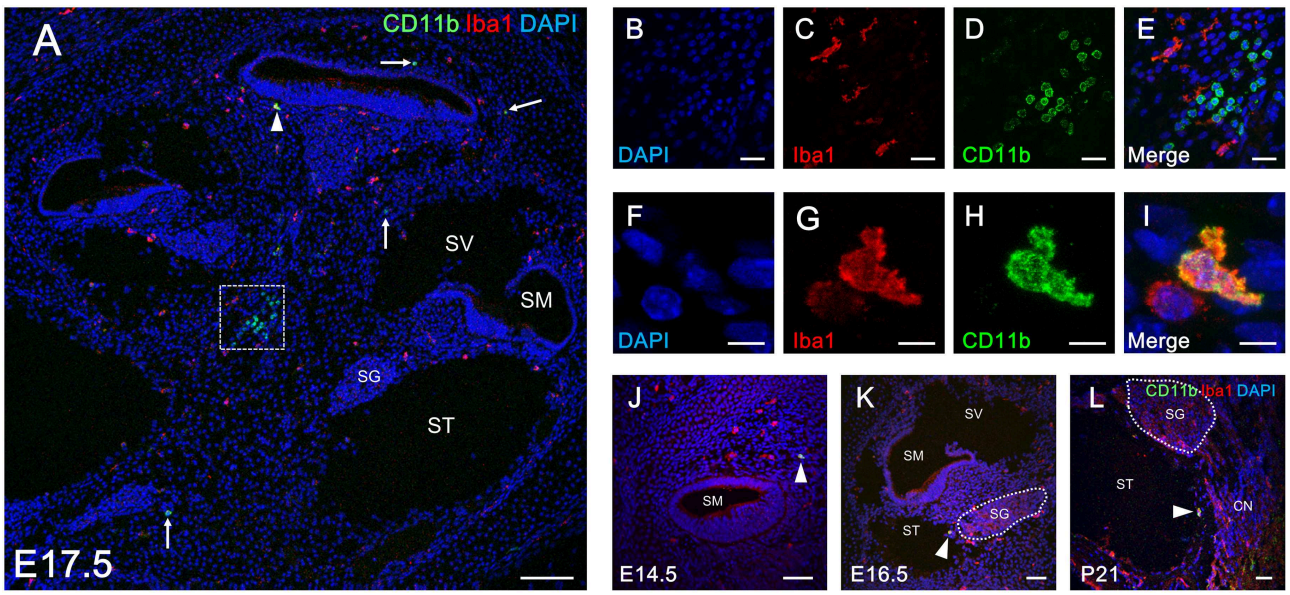

FIGURE 6 | Double immunostaining for Iba1 and CD11b in the cochlea at perinatal and adult stages. Distribution of Iba1-postive macrophages and CD11b-positive cells (**A**, arrows) throughout the entire cochlea at E17.5 **(A)**. Typical cells single-positive for Iba1 and CD11b in an inset of **(A)** are shown by immunostaining for DAPI **(B)**, Iba1 **(C)**, CD11b **(D)**, and Merge **(E)**. A portion of Iba1- or CD11b-positive cells in the cochlea at E17.5 were double-positive for both markers (**A**, arrowhead). A typical cell double positive for Iba1 and CD11b is shown by immunostaining for DAPI **(F)**, Iba1 **(G)**, CD11b **(H)**, and Merge **(I)**. Iba1 and CD11b double-positive cells in the cochlea were found at all developmental stages (from E14.5 to P21) (**J–L**, arrowheads). These findings suggest a direct transition in macrophage phenotype from CD11b-positive macrophage precursors to Iba1-positive macrophages. CN, cochlear nerve, SG, spiral ganglion; SM, scala media; ST, scala tympani; SV, scala vestibuli. Scale bars = 100 μm in **(A)**, 20 μm in **(B–E)**, 10 μm in **(F–I)**, and 50 μm in **(J–L)**.

findings revealed the heterogeneity of resident macrophages in the embryonic cochlea while also suggesting the heterogeneity of their hematopoietic origins.

Subtypes and Origins of Cochlear Resident Macrophages

The present study depicted the spatial and temporal distribution pattern of resident macrophages in the developing cochlea from E9 through postnatal stages. Regarding the emergence of cochlear macrophages, macrophage lineage cells expressing CX3CR1 have been observed around the otocyst at E10.5 in mice (35), which is consistent with the results presented herein. The ontogeny of resident fetal macrophages is believed to be categorized into two pathways (8). Firstly, macrophage progenitors arise from the blood island of the yolk sac at E7.5 and migrate through blood vessels directly to virtually all organs and tissues throughout the entire body at E10.5. Macrophages in other tissues, such as the brain (36) or developing skin (27), have also been observed as early as E10.5. Reports have shown that the development of primitive macrophages derived from the yolk sac depends on Csf1 signaling (17, 21). Secondly, in contrast to the yolk sac-derived primitive macrophages, monocyte progenitors arise from

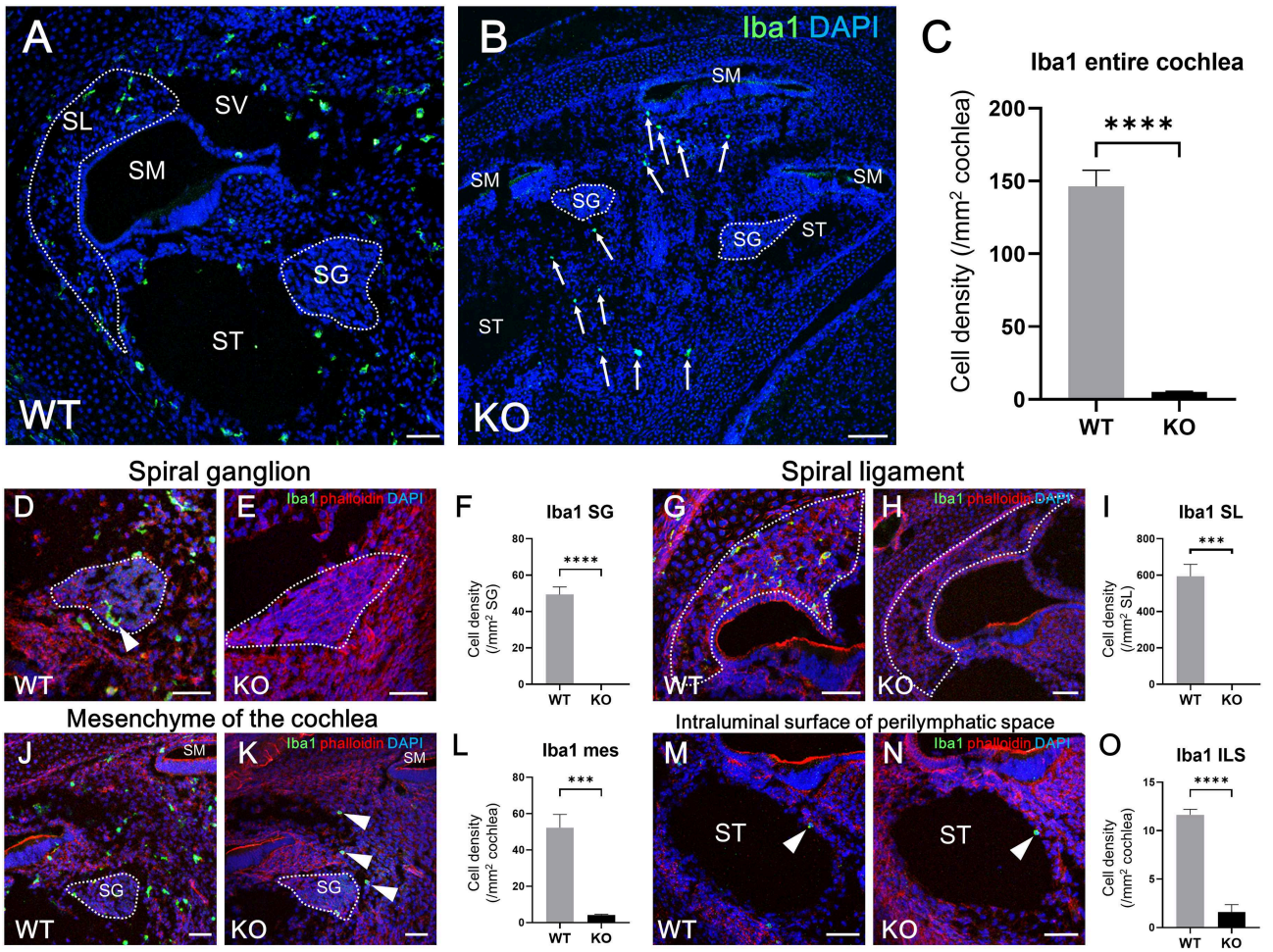

FIGURE 7 | Distribution and cell density of Iba1-positive cells in the cochlea of *Csf1r-null* mice at E17.5. Typical immunohistochemistry findings using anti-Iba1 antibody in the entire cochlea **(A,B)**, spiral ganglion **(D,E)**, spiral ligament **(G,H)**, mesenchyme **(J,K)**, and intraluminal surface of the perilymphatic space **(M,N)** in wildtype and *Csf1r*-null mice. The cell density of Iba1-positive macrophages in the entire cochlea **(C)**, spiral ganglion **(F)**, spiral ligament **(I)**, cochlear mesenchyme **(L)**, and intraluminal surface of the perilymphatic space **(O)** in both wildtype and *Csf1r*-null mice. *Csf1r*-null mice had a significantly lower Iba1-positive cell density than wildtype mice in any region of the cochlea, suggesting that Csf1 signaling plays essential roles in the development of cochlear resident macrophages originating from the yolk sac. WT, wildtype mice; KO, *Csf1r*-null mice; SG, spiral ganglion; SL, spiral ligament; SM, scala media; ST, scala tympani; SV, scala vestibuli; mes, mesenchyme; ILS, intraluminal surface of perilymphatic space. Scale bars = 50 μm. Statistical differences were assessed using unpaired *t*-tests. ***$p = 0.001$; ****$p < 0.0001$.

the yolk sac at E8.5 or from the aorta, gonads, and mesonephron regions at E10.5, migrate, and subsequently differentiate into fetal monocytes inside the fetal liver. These monocyte progenitors finally migrate to each tissue at E14.5 and differentiate into mature resident macrophages (8). The findings obtained herein suggest that a large portion of the cochlear resident macrophage population is derived from the yolk sac given that macrophages expressing Iba1, CD68, or F4/80 reside in the mesenchyme surrounding the otocyst at as early as E10.5. Moreover, cochlear analyses in *Csf1r*-null mice demonstrated that the number of macrophages in the spiral ganglion and spiral ligament were substantially decreased, suggesting that the supply of resident macrophages to such areas was dependent on the Csf1 signaling. These results also suggest that resident macrophages in the spiral ganglion and spiral ligament were derived from the yolk sac given that development of macrophages from the yolk sac were mainly promoted by the Csf1 signaling. Although Csf1r is expressed on macrophages derived from the yolk sac and fetal monocyte precursors derived from the fetal liver, migration and generation of macrophage precursors expressing CD11b appeared to be independent of the Csf1 signaling, which is consistent with previous reports (17, 21, 34). Taken together, our findings in *Csf1r*-null mice demonstrate that two subtypes of resident macrophages are present in the embryonic cochlea: one being Csf1r-dependent macrophages that originate from the yolk sac and the other being Csf1r-independent macrophages that migrate from the fetal liver via systemic circulation (**Figure 9**). Remarkable decrease of Langerhans cell precursors was observed

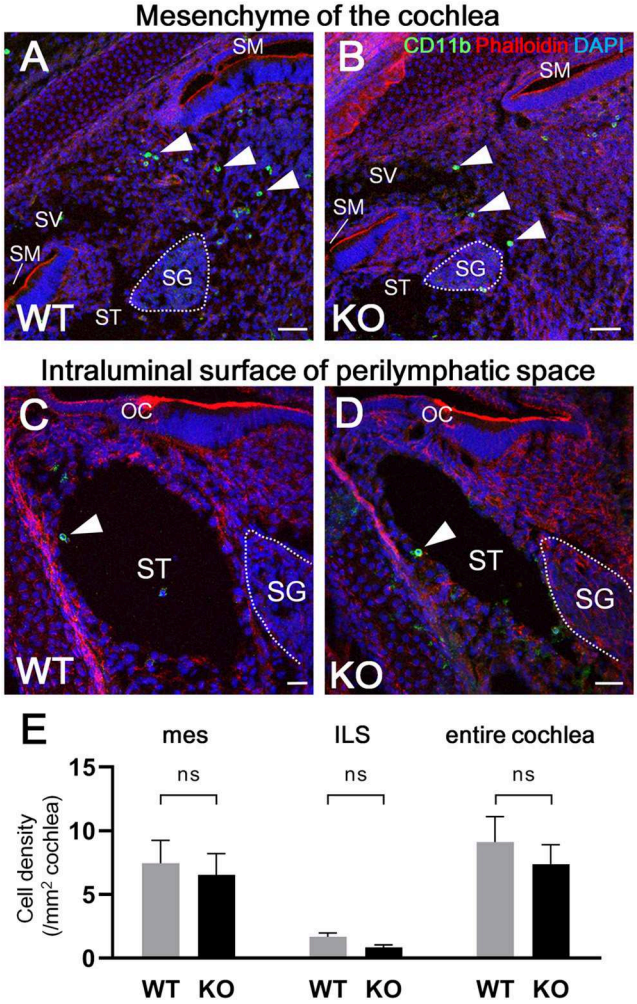

FIGURE 8 | Distribution of CD11b-positive cells in the cochlea of *Csf1r*-null mice. Typical immunohistochemistry findings using anti-CD11b antibody in the cochlear mesenchyme **(A,B)** and perilymphatic space **(C,D)** in wildtype and *Csf1r*-null mice. No significant differences in CD11b-positive cell density were observed between wildtype and *Csf1r*-null mice in any region, including the mesenchyme of the cochlear modiolus, intraluminal surface of the perilymphatic space, and entire cochlea **(E)**, suggesting that fetal liver hematopoiesis contributes to monocyte precursors in the cochlear modiolus independent of Csf1 signaling. mes, mesenchyme; ILS, intraluminal surface of perilymphatic space. Scale bars = 50 μm in **(A,B)** and 20 μm in **(C,D)**. Statistical differences were assessed using unpaired *t*-tests. WT, wildtype mice; KO, *Csf1r*-null mice.

in the skin of Csf1r-deficient mice while the absence of Csf1r did not affect monocyte development in the fetal liver and their recruitment to the skin, and Hoeffel et al. speculate that differentiation from fetal liver monocytes into Langerhans cell precursors is dependent on Csf1r (21). On the other hand, in the present study, we focused on the findings that a few Iba1-positive macrophages were still present in the cochlea of *Csf1r*-null mice and speculated that cochlear macrophages of *Csf1r*-null mice have differentiated from fetal liver monocytes. Csf1r-independent macrophages expressing Iba1 reside only in certain parts of the cochlea, such as the mesenchyme of the cochlear modiolus or the intraluminal surface of the perilymphatic space. Differences between the two types of cochlear macrophages are directly linked to the differences in the cochlear tissue site. In addition, quantitative assessment of resident macrophage density in wildtype and *Csf1r*-null mouse cochleae demonstrated that most of the cochlear macrophages during embryonic stage were Csf1r-dependent macrophages derived from the yolk sac.

Distribution and *in situ* Proliferative Capacity of Cochlear Resident Macrophages

Our findings on the *in situ* proliferative capacity of Iba1-positive cochlear macrophages suggest that the high density of macrophages in the neonatal cochlea might be due to *in situ* proliferation but not recruitment of macrophages from the systemic circulation. The percentage of pHH3-positive resident macrophages in the peritoneal cavity of mice has been reported to be 0.011% at 12–16 weeks of age to 0.25% at 2 weeks of age (37), with another report suggesting the same to be around 1.5% in the fetal lung (38). In addition, cardiac resident macrophages were reported to lose their self-renewal capacity with age (9). Accordingly, findings regarding the percentage of macrophages throughout the cell cycle presented in the aforementioned reports were consistent with those found herein. Concerning self-renewal of the macrophage lineage, two mechanisms of proliferation have been assumed. A number of resident macrophage-dedicated progenitor cells distinct from mature cells are thought to undergo asymmetrical cell division and subsequent terminal maturation into fully differentiated macrophages. In contrast, several studies have suggested that mature differentiated macrophages may undergo self-renewal through a mechanism whereby a fully differentiated macrophage proliferates and gives rise to equally mature macrophages (29, 39). In addition to self-renewal, Okano et al. reported that cochlear resident macrophages in adult mice are slowly replaced by circulating monocyte precursors supplied through hematopoiesis in the BM (6). Therefore, three major sources supplying resident macrophages in the cochlea seem to be present in adults: the yolk sac, fetal liver, and BM. The proportion of macrophages from the three different origins can change depending on the developmental stage of mice as has been reported in other tissues (8). Guilliams et al. quantitatively showed that alveolar fetal monocytes differentiate into mature alveolar macrophages with decreasing CD11b and increasing F4/80 expression using flow cytometry (40). Similarly, findings on double staining for CD11b and Iba1 in the present study suggested, at least in part, that CD11b single-positive fetal monocytes derived from the fetal liver undergo phenotype conversion into Iba1 single-positive mature macrophages through CD11b and Iba1 double-positive intermediate cells. Moreover, Iba1 and CD11b double-positive cells were observed from E14.5 to P21, which is consistent with results presented in previous reports that show fetal monocytes emerging in the fetal liver at around E12.5 and reaching systemic circulation by E13.5 to colonize every tissue except the brain (21,

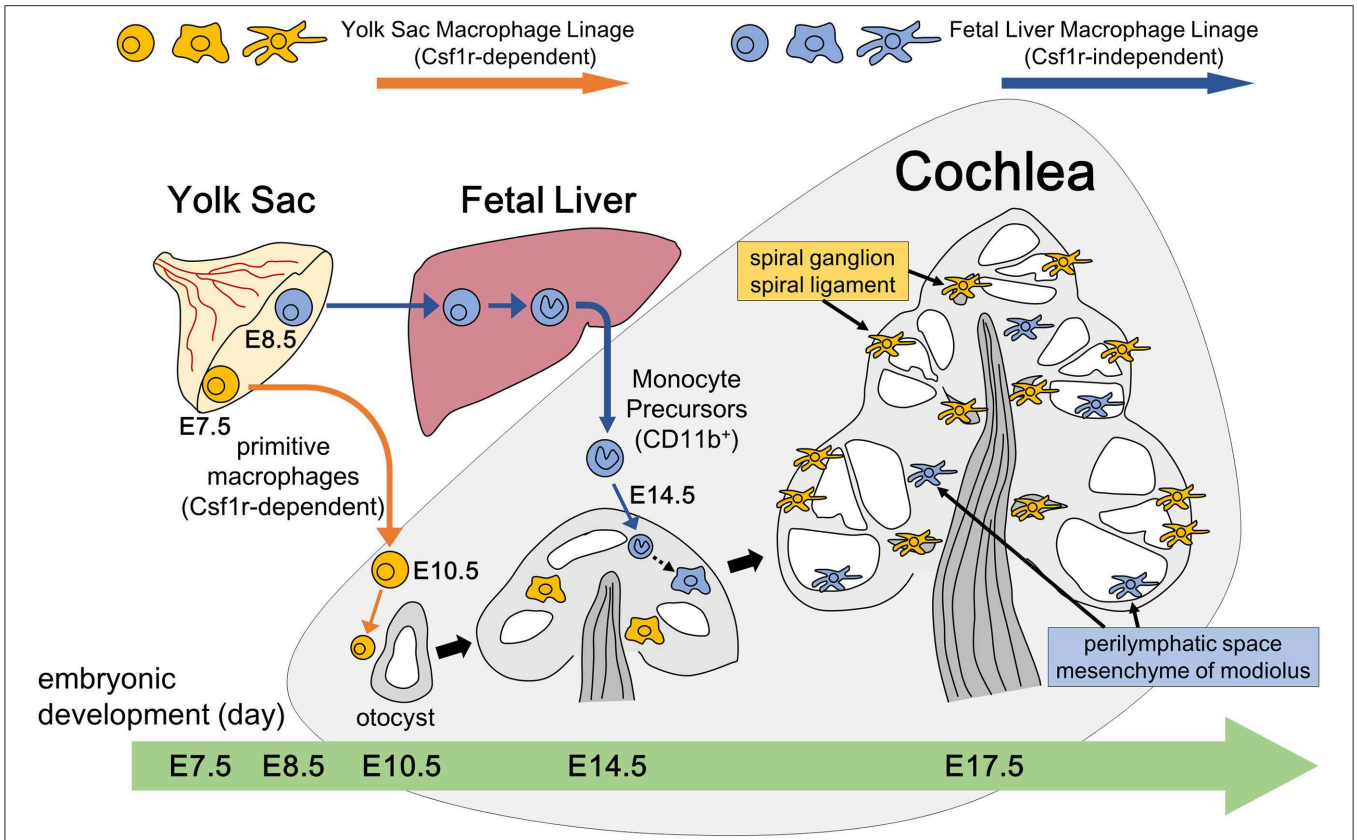

FIGURE 9 | Schematic representation of resident macrophage development in the embryonic cochlea through two different pathways. Two subtypes of resident macrophages are present in the embryonic cochlea: one being Csf1r-dependent macrophages that originate from the yolk sac and the other being Csf1r-independent macrophages that migrate from the fetal liver via systemic circulation. A large portion of the cochlear resident macrophage population is derived from the yolk sac given that macrophages expressing Iba1, CD68, or F4/80 reside in the mesenchyme surrounding the otocyst at as early as E10.5. These macrophages are distributed in the spiral ganglion and spiral ligament at E17.5, which is promoted by the Csf1 signaling. On the other hand, Csf1r-independent macrophages expressing CD11b migrate at as early as E14.5 and reside only in certain parts of the cochlea, such as the mesenchyme of the cochlear modiolus or the intraluminal surface of the perilymphatic space at E17.5.

34). Furthermore, the fact that CD11b-positive cells in wildtype mice were limited to the mesenchyme of the cochlear modiolus or intraluminal surface of the cochlea supports our hypothesis that macrophages derived from fetal liver monocytes are restricted to such areas.

Potential for Resident Macrophages in the Embryonic Cochlea to Be a Therapeutic Target

Previous studies have suggested that cochlear macrophages play different roles, such as the regulation of auditory glial cell number during postnatal development *in vivo* (41) and phagocytosis of damaged hair cells *in vitro* (35). However, specific macrophage roles in the embryonic cochlea currently remain unknown. Although the results presented herein do not directly demonstrate the roles of resident macrophages in the developing cochlea, the finding that two subtypes of cochlear resident macrophages reside in different parts of the cochlea may suggest different roles depending on the subtype. Regarding the development of a novel therapeutic treatment for congenital hearing loss, several studies have suggested macrophage-targeted therapies for the treatment of inflammatory diseases. One of the most exploited approaches has been facilitating macrophage phagocytosis of a loaded micro vehicle, which is then passively targeted to the site of inflammation due to mounting immune response (42). Modulation and reprogramming of macrophages is considered as a promising antitumor strategy. Hutter et al. showed that anti-CD47 treatment is efficacious against various brain tumors primarily by inducing tumor phagocytosis of macrophages (43). Macrophage depletion is another option to consider for therapeutic approach in pathologic condition, which based on the use of either depleting antibodies, such as anti-Csf1r, or molecules exerting a specific toxicity against macrophages, such as bisphosphonates and trabectedin (44). In cervical and mammary carcinoma mouse models, the depletion of tumor-associated macrophages, obtained by means of a highly selective Csf1r inhibitor, resulted in the arrest or delay of tumor growth (45). In conclusion, the modulation of the Csf1 signaling, which had a considerable impact on the number and distribution of cochlear macrophages in the present study, might lead to the therapeutic treatment of diseases by controlling the dynamics of cochlear resident macrophages later on.

DATA AVAILABILITY STATEMENT

The raw data supporting the conclusions of this manuscript will be made available by the authors, without undue reservation, to any qualified researcher.

ETHICS STATEMENT

The animal study was reviewed and approved by the Animal Research Committee, Kyoto University Graduate School of Medicine.

AUTHOR CONTRIBUTIONS

TO and KO designed and conceived the experiments. IK, KN, and TO performed the experiments and wrote the manuscript. TM developed mice used in the study. IK and TO analyzed the data. TO obtained funding.

FUNDING

This work was supported by a JSPS KAKENHI Grant (No. 16K11178 and No. 19K09908 to TO). The funders had no role in the study design, data collection, and analysis, decision to publish, or preparation of the manuscript.

ACKNOWLEDGMENTS

The authors would like to thank Dr. Issay Kitabayashi, Division of Hematological Malignancy, National Cancer Center Research Institute, Japan, and Dr. E. Richard Stanley, Department of Developmental and Molecular Biology, Albert Einstein College of Medicine, New York, USA, for providing *Csf1r*-null mice. We also thank Dr. Takayuki Nakagawa and Dr. Norio Yamamoto, Department of Otolaryngology, Head and Neck Surgery, Graduate School of Medicine, Kyoto University, Japan, for critical discussions related to the present study.

REFERENCES

1. Morton CC, Nance WE. Newborn hearing screening–a silent revolution. *N Engl J Med*. (2006) 354:2151–64. doi: 10.1056/NEJMra050700
2. Grosse SD, Ross DS, Dollard SC. Congenital cytomegalovirus (CMV) infection as a cause of permanent bilateral hearing loss: a quantitative assessment. *J Clin Virol*. (2008) 41:57–62. doi: 10.1016/j.jcv.2007.09.004
3. Mogi G, Lim DJ, Watanabe N. Immunological study on the inner-ear. Immunoglobulins in perilymph. *Arch Otolaryngol*. (1982) 108:270–5. doi: 10.1001/archotol.1982.00790530006003
4. Harris JP, Ryan AF. Immunobiology of the inner ear. *Am J Otolaryngol*. (1984) 5:418–25. doi: 10.1016/S0196-0709(84)80059-9
5. Hirose K, Discolo CM, Keasler JR, Ransohoff R. Mononuclear phagocytes migrate into the murine cochlea after acoustic trauma. *J Comp Neurol*. (2005) 489:180–94. doi: 10.1002/cne.20619
6. Okano T, Nakagawa T, Kita T, Kada S, Yoshimoto M, Nakahata T, et al. Bone marrow-derived cells expressing Iba1 are constitutively present as resident tissue macrophages in the mouse cochlea. *J Neurosci Res*. (2008) 86:1758–67. doi: 10.1002/jnr.21625
7. Epelman S, Lavine KJ, Beaudin AE, Sojka DK, Carrero JA, Calderon B, et al. Embryonic and adult-derived resident cardiac macrophages are maintained through distinct mechanisms at steady state and during inflammation. *Immunity*. (2014) 40:91–104. doi: 10.1016/j.immuni.2013.11.019
8. Ginhoux F, Guilliams M. Tissue-resident macrophage ontogeny and homeostasis. *Immunity*. (2016) 44:439–49. doi: 10.1016/j.immuni.2016.02.024
9. Molawi K, Wolf Y, Kandalla PK, Favret J, Hagemeyer N, Frenzel K, et al. Progressive replacement of embryo-derived cardiac macrophages with age. *J Exp Med*. (2014) 211:2151–8. doi: 10.1084/jem.20140639
10. Bain CC, Bravo-Blas A, Scott CL, Perdiguero EG, Geissmann F, Henri S, et al. Constant replenishment from circulating monocytes maintains the macrophage pool in the intestine of adult mice. *Nat Immunol*. (2014) 15:929–37. doi: 10.1038/ni.2967
11. Tamoutounour S, Guilliams M, Montanana Sanchis F, Liu H, Terhorst D, Malosse C, et al. Origins and functional specialization of macrophages and of conventional and monocyte-derived dendritic cells in mouse skin. *Immunity*. (2013) 39:925–38. doi: 10.1016/j.immuni.2013.10.004
12. Lavin Y, Winter D, Blecher-Gonen R, David E, Keren-Shaul H, Merad M, et al. Tissue-resident macrophage enhancer landscapes are shaped by the local microenvironment. *Cell*. (2014) 159:1312–26. doi: 10.1016/j.cell.2014.11.018
13. Bruttger J, Karram K, Wortge S, Regen T, Marini F, Hoppmann N, et al. Genetic cell ablation reveals clusters of local self-renewing microglia in the mammalian central nervous system. *Immunity*. (2015) 43:92–106. doi: 10.1016/j.immuni.2015.06.012
14. Bonnardel J, Guilliams M. Developmental control of macrophage function. *Curr Opin Immunol*. (2018) 50:64–74. doi: 10.1016/j.coi.2017.12.001
15. Bain CC, Scott CL, Uronen-Hansson H, Gudjonsson S, Jansson O, Grip O, et al. Resident and pro-inflammatory macrophages in the colon represent alternative context-dependent fates of the same Ly6Chi monocyte precursors. *Mucosal Immunol*. (2013) 6:498–510. doi: 10.1038/mi.2012.89
16. Askenase MH, Han SJ, Byrd AL, Morais da Fonseca D, Bouladoux N, Wilhelm C, et al. Bone-marrow-resident NK cells prime monocytes for regulatory function during infection. *Immunity*. (2015) 42:1130–42. doi: 10.1016/j.immuni.2015.05.011
17. Ginhoux F, Greter M, Leboeuf M, Nandi S, See P, Gokhan S, et al. Fate mapping analysis reveals that adult microglia derive from primitive macrophages. *Science*. (2010) 330:841–5. doi: 10.1126/science.1194637
18. Sato E, Shick HE, Ransohoff RM, Hirose K. Repopulation of cochlear macrophages in murine hematopoietic progenitor cell chimeras: the role of CX3CR1. *J Comp Neurol*. (2008) 506:930–42. doi: 10.1002/cne.21583
19. Shi X. Resident macrophages in the cochlear blood-labyrinth barrier and their renewal via migration of bone-marrow-derived cells. *Cell Tissue Res*. (2010) 342:21–30. doi: 10.1007/s00441-010-1040-2
20. Ryan GR, Dai XM, Dominguez MG, Tong W, Chuan F, Chisholm O, et al. Rescue of the colony-stimulating factor 1 (CSF-1)-nullizygous mouse [Csf1(op)/Csf1(op)] phenotype with a CSF-1 transgene and identification of sites of local CSF-1 synthesis. *Blood*. (2001) 98:74–84. doi: 10.1182/blood.V98.1.74
21. Hoeffel G, Wang Y, Greter M, See P, Teo P, Malleret B, et al. Adult Langerhans cells derive predominantly from embryonic fetal liver monocytes with a minor contribution of yolk sac-derived macrophages. *J Exp Med*. (2012) 209:1167–81. doi: 10.1084/jem.20120340
22. Dai XM, Ryan GR, Hapel AJ, Dominguez MG, Russell RG, Kapp S, et al. Targeted disruption of the mouse colony-stimulating factor 1 receptor gene results in osteopetrosis, mononuclear phagocyte deficiency, increased primitive progenitor cell frequencies, and reproductive defects. *Blood*. (2002) 99:111–20. doi: 10.1182/blood.V99.1.111
23. Wakaoka T, Motohashi T, Hayashi H, Kuze B, Aoki M, Mizuta K, et al. Tracing Sox10-expressing cells elucidates the dynamic development of the mouse inner ear. *Hear Res*. (2013) 302:17–25. doi: 10.1016/j.heares.2013.05.003
24. Imai Y, Ibata I, Ito D, Ohsawa K, Kohsaka S. A novel gene iba1 in the major histocompatibility complex class III region encoding an EF hand protein expressed in a monocytic lineage. *Biochem Biophys Res Commun*. (1996) 224:855–62. doi: 10.1006/bbrc.1996.1112

25. Dos Anjos Cassado A. F4/80 as a major macrophage marker: the case of the peritoneum and spleen. *Results Probl Cell Differ*. (2017) 62:161–79. doi: 10.1007/978-3-319-54090-0_7
26. Chistiakov DA, Killingsworth MC, Myasoedova VA, Orekhov AN, Bobryshev YV. CD68/macrosialin: not just a histochemical marker. *Lab Invest*. (2017) 97:4–13. doi: 10.1038/labinvest.2016.116
27. Ginhoux F, Merad M. Ontogeny and homeostasis of Langerhans cells. *Immunol Cell Biol*. (2010) 88:387–92. doi: 10.1038/icb.2010.38
28. Takahashi K, Yamamura F, Naito M. Differentiation, maturation, and proliferation of macrophages in the mouse yolk sac: a light-microscopic, enzyme-cytochemical, immunohistochemical, and ultrastructural study. *J Leukoc Biol*. (1989) 45:87–96. doi: 10.1002/jlb.45.2.87
29. Hashimoto D, Chow A, Noizat C, Teo P, Beasley MB, Leboeuf M, et al. Tissue-resident macrophages self-maintain locally throughout adult life with minimal contribution from circulating monocytes. *Immunity*. (2013) 38:792–804. doi: 10.1016/j.immuni.2013.04.004
30. Davies LC, Jenkins SJ, Allen JE, Taylor PR. Tissue-resident macrophages. *Nat Immunol*. (2013) 14:986–95. doi: 10.1038/ni.2705
31. Ajami B, Bennett JL, Krieger C, Tetzlaff W, Rossi FM. Local self-renewal can sustain CNS microglia maintenance and function throughout adult life. *Nat Neurosci*. (2007) 10:1538–43. doi: 10.1038/nn2014
32. Zhang W, Zheng J, Meng J, Neng L, Chen X, Qin Z. Macrophage migration inhibitory factor knockdown inhibit viability and induce apoptosis of PVM/Ms. *Mol Med Rep*. (2017) 16:8643–8. doi: 10.3892/mmr.2017.7684
33. Motohashi T, Yamanaka K, Chiba K, Miyajima K, Aoki H, Hirobe T, et al. Neural crest cells retain their capability for multipotential differentiation even after lineage-restricted stages. *Dev Dyn*. (2011) 240:1681–93. doi: 10.1002/dvdy.22658
34. Hoeffel G, Chen J, Lavin Y, Low D, Almeida FF, See P, et al. C-Myb(+) erythro-myeloid progenitor-derived fetal monocytes give rise to adult tissue-resident macrophages. *Immunity*. (2015) 42:665–78. doi: 10.1016/j.immuni.2015.03.011
35. Hirose K, Rutherford MA, Warchol ME. Two cell populations participate in clearance of damaged hair cells from the sensory epithelia of the inner ear. *Hear Res*. (2017) 352:70–81. doi: 10.1016/j.heares.2017.04.006
36. Ginhoux F, Lim S, Hoeffel G, Low D, Huber T. Origin and differentiation of microglia. *Front Cell Neurosci*. (2013) 7:45. doi: 10.3389/fncel.2013.00045
37. Davies LC, Rosas M, Smith PJ, Fraser DJ, Jones SA, Taylor PR. A quantifiable proliferative burst of tissue macrophages restores homeostatic macrophage populations after acute inflammation. *Eur J Immunol*. (2011) 41:2155–64. doi: 10.1002/eji.201141817
38. Stouch AN, Zaynagetdinov R, Barham WJ, Stinnett AM, Slaughter JC, Yull FE, et al. IκB kinase activity drives fetal lung macrophage maturation along a non-M1/M2 paradigm. *J Immunol*. (2014) 193:1184–93. doi: 10.4049/jimmunol.1302516
39. Aziz A, Soucie E, Sarrazin S, Sieweke MH. MafB/c-Maf deficiency enables self-renewal of differentiated functional macrophages. *Science*. (2009) 326:867–71. doi: 10.1126/science.1176056
40. Guilliams M, De Kleer I, Henri S, Post S, Vanhoutte L, De Prijck S, et al. Alveolar macrophages develop from fetal monocytes that differentiate into long-lived cells in the first week of life via GM-CSF. *J Exp Med*. (2013) 210:1977–92. doi: 10.1084/jem.20131199
41. Brown LN, Xing Y, Noble KV, Barth JL, Panganiban CH, Smythe NM, et al. Macrophage-mediated glial cell elimination in the postnatal mouse cochlea. *Front Mol Neurosci*. (2017) 10:407. doi: 10.3389/fnmol.2017.00407
42. Singh A, Talekar M, Raikar A, Amiji M. Macrophage-targeted delivery systems for nucleic acid therapy of inflammatory diseases. *J Control Release*. (2014) 190:515–30. doi: 10.1016/j.jconrel.2014.04.021
43. Hutter G, Theruvath J, Graef CM, Zhang M, Schoen MK, Manz EM, et al. Microglia are effector cells of CD47-SIRPalpha antiphagocytic axis disruption against glioblastoma. *Proc Natl Acad Sci USA*. (2019) 116:997–1006. doi: 10.1073/pnas.1721434116
44. Germano G, Frapolli R, Belgiovine C, Anselmo A, Pesce S, Liguori M, et al. Role of macrophage targeting in the antitumor activity of trabectedin. *Cancer Cell*. (2013) 23:249–62. doi: 10.1016/j.ccr.2013.01.008
45. Strachan DC, Ruffell B, Oei Y, Bissell MJ, Coussens LM, Pryer N, et al. CSF1R inhibition delays cervical and mammary tumor growth in murine models by attenuating the turnover of tumor-associated macrophages and enhancing infiltration by CD8(+) T cells. *Oncoimmunology*. (2013) 2:e26968. doi: 10.4161/onci.26968

Conflict of Interest: The authors declare that the research was conducted in the absence of any commercial or financial relationships that could be construed as a potential conflict of interest.

frontiers in Neurology

CASE REPORT
published: 12 November 2019
doi: 10.3389/fneur.2019.01172

Vertigo and Severe Balance Instability as Symptoms of Lyme Disease—Literature Review and Case Report

*Magdalena Jozefowicz-Korczynska[1], Ewa Zamyslowska-Szmytke[2], Anna Piekarska[3] and Oskar Rosiak[1]**

[1] Balance Disorders Unit, Department of Otolaryngology, Medical University of Lodz, The Norbert Barlicki Memorial Teaching Hospital, Lodz, Poland, [2] Nofer Institute of Occupational Medicine, Balance Disorders Unit, Department of Audiology and Phoniatrics, Lodz, Poland, [3] Department of Infectious Diseases and Hepatology, Medical University of Lodz, Lodz, Poland

Lyme disease is caused by a tick-borne bacterium *Borrelia* sp. This zoonotic infection is common in the Northern Hemisphere, e.g., Europe. Clinical presentation may involve multisystem symptoms and depends on the stage of the disease. The involvement of nervous system in Lyme disease is commonly referred to as neuroborreliosis. Neuroborreliosis may involve meningitis, mononeuritis multiplex, or cranial neuritis including the inflammation of vestibulocochlear nerve. In the late or chronic stage of Lyme disease, vestibular involvement may be the sole presentation, although such cases are rare. Our study was designed to present our own case and review the available literature reporting cases of neuroborreliosis with vertigo/dizziness and severe balance instability as a main disease symptom. The studies were obtained by searching the following databases: PubMed, Medline, and Embase. We included case reports of Lyme disease presenting with vertigo or gait disorders as the main symptom, written in the English language. Initially, 60 papers were identified. After analyzing the abstracts, seven manuscripts focusing on 13 clinical cases were included in this review. We conclude that the patients with neuroborreliosis sometimes present vertigo/dizziness, but rarely gait ataxia as a sole symptom. These complaints are usually accompanied by a hearing loss. Antibiotic treatment is usually effective. Balance instability in the patients with neuroborreliosis may persist but it responds well to vestibular rehabilitation.

Keywords: vertigo, Lyme disease, neuroborreliosis, vestibular rehabilitation, dizziness

OPEN ACCESS

Edited by:
Agnieszka J. Szczepek, Charité Medical University of Berlin, Germany

Reviewed by:
Katharina Stölzel, Charité Medical University of Berlin, Germany
Angel Batuecas-Caletrio, University of Salamanca Health Care Complex, Spain

****Correspondence:***
Oskar Rosiak
orosiak@gmail.com

Specialty section:
This article was submitted to Neuro-Otology, a section of the journal Frontiers in Neurology

Received: *12 September 2019*
Accepted: *21 October 2019*
Published: *12 November 2019*

Citation:
Jozefowicz-Korczynska M, Zamyslowska-Szmytke E, Piekarska A and Rosiak O (2019) Vertigo and Severe Balance Instability as Symptoms of Lyme Disease—Literature Review and Case Report. Front. Neurol. 10:1172. doi: 10.3389/fneur.2019.01172

INTRODUCTION

Lyme disease, caused by *Borrelia* sp. spirochete, is a zoonotic infection that spreads through tick bites. In Europe, the natural carrier for *Borrelia burgdorferi*, which is the most common species responsible for Lyme borreliosis, is a tick *Ixodes ricinus*. Epidemiological data suggest that the number of cases in Europe has increased steadily over the past two decades, reaching a total of 360,000 reported cases (1). Clinical manifestations of Lyme disease depend on its stage: early and late. The central nervous system is involved in ∼10–15% of Lyme disease patients and is referred to as neuroborreliosis. About 5% of infected individuals develop early onset neuroborreliosis that starts to be noticeable 4–6 weeks following tick bite, whereas over 95% of infected patients

develop neurological symptoms as late as 6 months from the initial infection (2). The patients with neuroborreliosis usually develop meningitis, mononeural neuritis, and cranial nerve palsy. Typically, if cranial nerves are involved, it is the facial nerve that is most affected. However, there were isolated reports describing cases of vestibulocochlear nerve involvement with hearing loss or vertigo (3, 4). Sole involvement of the vestibular system might present as dizziness and balance instability, whereas involvement of the cochlear nerve may be manifested by tinnitus and hearing loss. Gait ataxia is a very rare presentation and is usually accompanied by other symptoms. Such clinical manifestation can mimic a cerebellopontine lesion, and initially, such patients are often referred to neurologists and otorhinolaryngologists.

The diagnosis of neuroborreliosis may be problematic because the patients often do not recall being bitten by a tick. Additionally, if the bite occurred in a concealed area, there is a chance that the typical skin lesion (erythema) might not have been noticed. The diagnostic methods can be split into direct and indirect ones. Direct identification of pathogen involves diagnostic PCR with the cerebrospinal fluid (CSF) and material obtained from the skin lesion. The second direct diagnostic method is the bacterial culture. Unfortunately, the Borrelia culture is lengthy (up to several weeks) and still not internationally standardized. Indirect diagnosis involves identification of patient's antibodies directed against *Borrelia* sp. Two-tiered serological methods are usually used, the first being enzyme-linked immunoassay and the second being confirmatory test with use of Western blotting (or immunoblotting) technique. Detection of serum antibodies against *Borrelia* is a highly sensitive method but still not free of producing false-positive results, for instance due to infection with other bacteria, such as *Treponema pallidum* or *Helicobacter pylori* (5).

Bacterial infections of the nervous system are highly responsive to antimicrobial therapy; however, in rare cases, some symptoms may persist. The existence of chronic borreliosis or post-treatment Lyme disease syndrome has been the subject of debate in recent years (6).

In the present study, we review the available literature and summarize the case reports of neuroborreliosis with accompanying vertigo and balance instability and present one case report from our own clinical practice.

CASE DESCRIPTION

A 46-year-old male farmer was initially admitted to the Department of Neurology in 2018 with a sudden onset of tinnitus and hearing loss in the left ear, dizziness, severe balance instability, and gait ataxia. Neurological examination revealed no changes. Initially, a vestibular schwannoma was suspected, but the diagnostic imaging (CT, MRI, and angio-CT) revealed no pathologies. In addition, Doppler ultrasonography revealed no disturbances in a blood flow in vertebral or carotid arteries. However, lumbar puncture revealed an increased protein concentration (47 mg/dl) and cytosis (6.0/μl) in the CSF. Patient serum and CSF were tested for IgG and IgM *Borrelia*-specific antibodies using ELISA (LIAISON Borrelia, Manufacturer: DiaSorin). Positive results in ELISA were then confirmed with Western blot test (EUROLINE-RN-AT-adv for IgM and EUROLINE-RN-AT for IgG, Manufacturer: EUROIMMUN). Analysis by Western blot was positive for IgG antibodies in the CSF and serum. The antibody index (AI = QBb/QIg) was calculated from the ratio between CSF/serum for specific antibodies (QBb) and total immunoglobulins (QIg) and was negative for intrathecal antibody synthesis.

Following diagnosis, a 3-week course of doxycycline was initiated. Despite therapy, dizziness and gait impairment persisted. The patient was referred to the Balance Disorders Unit for vestibular evaluation. Audiometry revealed mild SNHL (sensory-neural hearing loss) in the right ear and mild to moderate SNHL for higher-frequency sounds, which was greater in the left ear. Speech discrimination was worse for the left ear (**Figure 1**) than the right ear (100% at 60 dB vs. 100% at 30 dB).

Upon examination, the patient presented with severe gait disturbance and imbalance. Romberg's test was positive. Unterberger sign was positive to the left side. Static and dynamic post-urography results were abnormal and the caloric test performed with videonystagmography (Ulmer SYNAPSIS 2008) determined canal paresis (87% left) with directional preponderance (7% right), and in addition, the saccadic pursuit eye movements and optokinetic tests were abnormal, confirming unilateral weakness on the left side and central vestibular system impairment. Clinical tests including Dynamic Gait Index (DGI), Berg Balance Scale (BBS), and Tinnetti test were conducted before and after rehabilitation (**Table 1**).

The patient underwent 10 consecutive, daily, 30-min sessions of vestibular rehabilitation therapy {individual rehabilitation program consisting of Cawthorne–Cooksey exercises and virtual reality rehabilitation [as per protocol described in our previous study (7)]} with significant balance improvement in eyes-open conditions. Improvement in DGI, BBS, and Tinnetti score was noted, shifting the patient from moderate to low risk of fall.

In control post-urography, a decrease in total length and mean velocity of COM was visible as well as an improvement in SOT score (30 vs. 52). The improvement in static post-urography was greater for eyes-closed conditions. The patient remains under close observation; tinnitus and hearing loss remained. The patient was not fitted with a hearing aid to the left ear because of satisfactory speech discrimination threshold.

LITERATURE REVIEW

Materials and Methods

The literature was collected during a comprehensive search of using the online databases PubMed, Medline on Ovid, and Embase on Ovid up until September 2019. The following search string was used: (Lyme Neuroborreliosis[Mesh] OR Neuroborreliosis[tw] OR "Nervous System Lyme Borreliosis"[tw] OR "Peripheral Nervous System Lyme Disease"[tw] OR "Lyme Meningoradiculitis"[tw] OR "Lyme Polyradiculitis"[tw] OR "Lyme Polyradiculopathy"[tw] OR "Central Nervous System Lyme Disease"[tw] OR "Lyme Meningoencephalitis"[tw] OR Lyme disease[mh] OR "Lyme disease"[tw] OR B. burgdorferi Infection[tw] OR "Lyme

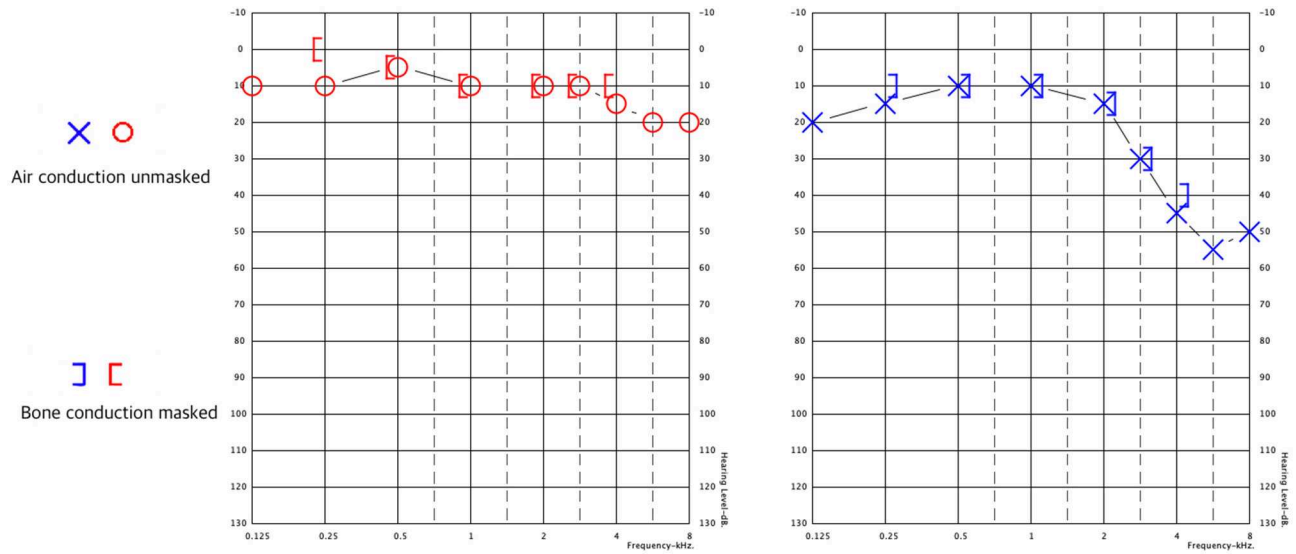

FIGURE 1 | Pure tone audiometry results. Right ear in red, left ear in blue. Both ears exhibit sensorineural hearing loss at 3–8 kHz, which is greater in the left ear.

TABLE 1 | Results of clinical tests and post-urography before and after vestibular rehabilitation therapy.

Test	Before rehabilitation	After rehabilitation
DGI (total score in pts.)	13	19
BBS (total score in pts.)	40 (medium risk of fall)	50 (low risk of fall)
Tinnetti (total score in pts.)	19 (moderate risk of fall)	24 (low risk of fall)
Static post-urography (total COM path length in mm) quiet stance, eyes open	183	92
Static post-urography (total COM mean velocity in mm/s) quiet stance, eyes open	0.73	0.55
Static post-urography (total COM path length in mm) quiet stance, eyes closed	314	201
Static post-urography (total COM mean velocity in mm/s) quiet stance, eyes closed	1.57	0.9
Dynamic post-urography SOT score	30	52

COM, center of mass; SOT, Sensory Organization test; DGI, Dynamic Gait Index; BBS, Berg Balance Scale.

Borreliosis"[tw] OR "Borrelia burgdorferi Infection"[tw] OR "Lyme Arthritis"[tw]) AND (Vertigo[Mesh] OR Vertigo[tw] OR Dizziness[Mesh] OR Dizziness[tw] OR Orthostasis[tw] OR Lightheadedness[tw] OR vestibular[tw] OR Light-Headedness[tw] OR "Light Headedness"[tw] OR "unsteady gait"[tw] OR Gait Ataxia[Mesh]).

In our review, the following inclusion criteria were established: (1) subject had to be human; (2) case report should provide a thorough patient history and laboratory findings including serum and CSF *Borrelia* antibody tests; (3) main complaint was vertigo or gait disturbance/ataxia; and (4) only full text studies written in English that were published in peer-reviewed journals were included in further analysis.

Two independent reviewers analyzed the abstracts and identified the papers meeting the inclusion and exclusion criteria. The cases were extracted from full-text manuscripts and summarized according to their clinical and laboratory findings. Furthermore, we include one case of neuroborreliosis with vertigo and gait ataxia diagnosed in our unit.

Results

Initial search result returned 60 non-duplicated results. Forty-three full-text articles were available in English. Six manuscripts were excluded because final diagnosis was different from Lyme disease, 8 studies reported other symptoms outside the scope of this analysis, 12 manuscripts presented pooled data, 2 were experimental studies, 2 were reviews, and 4 manuscripts not reporting CSF testing were excluded from further analysis. Review of full-text articles identified seven manuscripts describing case reports that met the inclusion criteria and one retrospective study reporting detailed results of eight individual cases of Lyme disease with vertigo, two of which were excluded due to lack of CSF testing. Clinical data were extracted by reviewers from the full-text manuscripts and are summarized in **Table 2** together with data from the case report described above.

DISCUSSION

We describe here a case that presented with neurological symptoms such as vertigo, gait ataxia, hearing impairment, and tinnitus. In addition, the patient had pathological parameters in the CSF and positive tests for *Borrelia*-specific IgG antibodies in the CSF and serum. According to the European Federation of Neurologic Societies (EFNS), at least two of the following diagnostic criteria should be met to consider possible

TABLE 2 | Summary of clinical and laboratory results in patients with neuroborreliosis presenting vertigo as the main symptom.

Patient age/sex	Study	Symptoms	Days to diagnosis	Borrelia antibody testing		Otological diagnostics	Outcome
				Serum	CSF		
46/M	Own case report	V, HL, T, I	10	IgM (–) IgG (+)	IgG (+)	SNHL VNG ab. POST ab.	V, I Imp. T, HL Per.
58/F	Huda et al. (8)	V, HL, I,OS	450	(–)	IgG (+) IgM (+)	SNHL	All.
62/M	Peltomaa et al. (9)	V, HL	90	IgM IgG (+)	(–)	SNHL	Sub.
50/F	Peltomaa et al. (9)	V, OS	284	IgG (+)	(–)	Audiometry no. POST no. ENG no.	H, A sub. V Imp.
52/F	Peltomaa et al. (9)	V, T	192	IgG (+)	(–)	SNHL POST ab. Caloric test ab.	Sub.
8/F	Peltomaa et al. (9)	V, T	150	IgM (+) IgG (+)	(–)	Audiometry no. POST ab.	Sub.
57/F	Peltomaa et al. (9)	V, T, HL	60	IgG (+)	(–)	ENG no. SNHL	H, V Imp. T, I Per.
38/F	Peltomaa et al. (9)	V,T,HL,OS	90	IgG (+)	(–)	SNHL ENG no.	Sub.
15/M	Curless et al. (10)	V, HL	30	IgG (–) IgM (–)	IgM (+)	N/A	Sub.
49/M	Ishizaki et al. (11)	V, T	30	IgG (+)	(–)	ENG ab. Caloric test no.	Sub.
12/M	Heininger et al. (12)	V, OS	7	IgM (+)	IgM (+)	ENG ab.	Sub.
69/M	Leeuwen et al. (13)	V, I	90	IgM (+) IgG (+)	(–)	VNG ab.	Sub.
28/F	Farshad et al. (14)	V, I	42	IgG (+) IgM (+)	IgG (+) IgM (+)	N/A	Sub.
80/F	Aboul-Enain et al. (15)	I, OS	N/A	IgG (–) IgM (–)	IgG (+) IgM (+)	N/A	Sub.

V, vertigo; T, tinnitus; HL, hearing loss; I, instability; OS, other symptoms; N/A, no data; SNHL, sensorineural hearing loss; no, normal; ab, abnormal; (+), positive; (–), negative; POST, posturography; Sub., Subsided; Imp., improved; Per., persistent.

neuroboreliosis and three for a definite neuroboreliosis: (i) neurological symptoms, (ii) CSF pleocytosis, and (iii) intrathecal *Borrelia*-specific antibodies (16). Thus, our patient fulfills the criteria for possible neuroboreliosis. Unfortunately, the antibiotic therapy was not successful in decreasing hearing loss or tinnitus, suggesting permanent damage to the hearing nerve and cochlea.

All cases extracted from the literature had vertigo or dizziness, which may be considered a neurological manifestation of neuroborreliosis and therefore fulfilling the first diagnostic criterion. The presence of anti-*Borrelia*-specific antibodies in the CSF was reported only in six cases, whereas in eight cases, no Bb antibodies in the CSF were detected. It should be mentioned that only three case reports (8, 13, 14) were published after the EFNS guidelines were introduced in 2010. Gait ataxia manifesting as complete inability to walk is very rare, and has only been reported in our case and one other case in literature, which did not report CSF antibody testing (17).

Despite not reaching a definite diagnosis of neuroborreliosis, in most cases, symptoms subsided after a course of antibiotic treatment. A course of oral or intravenous antibiotic as per EFNS guidelines should be considered in cases suspected of Lyme disease with solely vestibular manifestations, which fulfill at least the criteria for possible neuroborreliosis. Diagnostic imaging by MRI is highly recommended to exclude possible vestibular schwannoma or internal auditory canal tumors, which might account for similar symptoms (9).

CONCLUSIONS

Our review demonstrates that vertigo and gait ataxia may be a symptom of Lyme disease in some cases. Furthermore, antibiotic treatment of borreliosis is usually effective in reducing the otoneurological symptoms. Some balance instability may persist but responds well to the subsequent vestibular rehabilitation.

ETHICS STATEMENT

Ethical review and approval was not required for the study on human participants in accordance with the local legislation and

institutional requirements. The patients/participants provided their written informed consent to participate in this study. Written informed consent was obtained from the individual(s) for the publication of any potentially identifiable images or data included in this article.

AUTHOR CONTRIBUTIONS

MJ-K: conceived and designed the analysis, wrote the paper. EZ-S: contributed data, performed post-urographic assessments. AP: contributed data, analyzed laboratory results, participated in treatment. OR: collected the data, performed the analysis.

FUNDING

This project was supported by research funding from the National Centre for Research and Development under STRATEGMED2/266299/19/NCBR/2016. This study was supported by Medical University of Lodz Grant No. 503/1-036-02/503-21-002.

ACKNOWLEDGMENTS

This is a short text to acknowledge the contributions of specific colleagues, institutions, or agencies that aided the efforts of the authors.

REFERENCES

1. WHO. *Centralized Information System for Infectious Diseases (CisiD)* [Internet] (2019). Available online at: http://data.euro.who.int/cisid/ (cited Febuary 25, 2019).
2. Koedel U, Fingerle V, Pfister HW. Lyme neuroborreliosis - Epidemiology, diagnosis and management. *Nat Rev Neurol*. (2015) 11:446–56. doi: 10.1038/nrneurol.2015.121
3. Moscatello AL, Worden DL, Nadelman RB, Wormser G, Lucente F. Otolaryngologic aspects of Lyme disease. *Laryngoscope*. (1985) 101:592–5.
4. Goldfarb D, Sataloff RT. Lyme disease: a review for the otolaryngologist. *Ear Nose Throat J*. (1994) 73:824–9.
5. Ross Russell AL, Dryden MS, Pinto AA, Lovett JK. Lyme disease: diagnosis and management. *Pract Neurol*. (2018) 18:455–64. doi: 10.1136/practneurol-2018-001998
6. Halperin JJ. Chronic Lyme disease: misconceptions and challenges for patient management. *Infect Drug Resist*. (2015) 8:119–28. doi: 10.2147/IDR.S66739
7. Rosiak O, Krajewski K, Woszczak M, Jozefowicz-Korczynska M. Evaluation of the effectiveness of a virtual reality-based exercise program for unilateral peripheral vestibular deficit. *J Vestib Res*. (2018) 28:409–15. doi: 10.3233/VES-180647
8. Huda S, Wieshmann UC. Protracted neuroborreliosis - an unusual cause of encephalomyelitis. *Case Rep*. (2012) 2012:bcr1120115206. doi: 10.1136/bcr.11.2011.5206
9. Peltomaa M, Pyykkö I, Seppälä I, Viljanen M. Lyme borreliosis - An unusual cause of vertigo. *Auris Nasus Larynx*. (1998) 3:2330242. doi: 10.1016/S0385-8146(97)10039-6
10. Curless RG, Schatz NJ, Bowen BC, Rodriguez Z, Ruiz A. Lyme neuroborreliosis masquerading as a brainstem tumor in a 15-year- old. *Pediatr Neurol*. (1996) 3:258–60. doi: 10.1016/S0887-8994(96)00172-5
11. Ishizaki H, Pykö I, Nozue M. Neuroborreliosis in the etiology of vestibular neuronitis. *Acta Otolaryngol*. (1993) 503:67–69. doi: 10.3109/00016489309128076
12. Heininger U, Ries M, Christ P, Harms D. Simultaneous palsy of facial and vestibular nerve in a child with Lyme borreliosis. *Eur J Pediatr*. (1990) 149:781–2.
13. van Leeuwen RB, van Kooten B, de Cock AF. Bilateral vestibular hypofunction and Lyme disease: a causal link? *Acta Neurol Belg*. (2017) 117:367–8. doi: 10.1007/s13760-016-0658-6
14. Farshad-Amacker NA, Scheffel H, Frauenfelder T, Alkadhi H. Brainstem abnormalities and vestibular nerve enhancement in acute neuroborreliosis. *BMC Res Notes*. (2013) 6:551. doi: 10.1186/1756-0500-6-551
15. Aboul-Enein F, Kristoferitsch W. Normal pressure hydrocephalus or neuroborreliosis? *Wien Med Wochenschr*. (2009) 159:58–61. doi: 10.1007/s10354-008-0581-4
16. Mygland Å, Ljøstad U, Fingerle V, Rupprecht T, Schmutzhard E, Steiner I. EFNS guidelines on the diagnosis and management of European lyme neuroborreliosis. *Eur J Neurol*. (2010) 1:8–16. doi: 10.1111/j.1468-1331.2009.02862.x
17. Lopez M, Wise C. Acute ataxia in a 4-year-old boy: a case of Lyme disease neuroborreliosis. *Am J Emerg Med*. (2008) 26:1069.e5–6. doi: 10.1016/j.ajem.2008.03.029

Conflict of Interest: The authors declare that the research was conducted in the absence of any commercial or financial relationships that could be construed as a potential conflict of interest.

frontiers in Neurology

ORIGINAL RESEARCH
published: 21 November 2019
doi: 10.3389/fneur.2019.01244

Csf1 Signaling Regulates Maintenance of Resident Macrophages and Bone Formation in the Mouse Cochlea

Takayuki Okano and Ippei Kishimoto*

Department of Otolaryngology, Head and Neck Surgery, Graduate School of Medicine, Kyoto University, Kyoto, Japan

In the mammalian cochlea, resident macrophages settle in the spiral ligament, spiral ganglion, and stria vascularis, even at the steady state. Resident macrophages in the cochlea are believed to maintain homeostasis in the inner ear and become active, as part of the front line defense, following inner ear damage. However, the exact roles of cochlear resident macrophages require further clarification. Colony stimulating factor-1 (Csf1) signaling regulates survival, proliferation, and differentiation of resident macrophages and appears to be essential for resident macrophages in the inner ear. To examine the roles of Csf1 signaling in auditory function, we examined the ossicles and inner ear of homozygous *Csf1* mutant (*Csf1*$^{op/op}$) mice. The ossicles including the incus and stapes of *Csf1*$^{op/op}$ mice macroscopically demonstrated bone thickening, and the otic capsules of the inner ear were also thick and opaque. Histological analyses demonstrated that the otic capsules in *Csf1*$^{op/op}$ mice were thickened and showed spongy bone degeneration. Measurements of the auditory brainstem response revealed significant elevation of thresholds in 4-week old *Csf1*$^{op/op}$ mice compared with *wild-type* littermates, indicating that *Csf1*$^{op/op}$ mice demonstrate hearing loss due to, at least in part, deformity of the ossicles and bone capsule of the inner ear. Furthermore, *Csf1*$^{op/op}$ mice are deficient in the number of resident macrophages in the spiral ligament and stria vascularis, but not in the spiral ganglion. These data provide evidence that Csf1 signaling is important not only for bone formation in the inner ear, but also for the maintenance of resident macrophages in the spiral ligament and stria vascularis in the adult mouse cochlea.

Keywords: resident macrophages, inner ear, osteopetrosis, bone remodeling, hearing loss

OPEN ACCESS

Edited by:
Paola Perin,
University of Pavia, Italy

Reviewed by:
Sung Huhn Kim,
Yonsei University, South Korea
Juan Carlos Amor-Dorado,
Hospital Can Misses, Spain

****Correspondence:***
Takayuki Okano
tokano@ent.kuhp.kyoto-u.ac.jp

Specialty section:
This article was submitted to Neuro-Otology, a section of the journal Frontiers in Neurology

Received: *26 April 2019*
Accepted: *07 November 2019*
Published: *21 November 2019*

Citation:
Okano T and Kishimoto I (2019) Csf1 Signaling Regulates Maintenance of Resident Macrophages and Bone Formation in the Mouse Cochlea. Front. Neurol. 10:1244. doi: 10.3389/fneur.2019.01244

INTRODUCTION

The inner ear was once believed to be "immune-privileged," because the concentration of IgG in the perilymph is as low as in the cerebrospinal fluid and there is no lymphatic drainage or lymphoid tissue. However, a new era of inner ear immunology began following the discovery of intimate contacts between lymphocytes and macrophages in the endolymphatic sac of guinea pigs (1). In addition, previous studies have demonstrated the presence of immune-competent cells in specific parts of the inner ear such as the spiral ganglion and the spiral ligament, which are referred to as resident macrophages in the cochlea (2, 3).

Tissue resident macrophages are distributed in virtually all organs and tissues in the body and provide crucial innate immune defense and tissue-specific functions in the regulation and

maintenance of organ homeostasis (4). Recent studies revealed considerable heterogeneity of macrophages with respect to both development and metabolism and have provided convincing evidence that diverse lineages of tissue resident macrophages determine their responses to immune stimulation and environmental stressors (5). Under pathological conditions, macrophages acquire inflammatory effector functions, but they can also develop regulatory properties essential for tissue protection and repair. Moreover, macrophages recruited during inflammation are often functionally distinct from tissue resident macrophages (6). In the cochlea of adult mice, resident macrophages expressing Iba1 settle in both the spiral ligament and the spiral ganglion even in the steady state. Once inflammation caused by acoustic overstimulation or bacterial infection occurs in the cochlea, circulating monocytes migrate, and gather at wounded sites (3, 7–9). Cochlear resident macrophages are thought to be important for the immune system of the inner ear, including maintenance of the local environment and repair of damaged tissue or cells. However, many aspects regarding the functions of cochlear macrophages remain to be elucidated.

Colony stimulating factor-1 (Csf1, also known as MCSF or Csfm) signaling regulates survival, proliferation, and differentiation of resident macrophages (10). Mice homozygous for the naturally occurring *Csf1*^{op} (op: osteopetrosis) gene mutation lack *Csf1*, due to a spontaneous frameshift mutation, and have a reduced macrophage population in various organs (11). Due to a severe deficiency of osteoclasts that leads to a severe restriction in bone remodeling, *Csf1*$^{op/op}$ mice possess extensive skeletal deformities and a lower body weight in addition to a lower life-span and very poor breeding performance (12).

Thus, *Csf1*$^{op/op}$ mice offer the opportunity to understand the function of macrophages in the bony capsule (otic capsule) and organs surrounding the auditory sensory epithelium, such as the spiral ganglion and spiral ligament in the mouse cochlea. We herein examine and report the phenotypes in the inner ear of *Csf1*$^{op/op}$ mice and further clarify the roles of Csf1 signaling in the mouse inner ear.

MATERIALS AND METHODS

Animals

Mutant *Csf1*$^{op/op}$ mice were bred in our laboratory from breeding pairs of B6C3F1-a/a, *Csf1*$^{op/+}$ mice obtained from Dr. Toshio Suda, Keio University, Japan. *Csf1*$^{op/+}$ mice carry a spontaneous mutation of the *Csf1* gene, a single nucleotide (thymidine) insertion 262 bp downstream from the initiation codon. This results in a frameshift and the generation of a stop codon 21 bp downstream of the insertion. Genotyping using tail snip was performed with polymerase chain reaction (PCR) with a primer set of Forward 1 for wild type (*WT*) (ATCCTGTTTGCT ACCTAAAGAAGGCCATTT), Forward 2 for *Csf1*^{op} mutation (TCCTGTTTGCTACCTAAAGAAGGCCCATTT), and Reverse (CTTGTTCTGCTCCTCATAGTCCTTGGTGAA), followed by digestion with BstX-I. Mice were maintained in a pathogen-free microisolator environment in the Institute of Laboratory Animals, Kyoto University Graduate School of Medicine. Due to their lack of teeth, *Csf1*$^{op/op}$ pups were started on a powdered diet formula when 3 weeks old. All animal procedures were performed in accordance with the NIH Guide for the Care and Use of Laboratory Animals and were approved by the Animal Research Committee of Kyoto University Graduate School of Medicine (No. 170510, MedKyo18117).

Auditory Brainstem Responses and Noise Exposure

The auditory brainstem response (ABR) was measured under general anesthesia, through intraperitoneal injection of midazolam (10 mg/kg; Astellas Pharma Inc., Tokyo, Japan) and xylazine (10 mg/kg; Bayer DVM, Leverkusen, Germany). ABR waveforms were recorded using sound stimuli of tone bursts at 8, 16, and 32 kHz for 12.8 ms, at a sampling rate of 40 kHz, using 50–5,000 Hz band-pass filter settings, and were averaged from 1,000 stimuli. Stimulus intensity was decremented in 5-dB steps from high to subthreshold levels. The auditory threshold was defined as the lowest stimulus intensity that evoked a recognizable ABR wave pattern. All ABRs of experimental animals ($n = 4$, each genotype) were recorded at the age of 4 weeks and male and female mice were analyzed together.

To assess their susceptibility to acoustic overstimulation, animals were exposed to 8 kHz octave band noise at 120 dB sound pressure level (SPL) for 1 h in a ventilated sound exposure chamber while having free access to food and water. The sound levels were monitored and calibrated at multiple locations within the sound chamber to ensure uniformity of the stimulus. ABR measurements were performed pre-exposure and 2 h and 7 days after noise exposure.

Histological Assessments

Under general anesthesia with midazolam and xylazine, animals were perfused intracardially with ice-cooled phosphate-buffered saline (PBS) followed by 4% paraformaldehyde in phosphate buffer. The temporal bones were collected and immersed in the same fixative for 4 h at 4°C. Samples were decalcified with 10% EDTA in PBS and cryoprotected with 30% sucrose. Specimens were prepared as cryostat sections (10 μm in thickness). Midmodiolar sections were obtained for histological analyses. Histological assessments of the otic capsule were performed with hematoxylin-eosin staining. To quantify the thickness of otic capsule, the vertical thickness of the otic capsule was measured in the basal turn where the basement membrane of cochlea is attached. In addition, the cross-sectional area of Rosenthal's canal and the width of habenula perforata were also measured in the basal turn ($n = 4$ for each genotype).

For immunohistochemical assessment of cochlear resident macrophages, cryostat sections were immersed in blocking solution containing 10% goat serum for 30 min and incubated with a primary antibody at 4°C overnight. Cochlear macrophages were labeled by immunostaining for ionized calcium binding adapter molecule 1 (Iba1), which is specific for microglia/macrophages (3). The primary antibody used in this study was rabbit anti-Iba1 (1:1,000; Wako Pure Chemicals, Osaka, Japan). Visualization of primary antibodies

was performed using secondary antibodies conjugated with Alexa Fluor 555 (1:500; Molecular Probes, Eugene, OR). Nuclei were counterstained with 4′,6-diamidino,2-phenylindole dihydrochloride (DAPI, 1 μg/ml in PBS; Molecular Probes). Negative controls lacked primary antibody labeling. Specimens were viewed with a Nikon Eclipse E600 fluorescence microscope (Nikon, Tokyo, Japan).

Images were processed using Adobe Photoshop CS6 and Adobe Illustrator CS6 (Adobe Systems, San Jose, CA, USA). Image manipulations were limited to adjustments to brightness, hue, and saturation.

Quantification of Cochlear Macrophages

For the quantification of Iba1-positive cells, four sections were selected randomly from the 12 most midmodiolar sections for each *WT* or *Csf1*$^{op/op}$ animal. All cochlear macrophages, defined by coexpression of Iba1 and DAPI within the cochlea, were counted by two double-blinded examiners.

To investigate alterations in the number of Iba1-positive cells in the cochlea, the density of Iba1-positive cells in the spiral ganglion (SG, Rosenthal's canal), spiral ligament (SL, region occupied by type I-V fibrocytes), or stria vascularis (SV) was calculated by a modified method as described previously for evaluating the density of SG neurons (13). All Iba1-positive DAPI-stained cells within the SG, SL, or SV from the midbasal portion of the cochlea were counted. The SG, SL, and SV profiles were then traced under a bright field image to generate the area of SG with Image J (http://www.nist.gov/lispix/imlab/prelim/dnld.html). The density of Iba1-positive cells in SG, SL, or SV was expressed as the number of cells per 10,000 μm^2.

Statistical Analysis

Statistical analyses were performed by using one-way analysis of variance (ANOVA) followed by the Tukey-Kramer test for the analysis of ABR thresholds. An unpaired *t*-test was used in other statistical analyses. Data were expressed as the mean ± standard error. Differences with *p*-values below 0.05 were considered statistically significant.

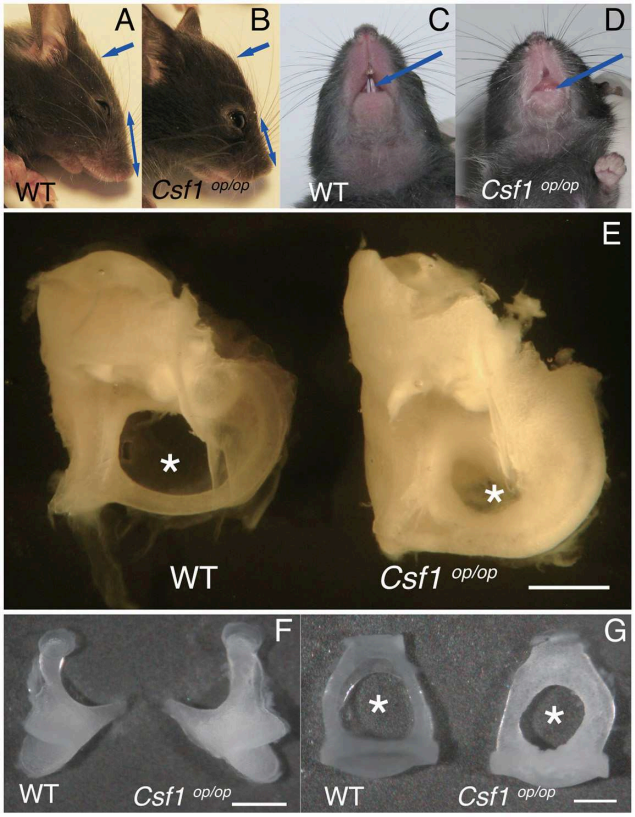

FIGURE 1 | Macroscopic phenotypes of the skull and ear in *Csf1*$^{op/op}$ mice. **(A–D)** *Csf1*$^{op/op}$ mice are clearly recognized by a distinctly domed skull and short snout (**A,B**, arrows and double headed arrows) and failure of eruption of the incisors (**C,D**, arrows). **(E)** Image of dissected cochleae from a representative set of *wild type* (*WT*) and *Csf1*$^{op/op}$ mice. The subarcuate fossa surrounded by the superior semicircular canal is remarkably small due to excessive bone formation of the inner ear in *Csf1*$^{op/op}$ mice (asterisks). Hypertrophy of the incus **(F)** and stapes **(G)** taken from *Csf1*$^{op/op}$ mice is shown in comparison to *WT* mice. The obturator foramen between the anterior and posterior crus is also remarkably small (asterisks). Bars: 1 mm for **(E)**, 500 μm for **(F)**, and 200 μm for **(G)**.

RESULTS

Excessive Bone Formation Is Pronounced in the Middle and Inner ear of *Csf1*$^{op/op}$ Mice

Csf1$^{op/op}$ mice could be clearly recognized by approximately 10 days of age by a distinctly domed skull and short snout (**Figures 1A,B**, arrows and double headed arrows), and by failure of eruption of the incisors (**Figures 1C,D**, arrows), as previously reported (12). We studied the macroscopic phenotype of the inner ear in *Csf1*$^{op/op}$ mice. Cleared inner ears from *WT* and *Csf1*$^{op/op}$ mice demonstrated that the otic capsules in *Csf1*$^{op/op}$ mice are thick and opaque. In particular, the subarcuate fossa surrounded by the superior semicircular canal showed shrinkage in *Csf1*$^{op/op}$ mice (**Figure 1E**, asterisks), reflecting excessive bone formation in the inner ear. Moreover, ossicles including the incus and the stapes demonstrated bone thickening (**Figures 1A,B**). The obturator foramen of the stapes pierced by the stapedial artery was also smaller in *Csf1*$^{op/op}$ mice compared with *WT* littermates due to excessive bone formation of the stapes (**Figures 1F,G**).

The Otic Capsules Surrounding the Membranous Labyrinth of *Csf1*$^{op/op}$ Mice Demonstrate Bone Thickening and Spongy Bone Degeneration

Cryostat sections of the inner ear stained with hematoxylin-eosin showed that the otic capsules surrounding the membranous labyrinth of *Csf1*$^{op/op}$ mice were thickened and demonstrated spongy bone degeneration (**Figures 2A,B** arrows, $n = 4$ for each genotype). Higher magnification images of the cochlear duct stained with hematoxylin-eosin also demonstrated excessive spongy bone formation in the lateral wall of the cochlea (**Figures 2C,D**, brackets and asterisks). The mean thickness of bony wall of the otic capsule was 37.5 ± 3.1 μm in *WT* mice in the

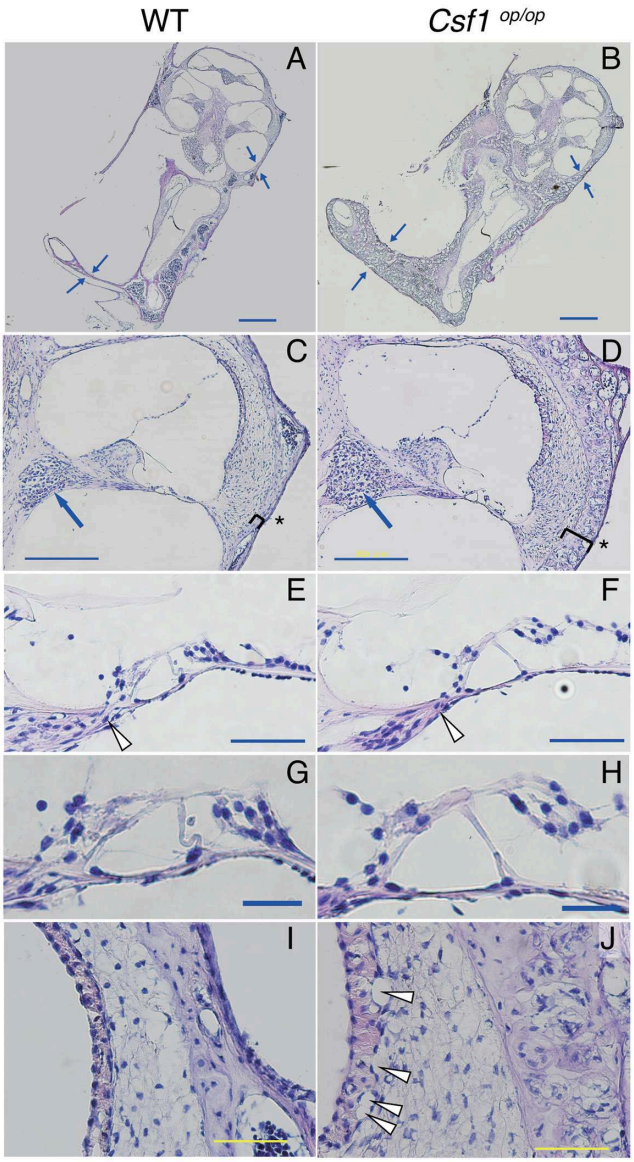

FIGURE 2 | Histological analyses demonstrated that the otic capsules of *Csf1*$^{op/op}$ mice have bone thickening and spongy bone degeneration. **(A,B)** Irregular lesions in *Csf1*$^{op/op}$ mice cause bone thickening of the otic capsule with spongy bone degeneration (arrows). Despite thickening of the otic capsule (parentheses), the spiral ganglion (arrows in **C,D**), the habenula perforata (arrowheads in **E,F**), and the organ of Corti **(G,H)** appear normal because at least one row of IHC, three rows of OHCs, and the triangle formed by two pillar cells appear to be preserved, whereas vacuolar formation in the basal cell layer of the stria vascularis was observed in *Csf1*$^{op/op}$ mice (arrowheads in **I,J**). The organ of Corti in the cochlear basal turn is shown. Bars: 500 μm for **(A,B)**, 200 μm for **(C,D)**, 50 μm for **(E,F,I,J)**, 20 μm for **(G,H)**.

basal turn, whereas that in *Csf1*$^{op/op}$ mice was 76.1 ± 2.3 μm. The difference in thickness of otic capsule was statistically significant (unpaired *t*-test, $p < 0.001$). In contrast, normal formation of Rosenthal's canal was observed, which contains the spiral ganglion in the cochlear modiolus (**Figures 2C,D**, arrows) and the osseous spiral lamina (**Figures 2E,F**, arrrowheads). The mean cross-sectional area of Rosenthal's canal in the basal turn was 1.85 ± 0.08 $\times 10^4$ μm^2 in *WT* mice while that in *Csf1*$^{op/op}$ mice was 1.94 ± 0.27 $\times 10^4$ μm^2. The difference in the cross-sectional area of Rosenthal's canal was not statistically significant (unpaired *t*-test, $p = 0.76$). In addition, the mean width of habenula perforata in the osseous spiral lamina of *WT* mice was 16.7 ± 1.3 μm, while that in *Csf1*$^{op/op}$ mice was 21.1 ± 2.0 μm. The difference in the width of habenula perforata was not statistically significant (unpaired *t*-test, $p = 0.11$). The gross morphology of the organ of Corti in the inner ear of *Csf1*$^{op/op}$ mice also appeared to be intact as one row of inner hair cells, three rows of outer hair cells, and the triangle formed by two pillar cells were at least preserved (**Figures 2E–H**). These findings are consistent with the development of the spiral ganglion and innervation of the auditory hair cells preceding the formation of the bone surrounding the cochlear duct. Finally, higher magnification images of SV revealed vacuole formation between the basal and intermediate cell layer of SV (**Figures 2I,J**, arrowheads).

Four-Week Old *Csf1*$^{op/op}$ Mice Show Significant Elevation of ABR Thresholds Compared With *WT* Littermates

To assess the auditory function of *Csf1*$^{op/op}$ mice, ABR thresholds in response to tone burst stimuli at 8, 16, and 32 kHz were measured in 4-week old *Csf1*$^{op/op}$ mice and *WT* littermates ($n = 4$ for each genotype). Thresholds in *WT* mice were 15.0 ± 2.9, 1.3 ± 1.3, and 26.3 ± 2.4 dB SPL at 8, 16, and 32 kHz, respectively, whereas thresholds in *Csf1*$^{op/op}$ mice were 38.8 ± 2.4, 30.0 ± 3.5, and 43.8 ± 2.4 dB SPL at 8, 16, and 32 kHz, respectively. Thresholds for all frequencies measured were significantly higher in *Csf1*$^{op/op}$ than in *WT* mice (**Figure 3A**), indicating that *Csf1*$^{op/op}$ mice show moderate hearing loss. When animals were exposed to 8 kHz octave band noise at 120 dB SPL for 1 h, the threshold shifts in *WT* mice were 61.3 ± 2.4, 66.3 ± 1.3, 58.8 ± 1.3 dB at 8, 16, and 32 kHz, respectively, while the threshold shifts in *Csf1*$^{op/op}$ mice were 13.8 ± 2.4, 7.5 ± 2.5, 13.8 ± 3.8 dB at 8, 16, and 32 kHz, respectively (**Figure 3B**). In addition to threshold shifts after noise exposure, raw data of ABR thresholds for all frequencies 2 h after noise exposure were significantly lower in *Csf1*$^{op/op}$ mice than in *WT* mice. Moreover, exposure to the 8 kHz octave band noise at 120 dB SPL for 1 h caused permanent threshold shifts in *WT* mice, whereas *Csf1*$^{op/op}$ mice showed only transient threshold shifts and recovery at 7 days after noise exposure to the same levels before noise exposure. Third, in *Csf1*$^{op/op}$ mice, the mean latencies of the wave I and the I-III interwave intervals at 8 kHz, 100 dB SPL were 2.74 ± 0.011 and 2.14 ± 0.016, and the mean latencies of the wave I and the I-III interwave intervals at 8 kHz, 70 dB SPL were 2.91 ± 0.028 and 2.19 ± 0.022, respectively. In *WT* mice, the mean latencies of the wave I and the I-III interwave intervals at 8 kHz, 70 dB SPL were 2.71 ± 0.016 and 2.13 ± 0.15, and the mean latencies of the wave I and the I-III interwave intervals at 8 kHz, 40 dB SPL were 2.92 ± 0.021 and 2.18 ± 0.15, respectively. The latencies of waves I and III were consistently delayed in *Csf1*$^{op/op}$ mice without any lengthening of interval between waves I and III, potentially suggesting conductive hearing loss in *Csf1*$^{op/op}$ mice.

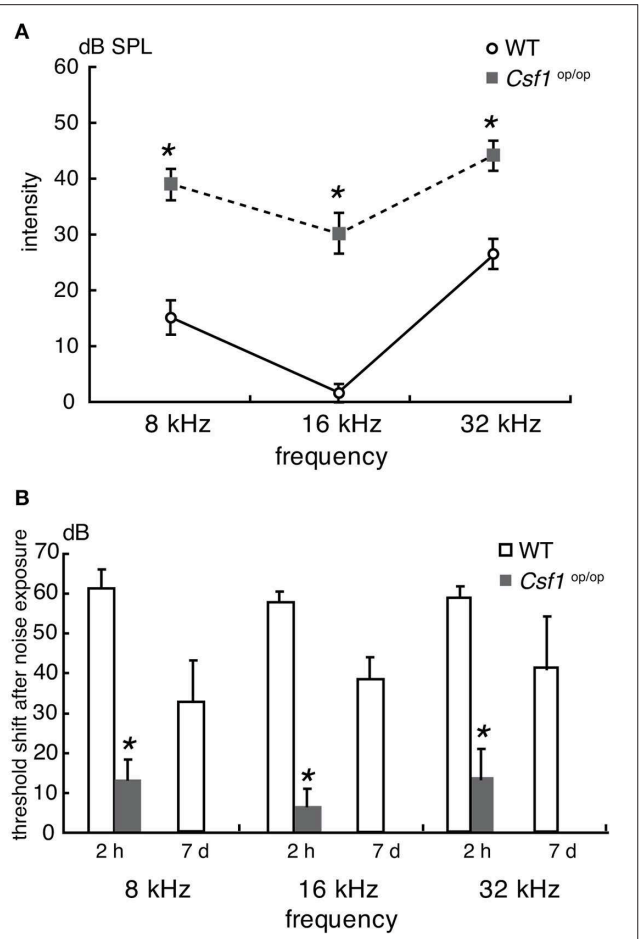

FIGURE 3 | Auditory brainstem response analyses revealed that *Csf1*$^{op/op}$ mice have mild to moderate hearing loss. **(A)** Auditory brainstem response (ABR) thresholds (decibels of sound pressure level, dB SPL) were measured in 4-week-old *Csf1*$^{op/op}$ mice and *wild type* (*WT*) littermates. Male and female mice were analyzed together. *Csf1*$^{op/op}$ mice show a higher ABR threshold at 8, 16, and 32 kHz, indicating that *Csf1*$^{op/op}$ mice have mild to moderate hearing loss. **(B)** ABR thresholds were also measured 2 h and 7 days after noise exposure to 8 kHz octave band noise at 120 dB SPL for 1 h. *Csf1*$^{op/op}$ mice are less susceptible to acoustic overstimulation, and the difference in the threshold shift in ABR 2 h after noise exposure compared with *WT* mice is statistically significant. Bars: mean ± SE. *$p < 0.05$.

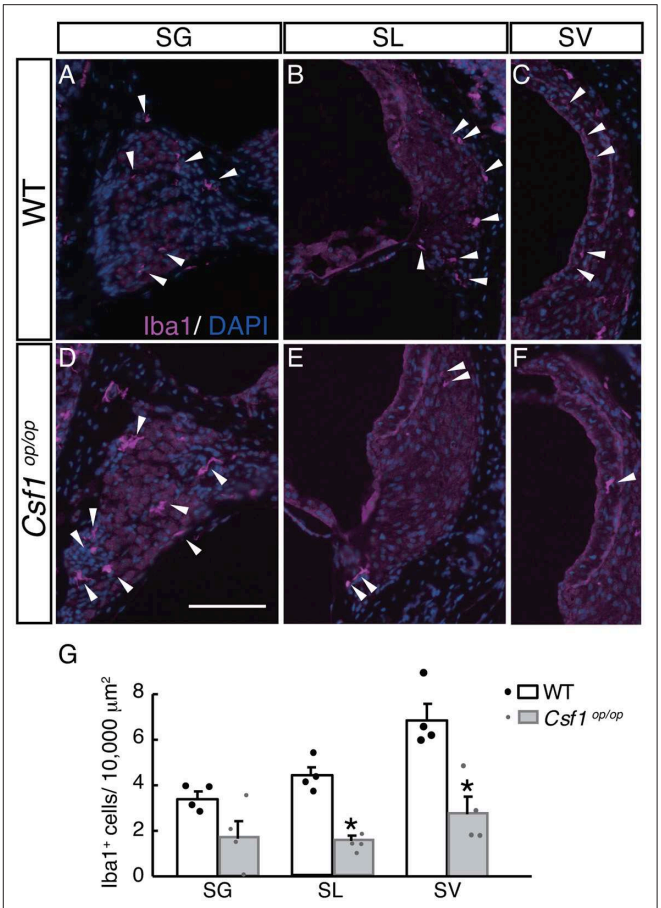

FIGURE 4 | Distribution and density of Iba1-positive macrophages in each part of the cochlea of *wild type* and *Csf1*$^{op/op}$ mice. Iba1-positive macrophages are found in the spiral ganglion **(A,D)**, spiral ligament **(B,E)**, and intermediate cell layer of the stria vascularis **(C,F)** in both *wild type* (*WT*) and *Csf1*$^{op/op}$ mice at the age of 4 weeks. While there is no statistically significant difference in the density of Iba1-positive macrophages in the spiral ganglion, a significant reduction in the density of Iba1-positive cells is observed in *Csf1*$^{op/op}$ mice, suggesting Csf1 dependency of resident macrophages in the spiral ligament and stria vascularis (**G**, single plots are also shown; $n = 4$ for each genotype). Bar: 200 μm for **(A–F)** (shown only in **D**). *$p < 0.05$.

Taken together, these findings suggest that moderate hearing loss shown in *Csf1*$^{op/op}$ mice was due to, at least in part, deformity of the ossicles and the otic capsule leading to a conductive hearing disorder, although the possibility of mixed hearing loss cannot be completely excluded.

Csf1$^{op/op}$ Mice Demonstrate a Significant Deficiency in the Number of Resident Macrophages in the Spiral Ligament and Stria Vascularis

To examine the roles of Csf1 signaling in the maintenance and distribution of resident macrophages in the mouse cochlea, the density of resident macrophages was examined with immunohistochemistry for Iba1 on the mid-modiolar section of 4-week old *WT* and *Csf1*$^{op/op}$ mice. Non-sensory parts of the cochlea including the SG, SL, and SV were densely populated with resident macrophages identified by Iba1 immunostaining, as previously shown (3) (**Figures 4A–C**). These cells had a characteristic morphology with several ramified processes that branched from the main axis of the cell body. However, the density of the cochlear macrophage population labeled with Iba1 was significantly decreased in *Csf1*$^{op/op}$ mice except in the SG (**Figures 4D–F**). The numbers of Iba1-positive cells per 10,000 μm^2 in the cochlea of *WT* mice were 3.42 ± 0.29, 4.35 ± 0.36, and 6.83 ± 0.69 in the SG, SL, and SV, respectively, whereas in *Csf1*$^{op/op}$ mice these numbers were 1.71 ± 0.71, 1.55 ± 0.17, 2.77 ± 0.71 in the SG, SL, and SV, respectively. The difference in density of Iba1-positive cells between *WT* and *Csf1*$^{op/op}$ mice was statistically significant in both SL and SV (**Figure 4G**, $n = 4$ for each genotype).

Taken together, Csf1 deficiency in the cochlea of 4-week old mice causes a significant decrease in the number of resident macrophages expressing Iba1, indicating that Csf1 signaling is required for the maintenance of cochlear resident macrophages in the SL and SV.

DISCUSSION

In this study, we examined the phenotype of the inner ear in *Csf1*$^{op/op}$ mice. The ossicles of *Csf1*$^{op/op}$ mice macroscopically showed bone thickening, and the otic capsules of *Csf1*$^{op/op}$ mice were also thick and opaque. Histological analyses demonstrated that the otic capsules of *Csf1*$^{op/op}$ mice were thickened and showed spongy bone degeneration. ABR measurements revealed significant elevation of thresholds in 4-week old *Csf1*$^{op/op}$ mice compared with their *WT* littermates, indicating that *Csf1*$^{op/op}$ mice demonstrate hearing loss due to, at least in part, deformity of the ossicles and bone capsule of the inner ear. Furthermore, *Csf1*$^{op/op}$ mice possess a significant deficiency in the number of resident macrophages in the spiral ligament and stria vascularis, but not in the spiral ganglion. These data provide evidence that Csf1 signaling is important not only for bone formation in the inner ear, but also for the maintenance of resident macrophages in the spiral ligament and stria vascularis of the adult mouse cochlea.

Interactions between the organ of Corti and the structures of the cochlea, such as the otic capsule and ossicles, are essential for hearing. In the embryo, the cochleae are formed through bidirectional signaling between the sensorineural structures and developing bone (14). Young *Csf1*$^{op/op}$ mice have excessive accumulation of bone without marrow cavities, increases in bone matrix formation (12), and, as demonstrated by our findings, spongy degeneration in the otic capsule that is associated with hearing impairment observed in ABR measurements. These observations show that *Csf1*$^{op/op}$ mice have a restricted capacity for bone remodeling, with severely reduced numbers of osteoclasts in the bone (15). *Csf1*$^{op/op}$ mice are used as a model for human hearing impairment observed in patients with osteopetrosis. Dozier et al. reported a case series of 32 patients with autosomal recessive osteopetrosis, which demonstrated that 26% of infants' ears showed hearing loss during the first year of life, and a total of 78% of children's ears demonstrated hearing loss during the study period. Of the children's ears with hearing loss, 100% had a conductive component and 26% had an additional sensorineural component (mixed hearing loss); cochleovestibular nerve conduction was normal in 100% of infants and 78% of children (16). While there are cases of osteopetrosis causing sensorineural hearing loss in humans, it has been hypothesized that this is due to auditory nerve compression from bony hypertrophy. In such cases, there are also reports that cochlear implants have been useful in patients with osteopetrosis who have deafness (17). Although osteopetrosis is genetically diverse, mutations in *CSF1* have been reported as autosomal recessive in humans (18). In the present study, *Csf1*$^{op/op}$ mice showed no nerve compression; therefore, hearing loss is thought to be largely due to conductive components such as spongy dysplasia of bone tissue in the ossicles and otic capsule. Our findings that *Csf1*$^{op/op}$ mice showed reduced elevation of ABR thresholds and quick recovery after acoustic overstimulation corroborates the presence of conductive hearing loss in *Csf1*$^{op/op}$ mice, although the possibility of mixed hearing loss cannot be completely excluded. Because *Csf1*$^{op/op}$ mice were analyzed at the age of 4 weeks in the present study, cochlear bony structures in *Csf1*$^{op/op}$ mice may change with age particularly with regard to nerve compression in the cochlear modiolus or osseous spiral lamina. In addition, recent studies on resident macrophages in the stria vascularis revealed specific roles as perivascular resident macrophage-like melanocytes (19, 20).

Csf1 is the most potent growth factor for macrophage differentiation (21, 22). In *Csf1*$^{op/op}$ mice, the production of functional M-CSF protein is impaired because of a defect in the coding region of the *Csf1* gene (15, 23). In *Csf1*$^{op/op}$ mice, the numbers of mature macrophages are reduced in many tissues, including the liver, spleen, lungs, and brain, because Csf1 deficiency results in widespread defects in monocyte/macrophage differentiation and osteoclast development. The failure of osteoclast development and differentiation in *Csf1*$^{op/op}$ mice results in impaired bone resorption and remodeling, leading to systemic osteopetrosis (15, 24–26). In our study, the otic capsules of *Csf1*$^{op/op}$ mice have histological changes in the inner ear, including bone thickening and spongy bone degeneration, which is compatible with previous studies (15, 24–26). In addition, *Csf1*$^{op/op}$ mice possess a significant deficiency in the number of resident macrophages in the spiral ligament and stria vascularis, but not in the spiral ganglion.

There are several reasons why *Csf1*$^{op/op}$ mice did not show complete loss of cochlear resident macrophages. Maternal Csf1, mainly produced from the uterus, is thought to support early development of *Csf1*$^{op/op}$ fetuses, which develop in the absence of Csf1 after birth. Milk-derived Csf1 does not seem to play a role in the development of macrophages in *Csf1*$^{op/op}$ mice. Accordingly, postnatal changes in macrophage subpopulations reflect a loss of Csf1 function (27). Another consideration is compensation of Csf1 signaling by IL-34. Most tissue macrophage populations are markedly reduced, but splenic macrophages are only slightly affected in *Csf1*$^{op/op}$ mice (28, 29), whereas *Il-34* null mice display a normal population of microglia and Langerhans cells (30). However, recent study revealed distinct requirement for Csf1 and IL-34 in the development and maintenance of microglia population (31), therefore further investigation should be required for elucidation of the detailed mechanisms of Csf1 signaling in the development of cochlear resident macrophages. According to previous studies in *Csf1*$^{op/op}$ mice and *Il-34* null mice, tissue resident macrophages are generally divided into two groups: Csf1-dependent macrophages and IL-34-dependent macrophages (32). Therefore, based on our results, the majority of resident macrophages in the spiral ligament and stria vascularis are Csf1-dependent, while the population of resident macrophages in the spiral ganglion is relatively Csf1-independent. Moreover, there is a possibility that a heterogeneous population of macrophages resides in each part of the mouse inner ear. Further studies are required to elucidate

the characteristics or mechanisms of differentiation of subtypes of cochlear resident macrophages.

In conclusion, our findings reveal unique roles for Csf1 signaling in bone morphogenesis and maintenance of resident macrophages in the mouse inner ear. These mechanisms could serve as a novel pharmacological target to treat the skeletal or hearing manifestations of osteopetrosis and other skeletal diseases.

DATA AVAILABILITY STATEMENT

The datasets generated for this study are available on request to the corresponding author.

ETHICS STATEMENT

This study was carried out in accordance with the recommendations of the NIH Guide for the Care and Use of Laboratory Animals. The protocol was approved by the Animal Research Committee of Kyoto University Graduate School of Medicine (No. 170510, MedKyo18117).

AUTHOR CONTRIBUTIONS

TO conceived and designed the experiments, performed the experiments, analyzed the data, wrote the paper. IK analyzed the results and prepared the manuscript.

FUNDING

This work was supported by a JSPS KAKENHI Grant (No. 16K11178 to TO). The funding organization had no role in the study design, data collection and analysis, decision to publish, or preparation of the manuscript.

ACKNOWLEDGMENTS

The authors would like to thank Dr. Toshio Suda, Keio University, Japan, for providing *Csf1*$^{op/op}$ mice. We also thank Dr. Juichi Ito, Dr. Takayuki Nakagawa, Kyoto University, Japan and Dr. Junko Okano, Shiga Medical University, Japan for critical discussion of the present study.

REFERENCES

1. Rask-Andersen H, Stahle J. Lymphocyte-macrophage activity in the endolymphatic sac. An ultrastructural study of the rugose endolymphatic sac in the guinea pig. ORL *J Otorhinolaryngol Relat Spec*. (1979) 41:177–92. doi: 10.1159/000275458
2. Hirose K, Discolo CM, Keasler JR, Ransohoff R. Mononuclear phagocytes migrate into the murine cochlea after acoustic trauma. *J Comp Neurol*. (2005) 489:180–94. doi: 10.1002/cne.20619
3. Okano T, Nakagawa T, Kita T, Kada S, Yoshimoto M, Nakahata T, et al. Bone marrow-derived cells expressing Iba1 are constitutively present as resident tissue macrophages in the mouse cochlea. *J Neurosci Res*. (2008) 86:1758–67. doi: 10.1002/jnr.21625
4. Lavin Y, Mortha A, Rahman A, Merad M. Regulation of macrophage development and function in peripheral tissues. *Nat Rev Immunol*. (2015) 15:731–44. doi: 10.1038/nri3920
5. Russell DG, Huang L, VanderVen BC. Immunometabolism at the interface between macrophages and pathogens. *Nat Rev Immunol*. (2019) 19:291–304. doi: 10.1038/s41577-019-0124-9
6. Guilliams M, Mildner A, Yona S. Developmental and functional heterogeneity of monocytes. *Immunity*. (2018) 49:595–613. doi: 10.1016/j.immuni.2018.10.005
7. Kaur T, Zamani D, Tong L, Rubel EW, Ohlemiller KK, Hirose K, et al. Fractalkine signaling regulates macrophage recruitment into the cochlea and promotes the survival of spiral ganglion neurons after selective hair cell lesion. *J Neurosci*. (2015) 35:15050–61. doi: 10.1523/JNEUROSCI.2325-15.2015
8. Wood MB, Zuo J. The contribution of immune infiltrates to ototoxicity and cochlear hair cell loss. *Front Cell Neurosci*. (2017) 11:106. doi: 10.3389/fncel.2017.00106
9. Yang W, Vethanayagam RR, Dong Y, Cai Q, Hu BH. Activation of the antigen presentation function of mononuclear phagocyte populations associated with the basilar membrane of the cochlea after acoustic overstimulation. *Neuroscience*. (2015) 303:1–15. doi: 10.1016/j.neuroscience.2015.05.081
10. Ryan GR, Dai XM, Dominguez MG, Tong W, Chuan F, Chisholm O, et al. Rescue of the colony-stimulating factor 1 (CSF-1)-nullizygous mouse (Csf1(op)/Csf1(op)) phenotype with a CSF-1 transgene and identification of sites of local CSF-1 synthesis. *Blood*. (2001) 98:74–84. doi: 10.1182/blood.V98.1.74
11. Michaelson MD, Bieri PL, Mehler MF, Xu H, Arezzo JC, Pollard JW, et al. CSF-1 deficiency in mice results in abnormal brain development. *Development*. (1996) 122:2661–72.
12. Marks SC Jr, Lane PW. Osteopetrosis, a new recessive skeletal mutation on chromosome 12 of the mouse. *J Hered*. (1976) 67:11–8. doi: 10.1093/oxfordjournals.jhered.a108657
13. Shinohara T, Bredberg G, Ulfendahl M, Pyykko I, Olivius NP, Kaksonen R, et al. Neurotrophic factor intervention restores auditory function in deafened animals. *Proc Natl Acad Sci USA*. (2002) 99:1657–60. doi: 10.1073/pnas.032677999
14. Driver EC, Kelley MW. Specification of cell fate in the mammalian cochlea. *Birth Defects Res C Embryo Today*. (2009) 87:212–21. doi: 10.1002/bdrc.20154
15. Naito M, Hayashi S, Yoshida H, Nishikawa S, Shultz LD, Takahashi K. Abnormal differentiation of tissue macrophage populations in 'osteopetrosis' (op) mice defective in the production of macrophage colony-stimulating factor. *Am J Pathol*. (1991) 139:657–67.
16. Dozier TS, Duncan IM, Klein AJ, Lambert PR, Key LL Jr. Otologic manifestations of malignant osteopetrosis. *Otol Neurotol*. (2005) 26:762–6. doi: 10.1097/01.mao.0000178139.27472.8d
17. Szymanski M, Zaslawska K, Trojanowska A, Szymanska A, Zadrozniak M. Osteopetrosis of the temporal bone treated with cochlear implant. *J Int Adv Otol*. (2015) 11:173–5. doi: 10.5152/iao.2015.449
18. Penna S, Capo V, Palagano E, Sobacchi C, Villa A. One disease, many genes: implications for the treatment of osteopetroses. *Front Endocrinol*. (2019) 10:85. doi: 10.3389/fendo.2019.00085
19. Zhang F, Dai M, Neng L, Zhang JH, Zhi Z, Fridberger A, et al. Perivascular macrophage-like melanocyte responsiveness to acoustic trauma–a salient feature of strial barrier associated hearing loss. *FASEB J*. (2013) 27:3730–40. doi: 10.1096/fj.13-232892
20. Zhang W, Zheng J, Meng J, Neng L, Chen X, Qin Z. Macrophage migration inhibitory factor knockdown inhibit viability and induce apoptosis of PVM/Ms. *Mol Med Rep*. (2017) 16:8643–8. doi: 10.3892/mmr.2017.7684
21. Stanley IJ, Burgess AW. Granulocyte macrophage-colony stimulating factor stimulates the synthesis of membrane and nuclear proteins in murine neutrophils. *J Cell Biochem*. (1983) 23:241–58. doi: 10.1002/jcb.240230121
22. Tushinski RJ, Oliver IT, Guilbert LJ, Tynan PW, Warner JR, Stanley ER. Survival of mononuclear phagocytes depends on a lineage-specific growth factor that the differentiated cells selectively destroy. *Cell*. (1982) 28:71–81. doi: 10.1016/0092-8674(82)90376-2

23. Takahashi K, Umeda S, Shultz LD, Hayashi S, Nishikawa S. Effects of macrophage colony-stimulating factor (M-CSF) on the development, differentiation, and maturation of marginal metallophilic macrophages and marginal zone macrophages in the spleen of osteopetrosis (op) mutant mice lacking functional M-CSF activity. *J Leukoc Biol.* (1994) 55:581–8. doi: 10.1002/jlb.55.5.581
24. Umeda S, Takahashi K, Naito M, Shultz LD, Takagi K. Neonatal changes of osteoclasts in osteopetrosis (op/op) mice defective in production of functional macrophage colony-stimulating factor (M-CSF) protein and effects of M-CSF on osteoclast development and differentiation. *J Submicrosc Cytol Pathol.* (1996) 28:13–26.
25. Umeda S, Takahashi K, Shultz LD, Naito M, Takagi K. Effects of macrophage colony-stimulating factor on macrophages and their related cell populations in the osteopetrosis mouse defective in production of functional macrophage colony-stimulating factor protein. *Am J Pathol.* (1996) 149:559–74.
26. Yoshida H, Hayashi S, Kunisada T, Ogawa M, Nishikawa S, Okamura H, et al. The murine mutation osteopetrosis is in the coding region of the macrophage colony stimulating factor gene. *Nature*. (1990) 345:442–4. doi: 10.1038/345442a0
27. Naito M. Macrophage heterogeneity in development and differentiation. *Arch Histol Cytol.* (1993) 56:331–51. doi: 10.1679/aohc.56.331
28. Nakamichi Y, Udagawa N, Takahashi N. IL-34 and CSF-1: similarities and differences. *J Bone Miner Metab*. (2013) 31:486–95. doi: 10.1007/s00774-013-0476-3
29. Yamamoto T, Kaizu C, Kawasaki T, Hasegawa G, Umezu H, Ohashi R, et al. Macrophage colony-stimulating factor is indispensable for repopulation and differentiation of Kupffer cells but not for splenic red pulp macrophages in osteopetrotic (op/op) mice after macrophage depletion. *Cell Tissue Res*. (2008) 332:245–56. doi: 10.1007/s00441-008-0586-8
30. Greter M, Lelios I, Pelczar P, Hoeffel G, Price J, Leboeuf M, et al. Stroma-derived interleukin-34 controls the development and maintenance of langerhans cells and the maintenance of microglia. *Immunity*. (2012) 37:1050–60. doi: 10.1016/j.immuni.2012.11.001
31. Easley-Neal C, Foreman O, Sharma N, Zarrin AA, Weimer RM. CSF1R Ligands IL-34 and CSF1 are differentially required for microglia development and maintenance in white and gray matter brain regions. *Front Immunol*. (2019) 10:2199. doi: 10.3389/fimmu.2019.02199
32. Cecchini MG, Dominguez MG, Mocci S, Wetterwald A, Felix R, Fleisch H, et al. Role of colony stimulating factor-1 in the establishment and regulation of tissue macrophages during postnatal development of the mouse. *Development*. (1994) 120:1357–72.

Conflict of Interest: The authors declare that the research was conducted in the absence of any commercial or financial relationships that could be construed as a potential conflict of interest.

frontiers in Neurology

ORIGINAL RESEARCH
published: 10 January 2020
doi: 10.3389/fneur.2019.01341

Correlations Between Vestibular Function and Imaging of the Semicircular Canals in DFNA9 Patients

Berina Ihtijarevic[1], Sebastien Janssens de Varebeke[2,3], Griet Mertens[1,3], Sven Dekeyzer[4], Paul Van de Heyning[1,3] and Vincent Van Rompaey[1,3]*

[1] Department of Otorhinolaryngology and Head and Neck Surgery, Antwerp University Hospital, Antwerp, Belgium, [2] Department of Otorhinolaryngology and Head and Neck Surgery, Jessa Hospital, Hasselt, Belgium, [3] Department of Translational Neurosciences, Faculty of Medicine and Health Sciences, University of Antwerp, Antwerp, Belgium, [4] Department of Radiology, Antwerp University Hospital, Antwerp, Belgium

OPEN ACCESS

Edited by:
Agnieszka J. Szczepek, Charité Medical University of Berlin, Germany

Reviewed by:
Nicolas Perez-Fernandez, University Clinic of Navarra, Spain
John Carey, Johns Hopkins University, United States
Samuel Gubbels, University of Colorado Denver, United States

Deepa Galaiya contributed to the review of John Carey

***Correspondence:**
Berina Ihtijarevic
berina.ihtijarevic@gmail.com

Specialty section:
This article was submitted to Neuro-Otology, a section of the journal Frontiers in Neurology

Received: *26 June 2019*
Accepted: *05 December 2019*
Published: *10 January 2020*

Citation:
Ihtijarevic B, Janssens de Varebeke S, Mertens G, Dekeyzer S, Van de Heyning P and Van Rompaey V (2020) Correlations Between Vestibular Function and Imaging of the Semicircular Canals in DFNA9 Patients. Front. Neurol. 10:1341. doi: 10.3389/fneur.2019.01341

Background and Purpose: Radiologic abnormalities on computed tomography (CT), including narrowing or sclerosis of the semicircular canals (SCCs), and T2-weighted magnetic resonance imaging (MRI), including signal loss in the SCC, have been reported as potential biomarkers in patients with P51S mutations in the *COCH* gene (i.e., DFNA9). The aim of our study was to correlate caloric responses through electronystagmography (ENG) data with imaging results in DFNA9 patients.

Materials and Methods: A retrospective study was performed in 45 patients; therefore, 90 ears with P51S mutations in the *COCH* gene were tested. Caloric responses and CT and MRI data were analyzed from June 2003 until May 2014. More than half of patients (54%) were candidates for cochlear implantation.

Results: In our population, 91% of tested ears had sclerotic lesions and/or narrowing in one or more SCCs on CT scan. All tested ears had narrowing or signal loss in at least one SCC on T2-weighted MRI. The lateral SCC was affected in 87% on CT scan and 92% on MRI. However, in 83% of tested ears, all three SCCs were affected on MRI. Furthermore, in 77% of tested ears, caloric responses were reduced bilaterally, while 11.5% showed unilateral hypofunction and the other 11.5% had normal caloric responses. CT abnormalities correlated with hypofunction of caloric responses. This statistically significant difference was present if abnormalities were observed in at least one of the SCCs as well as in ipsilateral lateral SCC function loss. MRI abnormalities in at least one of the SCCs correlated with ENG hypofunction, but there was no direct correlation between lateral SCC abnormalities on MRI and caloric responses of the investigated lateral canal.

Conclusion: Our retrospective analysis confirms the presence of CT and MRI abnormalities in DFNA9 patients with the P51S mutation in the *COCH* gene. A correlation between these radiologic features and vestibular function (tested by means of caloric response) was found in this population.

Keywords: DFNA9, electronystagmography, semicircular canal, magnetic resonance imaging, computed tomography

INTRODUCTION

DFNA9 is an autosomal dominant hereditary disorder characterized by progressive vestibular and cochlear deterioration. Patients typically become symptomatic in the third to fourth decade of life and usually present with oscillopsia and unsteadiness in darkness, due to bilateral vestibulopathy (1, 2). In a later stage, they develop severe-to-profound sensorineural hearing loss (3). DFNA9 is a non-syndromic form of hearing loss caused by a mutation in the coagulation factor C homology (*COCH*) gene (4). Many different mutations have been identified in the *COCH* gene worldwide, where P51S is a frequent mutation in Belgium and the Netherlands (4, 5). Histopathological studies show accumulation of eosinophilic glycosaminoglycan deposits with misfolded cochlin, which causes atrophy of fibrocytes, especially in the spiral ligament and limbus of the cochlea as well as the crista ampullaris of the semicircular canal (SCC) and the maculae of the vestibular system. This loss of fibrocytes leading to accumulation of acellular substance that probably consists of misfolded *COCH* protein may be the cause of cytotoxicity (6–8). Radiologic abnormalities on computed tomography (CT), including narrowing or sclerosis of the SCC, and T2-weighted magnetic resonance imaging (MRI), including signal loss in the SCC, have already been reported as a biomarker in carriers of the P51S mutations in the *COCH* gene (9). The authors have shown a correlation of these lesions with advanced stages of sensorineural hearing loss, suggesting these lesions to be secondary to an advanced inflammatory process.

The aim of our study was to correlate vestibular function, through caloric responses during electronystagmography (ENG) with CT and MRI abnormalities in the SCCs in DFNA9 patients.

MATERIALS AND METHODS

Ethics

The study was designed and conducted according to the Declaration of Helsinki (1996). The study was approved by the local ethics committee of the Antwerp University Hospital/University of Antwerp (protocol number 16/42/426).

Study Design

A retrospective study was performed in 45 patients with P51S mutations in the *COCH* gene, where 90 ears in total were investigated. ENG caloric responses and CT and MRI data were analyzed from June 2003 until May 2014. Both CT and MRI data were blinded to the investigators. A consultant neuroradiologist assessed all the CT and MRI blinded to the electronystagmography data.

Setting

Single tertiary referral otology department.

Audiometry

Hearing loss was defined by pure tone audiometry showing air-conducted hearing thresholds averaged for 500, 1,000, and 2,000 Hz higher than 16 dB HL (10). A subgroup of patients underwent evaluation for cochlear implantation candidacy. The criteria for reimbursement of cochlear implantation in Belgium are as follows: pure-tone average of 500, 1,000, and 2,000 Hz in unaided liminal audiometry exceeding 85 dB and speech discrimination with hearing aid <30%.

Vestibular Function Testing

Bilateral caloric irrigation was used to evaluate lateral SCC function. The methodology and normative values were reported earlier by Van der Stappen et al. (11) To summarize, subjects were seated in complete darkness, in a supine position with a head incline of 30°. Bithermal caloric irrigations (30°/44°) were performed in a 30 s time span, and nystagmus was recorded using ENG (Nystagliner Toennies, Germany). Caloric responses were categorized as follows:

- Caloric areflexia: sum of bithermal, 30° and 44°, max. peak slow phase velocity (SPV) < 6°/s per ear, in accordance with the Barany Society criteria for bilateral vestibulopathy (12).
- Caloric hypofunction: sum of bithermal, 30° and 44°, max. peak SPV < 10°/s and >6°/s.
- Normal caloric response: sum of bithermal max. peak SPV > 10°/s.

Computed Tomography

Multi-slice helical CT imaging of the temporal bone was performed on a 64-section CT scanner (LightSpeed VCT, GE Healthcare) with a 0.625 mm helical thickness. Tube voltage was 140 kV with a charge of 330 mA. A pitch of 0.531 mm per rotation was used with a rotation time of 1 s and an interval of 0.321 mm. Total acquisition time was 5.75 s. A field of view of 250 mm was used. Multiplanar reformation was performed with axial images reconstructed in the plane of the lateral SCC and coronal images reconstructed perpendicular to this plane. Additional reconstruction parallel to the superior SCC (Pöschl's plane) was performed. These reformations had a slice thickness of 0.2 mm with a field of view of 96 mm. Narrowing or sclerosis at the level of the SCC on CT imaging was defined when there was <50% of normal SCC diameter compared to the normal side or in consensus in case of bilateral pathology (**Figure 1**).

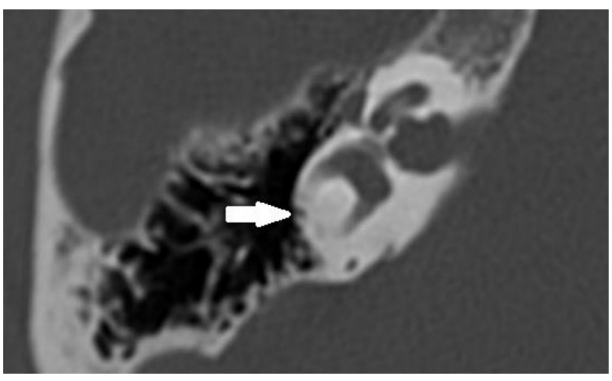

FIGURE 1 | Axial temporal bone CT scan of the right labyrinth demonstrating narrowing and ossification of the lateral semicircular canal (arrow).

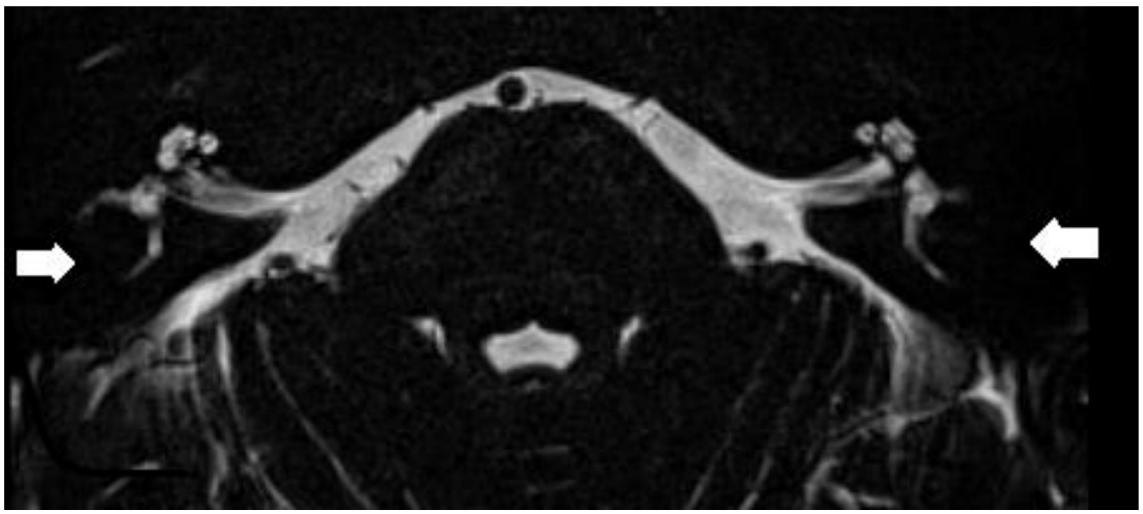

FIGURE 2 | Axial T2-weighted turbo spin echo MRI of the left and right labyrinth demonstrating signal loss in the lateral semicircular canal (arrow) corresponding to the axial CT slice in **Figure 1**.

Magnetic Resonance Imaging

MRI scans were performed on a 3-T system (Siemens Magnetom TIM Trio or Siemens Magnetom Skyra, Erlangen, Germany). The patients were positioned with their head in a 32-channel circularly polarized head coil. For each patient, an MRI scan of the brain and skull base was accomplished using the following sequences: axial T2-weighted turbo spin echo (T2 TSE) images and axial Fluid Attenuated Inversion Recovery (FLAIR) through the entire brain, followed by a 3D-turbo spin echo: "Sampling Perfection with Application optimized Contrasts using different flip angle Evolution" (SPACE) with TR/TE = 1,000/129 ms, 0.5 mm isometric voxels, a field of view of 200 mm, and a 384 × 384 matrix through the skull base. Also, sequences after gadolinium were included. The high spatial and contrast resolution of the 3D turbo spin echo images demonstrate an optimal contrast between the high intensity of the cerebrospinal fluid or labyrinthine fluid, and all other structures. The latter are outlined as low-intensity areas, such as cranial nerves, blood vessels, brainstem, cerebellum, and bony surroundings. Maximal intensity processing (MIP) of the 3D volume data acquired by the SPACE sequence produces 3D images of the high-intensity structures of the labyrinth. The 3D MIP of the SPACE sequence enables fast identification of abnormalities at the level of the SCCs. Narrowing or signal loss at the level of the SCC on MRI was defined when there was <50% of normal SCC diameter compared to the normal side or in consensus in case of bilateral pathology (**Figure 2**).

Statistics

Pearson chi-square tests were used to compare categorical variables. A logistic regression (ANOVA) was used for correction for age. A p-value of 0.05 or less was considered statistically significant.

RESULTS

Forty-five patients with P51S mutations in the *COCH* gene were included in the study (overall, 51% females and 49% males). In total, 90 ears were investigated. Missing data of caloric testing, audiometry, CT, and MRI results are provided in **Tables 1**, **2**. Age at caloric testing during ENG ranged from 44 to 77 years with a mean of 62 ± 10 years. Mean and median time interval between ENG and CT or MRI was 3 and 25 days, respectively. Two patients had their imaging 3 and 4 years after their first ENG. More than half of patients (54%) were candidates for cochlear implantation.

In our population, 91% of tested ears had sclerotic lesions and/or narrowing in one or more SCCs on CT scan. All tested ears had SCC narrowing or signal loss in at least one SCC on T2-weighted MRI. Moreover, in 83% of tested ears, all three SCCs were affected on MRI. The number affecting all SCCs per year on CT was 10%. On CT, 22% of tested ears had abnormalities of the posterior SCC, while 17% had abnormalities of the superior SCC and 87% had abnormalities of the lateral SCC. On MRI, 84% had abnormalities in the posterior canal, 87% had abnormalities in the superior canal, and 92% had abnormalities in the lateral canal (**Figure 3**).

We tested correlations between the ears with severe hearing loss >85 dB HL, therefore CI candidates, with CT and MRI. There was no correlation between audiometry and abnormalities on MRI in one of the SCCs. However, there was a correlation between audiometry and CT imaging abnormalities. This was statistically significant when there was an abnormality in one of the SCCs ($p = 0.001$) as well as in the posterior ($p < 0.001$), superior ($p = 0.001$) and lateral canal ($p = 0.001$) separately (**Tables 1**, **2**).

Moreover, 77% of tested ears showed a bilateral and 11.5% showed a unilateral hypofunction on ENG while 11.5% showed a normal result. CT abnormalities correlated with caloric

TABLE 1 | Overview of audiometry and caloric testing results with the missing data in all 90 ears.

	N	Normal/abnormal
Caloric testing	$n = 52$ Missing, $n = 38$	Normal, $n = 9$ (17%) Hypofunction, $n = 43$ (83%)
Audiometry	$n = 50$ Missing, $n = 40$	Non-CI candidates, $n = 23$ (46%) CI candidates, $n = 27$ (54%)

TABLE 2 | Correlation between lateral semicircular canal function loss (caloric testing) or pure tone audiometry and imaging abnormalities of the three SCC on CT and MRI.

	The different SCC	*n*	Audiometry (*p*-value)	Caloric testing (*p*-value)
CT $n = 23$ Missing, $n = 67$	Any abnormality	$n = 21$ (91%)	0.001	0.025
	Lateral	$n = 20$ (87%)	0.001	0.025
	Posterior	$n = 5$ (22%)	<0.001	NS
	Superior	$n = 4$ (17%)	0.001	NS
MRI $n = 38$ Missing, $n = 52$	Any abnormality	$n = 38$ (100%)	NS	0.042
	Lateral	$n = 35$ (92%)	NS	NS
	Posterior	$n = 32$ (84%)	NS	NS
	Superior	$n = 33$ (87%)	NS	NS

NS, not statistically significant difference.

hypofunction. This statistically significant difference was present if abnormalities were observed in at least one of the SCCs ($p = 0.025$) as well as in ipsilateral lateral SCC function loss ($p = 0.025$). MRI abnormalities in at least one of the SCC correlated with caloric hypofunction ($p = 0.042$), but there was no direct correlation with lateral SCC abnormalities on MRI and ENG (**Tables 1**, **2**). Finally, there was no statistically significant correlation between advanced age and the presence of caloric areflexia or the presence of any abnormalities on temporal bone CT scan or MRI.

DISCUSSION

During the last decades, many genotype–phenotype observational reports with auditory and vestibular testing have shown limited variability across subjects and helped to characterize DFNA9 (5, 13, 14). Recently, JanssensdeVarebeke et al. described a correlation between hearing loss and radiological abnormalities in patients with DFNA9, specifically with a P15S mutation in the *COCH* gene (9). This study suggested that radiological findings and the degree of hearing loss are both linked to the stage of this hereditary disease (9). However, vestibular function testing was not reported. Therefore, the radiological abnormalities observed in DFNA9 might also reflect the presence of vestibular function loss. Overall, correlations between vestibular function and imaging were not studied in the work by JanssensdeVarebeke et al.

Our analysis demonstrated a statistically significant correlation between CT and MRI abnormalities at the level of the SCC and caloric areflexia and hypofunction on ENG in patients with DFNA9. These imaging abnormalities are therefore of potential interest as biomarkers associated with a vestibular decay in DFNA9 patients. The only other published radiologic abnormality was reported in one patient with DFNA9 mutation presenting with bilateral superior semicircular canal dehiscence (SSCD) on CT imaging (4). While another case of SSCD was identified on histopathology in a DFNA9 patient, probably a circumstantial finding unrelated to DFNA9 (15).

A possible hypothesis for the radiologic abnormalities has been described as protein misfolding and eosinophilic containing deposits (6, 16). Another hypothesis suggests that these findings are the results of early stage fibrosis followed by end-stage ossification secondary to a slowly progressing inflammatory reaction. The study by JanssensdeVarebeke et al. demonstrated that 31% of the lesions on MRI were not detected on CT imaging, suggesting fibrosis (without sclerosis) at these sites (9). It is noteworthy that no enhancement of the SCC can be observed after administration of gadolinium on T1-weighted images. Our analysis also demonstrated sclerotic lesions and/or narrowing in one or more SCCs on CT scan in 91% of patients while all patients had SCC narrowing or signal loss on T2-weighted MRI. Therefore, MRI is more sensitive for detecting these radiologic abnormalities. Still, CT shows more significant correlations with audiometry as well as ENG results. These results might be explained by the pathophysiology of the fibrosis process. Possibly only the patients with more severe cochleovestibular deterioration show abnormalities on CT. Meaning that the process is started with fibrosis (sensitive on MRI) and ends with ossification (also easily seen on CT). Although this might be a possible explanation of the pathophysiology, there might be a contradiction with our correlation results. If fibrosis (which is easily seen on MRI) is the pathophysiology that explains the abnormal caloric responses in patients with DFNA9, we would expect strong correlations between these vestibular testings and MRI and not CT as we found (which easily shows the process of ossification).

Quesnel et al. described mechanisms that could explain delayed and progressive sensorineural hearing loss due to fibrous tissue deposition after hearing preservation cochlear implantation (17). They hypothesized that fibrous and bony tissue growth result in an increase in round window impedance and an occlusion of pressure outlets in the scala tympani. Afterwards, the pressure difference drops (pressures in both scalae are high) and a loss of input pressure drive occurs, finally causing sensorineural hearing loss (17). Van Rompaey et al. already suggested a correlation between these described fibrous tissue deposits and vestibular function loss (18, 19). Their study in patients with bilateral severe-to-profound SNHL, eligible for cochlear implantation, but excluding DFNA9 patients, showed abnormalities on T2-weighted MRI correlating to caloric areflexia. Thus, narrowing and/or signal loss in one or more SCCs is a finding not only in patients with DFNA9 but also in

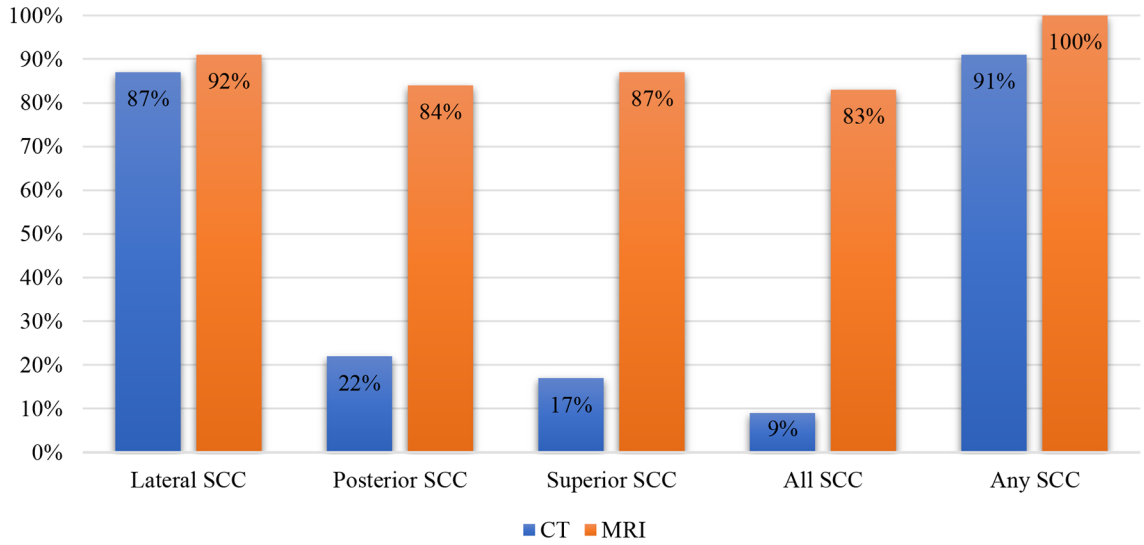

FIGURE 3 | A bar plot illustrating the percentages of the affected semicircular canals on CT and MRI.

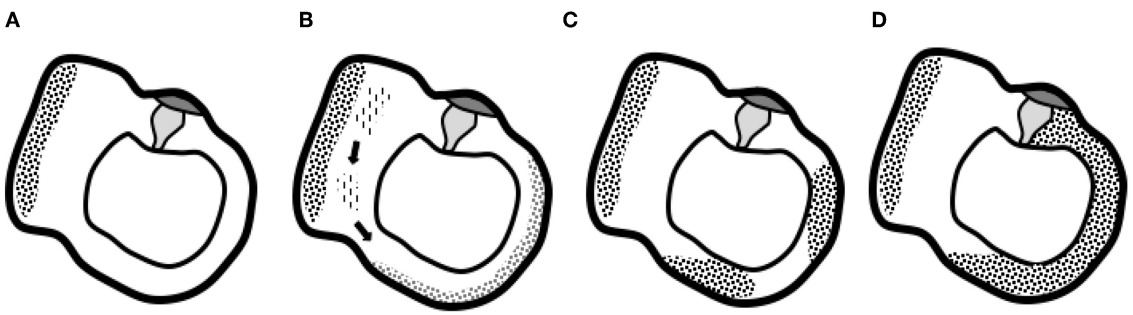

FIGURE 4 | Graphical representation of the suggested hypothesis. **(A)** Normal situation of the utricle and lateral semicircular canal with the utricle's macula and semicircular canal's cupula. **(B)** Progressive degeneration of the membranous labyrinth in the utricle might produce proteins that dislocate and accumulate in the semicircular canal. **(C)** Deposits eventually completely obstruct the semicircular canal and prevent the cupula from detecting angular acceleration of endolymph **(D)**, the end-stage ossification (18).

patients with vestibular hypofunction/areflexia without known hereditary etiology. The hypothesis suggested by Van Rompaey et al. (18) translates the theory put forward by Quesnel et al. from the cochlea to the vestibular system. More specifically, a progressive accumulation of fibrous tissue deposits toward the SCC membranous ampulla can decrease the impedance of the cupula and the convective current of the endolymph produced by caloric irrigation, which does not stimulate vestibular hair cells to send an afferent signal. Thus, the cupula is obstructed in its movement without the need for vestibular hair cell degeneration. Possibly, degeneration at the level of the utricle results in aggregates of protein that dislocate and accumulate at the cupula, which prevents it from detecting angular acceleration of endolymph (**Figure 4**) (18). A progressive accumulation of fibrous tissue deposits toward the SCC membranous ampulla can decrease the impedance of the cupula and the convective current of the endolymph produced by caloric irrigation, which does not stimulate vestibular hair cells to send an afferent signal. Alternatively, the impedance in the crista ampullaris may also be increased by remodeling of the extracellular matrix. Anyway, the cupula is obstructed in its movement and the apparent hypofunction is due to a hydrodynamic, mechanical cause, without the need for degeneration within the sensory epithelium.

Limitations of our study are the absence of a control group with unilateral or bilateral caloric areflexia without DFNA9. Another limitation is that caloric testing only evaluates lateral SCC function in its low frequencies, while video Head Impulse Testing (vHIT) can provide data on the function of all SCC in its high frequencies. Rabbitt has described that focal obstruction of the membranous labyrinth would not eliminate higher-frequency

responses, which has already been found after superior canal dehiscence plugging. In our study, we described acceleration sensitivity severely affected by complete occlusion of the lumen in the SCC, which would only hold for low-frequency stimuli like calorics. Therefore, a follow-up study using vHIT to test higher-frequency responses would be interesting (20). Moreover, all our patients had a symptomatic P15S *COCH* mutation; thus, future research should investigate correlations between hearing loss, vestibular testing, and imaging in mutations other than P51S. Finally, we did not subgrade our abnormalities of the SCC seen on imaging; we only defined more than 50% of the loss of the canal diameter as abnormal. Future studies using (semi-)automated analysis of the SCC would be helpful to confirm these findings.

To conclude, our retrospective analysis confirms the presence of CT and MRI abnormalities in DFNA9 patients that carry the P51S mutation in the *COCH* gene. A correlation between these radiologic features and vestibular function (tested by means of caloric response) was observed in this population and might also be a biomarker of vestibular decay in patients with P51S *COCH* mutation.

This might be interesting for future research using medical imaging data for algorithms such as Radiomics. Finally, in the future, these results could help diagnose patients in a pre-symptomatic stage as well as patients with normal hearing and bilateral vestibulopathy.

DATA AVAILABILITY STATEMENT

The datasets generated for this study are available on request to the corresponding author.

ETHICS STATEMENT

The studies involving human participants were reviewed and approved by local ethics committee of the Antwerp University Hospital/University of Antwerp (protocol number 16/42/426). Written informed consent for participation was not required for this study in accordance with the national legislation and the institutional requirements.

AUTHOR CONTRIBUTIONS

GM collected the data. SD and VV analyzed the CT and MRI and defined the abnormalities. BI did the analysis of the data. BI and VV drafted the manuscript. SJ and PV revised and corrected the manuscript.

FUNDING

Grants from Medel and Cochlear paid to institution and not related to the study.

REFERENCES

1. Lucieer F, Duijn S, Van Rompaey V, Perez Fornos A, Guinand N, Guyot JP, et al. Full spectrum of reported symptoms of bilateral vestibulopathy needs further investigation-a systematic review. *Front Neurol.* (2018) 9:352. doi: 10.3389/fneur.2018.00352
2. JanssensdeVarebeke S, Topsakal V, Van Camp G, Van Rompaey V. A systematic review of hearing and vestibular function in carriers of the Pro51Ser mutation in the COCH gene. *Eur Arch Otorhinolaryngol.* (2019) 276:1251–62. doi: 10.1007/s00405-019-05322-x
3. Vermeire K, Brokx JP, Wuyts FL, Cochet E, Hofkens A, De Bodt M, et al. Good speech recognition and quality-of-life scores after cochlear implantation in patients with DFNA9. *Otol Neurotol.* (2006) 27:44–9. doi: 10.1097/01.mao.0000187240.33712.01
4. Hildebrand MS, Gandolfo L, Shearer AE, Webster JA, Jensen M, Kimberling WJ, et al. A novel mutation in COCH-implications for genotype-phenotype correlations in DFNA9 hearing loss. *Laryngoscope.* (2010) 120:2489–93. doi: 10.1002/lary.21159
5. Pauw RJ, Huygen PL, Collin RW, Cruysberg JR, Hoefsloot LH, Kremer H, et al. Phenotype description of a novel DFNA9/COCH mutation, I109T. *Ann Otol Rhinol Laryngol.* (2007) 116:349–57. doi: 10.1177/000348940711600506
6. Merchant SN, Linthicum FH, Nadol JB Jr. Histopathology of the inner ear in DFNA9. *Adv Otorhinolaryngol.* (2000) 56:212–7. doi: 10.1159/000059105
7. Robertson NG, Hamaker SA, Patriub V, Aster JC, Morton CC. Subcellular localisation, secretion, and post-translational processing of normal cochlin, and of mutants causing the sensorineural deafness and vestibular disorder, DFNA9. *J Med Genet.* (2003) 40:479–86. doi: 10.1136/jmg.40.7.479
8. Street VA, Kallman JC, Robertson NG, Kuo SF, Morton CC, Phillips JO. A novel DFNA9 mutation in the vWFA2 domain of COCH alters a conserved cysteine residue and intrachain disulfide bond formation resulting in progressive hearing loss and site-specific vestibular and central oculomotor dysfunction. *Am J Med Genet A.* (2005) 139A:86–95. doi: 10.1002/ajmg.a.30980
9. de Varebeke SP, Termote B, Van Camp G, Govaerts PJ, Schepers S, Cox T, et al. Focal sclerosis of semicircular canals with severe DFNA9 hearing impairment caused by a P51S COCH-mutation: is there a link? *Otol Neurotol.* (2014) 35:1077–86. doi: 10.1097/MAO.0000000000000283
10. Clark JG. Uses and abuses of hearing loss classification. *ASHA.* (1981) 23:493–500.
11. Van Der Stappen A, Wuyts FL, Van De Heyning PH. Computerized electronystagmography: normative data revisited. *Acta Otolaryngol.* (2000) 120:724–30. doi: 10.1080/000164800750000243
12. Strupp M, Kim JS, Murofushi T, Straumann D, Jen JC, Rosengren SM, et al. Bilateral vestibulopathy: diagnostic criteria consensus document of the classification committee of the Barany society. *J Vestib Res.* (2017) 27:177–89. doi: 10.3233/VES-170619
13. Verstreken M, Declau F, Wuyts FL, D'Haese P, Van Camp G, Fransen E, et al. Hereditary otovestibular dysfunction and Meniere's disease in a large Belgian family is caused by a missense mutation in the COCH gene. *Otol Neurotol.* (2001) 22:874–81. doi: 10.1097/00129492-200111000-00028
14. Kemperman MH, De Leenheer EM, Huygen PL, van Duijnhoven G, Morton CC, Robertson NG, et al. Audiometric, vestibular, and genetic aspects of a DFNA9 family with a G88E COCH mutation. *Otol Neurotol.* (2005) 26:926–33. doi: 10.1097/01.mao.0000185062.12458.87
15. Kamakura T, Nadol JB Jr. Evidence of osteoclastic activity in the human temporal bone. *Audiol Neurootol.* (2017) 22:218–25. doi: 10.1159/000481279
16. Khetarpal U. DFNA9 is a progressive audiovestibular dysfunction with a microfibrillar deposit in the inner ear. *Laryngoscope.* (2000) 110:1379–84. doi: 10.1097/00005537-200008000-00030
17. Quesnel AM, Nakajima HH, Rosowski JJ, Hansen MR, Gantz BJ, Nadol JB Jr. Delayed loss of hearing after hearing preservation cochlear implantation:

Human temporal bone pathology and implications for etiology. *Hear Res.* (2016) 333:225–34. doi: 10.1016/j.heares.2015.08.018
18. Van Rompaey V, De Belder F, Parizel P, Van de Heyning P. Semicircular canal fibrosis as a biomarker for lateral semicircular canal function loss. *Front Neurol.* (2016) 7:43. doi: 10.3389/fneur.2016.00043
19. De Belder J, Matthysen S, Claes AJ, Mertens G, Van de Heyning P, Van Rompaey V. Does otovestibular loss in the autosomal dominant disorder DFNA9 have an impact of on cognition? A systematic review. *Front Neurosci.* (2017) 11:735. doi: 10.3389/fnins.2017.00735
20. Rabbitt RD. Semicircular canal biomechanics in health and disease. *J Neurophysiol.* (2019) 121:732–55. doi: 10.1152/jn.00708.2018

Conflict of Interest: The authors declare that the research was conducted in the absence of any commercial or financial relationships that could be construed as a potential conflict of interest.

frontiers in Neurology

ORIGINAL RESEARCH
published: 10 February 2020
doi: 10.3389/fneur.2019.01353

Intracochlear Perfusion of Tumor Necrosis Factor-Alpha Induces Sensorineural Hearing Loss and Synaptic Degeneration in Guinea Pigs

Sachiyo Katsumi[1,2†], *Mehmet I. Sahin*[1,2†], *Rebecca M. Lewis*[1,2†], *Janani S. Iyer*[1,2,3], *Lukas D. Landegger*[1,2] *and Konstantina M. Stankovic*[1,2,3,4*]

[1] Eaton Peabody Laboratories, Department of Otolaryngology—Head and Neck Surgery, Massachusetts Eye and Ear, Boston, MA, United States, [2] Department of Otolaryngology—Head and Neck Surgery, Harvard Medical School, Boston, MA, United States, [3] Program in Speech and Hearing Bioscience and Technology, Harvard Medical School, Boston, MA, United States, [4] Harvard Program in Therapeutic Science, Harvard Medical School, Boston, MA, United States

OPEN ACCESS

Edited by:
Agnieszka J. Szczepek, Charité Medical University of Berlin, Germany

Reviewed by:
Huib Versnel, University Medical Center Utrecht, Netherlands
Athanasia Warnecke, Hannover Medical School, Germany

***Correspondence:**
Konstantina M. Stankovic
konstantina_stankovic@meei.harvard.edu

[†] These authors have contributed equally to this work and share first authorship

Specialty section:
This article was submitted to Neuro-Otology, a section of the journal Frontiers in Neurology

Received: 09 August 2019
Accepted: 09 December 2019
Published: 10 February 2020

Citation:
Katsumi S, Sahin MI, Lewis RM, Iyer JS, Landegger LD and Stankovic KM (2020) Intracochlear Perfusion of Tumor Necrosis Factor-Alpha Induces Sensorineural Hearing Loss and Synaptic Degeneration in Guinea Pigs. Front. Neurol. 10:1353. doi: 10.3389/fneur.2019.01353

Tumor necrosis factor-alpha (TNF-α) is a proinflammatory cytokine that plays a prominent role in the nervous system, mediating a range of physiologic and pathologic functions. In the auditory system, elevated levels of TNF-α have been implicated in several types of sensorineural hearing loss, including sensorineural hearing loss induced by vestibular schwannoma, a potentially fatal intracranial tumor that originates from the eighth cranial nerve; however, the mechanisms underlying the tumor's deleterious effects on hearing are not well-understood. Here, we investigated the effect of acute elevations of TNF-α in the inner ear on cochlear function and morphology by perfusing the cochlea with TNF-α *in vivo* in guinea pigs. TNF-α perfusion did not significantly change thresholds for compound action potential (CAP) responses, which reflect cochlear nerve activity, or distortion product otoacoustic emissions, which reflect outer hair cell integrity. However, intracochlear TNF-α perfusion reduced CAP amplitudes and increased the number of inner hair cell synapses without paired post-synaptic terminals, suggesting a pattern of synaptic degeneration that resembles that observed in primary cochlear neuropathy. Additionally, etanercept, a TNF-α blocker, protected against TNF-α-induced synaptopathy when administered systemically prior to intracochlear TNF-α perfusion. Findings motivate further investigation into the harmful effects of chronically elevated intracochlear levels of TNF-α, and the potential for etanercept to counter these effects.

Keywords: sensorineural hearing loss, cochlear synaptopathy, tumor necrosis factor-alpha, vestibular schwannoma, unpaired (orphaned) ribbons

INTRODUCTION

Hearing loss is the most common sensory deficit in the world, affecting 466 million people today, and projected to affect 900 million by 2050 (1). The most common type of deafness is sensorineural hearing loss (SNHL), which is caused by damage to the delicate mechanosensory cells and auditory nerve fibers that reside within the inner ear's cochlea. The cochlea is a small, snail-shaped organ

that receives acoustic information from the environment and relays it to the brain. SNHL remains largely irreversible, incurable, and poorly understood in humans due primarily to the cochlea's inaccessibility and the fact that its sensory epithelium, the organ of Corti, cannot be biopsied without damaging hearing.

Although SNHL is typically caused by aging, overexposure to noise or ototoxic drugs, or genetic mutation, an additional potentially life-threatening cause of SNHL is vestibular schwannoma (VS), a non-malignant tumor arising from Schwann cells of the vestibular portion of the eighth cranial nerve, and extending into the cerebellopontine angle of the brain. A striking 95% of VS patients develop SNHL; additional symptoms can include tinnitus, balance difficulties, and facial paralysis (2). The conventional hypothesis regarding the mechanism underlying VS-induced SNHL is that the tumor compresses the vestibulocochlear nerve, preventing neural signals carrying hearing and balance information from traveling from the inner ear to the brain; however, evidence from multi-site, large cohort studies suggests that associations between tumor size and location and SNHL severity are weak (3–7), and that SNHL may (4, 8, 9) or may not (8, 10–13) worsen with tumor growth over time in VS patients. Furthermore, (1) increased outer hair cell-generated distortion product otoacoustic emission (DPOAE) thresholds are observed in VS patients with minimal SNHL, indicating that outer hair cell damage may occur as a primary event, rather than secondary to neuronal damage (14), (2) 90% of human temporal bones from patients with ipsilateral VS show hair cell and neuronal damage that do not correlate with tumor size (15), and (3) biochemically-measured and radiologically-inferred intracochlear fluid protein levels are elevated in ears from poor-hearing VS tumor patients independent of tumor size (16–18).

These reports motivate the hypothesis that VS-induced SNHL is caused, at least in part, by VS-secreted factors that directly damage cochlear hair cells and neurons. Indeed, our laboratory has previously shown that human VSs grouped based on patient hearing ability tend to have different gene expression profiles, suggesting molecular contributions to VS-induced SNHL (19). Focusing specifically on VS secretions that could alter cochlear function by traveling through the internal auditory canal, our group previously identified a significant correlation between levels of VS-secreted pro-inflammatory cytokine tumor necrosis factor alpha (TNF-α) and the degree of a patient's SNHL (20). We further demonstrated that when VS secretions from poor hearing-patients are added to murine cochlear organotypic cultures, the typically resulting cellular damage can be partially prevented by neutralizing TNF-α in these secretions (20). These results strongly implicate TNF-α as a mediator of cochlear degeneration in response to VS secretion exposure, and motivate further investigation into the mechanisms by which TNF-α exerts its impact on cochlear structure and function.

TNF-α is a pro-inflammatory cytokine with key functions in diverse cellular processes, including regulation of the pro-inflammatory responses and maintenance of cellular homeostasis. While the expression of TNF-α is typically undetectable in the normal cochlea (21), it can be induced with aging (22), inflammation (23), noise trauma (24, 25), vibration (21), and exposure to ototoxic drugs including cisplatin, a platinum-based chemotherapeutic, and gentamicin, an aminoglycoside antibiotic (26) in animal models. In humans, elevated TNF-α serum levels have been reported in patients with idiopathic sudden sensorineural hearing loss (ISSNHL) (27) and autoimmune inner ear disease (AIED) (28).

Here, we investigate the effects of *in vivo* intracochlear TNF-α perfusion on cochlear structure and function in guinea pigs. These experiments have implications for understanding the mechanisms of VS-induced SNHL in addition to other forms of SNHL, including ISSNHL, AIED, and noise-induced hearing loss. We perfused TNF-α via the round window, which opens into the perilymph-filled scala tympani, because (a) VS-secreted TNF-α is likely to reach the cochlea via the fundus of the internal auditory canal, which is continuous with the cochlea's perilymph-filled lumina, (b) perilymph bathes the vast majority of cochlear cells, and (c) the round window is surgically accessible in a minimally invasive fashion, using an approach that is similar to the approach routinely used in humans for cochlear implantation. We show that acute *in vivo* TNF-α perfusion leads to an increase in the number of synaptic ribbons without paired post-synaptic receptors, suggesting synaptic degeneration. We also demonstrate the efficacy of etanercept, a TNF-α-inhibitor, for protecting against TNF-α-induced synaptic damage when administered prior to TNF-α. Results suggest a TNF-α-induced pathologic profile that is similar to what is observed in primary cochlear neuropathy.

MATERIALS AND METHODS

Animals and Surgical Procedures

The experimental timeline is outlined in **Figure 1**. All procedures were approved by the Massachusetts Eye and Ear Institutional Animal Care and Use Committee.

Thirteen male albino guinea pigs (Hartley strain; 300–350 g; Charles River Laboratories, Inc., Wilmington, MA) were randomly assigned to one of three experimental groups: control (artificial perilymph, $n = 5$), TNF-α (TNF-α, $n = 4$), and prevention (etanercept + TNF-α, $n = 4$). Animals were anesthetized through intraperitoneal injections of pentobarbital sodium (Nembutal; 25 mg/kg), and intramuscular injections of fentanyl (0.2 mg/kg) and haloperidol (10 mg/kg) as described previously (29). Supplemental doses of 0.07 mg/kg Fentanyl and 3.0 mg/kg Droperidol alternating with 6.25 mg/kg Nembutal were administered as needed to maintain

Abbreviations: μL, microliter; μV, microvolts; ABR, auditory brainstem response; AMPA, α-amino-3-hydroxy-5-methyl-4-isoxazolepropionic acid; CAP, compound action potential; CtBP2, C-terminal-binding protein 2; dB, decibel; DPOAE, distortion product otoacoustic emission; EDTA, ethylenediaminetetraacetic acid; GluA2, glutamate ionotropic receptor AMPA type subunit 2; H&E, hematoxylin and eosin; h, hours; kg, kilogram; kHz, kilohertz; mg, milligram; mL, milliliter; mm, millimeter; mM, millimolar; ms, millisecond; NHS, normal horse serum; PBS, phosphate buffered saline; PFA, paraformaldehyde; SNHL, sensorineural hearing loss; SPL, sound pressure level; TNF-α, tumor necrosis factor-alpha; VS, vestibular schwannoma.

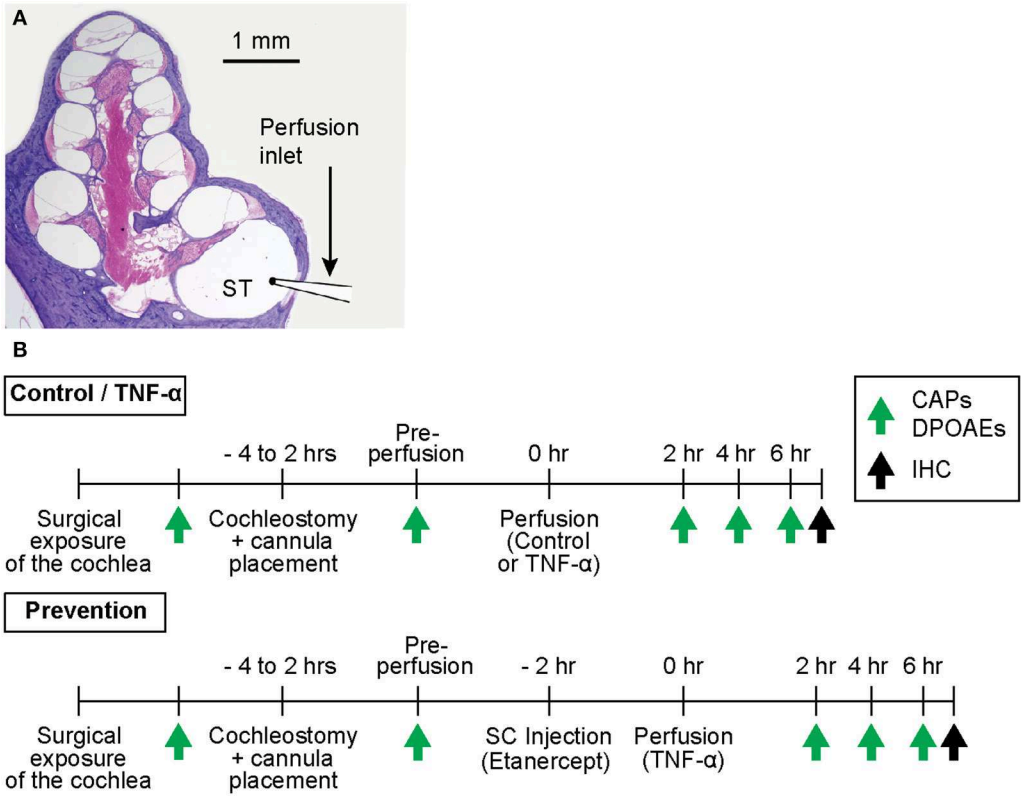

FIGURE 1 | (A) Mid-modiolar cross-section through a hematoxylin and eosin (H&E)-stained guinea pig cochlea, depicting its four spiraling turns. The microcannula is positioned through a cochleostomy adjacent to the round window to enable slow cochlear perfusion through scala tympani (ST). **(B)** Experimental timelines for control and TNF-α experiments vs. prevention experiments. The timelines are identical aside from the subcutaneous (SC) injection of a TNF-α-blocker (etanercept) prior to perfusion of TNF-α in prevention experiments. Green arrows indicate time points of hearing tests (CAPs and DPOAEs), black arrows indicate time point of post mortem immunohistochemistry (IHC).

deep anesthesia (30). A single subcutaneous injection of Atropine (0.04 mg/kg) was provided to minimize salivation and prevent airway edema. Lidocaine (<15 mg/kg, 1 mL) was administered subcutaneously in the periauricular region and external auditory canal (avoiding the middle ear region) to minimize local pain.

A retroauricular incision was made to expose the tympanic bulla. A sharp blade was used to open the bulla and expose the basal turn of the cochlea and the round window. A silver wire electrode was positioned at the round window niche to record CAPs as described below, and a small surgical pick was used to place a cochleostomy 0.5 mm anterior to the round window. A perfusion microcannula was inserted into the cochleostomy (**Figure 1A**) and was fixed to the bulla with glue. A silicon globe stopper was positioned 3 mm from the cannula's tip to prevent the cannula from entering too far into scala tympani, and to seal the cochleostomy. The distal end of the microcannula was connected to a Hamilton syringe filled with control artificial perilymph (130 mM NaCl, 3.5 mM KCl, 1.5 mM $CaCl_2$, 5.5 mM glucose, and 20 mM HEPES; at pH 7.5), or TNF-α (Recombinant Guinea Pig TNF-α Protein; 5035-TG-025 CF, R&D Systems, Inc., Minneapolis, MN; reconstituted to 100 μg/mL in phosphate buffered saline and diluted to 10 μg/mL in artificial perilymph) according to the condition being tested. The TNF-α concentration selected for the present experiments is higher than what we previously reported for human VS secretions (20) because we are using acute animal studies to model chronic and typically slowly-progressing VS-induced hearing loss in humans. Controlled perfusion was achieved using a pump (Harvard Apparatus PHD 2000, Harvard Apparatus, Holliston, MA) set to facilitate perfusion at a rate of 1.5 μL/min over the course of 50 min. For control and TNF-α experiments, a total volume of 7.5 μL of artificial perilymph or TNF-α, respectively, was perfused through scala tympani. For prevention experiments, 0.15 mL of etanercept (Enbrel, Amgen Inc., Thousand Oaks, CA) was injected subcutaneously 2 h prior to TNF-α perfusion (**Figure 1B**). Hearing was tested over the course of each experiment as described below. All experiments were carried out in an electrically- and acoustically-shielded, temperature-controlled chamber.

Animals were euthanized at the experiment's termination through intraperitoneal injections of Fatal Plus (Vortech Pharmaceuticals, Dearborn, MI), followed by intracardiac perfusion with 4% paraformaldehyde (PFA). Inner ears were

immediately extracted and prepared for histological assessment as described below.

Hearing Tests

Hearing was assessed via compound action potentials (CAPs), a measure of the synchronous firing of a population of auditory nerve fibers, and distortion product otoacoustic emissions, a proxy for outer hair cell function, over the course of each experiment. Specifically, hearing was tested just prior to cochleostomy placement, after positioning of the microcannula, and every 2 h after the first intracochlear perfusion until the experiment's termination (typically 6–8 h after the first perfusion).

All sound stimuli were delivered via a custom acoustic assembly comprising two dynamic drivers as sound sources and a miniature electret microphone to measure the sound pressure level (SPL) at the animal's ear (31, 32). Responses to auditory stimuli were monitored using a National Instruments PXI stimulus generation/data acquisition system (National Instruments, Austin, TX). The system was controlled and measurements were recorded using the Eaton Peabody Laboratories Cochlear Function Test Suite (33). All thresholds were measured and recorded at 8 frequencies from 2 to 32 kHz.

CAPs were recorded in response to tone-pip stimuli (0.5 ms duration, 0.5 ms rise-fall; $\cos^2$ onset envelope; 16/s) delivered at SPLs from 10 to 85 dB SPL proceeding in 5 dB steps. The electrode response was amplified (10,000X), filtered (0.3–3 kHz bandpass), and averaged (128 samples at each frequency-level combination). Threshold was defined as the lowest stimulus level at which a repeatable wave could be identified in the response waveform. The minimum input tone pip SPL that could generate a CAP amplitude of at least 0.4 μV was taken to be the CAP threshold of hearing; this value was empirically determined to be the voltage at which CAP amplitudes began to rise linearly with increasing SPL in our system. If the CAP amplitude was <0.4 μV at the maximum tone-pip SPL of 85 dB, the threshold was set to 85 dB.

When two primary tones f1 and f2 are simultaneously played to the inner ear, the cochlea generates acoustic distortion products that propagate back out through the inner and middle ear regions and can be recorded in the external auditory canal using a sensitive microphone. Distortion product otoacoustic emissions (DPOAEs) corresponding to the frequency 2f1–f2 are robust and are frequently measured to assess outer hair cell motility, which is required to generate the distortion products.

These DPOAEs were recorded as response amplitude vs. primary level functions (L1 = 10–80 dB; L2 = L1–10 dB; f1 and f2 incremented together in 5 dB steps); f2/f1 = 1.2 in the ear canal was amplified and digitally sampled at a rate of 200 kHz. Fourier analysis was used to determine the magnitudes of the DPOAE responses at f1, f2, and 2f1–f2. In a DPOAE magnitude spectrum, for a given frequency f, the noise floor was calculated as the average of the response magnitudes at the two frequencies above f and the two frequencies below f. The minimum input SPL required to generate a 2f1–f2 response with magnitude greater than the noise floor at 2f1–f2 was taken to be the DPOAE threshold.

Histology

Immediately following euthanasia and intracardiac perfusion with 4% PFA, inner ears were extracted and dissected to remove extraneous bulla and tissue. Both the round and oval windows were opened and PFA was perfused through the scala tympani and scala vestibuli to ensure thorough fixation of the organ of Corti. Cochleae remained in 4% PFA for 2 h on a shaker and were subsequently placed in 0.12 M EDTA for 2 weeks to decalcify the otic capsule for whole mount preparation.

Histologic sections of the organ of Corti were prepared as previously described (34). In brief, following decalcification, the otic capsule was removed from the cochlea and the spiraling cochlea was microdissected into 10 pieces. Each piece was further microdissected to fully expose the organ of Corti; the spiral ligament, stria vascularis, and tectorial and Reissner's membranes were removed. The resulting cochlear whole mount sections were blocked in 5% normal horse serum (NHS; Sigma-Aldrich, St. Louis, MO) in 1% Triton X-100 (Integra Chemical, Kent, WA) for 1 h, followed by overnight incubation with primary antibodies against hair cell cytoplasm and stereocilia (MYOVIIa rabbit anti-Myosin VIIa from Thermo Fisher Scientific at 1:100 dilution), neurofilament (NF-H, chicken anti-Neurofilament heavy chain from Millipore Sigma, Burlington, MA at 1:200), a synaptic ribbon protein (CtBP2, mouse IgG1 anti-C-terminal binding domain protein 2 from BD Transduction Laboratories at 1:200), and a post-synaptic receptor protein (GluA2, mouse IgG2a anti-Glutamate Receptor A2, from Millipore at 1:100). Following overnight primary incubation at 30°C, each piece was rinsed in PBS three times, and then incubated in secondary antibody diluted in 1% NHS with 1% Triton-X 100. Secondary antibodies included goat anti-rabbit Pacific Blue, goat anti-chicken Alexa 488, goat anti-mouse IgG1 Alexa 568, and goat anti-mouse IgG2a Alexa 647 (all secondaries from Thermo Fisher Scientific at 1:200). Cochlear whole mount pieces were incubated in secondary antibody for two 1-h sessions, and then rinsed in PBS three times. Stained tissue was mounted under coverslips on glass slides with Vectashield mounting media (Vector Laboratories, CA, #H1000).

Imaging and Synapse Quantification

Whole mounts were imaged using a Leica TCS SP8 laser-scanning confocal microscope. Preliminary low magnification (10X) images were acquired and subsequently arranged from base to apex and labeled according to frequency region (5.6, 8, 16, 24, and 32 kHz) using a custom ImageJ plug-in (35). In each dissected piece of the cochlea, a series of arcs is traced over the heads of the pillar cells with this plug-in to compute relative distances along the spiral. These distances are converted into best frequency based on a published cochlear frequency map for the guinea pig (36). The generated frequency maps guided subsequent high magnification (63X) imaging to visualize pre- and post-synaptic processes in the basal region of each inner hair cell.

High magnification z-stacks were uploaded to Amira 3D Software for Life Sciences (Thermo Fisher Scientific) for automated identification and segmentation of ribbons.

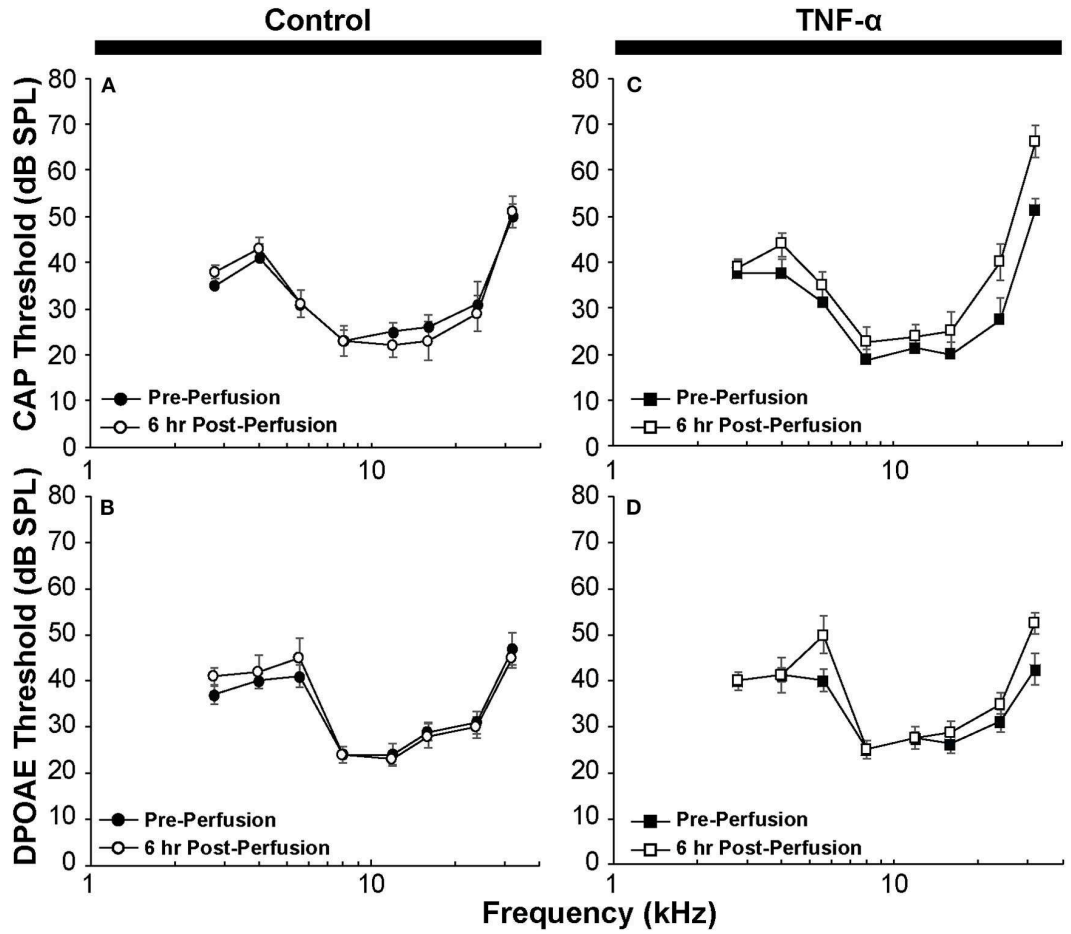

FIGURE 2 | (A) CAP thresholds and **(B)** DPOAE thresholds in control guinea pig before vs. 6 h after perfusion of artificial perilymph through scala tympani demonstrate minimal impact of the surgical and perfusion techniques; $N = 5$ animals. **(C)** CAP thresholds and **(D)** DPOAE thresholds in the TNF-α group before vs. 6 h after intracochlear perfusion of TNF-α; $N = 4$ animals. Error bars represent standard errors of the mean. Differences in thresholds were not statistically significant ($p > 0.05$).

Specifically, custom software (35) was used to locate each CtBP2-representative punctum and display the voxel space immediately surrounding it as a separate image, facilitating clear visualization of paired (with post-synaptic GluA2 receptor) vs. unpaired (orphaned) ribbons. Paired and orphaned ribbons were then counted manually for each frequency region and for each experimental condition.

Statistical Analysis

Differences in DPOAE and CAP thresholds before and after intracochlear perfusion were assessed by two-way ANOVA. Error bars in **Figure 2** indicate standard errors of the mean. When comparing differences in CAP amplitudes and the number of orphaned ribbons per inner hair cell among the three groups, Kruskal Wallis *H*-tests were applied using IBM SPSS and Microsoft Excel software.

RESULTS

CAP thresholds (**Figure 2A**) and DPOAE thresholds (**Figure 2B**) did not change in response to intracochlear perfusion with artificial perilymph, indicating a consistent technique. While CAP (**Figure 2C**) and DPOAE (**Figure 2D**) thresholds 6 h post-TNF-α perfusion did not significantly change in the TNF-α group relative to control, and the growth of DPOAE as a function of sound level was not significantly affected among the groups (**Supplemental Figure 1**), there was a trend indicating an increase in CAP thresholds pre- vs. 6 h post-perfusion at 24 and 32 kHz in the TNF-α group (**Figure 2C**). This trend motivated subsequent analysis of physiologic and morphologic changes in these frequency regions. Specifically, we analyzed CAP amplitudes and afferent synapses between inner hair cells and auditory nerve fibers because previous research has shown that (a) CAP amplitude is a more sensitive metric of neuronal damage than CAP threshold (37), (b) TNF-α-mediated sensorineural damage localizes to the basal turn (38, 39), and (c) these synapses may be damaged even when audiometric thresholds are normal or near-normal (40, 41). For each animal, CAP amplitudes were normalized to the 80 dB SPL pre-intracochlear perfusion response (**Figure 3**). At 32 kHz, there were statistically significant differences in CAP amplitudes across the three experimental groups at multiple sound levels between 70 and 80 dB SPL.

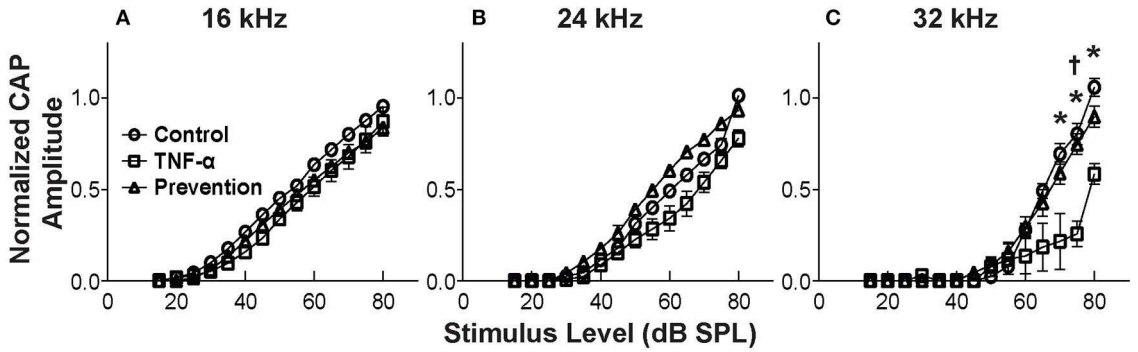

FIGURE 3 | Mean CAP amplitude vs. level functions for 16 kHz **(A)**, 24 kHz **(B),** and 32 kHz **(C)** for the control group (perfused with artificial perilymph), the TNF-α group and the prevention group (animals received etanercept 2 h prior to receiving TNF-α). Amplitudes are normalized to the 80 dB SPL pre-intracochlear perfusion response for each animal. Normalized amplitudes in TNF-α group are significantly decreased relative to control and prevention group at 32 kHz. *, † = statistically significant at $p < 0.05$ for control vs. TNF-α and TNF-α vs. prevention groups, respectively. Error bars represent SEM. Figure legend in **(A)** also applies to **(B,C)**.

Specifically, the analysis at 80 dB SPL revealed χ^2 (2) = 7.517, p = 0.01. Further analysis revealed a significant difference between the TNF-α and control groups [χ^2 (1) = 6.05, p = 0.01], and a similar trend between the TNF-α and prevention groups [χ^2 (1) = 4.133, p = 0.05], but importantly, not between the control and prevention groups [χ^2 (1) = 0.96, p = 0.41]. Similarly, at 75 dB SPL, there was a significant difference in the normalized CAP amplitudes across the three groups [χ^2 (2) = 7.736, p = 0.01]. Further, CAP amplitude was significantly reduced in the TNF-α group relative to the control group [χ^2 (1) = 6.05, p = 0.01] and prevention group [χ^2 (1) = 5.398, p = 0.02]; there was no difference between the control and prevention groups [χ^2 (1) = 0, p = 1]. Finally, at 70 dB SPL, there was statistically significant difference across the three experimental groups [χ^2 (2) = 9.972, p = 0.01]. Additional analysis revealed a significant difference between the TNF-α and control groups [χ^2 (1) = 6.05, p = 0.01], and a similar trend between the TNF-α and prevention groups [χ^2 (1) = 4.133, p = 0.05], but not between the control and prevention groups [χ^2 (1) = 0.06, p = 0.90]. The reduced CAP amplitudes in the TNF-α group compared to the control group indicate a neurotoxic effect of TNF-α. In addition, the observed difference between the control and prevention groups is minimal, demonstrating the efficacy of etanercept for protecting against TNF-α-induced neurotoxicity.

The observed functional effects of TNF-α and etanercept were corroborated by findings from morphologic assessment of inner hair cell synapses (**Figure 4**). The active region of a healthy inner hair cell afferent synapse is characterized by the presence of both (1) an electron-dense pre-synaptic ribbon, and (2) a post-synaptic AMPA glutamate receptor, located at the proximal end of the spiral ganglion auditory nerve fiber that receives an auditory signal from the hair cell and sends it to the brain (**Figures 4A–C**). In our study, ribbon synapses were immunolabeled with an antibody to CtBP2, an important synaptic ribbon protein, and post-synaptic receptors were labeled with an antibody to GluA2, an AMPA receptor protein. The respective signals are shown in red and green in Control (**Figure 4A**), TNF-α (**Figure 4B**), and Prevention (**Figure 4C**) groups where Myosin VIIa-expressing inner hair cells are labeled in blue. Custom software (29) automatically detected and segmented CtBP2-expressing ribbons into separate squares, each depicting the x-y-projection of a 1 μm^3 voxel space centered at a detected ribbon (**Figures 4D–F**). Such segmentation analyses and subsequent counting of projections including CtBP2 signal but not GluA2 signal (i.e., unpaired ribbon synapses, or "orphaned" synapses) was performed at 5.6, 8, 16, 24, and 32 kHz regions (**Figures 4G–I**) and revealed a statistically significant difference in the number of orphaned ribbons per inner hair cell between the three experimental groups at 24 kHz [χ^2 (2) = 9.05, p = 0.001] and 32 kHz [χ^2 (2) = 7.06, p = 0.018] but not at 5.6 kHz [χ^2 (2) = 5.01, p = 0.07], 8 kHz [χ^2 (2) = 2.83, p = 0.26], or 16 kHz [χ^2 (2) = 4.02, p = 0.14]. Further analysis at 32 kHz revealed a statistically significant increase in the number of orphans in the TNF-α group compared to the control group [χ^2 (1) = 4.86, p = 0.03] and prevention group [χ^2 (1) = 5.33, p = 0.03]; importantly, there was no difference between the control and prevention groups [χ^2 (1) = 0.24, p = 0.73]. Similarly, at 24 kHz, there was a statistically significant difference in the number of orphans between the TNF-α and control groups [χ^2 (1) = 6.0, p = 0.02] and a similar trend between the TNF-α and prevention groups [χ^2 (1) = 4.08, p = 0.05], but not between the control and prevention groups [χ^2 (1) = 3.84, p = 0.06]. No significant differences were observed in number of inner or outer hair cells or in the overall number of ribbons across groups. This finding is consistent with our physiologic result, and the previously published results that TNF-α preferentially damages the basal turn of the cochlea (38, 39), supporting the hypotheses that TNF-α has the potential to exert a toxic effect on inner ear structure when present at high concentrations in the inner ear, and that etanercept may protect against the associated degenerative effects if administered in a timely manner.

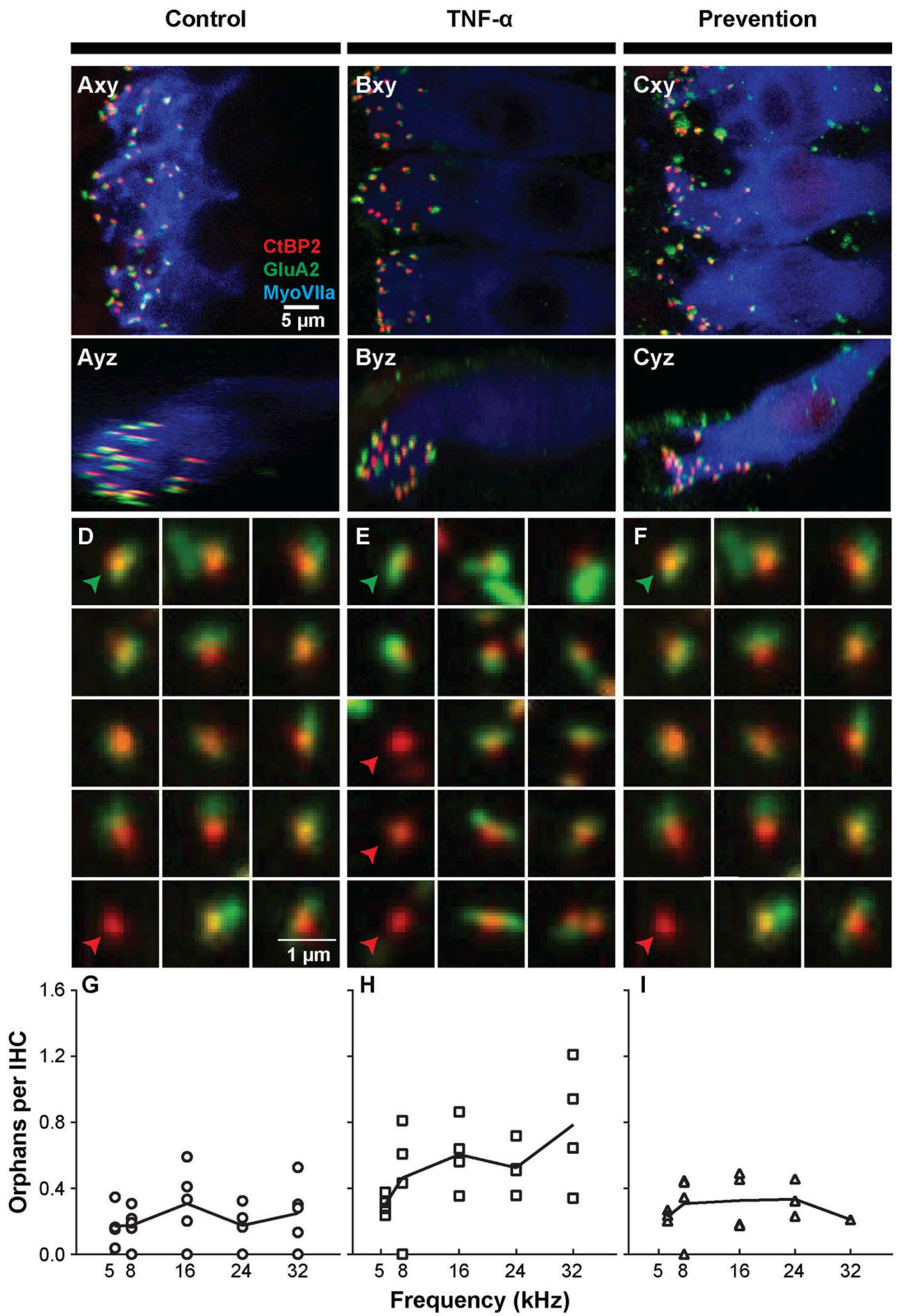

FIGURE 4 | Intracochlear TNF-α perfusion increases the number of orphaned synapses at the basal pole of inner hair cells. Left column shows results from the control group (perfused with artificial perilymph); middle column shows results from the TNF-α group; right column shows results from the prevention group (animals received

(Continued)

FIGURE 4 | etanercept 2 h prior to receiving TNF-α). **(A–C)** Representative confocal images of inner hair cells (IHCs) immunostained for myosin VIIa (blue) with pre-synaptic ribbons stained for CtBP2 (red) and post-synaptic terminals stained for GluA2 (green). Images from the 32-kHz region show maximum projections from "surface" views (*xy*) of three adjacent IHCs and side views (*yz*) of the same confocal image stacks. Green arrowheads point to a paired synapse, i.e., CtBP2- and GluA2-positive puncta, indicating presence of a communicating post-synaptic terminal. Red arrowheads point to unpaired (orphaned) synapses, i.e., CtBP2-positive puncta. Scale bar in **(A)** also applies to **(B,C)**. **(D–F)** Custom software automatically detects and segments ribbon synapses based on presence of the CtBP2 label and associated fluorescence signal. Representative "thumbnail" images depicting detected ribbons in control **(D)**, TNF-α **(E)**, and prevention **(F)** conditions demonstrate the reduced number of ribbons with paired post-synaptic terminals in the TNF-α condition relative to the control and prevention conditions. Each thumbnail depicts the x-y projection of the voxel space within 1 μm of a CtBP2-indicative punctum. Green arrowhead, paired synapses; red arrowhead, unpaired (orphaned) synapse. **(G–I)** The number of orphaned ribbon synapses per inner hair cell at 5.6, 8, 16, 24, 32 kHz in control (**G**; $n = 5$), TNF-α (**H**; $n = 4$), and prevention (**I**; $n = 4$) groups. Each symbol in a panel represents an individual animal. There is a significant difference between the three experimental groups at 24 kHz [χ^2 (2) = 9.05, $p = 0.001$] and 32 kHz [χ^2 (2) = 7.06, $p = 0.018$]. Further, the number of orphaned synapses at 32 kHz is statistically greater in the TNF-α group relative to the control group [χ^2 (1) = 4.86, $p = 0.03$] and prevention group [χ^2 (1) = 5.33, $p = 0.03$]. Similarly, the number of orphaned synapses at 24 kHz is statistically greater in the TNF-α group relative to the control group [χ^2 (1) = 6.0, $p = 0.02$].

DISCUSSION

Here we investigate the structural and functional effects of *in vivo* intracochlear perfusion of TNF-α through the cochlea in guinea pigs to further elucidate the role of TNF-α in SNHL. Our results show that acute elevations in intracochlear levels of TNF-α cause a reduction in the CAP amplitude at 32 kHz in addition to synaptic degeneration along the cochlear length within 6 h of TNF-α administration, without significantly affecting audiometric thresholds. Importantly, these effects were abrogated when etanercept, a TNF-α-blocker, was administered systemically prior to TNF-α perfusion. These findings support the hypothesis that VS-induced SNHL may result in part from TNF-α-containing tumor secretions passing into the cochlea via the internal auditory canal.

The hypothesis that TNF-α may play a role in VS-induced SNHL comes from several studies showing that (a) VS tumor secretions contain high levels of TNF-α (20), (b) VS tumor size and proximity to the inner ear are poorly correlated with SNHL in VS patients (3), and (c) upregulation of TNF-α in the cochlea in response to a variety of etiologies of inner ear disease causes hearing loss (21–25, 42–46). Previous studies have shown upregulated levels of TNF-α following exposure to high levels of noise, implicating TNF-α in acoustic trauma (24, 25, 46). In addition, increased expression of TNF-α has been observed in the modiolus, spiral ganglion, and stria vascularis in mouse models of presbycusis (22), and other groups have shown that vibration-induced SNHL results in upregulation of intracochlear levels of TNF-α (21). Direct inoculation of cerebrospinal fluid with Streptococcus pneumoniae in Mongolian gerbil model led to an increase in TNF-α circulation that was directly associated with bacterial meningitis and elevations in auditory brainstem response (ABR) thresholds (23). Activation of TNF-α is also observed in rodents treated with cisplatin (42, 43) and gentamicin (44, 45), both of which have known structural and functional ototoxic effects. Our findings contribute to this body of work by suggesting that the acute effects of TNF-α exposure on cochlear structure and function may be specific to synaptic degeneration and reduction in CAP amplitudes, respectively. Future work should aim to systematically document the effects of TNF-α exposure on intracochlear structure and function in all of the aforementioned etiologies of SNHL to reveal a potential pattern across diseases, and investigate the longer-term otologic effects of TNF-α upregulation in the inner ear.

The present *in vivo* experiments follow up on our previous *ex vivo* investigations into the effects of applying both recombinant TNF-α and human VS secretions to murine cochlear explants (20). In the *ex vivo* studies, while secretions from specific VS tumors caused inner hair cell damage, outer hair cell damage, and nerve fiber disorganization, application of recombinant TNF-α caused nerve fiber disorganization and a decrease in neurite counts without evidence of any hair cell damage. The present *in vivo* studies were also conducted using recombinant TNF-α, and the observed synaptic degeneration corroborates the findings of nerve fiber disorganization in the previous *ex vivo* studies. Thus, it is likely that the VS secretion-induced hair cell damage observed in our previous *ex vivo* studies occurred due to a longer or different method of exposure, and/or was mediated by a different ototoxic secreted factor or some other mechanism altogether. Relevantly, it is known from studies conducted in the central nervous system that overexpression of TNF-α can cause acute synaptic degeneration via glutamate-mediated cytotoxicity. Specifically, excess TNF-α production has been shown to lead to neuronal death (47) mediated predominantly by TNF receptor 1 activation (48), and it has been demonstrated that TNF-α's neurotoxic action most likely targets the glutamatergic system, potentiating AMPA-induced excitotoxicity (49). In particular, Cueva Vargas et al. (50) reported that TNF-α-induced retinal ganglion cell death in glaucoma may be specifically mediated by increased expression of Ca^{2+}-permeable AMPA receptors that is caused by selective downregulation of the GluA2 subunit of the AMPA receptors in these neurons. Returning to the peripheral auditory system, it is widely accepted that glutamate is the afferent neurotransmitter responsible for communication between inner hair cells and spiral ganglion neuron terminals in the cochlea (51) and that AMPA receptors are abundant and critically important for fast synaptic transmission in the guinea pig cochlea (52). Because we specifically immunostained for presence of the GluA2 subunit of AMPA receptors, our observation of a reduced number of paired synapses in the TNF-α group relative to the artificial perilymph and prevention experimental groups is consistent with Cueva Vargas et al.'s finding in retinal ganglion cells. Importantly, it is likely that we would have observed more widespread degeneration if we had performed longitudinal experiments to study the long-term

effects of chronic overexposure of the inner ear to TNF-α, as other reports (including those from our own lab as described above) have demonstrated deleterious effects on hair cells as well. Future studies should further investigate the mechanisms underlying both hair cell and neuronal damage observed in response to VS secretion exposure, and should be designed to distinguish between acute and chronic effects of the presence of VS secretions in the inner ear.

In a previous *in vivo* study on TNF-α-induced intracochlear cytotoxicity, Keithley et al. (53) investigated whether the mechanism underlying TNF-α-induced SNHL may involve TNF-α-induced recruitment of circulatory leukocytes to the inner ear, as it is known that the inner ear's rapid inflammatory response to antigen/pathogen invasion can cause hearing loss and irreversible damage to the inner ear's mechanosensory structures (54, 55). While they did find that perfusion of high concentrations (2 μg/mL administered over the course of 4 days) of TNF-α induced recruitment of inflammatory cells to the perivascular space around the spiral modiolar vein, they did not observe significant differences between the TNF-α and vehicle experimental groups in click-evoked ABR thresholds *in vivo*, and they observed only minimal differences between these groups in inner and outer hair cell counts *in vitro*. These findings are consistent with our present results; specifically, we also did not observe significant differences in CAP thresholds between the TNF-α and control groups, and did not observe significant differences between these groups in hair cell counts. Keithley et al. did not comment on CAP amplitudes or synaptic integrity in their report. While we cannot directly compare Keithley et al.'s results with ours, because we measured tone-evoked CAPs, both studies nonetheless have important parallels, and reach similar conclusions. Taken together, our current *in vivo* results and previously published *ex vivo* results on application of human VS secretions to mouse cochlear explants suggest that in cases of VS-induced SNHL where inner and outer hair cell death are observed, the hair cell degeneration cannot be explained by acute TNF-α-mediated cytotoxicity alone.

Our finding that administration of etanercept, a TNF-α-blocker, protected the inner ear from TNF-α induced structural and functional transformation is consistent with a large body of literature showing that blocking TNF-α in several contexts of SNHL can prevent subsequent SNHL (56–59). One hypothesis regarding the mechanism of action of TNF-α is that it induces a pre-constrictive state throughout the cochlea's microcirculatory system, thereby decreasing cochlear blood flow and inducing cochlear ischemia. Etanercept has been shown to protect against this vasoconstriction by increasing cochlear blood flow when administered both pre- and post-trauma-inducing stimulus exposure, suggesting its utility for both protection against and rescue from the harmful effects of TNF-α exposure. Ihler et al. (60) demonstrated etanercept's protective effect against TNF-α mediated reductions in cochlear blood flow, while Arpornchayanon et al. (56) showed that systemic administration of etanercept following high noise exposure increased strial capillary blood flow and preserved ABR thresholds relative to animals that were exposed to noise without subsequent etanercept treatment. Importantly, etanercept has already been used pre-clinically for treating classic inflammatory types of SNHL such as labyrinthitis (59). However, a small pilot clinical study did not find etanercept effective for treating autoimmune inner ear disease (57). Our findings are consistent with those showing etanercept's protective effect—we found that providing etanercept prior to TNF-α perfusion promoted preservation of CAP amplitudes and synaptic integrity. Indeed, the animals that received etanercept were not significantly different from the artificial perilymph-receiving controls in their CAP amplitudes and number of orphaned ribbon synapses. Taken together, our results suggest that TNF-α-induced synaptopathy may be prevented by etanercept administration. Although precise mechanisms of this therapeutic effect remain to be determined, it is possible that etanercept prevents TNF-α-induced reduction in cochlear blood flow and local anoxia. These findings motivate further investigation into whether and how etanercept can be used to mediate the effects of trauma-induced TNF-α upregulation in the inner ear to prevent the subsequent irreversible damage.

An important limitation of the present study is the acute nature of the experimental design; specifically, hearing was assessed up to 6 h post-TNF-α perfusion, when animals were immediately sacrificed and ears extracted for histology. By contrast, in previous *in vivo* and *in vitro* studies assessing TNF-α's ototoxic effect on the organ of Corti, animals or cochlear explants, respectively, were kept alive for several days during or after TNF-α treatment before histological processing and assessment (38, 53). The *in vitro* studies showed significant deterioration over the course of several days of incubation in TNF-α-doped culture medium, and significant differences between 2, 4, and 8 days specifically (38). The acute exposure and short experimental timeline in the present studies may explain the observed minimal changes in hearing sensitivity, and inner and outer hair cell integrity.

In summary, although we did not observe any direct effects of TNF-α on CAP or DPOAE thresholds or on hair cell counts, our experiments did reveal that TNF-α specifically caused a decrease in CAP amplitudes accompanied by an increase in the number of unpaired or orphaned ribbon synapses within 6 h of exposure. This finding suggests a pathologic profile that is similar to what is observed in primary cochlear neuropathy—in the latter disease, reductions in ABR Wave I amplitudes and synaptic degeneration are observed with minimal changes in ABR Wave I and DPOAE thresholds and minimal loss of inner and outer hair cells in mice (34, 40) and guinea pigs (29). These synaptic changes occur rapidly, within hours of noise exposure. Moreover, age-related synaptic degeneration long precedes age-related changes in audiometric thresholds or hair cell counts in mice (41). Importantly, both cochlear neuropathy patients and VS patients typically experience difficulties with word recognition and speech-in-noise tasks, which are thought to reflect loss of peripheral axons (37). Future work should investigate the effects of *in vivo* chronic intracochlear exposure to TNF-α and assessment of hearing and cochlear morphology at several sequential time points, in addition to further exploring etanercept's ability to protect against TNF-α-induced SNHL, and rescue hearing function post-exposure to TNF-α. Given that

the brainstem is also located near the cerebellopontine angle, future *in vitro* and *in vivo* brain studies should investigate the brainstem's potential vulnerability to high levels of TNF-α in VS secretions.

DATA AVAILABILITY STATEMENT

The datasets generated for this study are available on request to the corresponding author.

ETHICS STATEMENT

The animal study was reviewed and approved by Massachusetts Eye and Ear Institutional Animal Care and Use Committee.

AUTHOR CONTRIBUTIONS

KS conceived of the project and supervised all the work. KS and MS designed experiments. MS and SK performed electrophysiological measurements. SK and RL performed confocal immunohistochemistry and synaptic counting. SK, RL, and LL performed cochlear microdissections. SK, JI, MS, RL, and KS analyzed data. JI and KS wrote the manuscript. All authors edited the manuscript and approved the final version.

FUNDING

This work was supported by National Institute on Deafness and Other Communication Disorders (R01DC015824), Nancy Sayles Day Foundation, the Lauer Tinnitus Research Center, the Zwanziger Foundation, the Barnes Foundation (all awarded to KS), and the National Defense Science and Engineering Graduate Fellowship (JI).

ACKNOWLEDGMENTS

The authors thank William Sewell, M. Charles Liberman, Tyler Hickman, and Ishmael Stefanov-Wagner for very helpful discussions.

SUPPLEMENTARY MATERIAL

The Supplementary Material for this article can be found online at: https://www.frontiersin.org/articles/10.3389/fneur.2019.01353/full#supplementary-material

Supplemental Figure 1 | Mean DP amplitude (2f1-f2) vs. level functions for f2 =16 kHz **(A)**, 24 kHz **(B)** and 32 kHz **(C)** at 6 h post-perfusion for the three groups. The control group was perfused with artificial perilymph. The prevention group received etanercept 2 h prior to intracochlear TNF-α perfusion. The differences among groups were not statistically significant. Error bars represent SEM. Figure legend in **(A)** also applies to **(B,C)**.

REFERENCES

1. World Health Organization. *Deafness and Hearing Loss*. World Health Organization Fact Sheets (2018). Available online at: https://www.who.int/health-topics/hearing-loss (accessed December 18, 2019).
2. Ren Y, Stankovic KM. The role of tumor necrosis factor alpha (TNFα)in hearing loss and vestibular schwannomas. *Curr Otorhinolaryngol Rep*. (2018) 6:15–23. doi: 10.1007/s40136-018-0186-4
3. Nadol JB Jr, Diamond PF, Thornton AR. Correlation of hearing loss and radiologic dimensions of vestibular schwannomas (acoustic Neuromas). *Am J Otol*. (1996) 17:312–6.
4. Fayad JN, Semaan MT, Lin J, Berliner KI, Brackmann DE. Conservative management of vestibular schwannoma: expectations based on the length of the observation period. *Otol Neurotol*. (2014) 35:1258–65. doi: 10.1097/mao.0000000000000285
5. van de Langenberg R, de Bondt BJ, Nelemans PJ, Dohmen AJ, Baumert BG, Stokroos RJ. Predictors of volumetric growth and auditory deterioration in vestibular schwannomas followed in a wait and scan policy. *Otol Neurotol*. (2011) 32:338–44. doi: 10.1097/MAO.0b013e3182040d9f
6. Yang I, Sughrue ME, Han SJ, Aranda D, Pitts LH, Cheung SW, et al. A comprehensive analysis of hearing preservation after radiosurgery for vestibular schwannoma. *J Neurosurg*. (2010) 112:851–9. doi: 10.3171/2009.8.jns0985
7. van Linge A, Borsboom GJ, Wieringa MH, and Goedegebure A. Hearing loss progresses faster in patients with growing intracanalicular vestibular schwannomas. *Otol Neurotol*. (2016) 37:1442–8. doi: 10.1097/mao.0000000000001190
8. Hajioff D, Raut VV, Walsh RM, Bath AP, Bance ML, Guha A, et al. Conservative management of vestibular schwannomas: third review of a 10-year prospective study. *Clin Otolaryngol*. (2008) 33:255–9. doi: 10.1111/j.1749-4486.2008.01705.x
9. Sughrue ME, Kane AJ, Kaur R, Barry JJ, Rutkowski MJ, Pitts LH, et al. A prospective study of hearing preservation in untreated vestibular schwannomas. *J Neurosurg*. (2011) 114:381–5. doi: 10.3171/2010.4.jns091962
10. Caye-Thomasen P, Dethloff T, Hansen S, Stangerup SE, and Thomsen J. Hearing in patients with intracanalicular vestibular schwannomas. *Audiol Neurootol*. (2007) 12:1–12. doi: 10.1159/000096152
11. Ferri GG, Modugno GC, Pirodda A, Fioravanti A, Calbucci F, and Ceroni AR. Conservative management of vestibular schwannomas: an effective strategy. *Laryngoscope*. (2008) 118:951–7. doi: 10.1097/MLG.0b013e31816a8955
12. Younes E, Montava M, Bachelard-Serra M, Jaloux L, Salburgo F, Lavieille JP. Intracanalicular vestibular schwannomas: initial clinical manifestation, imaging classification, and risk stratification for management proposal. *Otol Neurotol*. (2017) 38:1345–50. doi: 10.1097/mao.0000000000001538
13. Pennings RJ, Morris DP, Clarke L, Allen S, Walling S, Bance ML. Natural history of hearing deterioration in intracanalicular vestibular schwannoma. *Neurosurgery*. (2011) 68:68–77. doi: 10.1227/NEU.0b013e3181fc60cb
14. Gouveris HT, Victor A, and Mann WJ. Cochlear origin of early hearing loss in vestibular schwannoma. *Laryngoscope*. (2007) 117:680–3. doi: 10.1097/MLG.0b013e31803146c5
15. Roosli C, Linthicum FH Jr, Cureoglu S, Merchant SN. Dysfunction of the cochlea contributing to hearing loss in acoustic neuromas: an underappreciated entity. *Otol Neurotol*. (2012) 33:473–80. doi: 10.1097/MAO.0b013e318248ee02
16. Silverstein H. A rapid protein test for acoustic neurinoma. *Arch Otolaryngol*. (1972) 95:202–4. doi: 10.1001/archotol.1972.00770080344003
17. Silverstein H. Labyrinthine tap as a diagnostic test for acoustic neurinoma. *Otolaryngol Clin North Am*. (1973) 6:229–44.
18. Lassaletta L, Martinez-Glez V, Torres-Martin M, Rey JA, Gavilan J. cDNA microarray expression profile in vestibular schwannoma: correlation with clinical and radiological features. *Cancer Genet Cytogenet*. (2009) 194:125–7. doi: 10.1016/j.cancergencyto.2009.06.016
19. Stankovic KM, Mrugala MM, Martuza RL, Silver M, Betensky RA, Nadol JB Jr, et al. Genetic determinants of hearing loss associated with vestibular schwannomas. *Otol Neurotol*. (2009) 30:661–7. doi: 10.1097/MAO.0b013e3181a66ece

20. Dilwali S, Landegger LD, Soares VY, Deschler DG, Stankovic KM. Secreted factors from human vestibular schwannomas can cause cochlear damage. *Sci Rep*. (2015) 5:18599. doi: 10.1038/srep18599
21. Zou J, Pyykko I, Sutinen P, Toppila E. Vibration induced hearing loss in guinea pig cochlea: expression of TNF-alpha and VEGF. *Hear Res*. (2005) 202:13–20. doi: 10.1016/j.heares.2004.10.008
22. Riva C, Donadieu E, Magnan J, Lavieille JP. Age-related hearing loss in CD/1 mice is associated to ROS formation and HIF target proteins up-regulation in the cochlea. *Exp Gerontol*. (2007) 42:327–36. doi: 10.1016/j.exger.2006.10.014
23. Aminpour S, Tinling SP, Brodie HA. Role of tumor necrosis factor-alpha in sensorineural hearing loss after bacterial meningitis. *Otol Neurotol*. (2005) 26:602–9. doi: 10.1097/01.mao.0000178121.28365.0d
24. Fujioka M, Kanzaki S, Okano HJ, Masuda M, Ogawa K, Okano H. Proinflammatory cytokines expression in noise-induced damaged cochlea. *J Neurosci Res*. (2006) 83:575–83. doi: 10.1002/jnr.20764
25. Landegger LD, Vasilijic S, Fujita T, Soares VY, Seist R, Xu L, et al. Cytokine levels in inner ear fluid of young and aged mice as molecular biomarkers of noise-induced hearing loss. *Front Neurol*. (2019) 10:977. doi: 10.3389/fneur.2019.00977
26. So H, Kim H, Lee JH, Park C, Kim Y, Kim E, et al. Cisplatin cytotoxicity of auditory cells requires secretions of proinflammatory cytokines via activation of ERK and NF-kappaB. *J Assoc Res Otolaryngol*. (2007) 8:338–55. doi: 10.1007/s10162-007-0084-9
27. Demirhan E, Eskut NP, Zorlu Y, Cukurova I, Tuna G, Kirkali FG. Blood levels of TNF-alpha, IL-10, and IL-12 in idiopathic sudden sensorineural hearing loss. *Laryngoscope*. (2013) 123:1778–81. doi: 10.1002/lary.23907
28. Svrakic M, Pathak S, Goldofsky E, Hoffman R, Chandrasekhar SS, Sperling N, et al. Diagnostic and prognostic utility of measuring tumor necrosis factor in the peripheral circulation of patients with immune-mediated sensorineural hearing loss. *Arch Otolaryngol Head Neck Surg*. (2012) 138:1052–8. doi: 10.1001/2013.jamaoto.76
29. Lin HW, Furman AC, Kujawa SG, Liberman MC. Primary neural degeneration in the Guinea pig cochlea after reversible noise-induced threshold shift. *J Assoc Res Otolaryngol*. (2011) 12: 605–16. doi: 10.1007/s10162-011-0277-0
30. Brown MC. Recording and labeling at a site along the cochlea shows alignment of medial olivocochlear and auditory nerve tonotopic mappings. *J Neurophysiol*. (2016) 115:1644–53. doi: 10.1152/jn.00842.2015
31. Kang WS, Nguyen K, McKenna CE, Sewell WF, McKenna MJ, Jung DH. Measurement of ototoxicity following intracochlear bisphosphonate delivery. *Otol Neurotol*. (2016) 37: 621–6. doi: 10.1097/mao.0000000000001042
32. Kang WS, Sun S, Nguyen K, Kashemirov B, McKenna CE, Hacking SA, et al. Non-ototoxic local delivery of bisphosphonate to the mammalian cochlea. *Otol Neurotol*. (2015) 36:953–60. doi: 10.1097/mao.0000000000000786
33. Massachusetts Eye and Ear. *Eaton Peabody Laboratories Cochlear Function Testing*. Available online at: https://www.masseyeandear.org/research/otolaryngology/investigators/laboratories/eaton-peabody-laboratories/epl-engineering-resources (accessed September 1, 2019).
34. Jensen JB, Lysaght AC, Liberman MC, Qvortrup K, Stankovic KM. Immediate and delayed cochlear neuropathy after noise exposure in pubescent mice. *PLoS ONE*. (2015) 10:e0125160. doi: 10.1371/journal.pone.0125160
35. Massachusetts Eye and Ear. *ImageJ Plugin for Cochlear Frequency Mapping in Whole Mounts*. Available online at: https://www.masseyeandear.org/research/otolaryngology/investigators/laboratories/eaton-peabody-laboratories/epl-histology-resources/imagej-plugin-for-cochlear-frequency-mapping-in-whole-mounts (accessed September 1, 2019).
36. Tsuji J, Liberman MC. Intracellular labeling of auditory nerve fibers in guinea pig: central and peripheral projections. *J Comp Neurol*. (1997) 381:188–202.
37. Liberman MC, Kujawa SG. Cochlear synaptopathy in acquired sensorineural hearing loss: manifestations and mechanisms. *Hear Res*. (2017) 349:138–47. doi: 10.1016/j.heares.2017.01.003
38. Wu Q, Wang GP, Xie J, Guo JY, Gong SS. Tumor necrosis factor-alpha-induced ototoxicity in mouse cochlear organotypic culture. *PLoS ONE*. (2015) 10:e0127703. doi: 10.1371/journal.pone.0127703
39. Haake SM, Dinh CT, Chen S, Eshraghi AA, Van De Water TR. Dexamethasone protects auditory hair cells against TNFalpha-initiated apoptosis via activation of PI3K/Akt and NFkappaB signaling. *Hear Res*. (2009) 255:22–32. doi: 10.1016/j.heares.2009.05.003
40. Kujawa SG, Liberman MC. Adding insult to injury: cochlear nerve degeneration after "temporary" noise-induced hearing loss. *J Neurosci*. (2009) 29:14077–85. doi: 10.1523/jneurosci.2845-09.2009
41. Sergeyenko Y, Lall K, Liberman MC, Kujawa SG. Age-related cochlear synaptopathy: an early-onset contributor to auditory functional decline. *J Neurosci*. (2013) 33:13686–94. doi: 10.1523/jneurosci.1783-13.2013
42. Altun Z, Olgun Y, Ercetin P, Aktas S, Kirkim G, Serbetcioglu B, et al. Protective effect of acetyl-l-carnitine against cisplatin ototoxicity: role of apoptosis-related genes and pro-inflammatory cytokines. *Cell Prolif*. (2014) 47:72–80. doi: 10.1111/cpr.12080
43. Kaur T, Mukherjea D, Sheehan K, Jajoo S, Rybak LP, Ramkumar V. Short interfering RNA against STAT1 attenuates cisplatin-induced ototoxicity in the rat by suppressing inflammation. *Cell Death Dis*. (2011) 2:e180. doi: 10.1038/cddis.2011.63
44. Bas E, Van De Water TR, Gupta C, Dinh J, Vu L, Martinez-Soriano F, et al. Efficacy of three drugs for protecting against gentamicin-induced hair cell and hearing losses. *Br J Pharmacol*. (2012) 166:1888–904. doi: 10.1111/j.1476-5381.2012.01890.x
45. Wood JW, Bas E, Gupta C, Selman Y, Eshraghi A, Telischi FF, et al. Otoprotective properties of mannitol against gentamicin induced hair cell loss. *Otol Neurotol*. (2014) 35:e187–94. doi: 10.1097/mao.0000000000000342
46. Min JH, Kim CJ, Koh SH, Nam JS, Jeong HM, Lee JH, et al. Expression and distribution of tumor necrosis factor-alpha in mice cochlea exposed to noise. *Korean J Otorhinolaryngol*. (2010) 53:527–33. doi: 10.3342/kjorl-hns.2010.53.9.527
47. Li R, Yang L, Lindholm K, Konishi Y, Yue X, Hampel H, et al. Tumor necrosis factor death receptor signaling cascade is required for amyloid-beta protein-induced neuron death. *J Neurosci*. (2004) 24:1760–71. doi: 10.1523/jneurosci.4580-03.2004
48. Yang L, Lindholm K, Konishi Y, Li R, Shen Y. Target depletion of distinct tumor necrosis factor receptor subtypes reveals hippocampal neuron death and survival through different signal transduction pathways. *J Neurosci*. (2002) 22:3025–32. doi: 10.1523/JNEUROSCI.22-08-03025.2002
49. Bernardino L, Xapelli S, Silva AP, Jakobsen B, Poulsen FR, Oliveira CR, et al. Modulator effects of interleukin-1beta and tumor necrosis factor-alpha on AMPA-induced excitotoxicity in mouse organotypic hippocampal slice cultures. *J Neurosci*. (2005) 25:6734–44. doi: 10.1523/jneurosci.1510-05.2005
50. Cueva Vargas JL, Osswald IK, Unsain N, Aurousseau MR, Barker PA, Bowie D, et al. Soluble tumor necrosis factor alpha promotes retinal ganglion cell death in glaucoma via calcium-permeable AMPA receptor activation. *J Neurosci*. (2015) 35:12088–102. doi: 10.1523/jneurosci.1273-15.2015
51. Puel JL. Chemical synaptic transmission in the cochlea. *Prog Neurobiol*. (1995) 47:449–76.
52. Ruel J, Chen C, Pujol R, Bobbin RP, Puel JL. AMPA-preferring glutamate receptors in cochlear physiology of adult guinea-pig. *J Physiol*. (1999) 518(Pt 3):667–80. doi: 10.1111/j.1469-7793.1999.0667p.x
53. Keithley EM, Wang X, Barkdull GC. Tumor necrosis factor alpha can induce recruitment of inflammatory cells to the cochlea. *Otol Neurotol*. (2008) 29:854–9. doi: 10.1097/MAO.0b013e31818256a9
54. Keithley EM, Woolf NK, Harris JP. Development of morphological and physiological changes in the cochlea induced by cytomegalovirus. *Laryngoscope*. (1989) 99:409–14. doi: 10.1288/00005537-198904000-00010
55. Ma C, Billings P, Harris JP, Keithley EM. Characterization of an experimentally induced inner ear immune response. *Laryngoscope*. (2000) 110:451–6. doi: 10.1097/00005537-200003000-00024
56. Arpornchayanon W, Canis M, Ihler F, Settevendemie C, Strieth S. TNF-alpha inhibition using etanercept prevents noise-induced hearing loss by improvement of cochlear blood flow *in vivo*. *Int J Audiol*. (2013) 52:545–52. doi: 10.3109/14992027.2013.790564
57. Cohen S, Shoup A, Weisman MH, Harris J. Etanercept treatment for autoimmune inner ear disease: results of a pilot placebo-controlled study. *Otol Neurotol*. (2005) 26:903–7. doi: 10.1097/01.mao.0000185082.28598.87

58. Satoh H, Firestein GS, Billings PB, Harris JP, Keithley EM. Tumor necrosis factor-alpha, an initiator, and etanercept, an inhibitor of cochlear inflammation. *Laryngoscope*. (2002) 112:1627–34. doi: 10.1097/00005537-200209000-00019
59. Wang X, Truong T, Billings PB, Harris JP, Keithley EM. Blockage of immune-mediated inner ear damage by etanercept. *Otol Neurotol*. (2003) 24:52–7. doi: 10.1097/00129492-200301000-00012
60. Ihler F, Sharaf K, Bertlich M, Strieth S, Reichel CA, Berghaus A, et al. Etanercept prevents decrease of cochlear blood flow dose-dependently caused by tumor necrosis factor alpha. *Ann Otol Rhinol Laryngol*. (2013). 122:468–73. doi: 10.1177/000348941312200711

Conflict of Interest: The authors declare that the research was conducted in the absence of any commercial or financial relationships that could be construed as a potential conflict of interest.

frontiers in Neurology

REVIEW
published: 05 March 2020
doi: 10.3389/fneur.2020.00141

Genetic Hearing Loss Associated With Autoinflammation

Hiroshi Nakanishi[1,2], *Pragya Prakash*[2], *Taku Ito*[2,3], *H. Jeffrey Kim*[4], *Carmen C. Brewer*[2], *Danielle Harrow*[2], *Isabelle Roux*[2], *Seiji Hosokawa*[1] *and Andrew J. Griffith*[2]*

[1] *Department of Otorhinolaryngology/Head & Neck Surgery, Hamamatsu University School of Medicine, Hamamatsu, Japan,* [2] *Otolaryngology Branch, National Institute on Deafness and Other Communication Disorders, National Institutes of Health, Bethesda, MD, United States,* [3] *Department of Otorhinolaryngology, Tokyo Medical and Dental University, Tokyo, Japan,* [4] *Office of the Clinical Director, National Institute on Deafness and Other Communication Disorders, National Institutes of Health, Bethesda, MD, United States*

Sensorineural hearing loss can result from dysfunction of the inner ear, auditory nerve, or auditory pathways in the central nervous system. Sensorineural hearing loss can be associated with age, exposure to ototoxic drugs or noise, or mutations in nuclear or mitochondrial genes. However, it is idiopathic in some patients. Although these disorders are mainly caused by dysfunction of the inner ear, little of the pathophysiology in sensorineural hearing loss is known due to inaccessibility of the living human inner ear for biopsy and pathological analysis. The inner ear has previously been thought of as an immune-privileged organ. We recently showed that a missense mutation of the *NLRP3* gene is associated with autosomal-dominant sensorineural hearing loss with cochlear autoinflammation in two unrelated families. *NLRP3* encodes the NLRP3 protein, a key component of the NLRP3 inflammasome that is expressed in immune cells, including monocytes and macrophages. Gain-of-function mutations of *NLRP3* cause abnormal activation of the NLRP3 inflammasome leading to IL-1β secretion in a spectrum of autosomal dominant systemic autoinflammatory phenotypes termed cryopyrin-associated periodic syndromes. The affected subjects of our two families demonstrated atypical phenotypes compared with those reported for subjects with cryopyrin-associated periodic syndromes. These observations led us to test the hypothesis that macrophage/monocyte-like cells in the cochlea can mediate local autoinflammation via activation of the NLRP3 inflammasome. The inflammasome can indeed be activated in macrophage/monocyte-like cells of the mouse cochlea, with secretion of IL-1β. The macrophage/monocyte-like cells in the cochlea were also found to be associated with hearing loss in a *Slc26a4*-insufficient mouse model of human deafness. This review addresses our understanding of genetic hearing loss mediated by autoinflammation and macrophage/monocyte-like cells in the cochlea.

Keywords: cryopyrin-associated periodic syndromes, hearing loss, interleukin-1β, macrophage, *NLRP3*, Pendred syndrome, *SLC26A4*

OPEN ACCESS

Edited by:
Agnieszka J. Szczepek, Charité Medical University of Berlin, Germany

Reviewed by:
Peter S. Steyger, Creighton University, United States
Teresa Requena, University of Edinburgh, United Kingdom

***Correspondence:**
Andrew J. Griffith
griffita@nidcd.nih.gov

Specialty section:
This article was submitted to Neuro-Otology, a section of the journal Frontiers in Neurology

Received: *04 November 2019*
Accepted: *07 February 2020*
Published: *05 March 2020*

Citation:
Nakanishi H, Prakash P, Ito T, Kim HJ, Brewer CC, Harrow D, Roux I, Hosokawa S and Griffith AJ (2020) Genetic Hearing Loss Associated With Autoinflammation. Front. Neurol. 11:141. doi: 10.3389/fneur.2020.00141

INTRODUCTION

Sensorineural hearing loss can result from dysfunction of the inner ear, auditory nerve or higher auditory pathways in the central nervous system. Sensorineural hearing loss includes a wide variety of disorders, such as idiopathic sudden sensorineural hearing loss, age-related hearing loss, hearing loss associated with exposure to ototoxic drugs or noise, and almost all heritable forms of non-syndromic hearing loss. Although these disorders are usually caused by dysfunction of the inner ear, the pathophysiology in sensorineural hearing loss is usually unknown due to inaccessibility of the living human inner ear for biopsy and pathological analysis.

In this review, we focus on the hearing loss caused by dysregulation of the NLRP3 inflammasome. The NLRP3 inflammasome is a critical component of a widely studied, canonical inflammatory signaling pathway in the innate immune system. We review syndromic and non-syndromic hearing loss phenotypes caused by an *NLRP3* mutation. We also review the role of cochlear macrophages in a mouse model of genetic hearing loss phenotypes, non-syndromic recessive deafness DFNB4 and Pendred syndrome, caused by variants of the *SLC26A4* gene.

NLRP3 INFLAMMASOME AND ITS ACTIVATION PATHWAY

The *NLRP3* gene (NLR family, pyrin domain containing three, MIM 606416) encodes the NLRP3 protein (also called cryopyrin), a key and eponymous component of the NLRP3 inflammasome (1). The NLRP3 inflammasome is an innate immune sensor expressed in immune cells, such as monocytes, macrophages, and dendritic cells (2–4). The NLRP3 protein consists of an N-terminal pyrin domain (PYD), a central nucleotide-binding oligomerization (NACHT) domain, and a leucine-rich repeat (LRR) domain at the C terminus (5). When the NLRP3 inflammasome is activated, the PYD domain mediates recruitment of ASC (apoptosis-associated speck-like protein containing CARD) and procaspase-1 to form an NLRP3

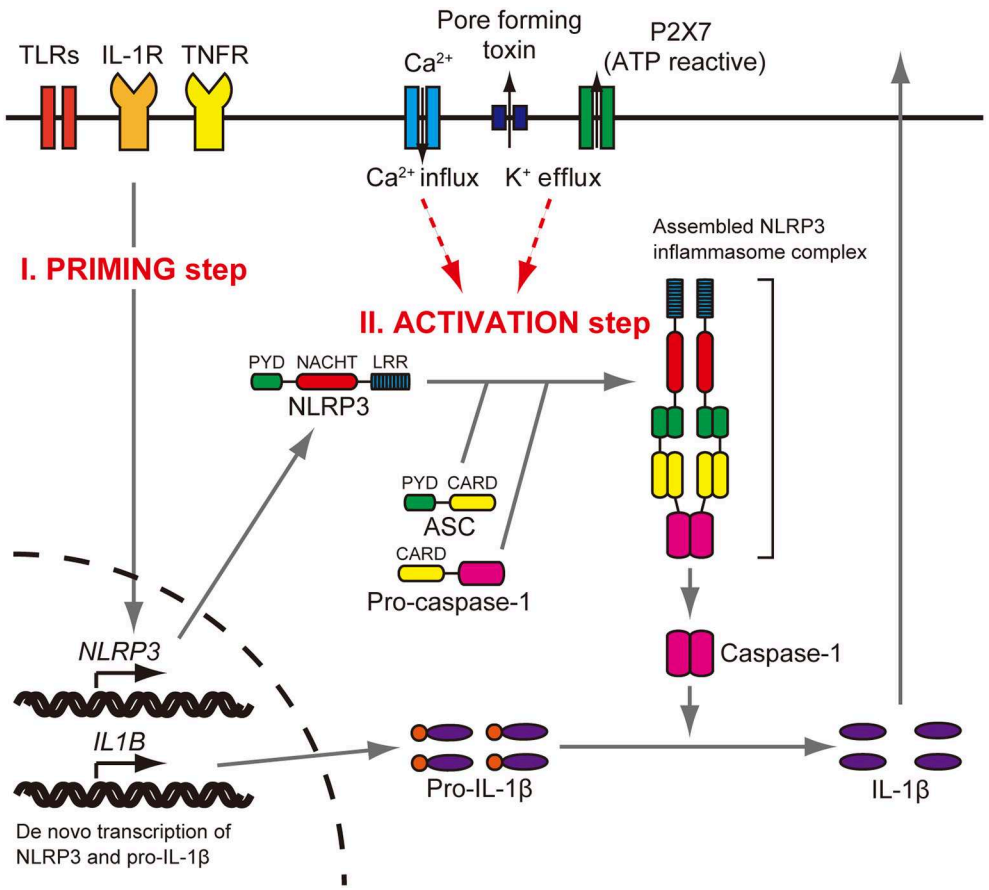

FIGURE 1 | NLRP3 inflammasome activation. Stimulation of Toll-like receptors (TLRs), IL-1 receptor (IL-1R), or tumor necrosis factor receptor (TNFR) increases NLRP3 and pro–IL-1β protein expression (priming step). The activation step involves efflux of K^+, which can be initiated by pore-forming toxin or ATP-triggered channel P2X7, or Ca^{2+} influx. When the NLRP3 inflammasome is activated, the PYD domain mediates recruitment of ASC and procaspase-1 to form a complex that cleaves inactive procaspase-1 to generate active caspase-1. Caspase-1 can process pro–IL-1β to mature IL-1β, which is secreted. Reproduced from Figure S1, Nakanishi et al. (6).

inflammasome complex that cleaves inactive procaspase-1 to form active caspase-1 (**Figure 1**). Caspase-1 can process pro–IL-1β to mature IL-1β, a secreted proinflammatory cytokine (1, 7, 8). Activation of the NLRP3 inflammasome requires at least two signals (9). The initial priming signal includes Toll-like receptor ligands, such as bacterial lipopolysaccharide (LPS), that result in increased NLRP3 and pro–IL-1β mRNA and protein expression (3). The second signal can be one of a variety of activators that include adenosine triphosphate (ATP), extracellular calcium, crystalline molecules, or pore-forming toxins (10, 11). Other second signals include heme, or pathogen associated RNA (12, 13), with further details provided in a recent review (14).

MUTATIONS OF *NLRP3* CAUSE CRYOPYRIN-ASSOCIATED PERIODIC SYNDROMES (CAPS)

Gain-of-function mutations of *NLRP3* cause a spectrum of autosomal-dominant systemic autoinflammatory diseases called cryopyrin-associated periodic syndromes (CAPS). The CAPS spectrum includes three classical clinical subtypes: neonatal-onset multisystem inflammatory disease (NOMID, MIM 607115), Muckle-Wells syndrome (MWS, MIM 191900), and familial cold autoinflammatory syndrome (FCAS, MIM 120100). These phenotypes share signs and symptoms including recurrent fever, rash, headache, conjunctivitis, and arthralgia or arthritis. All of the CAPS subtypes include serologic evidence of systemic inflammation.

NLRP3 mutations lead to CAPS via constitutive activation of the NLRP3 inflammasome and increased IL-1β production (5, 15–18). Monocytes from patients with *NLRP3* mutations only require the initial priming signal, not a second activating signal, to induce IL-1β secretion (15). IL-1β activates cells by binding and signaling through IL-1 receptor type I and the IL-1 receptor accessory protein. Anakinra, a non-glycosylated recombinant version of the endogenous human IL-1 receptor antagonist, significantly improves the clinical signs and symptoms and inflammatory markers of NOMID, MWS, and FCAS (19–21).

AUDITORY PHENOTYPES ASSOCIATED WITH CAPS

Hearing loss is one of the most common manifestations of CAPS (20). Ahmadi et al. reported the prevalence of hearing loss to be 76, 86, 33, and 25% in NOMID, NOMID/MWS, MWS, and FCAS subjects, respectively, among a cohort of 57 patients diagnosed with CAPS (22). Hearing loss was characteristically worse in the higher frequencies and appeared to progress with age. Sensorineural hearing loss was the most common type of hearing loss in all groups: 61% of NOMID, 71% of NOMID/MWS, 33% of MWS, and 25% of FCAS patients.

On MRI- FLAIR examination, cochlear enhancement was detected in 90% of NOMID, 55% of NOMID/MWS, 33% of MWS and 17% of FCAS patients (22). Cochlear enhancement is thought to represent diffusion of contrast material into cochlear tissues from blood vessels comprising the blood-labyrinth barrier that are rendered permeable by inflammation (20, 22).

There are several reports of hearing loss caused by NLRP3-mediated inflammation that was successfully treated with anakinra, an IL-1 receptor antagonist (19–21). After 60 months of anakinra therapy for 26 patients with NOMID, the hearing improved in 30% of ears (23). Hearing loss was stabilized with anakinra therapy in the majority of the patients, but 13 ears developed further hearing loss over 60 months. Cochlear enhancement on MRI-FLAIR was initially observed in 22 of 25 patients. Cochlear enhancement was reduced over 60 months but it was persistent in 14 of 25 patients at 36 months and 10 of 19 patients at 60 months. The incomplete hearing improvement in response to anakinra therapy likely reflects irreversible cochlear damage from prior chronic inflammation, so prompt initiation of therapy at or soon after the onset of SNHL might be essential for preventing or reversing cochlear damage from uncontrolled NLPR3-mediated autoinflammation.

AN *NLRP3* MUTATION CAUSES NON-SYNDROMIC AND SYNDROMIC HEARING LOSS

We recently reported a gain-of-function mutation, c.2753G > A (p.Arg918Gln) in *NLRP3*, that causes autosomal dominant non-syndromic hearing loss (DFNA34) in a North American Caucasian family (LMG113) (6). There were no symptoms or physical signs of systemic inflammation. Their hearing loss was symmetric, bilateral, and progressive. The age of onset varied from the second to fourth decade of life. Post-contrast MRI-FLAIR examination of the temporal bones of two affected members of LMG113 revealed pathologic enhancement of the cochlea that was similar but less severe than that observed in NOMID or MWS patients with sensorineural hearing loss. These results indicate that the subjects had sensorineural hearing loss associated with radiologic evidence of cochlear inflammation.

The c.2753G > A (p.Arg918Gln) mutation of *NLRP3* also causes sensorineural hearing loss with mixed signs and symptoms of systemic autoinflammation in affected members of an unrelated North American family, LMG446, of mixed Caucasian and Hispanic ancestry (6). The 35 year-old father had a history of progressive bilateral sensorineural hearing loss and symptoms of systemic autoinflammation. His three offspring all carried the p.Arg918Gln mutation and had symptoms and signs of systemic autoinflammation. Thus, the affected members of LMG446 had systemic autoinflammatory phenotypes, but none of them met diagnostic criteria for NOMID, MWS, or FCAS. One sibling (13 yo) had bilateral hearing loss at high frequencies, another (10 yo) had right-sided hearing loss at high frequencies, whereas the youngest (6 yo) had hearing thresholds within normal limits, that may reflect his young age and presymptomatic status. MRI-FLAIR pre-contrast evaluations demonstrated abnormally increased signal in all the affected subjects. This finding was considered to reflect probable evidence of prior inflammation. Family LMG446 thus co-segregates the p.Arg918Gln mutation of *NLRP3* with a novel atypical form of CAPS.

IL-1β BLOCKADE REVERSES HEARING LOSS IN FAMILY LMG446

Three affected members of family LMG446 were treated with subcutaneous anakinra. After 5 months of therapy, the pure-tone audiometric thresholds of two members were completely within normal limits (6). The thresholds of the third family member improved to within the range of age- and sex-adjusted normative thresholds for the left ear. The improvements in hearing correlated with a decrease in MRI-FLAIR signals. These results indicate that hearing loss is associated with cochlear inflammation caused by NLRP3 inflammasome activation.

INNER EAR MACROPHAGES EXPRESS *NLRP3*

All of these observations strongly implicate cochlear inflammation in the pathogenesis of hearing loss. This raises the question of whether the hearing loss is secondary to systemic autoinflammation with cochlear infiltration of circulating immune cells, or primary autoinflammation with pathologic activation of the NLRP3 inflammasome within the resident immune cells of the cochlea.

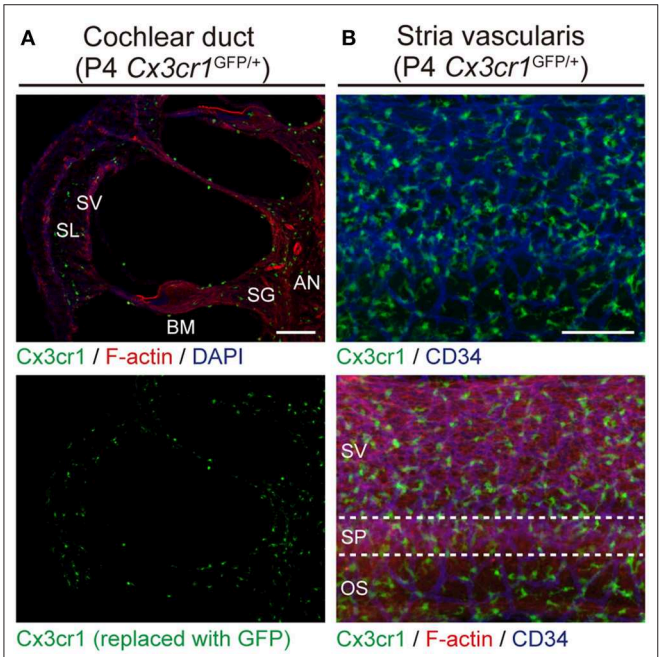

FIGURE 2 | Resident macrophage-like cells in mouse cochlea. **(A)** P4 *Cx3cr1*$^{GFP/+}$ cochleae have GFP$^+$ cells scattered throughout the cochlea, including the auditory nerve (AN), spiral ganglion (SG), basilar membrane (BM), stria vascularis (SV), and spiral ligament (SL). Phalloidin (red) and DAPI (blue) label F-actin and nuclei, respectively. **(B)** Lateral wall of a P4 *Cx3cr1*$^{GFP/+}$ cochlea with GFP$^+$ cells mainly localized around blood vessels (blue, labeled with anti-CD34 antibody). SV, stria vascularis; SP, spiral prominence; OS, outer sulcus; scale bars, 100 μm. Reproduced from Figure 7, Nakanishi et al. (6). GFP$^+$ cells are similarly distributed in all parts of the cochlea at P30 (6).

Cx3cr1^{GFP} mice can be used to identify monocytes, as well as subsets of NK cells, dendritic cells, and resident macrophages (24). Adult *Cx3cr1*$^{GFP/GFP}$ mouse cochleae have GFP$^+$ cells which also express a lymphocyte marker CD45 and macrophage markers CD68 and Iba1 (25). We also found GFP$^+$ cells scattered throughout the auditory nerve, spiral ganglion, basilar membrane, stria vascularis, and spiral ligament (**Figure 2**) (6). The GFP$^+$ cells were primarily localized adjacent to or near blood vessels in the lateral wall and basilar membrane (**Figure 2**). These GFP$^+$ cells also express the macrophage marker F4/80. These studies demonstrate that these GFP$^+$ cells are tissue-resident macrophage-like cells that exist in the adult mouse cochlea.

We have shown that *Nlrp3* is expressed in cochlea-resident cells expressing *Cx3cr1* (6). *Nlrp3* mRNA was detected in GFP$^+$ cells but not in GFP$^-$ cells, indicating that normal mouse cochlear macrophage-like cells express *Nlrp3*. We did not try to detect or analyze NLRP3 protein since we were unaware of any commercial or custom antibodies that were specific.

NLRP3 INFLAMMASOME CAN BE ACTIVATED IN INNER EAR MACROPHAGES

To determine if the NLRP3 inflammasome can be activated in wild-type mouse cochleae (postnatal day 3–4, C57BL/6J mouse strain), we measured levels of IL-1β in supernatants of cultured wild-type mouse cochlear tissues. Higher levels of IL-1β were secreted from cultured cochleae stimulated with LPS and ATP, in comparison to cochleae cultured with

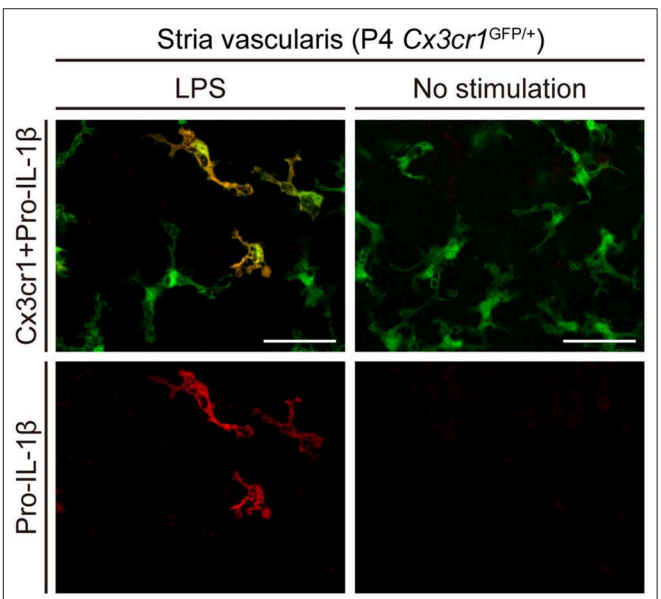

FIGURE 3 | Cultured lateral wall of a P4 *Cx3cr1*$^{GFP/+}$ cochlea stained with anti-IL-1β antibody (red). Pro-IL-1β immunoreactivity is present in a subset of GFP$^+$ cells from cultured cochleae stimulated with LPS, whereas no immunoreactivity is detected without stimulation. Scale bars, 50 μm. Reproduced from Figure 10, Nakanishi et al. (6).

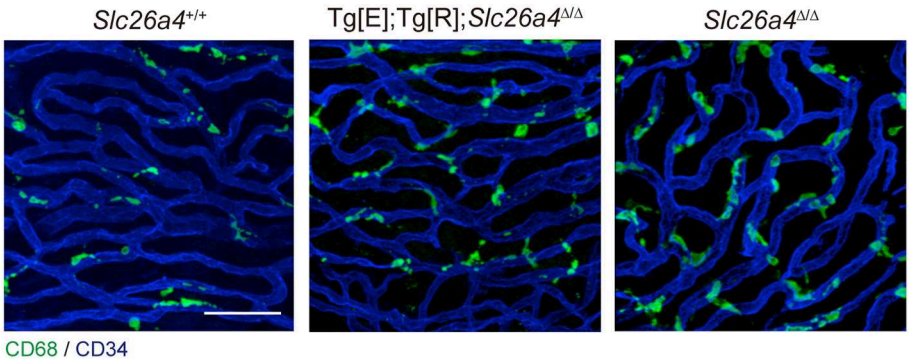

FIGURE 4 | Whole-mount preparation of stria vascularis at 1 month of age stained with anti-CD68 (green) and anti-CD34 antibodies (blue). Anti-CD68 antibodies stain cells of the macrophage–monocyte lineage in control (*Slc26a4*$^{+/+}$; left), *Slc26a4*-insufficient (Tg[E];Tg[R];*Slc26a4*$^{\Delta/\Delta}$; middle) and *Slc26a4*-null (*Slc26a4*$^{\Delta/\Delta}$; right) stria vascularis. The area of anti-CD68 staining was higher in *Slc26a4*-insufficient ears compared to control ears, and the area of staining was even higher in *Slc26a4*-null ears. *Slc26a4*-insufficient (Tg[E];Tg[R];*Slc26a4*$^{\Delta/\Delta}$) mice have the effector transgene (Tg[E]) and the responder transgene (Tg[R]). All *Slc26a4* expression is under the control of doxycycline (33). Blood vessels were stained with anti-CD34 antibodies (blue). Scale bar, 40 μm. Reproduced from Figure 7, Ito et al. (32).

LPS but not ATP (6). Furthermore, intracellular pro-IL-1β expression was elevated in some cochlear *Cx3cr1*$^{+}$ cells in response to LPS stimulation (**Figure 3**). Mature IL-1β could not be detected in this experiment since it is secreted extracellularly. These findings indicate that macrophage/monocyte-like cells in the cochlea are cells in which the NLRP3 inflammasome exists and can be activated. Thus, these data indicate that some macrophage/monocyte-like cells in the cochlea can be associated with an innate immune response and hearing loss.

COCHLEAR INFLAMMATION AND HEARING LOSS FLUCTUATION IN A MOUSE MODEL OF PENDRED SYNDROME

The stria vascularis is located in the lateral wall of the cochlea and is composed of three layers of cells: marginal cells, intermediate cells, and basal cells. The stria vascularis contains an extensive vascular network that is physiologically compartmentalized from surrounding strial cells by the blood-labyrinth barrier. The blood-labyrinth barrier includes a layer of endothelial cells connected by tight junctions within the walls of strial blood vessels. The stria vascularis produces endolymph and generates the endocochlear potential that is required for inner ear sensory hair cell function. The normally functioning tight junction-based blood-labyrinth barrier is believed to prevent or restrict the diffusion of immune cells, inner ear antigens, and antibodies between the circulation and the strial tissue (26, 27). Macrophages also exist adjacent to or near blood vessels in the stria vascularis, and have been referred to as perivascular macrophage/monocyte-like cells in some publications (28, 29). The integrity of the blood-labyrinth barrier in the stria vascularis is thought to be maintained by vascular endothelial cells, intermediate cells and perivascular macrophages. In fact, depletion of perivascular macrophage by gene targeting produced leaky capillaries and elevated hearing thresholds *in vivo* (30).

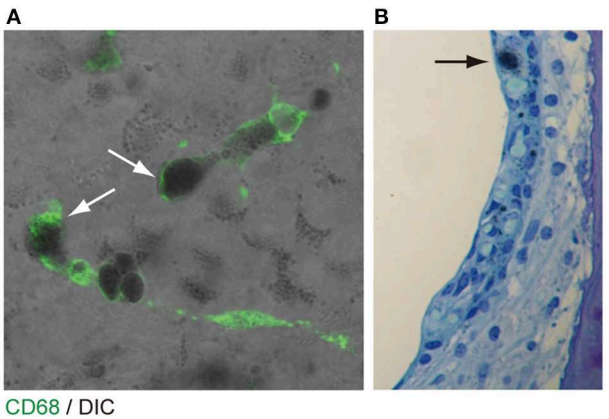

FIGURE 5 | Pigmentation granules and macrophages in the stria vascularis. **(A)** Whole mount preparation of P30 *Slc26a4*-insufficient (Tg[E];Tg[R];*Slc26a4*$^{\Delta/\Delta}$) stria vascularis stained with anti-CD68 antibody (green). Many pigmentations granules of variable size and shape were observed, some of which were associated with macrophages labeled by CD68 antibody (arrows). Macrophages appear to phagocytose parts of aggregated pigmentation and degenerated intermediate cells. **(B)** P30 *Slc26a4*-insufficient cochlear section stained with toluidine blue. Pigmentation is localized in the intermediate cell layer. *Slc26a4*-insufficient (Tg[E];Tg[R];*Slc26a4*$^{\Delta/\Delta}$) mice have the effector transgene (Tg[E]) and the responder transgene (Tg[R]). All *Slc26a4* expression is under the control of doxycycline (33). Reproduced from Figure 9, Ito et al. (32).

The origin of the perivascular macrophages in the normal resting stria vascularis is controversial (30, 31). However, significant macrophage invasion or proliferation or both are observed in the *Slc26a4*-null mouse, a model of Pendred syndrome (31). We characterized macrophages in an *Slc26a4*-insufficient mouse with fluctuation of hearing and endocochlear potential (32). The area of staining with anti-CD68 antibodies in the stria vascularis was correlated with the severity of hearing loss (**Figure 4**). Also, there was a strong correlation of click

ABR thresholds with *Cd68* mRNA levels. These data support the hypothesis that macrophage activity is affecting hearing by influencing the function of the stria vascularis. Additionally, we observed that macrophages appeared to phagocytose pigment granules, which are increased in the stria vascularis of *Slc26a4*-insufficient cochleae (**Figure 5**). The roles of hyperpigmentation and macrophage invasion, activation or proliferation within the stria vascularis of the *Slc26a4*-insufficient cochlea remain undetermined. However, similar observations were reported for macrophages in the iris and ciliary body of the anterior chamber of the eye, presumably to ensure excess pigment granules are retained in the tissue and not released into the anterior chamber of the eye (34).

CONCLUSION

Macrophage-like cells are scattered throughout all cochlear tissues, including the auditory nerve, spiral ganglion, basilar membrane, stria vascularis, and spiral ligament. The p.Arg918Gln mutation in *NLRP3* can cause non-syndromic sensorineural hearing loss as well as an atypical presentation of CAPS. In wild-type mouse cochlea, the NLRP3 inflammasome exists and can be activated in the macrophages. These results support the hypothesis that local cochlear activation of the NLRP3 inflammasome can induce cochlear autoinflammation and sensorineural hearing loss in the affected subjects. In an *Slc26a4*-insufficient mouse model of sensorineural hearing loss, macrophage activity is likely affecting hearing by influencing the function of the stria vascularis. Thus, macrophages in the cochlea can affect cochlear and auditory function in more than one disorder and, possibly, in many disorders of hearing.

AUTHOR CONTRIBUTIONS

All authors listed have made a substantial, direct and intellectual contribution to the work, and approved it for publication.

ACKNOWLEDGMENTS

We thank Thomas Friedman and Michael Hoa for critical review of this manuscript. This research was supported (in part) by the Intramural Research Program of the NIH, NIDCD (Z01-DC000060 to AG).

REFERENCES

1. Agostini L, Martinon F, Burns K, McDermott MF, Hawkins PN, Tschopp J. NALP3 forms an IL-1beta-processing inflammasome with increased activity in Muckle-Wells autoinflammatory disorder. *Immunity.* (2004) 20:319–25. doi: 10.1016/S1074-7613(04)00046-9
2. Sutterwala FS, Ogura Y, Szczepanik M, Lara-Tejero M, Lichtenberger GS, Grant EP, et al. Critical role for NALP3/CIAS1/Cryopyrin in innate and adaptive immunity through its regulation of caspase-1. *Immunity.* (2006) 24:317–27. doi: 10.1016/j.immuni.2006.02.004
3. Guarda G, Zenger M, Yazdi AS, Schroder K, Ferrero I, Menu P, et al. Differential expression of NLRP3 among hematopoietic cells. *J Immunol.* (2011) 186:2529–34. doi: 10.4049/jimmunol.1002720
4. Gross O, Yazdi AS, Thomas CJ, Masin M, Heinz LX, Guarda G, et al. Inflammasome activators induce interleukin-1α secretion via distinct pathways with differential requirement for the protease function of caspase-1. *Immunity.* (2012) 36:388–400. doi: 10.1016/j.immuni.2012.01.018
5. Hoffman HM, Mueller JL, Broide DH, Wanderer AA, Kolodner RD. Mutation of a new gene encoding a putative pyrin-like protein causes familial cold autoinflammatory syndrome and Muckle-Wells syndrome. *Nat Genet.* (2001) 29:301–5. doi: 10.1038/ng756
6. Nakanishi H, Kawashima Y, Kurima K, Chae JJ, Ross AM, Pinto-Patarroyo G, et al. NLRP3 mutation and cochlear autoinflammation cause syndromic and nonsyndromic hearing loss DFNA34 responsive to anakinra therapy. *Proc Natl Acad Sci USA.* (2017) 114:E7766–75. doi: 10.1073/pnas.1702946114
7. Martinon F, Burns K, Tschopp J. The inflammasome: a molecular platform triggering activation of inflammatory caspases and processing of proIL-beta. *Mol Cell.* (2002) 10:417–26. doi: 10.1016/S1097-2765(02)00599-3
8. Mariathasan S, Newton K, Monack DM, Vucic D, French DM, Lee WP, et al. Differential activation of the inflammasome by caspase-1 adaptors ASC and Ipaf. *Nature.* (2004) 430:213–8. doi: 10.1038/nature02664
9. Sutterwala FS, Haasken S, Cassel SL. Mechanism of NLRP3 inflammasome activation. *Ann N Y Acad Sci.* (2014) 1319:82–95. doi: 10.1111/nyas.12458
10. Horvath GL, Schrum JE, De Nardo CM, Latz E. Intracellular sensing of microbes and danger signals by the inflammasomes. *Immunol Rev.* (2011) 243:119–35. doi: 10.1111/j.1600-065X.2011.01050.x
11. Lee GS, Subramanian N, Kim AI, Aksentijevich I, Goldbach-Mansky R, Sacks DB, et al. The calcium-sensing receptor regulates the NLRP3 inflammasome through Ca2+ and cAMP. *Nature.* (2012) 492:123–7. doi: 10.1038/nature11588
12. Gupta R, Ghosh S, Monks B, DeOliveira RB, Tzeng TC, Kalantari P, et al. RNA and β-hemolysin of group B Streptococcus induce interleukin-1β (IL-1β) by activating NLRP3 inflammasomes in mouse macrophages. *J. Biol. Chem.* (2014) 289:13701–5. doi: 10.1074/jbc.C114.548982
13. Erdei J, Tóth A, Balogh E, Nyakundi BB, Bányai E, Ryffel B, et al. Induction of NLRP3 inflammasome activation by heme in human endothelial cells. *Oxid Med Cell Longev.* (2018) 20:4310816. doi: 10.1155/2018/4310816
14. Kelley N, Jeltema D, Duan Y, He Y. The NLRP3 Inflammasome: An Overview of Mechanisms of Activation and Regulation. *Int J Mol Sci.* (2019) 20:E3328. doi: 10.3390/ijms20133328
15. Aksentijevich I, Nowak M, Mallah M, Chae JJ, Watford WT, Hofmann SR, et al. De novo CIAS1 mutations, cytokine activation, and evidence for genetic heterogeneity in patients with neonatal-onset multisystem inflammatory disease (NOMID): a new member of the expanding family of pyrin-associated autoinflammatory diseases. *Arthritis Rheum.* (2002) 46:3340–8. doi: 10.1002/art.10688
16. Feldmann J, Prieur AM, Quartier P, Berquin P, Certain S, Cortis E, et al. Chronic infantile neurological cutaneous and articular syndrome is caused by mutations in CIAS1, a gene highly expressed in polymorphonuclear cells and chondrocytes. *Am J Hum Genet.* (2002) 71:198–203. doi: 10.1086/341357
17. Conforti-Andreoni C, Ricciardi-Castagnoli P, Mortellaro A. The inflammasomes in health and disease: from genetics to molecular mechanisms of autoinflammation and beyond. *Cell Mol Immunol.* (2011) 8:135–45. doi: 10.1038/cmi.2010.81
18. Booshehri LM, Hoffman HM. CAPS and NLRP3. *J Clin Immunol.* (2019) 39:277–86. doi: 10.1007/s10875-019-00638-z
19. Hoffman HM, Rosengren S, Boyle DL, Cho JY, Nayar J, Mueller JL, et al. Prevention of cold-associated acute inflammation in familial cold autoinflammatory syndrome by interleukin-1 receptor antagonist. *Lancet.* (2004) 364:1779–85. doi: 10.1016/S0140-6736(04)17401-1
20. Goldbach-Mansky R, Dailey NJ, Canna SW, Gelabert A, Jones J, Rubin BI, et al. Neonatal-onset multisystem inflammatory disease responsive to interleukin-1beta inhibition. *N Engl J Med.* (2006) 355:581–92. doi: 10.1056/NEJMoa055137
21. Kuemmerle-Deschner JB, Tyrrell PN, Koetter I, Wittkowski H, Bialkowski A, Tzaribachev N, et al. Efficacy and safety of anakinra therapy in pediatric and

adult patients with the autoinflammatory Muckle-Wells syndrome. *Arthritis Rheum.* (2011) 63:840–9. doi: 10.1002/art.30149
22. Ahmadi N, Brewer CC, Zalewski C, King KA, Butman JA, Plass N, et al. Cryopyrin-associated periodic syndromes: otolaryngologic and audiologic manifestations. *Otolaryngol Head Neck Surg.* (2011) 145:295–302. doi: 10.1177/0194599811402296
23. Sibley CH, Plass N, Snow J, Wiggs EA, Brewer CC, King KA, et al. Sustained response and prevention of damage progression in patients with neonatal-onset multisystem inflammatory disease treated with anakinra: a cohort study to determine three- and five-year outcomes. *Arthritis Rheum.* (2012) 64:2375–86. doi: 10.1002/art.34409
24. Jung S, Aliberti J, Graemmel P, Sunshine MJ, Kreutzberg GW, Sher A, et al. Analysis of fractalkine receptor CX(3)CR1 function by targeted deletion and green fluorescent protein reporter gene insertion. *Mol Cell Biol.* (2000) 20:4106–14. doi: 10.1128/MCB.20.11.4106-4114.2000
25. Hirose K, Discolo CM, Keasler JR, Ransohoff R. Mononuclear phagocytes migrate into the murine cochlea after acoustic trauma. *J Comp Neurol.* (2005) 489:180–94. doi: 10.1002/cne.20619
26. Harris JP. Immunology of the inner ear: response of the inner ear to antigen challenge. *Otolaryngol Head Neck Surg.* (1983) 91:18–32. doi: 10.1177/019459988309100105
27. Harris JP. Immunology of the inner ear: evidence of local antibody production. *Ann Otol Rhinol Laryngol.* (1984) 93:157–62. doi: 10.1177/000348948409300211
28. Dai M, Yang Y, Omelchenko I, Nuttall AL, Kachelmeier A, Xiu R, et al. Bone marrow cell recruitment mediated by inducible nitric oxide synthase/stromal cell-derived factor-1alpha signaling repairs the acoustically damaged cochlear blood-labyrinth barrier. *Am J Pathol.* (2010) 177:3089–99. doi: 10.2353/ajpath.2010.100340
29. Shi X. Resident macrophages in the cochlear blood-labyrinth barrier and their renewal via migration of bone-marrow-derived cells. *Cell Tissue Res.* (2010) 342:21–30. doi: 10.1007/s00441-010-1040-2
30. Zhang W, Dai M, Fridberger A, Hassan A, Degagne J, Neng L, et al. Perivascular-resident macrophage-like melanocytes in the inner ear are essential for the integrity of the intrastrial fluid-blood barrier. *Proc Natl Acad Sci USA.* (2012) 109:10388–93. doi: 10.1073/pnas.1205210109
31. Jabba SV, Oelke A, Singh R, Maganti RJ, Fleming S, Wall SM, et al. Macrophage invasion contributes to degeneration of stria vascularis in Pendred syndrome mouse model. *BMC Med.* (2006) 4:37. doi: 10.1186/1741-7015-4-37
32. Ito T, Li X, Kurima K, Choi BY, Wangemann P, Griffith AJ. Slc26a4-insufficiency causes fluctuating hearing loss and stria vascularis dysfunction. *Neurobiol Dis.* (2014) 66:53–65. doi: 10.1016/j.nbd.2014.02.002
33. Choi BY, Kim HM, Ito T, Lee KY, Li X, Monahan K, et al. Mouse model of enlarged vestibular aqueducts defines temporal requirement of Slc26a4 expression for hearing acquisition. *J Clin Invest.* (2012) 121:4516–25. doi: 10.1172/JCI59353
34. Chinnery HR, McMenamin PG, Dando SJ. Macrophage physiology in the eye. *Pflugers Arch.* (2017) 469:501–15. doi: 10.1007/s00424-017-1947-5

Conflict of Interest: The authors declare that the research was conducted in the absence of any commercial or financial relationships that could be construed as a potential conflict of interest.

frontiers in Neurology

ORIGINAL RESEARCH
published: 14 May 2020
doi: 10.3389/fneur.2020.00341

Immune Response After Cochlear Implantation

Edi Simoni[1,2,3], *Erica Gentilin*[1,2], *Mariarita Candito*[1,2], *Giulia Borile*[4,5], *Filippo Romanato*[4,5], *Milvia Chicca*[6], *Sara Nordio*[7], *Marta Aspidistria*[8], *Alessandro Martini*[1,2], *Diego Cazzador*[1,2,3] *and Laura Astolfi*[1,2]*

[1] Bioacoustics Research Laboratory, Department of Neurosciences, University of Padua, Padua, Italy, [2] Otorhinolaryngology Unit, Department of Neurosciences, University of Padua, Padua, Italy, [3] Section of Human Anatomy, Department of Neuroscience, University of Padua, Padua, Italy, [4] Department of Physics and Astronomy "G. Galilei", University of Padua, Padua, Italy, [5] Laboratory for Nanofabrication of Nanodevices, Padua, Italy, [6] Department of Life Sciences and Biotechnology, University of Ferrara, Ferrara, Italy, [7] Fondazione Ospedale San Camillo IRCCS, Venice, Italy, [8] Department of Statistical Sciences, University of Padua, Padova, Italy

A cochlear implant (CI) is an electronic device that enables hearing recovery in patients with severe to profound hearing loss. Although CIs are a successful treatment for profound hearing impairment, their effectivity may be improved by reducing damages associated with insertion of electrodes in the cochlea, thus preserving residual hearing ability. Inner ear trauma leads to inflammatory reactions altering cochlear homeostasis and reducing post-operative audiological performances and electroacoustic stimulation. Strategies to preserve residual hearing ability led to the development of medicated devices to minimize CI-induced cochlear injury. Dexamethasone-eluting electrodes recently showed positive outcomes. In previous studies by our research group, intratympanic release of dexamethasone for 14 days was able to preserve residual hearing from CI insertion trauma in a Guinea pig model. Long-term effects of dexamethasone-eluting electrodes were therefore evaluated in the same animal model. Seven Guinea pigs were bilaterally implanted with medicated rods and four were implanted with non-eluting ones. Hearing threshold audiograms were acquired prior to implantation and up to 60 days by recording compound action potentials. For each sample, we examined the amount of bone and fibrous connective tissue grown within the scala tympani in the basal turn of the cochlea, the cochleostomy healing, the neuronal density, and the correlation between electrophysiological parameters and histological results. Detection of tumor necrosis factor alpha, interleukin-6, and foreign body giant cells showed that long-term electrode implantation was not associated with an ongoing inflammation. Growth of bone and fibrous connective tissue around rods induced by CI was reduced in the scala tympani by dexamethasone release. For cochleostomy sealing, dexamethasone-treated animals showed less bone tissue growth than negative. Dexamethasone did not affect cell density in the spiral ganglion. Overall, these results support the use of dexamethasone as anti-inflammatory additive for eluting electrodes able to protect the cochlea from CI insertion trauma.

Keywords: drug delivery, fibrosis, cochleostomy, neuronal degeneration, steroids, dexamethasone

OPEN ACCESS

Edited by:
Isabel Varela-Nieto, Consejo Superior de Investigaciones Científicas (CSIC), Spain

Reviewed by:
Sung Huhn Kim, Yonsei University, South Korea
Miryam Calvino, University Hospital La Paz, Spain

***Correspondence:**
Laura Astolfi
laura.astolfi@unipd.it

Specialty section:
This article was submitted to Neuro-Otology, a section of the journal Frontiers in Neurology

Received: *18 October 2019*
Accepted: *07 April 2020*
Published: *14 May 2020*

Citation:
Simoni E, Gentilin E, Candito M, Borile G, Romanato F, Chicca M, Nordio S, Aspidistria M, Martini A, Cazzador D and Astolfi L (2020) Immune Response After Cochlear Implantation. Front. Neurol. 11:341. doi: 10.3389/fneur.2020.00341

INTRODUCTION

The loss of cochlear hair cells invariably leads to sensorineural hearing loss because no niches of stem cells able to renew this tissue have been identified to date in the organ of Corti (1). Thus, the only way to restore hearing ability is to undergo a cochlear implant (CI) surgery, and currently, the application of this device is useful for young as well as old patients (2, 3). Unfortunately, this advanced electroacoustic device may cause adverse effects, among which damages due to insertion of the electrode into the cochlea. Such damages may be mechanical (disruption of basal membrane and spiral ligament) or physiological (residual hearing impairment, inflammatory foreign body reaction, and neuronal degeneration). In order to prevent or reduce these adverse effects, several innovative surgical approaches have been developed, such as different accesses for CI insertion (round window or cochleostomy) (4) and less traumatic (thinner and shorter) electrodes (5, 6). Anti-inflammatory drugs have been applied to prevent foreign body reaction (7–11) and to prevent neuronal degeneration (12). In a recent review on the complications of CI surgery, cochlear complications are defined as unusual, accounting for 1%. Only three cases of chronic granulating labyrinthitis and 19 cases of cochlear fibrosis/osteoneogenesis were found over 7,132 surgical procedures (13). Explantation of the array was necessary in all the abovementioned cases.

The inflammatory response to CI has been investigated in both animal models and humans, showing that it may cause tissue growth around the electrode (7, 11, 14, 15), inducing fluctuations or increase of the impedance level (16) or even electrode extrusion (13, 14, 17). The disruption of cochlear structures may also increase local inflammation, in turn leading to further tissue growth (16). The main cause for inflammatory reaction to the foreign body is thought to be silicone embedding the electrode (14). Previous studies by our research group showed that the inflammatory reaction was not due to toxicity of silicone or of its polydimethylsiloxane components, because these compounds were found biocompatible in an inner ear cell line derived from Immortomouse™ organ of Corti (OC-k3) and in a neuronal cell line derived from rat pheochromocytoma (PC12) (18, 19). Concerning cell adhesion, silicone-derived compounds have been shown able to support growth and surface cell adhesion in PC12 (20), but opposite results have also been reported (21).

The use of glucocorticoids is known to reduce cochlear damage and hearing loss caused by a traumatic lesion or by ototoxic drugs (22–25). Among drugs currently employed in auditory therapies, there is dexamethasone, recognized by glucocorticoid receptors, thus able to activate anti-inflammatory and anti-apoptotic pathways (26–30). Previous studies on a new dexamethasone-eluting electrode designed by MED-EL Hearing Implants (Innsbruck, Austria) showed an *in vitro* continuous release of the drug up to 60 days (7, 31) and *in vivo* in a Guinea pig model anti-inflammatory effects up to 14 days after cochleostomy (acute reaction) (7). Based on these results, we examined the *in vivo* long-term anti-inflammatory effects (chronic reaction) in the same animal model up to 60 days after cochleostomy.

MATERIALS AND METHODS

Animals

Eleven tricolor Guinea pigs obtained from Charles River (Lecco, Italy) underwent cochleostomy and were implanted with medical grade silicone rods without any contact or wire. The animals were randomly divided into two experimental groups: the first one was implanted with 10% dexamethasone-eluting rods (DERs, 7 animals, 14 ears), and the second one was implanted with non-eluting rods (NERs, 4 animals, 8 ears).

All animal tests were approved according to Italian guidelines provided in DL 116/92, with reference to European Economic Community directive 86–609. The animals were treated by accepted veterinary standards and housed under the same living conditions.

Drug Delivery Rods

The silicone rods were 25 mm long and 0.6 mm in diameter, with a 5-mm-long tip decreasing in diameter from 0.6 to 0.3 mm. In the DER group, the 5 mm tip of the silicone rod was composed of silicone mixed with 10% dexamethasone, while in the NER group, no drug was added to silicone as previously reported (7).

Electrophysiological Measurements and Surgical Procedure

In order to verify the absence of hearing problems, the auditory threshold was measured before surgery by the auditory brainstem responses (ABRs) in all animals. The compound action potential (CAP) was used to assess the auditory threshold immediately before (pre-op) and after cochleostomy at days 0, 3, 7, 14, 30, and 60. Each animal was handled under strict aseptic conditions, and the CAP recording and the surgery approach were performed as previously described (6, 7).

Briefly, as anesthesia, 0.5 ml atropinsulfate (0.5 mg/ml) was intraperitoneally injected while 10 mg/kg enrofloxacin (5%) was subcutaneously administered. The cochleostomy was performed by retroauricolar approach, the hole diameter was 0.7 mm, and the rod was inserted at a depth of 3 mm. In order to record the CAP threshold, a gold wire was placed near the round window. To measure CAP thresholds, the stimuli were clicks and Gaussian-shaped tone pips presented in the frequency range of 0.5–32 kHz (2 points/octave) and at an intensity range from 10 to 100 dB (in 2-dB steps, 30 averages per step). During the recording procedure, the contralateral ear was blocked with a foam insert.

The CAP threshold evoked by click, low-frequency band (4- and 8-kHz tone pips) and high-frequency band (16- and 32-kHz tone pips), and the thresholds were measured immediately before (pre-op) and after cochleostomy at days 0, 3, 7, 14, 30, and 60. The threshold shifts (TSs) were calculated subtracting the pre-op CAP value from each CAP value measured after cochleastomy. A positive value of TS indicated a hearing loss while a negative one indicated a hearing recovery after cochleostomy.

The insertion trauma was evaluated by comparing CAP recordings between pre-op and day 0, and the possible damage

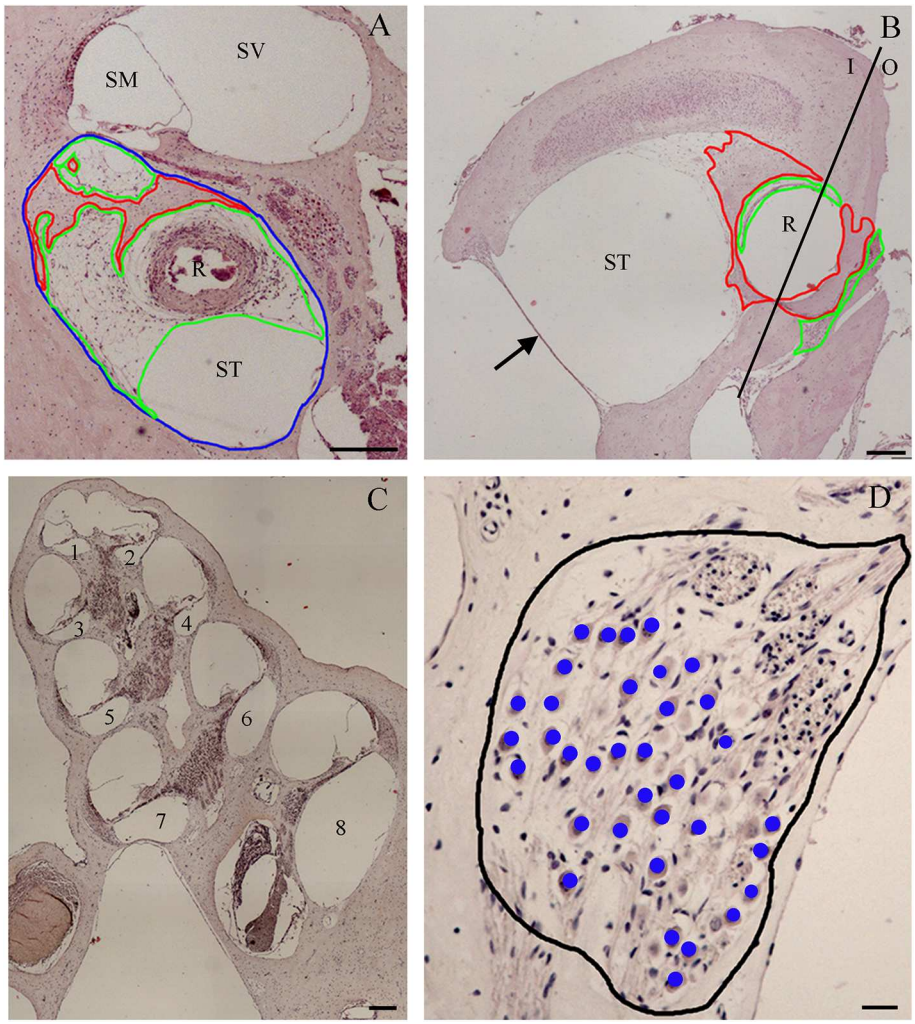

FIGURE 1 | Tissue growth within the scala tympani **(A)** and around cochleostomy **(B)**. Section of the cochlear duct suitable to measure the neuron density in the spiral ganglion **(C)** and spiral ganglion neuron density **(D)**. Blue outline, scala tympani area; red outline, bone area; green outline, fibrotic area; R rod site; ST, scala tympani space; SV, scala vestibuli; SM, scala media; I, inside; O, outside; 1–4, apical regions; 5–6, medial regions; 7–8, basal regions; black outline, ganglion area; blue dots, neurons. Scale bars, 200 μm **(A–C)** and 20 μm **(D)**. Arrow, round window.

or recovery was evaluated by comparing CAP recordings between pre-op and all the other time intervals.

Histology

All animals were painlessly sacrificed by decapitation after the last CAP recording, when they were still anesthetized. The removed bullae were placed in Shandon Glyo-Fixx™ (Thermo Scientific, Milan, Italy) and incubated at 4°C up to 20 h. After fixation, the samples were decalcified by an EDTA solution (10% ethylene diamine tetra acetic acid in phosphate buffer, pH 7.4) for 28 days in an incubator at 37°C. The EDTA solution was changed every 2 days. After decalcification, the bullae were washed, dehydrated, and embedded in paraffin (Diapath S.p.A, Bergamo, Italy). Once oriented with the modiolus axis parallel to the longitudinal axis of the paraffin block, the samples were cut by a semiautomatic microtome CUT 5062 (SLEE medical GmbH, Mainz, Germany) in 5-μm sections that were sequentially collected on Superfrost ® Plus microscope slides (Diapath S.p.A), and each section was spaced 50 μm from the next one, to analyze the entire cochlea. For each cochlea, about 60 sections were stained with hematoxylin–eosin (EE). The Nis-Elements 3.0 Image Analysis System software (Nikon, Amsterdam, Netherlands) was employed for histological and biometrical analyses. The parameters analyzed for each cochlea section stained with EE were the following:

A. The amount of tissue growth within the scala tympani in the basal turn of the cochlea (TG, "occlusion"), expressed in μm^2 and percentage (tissue area/scala tympani area). Both the fibrous and bone components of the tissue were included in the tissue growth (**Figure 1A**).
B. The amount of tissue growth around the cochleostomy hole ("healing") expressed in μm^2 (**Figure 1B**). For each section,

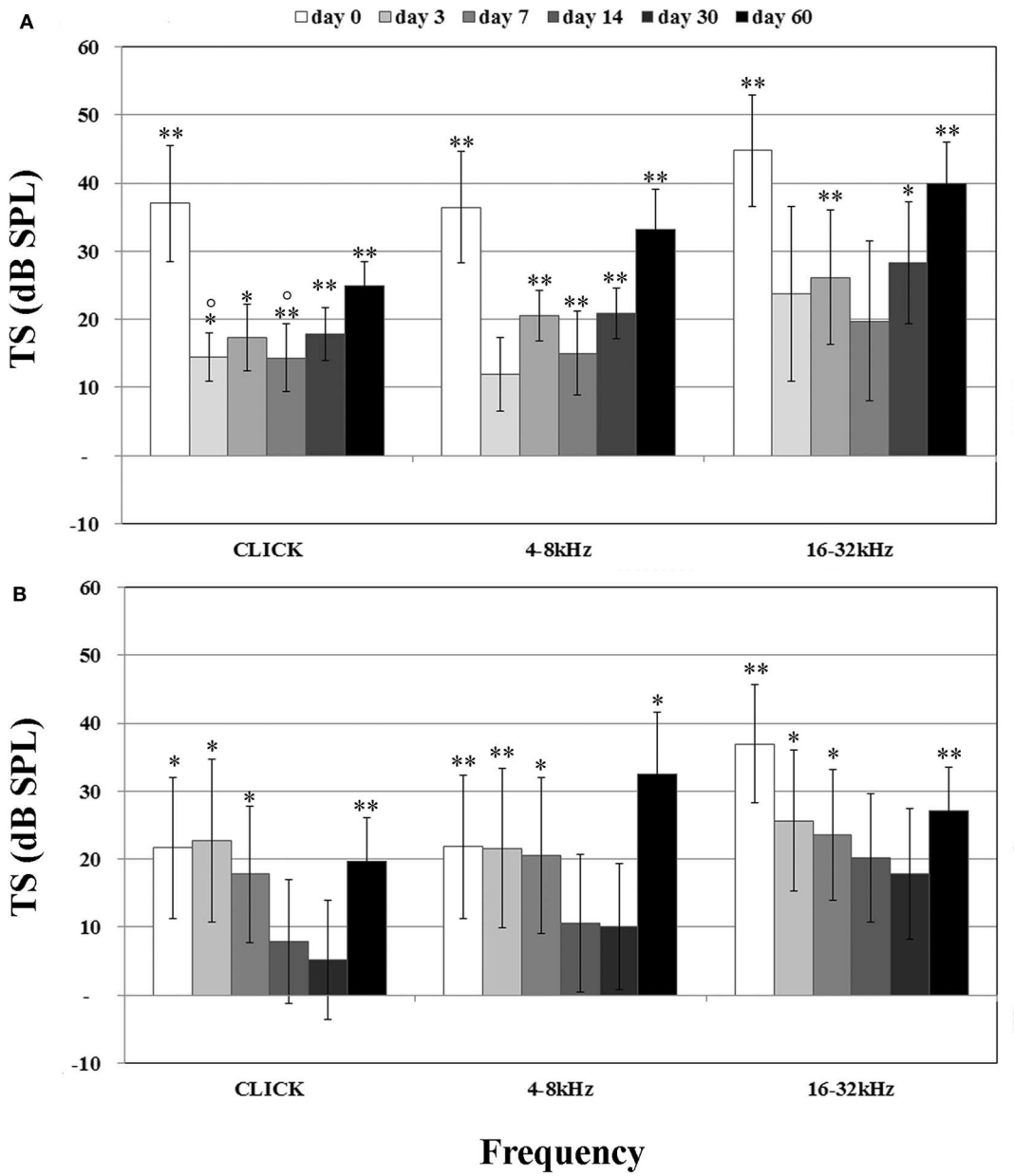

FIGURE 2 | Compound action potential (CAP) related to treatment, reported as threshold shift (TS) and evaluated in comparison with CAP before cochleostomy (pre-op). **(A)** Negative eluting rod (NER) group. **(B)** Dexamethasone-eluting rod (DER) group. Significant differences referred to pre-op CAP measured before cochleostomy (insertion trauma): $^{*}p < 0.05$, $^{**}p < 0.01$. Significant differences referred to day 0 after cochleostomy (recovery): $^{\circ}p < 0.05$. Values are shown as averages with standard error bars.

the cochleostomy hole was divided in an internal and an external region (**Figure 1B**). Measurements were performed in all sections in which the cochleostomy hole was visible.

C. The neuronal density, expressed as the number of neurons/10,000 μm^2. In order to measure the number of neurons, slices including the modiolus (the conic central axis of the cochlea) were divided into three regions, apical, medial, and basal, respectively, with four (1–4), two (5–6), and two (7–8) sections of the membranous labyrinth (**Figure 1C**). The neuronal density was calculated on three consecutive slices containing the modiolus: only neurons with nuclei were counted (**Figure 1D**). The number of neurons was divided by the area of the Rosenthal's canal.

The Nis-Elements 3.0 Image Analysis System software (Nikon) converts the pixels in micrometers based on the objective magnification and then calculates the size of a given distance or area. Based on these data, the amount of tissue growth within the scala tympani (expressed in area) was measured at

the basal turn of the cochlea and correlated to the distance from the cochleostomy hole. The size of the cochleostomy hole and the thickness and the area of tissue growth around it were also measured.

Masson's trichrome staining (Bio-Optica, Milan, Italy) was applied to highlight the fibrotic reaction products in the scala tympani and around the cochleostomy hole (two samples: about 60 sections each, per group).

The label-free second harmonic generation analyses (detected by the two-photon microscope optimized as previously reported by Filippi and collaborators) (32) were applied to highlight the collagen and elastin production around the cochleostomy hole (two samples: about 10 sections each, per group).

Immunohistochemistry

The sections were permeabilized with a 0.1% Tween 20 (Sigma-Aldrich, Milan, Italy) solution in PBS, endogenous peroxidase was blocked with 1% hydrogen peroxide (Marco Viti Pharmaceutical, Sandrigo, Vicenza, Italy), and non-specific sites were saturated with the blocking buffer Vecstain Elite ABC kit (Vector Laboratories, Burlingame, CA, USA). Sections were then incubated with the primary antibody at the concentrations 1:250 for IL-6 (bs-0782R, Bioss Inc, Woburn, Massachusetts, USA) and 1:200 for TNFalfa (ab1793, abcam, San Francisco, USA) overnight at 4°C.

After 24 h, the incubation with the appropriate secondary antibody Vecstain Elite ABC kit (Vector Laboratories) was performed, followed by signal amplification and detection with Vector SG Peroxidase substrate kit (Vector) and the Nuclear Fast Red (Vector Laboratories). Finally, after dehydration and a passage in xylene, the slides were mounted with Surgipath® Micromount (Leica Biosystem, Buccinasco, Milan, Italy) and observed with the optical microscope ECLIPSE 50i (Nikon). Two samples per groups were analyzed at the cochleostomy and mid-modiolar region (about 15 sections each). The images were acquired with Nis Elements D 3.2 software (Nikon).

Statistical Analyses

Concerning the CAP TSs, the statistical significance among time intervals and experimental groups was measured by the Mann–Whitney U test (significant with $p \leq 0.05$, highly significant with $p \leq 0.01$).

The correlations between tissue growth (as scala tympani occlusion or cochleostomy healing) and hearing ability (as insertion trauma or TS recorded at day 60) were measured by Spearman non-parametric rank correlation. Statistical significance between experimental groups was measured by the Kruskal–Wallis one-way analysis assessing the differences between multiple groups. Correlations were established among the hearing TSs (expressed in dB and measured both at the click and at 32 kHz), the tissue growth (measured as both occlusion and healing), and the neuronal density at the insertion site. Linear regression models were applied to identify the influence of the tested variables on the TS at day 60. Statistical analyses were performed by the STATISTICA 7.1 software (Stat Soft Italia srl, Padua, Italy) and R software version 3.2.5 (33).

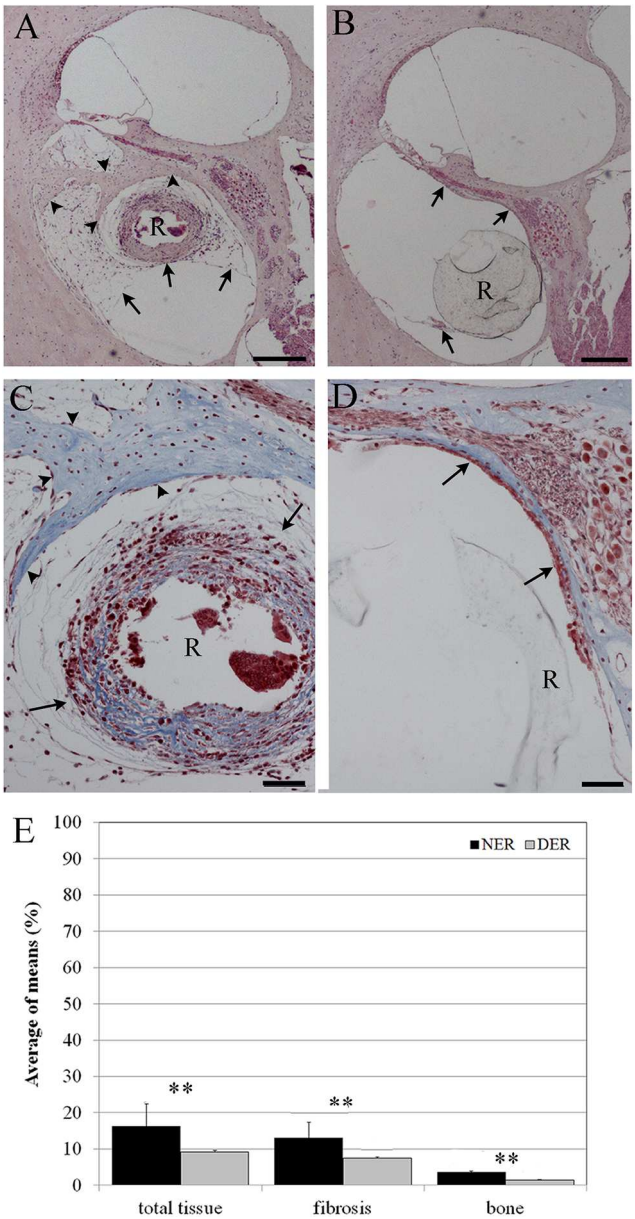

FIGURE 3 | Tissue growth in the scala tympani according to treatment after 60 days. **(A,C)** NER group. **(B,D)** DER group. **(E)** Bar graph represents the scala tympani occlusion expressed as percentage of tissue growth in the scala tympani 60 days after surgery, according to treatment. Significant differences $^{**}p < 0.01$. **(A,B)** Hematoxylin–eosin staining; scale bars, 200 μm. **(C,D)** Masson's trichrome staining; scale bars, 50 μm. Arrowheads, new bone growth; arrows, fibrotic tissue; R, rod site or silicon rod.

RESULTS

Electrophysiology

Before treatments, all Guinea pigs had normal hearing thresholds. When the animals were assigned to the experimental groups, no significant difference in hearing thresholds was detected among groups ($p > 0.05$). In the NER group, the

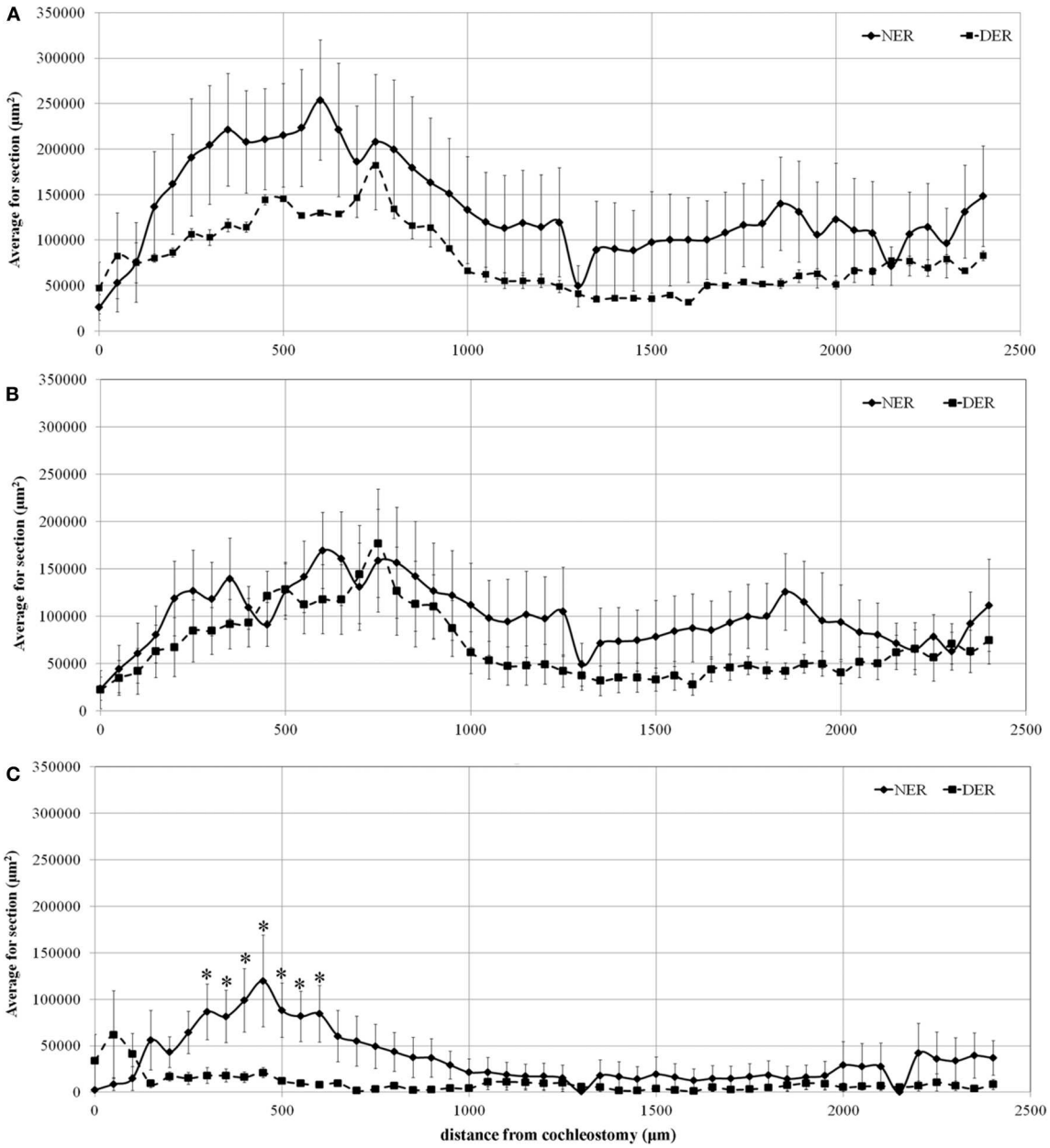

FIGURE 4 | Tissue growth in the scala tympani along the basal turn of the cochlea. **(A)** Total tissue growth; **(B)** fibrotic tissue growth; **(C)** new bone formation. Significant differences between NER and DER groups: $^*p < 0.05$. Values are shown as averages with standard error bars.

significant TSs observed at day 0 were higher than 35 dB at all frequencies tested (**Figure 2A**). Over time, a quick recovery of TSs was observed after cochleostomy but also a significant increase 60 days post-surgery, with values similar to those detected at day 0. In the DER group immediately after cochleostomy, significant TSs (day 0) were observed at the high frequencies of about 35 dB, and at the click and lower frequencies of about 20 dB of TSs (**Figure 2B**). Over time, at all frequencies tested, the TSs decreased up to day 30 and then increased up to 60 days post-surgery (**Figure 2B**). Comparing the two treatment groups, although not statistically significant, at all frequencies tested after cochleostomy and over time, the DER group showed lower TSs than the NER one (**Figure 2**).

Tissue Growth in the Scala Tympani

In order to evaluate the occlusion due to the formation of new tissue, we measured the amount of tissue growth as percentage of the scala tympani area. In the scala tympani of the NER group, a strong inflammatory reaction was observed around the electrode occluding almost all the scala tympani (**Figure 3A**). A high number of fibrotic cells and extracellular matrix deposition were observed nearby the rod site (**Figure 3C**), and outwardly a

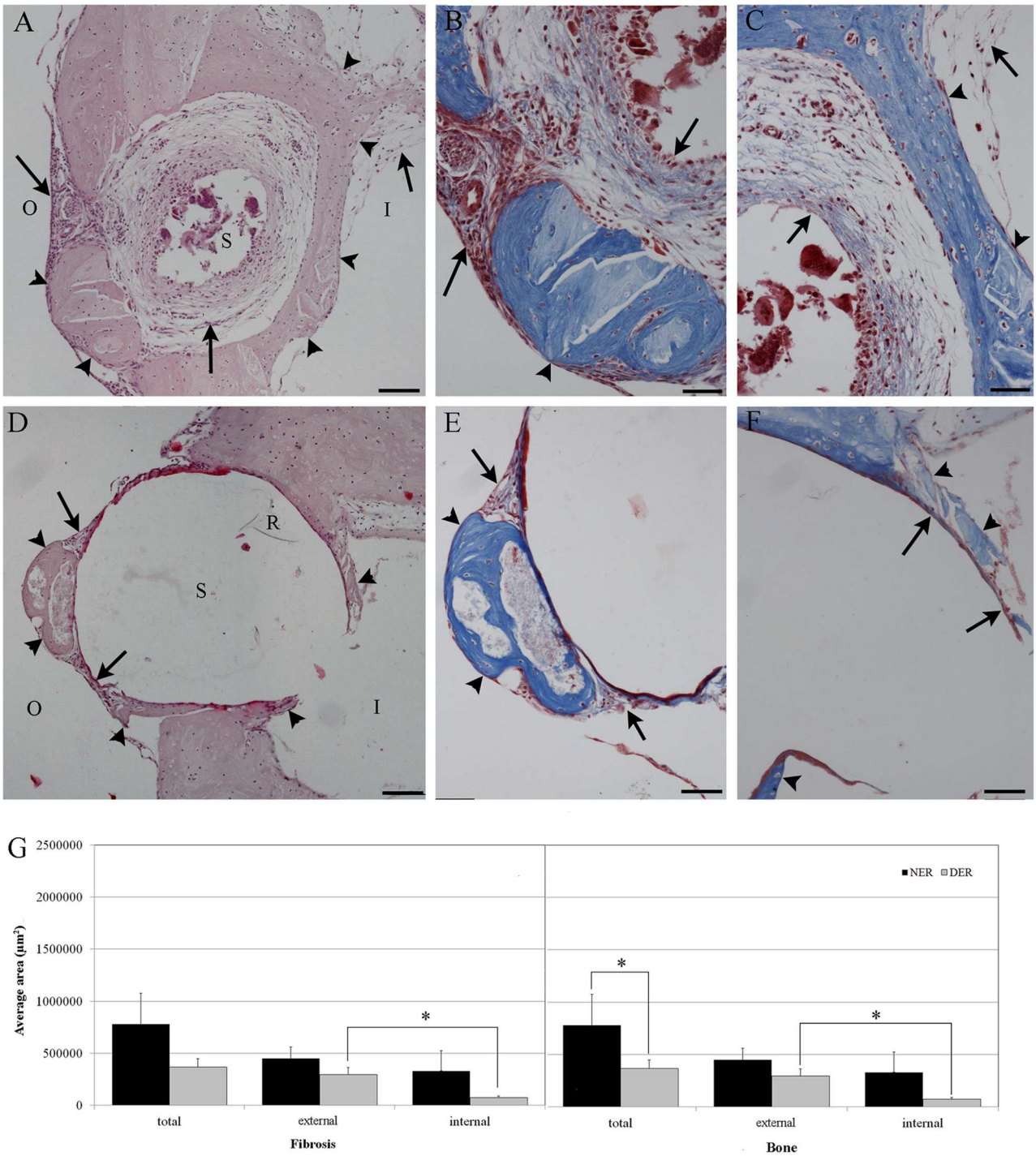

FIGURE 5 | Cochleostomy sealing measured as tissue growth around the cochleostomy site after 60 days, according to treatment. **(A,D)** HEmatosillin-Eosin staining, **(B,C,E,F)** Masson's trichrome staining. **(A–C)** NER group. **(D–F)** DER group. **(G)** Bar graph represents the cochleostomy sealing expressed as areas (μm^2) of fibrotic tissue and new bone growth around the cochleostomy site 60 days after surgery, according to treatment. Significant differences $^*p < 0.05$. **(A,D)** Hematoxylin-eosin staining; scale bars, 100 µm. **(B,C,E,F)** Masson's trichrome staining; scale bars, 50 µm. I, inside cochleostomy; O, outside cochleostomy; S, rod site; R, silicon rod. Arrowheads, new bone growth; arrows, fibrotic tissue.

growth of new tissue bone was observed until the edge of scala tympani (**Figures 3A,C**). In the DER group, the inflammatory reaction was markedly reduced and characterized by fibrotic tissue mostly composed of fibroblasts tight to the edge of scala tympani (**Figure 3D**). In the same group, the average tissue growth measured in the scala tympani was significantly lower

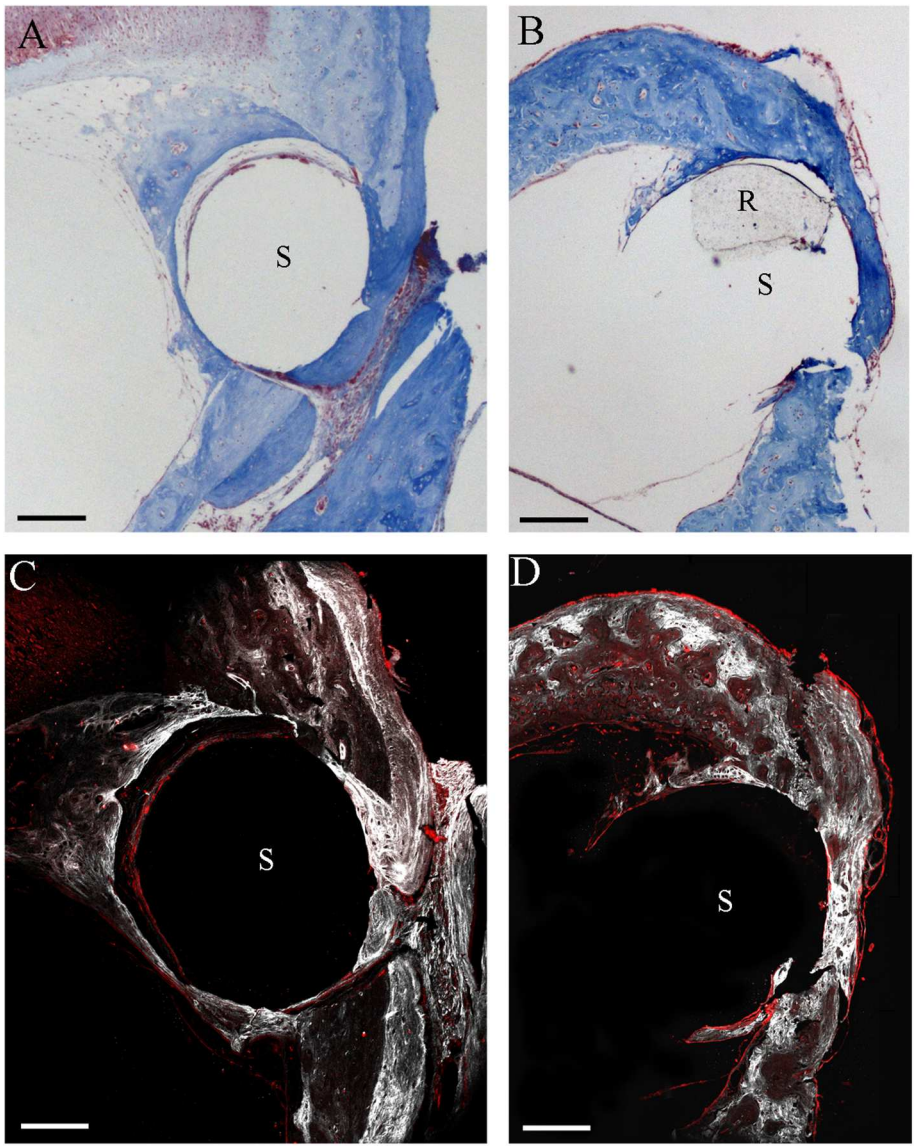

FIGURE 6 | Two-photon microscope analysis. Masson's trichrome staining in NER **(A)** and DER **(B)** groups, respectively. Images obtained through label-free second harmonic generation captured at the same cochleostomy region, respectively, in a NER **(C)** and a DER **(D)** implant. In white, signal from collagen; in red, elastin (autofluorescence). S, rod site; R, silicon rod. Scale bars, 200 μm.

in comparison to NER; moreover, a significant reduction was observed in fibrotic tissue growth (fibrosis) and new bone formation (**Figure 3E**). In the DER group, the rod was still present, while in the NER group, it seemed to be replaced with fibrotic tissue (**Figures 3A,B**).

Concerning the correlation between the percentage of TG and its distance from the cochleostomy, the total TG, the fibrosis, and the area of new bone formation (expressed in μm^2) are shown in **Figure 4**, plotted according to their distance from the cochleostomy site.

The data show that the areas of total TG progressively increased from the site of cochleostomy, peaking at about 600 μm. Tissue growth area until the end of the basal turn was always higher in NER than in DER, although not significant (**Figure 4A**). A similar amount of fibrotic tissue growth was observed near the cochleostomy, increasing in the NER group until the end of the basal turn at the cochlea, without reaching statistical significance (**Figure 4B**). The formation of new bone was significantly higher in NER in comparison to DER near the cochleostomy site, although there was a high variability within the groups. At a distance higher than 1,000 μm from the cochleostomy hole, the amount of new bone formation was similar between the groups (**Figure 4C**).

Effects of Dexamethasone Elution on Cochleostomy Healing

After 60 days from surgery, new bone formation mixed with fibrotic tissue around the cochleostomy site was detected in

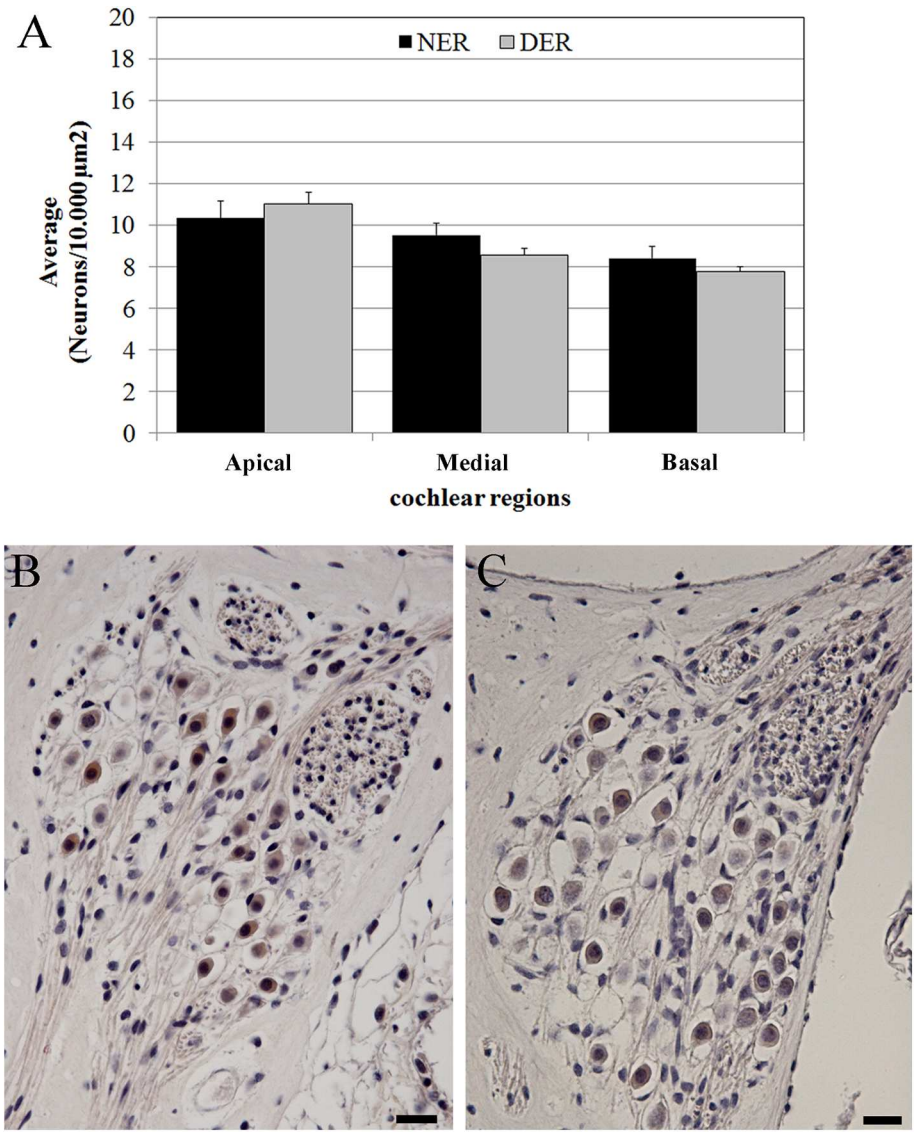

FIGURE 7 | Neuronal density. **(A)** Average neuronal density measured in three regions of the cochlear turns. Bars represent standard errors. **(B)** NER, spiral ganglion in the basal turn. **(C)** DER, spiral ganglion in the basal turn. Scale bars, 20 µm.

all samples. The EE and Masson's trichrome staining showed a higher inflammatory reaction in NER (**Figures 5A–C**) in comparison to DER (**Figures 5D–F**). The cochleostomy sealing was also measured for each cochlea as the amount of tissue growth, fibrosis, and new bone formation in the area inside and outside of the cochleostomy (**Figure 1B**). In the DER group, the amount of total new bone formation was significantly lower than in NER. Moreover, DER showed significantly lower amounts of fibrotic tissue and new bone formation inside the cochleostomy area than in the outside ($p < 0.01$), while in the NER group, the amount of these tissues was similar in both inside and outside areas (**Figure 5G**).

By the two-photon microscope analysis, it was possible to detect a larger second harmonic generation signal proportional to a higher deposition of collagen in the NER group than in the DER one around cochleostomy. Starting from the rod site, elastin and, outwardly, collagen were observed (**Figure 6**).

Spiral Ganglion Integrity

The neuronal density was measured according to the cochlear region (basal, medial and apical turn) (**Figures 1C,D**) and no significant differences were detected between NER and DER in any region ($p > 0.05$) (**Figure 7**).

Immunoreaction

No TNFalfa staining was detected in the tissue growth in both groups of treatment (data not shown). In NER, it was possible to recognize immune cells [lymphocytes and foreign body giant cells (FBGCs)] in the inflammatory tissue, mostly composed of fibroblasts and bone, both in scala tympani

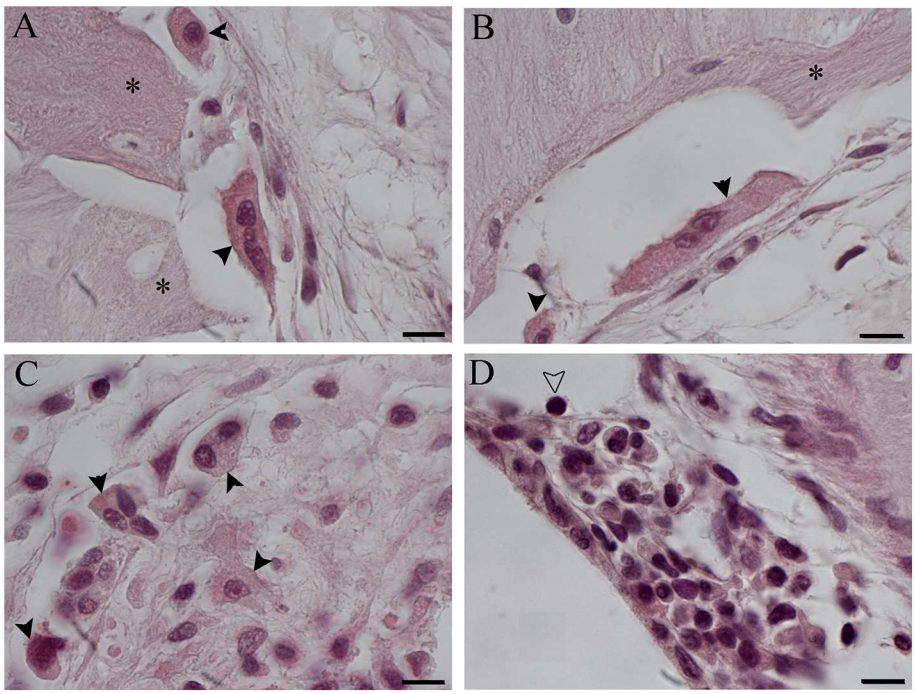

FIGURE 8 | Foreign body giant cells (FBGCs) in proximity of new bone growth in the outer **(A)** and inner **(B)** side of the cochelostomy. Numerous FBGCs are visible also inside the inflammatory reaction around the electrode **(C)**. An inflammatory infiltration is visible near the cochleostomy **(D)**. Hematoxylin–eosin staining. Scale bars, 10 μm. *, new bone; black arrowheads, FGBC; white arrowhead, lymphocyte.

and around the cochleostomy (**Figures 8–10**). The FBGCs are mostly found near new bone growth (**Figure 8**). In the NER group, IL-6 staining was present in all inflammatory tissue growth around the cochleostomy and in the scala tympani, mostly in the fibrotic tissue surrounding the silicon rod (**Figures 9A–E** and **10A–E**), into the FBGCs close to new bone growth (**Figure 9E**) and in the cells surrounding the marginal cochleostomy area (**Figure 9C**). In the DER group, the inflammatory reaction was significantly lower (**Figures 9F,G** and **10F–H**).

Correlation of Hearing Loss in Animal Studies With Histological Findings

The NER group showed a positive correlation between the CAP recorded at all frequencies (at day 0 and day 60) and the amount of tissue detected around the cochleostomy hole [fibrosis with $R_{(6)} = 0.8286$, $p < 0.05$ and new bone with $R_{(6)} = 0.8986$, $p < 0.05$]. Concerning the scala tympani occlusion, the fibrosis was positively correlated only with the CAP higher frequencies recorded at the day 60 [$R_{(6)} = 0.8117$, $p < 0.05$]. In the DER group, a significant correlation between tissue growth in the scala tympani [total tissue with $R_{(7)} = 0.8929$, $p < 0.05$ and fibrosis $R_{(7)} = 0.8571$, $p < 0.05$] and the CAP click was recorded at day 0.

At linear regression, DERs did not impact TS outcomes at post-operative day 60 for the 4–8 kHz frequencies. On the contrary, for the 16–32 kHz frequencies, the positioning of DERs was associated with a hearing recovery of 26.6 dB (95%CI −42, −11 dB; $p < 0.01$). Furthermore, the area of bone formation on the cochleostomy external surface positively impacted TS, while a negative effect on hearing was observed in the case of fibrous tissue formation on the external surface of the cochleostomy and fibrosis area in the scala tympani, at 1,000 μm from the cochleostomy (**Table 1**).

DISCUSSION

Electrophysiology

The main issue in CI electrode arrays is to design new less traumatic electrodes, able to avoid all side effects leading to CI outcome failures (34). In the DER group, the CI insertion trauma caused about 20 dB SPL of TS at click and at the 4–8 kHz frequencies, and about 35 dB SPL at the 16–32 kHz frequencies. This damage was higher than that detected in previous studies in the same animal model (7); thus, it was suitable for studies of chronic effects of dexamethasone-eluting CI rods. In the course of time, at all frequencies tested, a decrease in TS was detected up to 30 days; there was also an increase at 60 days, although not significant. Similar results were previously reported in the same animal model treated with dexamethasone but with a different surgical approach (8–10). In the NER group, the TS caused by CI insertion trauma was higher than in the DER one; thus, it is possible that DERs have exerted a positive effect in hearing ability preservation.

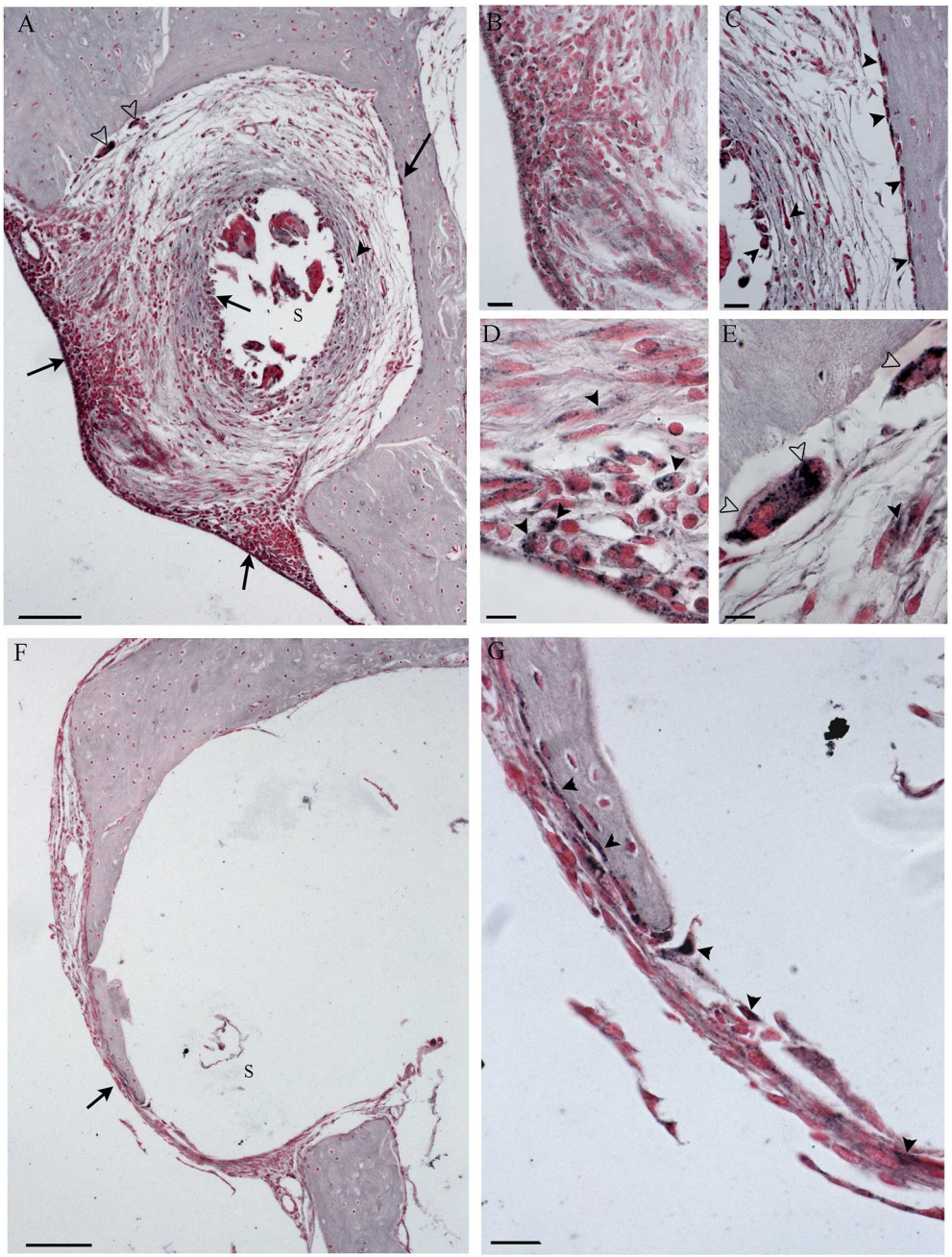

FIGURE 9 | Immunohistochemistry with IL-6 in the cochleostomy site after 60 days, according to treatment. NER group **(A–E)**; DER group **(F,G)**. Arrows indicate staining inside the fibrotic tissue; black arrowheads indicate stained cells; white arrowheads indicate stained FGB. S, rod site; Scale bars, 100 μm **(A,F)**, 50 μm **(B,C,G)**, and 10 μm **(D,E)**.

Tissue Growth and Immunoreaction

The histological analyses supported the hypothesis that dexametasone protected the cochlea from the inflammatory reaction, because a lower tissue growth was observed in the scala tympani in the DER group in comparison to the NER one. Moreover, only in NER was a significant positive correlation detected between the occlusion of scala tympani and the hearing loss detected at day 60, while in the DER group, a significant positive correlation was detected between the occlusion and the insertion trauma. In a previous study, it was demonstrated that Guinea pigs implanted with eluting silicon electrode arrays (containing from 0.1 to 10% of dexamethasone) showed

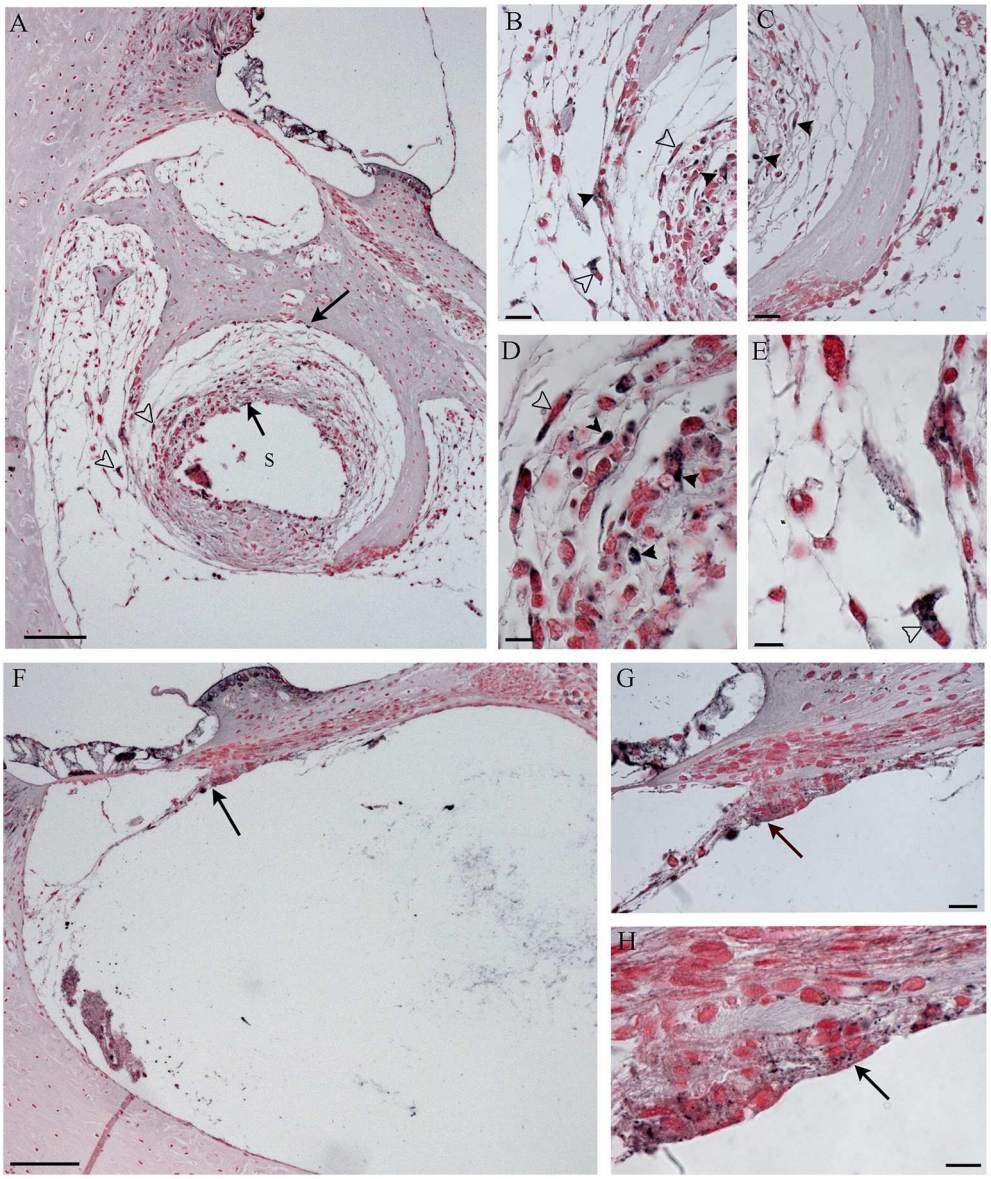

FIGURE 10 | Immunohistochemistry with IL-6 in the scala tympani along the basal turn of the cochlea, according to treatment. NER group **(A–E)**; DER group **(F–H)**. Arrows indicate staining inside the fibrotic tissue; black arrowheads indicate stained cells; white arrowheads indicate stained FGB. S, rod site; Scale bars, 100 μm **(A,F)**, 20 μm **(B,C,G)**, and 10 μm **(D,E,H)**.

significantly less fibrosis in the scala tympani and reduced loss of number of synapses and nerve fibers. The ABR and CAP thresholds were parallel. In addition, in Guinea pigs implanted with the array containing 10% of dexamethasone, CAP thresholds were significantly reduced after 90 days post-surgery (8). In humans, it was shown that when used for a long time, CI often causes fibrotic reaction (16) and affects the inner ear tissues, mostly hair cells and dendritic processes (residual hearing) (35).

Concerning the tissue growth, an immunoreaction was observed in both treatment groups. The tissue growth observed after CI insertion may be due to foreign body reaction to the rod, triggered by monocytes and bone fragments carried inside the scala tympani after CI insertion (15, 36). In humans, the histological analyses showed the presence of lymphocytes (B and T), macrophages, and FBGCs in the tissue growth around platinum or silicon particulate, supposedly derived from electrode degeneration (14, 15, 35). In the present study, the infiltration of immune cells was confirmed. In addition, in the NER group, which showed higher immunoreaction, the silicon rod seemed to be replaced with the fibrous tissue, although no silicon particles were detected within the FBGCs. In the DER group, the release of dexamethasone apparently reduced the inflammation.

TABLE 1 | Linear regression.

Variable	Coefficient	95% CI	*p*-value
DER	−26.6	[−42, −11]	< 0.01
Bone area (μm^2), external cochlear surface	−0.0001	[−0.00012, 0.0000093]	0.03
Fibrosis area (μm^2), external cochlear surface	0.00004	[−0.000069, −0.0000083]	0.02
Fibrosis area (μm^2), scala tympani, at 1,000 μm	2.24	[0.93, 3.6]	<0.01

Multiple R^2, 0.788; F statistic, 7.41 on 4 and 8 DF; p-value, 0.00845.

In the DER group, the new bone formation was significantly lower than in the NER group, especially near the cochleostomy hole, as reported by other authors (10, 14, 16). Development of the extracellular matrix is promoted by fibroblast secretion triggered by macrophages (37): new bone formation is directly related to fibrosis and to the damage extent (35). Our results support the hypothesis that dexamethasone successfully interferes with new bone formation. According to previous studies, dexamethasone is able to inhibit the production of collagen and fibronectin promoting osteoblast apoptosis and autophagy of osteoblast-like cells (38).

In the DER group, the severity of the inflammatory reaction was lower than that in the NER group, with less IL-6 expression and infiltration of immune cells such as FBGCs. The IL-6 is an inflammatory cytokine expressed by several cell types, such as damage-associated molecular patterns (DAMPs), endothelial cells, macrophages, and fibroblasts: its expression is significantly reduced by glucocorticoids (39, 40). The expression of IL-6 detected in the tissue growth around the rod in the NER group may be related to DAMP cells, fibroblasts, or FBGC activity, and the presence of dexamethasone in the DER group prevents their activation and then the recruitment of immune cells. The lower production of new bone in the DER group is then supported by the lower amount of FBGCs that are known to exhibit osteoblast-like activity (41). The formation of FBGC is due to macrophage fusion triggered by chronic inflammation developed around the foreign material (40), supporting the minor side effects in the DER group.

Correlation of Hearing Loss in Animal Studies With Histological Findings

The significant positive correlation between CAP TSs, recorded as insertion trauma at day 0 and hearing loss at day 60, and tissue growth around the cochleostomy in the NER group may support the use of dexamethasone to reduce these side effects, since a significant lower amount of new bone has been detected in the DER group. Moreover, the significant positive correlation between the hearing loss at day 60 and the scala tympani occlusion in the NER group is apparently prevented by dexamethasone release. However, the significant positive correlation between the tissue growth in the scala tympani after 60 days and the insertion trauma recorded at click supports the hypothesis that this chronic reaction may be avoided by increasing the amount of dexamethasone administered during the surgery. In a previous study, a significant correlation between the tissue growth and the impedance was detected in Guinea pigs implanted with similar DERs for 90 days, but no correlation was detected between the hearing loss and the tissue growth (10). This discrepancy may be due to a different study design, for example, to the method by which the hearing ability was measured (CAP vs. acoustically evoked auditory brainstem response). In our animal model, no significant reduction in neuronal density was detected in both groups, supporting the hypothesis that the addition or not of dexamethasone to CI electrodes had no effect on neurons of the spiral ganglion. Similar results were shown in the same animal model implanted with dexamethasone-eluting electrodes embedded with a range of drug from 1 to 10% (11) and in cat models, in which no relation between the degree of cochlear inflammation and the ganglion cell density was found (42). The neuronal density of NER and DER groups was similar to neuronal density observed in normal Guinea pigs by Wrzeszcz et al. (43), supporting the hypothesis that soft surgery did not damage spiral ganglion neurons. Bas and colleagues demonstrated that electrode insertion trauma causes the loss of synapses and damages of nerve fibers (8), probably because they used a different and invasive surgery approach.

CONCLUSIONS

In humans, fibrotic tissue and new bone formation constantly detected around the cochleostomy hole did not appear to impair CI outcome, except in the case of hybrid implants, and the lower density of neurons did not significantly reduce speech perception (4). Nonetheless, a thicker fibrous tissue within the cochlea may play a role in loss of residual hearing, and the preservation of low frequencies has a pivotal role in improving speech perception (44). In conclusion, the dexamethasone release is a good strategy to counteract the inflammatory reaction, but further studies on mechanisms underlying these side effects is essential to develop improved electrodes based on dexamethasone release that will be able to completely avoid the occurrence of inflammation.

DATA AVAILABILITY STATEMENT

The datasets generated for this study are available on request to the corresponding author.

ETHICS STATEMENT

The animal study was reviewed and approved by All animal tests were approved according to Italian guidelines provided in DL 116/92, with reference to European Economic Community directive 86-609.All experiments were approved by the Ethics Committee for Animal Usage

of the University of Ferrara (Ferrara, Italy), registration no. 9982/2010.

AUTHOR CONTRIBUTIONS

ES, AM, and LA contributed to the conception and design of the study. LA and ES performed the electrophysiological and histological analyses. DC, SN, and MA performed the statistical analysis. LA wrote the first draft of the manuscript. MC, GB, FR, EG, and MC wrote sections of the manuscript. All authors contributed to manuscript revision, and read and approved the submitted version.

FUNDING

This research has been sponsored by MED-EL Hearing Implants (Innsbruck, Austria; Grant number R/MED/MAR13/2007).

ACKNOWLEDGMENTS

The authors would like to thank Dr. Susanne Braun, Dr. Jochen Tillein (MED-EL Hearing Implants), Dr. Pietro Giordano, and Dr. Sathiyaseelan Theneshkumar for helpful discussions and expert surgical assistance.

REFERENCES

1. Simoni E, Orsini G, Chicca M, Bettini S, Franceschini V, Martini A, et al. Regenerative medicine in hearing recovery. *Cytotherapy*. (2017) 19:909–15. doi: 10.1016/j.jcyt.2017.04.008
2. Ghiselli S, Nedic S, Montino S, Astolfi L, Bovo R. Cochlear implantation in post-lingually deafened adults and elderly patients: analysis of audiometric and speech perception outcomes during the first year of use. *Acta Otorhinolaryngol Ital*. (2016) 36:513–9. doi: 10.14639/0392-100X-1222
3. Bovo R, Trevisi P, Ghiselli S, Benatti A, Martini A. Is very early hearing assessment always reliable in selecting patients for cochlear implants? A case series study. *Int J Pediatr Otorhinolaryngol*. (2015) 79:725–31. doi: 10.1016/j.ijporl.2015.02.033
4. Linthicum FH Jr, Doherty JK, Lopez IA, Ishiyama A. Cochlear implant histopathology. *World J Otorhinolaryngol Head Neck Surg*. (2018) 3:211–3. doi: 10.1016/j.wjorl.2017.12.008
5. Gifford RH, Dorman MF, Spahr AJ, Bacon SP, Skarzynski H, Lorens A. Hearing preservation surgery: psychophysical estimates of cochlear damage in recipients of a short electrode array. *J Acoust Soc Am*. (2008) 124:2164–73. doi: 10.1121/1.2967842
6. Giordano P, Hatzopoulos S, Giarbini N, Prosser S, Petruccelli J, Simoni E, et al. A soft-surgery approach to minimize hearing damage caused by the insertion of a cochlear implant electrode: a guinea pig animal model. *Otol Neurotol*. (2014) 35:1440–5. doi: 10.1097/MAO.0000000000000440
7. Astolfi L, Simoni E, Giarbini N, Giordano P, Pannella M, Hatzopoulos S, et al. Cochlear implant and inflammation reaction: safety study of a new steroid-eluting electrode. *Hear Res*. (2016) 336:44–52. doi: 10.1016/j.heares.2016.04.005
8. Bas E, Bohorquez J, Goncalves S, Perez E, Dinh CT, Garnham C, et al. Electrode array-eluted dexamethasone protects against electrode insertion trauma induced hearing and hair cell losses, damage to neural elements, increases in impedance and fibrosis: a dose response study. *Hear Res*. (2016) 337:12–24. doi: 10.1016/j.heares.2016.02.003
9. Honeder C, Zhu C, Schöpper H, Gausterer JC, Walter M, Landegger LD, et al. Effects of sustained release dexamethasone hydrogels in hearing preservation cochlear implantation. *Hear Res*. (2016) 341:43–9. doi: 10.1016/j.heares.2016.08.001
10. Wilk M, Hessler R, Mugridge K, Jolly C, Fehr M, Lenarz T, et al. Impedance changes and fibrous tissue growth after cochlear implantation are correlated and can be reduced using a dexamethasone eluting electrode. *PLoS ONE*. (2016) 11:e0147552. doi: 10.1371/journal.pone.0147552
11. Lyu AR, Kim DH, Lee SH, Shin DS, Shin SA, Park YH. Effects of dexamethasone on intracochlear inflammation and residual hearing after cochleostomy: a comparison of administration routes. *PLoS ONE*. (2018) 13:e0195230. doi: 10.1371/journal.pone.0195230
12. Scheper V, Hessler R, Hütten M, Wilk M, Jolly C, Lenarz T, et al. Local inner ear application of dexamethasone in cochlear implant models is safe for auditory neurons and increases the neuroprotective effect of chronic electrical stimulation. *PLoS ONE*. (2017) 12:e0183820. doi: 10.1371/journal.pone.0183820
13. Benatti A, Castiglione A, Trevisi P, Bovo R, Rosignoli M, Manara R, et al. Endocochlear inflammation in cochlear implant users: case report and literature review. *Int J Pediatr Otorhinolaryngol*. (2013) 77:885–93. doi: 10.1016/j.ijporl.2013.03.016
14. Nadol JB Jr, O'Malley JT, Burgess BJ, Galler D. Cellular immunologic responses to cochlear implantation in the human. *Hear Res*. (2014) 318:11–7. doi: 10.1016/j.heares.2014.09.007
15. O'Malley JT, Burgess BJ, Galler D, Nadol JB Jr. Foreign body response to silicone in cochlear implant electrodes in the human. *Otol Neurotol*. (2017) 38:970–7. doi: 10.1097/MAO.0000000000001454
16. Ishai R, Herrmann BS, Nadol JB Jr, Quesnel AM. The pattern and degree of capsular fibrous sheaths surrounding cochlear electrode arrays. *Hear Res*. (2017) 348:44–53. doi: 10.1016/j.heares.2017.02.012
17. Ciorba A, Astolfi L, Jolly C, Martini A. Cochlear implants and inner ear based therapy. *Eur J Nanomed*. (2009) 2:25–8. doi: 10.1515/EJNM.2009.2.2.25
18. Astolfi L, Simoni E, Martini A. OC-k3 cells, an *in vitro* model for cochlear implant biocompatibility. *Hear Balance Commun*. (2015) 13:166–74 doi: 10.3109/21695717.2015.1063232
19. Simoni E, Gentilin E, Candito M, Martini A, Astolfi L. Polydimethylsiloxanes biocompatibility in PC12 neuronal cell line. *Colloids Surf B Biointerfaces*. (2019)173:400–6. doi: 10.1016/j.colsurfb.2018.10.005
20. Palchesko RN, Zhang L, Sun Y, Feinberg AW. Development of polydimethylsiloxane substrates with tunable elastic modulus to study cell mechanobiology in muscle and nerve. *PLoS ONE*. (2012) 7:e51499. doi: 10.1371/journal.pone.0051499
21. Yue Z, Liu X, Molino PJ, Wallace GG. Bio-functionalisation of polydimethylsiloxane with hyaluronic acid and hyaluronic acid-collagen conjugate for neural interfacing. *Biomaterials*. (2011) 32:4714–24. doi: 10.1016/j.biomaterials.2011.03.032
22. Takemura K, Komeda M, Yagi M, Himeno C, Izumikawa M, Doi T, et al. Direct inner ear infusion of dexamethasone attenuates noise-induced trauma in the Guinea pig. *Hear Res*. (2004) 196:56–68. doi: 10.1016/j.heares.2004.06.003
23. Zou J, Pyykko I, Sutinen P, Toppila E. Vibration induced hearing loss in guinea pig cochlea: expression of TNF-alpha and VEGF. *Hear Res*. (2005) 202:13–20. doi: 10.1016/j.heares.2004.10.008
24. Tabuchi K, Murashita H, Tobita T, Oikawa K, Tsuji S, Uemaetomari I, et al. Dheydroepiandrosterone sulfate reduces acoustic injury of Guinea pig cochlea. *J Pharmacol Sci*. (2005) 115:1219–22. doi: 10.1254/jphs.SCZ050443
25. Tabuchi K, Oikawa K, Murashita H, Hoshino T, Tsuji S, Hara A. Protective effect of glucocorticoids on ischemia-reperfusion injury of outer hair cells. *Laryngoscope*. (2006) 116:627–9. doi: 10.1097/01.mlg.0000200963.69342.d7
26. Chandrasekhar SS. Intratympanic dexamethasone for sudden sensorineural hearing loss: clinical and laboratory evaluation. *Otol Neurotol*. (2001) 22:18–23. doi: 10.1097/00129492-200101000-00005
27. Himeno C, Komeda M, Izumikawa M, Takemura K, Yagi M, Weiping Y, et al. Intra-cochlear administration of Dexamethasone attenuates aminoglycoside ototoxicity in the guinea pig. *Hear Res*. (2002) 167:61–70. doi: 10.1016/S0378-5955(02)00345-3
28. Daldal A, Odabasi O, Serbetcioglu B. The protective effect of intratympanic dexamethasone on cisplatin-induced ototoxicity in guinea pigs. *Otolaryngol Head Neck Surg*. (2007) 137:747–52. doi: 10.1016/j.otohns.2007.05.068

29. Phillips JS, Westerberg B. Intratympanic steroids for Ménière's disease or syndrome. *Cochrane Database Syst Rev*. (2011) 6:CD008514. doi: 10.1002/14651858.CD008514.pub2
30. Liebau A, Pogorzelski O, Salt AN, Plontke SK. Hearing changes after intratympanically applied steroids for primary therapy of sudden hearing loss: a meta-analysis using mathematical simulations of drug delivery protocols. *Otol Neurotol*. (2017) 38:19–30. doi: 10.1097/MAO.0000000000001254
31. Astolfi L, Guaran V, Marchetti N, Olivetto E, Simoni E, Cavazzini A, et al. Cochlear implants and drug delivery: *in vitro* evaluation of dexamethasone release. *J Biomed Mater Res B Appl Biomater*. (2014) 102:267–73. doi: 10.1002/jbm.b.33004
32. Filippi A, Dal Sasso E, Iop L, Armani A, Gintoli M, Sandri M, et al. Multimodal label-free *ex vivo* imaging using a dual-wavelength microscope with axial chromatic aberration compensation. *J Biomed Opt*. (2018) 23:1–9. doi: 10.1117/1.JBO.23.9.091403
33. R Core Team. R Foundation for Statistical Computing. (2013) Vienna.
34. Dhanasingh A, Jolly C. An overview of cochlear implant electrode array designs. *Hear Res*. (2017) 356:93–103. doi: 10.1016/j.heares.2017.10.005
35. Kamakura T, O'Malley JT, Nadol JB Jr. Preservation of cells of the organ of corti and innervating dendritic processes following cochlear implantation in the human: an immunohistochemical study. *Otol Neurotol*. (2018) 39:284–93. doi: 10.1097/MAO.0000000000001686
36. Radeloff A, Unkelbach MH, Tillein J, Braun S, Helbig S, Gstöttner W, et al. Impact of intrascalar blood on hearing. *Laryngoscope*. (2007) 117:58–62. doi: 10.1097/01.mlg.0000242073.02488.f4
37. Witherel CE, Abebayehu D, Barker TH, Spiller KL. Macrophage and fibroblast interactions in biomaterial-mediated fibrosis. *Adv Healthc Mater*. (2019) 8:e1801451. doi: 10.1002/adhm.201801451
38. Liu W, Zhao Z, Na Y, Meng C, Wang J, Bai R. Dexamethasone-induced production of reactive oxygen species promotes apoptosis via endoplasmic reticulum stress and autophagy in MC3T3-E1 cells. *Int J Mol Med*. (2018) 41:2028–36. doi: 10.3892/ijmm.2018.3412
39. Tanaka T, Narazaki M, Kishimoto T. IL-6 in inflammation, immunity, and disease. *Cold Spring Harb Perspect Biol*. (2014) 6:a016295. doi: 10.1101/cshperspect.a016295
40. Harlim A, Kanoko M, Aisah S. Classification of foreign body reactions due to industrial silicone injection. *Dermatol Surg*. (2018) 44:1174–82. doi: 10.1097/DSS.0000000000001531
41. Barbeck M, Booms P, Unger R, Hoffmann V, Sader R, Kirkpatrick CJ, et al. Multinucleated giant cells in the implant bed of bone substitutes are foreign body giant cells-New insights into the material-mediated healing process. *J Biomed Mater Res A*. (2017) 105:1105–11. doi: 10.1002/jbm.a.36006
42. Moralee SJ. The effect of inflammation on spiral ganglion cell density measurements in the cat cochlea. *Clin Otolaryngol Allied Sci*. (2000) 25:492–4. doi: 10.1046/j.1365-2273.2000.00373.x
43. Wrzeszcz A, Reuter G, Nolte I, Lenarz T, Scheper V. Spiral ganglion neuron quantification in the guinea pig cochlea using confocal laser scanning microscopy compared to embedding methods. *Hear Res*. (2013) 306:145–55. doi: 10.1016/j.heares.2013.08.002
44. Welch C, Dillon MT, Pillsbury HC. Electric and acoustic stimulation in cochlear implant recipients with hearing preservation. *Semin Hear*. (2018) 39:414–27. doi: 10.1055/s-0038-1670707

Conflict of Interest: The authors declare that this study received funding from MED-EL Hearing Implants (Innsbruck, Austria). The funder was partially involved in the study design, and provided the electrode used in the experiments. The funder was not involved in collection, analysis, interpretation of data, the writing of this article or the decision to submit it for publication. The authors declare that the research was conducted in the absence of any commercial or financial relationships that could be construed as a potential conflict of interest.

frontiers in Neurology

REVIEW
published: 23 November 2020
doi: 10.3389/fneur.2020.505995

Cannabinoids, Inner Ear, Hearing, and Tinnitus: A Neuroimmunological Perspective

Paola Perin[1], Alex Mabou Tagne[2], Paolo Enrico[3], Franca Marino[2], Marco Cosentino[2], Roberto Pizzala[4] and Cinzia Boselli[5]*

[1] Department of Brain and Behavioural Sciences, University of Pavia, Pavia, Italy, [2] University of Insubria, Varese, Italy, [3] University of Sassari, Sassari, Italy, [4] Department of Molecular Medicine, University of Pavia, Pavia, Italy, [5] Department of Drug Sciences, University of Pavia, Pavia, Italy

Cannabis has been used for centuries for recreational and therapeutic purposes. Whereas, the recreative uses are based on the psychotropic effect of some of its compounds, its therapeutic effects range over a wide spectrum of actions, most of which target the brain or the immune system. Several studies have found cannabinoid receptors in the auditory system, both at peripheral and central levels, thus raising the interest in cannabinoid signaling in hearing, and especially in tinnitus, which is affected also by anxiety, memory, and attention circuits where cannabinoid effects are well described. Available studies on animal models of tinnitus suggest that cannabinoids are not likely to be helpful in tinnitus treatment and could even be harmful. However, the pharmacology of cannabinoids is very complex, and most studies focused on neural CB1R-based responses. Cannabinoid effects on the immune system (where CB2Rs predominate) are increasingly recognized as essential in understanding nervous system pathological responses, and data on immune cannabinoid targets have emerged in the auditory system as well. In addition, nonclassical cannabinoid targets (such as TRP channels) appear to play an important role in the auditory system as well. This review will focus on neuroimmunological mechanisms for cannabinoid effects and their possible use as protective and therapeutic agents in the ear and auditory system, especially in tinnitus.

Keywords: cannabinoids, tinnitus, auditory, neuroimmune, hearing

OPEN ACCESS

Edited by:
Jose Antonio Lopez-Escamez, Andalusian Autonomous Government of Genomics and Oncological Research (GENYO), Spain

Reviewed by:
Paula Morales, Instituto de Química Médica (IQM), Spain
Zheng-Xiong Xi, National Institute on Drug Abuse (NIDA), United States

****Correspondence:***
Paola Perin
pperin@unipv.it

Specialty section:
This article was submitted to Neuro-Otology, a section of the journal Frontiers in Neurology

Received: *18 October 2019*
Accepted: *18 August 2020*
Published: *23 November 2020*

Citation:
Perin P, Mabou Tagne A, Enrico P, Marino F, Cosentino M, Pizzala R and Boselli C (2020) Cannabinoids, Inner Ear, Hearing, and Tinnitus: A Neuroimmunological Perspective. Front. Neurol. 11:505995. doi: 10.3389/fneur.2020.505995

INTRODUCTION

Endocannabinoids (ECs; **Figure 1**) are a class of ubiquitous endogenous lipids regulating essential processes ranging from energy balance, to pain, to motor control, and involved in pathologies as diverse as (among others) schizophrenia, glaucoma, multiple sclerosis, and obesity (20). In the CNS, ECs influence synaptic plasticity (21, 22), modulate neuroinflammation (23), and affect neurogenesis (24) and may also affect neuronal activity by binding to neurotransmitter receptors and ion channels (25). These cellular effects are reflected in the EC modulation of several brain functions, including fear and anxiety (26), or memory (27). Overall, the standard arrangement in the brain appears to be the presence of multiple EC pathways affecting the same circuits, often with different or even opposing effect.

In the immune system, ECs affect cell proliferation, migration, differentiation, cytokine production, and apoptosis (28). The two responses, immune and neural, interact in neuroinflammation, where ECs play major roles (29). Earlier studies suggested that neural

effects of cannabinoids are mediated by CB1R activation (30) whereas immune effects are mediated by CB2R (31). However, it is important to stress that the separation of these biological actions is not as clear-cut as initially suggested (32), and other receptors can also be activated by ECs. The dizzying complexity of cannabinoid pharmacology (see **Supplementary Tables 1, 2**) requires a deep knowledge of the precise "fingerprint" of the molecular pathways affected by each compound, in each organ and each species, to dissect its effects.

Cannabinoid Pharmacology

The pharmacology of cannabinoids is very complex, for several reasons. First, more than one hundred phytocannabinoids (33) and at least 13 ECs (25) have been identified. Second, their lipidic nature makes unraveling their molecular interactions more difficult than for conventional transmitters (34). Third, CBRs are connected to several intracellular pathways (**Figure 1B**) and may produce different (even opposite) results depending on the particular ligand and its concentration (8, 9, 35) and on the cell repertoire of signal transduction molecules (36).

ECs are one of the four families of bioactive lipids (together with classical eicosanoids, SPMs, and lysoglycerophospholipids/sphingolipids), which are generated from PUFA precursors esterified into membrane lipids (37). The EC system includes CBRs, their endogenous ligands, and the proteins involved in EC formation, transport, and degradation.

The first discovered and best-characterized ECs are AEA and 2-AG (38–40). Several other EC lipid mediators (41–43) [and a family of EC peptides, named "pepcans" (44)] have also been described (see also **Supplementary Table 1**), but their endogenous functions have been less characterized.

ECs (**Figure 1C**) are produced "on demand" from membrane lipids by several Ca^{2+}-dependent enzymes (17), and metabolic pathways for production, transport, and degradation differ for the various ECs, making it possible for cells to tailor their local EC repertoire (45) by regulating their local concentrations through modulation of their biosynthesis, transport, and degradation (46). Once released, ECs are rapidly deactivated by intracellular enzymes (47): AEA by FAAH1 and 2 [the latter not expressed in rodents (1)], and 2-AG mainly by MAGL, and less by ABHD6 and ABHD12 (19). In addition, ECs may be transformed in non-EC bioactive metabolites [e.g., by COX-2 (48)].

ECs (**Figure 1B**) bind and activate two specific G-protein-coupled cannabinoid receptors, CB1R and CB2R (49–51), plus additional targets (52), such as TRP channels (53), PPARs (54–57), and "orphan" G-protein coupled receptors such as GPR18 and GPR55 (58, 59). Most EC are able to activate both CB1R and CB2R, although with different potency and effects (60), whereas nonclassical targets may interact with limited EC subsets (**Supplementary Table 1**) and also non-EC ligands. A clear example is TRPV1, which is activated by AEA binding to a cytoplasmic site (16) but is also sensitive to other stimuli such as heat, vanilloids, protons, N-acyl amides, and arachidonic acid derivatives (61).

CB1R and CB2R are class A (rhodopsin-like) GPCRs (4), and both couple to Gi/o G-proteins (5, 6), reducing cAMP concentration (7). However, the coupling between CBRs and biochemical pathways is complex and context-dependent. First, CB1Rs may form homo- or heterodimers with other GPCRs (62), such as (among others) CB2Rs (63), A2A adenosine receptors (64), D2 dopamine receptors (65), μ opioid receptors (66), and orexin-1 receptors (67), whereas CB2R may dimerize with the CXCR4 chemokine receptor (68) and GPR55 (69). The presence of CB1R/CB2R heteromers makes it impossible to clearly separate the biological responses of CB1R and CB2R *in vivo*.

Second, CBRs show dimerization- and agonist-biased response, due to conformation-dependent binding by β-arrestins (10). Besides blocking interactions with Gi/o proteins, β-arrestin effects include CBR internalization and ERK pathway/Gs protein activation (9), so that cAMP levels may increase instead of decreasing depending on CBR receptor bias. Receptor coupling flexibility appears more limited (although not absent) for CB2Rs, which mainly activate Gi proteins, whereas CB1Rs may couple to Go, Gs, Gq, and G12/13, thus activating a very diverse network of responses (8). Both receptors are in addition able to activate ER stress pathways linked to autophagy (70).

The β-arrestin-dependent internalization of plasma membrane CBRs is linked to receptor degradation (9); however, functional CBRs have been found in the outer mitochondrial membrane (12), and in the endoplasmic reticulum, endosomes, lysosomes, and nuclear membrane (3). Subcellular localization affect CB-related responses: mitochondrial localization allows CBRs to modulate cell energetic balance (13), and ROS production (14), whereas endolysosomal localization is correlated with inflammation and phagocytosis (71). Moreover, intracellular receptor sites will be inaccessible to membrane-impermeant cannabinoid agonists and antagonists.

Besides G-protein-coupled receptors, TRP nonselective cation channels are being increasingly recognized as an integral part of the EC system (ionotropic EC receptors): six of the 28 TRP channels are sensitive to cannabinoids (53). Among these, TRPV1 is the most studied, mainly due to its expression in nociceptors and role in pain-related processes: TRPV1 channels are colocalized with CB1R and/or CB2R in several types of cells, and TRPV1 block or desensitization underlies analgesia (72); the

Abbreviations: 2-AG, 2-arachidonoylglycerol; ABHD4, ABHD6, ABHD12, αβ-hydrolase domain 4,6,12; ACEA, arachidonyl-2'-chloroethylamide; AEA, N-arachidonoylethanolamide (anandamide); BDNF, brain-derived nerve factor; BNST, bed nucleus of the stria terminalis; CBR; CB1R; CB2R, cannabinoid receptor, type 1, type 2; CBD, cannabidiol; COX-2, cyclooxygenase type 2; CREB, cAMP response element binding protein; DAG diacylglycerol; DAGL, DAG lipase; DCN, dorsal cochlear nucleus; DSE, Depolarization-induced suppression of excitation; DSI, Depolarization-induced suppression of inhibition; EC, endocannabinoid; EMT, endocannabinoid membrane transporter; ERK, Extracellular signal-Regulated Kinase; FAAH, fatty acid amide hydrolase; GDE1, glycerophosphodiesterase 1; GPCR, G-protein-coupled receptor; HPA, hypothalamic-pituitary-adrenal; MAGL, monoacylglycerol lipase; NAPE, N-arachidoylphosphatidyletanolamine; NAT, N-acyltransferase; NR3C1, glucocorticoid receptor; PHARC, Polyneuropathy, Hearing loss, Ataxia, Retinitis pigmentosa, and Cataracts; PLA2, phospholipase A2; PLD, phospholipase D; PPAR, Peroxisome proliferator-activated receptors; PUFA, polyunsaturated fatty acids; SPM, specialized pro-resolving mediators; TRP, Transient receptor potential; Δ9-THC, Δ9-tetrahydrocannabinol; VCN, ventral cochlear nucleus.

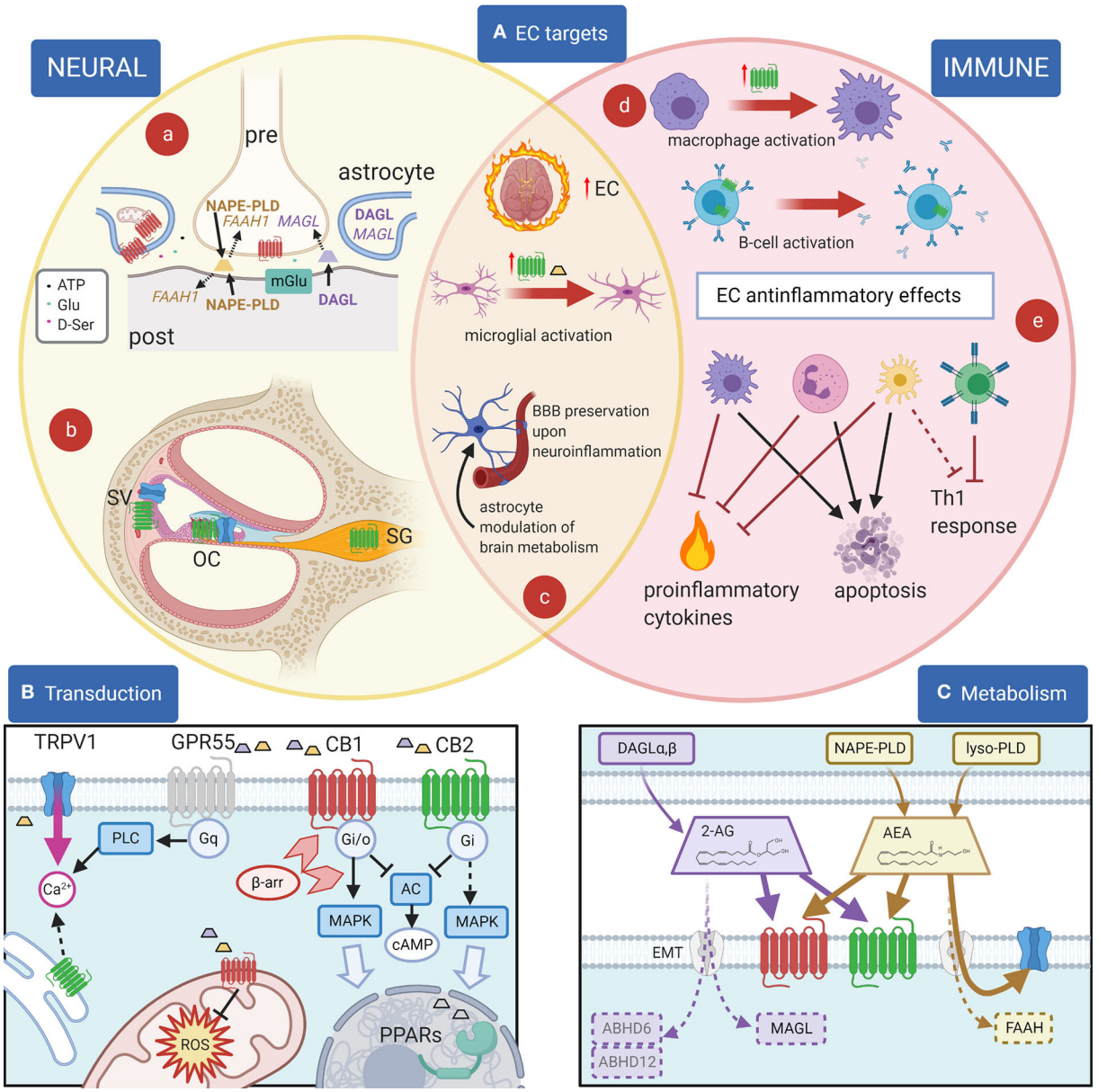

FIGURE 1 | EC and their effects. **(A)**: Principal EC targets in neural and immune systems, and in the cochlea. (a) In most brain areas, 2-AG (purple) is synthetized by DAGL-α in neuronal dendrites and somata and catabolized by MAGL in presynaptic terminals, where CB1R (red) are also present. 2-AG is produced postsynaptically in a Ca^{2+}-dependent way upon activation of metabotropic receptors (blue) and inactivated presynaptically near its target (1). For AEA (yellow), on the other hand, the biosynthetic enzyme NAPE-PLD is both pre- and postsynaptic, and the catabolic enzyme FAAH-1 is predominantly postsynaptic (1). Astrocytes are also involved in synaptic effects through an EC modulation of gliotransmission, and in addition EC effects on astrocyte mitochondria contribute to neuronal metabolism regulation. (b) In the cochlea, CB2R (green) are found in the organ of Corti (OC), basal cells of the stria vascularis (SV) and spiral ganglion (SG), whereas TRPV1 channels (blue) are found in the organ of Corti and marginal cells of the stria vascularis. (c) During neuroinflammation, several changes are seen in the EC system. The overall EC production increases. Activated microglia increases AEA production (yellow trapezoid) and CB2R expression (green). Astrocytes become activated and BBB is affected (both effects are counteracted by EC responses). (d) Cell activation may change CB2R expression as in macrophages (purple) (2) or CB2R subcellular localization as in B lymphocytes (blue) (3). (e) Anti-inflammatory EC responses in immune cells include the block of Th1 responses due to direct effects on T cells (green) and indirect effects on dendritic cells (yellow), apoptosis induction on several cell types, and the inhibition of proinflammatory cytokines and factors. **(B)**: Principal EC receptors and their main intracellular pathways. Both 2-AG (purple trapezoid) and AEA (yellow trapezoid) act on CB1R and CB2R, which are class A GPCRs (4) coupled to Gi/o G-proteins (5, 6), reducing cAMP concentration (7). β-Arrestin binding (light red arrowheads) induces CBR internalization and switches receptor coupling, especially for CB1, also activating MAP kinase pathways (8–10) linked to nuclear effects (large light blue arrow). MAPK pathways are also activated through Gi βγ action (dotted line), both by CB1R and by CB2R (11). Functional CBRs have been also found in intracellular compartments such as the outer mitochondrial membrane (12), where they modulate cell energetic balance (13), and ROS production (14) or endoplasmic reticulum, where they may induce Gq-related Ca2+ release from intracellular stores (3). Moreover, ECs or related lipids activate nuclear PPARs (15). TRPV1 channels are often colocalized with CB1R

(Continued)

FIGURE 1 | and/or CB2R and activated by cytoplasmic ECs (16), increasing cytosolic Ca2+. Finally, orphan receptors may activate other pathways, e.g., GPR55 is linked to Gq-PLC and therefore contributes to cytosolic Ca2+ increase. Most cells only express a subset of these pathways. **(C)**: Metabolism of 2-AG and anandamide (AEA). 2-AG (purple) is produced from DAG by DAG lipases (DAGLα and β). Biosynthesis of AEA (yellow) is more complex and may involve hydrolysis of NAPE membrane phospholipids by NAPE-PLD (which directly generates AEA) or sequential action of several enzymes (not shown), followed by a lyso-PLD (17). Although lipophilic, ECs have membrane transport mechanisms (EMT, light gray) (18). EC binding sites on CB1 (red) and CB2 (green) are extracellular, whereas on TRP channels (blue) the site is intracellular. Degradation of AEA is mainly due to FAAH, whereas 2-AG is primarily degraded by MAGL, and less by ABHD6 and ABHD12 (19). Created with Biorender.

analgesic and antihyperalgesic effects of phytocannabinoids are, at least in part, mediated by this channel (53).

EC System in the Brain

CBRs are expressed in most tissues of the body (73) and are by far the most abundant type of G-protein-coupled receptors in the mammalian brain (74). CB1R is predominantly expressed in the CNS (75), at comparable levels as glutamate and GABA receptors (74, 76). On the other hand, CB2R was originally thought to be restricted to immune and hematopoietic cells (77, 78), but more precise localization tools have subsequently allowed to assess its expression in other systems, including the nervous system (79) and the inner ear (80). CB2R expression in the healthy brain is in fact hundreds of times less than for CB1R but is strongly upregulated under pathological conditions (81). Localization, splice variants, and physiology of CBRs appear to be highly species-dependent (73), thus complicating result comparisons between animal and human studies.

CB1R neuronal effects are well known and have been extensively covered in several exhaustive reviews (49, 82, 83). Glial responses are less completely characterized but appear important especially in the presence of neuroinflammation (84), where EC tone is elevated (85). Neuroinflammation is a protective brain defense response that can however degenerate into a chronical state involved in the pathophysiology of several neurological and psychiatric disorders (86).

In neurons (**Figure 1A**a), the classical EC effect is retrograde inhibition mediated by presynaptic neuronal CB1Rs and postsynaptically produced 2-AG: CB1R activation inhibits the release of the presynaptic transmitter (22), causing short-term DSE on excitatory neurons, or DSI on inhibitory neurons (87). This mechanism has been dissected in the DCN molecular layer, where glutamatergic parallel fibers carrying non-auditory signals contact fusiform cells and glycinergic cartwheel cells (which in turn provide feedforward inhibition to fusiform cells) (88). Fusiform cell output is shaped by plasticity in the molecular layer circuits, which collectively generate "negative images" of expected sounds to be attenuated at fusiform apical dendrites (89). Plasticity changes in this circuit have been correlated with tinnitus onset (90, 91). Cartwheel cells release EC from their dendrites upon stimulation, thus inducing DSE at parallel fibers (92), whereas fusiform cells do not; therefore, activation of cartwheel cells depresses its parallel fiber input, gradually reducing their feedforward inhibition (93). In fusiform cells, ECs are involved in acetylcholine-induced plasticity changes at parallel fiber synapses (94) which have been correlated with tinnitus (95). Prolonged exposure to high doses of salicylate (a well-known tinnitus inducer) increases EC release in the DCN, thus changing molecular layer plasticity (96). Unfortunately, cannabinoid modulation of this circuit has not yielded effective tinnitus treatments [see discussion in (97)].

For AEA, on the other hand, the biosynthetic enzyme NAPE-PLD is both pre- and postsynaptic, and the catabolic enzyme FAAH-1 is predominantly postsynaptic (1). Postsynaptic production of AEA produces a "tonic" retrograde inhibition at some synapses, which is shut down by neuronal inactivity through upregulation of FAAH1 (98); presynaptic production feeds instead into an anterograde mechanism. In addition, in the hippocampus, NAPE-PLD is localized in intracellular membrane cisternae of axonal Ca^{2+} stores (99) and AEA may act as an intracellular messenger by activating TRPV1 intracellular binding site.

Like neurons, glial cells can synthesize ECs in response to physiological or pathological stimuli (100, 101). In astrocytes, more than 70% of CB1Rs are found at perivascular endfeet, and EC activation has been found to modulate brain energy consumption (102) through EC effects on astrocyte mitochondria (103). At synapses, astrocytes express both DAGLα and MAGL and may display Ca^{2+}-dependent EC release, which modulates synaptic response (104); conversely, astrocytic CB1R activation may induce Ca^{2+}-dependent release of Glu (105), ATP, or D-serine (106) in response to synaptic EC. Astrocyte EC effects have been found to be involved in the regulation of sleep in the PPT (107) and in the regulation of circadian rhythms in the suprachiasmatic nucleus (108). These latter effects may be relevant for tinnitus given its association with sleep disturbances (109) and its circadian modulation (110).

Neuroinflammation is a brain reaction aimed at counteracting acute damage, restoring the homeostasis and limiting brain parenchyma injury, and includes microglial activation, reactive astrogliosis, production of inflammatory mediators, BBB breakdown, and subsequent brain infiltration of circulating immune cells (111). Neuroinflammation dysregulation may turn microglia and astrocytes in uncontrolled sources of inflammatory mediators, which may worsen damage progression.

A growing body of data suggest that EC are able to exert immunoregulatory and anti-inflammatory properties (112–114), by decreasing the production of NO, ROS/RNS, free radicals, and pro-inflammatory cytokines in activated glial cells, while switching microglia toward anti-inflammatory phenotypes (115–118). Remarkably, the increase in EC concentration and microglial CB receptors during neuroinflammation may yield a neuroprotective negative feedback mechanism aimed at limiting inflammatory responses.

The main brain source of ECs in neuroinflammatory conditions is microglia (119, 120), the resident immune cells of the CNS (121–123). Consistently with its immune role

and nature, microglia express DAGL-β and (mainly) ABHD12 instead of the neuronal DAGL-α and MAGL (124), and while CB1Rs are expressed at low levels and mostly located intracellularly (120), microglia is the main CB2R-expressing cell in the brain (125). Microglial CB2R expression may increase up to 100 fold upon inflammation or tissue injury (126), and microglial Ca^{2+} increases [e.g., from P2X7 receptor activation (127)] and directly increases DAGL, thus increasing the production of 2-AG (128), which during neuroinflammation becomes 20-fold higher in microglia than in other brain cells (120). Mounting evidence suggests that the EC system might represent a promising tool to modify (micro)glial activity and profiles in order to achieve benefits for neuroinflammatory diseases (104). Indeed, CB2Rs can downregulate astrocyte and microglial cell overactivation during neuroinflammatory disorders, thus protecting them (129); selective depletion of MAGL in astrocytes attenuates LPS-induced neuroinflammation [(130), and CB2R upregulation and activation of EC signaling pathways have been associated with a restoration of tissue homeostasis in neuroinflammatory conditions (118, 131).

Brain CB2Rs have been less studied than CB1Rs (79), mainly due to the delay in the availability of sensitive genetic and molecular tools (126, 132, 133). In the CNS, CB2Rs are chiefly expressed on microglia (134, 135), and to some extent on astrocytes, oligodendrocytes, progenitor neural cells, and neurons (136–138); neuronal CB2R is mainly postsynaptic, differently from CB1R (137). In human, the brain only expresses one CB2R isoform (CB2RA) whereas a second one (CB2RB) is expressed in the immune system (139); rats express two additional isoforms (CB2RC and CB2RD) present neither in mice nor in humans (126), and their CB2R expression is lower and with a different distribution from mice (140). Lack of CB2R brain expression was incorrectly inferred by methods only evidencing non-brain isoforms or with insufficient sensitivity (126).

Microglial actions range from protection against damaging signals altering CNS homeostasis through phagocytosis, release of proinflammatory cytokines, and recruitment of circulating immune cells [reviewed in (141)], to controlling neuronal proliferation and differentiation [through selective neuronal phagocytosis and release of neurotrophic and neurotoxic factors reviewed in (142)], to modulating neuronal plasticity and memory [through neurotrophin release and selective synaptic pruning reviewed in (141, 142)]. In order to fulfill all these tasks, microglia are extremely plastic cells that readily change their phenotypes on demand; microglial phenotypes, previously crammed into an M1–M2 gradient to fit a classical macrophage activation model (143), are now recognized to be much more diverse (144) and influenced by the brain region (145), species (146), age (147), gender (148), and physiopathological state (149). In particular, neurodegenerative diseases appear to associate with specific microglial phenotypes which release pro-inflammatory mediators, as well as contributing to prolonged oxidative stress, leading to chronic neuroinflammation, which in turn drives neurodegeneration (141, 150, 151).

As regards hearing loss, which is a risk factor for tinnitus, chronic inflammation is seen as a major player in presbycusis [reviewed in (152)] and has been found to be associated with poorer hearing in a population-based cross-sectional study (153). Moreover, in mice, microglial ablation and TNF-alpha antagonism (154) both decrease tinnitus signs, and TNF-alpha KO mice are resilient to noise trauma-induced tinnitus (154). In human, gene polymorphisms in both TNF-alpha (155) and IL-6 (156) have been found to increase tinnitus risk in an elderly population with a history of occupational noise exposure. Neuroinflammation (and its dysregulation) appears therefore as a promising candidate mechanism for tinnitus susceptibility, and its modulation by cannabinoids may provide novel therapeutic targets. A caveat regarding neuroinflammation as a target is the complexity emerging from single-cell studies (157), which could underlie a heterogeneity similar to that observed in most multifactorial inflammatory disorders [e.g., rheumatoid arthritis (158), Menière's disease (159), and IBD (160)].

Besides neurons and glial cells, neuroinflammation involves cells of the immune system, where EC cellular mechanisms differ from neuronal ones. Cannabinoid immunomodulatory effects are complex but appear to be largely mediated through CB2Rs, whose expression on immune cells is usually higher than that of CB1R (161, 162). Moreover, nonclassical cannabinoid targets such as TRP channels (53) and PPARs (15) are well-known as key regulators of the immune response (163–165). It is interesting that EC responses in the cochlea (see below) appear more similar to those observed in the immune system than in the nervous system.

In human immune cells, CB2R is expressed most in B cells, followed by NK cells, monocytes, neutrophils, and finally T cells (134, 166, 167). Peripheral blood T cells, monocytes, and dendritic cells only express intracellular CB2R (168), whereas naïve peripheral blood B cells also express these receptors on the cell surface and lose it upon activation (169). Intracellular CB2Rs in immune cells have been associated with Ca^{2+} release from stores (3).

CB2R activation in immune cells regulates all three major MAPKs (12) and decreases DNA binding for various nuclear factors (170), which results in the downregulation of critical immunoregulatory genes including IL-2 (171, 172). Overall, these major signaling networks play important roles in CB2R-mediated effects on immune cell functions including migration, proliferation, differentiation, apoptosis, and cytokine production (28). Generally, effects of the EC system on immune cells appear directed toward an anti-inflammatory action, although the context-dependent action of cannabinoids may support different responses in different cell types and states (62, 173–176).

As regards neuroinflammatory responses, a major player is the Toll-like receptor (TLR) system (177). TLRs are able to recognize pathogen-associated and damage-associated molecular patterns (PAMPs and DAMPs), and several of their effects appear to be counteracted by ECs [especially through CB2R-related mechanisms (11)]. Since cochlear damage has also been found to induce TLR4-responses (178), similar protective effects could be expected on the cochlea.

Cannabinoids and Tinnitus

Cannabinoids have been considered as potential treatment for tinnitus percept and/or distress, and with the legalization of light cannabis (L.242/2016 as regards Italy), several tinnitus sufferers are turning to it as a possible DIY remedy. Interest in cannabinoids as possible treatment for tinnitus has been motivated by several reasons. Early models of tinnitus stressed its similarities with neuropathic pain (179) and with epilepsy (180), both of which can be modulated by cannabinoids (181, 182).

The association between tinnitus and marijuana use in humans has been studied with contrasting results. In one study on health problems related to illicit drug use from the NSDUH database (n = 29,195) (183), tinnitus did not show any association to marijuana use (whereas an association was found with hallucinogens and inhalants); in a second, cross-sectional study on the NHANES database (n = 2,705) (184), a correlation was found between tinnitus and cannabis use, although not between cannabis use frequency and tinnitus severity, and the authors concluded that it was not possible to differentiate between causal association (cannabis use increases tinnitus prevalence), reverse causal association (tinnitus sufferers use more cannabis than non-sufferers), and association due to external common cause (i.e., anxiety, which increases both tinnitus risk and cannabis use).

Animal studies [reviewed in (97)] suggest that cannabinoids do not reduce, and may even favor, tinnitus percept. Similarly, tinnitus in humans has been sporadically observed in association with abuse of synthetic cannabinoid mixtures (185, 186).

These seemingly contradictory results arise from two inherent complexities in the problem under study. First, the responses to cannabinoids (even for the same compound mixtures) strongly depend on drug formulation, administration route, and concentration. Second (**Figure 2**), tinnitus can result from many different mechanisms which are often hard to identify.

As regards the first complexity, it is important to stress that isolated and characterized phytocannabinoids, present in *Cannabis sativa* L. and a few other plant species (187, 188), include about 120 molecules (189), the most studied of which are Δ9-THC, mainly responsible for cannabis psychoactive effects (55), and cannabidiol (CBD), the major non-psychotropic component (190).

After the explanation of the structure–activity relationships in the Δ9-THC series (191, 192), a large and heterogeneous array of cannabimimetic compounds (**Supplementary Tables 1, 2**) have been synthesized (193, 194) including cannabinoid receptor agonists and antagonists (195), as well as drugs acting on EC metabolism (18, 196). Although, for several of them, dangerous health effects and strong potential for abuse and addiction greatly limit therapeutic use (197–199), several synthetic and phyto-cannabinoids are currently under clinical evaluation for different pathological conditions (see **Table 1**).

Cannabinoid bioavailability varies significantly by their formulation and route of administration (200, 201) and is also affected by poorly controllable factors such as subjective inhalation characteristics (200, 202, 203) or hepatic first-pass metabolism (202, 204–206). This is particularly relevant because the expansion of legal use of cannabinoids, for medical and nonmedical purposes, has substantially increased the types of commercially available preparations (207).

Second, besides the intrinsic complexities of cannabinoid pharmacology, the main problem in attempting a pharmacological approach to tinnitus is the lack of a clear unifying causative hypothesis for this condition (208, 209). Current models of tinnitus include (1) a peripheral trigger [which is assumed to be reduced or altered cochlear input (210), even if transient (211) or "hidden" [but see (212)], or possibly a somatosensory trigger (210, 213)]; (2) an aberrant compensatory response in the brainstem [most likely more complex than a simple "gain increase" (91, 210, 214) as was initially postulated to compensate for reduced input (215)]; and (3) a reconfiguration of cortical pathways including auditory, attentional, salience-related, and emotion-processing networks [which is thought to be necessary for the tinnitus percept to emerge to consciousness (216, 217)]. Given the absence of a causative hypothesis for tinnitus, in this review we will consider cannabinoid effects linked to both tinnitus and its main risk factors such as hearing loss or anxiety.

In animal models, tinnitus may be induced by noise trauma or ototoxic drugs such as salicylate (218). In humans, tinnitus is associated with several risk factors such as hearing loss, head trauma, and endocrine and immune dysregulation (208); however, the association between risk factors and tinnitus is far from linear. For example, although hearing loss is the main risk factor for tinnitus, it is not always accompanied by it, and tinnitus may be present without hearing loss (208). Non-auditory brain circuits also play important roles: in particular, tinnitus shows comorbidity with anxiety and depression (208, 219) and chronic tinnitus is associated with changes in attentional, memory, and limbic circuits (220, 221). The hypothesis explaining the involvement of non-auditory circuits includes a misdirection of attention which stays anomalously focused on the tinnitus percept (216), the involvement of limbic circuits encoding distress (220, 221) and the "replaying" of phantom sounds from memory in the absence of real percepts (220, 221).

At each of the levels thought to be associated with tinnitus onset and chronicization there are both well-known and potential cannabinoid targets. EC mechanisms have been found in the auditory brainstem, and particularly in the DCN, which is thought to be a major site of tinnitus onset (91, 222, 223). These neuronal, CB1R-based mechanisms (see previous section for a discussion of DCN effects) were considered very promising for a cannabinoid-based tinnitus treatment; unfortunately, animal studies displayed no effects, or even tinnitus increase, upon treatment [see discussion in (97)].

In addition to these targets, however, several other EC mechanisms (mainly related to inflammation) are present in the auditory system and in other CNS regions important for tinnitus (**Figure 2**). A protective EC mechanism is present in the cochlea (224, 225). Moreover, animal studies show inflammatory responses in the auditory cortex after tinnitus induction (154, 226), and inflammatory responses in the cochlea (154, 227, 228)

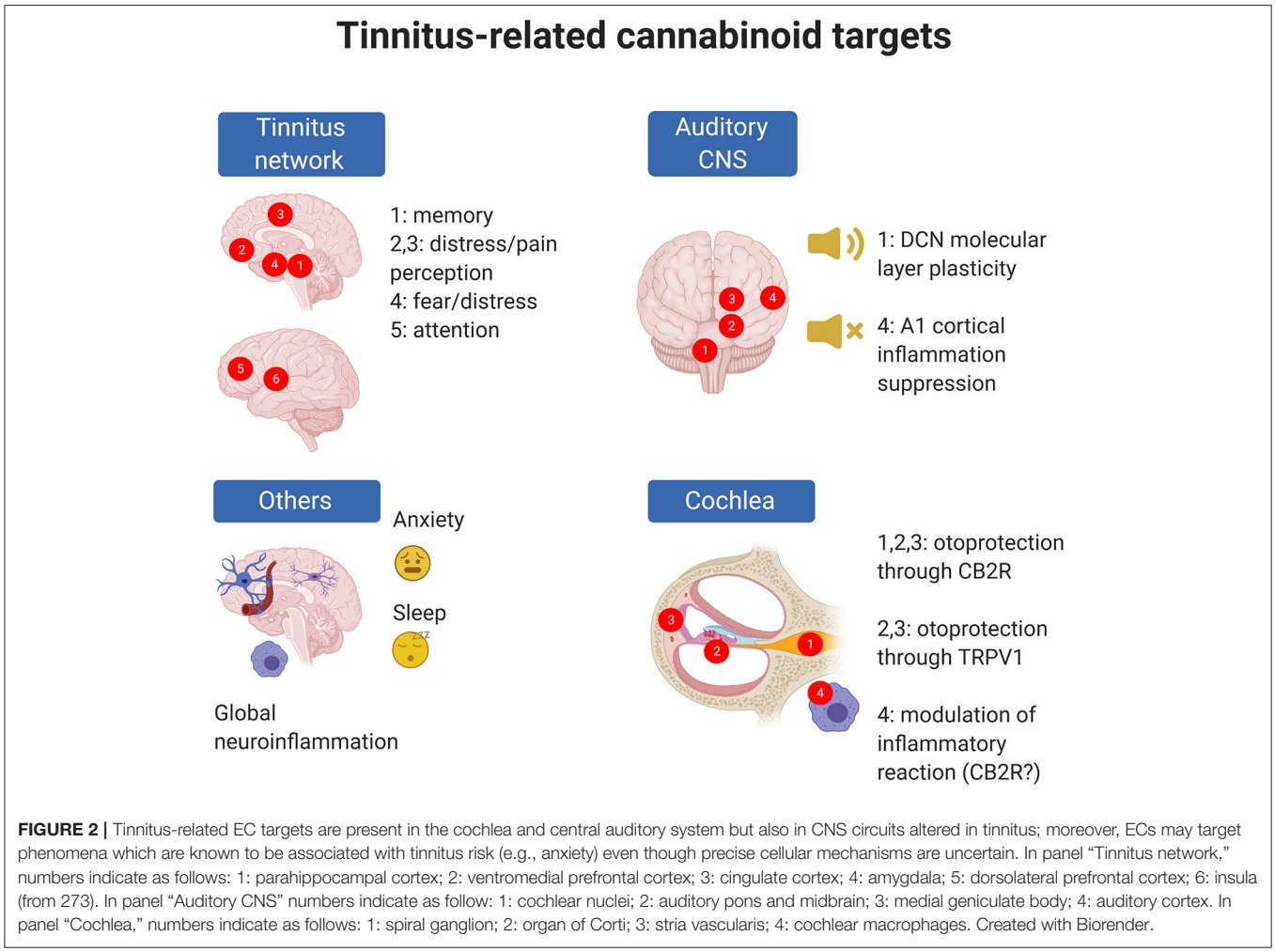

FIGURE 2 | Tinnitus-related EC targets are present in the cochlea and central auditory system but also in CNS circuits altered in tinnitus; moreover, ECs may target phenomena which are known to be associated with tinnitus risk (e.g., anxiety) even though precise cellular mechanisms are uncertain. In panel "Tinnitus network," numbers indicate as follows: 1: parahippocampal cortex; 2: ventromedial prefrontal cortex; 3: cingulate cortex; 4: amygdala; 5: dorsolateral prefrontal cortex; 6: insula (from 273). In panel "Auditory CNS" numbers indicate as follow: 1: cochlear nuclei; 2: auditory pons and midbrain; 3: medial geniculate body; 4: auditory cortex. In panel "Cochlea," numbers indicate as follows: 1: spiral ganglion; 2: organ of Corti; 3: stria vascularis; 4: cochlear macrophages. Created with Biorender.

and cochlear nuclei (229–232) after tinnitus-inducing treatments. Neuroinflammation may uncover novel EC-related therapeutic strategies, given the well-known anti-inflammatory effect of several cannabinoid drugs and pathways (see previous section).

In the auditory system, EC receptors and biosynthetic enzymes have been observed in several species and at several levels, and EC system modulation affects hearing at various levels. Moreover, several immune components and mechanisms known to be affected by EC modulation are also present in the auditory system, both peripheral and central. In the mammalian auditory system, EC system components or effects have been found in the cochlea (80), cochlear nuclei (93, 96, 233), MNTB (234), inferior colliculus (235, 236), and auditory cortex (237).

The hearing phenotypes of knockout mice for CB1R (238) and ABHD12 (239) have been characterized. In CB1R KO mice, high-frequency hearing is reduced but gap detection is improved, suggesting a change in auditory processing (238) or attentional modulation of perception, since in humans, chronic cannabis use is associated with attention-modulated deficit in PPI (240). Of relevance for tinnitus, CB1R KO mice also exhibit increased anxiety responses (241).

ABHD12 KO mice (239) and human ABHD12 nonsense mutations (242) display progressive hearing loss within PHARC syndrome. The absence of functional ABHD12 removes a catabolic pathway for 2-AG (see **Figure 1**); although the causative link between mutation and phenotype is still missing, a pro-inflammatory phenotype displaying microglial activation is observed (243), consistent with the expression of ABHD12 in both resting and activated microglia (242). Moreover, in the ABHD12 KO mouse the AA-related lipidome displays significant brain region-dependent changes (239) and macrophages increase LPS-induced cytokine production (244). On the other hand, the selective block of ABHD12 in adult mice does not induce hearing loss, suggesting developmental effects (245).

KO mice for CB2R (246) and other EC system components (239) are available, but their hearing has not been characterized; CB2R KO mice, on the other hand, display significant memory alterations (247).

In the cochlea, CB1R mRNA has been detected, and it decreases upon tinnitus-inducing salicylate treatment (248). However, the role of CB1Rs in the cochlea is still uncertain.

TABLE 1 | Major clinical trials based on pharmacological treatment targeting the endocannabinoid system (updated to July 21, 2020).

Drug	Pharmacology	Phase	Conditions	Completion date (*estimated date for ongoing studies)	National clinical trials (NCT) number
AZD1940	CB_1/CB_2 non-selective agonist	1 2	Back pain Pain	November 2008 May 2008	NCT00689780, NCT00659490
Org 28611	CB_1/CB_2 non-selective agonist	2	Pain	August 2007	NCT00782951
SAB378	CB_1/CB_2 non-selective agonist	2	Pain	January 2010	NCT00723918
APD-371	CB_2 selective agonist	2 2	Abdominal Pain, Crohn disease Abdominal pain	September 2018 *February 2022	NCT03155945 NCT04043455
GW-842,166X	CB_2 selective agonist	**1** **2**	Inflammatory pain Pain	July 2007 May 2009	NCT00511524 NCT00444769
Lenabasum	CB_2 selective agonist	**2** **3** **3** **2** **2** **2** **2**	Chronic inflammation	*August 2020 *December 2021 March 2020 December 2016 *July 2023 *December 2020 *December 2021	NCT03451045 NCT03813160 NCT03398837 NCT02465450 NCT02466243 NCT03093402 NCT02465437
Cannabidiol (Epidiolex)	See cannabidiol section for details	1,2 3 3 3 1 3 3 3 1	Seizures	May 2016 June 2017 February 2019 *February 2022 August 2019 March 2016 May 2016 *January 2021 June 2019	NCT02324673 NCT02318602 NCT02544763 NCT02544750 NCT02700412 NCT02224690 NCT02224560 NCT03808935 NCT02286986
		1 **1** **1** **1** **1** **1,2** **2** **3** **2** **2** **3** **3** **3** **3** **3** **3** **3** **3** **1** **2** **3** 2 4	Pain Chronic pain Neuropathic pain	December 2019 December 2020 *December 2021 *December 2021 January 2015 *December 2021 December 2019 August 2002 *December 2020 January 2010 January 2016 September 2006 January 2005 November 2014 July 2015 December 2015 August 2002 September 2002 September 2008 March 2004 *September 2022 November 2018 December 2004 July 2020 June 2020	NCT04193631 NCT03215940 NCT04044729 NCT04030442 NCT01893424 NCT02751359 NCT04088929 NCT01606176 NCT03099005 NCT00530764 NCT01337089 NCT00675948 NCT01606202 NCT01361607 NCT01262651 NCT01424566 NCT01604265 NCT01606189 NCT00391079 NCT00674609 NCT03679949 NCT03763851 NCT01606137 NCT04195269 NCT03891264
		2 **2** **2**	Anxiety	*August 2021 *February 2021 *March 2022	NCT02548559 NCT04267679 NCT04286594

(Continued)

TABLE 1 | Continued

Drug	Pharmacology	Phase	Conditions	Completion date (*estimated date for ongoing studies)	National clinical trials (NCT) number
		2		*January 2021	NCT04086342
		1		*November 2021	NCT04075435
		2		*July 2021	NCT03948074
		2		November 2017	NCT02818777
		2		*June 2021	NCT03582137
		2,3		February 2017	NCT02283281
		3		*October 2020	NCT03549819
ABX-1431	MAGL inhibitor	1	Pain	March 2018	NCT02929264
		1	Neurodegerative	July 2018	NCT03138421
		1	disorders	May 2019	NCT03447756
		1		October 2017	NCT03058562
		1		July 2018	NCT03138421
		2		January 2020	NCT03625453
ASP8477	FAAH inhibitor	2	Neuropathic pain	February 2015	NCT02065349
JNJ-42165279	FAAH inhibitor	1	Anxiety	July 2014	NCT02169973
		1		August 2014	NCT01826786
		2		August 2018	NCT02432703
		2		February 2019	NCT02498392
		2		*March 2022	NCT03664232
PF-04457845	FAAH inhibitor	1	Pain	July 2009	NCT00836082
		1		March 2017	NCT02134080
		2		May 2010	NCT00981357
		2		March 2015	NCT02216097
		2		June 2020	NCT01618656
		2		June 2020	NCT01665573
		2		*December 2022	NCT03386487
SSR411298	FAAH inhibitor	2	Pain	February 2010	NCT00822744
		2		February 2012	NCT01439919
V158866	FAAH inhibitor	1	Neuropathic pain	July 2011	NCT01634529
		2		July 2015	NCT01748695

On the other hand, CB2Rs have been found in rodent hair cells and pillar and Deiters' cells, spiral ganglion and nerve, and stria vascularis basal cells (224), and their expression increases upon cisplatin administration (80). Cisplatin is known to be strongly ototoxic by inducing cochlear inflammation (249), and CB2R block or knockdown makes the cochlea more sensitive to cisplatin ototoxicity (224): moreover, treatment with the CB2R antagonist AM630 is in itself proinflammatory, suggesting the presence of a cytoprotective EC tone in the cochlea (224). In addition, EC protective role in the cochlea has been found to involve TRPV1 activation: TRPV1 channels are expressed in hair cells (especially toward the apical pole), pillar, and Deiters' cells and in the marginal cells of the stria vascularis (250). The TRPV1 agonist capsaicin increases cochlear CB2R expression, and a CB2R-dependent mechanism induces the activation of STAT3; on the other hand, cisplatin induces the activation of proapoptotic factor STAT1 (225). The protective effect of capsaicin, which transiently induces STAT1 and TTS (225), is most likely due to the strong desensitization it induces on TRPV1 channels after a transient activation, similar to its effect in pain treatment (251).

CB1Rs are present in both ventral (VCN) and dorsal (DCN) cochlear nuclei of the rat; in the VCN, their role is unclear, but their expression decreases upon salicylate treatment, which induces tinnitus (233). In the DCN, salicylate does not change CB1R expression (233) but alters EC response on cartwheel cells (96). It is interesting to note the presence of CB1R (252) and CB2R (253) in the IV ventricle choroid plexus, especially because CB2R promote neural stem cell proliferation (254) and neurogenesis was observed in cochlear nuclei after deafferentation (255). In both man (256) and rat (257), there is a variable direct contact between the DCN surface and branches of the choroid plexus, where ECs released in the DCN molecular layer (92) could reach the plexus, possibly modulating its immune gate function (258).

As regards cortical effects important for tinnitus treatment, it is well known that anxiety (181) and attention (259) are strongly affected by cannabinoids. A point to be remembered is that, although cannabis use is associated with an acute anti-anxiety effect (260), chronic cannabis use may dramatically worsen anxiety (261, 262), thus exacerbating tinnitus severity. The anxiety-inducing effect of cannabis is correlated with its

Δ9-THC content, and Δ9-THC alone may induce anxiety and paranoia (263); on the other hand, CBD appears to have opposite effects on anxiety (264) and is currently under clinical evaluation for the treatment of anxiety, psychosis, and posttraumatic stress disorder (190, 265, 266).

These data show that cannabinoid effects of possible relevance for tinnitus are very diverse and include anti-inflammatory, protective reactions and selective circuit modulation of "auditory context." Since the anti-inflammatory route is starting to be explored as a possible therapeutic target in hearing loss (152) and tinnitus (154), interest has been raised for cannabinoids as a treatment option, and in particular for CBD, owing to its good toxicological profile in humans and lack of psychotropic effects. The recent availability of CBD preparations underlies anecdotal use reports by tinnitus patients; however, no controlled human studies have been performed yet.

Cannabidiol (CBD) is currently under clinical evaluation for the treatment of pain, anxiety, depression, sleep disorders, PTSD, headaches, and seizures (see **Supplementary Table 1**), all conditions which display analogies or associations with tinnitus (97, 179, 208). Despite such a wide spectrum of potentially interesting pharmacological properties, the practical effects of CBD on tinnitus are still underexplored.

Indeed, as of today the only study using CBD investigated the effects of a THC-CBD 1:1 mixture on noise trauma-induced tinnitus in the rat, showing no effects of daily treatment on tinnitus animals, and actually suggesting that cannabinoids might favor tinnitus onset, since treatment increased the fraction of animals showing tinnitus signs (267). These results agree with the effects of synthetic CB1R agonists (WIN55, 212-2, CP55,940, and ACEA) which have been tested in animal models of salicylate-induced tinnitus, with negative results [rat: (268); guinea pig: (269)]. It has to be remembered, however, that co-administered CBD and THC interact in a very complex way, and cannabinoid mixtures exert effects which may be very different from the simple combination of the effects of each drug *per se* (270). One example is CB1R activation in the cerebral cortex and hippocampus, associated with effects on cognition and memory (271): in this model, CBD is able to counteract THC-induced memory impairment (272).

In general, the pharmacodynamic of CBD appears particularly complex, with over 65 identified molecular targets, and different mechanisms proposed to explain its actions (190, 273, 274). Here we summarize only the CBD targets which may bear relevance for tinnitus.

On CB1R/CB2R, CBD has a very low affinity (in the μM range) and shows little agonist activity; on the other hand, it seems to antagonize CB1/CB2 synthetic agonist action with KB values in the nM range (275). It has been suggested that CBD acts as negative allosteric modulator of CB1R and as antagonist/inverse agonist of CB2R (276); in addition, it may indirectly affect CBR function by inhibiting FAAH activity, thus increasing endogenous anandamide levels (277, 278). For example, CBD neuroprotective effect after cerebral hypoxia–ischemia in immature pigs involves CB2R activation (279) and may be therefore due to EC increase rather than to a direct receptor effect.

Besides these effects, CBD acts as antagonist/inverse agonist of GPCR3, GPCR6, GPCR18, and GPCR55 (33, 280) and modulates serotonergic transmission acting as an allosteric agonist of 5HT1A receptor, a partial agonist of 5HT2A, and an allosteric inhibitor of 5HT3A (281–283). CBD protective effects on a BBB permeability model (284) required PPARγ and 5HT1A and were independent of CBRs. Similarly, CBD anti-depressant and anxiolytic effects also appear independent from CB2R (285) and linked to 5HT1A activation.

In the μM range, CBD may also activate adenosine A1 (286) and A2A receptors (287), activate glycine α1 (288) and α3 receptors (289), inhibit α7 nicotinic acetylcholine receptors (290), and allosterically modulate μ and δ opioid receptors (half maximal inhibition was observed at ∼10 μM) (291). As a caveat, since CBD concentrations $> 20\,\mu M$ are unlikely to be attained *in vivo* (292), not all the described CBD pharmacological activities are likely to be physiologically meaningful.

Modulation of α7 nAChRs may be relevant for tinnitus since these receptors are expressed in cortical and hippocampal neurons and affect cognition and memory [reviewed in (293)]; moreover, these receptors are also expressed in microglia (294) and macrophages (295) and are involved in the vagal-mediated cholinergic anti-inflammatory response signaling through the JAK2/STAT3 pathway, decreasing levels of pro-inflammatory cytokines, such as TNF-α, IL-1β, and IL-6 and increasing levels of anti-inflammatory cytokines such as IL-10 (295–298).

Finally, CBD may affect several ion channels including voltage-dependent Na channels (299), T-type Ca channels (300), and TRPV1 and TRPV2 channels (301). In particular, CBD can act on TRPV-1, exhibiting an action similar to capsaicin, both *in vitro* (302) and in an animal model of acute inflammation (303). This is relevant since capsaicin is able to exert protective effects on cochlear inflammatory damage (225), and therefore, CBD may exert similar otoprotective actions.

CONCLUSIONS

1. Cannabinoids are involved in neural processing in the healthy auditory system, in protective reaction to auditory damage, and in most non-auditory circuits known to be associated with tinnitus.
2. Given the availability of a large number of drugs with a wide spectrum of different effects on the EC system, it appears possible that some of them may reduce tinnitus percept or risk factors rather than increase them, similar to what is seen, e.g., for anxiety (where EC-targeting drugs may either worsen or ameliorate it).
3. EC modulation of neuroinflammatory responses in the auditory system, in particular by CBD, which is neuroprotective, is anti-inflammatory, undergoes clinical trial as an anxiolytic, and acts on pathways involved in cochlear damage protection, may represent a novel pharmacological approach to hearing loss and tinnitus, although more data

are necessary (especially on humans) to assess the therapeutic value of this or other EC drugs.

AUTHOR CONTRIBUTIONS

All authors listed have made a substantial, direct and intellectual contribution to the work, and approved it for publication. PP, RP, and PE contributed auditory expertise. AMT, FM, and MC neuroimmunological expertise. PE and CB pharmacological and clinical expertise.

FUNDING

This work was supported by AIT ONLUS donations to PP and FRG2019 grant to CB.

SUPPLEMENTARY MATERIAL

The Supplementary Material for this article can be found online at: https://www.frontiersin.org/articles/10.3389/fneur.2020.505995/full#supplementary-material

REFERENCES

1. Di Marzo V, De Petrocellis L. Why do cannabinoid receptors have more than one endogenous ligand? *Philos Trans R Soc Lond B Biol Sci*. (2012) 367:3216–28. doi: 10.1098/rstb.2011.0382
2. Carlisle SJ, Marciano-Cabral F, Staab A, Ludwick C, Cabral GA. Differential expression of the CB2 cannabinoid receptor by rodent macrophages and macrophage-like cells in relation to cell activation. *Int Immunopharmacol*. (2002) 2:69–82. doi: 10.1016/S1567-5769(01)00147-3
3. Brailoiu GC, Deliu E, Marcu J, Hoffman NE, Console-Bram L, Zhao P, et al. Differential activation of intracellular versus plasmalemmal CB2 cannabinoid receptors. *Biochemistry*. (2014) 53:4990–9. doi: 10.1021/bi500632a
4. Console-Bram L, Marcu J, Abood ME. Cannabinoid receptors: nomenclature and pharmacological principles. *Prog Neuropsychopharmacol Biol Psychiatry*. (2012) 38:4–15. doi: 10.1016/j.pnpbp.2012.02.009
5. Mackie K, Lai Y, Westenbroek R, Mitchell R. Cannabinoids activate an inwardly rectifying potassium conductance and inhibit Q-type calcium currents in AtT20 cells transfected with rat brain cannabinoid receptor. *J Neurosci*. (1995) 15:6552–61. doi: 10.1523/JNEUROSCI.15-10-06552.1995
6. Mackie K, Hille B. Cannabinoids inhibit N-type calcium channels in neuroblastoma-glioma cells. *Proc Natl Acad Sci USA*. (1992) 89:3825–9. doi: 10.1073/pnas.89.9.3825
7. Zou S, Kumar U. Cannabinoid receptors and the endocannabinoid system: signaling and function in the central nervous system. *Int J Mol Sci*. (2018) 19:833. doi: 10.3390/ijms19030833
8. Ibsen MS, Connor M, Glass M. Cannabinoid CB(1) and CB(2) receptor signaling and bias. *Cannabis Cannabinoid Res*. (2017) 2:48–60. doi: 10.1089/can.2016.0037
9. Ibsen MS, Finlay DB, Patel M, Javitch JA, Glass M, Grimsey NL. Cannabinoid CB1 and CB2 receptor-mediated arrestin translocation: species, subtype, and agonist-dependence. *Front Pharmacol*. (2019) 10:350. doi: 10.3389/fphar.2019.00350
10. Smith JS, Rajagopal S. The β-arrestins: multifunctional regulators of G protein-coupled receptors. *J Biol Chem*. (2016) 291:8969–77. doi: 10.1074/jbc.R115.713313
11. McCoy KL. Interaction between cannabinoid system and toll-like receptors controls inflammation. *Mediat Inflamm*. (2016) 2016:5831315. doi: 10.1155/2016/5831315
12. Hebert-Chatelain E, Desprez T, Serrat R, Bellocchio L, Soria-Gomez E, Busquets-Garcia A, et al. A cannabinoid link between mitochondria and memory. *Nature*. (2016) 539:555–9. doi: 10.1038/nature20127
13. Silvestri C, Di Marzo V. The endocannabinoid system in energy homeostasis and the etiopathology of metabolic disorders. *Cell Metab*. (2013) 17:475–90. doi: 10.1016/j.cmet.2013.03.001
14. Gallelli CA, Calcagnini S, Romano A, Koczwara JB, de Ceglia M, Dante D, et al. Modulation of the oxidative stress and lipid peroxidation by endocannabinoids and their lipid analogues. *Antioxidants*. (2018) 7:93. doi: 10.3390/antiox7070093
15. Pistis M, O'Sullivan SE. The role of nuclear hormone receptors in cannabinoid function. *Adv Pharmacol*. (2017) 80:291–328. doi: 10.1016/bs.apha.2017.03.008
16. Starkus J, Jansen C, Shimoda LMN, Stokes AJ, Small-Howard AL, Turner H. Diverse TRPV1 responses to cannabinoids. *Channels*. (2019) 13:172–91. doi: 10.1080/19336950.2019.1619436
17. Di Marzo V. Targeting the endocannabinoid system: to enhance or reduce? *Nat Rev Drug Discov*. (2008) 7:438–55. doi: 10.1038/nrd2553
18. Chicca A, Arena C, Manera C. Beyond the direct activation of cannabinoid receptors: new strategies to modulate the endocannabinoid system in CNS-related diseases. *Recent Pat CNS Drug Discov*. (2016) 10:122–41. doi: 10.2174/1574889810999160603185126
19. Savinainen JR, Saario SM, Laitinen JT. The serine hydrolases MAGL, ABHD6 and ABHD12 as guardians of 2-arachidonoylglycerol signalling through cannabinoid receptors. *Acta Physiol*. (2012) 204:267–76. doi: 10.1111/j.1748-1716.2011.02280.x
20. Kaur R, Ambwani SR, Singh S. Endocannabinoid system: a multi-facet therapeutic target. *Curr Clin Pharmacol*. (2016) 11:110–7. doi: 10.2174/1574884711666160418105339
21. Wilson RI, Nicoll RA. Endogenous cannabinoids mediate retrograde signalling at hippocampal synapses. *Nature*. (2001) 410:588–92. doi: 10.1038/35069076
22. Kano M, Ohno-Shosaku T, Hashimotodani Y, Uchigashima M, Watanabe M. Endocannabinoid-mediated control of synaptic transmission. *Physiol Rev*. (2009) 89:309–80. doi: 10.1152/physrev.00019.2008
23. Labra VC, Santibáñez CA, Gajardo-Gómez R, Díaz EF, Gómez GI, Orellana JA. The neuroglial dialog between cannabinoids and hemichannels. *Front Mol Neurosci*. (2018) 11:79. doi: 10.3389/fnmol.2018.00079
24. Oddi S, Scipioni L, Maccarrone M. Endocannabinoid system and adult neurogenesis: a focused review. *Curr Opin Pharmacol*. (2019) 50:25–32. doi: 10.1016/j.coph.2019.11.002
25. Pertwee RG. Endocannabinoids and their pharmacological actions. *Handb Exp Pharmacol*. (2015) 231:1–37. doi: 10.1007/978-3-319-20825-1_1
26. Lutz B. Lipid mediators in the regulation of emotions, memory, and cognitive functions. In: Melis M, editor. *Endocannabinoids and Lipid Mediators in Brain Functions*. Cham: Springer International Publishing, A. G. (2017).
27. Lisboa SF, Vila-Verde C, Rosa J, Uliana DL, Stern CAJ, Bertoglio LJ, et al. Tempering aversive/traumatic memories with cannabinoids: a review of evidence from animal and human studies. *Psychopharmacology*. (2019) 236:201–26. doi: 10.1007/s00213-018-5127-x
28. Turcotte C, Blanchet MR, Laviolette M, Flamand N. The CB2 receptor and its role as a regulator of inflammation. *Cell Mol Life Sci*. (2016) 73:4449–70. doi: 10.1007/s00018-016-2300-4
29. Mastinu A, Premoli M, Ferrari-Toninelli G, Tambaro S, Maccarinelli G, Memo M, et al. Cannabinoids in health and disease: pharmacological potential in metabolic syndrome and neuroinflammation. *Horm Mol Biol Clin Investig*. (2018) 36:1–15. doi: 10.1515/hmbci-2018-0013
30. Marco EM, García-Gutiérrez MS, Bermúdez-Silva FJ, Moreira FA, Guimarães F, Manzanares J, et al. Endocannabinoid system and psychiatry: in search of a neurobiological basis for detrimental and potential therapeutic effects. *Front Behav Neurosci*. (2011) 5:63. doi: 10.3389/fnbeh.2011.00063
31. Basu S, Dittel BN. Unraveling the complexities of cannabinoid receptor 2 (CB2) immune regulation in health and disease Immunol. *Res*. (2011) 51:26–38. doi: 10.1007/s12026-011-8210-5

32. Onaivi ES, Ishiguro H, Gu S, Liu QR. CNS effects of CB2 cannabinoid receptors: beyond neuro-immuno-cannabinoid activity. *J Psychopharmacol*. (2012) 26:92–103. doi: 10.1177/0269881111400652
33. Morales P, Hurst DP, Reggio PH. Molecular targets of the phytocannabinoids: a complex picture. *Prog Chem Org Nat Prod*. (2017) 103:103–31. doi: 10.1007/978-3-319-45541-9_4
34. Lynch DL, Hurst DP, Shore DM, Pitman MC, Reggio PH. Molecular dynamics methodologies for probing cannabinoid ligand/receptor interaction. *Methods Enzymol*. (2017) 593:449–90. doi: 10.1016/bs.mie.2017.05.004
35. Di Marzo V, Piscitelli F. The endocannabinoid system and its modulation by phytocannabinoids. *Neurotherapeutics*. (2015) 12:692–8. doi: 10.1007/s13311-015-0374-6
36. Hryhorowicz S, Walczak M, Zakerska-Banaszak O, Słomski R, Skrzypczak-Zielińska M. Pharmacogenetics of cannabinoids. *Eur J Drug Metab Pharmacokin*. (2018) 43:1–12. doi: 10.1007/s13318-017-0416-z
37. Chiurchiù V, Leuti A, Maccarrone M. Bioactive lipids and chronic inflammation: managing the fire within. *Front Immunol*. (2018) 9:38. doi: 10.3389/fimmu.2018.00038
38. Devane WA, Hanus L, Breuer A, Pertwee RG, Stevenson LA, Griffin G, et al. Isolation and structure of a brain constituent that binds to the cannabinoid receptor. *Science*. (1992) 258:1946–9. doi: 10.1126/science.1470919
39. Mechoulam R, Ben-Shabat S, Hanus L, Ligumsky M, Kaminski NE, Schatz AR, et al. Identification of an endogenous 2-monoglyceride, present in canine gut, that binds to cannabinoid receptors. *Biochem Pharmacol*. (1995) 50:83–90. doi: 10.1016/0006-2952(95)00109-D
40. Sugiura T, Kishimoto S, Oka S, Gokoh M. Biochemistry, pharmacology and physiology of 2-arachidonoylglycerol, an endogenous cannabinoid receptor ligand. *Prog Lipid Res*. (2006) 45:405–46. doi: 10.1016/j.plipres.2006.03.003
41. Pagotto U, Marsicano G, Cota D, Lutz B, Pasquali R. The emerging role of the endocannabinoid system in endocrine regulation and energy balance. *Endocr Rev*. (2006) 27:73–100. doi: 10.1210/er.2005-0009
42. Wang J, Ueda N. Biology of endocannabinoid synthesis system. *Prostaglandins Other Lipid Mediat*. (2009) 89:112–9. doi: 10.1016/j.prostaglandins.2008.12.002
43. Hanus L, Abu-Lafi S, Fride E, Breuer A, Vogel Z, Shalev DE, et al. 2-arachidonyl glyceryl ether, an endogenous agonist of the cannabinoid CB1 receptor. *Proc Natl Acad Sci USA*. (2001) 98:3662–5. doi: 10.1073/pnas.061029898
44. Bauer M, Chicca A, Tamborrini M, Eisen D, Lerner R, Lutz B, et al. Identification and quantification of a new family of peptide endocannabinoids (Pepcans) showing negative allosteric modulation at CB1 receptors. *J Biol Chem*. (2012) 287:36944–67. doi: 10.1074/jbc.M112.382481
45. Leishman E, Cornett B, Spork K, Straiker A, Mackie K, Bradshaw HB. Broad impact of deleting endogenous cannabinoid hydrolyzing enzymes and the CB1 cannabinoid receptor on the endogenous cannabinoid-related lipidome in eight regions of the mouse brain. *Pharmacol Res*. (2016) 110:159–72. doi: 10.1016/j.phrs.2016.04.020
46. Alger BE, Kim J. Supply and demand for endocannabinoids. *Trends Neurosci*. (2011) 34:304–15. doi: 10.1016/j.tins.2011.03.003
47. Marrs WR, Horne EA, Ortega-Gutierrez S, Cisneros JA, Xu C, Lin YH, et al. Dual inhibition of alpha/beta-hydrolase domain 6 and fatty acid amide hydrolase increases endocannabinoid levels in neurons. *J Biol Chem*. (2011) 286:28723–8. doi: 10.1074/jbc.M110.202853
48. Gatta L, Piscitelli F, Giordano C, Boccella S, Lichtman A, Maione S, et al. Discovery of prostamide F2α and its role in inflammatory pain and dorsal horn nociceptive neuron hyperexcitability. *PLoS ONE*. (2012) 7:e31111. doi: 10.1371/journal.pone.0031111
49. Mechoulam R, Parker LA. The endocannabinoid system and the brain. *Ann Rev Psychol*. (2013) 64:21–47. doi: 10.1146/annurev-psych-113011-143739
50. Fonseca BM, Costa MA, Almada M, Correia-da-Silva G, Teixeira NA. Endogenous cannabinoids revisited: a biochemistry perspective. *Prostaglandins Other Lipid Mediat*. (2013) 102–3:13–30. doi: 10.1016/j.prostaglandins.2013.02.002
51. Lu HC, Mackie K. An introduction to the endogenous cannabinoid system. *Biol Psychiatry*. (2016) 79:516–25. doi: 10.1016/j.biopsych.2015.07.028
52. Begg M, Pacher P, Bátkai S, Osei-Hyiaman D, Offertáler L, Mo FM, et al. Evidence for novel cannabinoid receptors. *Pharmacol Ther*. (2005) 106:133–45. doi: 10.1016/j.pharmthera.2004.11.005
53. Muller C, Morales P, Reggio PH. Cannabinoid ligands targeting TRP channels. *Front Mol Neurosci*. (2019) 11:487. doi: 10.3389/fnmol.2018.00487
54. O'Sullivan SE. Cannabinoids go nuclear: evidence for activation of peroxisome proliferator-activated receptors. *Br J Pharmacol*. (2007) 152:576–82. doi: 10.1038/sj.bjp.0707423
55. Pertwee RG. Cannabinoid pharmacology: the first 66 years. *Br J Pharmacol*. (2006) 147 (Suppl. 1):S163–71. doi: 10.1038/sj.bjp.0706406
56. Pertwee RG. Cannabinoid receptor ligands: clinical and neuropharmacological considerations, relevant to future drug discovery and development. *Expert Opin Investig Drugs*. (2000) 9:1553–71. doi: 10.1517/13543784.9.7.1553
57. Pistis M, Melis M. From surface to nuclear receptors: the endocannabinoid family extends its assets. *Curr Med Chem*. (2010) 17:1450–67. doi: 10.2174/092986710790980014
58. Irving A, Abdulrazzaq G, Chan SLF, Penman J, Harvey J, Alexander SPH. Cannabinoid receptor-related orphan G protein-coupled receptors. *Adv Pharmacol*. (2017) 80:223–47. doi: 10.1016/bs.apha.2017.04.004
59. Morales P, Reggio PH. An Update on Non-CB1, Non-CB2 cannabinoid related G-protein-coupled receptors. *Cannabis Cannabinoid Res*. (2017) 2:265–73. doi: 10.1089/can.2017.0036
60. Pertwee RG, Howlett AC, Abood ME, Alexander SPH, Di Marzo V, Elphick MR, et al. International Union of Basic and Clinical Pharmacology. LXXIX. Cannabinoid receptors and their ligands: beyond CB1 and CB_2. *Pharmacol Rev*. (2010) 62:588–631. doi: 10.1124/pr.110.003004
61. De Petrocellis L, Nabissi M, Santoni G, Ligresti A. Actions and regulation of ionotropic cannabinoid receptors. *Adv Pharmacol*. (2017) 80:249–89. doi: 10.1016/bs.apha.2017.04.001
62. Oláh A, Szekanecz Z, Bíró T. Targeting cannabinoid signaling in the immune system: "high"-ly exciting questions, possibilities, and challenges. *Front Immunol*. (2017) 8:1487. doi: 10.3389/fimmu.2017.01487
63. Callén L, Moreno E, Barroso-Chinea P, Moreno-Delgado D, Cortés A, Mallol J, et al. Cannabinoid receptors CB1 and CB2 form functional heteromers in brain. *J Biol Chem*. (2012) 287:20851–65. doi: 10.1074/jbc.M111.335273
64. Moreno E, Chiarlone A, Medrano M, Puigdellívol M, Bibic L, Howell LA, et al. Singular location and signaling profile of adenosine A2A-cannabinoid CB1 receptor heteromers in the dorsal striatum. *Neuropsychopharmacology*. (2018) 43:964–77. doi: 10.1038/npp.2017.12
65. Kearn CS, Blake-Palmer K, Daniel E, Mackie K, Glass M. Concurrent stimulation of cannabinoid CB1 and dopamine D2 receptors enhances heterodimer formation: a mechanism for receptor cross-talk? *Mol Pharmacol*. (2005) 67:1697–704. doi: 10.1124/mol.104.006882
66. Hojo M, Sudo Y, Ando Y, Minami K, Takada M, Matsubara T, et al. mu-Opioid receptor forms a functional heterodimer with cannabinoid CB1 receptor: electrophysiological and FRET assay analysis. *J Pharmacol Sci*. (2008). 108:308–19. doi: 10.1254/jphs.08244fp
67. Ward RJ, Pediani JD, Milligan G. Heteromultimerization of cannabinoid CB(1) receptor and orexin OX(1) receptor generates a unique complex in which both protomers are regulated by orexin, A. *J Biol Chem*. (2011) 286:37414–28. doi: 10.1074/jbc.M111.287649
68. Coke CJ, Scarlett KA, Chetram MA, Jones KJ, Sandifer BJ, Davis AS, et al. Simultaneous activation of induced heterodimerization between CXCR4 chemokine receptor and cannabinoid receptor 2 (CB2) reveals a mechanism for regulation of tumor progression. *J Biol Chem*. (2016) 291:9991–10005. doi: 10.1074/jbc.M115.712661
69. Balenga NA, Martínez-Pinilla E, Kargl J, Schröder R, Peinhaupt M, Platzer W, et al. Heteromerization of GPR55 and cannabinoid CB2 receptors modulates signalling. *Br J Pharmacol*. (2014). 171:5387–406. doi: 10.1111/bph.12850
70. Costa L, Amaral C, Teixeira N, Correia-da-Silva G, Fonseca BM. Cannabinoid-induced autophagy: protective or death role?, prostaglandins & other lipid. *Mediators*. (2016) 122:54–63. doi: 10.1016/j.prostaglandins.2015.12.006
71. Hiebel C, Behl C. The complex modulation of lysosomal degradation pathways by cannabinoid receptors 1 and 2. *Life Sci*. (2015) 138:3–7. doi: 10.1016/j.lfs.2015.03.020

72. Premkumar LS, Abooj M. TRP channels and analgesia. *Life Sci*. (2013) 92:415–24. doi: 10.1016/j.lfs.2012.08.010
73. Joshi N, Onaivi ES. Endocannabinoid system components: overview and tissue distribution. *Adv Exp Med Biol*. (2019) 1162:1–12. doi: 10.1007/978-3-030-21737-2_1
74. Howlett AC. The cannabinoid receptors. *Prostaglandins Other Lipid Mediat*. (2002) 68–9:619–31. doi: 10.1016/S0090-6980(02)00060-6
75. Pacher P, Bátkai S, Kunos G. The endocannabinoid system as an emerging target of pharmacotherapy. *Pharmacol Rev*. (2006) 58:389–462. doi: 10.1124/pr.58.3.2
76. Herkenham M, Lynn AB, Johnson MR, Melvin LS, de Costa BR, Rice KC. Characterization and localization of cannabinoid receptors in rat brain: a quantitative *in vitro* autoradiographic study. *J Neurosci*. (1991) 11:563–83. doi: 10.1523/JNEUROSCI.11-02-00563.1991
77. Munro S, Thomas KL, Abu-Shaar M. Molecular characterization of a peripheral receptor for cannabinoids. *Nature*. (1993). 365:61–5. doi: 10.1038/365061a0
78. Pacher P, Mechoulam R. Is lipid signaling through cannabinoid 2 receptors part of a protective system? *Prog Lipid Res*. (2011). 50:193–211. doi: 10.1016/j.plipres.2011.01.001
79. Atwood BK, Mackie K. CB2: a cannabinoid receptor with an identity crisis. *Br J Pharmacol*. (2010) 160:467–79. doi: 10.1111/j.1476-5381.2010.00729.x
80. Martín-Saldaña S, Trinidad A, Ramil E, Sánchez-López AJ, Coronado MJ, Martínez-Martínez E, et al. Spontaneous cannabinoid receptor 2 (CB2) expression in the cochlea of adult albino rat and its up-regulation after cisplatin treatment. *PLoS ONE*. (2016) 11:e0161954. doi: 10.1371/journal.pone.0161954
81. Yu SJ, Reiner D, Shen H, Wu KJ, Liu QR, Wang Y. Time-dependent protection of CB2 receptor agonist in stroke. *PLoS ONE*. (2015) 10:e0132487. doi: 10.1371/journal.pone.0132487
82. Katona I, Freund TF. Multiple functions of endocannabinoid signaling in the brain. *Annu Rev Neurosci*. (2012) 35:529–58. doi: 10.1146/annurev-neuro-062111-150420
83. Busquets-Garcia A, Bains J, Marsicano G. CB(1) receptor signaling in the brain: extracting specificity from ubiquity. *Neuropsychopharmacology*. (2018) 43:4–20. doi: 10.1038/npp.2017.206
84. Narayanaswami V, Dahl K, Bernard-Gauthier V, Josephson L, Cumming P, Vasdev N. Emerging PET radiotracers and targets for imaging of neuroinflammation in neurodegenerative diseases: outlook beyond TSPO. *Mol Imaging*. (2018) 17:1536012118792317. doi: 10.1177/1536012118792317
85. Toczek M, Malinowska B. Enhanced endocannabinoid tone as a potential target of pharmacotherapy. *Life Sci*. (2018) 204:20–45. doi: 10.1016/j.lfs.2018.04.054
86. Chen WW, Zhang X, Huang WJ. Role of neuroinflammation in neurodegenerative diseases. *Mol Med Rep*. (2016) 13:3391–6. doi: 10.3892/mmr.2016.4948
87. Diana MA, Marty A. Endocannabinoid-mediated short-term synaptic plasticity: depolarization-induced suppression of inhibition (DSI) and depolarization-induced suppression of excitation (DSE). *Br J Pharmacol*. (2004) 142:9–19. doi: 10.1038/sj.bjp.0705726
88. Oertel D, Young ED. What's a cerebellar circuit doing in the auditory system? *Trends Neurosci*. (2004) 27:104–10. doi: 10.1016/j.tins.2003.12.001
89. Singla S, Dempsey C, Warren R, Enikolopov AG, Sawtell NB. A cerebellum-like circuit in the auditory system cancels responses to self-generated sounds. *Nat Neurosci*. (2017) 20:943–50. doi: 10.1038/nn.4567
90. Tzounopoulos T. Mechanisms of synaptic plasticity in the dorsal cochlear nucleus: plasticity-induced changes that could underlie tinnitus. *Am J Audiol*. (2008). 17:S170–5. doi: 10.1044/1059-0889(2008/07-0030)
91. Shore SE, Wu C. Mechanisms of noise-induced tinnitus: insights from cellular studies. *Neuron*. (2019) 103:8–20. doi: 10.1016/j.neuron.2019.05.008
92. Sedlacek M, Tipton PW, Brenowitz SD. Sustained firing of cartwheel cells in the dorsal cochlear nucleus evokes endocannabinoid release and retrograde suppression of parallel fiber synapses. *J Neurosci*. (2011) 31:15807–17. doi: 10.1523/JNEUROSCI.4088-11.2011
93. Zhao Y, Rubio ME, Tzounopoulos T. Distinct functional and anatomical architecture of the endocannabinoid system in the auditory brainstem. *J Neurophysiol*. (2009) 101:2434–46. doi: 10.1152/jn.00047.2009
94. Zhao Y, Tzounopoulos T. Physiological activation of cholinergic inputs controls associative synaptic plasticity via modulation of endocannabinoid signaling. *J Neurosci*. (2011) 31:3158–68. doi: 10.1523/JNEUROSCI.5303-10.2011
95. Stefanescu RA, Shore SE. Muscarinic acetylcholine receptors control baseline activity and Hebbian stimulus timing-dependent plasticity in fusiform cells of the dorsal cochlear nucleus. *J Neurophysiol*. (2017) 117:1229–38. doi: 10.1152/jn.00270.2016
96. Zugaib J, Leão RM. Enhancement of endocannabinoid-dependent depolarization-induced suppression of excitation in glycinergic neurons by prolonged exposure to high doses of salicylate. *Neuroscience*. (2018) 376:72–9. doi: 10.1016/j.neuroscience.2018.02.016
97. Zheng Y, Smith PF. Cannabinoid drugs: will they relieve or exacerbate tinnitus? *Curr Opin Neurol*. (2019) 32:131–6. doi: 10.1097/WCO.0000000000000631
98. Kim J, Alger BE. Reduction in endocannabinoid tone is a homeostatic mechanism for specific inhibitory synapses. *Nat Neurosci*. (2010). 13:592–600. doi: 10.1038/nn.2517
99. Nyilas R, Dudok B, Urbán GM, Mackie K, Watanabe M, Cravatt BF, et al. Enzymatic machinery for endocannabinoid biosynthesis associated with calcium stores in glutamatergic axon terminals. *J Neurosci*. (2008) 28:1058–63. doi: 10.1523/JNEUROSCI.5102-07.2008
100. Freund TF, Katona I, Piomelli D. Role of endogenous cannabinoids in synaptic signaling. *Physiol Rev*. (2003) 83:1017–66. doi: 10.1152/physrev.00004.2003
101. Hillard CJ. Biochemistry and pharmacology of the endocannabinoids arachidonylethanolamide and 2-arachidonylglycerol. *Prostaglandins Other Lipid Mediat*. (2000) 61:3–18. doi: 10.1016/S0090-6980(00)00051-4
102. Stella N. Cannabinoid signaling in glial cells. *Glia*. (2004) 48:267–77. doi: 10.1002/glia.20084
103. Jimenez-Blasco D, Busquets-Garcia A, Hebert-Chatelain E, Serrat R, Vicente-Gutierrez C, Ioannidou C, et al. Glucose metabolism links astroglial mitochondria to cannabinoid effects. *Nature*. (2020) 583:603–8. doi: 10.1038/s41586-020-2470-y
104. Viader A, Blankman JL, Zhong P, Liu X, Schlosburg JE, Joslyn CM, et al. Metabolic interplay between astrocytes and neurons regulates endocannabinoid action. *Cell Rep*. (2015) 12:798–808. doi: 10.1016/j.celrep.2015.06.075
105. Navarrete M, Araque A. Endocannabinoids potentiate synaptic transmission through stimulation of astrocytes. *Neuron*. (2010) 68:113–26. doi: 10.1016/j.neuron.2010.08.043
106. Rasooli-Nejad S, Palygin O, Lalo U, Pankratov Y. Cannabinoid receptors contribute to astroglial Ca2+-signalling and control of synaptic plasticity in the neocortex *Phil. Trans, R Soc B*. (2014) 369:20140077. doi: 10.1098/rstb.2014.0077
107. Kovács A, Bordás C, Bíró T, Hegyi Z, Antal M, Szücs P, et al. Direct presynaptic and indirect astrocyte-mediated mechanisms both contribute to endocannabinoid signaling in the pedunculopontine nucleus of mice. *Brain Struct Funct*. (2017) 222:247–66. doi: 10.1007/s00429-016-1214-0
108. Hablitz LM, Gunesch AN, Cravetchi O, Moldavan M, Allen CN. Cannabinoid signaling recruits astrocytes to modulate presynaptic function in the suprachiasmatic nucleus. *eNeuro*. (2020) 7:ENEURO.0081-19.2020. doi: 10.1523/ENEURO.0081-19.2020
109. Koning HM. Sleep disturbances associated with tinnitus: reduce the maximal intensity of tinnitus. *Int Tinnitus J*. (2019) 23:64–8. doi: 10.5935/0946-5448.20190018
110. Probst T, Pryss RC, Langguth B, Rauschecker JP, Schobel J, Reichert M, et al. Does tinnitus depend on time-of-day? An ecological momentary assessment study with the "TrackYourTinnitus" *Application Front Aging Neurosci*. (2017) 9:253. doi: 10.3389/fnagi.2017.00253
111. Becher B, Spath S, Goverman J. Cytokine networks in neuroinflammation. *Nat Rev Immunol*. (2017) 17:49–59. doi: 10.1038/nri.2016.123
112. Walter L, Stella N. Endothelin-1 increases 2-arachidonoyl glycerol (2-AG) production in astrocytes. *Glia*. (2003) 44:85–90. doi: 10.1002/glia.10270
113. Rom S, Persidsky Y. Cannabinoid receptor 2: potential role in immunomodulation and neuroinflammation. *J Neuroimmune Pharmacol*. (2013) 8:608–20. doi: 10.1007/s11481-013-9445-9

114. Turcotte C, Chouinard F, Lefebvre JS, Flamand N. Regulation of inflammation by cannabinoids, the endocannabinoids 2-arachidonoyl-glycerol and arachidonoyl-ethanolamide and their metabolites. *J Leukoc Biol*. (2015) 97:1049–70. doi: 10.1189/jlb.3RU0115-021R
115. Waksman Y, Olson JM, Carlisle SJ, Cabral GA. The central cannabinoid receptor (CB1) mediates inhibition of nitric oxide production by rat microglial cells. *J Pharmacol Exp Ther*. (1999) 288:1357–66.
116. Molina-Holgado F, Molina-Holgado E, Guaza C, Rothwell NJ. Role of CB1 and CB2 receptors in the inhibitory effects of cannabinoids on lipopolysaccharide-induced nitric oxide release in astrocyte cultures. *J Neurosci Res*. (2002) 67:829–36. doi: 10.1002/jnr.10165
117. Molina-Holgado F, Pinteaux E, Moore JD, Molina-Holgado E, Guaza C, Gibson RM, et al. Endogenous interleukin-1 receptor antagonist mediates anti-inflammatory and neuroprotective actions of cannabinoids in neurons and glia. *J Neurosci*. (2003) 23:6470–4. doi: 10.1523/JNEUROSCI.23-16-06470.2003
118. Mecha M, Feliú A, Carrillo-Salinas FJ, Rueda-Zubiaurre A, Ortega-Gutiérrez S, de Sola RG, et al. Endocannabinoids drive the acquisition of an alternative phenotype in microglia. *Brain Behav Immun*. (2015) 49:233–45. doi: 10.1016/j.bbi.2015.06.002
119. Stella N. Endocannabinoid signaling in microglial cells. *Neuropharmacology*. (2009) 56:244–53. doi: 10.1016/j.neuropharm.2008.07.037
120. Walter L, Franklin A, Witting A, Wade C, Xie Y, Kunos G, et al. Nonpsychotropic cannabinoid receptors regulate microglial cell migration. *J Neurosci*. (2003) 23:1398–405. doi: 10.1523/JNEUROSCI.23-04-01398.2003
121. Bruttger J, Karram K, Wörtge S, Regen T, Marini F, Hoppmann N, et al. Genetic cell ablation reveals clusters of local self-renewing microglia in the mammalian central nervous system. *Immunity*. (2015) 43:92–106. doi: 10.1016/j.immuni.2015.06.012
122. Askew K, Li K, Olmos-Alonso A, Garcia-Moreno F, Liang Y, Richardson P, et al. Coupled proliferation and apoptosis maintain the rapid turnover of microglia in the adult brain. *Cell Rep*. (2017) 18:391–405. doi: 10.1016/j.celrep.2016.12.041
123. Huang Y, Xu Z, Xiong S, Sun F, Qin G, Hu G, et al. Repopulated microglia are solely derived from the proliferation of residual microglia after acute depletion. *Nat Neurosci*. (2018) 21:530–40. doi: 10.1038/s41593-018-0090-8
124. Viader A, Ogasawara D, Joslyn CM, Sanchez-Alavez M, Mori S, Nguyen W, et al. A chemical proteomic atlas of brain serine hydrolases identifies cell type-specific pathways regulating neuroinflammation. *Elife*. (2016) 5:e12345. doi: 10.7554/eLife.12345
125. Stella N. Cannabinoid and cannabinoid-like receptors in microglia, astrocytes, and astrocytomas. *Glia*. (2010) 58:1017–30. doi: 10.1002/glia.20983
126. Jordan CJ, Xi ZX. Progress in brain cannabinoid CB(2) receptor research: From genes to behavior. *Neurosci Biobehav Rev*. (2019) 98:208–20. doi: 10.1016/j.neubiorev.2018.12.026
127. Lemos JR, Ortiz-Miranda SI, Cuadra AE, Velázquez-Marrero C, Custer EE, Dad T, et al. Modulation/physiology of calcium channel subtypes in neurosecretory terminals. *Cell Calcium*. (2012) 51:284–92. doi: 10.1016/j.ceca.2012.01.008
128. Witting A, Walter L, Wacker J, Möller T, Stella N. P2X7 receptors control 2-arachidonoylglycerol production by microglial cells. *Proc Natl Acad Sci USA*. (2004) 101:3214–9. doi: 10.1073/pnas.0306707101
129. Cassano T, Calcagnini S, Pace L, De Marco F, Romano A, Gaetani S. Cannabinoid receptor 2 signaling in neurodegenerative disorders: from pathogenesis to a promising therapeutic target. *Front Neurosci*. (2017) 11:30. doi: 10.3389/fnins.2017.00030
130. Grabner GF, Eichmann TO, Wagner B, Gao Y, Farzi A, Taschler U, et al. Deletion of monoglyceride lipase in astrocytes attenuates lipopolysaccharide-induced neuroinflammation. *J Biol Chem*. (2016) 291:913–23. doi: 10.1074/jbc.M115.683615
131. Miller LK, Devi LA. The highs and lows of cannabinoid receptor expression in disease: mechanisms and their therapeutic implications. *Pharmacol Rev*. (2011) 63:461–70. doi: 10.1124/pr.110.003491
132. Baek JH, Darlington CL, Smith PF, Ashton JC. Antibody testing for brain immunohistochemistry: brain immunolabeling for the cannabinoid CB_2 receptor. *J Neurosci Methods*. (2013) 216:87–95. doi: 10.1016/j.jneumeth.2013.03.021
133. Zhang HY, Shen H, Jordan CJ, Liu QR, Gardner EL, Bonci A, et al. CB2 receptor antibody signal specificity: correlations with the use of partial CB2-knockout mice and anti-rat CB2 receptor antibodies. *Acta Pharmacol Sin*. (2019) 40:398–409. doi: 10.1038/s41401-018-0037-3
134. Galiègue S, Mary S, Marchand J, Dussossoy D, Carrière D, Carayon P, et al. Expression of central and peripheral cannabinoid receptors in human immune tissues and leukocyte subpopulations. *Eur J Biochem*. (1995) 232:54–61. doi: 10.1111/j.1432-1033.1995.tb20780.x
135. Ofek O, Karsak M, Leclerc N, Fogel M, Frenkel B, Wright K, et al. Peripheral cannabinoid receptor, CB2, regulates bone mass. *Proc Natl Acad Sci USA*. (2006) 103:696–701. doi: 10.1073/pnas.0504187103
136. Benito C, Romero JP, Tolón RM, Clemente D, Docagne F, Hillard CJ, et al. Cannabinoid CB1 and CB2 receptors and fatty acid amide hydrolase are specific markers of plaque cell subtypes in human multiple sclerosis. *J Neurosci*. (2007) 27:2396–402. doi: 10.1523/JNEUROSCI.4814-06.2007
137. Brusco A, Tagliaferro P, Saez T, Onaivi ES. Postsynaptic localization of CB2 cannabinoid receptors in the rat hippocampus. *Synapse*. (2008) 62:944–9. doi: 10.1002/syn.20569
138. Molina-Holgado E, Vela JM, Arévalo-Martín A, Almazán G, Molina-Holgado F, Borrell J, et al. Cannabinoids promote oligodendrocyte progenitor survival: involvement of cannabinoid receptors and phosphatidylinositol-3 kinase/Akt signaling. *J Neurosci*. (2002) 22:9742–53. doi: 10.1523/JNEUROSCI.22-22-09742.2002
139. Liu QR, Pan CH, Hishimoto A, Li C-Y, Xi Z-X, Llorente-Berzal A, et al. Species differences in cannabinoid receptor 2 (CNR2 gene): identification of novel human and rodent CB2 isoforms, differential tissue expression and regulation by cannabinoid receptor ligands. *Genes Brain Behav*. (2009). 8:519–30. doi: 10.1111/j.1601-183X.2009.00498.x
140. Zhang HY, Bi GH, Li X, Li J, Qu H, Zhang S-J, et al. Species differences in cannabinoid receptor 2 and receptor responses to cocaine self-administration in mice and rats. *Neuropsychopharmacology*. (2015). 40:1037–51. doi: 10.1038/npp.2014.297
141. Colonna M, Butovsky O. Microglia function in the central nervous system during health and neurodegeneration. *Annu Rev Immunol*. (2017) 35:441–68. doi: 10.1146/annurev-immunol-051116-052358
142. Casano AM, Peri F. Microglia: multitasking specialists of the brain. *Dev Cell*. (2015) 32:469–77. doi: 10.1016/j.devcel.2015.01.018
143. Ransohoff RM. A polarizing question: do M1 and M2 microglia exist? *Nat Neurosci*. (2016) 19:987–91. doi: 10.1038/nn.4338
144. Masuda T, Sankowski R, Staszewski O, Prinz M. Microglia heterogeneity in the single-cell era. *Cell Rep*. (2020) 30:1271–81. doi: 10.1016/j.celrep.2020.01.010
145. De Biase LM, Bonci A. Region-specific phenotypes of microglia: the role of local regulatory cues. *Neuroscientist*. (2019) 25:314–33. doi: 10.1177/1073858418800996
146. Geirsdottir L, David E, Keren-Shaul H, Weiner A, Bohlen SC, Neuber J, et al. Cross-species single-cell analysis reveals divergence of the primate microglia program. *Cell*. (2019) 179:1609–22.e16. doi: 10.1016/j.cell.2019.11.010
147. Galatro TF, Holtman IR, Lerario AM, Vainchtein ID, Brouwer N, Sola PR, et al. Transcriptomic analysis of purified human cortical microglia reveals age-associated changes. *Nat Neurosci*. (2017) 20:1162–71. doi: 10.1038/nn.4597
148. Villa A, Della Torre S, Maggi A. Sexual differentiation of microglia. *Front Neuroendocrinol*. (2019) 52:156–64. doi: 10.1016/j.yfrne.2018.11.003
149. Butovsky O, Weiner HL. Microglial signatures and their role in health and disease. *Nat Rev Neurosci*. (2018) 19:622–35. doi: 10.1038/s41583-018-0057-5
150. Rivest S. Regulation of innate immune responses in the brain. *Nat Rev Immunol*. (2009) 9:429–39. doi: 10.1038/nri2565
151. Tansey MG, McCoy MK, Frank-Cannon TC. Neuroinflammatory mechanisms in Parkinson's disease: potential environmental triggers, pathways, and targets for early therapeutic intervention. *Exp Neurol*. (2007) 208:1–25. doi: 10.1016/j.expneurol.2007.07.004
152. Watson N, Ding B, Zhu X, Frisina RD. Chronic inflammation - inflammaging - in the ageing cochlea: a novel target for future presbycusis therapy. *Ageing Res Rev*. (2017) 40:142–8. doi: 10.1016/j.arr.2017.10.002

153. Wang J, Sung V, Carew P, Liu RS, Burgner D, Wake M. Inflammation and hearing status in mid-childhood and mid-life: a population-based cross-sectional study. *Int J Epidemiol*. (2019) 48:1556–66. doi: 10.1093/ije/dyz023
154. Wang W, Zhang LS, Zinsmaier AK, Patterson G, Leptich EJ, Shoemaker SL, et al. Neuroinflammation mediates noise-induced synaptic imbalance and tinnitus in rodent models. *PLoS Biol*. (2019) 17:e3000307. doi: 10.1371/journal.pbio.3000307
155. Marchiori LL, Dias AC, Gonçalvez AS, Poly-Frederico RC, doi MY. Association between polymorphism of tumor necrosis factor alpha (tnfα) in the region−308 g/a with tinnitus in the elderly with a history of occupational noise exposure. *Noise Health*. (2018) 20:37−41. doi: 10.4103/nah.NAH_34_17
156. Doi MY, Dias AC, Poly-Frederico RC, Maria MG, de Oliveira MN, de Moraes Marchiori LL. Association between polymorphism of interleukin-6 in the region−174G/C and tinnitus in the elderly with a history of occupational noise exposure. *Noise Health*. (2015) 17:406–10. doi: 10.4103/1463-1741.169703
157. Masgrau R, Guaza C, Ransohoff RM, Galea E. Should we stop saying 'glia' and 'neuroinflammation'? *Trends Mol Med*. (2017) 23:486–500. doi: 10.1016/j.molmed.2017.04.005
158. Petrackova A, Horak P, Radvansky M, Fillerova R, Smotkova Kraiczova V, Kudelka M, et al. Revealed heterogeneity in rheumatoid arthritis based on multivariate innate signature analysis. *Clin Exp Rheumatol*. (2019) 13:1–7. doi: 10.1155/2019/3575803
159. Lopez-Escamez JA, Batuecas-Caletrio A, Bisdorff A. Towards personalized medicine in Ménière's disease. *F1000Res*. (2018) 7:F1000. doi: 10.12688/f1000research.14417.1
160. Borg-Bartolo SP, Boyapati RK, Satsangi J, Kalla R. Precision medicine in inflammatory bowel disease: concept, progress and challenges. *F1000Res*. (2020) 9:F1000. doi: 10.12688/f1000research.20928.1
161. Galve-Roperh I, Chiurchiù V, Díaz-Alonso J, Bari M, Guzmán M, Maccarrone M. Cannabinoid receptor signaling in progenitor/stem cell proliferation and differentiation. *Prog Lipid Res*. (2013) 52:633–50. doi: 10.1016/j.plipres.2013.05.004
162. Patel KD, Davison JS, Pittman QJ, Sharkey KA. Cannabinoid CB(2) receptors in health and disease. *Curr Med Chem*. (2010) 17:1393–410. doi: 10.2174/092986710790980041
163. O'Sullivan SE, Kendall DA. Cannabinoid activation of peroxisome proliferator-activated receptors: potential for modulation of inflammatory disease. *Immunobiology*. (2010) 215:611–6. doi: 10.1016/j.imbio.2009.09.007
164. Parenti A, De Logu F, Geppetti P, Benemei S. What is the evidence for the role of TRP channels in inflammatory and immune cells? *Br J Pharmacol*. (2016) 173:953–69. doi: 10.1111/bph.13392
165. Santoni G, Cardinali C, Morelli MB, Santoni M, Nabissi M, Amantini C. Danger- and pathogen-associated molecular patterns recognition by pattern-recognition receptors and ion channels of the transient receptor potential family triggers the inflammasome activation in immune cells and sensory neurons. *J Neuroinflammation*. (2015) 12:21. doi: 10.1186/s12974-015-0239-2
166. Klein TW, Newton C, Zhu W, Daaka Y, Friedman H. delta 9-Tetrahydrocannabinol, cytokines, and immunity to Legionella pneumophila. *Proc Soc Exp Biol Med*. (1995) 209:205–12. doi: 10.3181/00379727-209-43897b
167. Lee SF, Newton C, Widen R, Friedman H, Klein TW. Differential expression of cannabinoid CB(2) receptor mRNA in mouse immune cell subpopulations and following B cell stimulation. *Eur J Pharmacol*. (2001) 423:235–41. doi: 10.1016/S0014-2999(01)01122-0
168. Castaneda JT, Harui A, Kiertscher SM, Roth JD, Roth MD. Differential expression of intracellular and extracellular CB(2) cannabinoid receptor protein by human peripheral blood leukocytes. *J Neuroimmune Pharmacol*. (2013) 8:323–32. doi: 10.1007/s11481-012-9430-8
169. Castaneda JT, Harui A, Roth MD. Regulation of cell surface CB2 receptor during human B cell activation and differentiation. *J Neuroimmune Pharmacol*. (2017) 12:544–54. doi: 10.1007/s11481-017-9744-7
170. Massi P, Vaccani A, Parolaro D. Cannabinoids, immune system and cytokine network. *Curr Pharm Des*. (2006) 12:3135–46. doi: 10.2174/138161206777947425
171. Herring AC, Koh WS, Kaminski NE. Inhibition of the cyclic AMP signaling cascade and nuclear factor binding to CRE and κB elements by cannabinol, a minimally CNS-active cannabinoid. *Biochem Pharmacol*. (1998) 55:1013–23. doi: 10.1016/S0006-2952(97)00630-8
172. Kaminski NE. Immune regulation by cannabinoid compounds through the inhibition of the cyclic AMP signaling cascade and altered gene expression. *Biochem Pharmacol*. (1996) 52:1133–40. doi: 10.1016/0006-2952(96)00480-7
173. Chiurchiù V. Endocannabinoids and immunity. *Cannabis Cannabinoid Res*. (2016) 1:59–66. doi: 10.1089/can.2016.0002
174. Chiurchiù V, Battistini L, Maccarrone M. Endocannabinoid signalling in innate and adaptive immunity. *Immunology*. (2015) 144:352–64. doi: 10.1111/imm.12441
175. Croxford JL, Yamamura T. Cannabinoids and the immune system: potential for the treatment of inflammatory diseases? *J Neuroimmunol*. (2005) 166:3–18. doi: 10.1016/j.jneuroim.2005.04.023
176. Tanasescu R, Constantinescu CS. Cannabinoids and the immune system: an overview. *Immunobiology*. (2010) 215:588–97. doi: 10.1016/j.imbio.2009.12.005
177. Kumar V. Toll-like receptors in the pathogenesis of neuroinflammation. *J Neuroimmunol*. (2019) 332:16–30. doi: 10.1016/j.jneuroim.2019.03.012
178. Zhang G, Zheng H, Pyykko I, Zou J. The TLR-4/NF-κB signaling pathway activation in cochlear inflammation of rats with noise-induced hearing loss. *Hear Res*. (2019) 379:59–68. doi: 10.1016/j.heares.2019.04.012
179. Møller AR. Tinnitus and pain. *Prog Brain Res*. (2007) 166:47–53. doi: 10.1016/S0079-6123(07)66004-X
180. Jastreboff PJ, Sasaki CT. An animal model of tinnitus: a decade of development. *Am J Otol*. (1994) 15:19–27.
181. Donvito G, Nass SR, Wilkerson JL, Curry ZA, Schurman LD, Kinsey SG, et al. The endogenous cannabinoid system: a budding source of targets for treating inflammatory and neuropathic pain. *Neuropsychopharmacology*. (2018) 43:52–79. doi: 10.1038/npp.2017.204
182. Billakota S, Devinsky O, Marsh E. Cannabinoid therapy in epilepsy. *Curr Opin Neurol*. (2019) 32:220–6. doi: 10.1097/WCO.0000000000000660
183. Han B, Gfroerer JC, Colliver JD. Associations between duration of illicit drug use and health conditions: results from the 2005-2007 national surveys on drug use and health. *Ann Epidemiol*. (2010) 20:289–97. doi: 10.1016/j.annepidem.2010.01.003
184. Qian ZJ, Alyono JC. An association between marijuana use and tinnitus. *Am J Otolaryngol*. (2020) 41:2314. doi: 10.1016/j.amjoto.2019.102314
185. Spaderna M, Addy PH, D'Souza DC. Spicing things up: synthetic cannabinoids. *Psychopharmacology*. (2013) 228:525–40. doi: 10.1007/s00213-013-3188-4
186. Sutlović D, Prkačin I, Vaiano F, Bertol E, Bratinčević MV, Definis-Gojanović M. A case of synthetic cannabinoid poisoning in Croatia. *Arh Hig Rada Toksikol*. (2018) 69:186–90. doi: 10.2478/aiht-2018-69-3100
187. Gertsch J, Pertwee RG, Di Marzo V. Phytocannabinoids beyond the Cannabis plant- do they exist? *Br J Pharmacol*. (2010) 160:523–9. doi: 10.1111/j.1476-5381.2010.00745.x
188. Woelkart K, Salo-Ahen OM, Bauer R. CB receptor ligands from plants. *Curr Top Med Chem*. (2008) 8:173–86. doi: 10.2174/156802608783498023
189. ElSohly MA, Radwan MM, Gul W, Chandra S, Galal A. Phytochemistry of *Cannabis sativa*, L. *Prog Chem Org Nat Prod*. (2017) 103:1–36. doi: 10.1007/978-3-319-45541-9_1
190. Pisanti S, Malfitano AM, Ciaglia E, Lamberti A, Ranieri R, Cuomo G, et al. Cannabidiol: state of the art and new challenges for therapeutic applications. *Pharmacol Ther*. (2017) 175:133–50. doi: 10.1016/j.pharmthera.2017.02.041
191. Edery H, Grunfeld Y, Porath G, Ben-Zvi Z, Shani A, Mechoulam R. Structure-activity relationships in the tetrahydrocannabinol series. Modifications on the aromatic ring and it the side-chain. *Arzneimittelforschung*. (1972) 22:1995–2003.
192. Mechoulam R, Braun P, Gaoni Y. Syntheses of 1-tetrahydrocannabinol and related cannabinoids. *J Am Chem Soc*. (1972) 94:6159–65. doi: 10.1021/ja00772a038

193. ElSohly MA, Gul W, Wanas AS, Radwan MM. Synthetic cannabinoids: analysis and metabolites. *Life Sci*. (2014) 97:78–90. doi: 10.1016/j.lfs.2013.12.212
194. Shevyrin V, Melkozerov V, Endres GW, Safran Y, Morzherin Y. On a new cannabinoid classification system: a sight on the illegal market of novel psychoactive substances. *Cannabis Cannabinoid Res.* (2016) 1:186–94. doi: 10.1089/can.2016.0004
195. Pertwee RG. Targeting the endocannabinoid system with cannabinoid receptor agonists: pharmacological strategies and therapeutic possibilities. *Philos Trans R Soc Lond B Biol Sci*. (2012) 367:3353–63. doi: 10.1098/rstb.2011.0381
196. Kohnz RA, Nomura DK. Chemical approaches to therapeutically target the metabolism and signaling of the endocannabinoid 2-AG and eicosanoids. *Chem Soc Rev*. (2014) 43:6859–69. doi: 10.1039/C4CS00047A
197. Le Boisselier R, Alexandre J, Lelong-Boulouard V, Debruyne D. Focus on cannabinoids and synthetic cannabinoids. *Clin Pharmacol Ther*. (2017) 101:220–9. doi: 10.1002/cpt.563
198. De Luca MA, Fattore L. Therapeutic use of synthetic cannabinoids: still an open issue? *Clin Ther*. (2018) 40:1457–66. doi: 10.1016/j.clinthera.2018.08.002
199. Tai S, Fantegrossi WE. Synthetic cannabinoids: pharmacology, behavioral effects, and abuse potential. *Curr Addict Rep*. (2014) 1:129–36. doi: 10.1007/s40429-014-0014-y
200. Swortwood MJ, Newmeyer MN, Andersson M, Abulseoud OA, Scheidweiler KB, Huestis MA. Cannabinoid disposition in oral fluid after controlled smoked, vaporized, and oral cannabis administration. *Drug Test Anal*. (2017) 9:905–15. doi: 10.1002/dta.2092
201. Lucas CJ, Galettis P, Schneider J. The pharmacokinetics and the pharmacodynamics of cannabinoids. *Br J Clin Pharmacol*. (2018) 84:2477–82. doi: 10.1111/bcp.13710
202. Grotenhermen F. Clinical pharmacokinetics of cannabinoids. *J Cannabis Ther*. (2003) 3:3–51. doi: 10.1300/J175v03n01_02
203. Toennes SW, Ramaekers JG, Theunissen EL, Moeller MR, Kauert GF. Comparison of cannabinoid pharmacokinetic properties in occasional and heavy users smoking a marijuana or placebo joint. *J Anal Toxicol*. (2008) 32:470–7. doi: 10.1093/jat/32.7.470
204. Huestis MA. Human cannabinoid pharmacokinetics. *Chem Biodivers*. (2007) 4:1770–804. doi: 10.1002/cbdv.200790152
205. Badowski ME. A review of oral cannabinoids and medical marijuana for the treatment of chemotherapy-induced nausea and vomiting: a focus on pharmacokinetic variability and pharmacodynamics. *Cancer Chemother Pharmacol*. (2017) 80:441–9. doi: 10.1007/s00280-017-3387-5
206. Siemens AJ, Walczak D, Buckley FE. Characterization of blood disappearance and tissue distribution of [3H]cannabidiol. *Biochem Pharmacol*. (1980) 29:462–4. doi: 10.1016/0006-2952(80)90532-8
207. Hazekamp A, Ware MA, Muller-Vahl KR, Abrams D, Grotenhermen F. The medicinal use of cannabis and cannabinoids-an international cross-sectional survey on administration forms. *J Psychoactive Drugs*. (2013) 45:199–210. doi: 10.1080/02791072.2013.805976
208. Baguley D, McFerran D, Hall D. Tinnitus. *Lancet*. (2013) 382:1600–7. doi: 10.1016/S0140-6736(13)60142-7
209. McFerran DJ, Stockdale D, Holme R, Large CH, Baguley DM. Why is there no cure for tinnitus? *Front Neurosci*. (2019) 13:802. doi: 10.3389/fnins.2019.00802
210. Shore SE, Roberts LE, Langguth B. Maladaptive plasticity in tinnitus–triggers, mechanisms and treatment. *Nat Rev Neurol*. (2016) 12:150–60. doi: 10.1038/nrneurol.2016.12
211. Brotherton H, Turtle C, Plack CJ, Munro KJ, Schaette R. Earplug-induced changes in acoustic reflex thresholds suggest that increased subcortical neural gain may be necessary but not sufficient for the occurrence of tinnitus. *Neuroscience*. (2019) 407:192–9. doi: 10.1016/j.neuroscience.2019.03.017
212. Guest H, Munro KJ, Prendergast G, Howe S, Plack CJ. Tinnitus with a normal audiogram: Relation to noise exposure but no evidence for cochlear synaptopathy. *Hear Res*. (2017) 344:265–74. doi: 10.1016/j.heares.2016.12.002
213. Hullfish J, Sedley W, Vanneste S. Prediction and perception: Insights for (and from) tinnitus. *Neurosci Biobehav Rev*. (2019) 102:1–12. doi: 10.1016/j.neubiorev.2019.04.008
214. Möhrle D, Hofmeier B, Amend M, Wolpert S, Ni K, Bing D, et al. Enhanced central neural gain compensates acoustic trauma-induced cochlear impairment, but unlikely correlates with tinnitus and hyperacusis. *Neuroscience*. (2019) 407:146–69. doi: 10.1016/j.neuroscience.2018.12.038
215. Sedley W. Tinnitus: does gain explain? *Neuroscience*. (2019) 407:213–28. doi: 10.1016/j.neuroscience.2019.01.027
216. Rauschecker JP, May ES, Maudoux A, Ploner M. Frontostriatal gating of tinnitus and chronic pain. *Trends Cogn Sci*. (2015) 19:567–78. doi: 10.1016/j.tics.2015.08.002
217. Sedley W, Friston KJ, Gander PE, Kumar S, Griffiths TD. An integrative tinnitus model based on sensory precision. *Trends Neurosci*. (2016) 39:799–812. doi: 10.1016/j.tins.2016.10.004
218. Brozoski TJ, Bauer CA. Animal models of tinnitus. *Hear Res*. (2016) 338:88–97. doi: 10.1016/j.heares.2015.10.011
219. Wallhäusser-Franke E, D'Amelio R, Glauner A, Delb W, Servais JJ, Hörmann K, et al. Transition from acute to chronic tinnitus: predictors for the development of chronic distressing tinnitus. *Front Neurol*. (2017) 8:605. doi: 10.3389/fneur.2017.00605
220. Husain FT. Neural networks of tinnitus in humans: Elucidating severity and habituation. *Hear Res*. (2016) 334:37–48. doi: 10.1016/j.heares.2015.09.010
221. Elgoyhen AB, Langguth B, De Ridder D, Vanneste S. Tinnitus: perspectives from human neuroimaging. *Nat Rev Neurosci*. (2015) 16:632–42. doi: 10.1038/nrn4003
222. Baizer JS, Manohar S, Paolone NA, Weinstock N, Salvi RJ. Understanding tinnitus: the dorsal cochlear nucleus, organization and plasticity. *Brain Res*. (2012) 1485:40–53. doi: 10.1016/j.brainres.2012.03.044
223. Zhao Y, Rubio M, Tzounopoulos T. Mechanisms underlying input-specific expression of endocannabinoid-mediated synaptic plasticity in the dorsal cochlear nucleus. *Hear Res*. (2011) 279:67–73. doi: 10.1016/j.heares.2011.03.007
224. Ghosh S, Sheth S, Sheehan K, Mukherjea D, Dhukhwa A, Borse V, et al. The endocannabinoid/cannabinoid receptor 2 system protects against cisplatin-induced hearing loss. *Front Cell Neurosci*. (2018) 12:271. doi: 10.3389/fncel.2018.00271
225. Bhatta P, Dhukhwa A, Sheehan K, Al Aameri RFH, Borse V, Ghosh S, et al. Capsaicin protects against cisplatin ototoxicity by changing the STAT3/STAT1 ratio and activating cannabinoid (CB2) receptors in the cochlea. *Sci Rep*. (2019) 9:4131. doi: 10.1038/s41598-019-40425-9
226. Chen YC, Li X, Liu L, Wang J, Lu CQ, Yang M, et al. Tinnitus and hyperacusis involve hyperactivity and enhanced connectivity in auditory-limbic-arousal-cerebellar network. *Elife*. (2015) 4:e06576. doi: 10.7554/eLife.06576.012
227. He W, Yu J, Sun Y, Kong W. Macrophages in noise-exposed cochlea: changes, regulation and the potential role. *Aging Dis*. (2020) 11:191–9. doi: 10.14336/AD.2019.0723
228. Miyao M, Firestein GS, Keithley EM. Acoustic trauma augments the cochlear immune response to antigen. *Laryngoscope*. (2008) 118:1801–8. doi: 10.1097/MLG.0b013e31817e2c27
229. Baizer JS, Wong KM, Manohar S, Hayes SH, Ding D, Dingman R, et al. Effects of acoustic trauma on the auditory system of the rat: the role of microglia. *Neuroscience*. (2015) 303:299–311. doi: 10.1016/j.neuroscience.2015.07.004
230. Hu SS, Mei L, Chen JY, Huang ZW, Wu H. Effects of salicylate on the inflammatory genes expression and synaptic ultrastructure in the cochlear nucleus of rats. *Inflammation*. (2014) 37:365–73. doi: 10.1007/s10753-013-9748-2
231. Manohar S, Dahar K, Adler HJ, Dalian D, Salvi R. Noise-induced hearing loss: neuropathic pain via Ntrk1 signaling. *Mol Cell Neurosci*. (2016) 75:101–12. doi: 10.1016/j.mcn.2016.07.005
232. Fuentes-Santamaría V, Alvarado JC, Melgar-Rojas P, Gabaldón-Ull MC, Miller JM, Juiz JM. The role of glia in the peripheral and central auditory system following noise overexposure: contribution of TNF-α and IL-1β to the pathogenesis of hearing loss. *Front Neuroanat*. (2017) 11:9. doi: 10.3389/fnana.2017.00009

233. Zheng Y, Baek JH, Smith PF, Darlington CL. Cannabinoid receptor down-regulation in the ventral cochlear nucleus in a salicylate model of tinnitus. *Hear Res*. (2007) 228:105–11. doi: 10.1016/j.heares.2007.01.028
234. Curry RJ, Peng K, Lu Y. Neurotransmitter- and release-mode-specific modulation of inhibitory transmission by group I metabotropic glutamate receptors in central auditory neurons of the mouse. *J Neurosci*. (2018) 38:8187–99. doi: 10.1523/JNEUROSCI.0603-18.2018
235. Valdés-Baizabal C, Parras GG, Ayala YA, Malmierca MS. Endocannabinoid modulation of stimulus-specific adaptation in inferior colliculus neurons of the rat. *Sci Rep*. (2017). 7:6997. doi: 10.1038/s41598-017-07460-w
236. Medeiros P, de Freitas RL, Silva MO, Coimbra NC, Melo-Thomas L. CB1 cannabinoid receptor-mediated anandamide signaling mechanisms of the inferior colliculus modulate the haloperidol-induced catalepsy. *Neuroscience*. (2016) 337:17–26. doi: 10.1016/j.neuroscience.2016.08.047
237. Trettel J, Levine ES. Cannabinoids depress inhibitory synaptic inputs received by layer 2/3 pyramidal neurons of the neocortex. *J Neurophysiol*. (2002) 88:534–9. doi: 10.1152/jn.2002.88.1.534
238. Toal KL, Radziwon KE, Holfoth DP, Xu-Friedman MA, Dent ML. Audiograms, gap detection thresholds, and frequency difference limens in cannabinoid receptor 1 knockout mice. *Hear Res*. (2016) 332:217–22. doi: 10.1016/j.heares.2015.09.013
239. Leishman E, Mackie K, Bradshaw HB. Elevated levels of arachidonic acid-derived lipids including prostaglandins and endocannabinoids are present throughout ABHD12 knockout brains: novel insights into the neurodegenerative phenotype. *Front Mol Neurosci*. (2019) 12:142. doi: 10.3389/fnmol.2019.00142
240. Kedzior KK, Martin-Iverson MT. Chronic cannabis use is associated with attention-modulated reduction in prepulse inhibition of the startle reflex in healthy humans. *J Psychopharmacol*. (2006) 20:471–84. doi: 10.1177/0269881105057516
241. Lisboa SF, Gomes FV, Terzian AL, Aguiar DC, Moreira FA, Resstel LB, et al. The endocannabinoid system and anxiety. *Vitam Horm*. (2017) 103:193–279. doi: 10.1016/bs.vh.2016.09.006
242. Fiskerstrand T, H'mida-Ben Brahim D, Johansson S, et al. Mutations in ABHD12 cause the neurodegenerative disease PHARC: An inborn error of endocannabinoid metabolism. *Am J Hum Genet*. (2010). 87:410–7. doi: 10.1016/j.ajhg.2010.08.002
243. Blankman JL, Long JZ, Trauger SA, Siuzdak G, Cravatt BF. ABHD12 controls brain lysophosphatidylserine pathways that are deregulated in a murine model of the neurodegenerative disease PHARC. *Proc Natl Acad Sci USA*. (2013). 110:1500–5. doi: 10.1073/pnas.1217121110
244. Kamat SS, Camara K, Parsons WH, et al. Immunomodulatory lysophosphatidylserines are regulated by ABHD16A and ABHD12 interplay. *Nat Chem Biol*. (2015). 11:164–71. doi: 10.1038/nchembio.1721
245. Ogasawara D, Ichu TA, Vartabedian VF, Benthuysen J, Jing H, Reed A, et al. Selective blockade of the lyso-PS lipase ABHD12 stimulates immune responses *in vivo*. *Nat Chem Biol*. (2018) 14:1099–108. doi: 10.1038/s41589-018-0155-8
246. Tschöp J, Kasten KR, Nogueiras R, Goetzman HS, Cave CM, England LG, et al. The cannabinoid receptor 2 is critical for the host response to sepsis. *J Immunol*. (2009) 183:499–505. doi: 10.4049/jimmunol.0900203
247. Li Y, Kim J. CB2 cannabinoid receptor knockout in mice impairs contextual long-term memory and enhances spatial working memory. *Neural Plast*. (2016). 2016:9817089. doi: 10.1155/2016/9817089
248. Hwang JH, Chan YC. Expression of dopamine receptor 1A and cannabinoid receptor 1 genes in the cochlea and brain after salicylate-induced tinnitus. *ORL J Otorhinolaryngol Relat Spec*. (2016) 78:268–75. doi: 10.1159/000449170
249. Sheth S, Mukherjea D, Rybak LP, Ramkumar V. Mechanisms of cisplatin-induced ototoxicity and otoprotection. *Front Cell Neurosci*. (2017) 11:338. doi: 10.3389/fncel.2017.00338
250. Jiang M, Li H, Johnson A, Karasawa T, Zhang Y, Meier WB, et al. Inflammation up-regulates cochlear expression of TRPV1 to potentiate drug-induced hearing loss. *Sci Adv*. (2019) 5:eaaw1836. doi: 10.1126/sciadv.aaw1836
251. Blair HA. Capsaicin 8% dermal patch: a review in peripheral neuropathic pain. *Drugs*. (2018) 78:1489–500. doi: 10.1007/s40265-018-0982-7
252. Ashton JC, Appleton I, Darlington CL, Smith PF. Cannabinoid CB1 receptor protein expression in the rat choroid plexus: a possible involvement of cannabinoids in the regulation of cerebrospinal fluid. *Neurosci Lett*. (2004) 364:40–2. doi: 10.1016/j.neulet.2004.04.016
253. Baek JH, Zheng Y, Darlington CL, Smith PF. Cannabinoid CB2 receptor expression in the rat brainstem cochlear and vestibular nuclei. *Acta Otolaryngol*. (2008) 128:961–7. doi: 10.1080/00016480701796944
254. Molina-Holgado F, Rubio-Araiz A, García-Ovejero D, Williams RJ, Moore JD, Arévalo-Martín A, et al. CB2 cannabinoid receptors promote mouse neural stem cell proliferation. *Eur J Neurosci*. (2007) 25:629–34. doi: 10.1111/j.1460-9568.2007.05322.x
255. Tighilet B, Dutheil S, Siponen MI, Noreña AJ. Reactive neurogenesis and down-regulation of the potassium-chloride cotransporter KCC2 in the cochlear nuclei after cochlear deafferentation. *Front Pharmacol*. (2016) 7:281. doi: 10.3389/fphar.2016.00281
256. Terr LI, Edgerton BJ. Physical effects of the choroid plexus on the cochlear nuclei in man. *Acta Otolaryngol*. (1985) 100:210–7. doi: 10.3109/00016488509104783
257. Perin P, Voigt FF, Bethge P, Helmchen F, Pizzala R. iDISCO+ for the study of neuroimmune architecture of the rat auditory brainstem. *Front Neuroanat*. (2019) 13:15. doi: 10.3389/fnana.2019.00015
258. Marques F, Sousa JC, Brito MA, Pahnke J, Santos C, Correia-Neves M, et al. The choroid plexus in health and in disease: dialogues into and out of the brain. *Neurobiol Dis*. (2017). 107:32–40. doi: 10.1016/j.nbd.2016.08.011
259. Bhattacharyya S, Falkenberg I, Martin-Santos R, Atakan Z, Crippa JA, Giampietro V, et al. Cannabinoid modulation of functional connectivity within regions processing attentional salience. *Neuropsychopharmacology*. (2015) 40:1343–52. doi: 10.1038/npp.2014.258
260. Bonn-Miller MO, Zvolensky MJ, Bernstein A. Marijuana use motives: concurrent relations to frequency of past 30-day use and anxiety sensitivity among young adult marijuana smokers. *Addict Behav*. (2007) 32:49–62. doi: 10.1016/j.addbeh.2006.03.018
261. Hall W, Solowij N. Adverse effects of cannabis. *Lancet*. (1998) 352:1611–6. doi: 10.1016/S0140-6736(98)05021-1
262. Viveros MP, Llorente R, Moreno E, Marco EM. Behavioural and neuroendocrine effects of cannabinoids in critical developmental periods. *Behav Pharmacol*. (2005) 16:353–62. doi: 10.1097/00008877-200509000-00007
263. Fusar-Poli P, Crippa JA, Bhattacharyya S, Borgwardt SJ, Allen P, Martin-Santos R, et al. Distinct effects of {delta}9-tetrahydrocannabinol and cannabidiol on neural activation during emotional processing. *Arch Gen Psychiatry*. (2009) 66:95–105. doi: 10.1001/archgenpsychiatry.2008.519
264. Papagianni EP, Stevenson CW. Cannabinoid regulation of fear and anxiety: an update. *Curr Psychiatry Rep*. (2019) 21:38. doi: 10.1007/s11920-019-1026-z
265. White CM. A Review of human studies assessing Cannabidiol's (CBD) therapeutic actions and potential. *J Clin Pharmacol*. (2019) 47:10. doi: 10.1002/jcph.1387
266. Elms L, Shannon S, Hughes S, Lewis N. Cannabidiol in the treatment of post-traumatic stress disorder: a case series. *J Altern Complement Med*. (2019) 25:392–7. doi: 10.1089/acm.2018.0437
267. Zheng Y, Reid P, Smith PF. Cannabinoid CB1 receptor agonists do not decrease, but may increase acoustic trauma-induced tinnitus in rats. *Front Neurol*. (2015) 6:60. doi: 10.3389/fneur.2015.00060
268. Zheng Y, Stiles L, Hamilton E, Smith PF, Darlington CL. The effects of the synthetic cannabinoid receptor agonists, WIN55,212-2 and CP55,940, on salicylate-induced tinnitus in rats. *Hear Res*. (2010) 268:145–50. doi: 10.1016/j.heares.2010.05.015
269. Berger JI, Coomber B, Hill S, Alexander SPH, Owen W, Palmer AR, et al. Effects of the cannabinoid CB_1 agonist ACEA on salicylate ototoxicity, hyperacusis and tinnitus in guinea pigs. *Hear Res*. (2017) 356:51–62. doi: 10.1016/j.heares.2017.10.012

270. Boggs DL, Nguyen JD, Morgenson D, Taffe MA, Ranganathan M. Clinical and preclinical evidence for functional interactions of cannabidiol and Δ9-tetrahydrocannabinol. *Neuropsychopharmacology*. (2018) 43:142–54. doi: 10.1038/npp.2017.209
271. Bow EW, Rimoldi JM. The structure-function relationships of classical cannabinoids: CB1/CB2 modulation. *Perspect Medicin Chem*. (2016) 8:17–39. doi: 10.4137/PMC.S32171
272. Morgan CJ, Schafer G, Freeman TP, Curran HV. Impact of cannabidiol on the acute memory and psychotomimetic effects of smoked cannabis: naturalistic study: naturalistic study [corrected]. *Br J Psychiatry*. (2010) 197:285–90. doi: 10.1192/bjp.bp.110.077503
273. Ibeas Bih C, Chen T, Nunn AV, Bazelot M, Dallas M, Whalley BJ. Molecular targets of cannabidiol in neurological disorders. *Neurotherapeutics*. (2015) 12:699–730. doi: 10.1007/s13311-015-0377-3
274. Elsaid S, Kloiber S, Le Foll B. Effects of cannabidiol (CBD) in neuropsychiatric disorders: a review of pre-clinical and clinical findings. *Prog Mol Biol Transl Sci*. (2019) 167:25–75. doi: 10.1016/bs.pmbts.2019.06.005
275. Thomas A, Baillie GL, Phillips AM, Razdan RK, Ross RA, Pertwee RG. Cannabidiol displays unexpectedly high potency as an antagonist of CB1 and CB2 receptor agonists *in vitro*. *Br J Pharmacol*. (2007) 150:613–23. doi: 10.1038/sj.bjp.0707133
276. Laprairie RB, Bagher AM, Kelly MEM, Denovan-Wright EM. Cannabidiol is a negative allosteric modulator of the cannabinoid CB1 receptor. *Br J Pharmacol*. (2015) 172:4790–805. doi: 10.1111/bph.13250
277. Bisogno T, Sepe N, Melck D, Maurelli S, De Petrocellis L, Di Marzo V. Biosynthesis, release and degradation of the novel endogenous cannabimimetic metabolite 2-arachidonoylglycerol in mouse neuroblastoma cells. *Biochem J*. (1997) 322 (Pt 2)(Pt 2):671–7. doi: 10.1042/bj3220671
278. Massi P, Valenti M, Vaccani A, Gasperi V, Perletti G, Marras E, et al. 5-Lipoxygenase and anandamide hydrolase (FAAH) mediate the antitumor activity of cannabidiol, a non-psychoactive cannabinoid. *J Neurochem*. (2008) 104:1091–100. doi: 10.1111/j.1471-4159.2007.05073.x
279. Pazos MR, Mohammed N, Lafuente H, Santos M, Martínez-Pinilla E, Moreno E, et al. Mechanisms of cannabidiol neuroprotection in hypoxic-ischemic newborn pigs: role of 5HT(1A) and CB2 receptors. *Neuropharmacology*. (2013) 71:282–91. doi: 10.1016/j.neuropharm.2013.03.027
280. Laun AS, Song Z-H. GPR3 and GPR6, novel molecular targets for cannabidiol. *Biochem Biophys Res Commun*. (2017) 490:17–21. doi: 10.1016/j.bbrc.2017.05.165
281. Russo EB, Burnett A, Hall B, Parker KK. Agonistic properties of cannabidiol at 5-HT1a receptors. *Neurochem Res*. (2005) 30:1037–43. doi: 10.1007/s11064-005-6978-1
282. Austgen JR, Kline DD. Endocannabinoids blunt the augmentation of synaptic transmission by serotonin 2A receptors in the nucleus tractus solitarii (nTS). *Brain Res*. (2013) 1537:27–36. doi: 10.1016/j.brainres.2013.09.006
283. Yang KH, Galadari S, Isaev D, Petroianu G, Shippenberg TS, Oz M. The nonpsychoactive cannabinoid cannabidiol inhibits 5-hydroxytryptamine3A receptor-mediated currents in Xenopus laevis oocytes. *J Pharmacol Exp Ther*. (2010) 333:547–54. doi: 10.1124/jpet.109.162594
284. Hind WH, England TJ, O'Sullivan SE. Cannabidiol protects an in vitro model of the blood-brain barrier from oxygen-glucose deprivation via PPARγ and 5-HT1A receptors. *Br J Pharmacol*. (2016) 173:815–25. doi: 10.1111/bph.13368
285. de Mello Schier RA, de Oliveira Ribeiro PN, Coutinho SD, Machado S, Arias-Carrión O, Crippa AJ, et al. Antidepressant-like and anxiolytic-like effects of cannabidiol: a chemical compound of cannabis sativa. *CNS Neurol Disord Drug Targets*. (2014) 13:953–60. doi: 10.2174/1871527313666140612114838
286. Gonca E, Darici F. The effect of cannabidiol on ischemia/reperfusion-induced ventricular arrhythmias: the role of adenosine A1 receptors. *J Cardiovasc Pharmacol Ther*. (2015) 20:76–83. doi: 10.1177/1074248414532013
287. Castillo A, Tolón MR, Fernández-Ruiz J, Romero J, Martinez-Orgado J. The neuroprotective effect of cannabidiol in an in vitro model of newborn hypoxic-ischemic brain damage in mice is mediated by CB(2) and adenosine receptors. *Neurobiol Dis*. (2010) 37:434–40. doi: 10.1016/j.nbd.2009.10.023
288. Ahrens J, Demir R, Leuwer M, De La Roche J, Krampfl K, Foadi N, et al. The nonpsychotropic cannabinoid cannabidiol modulates and directly activates alpha-1 and alpha-1-beta glycine receptor function. *Pharmacology*. (2009) 83:217. doi: 10.1159/000201556
289. Xiong W, Cui T, Cheng K, Yang F, Chen SR, Willenbring D, et al. Cannabinoids suppress inflammatory and neuropathic pain by targeting alpha3 glycine receptors. *J Exp Med*. (2012) 209:1121. doi: 10.1084/jem.20120242
290. Mahgoub M, Keun-Hang SY, Sydorenko V, Ashoor A, Kabbani N, Al Kury L, et al. Effects of cannabidiol on the function of α7-nicotinic acetylcholine receptors. *Eur J Pharmacol*. (2013) 720:310–9. doi: 10.1016/j.ejphar.2013.10.011
291. Kathmann M, Flau K, Redmer A, Tränkle C, Schlicker E. Cannabidiol is an allosteric modulator at mu- and delta-opioid receptors. *Naunyn Schmiedebergs Arch Pharmacol*. (2006) 372:354–61. doi: 10.1007/s00210-006-0033-x
292. Deiana S, Watanabe A, Yamasaki Y, Amada N, Arthur M, Fleming S, et al. Plasma and brain pharmacokinetic profile of cannabidiol (CBD), cannabidivarine (CBDV), Δ^9-tetrahydrocannabivarin (THCV) and cannabigerol (CBG) in rats and mice following oral and intraperitoneal administration and CBD action on obsessive-compulsive behaviour. *Psychopharmacology*. (2012). 219:859–73. doi: 10.1007/s00213-011-2415-0
293. Papke RL, Jon M. Lindstrom, Nicotinic acetylcholine receptors: conventional and unconventional ligands and signaling, *Neuropharmacology*. (2020) 168:8021. doi: 10.1016/j.neuropharm.2020.108021
294. Egea JI, Buendia E, Parada E, Navarro R, Leon MG. Lopez Anti-inflammatory role of microglial alpha, nAChRs and its role in neuroprotection. *Biochem Pharmacol*. (2015) 97:463–72. doi: 10.1016/j.bcp.2015.07.032
295. de Jonge WJ, van der Zanden EP, The FO, Bijlsma MF, van Westerloo DJ, Bennink RJ, et al. Stimulation of the vagus nerve attenuates macrophage activation by activating the Jak2-STAT3 signaling pathway. *Nat Immunol*. (2005) 6:844–51. doi: 10.1038/ni1229
296. Chatterjee PK, Al-Abed YB, Sherry CN. Metz Cholinergic agonists regulate JAK2/STAT3 signaling to suppress endothelial cell activation. *Am J Physiol Cell Physiol*. (2009) 297:C1294–306. doi: 10.1152/ajpcell.00160.2009
297. Marrero MB, Bencherif M. Convergence of alpha 7 nicotinic acetylcholine receptor-activated pathways for anti-apoptosis and anti-inflammation: central role for JAK2 activation of STAT3 and NF-kappaB. *Brain Res*. (2009) 1256:1–7. doi: 10.1016/j.brainres.2008.11.053
298. Zhang Q, Lu Y, Bian H, Guo L, Zhu H. Activation of the alpha7 nicotinic receptor promotes lipopolysaccharide-induced conversion of M1 microglia to M2. *Am J Transl Res*. (2017) 9:971–85.
299. Watkins AR. Cannabinoid interactions with ion channels and receptors. *Channels*. (2019) 13:162–7. doi: 10.1080/19336950.2019.1615824
300. Ross HR, Napier I, Connor M. Inhibition of recombinant human T-type calcium channels by Delta9-tetrahydrocannabinol and cannabidiol. *J Biol Chem*. (2008) 283:16124–34. doi: 10.1074/jbc.M707104200
301. De Petrocellis L, Ligresti A, Moriello AS, Allarà M, Bisogno T, Petrosino S, et al. Effects of cannabinoids and cannabinoid-enriched Cannabis extracts on TRP channels and endocannabinoid metabolic enzymes. *Br J Pharmacol*. (2011) 163:1479–94. doi: 10.1111/j.1476-5381.2010.01166.x
302. Bisogno TL, Hanus L, De Petrocellis S, Tchilibon DE, Ponde I, et al. Molecular targets for cannabidiol and its synthetic analogues: effect on vanilloid VR1 receptors and on the cellular uptake and enzymatic hydrolysis of anandamide. *Br J Pharmacol*. (2001) 134:845–52. doi: 10.1038/sj.bjp.0704327
303. Costa B, Giagnoni G, Franke C, Trovato AE, Colleoni M. Vanilloid TRPV1 receptor mediates the antihyperalgesic effect of the

nonpsychoactive cannabinoid, cannabidiol, in a rat model of acute inflammation. *Br J Pharmacol*. (2004) 143:247–50. doi: 10.1038/sj.bjp.0705920

Conflict of Interest: The authors declare that the research was conducted in the absence of any commercial or financial relationships that could be construed as a potential conflict of interest.

Advantages of publishing in Frontiers

OPEN ACCESS
Articles are free to read for greatest visibility and readership

FAST PUBLICATION
Around 90 days from submission to decision

HIGH QUALITY PEER-REVIEW
Rigorous, collaborative, and constructive peer-review

TRANSPARENT PEER-REVIEW
Editors and reviewers acknowledged by name on published articles

Frontiers
Avenue du Tribunal-Fédéral 34
1005 Lausanne | Switzerland

Visit us: www.frontiersin.org
Contact us: frontiersin.org/about/contact

REPRODUCIBILITY OF RESEARCH
Support open data and methods to enhance research reproducibility

DIGITAL PUBLISHING
Articles designed for optimal readership across devices

FOLLOW US
@frontiersin

IMPACT METRICS
Advanced article metrics track visibility across digital media

EXTENSIVE PROMOTION
Marketing and promotion of impactful research

LOOP RESEARCH NETWORK
Our network increases your article's readership